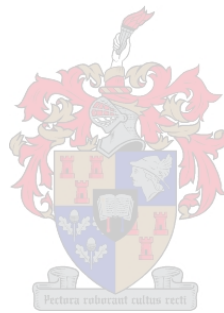


# Geotechnical Characterisation of the Upper Quaternary Sands of the Cape Flats

By Nanine Fouche



Dissertation presented for the degree of Doctor of Philosophy in the Faculty of Engineering at Stellenbosch University

Supervisors:

Prof. Peter W Day

Dr Marius de Wet

March 2021

## **Declaration**

By submitting this thesis electronically, I declare that the entirety of the work contained therein is my own, original work, that I am the sole author thereof (save to the extent explicitly otherwise stated), that reproduction and publication thereof by Stellenbosch University will not infringe any third party rights and that I have not previously in its entirety or in part submitted it for obtaining any qualification.

March 2021

## Abstract

The sand-covered coastal plain connecting the Cape Peninsula mountain chain to the South-Western Cape mainland, is known as the Cape Flats (Hill and Theron, 1981). The area is home to many residents of the greater Cape Town area and is characterised by densely populated townships comprising an amalgamation of formal and informal housing. Rapid on-going civil development is taking place in the Cape Flats to improve existing infrastructure and to develop new facilities for the local communities. The construction of educational, community and public transport facilities and housing developments, are some of the recent and future envisaged improvement projects.

The whitish windblown sands covering this area of approximately 460 km<sup>2</sup>, referred to as the upper Quaternary sands of the Cape Flats, will provide founding material for the proposed infrastructure. A knowledge of the geotechnical properties and engineering behaviour of these sands is essential for design of suitable foundations for proposed structures and earthworks associated with such developments. During the initial planning stages of a project, when assumptions must be made regarding investigation and construction methods best suited to the project, a knowledge of general characterisation can also be beneficial.

This research is the first major contribution towards comprehensively characterising the Quaternary-aged sands of the Witzand, Springfontyn and Langebaan Formations from the Cape Flats in terms of their physical properties and engineering behaviour. By combining, analysing and interpreting the wealth of existing and available geotechnical information from previous and new soil investigations undertaken in the area, this aim was achieved. In-situ and laboratory data from 155 site investigations undertaken in the study area were collected and documented. In addition, new or different methods of investigation and testing not commonly used in the area have been researched, including, but not limited to piezocone penetrometer tests (CPTu), continuous surface wave (CSW) tests, and monotonic and repeated load triaxial tests.

The sands from the study area were classified based on their grading properties, Atterberg limits, maximum dry density and optimum moisture content, minimum dry density, California Bearing Ratio (CBR), erodibility and corrosivity, and characterised in terms of its compressibility, shear strength, permeability, volumetric behaviour during shear including liquefaction potential, in-situ density and moisture content and specific gravity. The geotechnical properties that characterise the distinctive sand formations were explored to produce statistical results, revealing underlying patterns, distinctive trends, distributions and correlations, and the resultant practical importance and probable implications explored. Focus was placed upon determining the nature of the relationships between the soil parameters, specifically for the sands of the Cape Flats, and any inter-formation variation in such relationships.

The typically steep particle size distribution (PSD) curve associated with the shallow Cape Flats sands reflects the predominance of particles with sizes between 0.075mm and 0.6mm (fine and medium sand). The aeolian sands are typically non-plastic or slightly plastic with a typical fines content (<0.075mm) of around 5%. It is the predominance of fine, and to a lesser degree, medium sand size particles, and the shape of these quartzose particles, that typically govern the engineering behaviour of the windblown deposits. In this regard, typical descriptions for some of the soil properties are given below:

- Mainly G7, G8 and G9 quality “gravel-soil” (TRH14 system), Class A-3 materials (AASHTO system), and SP materials (USCS).
- Rarely compacted to densities exceeding  $1850\text{kg/m}^3$  using modified AASHTO compaction effort (owed to the uniform gradation).
- Minimum index density ranging from approximately  $1420\text{kg/m}^3$  to  $1590\text{kg/m}^3$ .
- Specific gravity ( $G_s$ ) of soils with predominantly sand-size grains ranging from 2.62 to 2.69.
- Buried structures susceptible to deterioration via electrochemical processes in certain areas of the Cape Flats.
- Typically, low susceptibility of soil grains to detach and be transported by rainfall and runoff.
- Mostly semi-pervious ( $k = 5.9 \times 10^{-4}$  to  $5.7 \times 10^{-6}$  m/s).
- Typically, moderate to high surface infiltration rates.
- Highly compressible, and either non-collapsible or possessing a low collapse potential.
- Peak friction angles varying from about  $30^\circ$  to  $40^\circ$ , with cohesion values up to about 13kPa.
- Predominantly dilative and locally prone to cyclic liquefaction during dynamic loading (e.g. an earthquake).

These descriptions, which provide a broad and simplified indication of the engineering properties of the material underlying the Cape Flats, could create the impression of a uniform deposit of mainly sandy soils. However, the soils were found to be highly variable (with both inter- and intra-formation variation), with a wide range of values assigned to many material properties; principally a function of soil texture, gradation and degree of cementation. For instance, the calcretised sands of the Witzand and Langebaan Formations will be associated with significantly decreased permeabilities and infiltration rates (thereby increasing run-off and erosion potential of the overlying sands), a potentially collapsible soil fabric (calcium carbonate as bonding agent), increased bearing strength, and shallow perched water tables. The higher fines content associated with the Springfontyn Formation sands resulted in higher compacted densities, whereas peaty layers from the same formation are associated with lower specific gravities (ranging between 2.4 and 2.64), and acidic and potentially corrosive soils. The consistency of the Cape Flats sands varies substantially, both vertically and horizontally (over short distances), and so also its susceptibility to settlement. The variability also showed in the proposed predictive models. Grading parameters were found to be relatively poor predictors of maximum dry density and optimum moisture content, and the relationship between individual California Bearing Ratio and dry density values was weak and only marginally improved by including the grading modulus. In addition, SPT blow count and overburden pressure are not very efficient predictors of shear wave velocity ( $V_s$ ) in the non-uniform sands. Settlement predictions based on small-strain stiffness (obtained from  $V_s$ ) have the advantage of considering non-linear stress-strain behaviour of soil and the degradation of stiffness with increasing strain.

From the above it is evident that the physical properties of the Cape Flats sands are far from simple and cannot be narrowed to a general definition. The findings of this research may be used to form initial appreciation of the likely properties of the material and potential problem areas. This will guide the planning and execution of appropriate site-specific investigations and aid the interpretation of results. This research has shown that there is merit in broadening the current approach to site investigations of the Cape Flats, which traditionally rely heavily on shallow test pits and penetrometer testing. In particular, increased use of CPTu testing and the determination of shear wave velocity by means of CSW or MASW testing should be considered.

## Opsomming

Die sandbedekte gelyktes van die kusgebied wat die Kaap Peninsula bergreeks verbind met die Suidwes-Kaapse vasteland is bekend as die Kaapste Vlakte (Hill en Theron, 1981). Hierdie streek is die tuiste van baie inwoners van die groter Kaapstad area en word gekenmerk deur digbevolkte dorpsgebiede, bestaande uit 'n samestelling van formele en informele behuising. Siviele ontwikkeling op die Kaapse Vlakte vind vining en deurlopend plaas om die bestaande infrastruktuur te verbeter en om nuwe fasiliteite vir die plaaslike bevolking daar te stel. Die konstruksie van opvoedkundige, gemeenskap en openbare vervoer fasiliteite en behuisingsontwikkeling is sommige van die huidige en toekomstige verbeteringsprojekte wat beplan word.

Die witterige, eoliese sand wat hierdie area van ongeveer 460km<sup>2</sup> bedek, is bekend as die boonste Kwartêrne sand van die Kaapse Vlakte en sal fondamentmateriaal vir die voorgestelde infraskruktuur voorsien. 'n Kennis van die geotegniese eienskappe en ingenieursgedrag van hierdie sand is noodsaaklik vir die ontwerp van geskikte fondamente vir voorgestelde strukture en grondwerke wat met die sodanige ontwikkelings gepaardgaan. Gedurende die aanvanklike beplanningsfases van 'n projek, wanneer aannames gemaak moet word rakende ondersoek- en konstruksiemetodes mees geskik vir die projek, kan 'n kennis van die algemene karakterisering ook voordelig wees.

Hierdie navorsing is die eerste grootskaalse bydrae tot omvangryke karakterisering van die Kwartêrne sand van die Witzand, Springfontyn en Langebaan Formasies van die Kaapse Vlakte, in terme van hul fisiese eienskappe en ingenieursgedrag. Deur die kombinerende, analise en interpretasie van die groot hoeveelheid bestaande beskikbare geotegniese data van vorige en nuwe grondondersoeke in die area, is hierdie doelwit bereik. In-situ en laboratorium data van 155 terreinondersoeke in die studie-area is bymekaar gemaak en gedokumenteer. Voeg hierby dat nuwe of verskillende ondersoek- en toetsmetodes, wat nie algemeen gebruik is in die area nie, nagevors is, insluitend maar nie beperk tot piësokegel penetrasie toetse (CPTu), deurlopende oppervlaktgolf (CSW) toetse en monotoniese en herhaalde las drieassige toetse nie.

Die sand van die studie-area is geklassifiseer, gebaseer op hul graderingseienskappe, Atterberg grense, maksimum droë digtheid en optimum voginhoud, minimum droë digtheid, Kaliforniese drakragverhouding (KDV), erodeerbaarheid en korrosiwiteit. Die sand is gekarakteriseer in terme van saamdrukbaarheid, skuifsterkte, deurlatendheid, volumetriese gedrag tydens skuifbeweging insluitend vervloeiings potensiaal, in-situ digtheid en voginhoud en spesifieke digtheid. Die geotegniese eienskappe wat die spesifieke sandformasies kenmerk, is ondersoek om statistiese uitslae te produseer, en dui op onderliggende patrone, spesifieke tendense, verspreiding en korrelasies. Die gevolglike praktiese belangrikheid, asook moontlike implikasies, is ondersoek. Fokus is geplaas op die bepaling van die verhouding tussen grondparameters, spesifiek vir die sand van die Kaapse Vlakte en enige inter-formasie variasies in sodanige verhoudings.

Die tipiese styl partikelgrootteverdeling-kurwe wat met die Kaapse Vlakte sand geassosieer word, toon die oorheersing van deeltjies in grootte tussen 0.075mm en 0.6mm (fyn en medium sand). Die Aeoliese sand is tipies nie-plasties of effens plasties met 'n tipiese fynstof inhoud (<0.075mm) van ongeveer 5%. Dit is die oorheersing van fyn, en in 'n mindere mate, medium sandgrootte deeltjies wat tipies die ingenieursgedrag van die windverwaide afsettings beheer. In die opsig word tipiese beskrywings van sommige grondeienskappe hieronder aangedui.

- Hoofsaaklik G7, G8 en G9 kwaliteit gruisgrond (TRH14 sisteem), klas A-3 materiaal (AASHTO sisteem), en SP materiale (USCS).
- Selde gekompakteer tot digthede wat  $1850\text{kg/m}^3$  oorskry, deur gebruik te maak van gewysigde AASHTO kompaksie energie (as gevolg van die eenvormige gradering).
- Minimum droë digtheid wat varieer van ongeveer  $1420\text{kg/m}^3$  tot  $1590\text{kg/m}^3$ .
- Spesifieke digtheid ( $G_s$ ) van grond wat grootliks sandgrootte korrels bevat varieer van 2.62 tot 2.69.
- Ondergrondse strukture vatbaar vir verswakking via elektro-chemiese prosesse in sekere areas van die Kaapse Vlakte.
- Tipiese lae vatbaarheid van grondkorrels om los te raak en weggevoer te word deur reënval en afloop water.
- Hoofsaaklik semi-deurlatend ( $k = 5.9 \times 10^{-4}$  tot  $5.7 \times 10^{-6}$  m/s).
- Meestal 'n matige tot hoë infiltrasietempo.
- Hoogs saamdrukbaar en nie-swigbaar of 'n lae potensiaal om swigbaar te wees.
- Maksimum wrywingshoeke wat varieer tussen ongeveer  $30^\circ$  en  $40^\circ$  met kohesiewaardes tot en met 13kPa.
- Hoofsaaklike uitdyend gedurende skuif en lokaal geneig tot sikliese vervloeiing gedurende dinamiese belasting (bv. 'n aardbewing).

Bogenoemde beskrywings, wat 'n breë en vereenvoudige aanduiding van die ingenieurseienskappe van die materiaal wat die Kaapse Vlakte onderlê verskaf, kan die indruk skep van 'n eenvormige afsetting van hoofsaaklik sandgrond. Dit is egter gevind dat die grond hoogs veranderlik is (met beide inter- en intra-formasie variasie) met 'n wye verskeidenheid van waardes geassosieer met heelwat materiaal eienskappe, hoofsaaklik 'n funksie van gradering en graad van sementasie. Byvoorbeeld, die gesementeerde (kalkhoudende) sand van die Witzand en Langebaan Formasies sal geassosieer word met 'n laer deurlatendheid en infiltrasietempo (daarby toenemende afloop en erosie van die oorliggende sand), 'n potensiële swigbare grondstruktuur (kalsiumkarbonaat as bindingsstof), verhoogde dravermoë en vlak tydenlike grondwatervlakke. Die hoër fynstof inhoud wat geassosieer word met die Springfontyn Formasie sand het gelei tot hoër kompaksie digtheid, terwyl grond met 'n hoë inhoud organise materiaal in dieselfde formasie met laer spesifieke digtheid (tussen 2.4 en 2.64) geassosieer word, en suur en potensieel korrosief is. Die digtheid van die Kaapse Vlakte sand wissel beduidend, beide vertikaal en horisontaal (oor kort afstande), asook die vatbaarheid vir versakking. Die wisselbaarheid is ook getoon in die voorgestelde transformasie modelle, met die graderingsparameters wat maksimum droë digtheid en optimum voginhoud swak voorspel, asook 'n swak verhouding tussen individuele Kaliforniese drakragverhouding en droë digtheid waardes (ietwat verbeter deur die graderingsmodulus in te sluit). Bykomend, is SPT houtelling en bo-gronddruk nie goeie aanduiders van skuifgolf snelheid ( $V_s$ ) in die nie-eenvormige sand nie. Sullke aanduiders het die voordeel dat dit die nie-lineêre spanning-vervormings gedrag in ag neem wanneer elastiese versakking bereken word.

Uit die bogenoemde is dit duidelik dat die fisiese eienskappe van die Kaapse Vlakte sand vêr van eenvoudig is en kan nie vereenvoudig word tot 'n enkele definisie nie. Die bevindinge van hierdie navorsing kan gebruik word om 'n aanvanklike idee van die waarskynlike eienskappe van die materiaal en potensiële probleemareas te vorm. Hierdie sal die beplanning en uitvoering van terrein-spesifieke ondersoeke lei en die interpretasie van die resultate aanhelp. Hierdie navorsing het aangedui dat daar meriete is in die verbreding van die huidige benadering tot

terreinondersoeke in die Kaapse Vlakte, wat tradisioneel meestal staatmaak op toetsgate en penetrasie toetse. Die vermeerde gebruik van veral CPTu toetse en die bepaling van skuifgolf snelheid ( $V_s$ ) by wyse van CSW of MASW toetse moet oorweeg word.

This thesis is dedicated to my children, Mari and Sois

## Acknowledgements

*~Your grace has brought me here~*

This thesis would have remained an unachievable goal without the selfless and unwavering support of my husband, Francois Fouche. I am grateful for all you have done during this long and sometimes difficult journey. I would like to thank my parents, Petrus and Marianne Gildenhuis, who have encouraged and supported me from the first day of primary school. I hope I have made you proud.

I would like to thank Prof. Peter Day, who has guided me along the way and inspired me to be the best I can be. Thank you for the time you have invested in me and this research. I would also like to thank my co-supervisor, Dr Marius de Wet, for his support and guidance (even after retirement). My interest in geotechnics started in your class. I am also grateful for the support of my colleagues, especially, Dr Charles MacRobert and Prof. Marion Sinclair.

The research would not have been possible without the geotechnical data from past investigations made available by the following companies: Aurecon South Africa (Cape Town), Roadlab (Cape Town), Geoscience Laboratories, Fairbrother Geotechnical Engineering, Council for Geoscience (Cape Town), M. van Wieringen and Associates, Core Geotechnical Consultants, Kantey and Templer Consulting Engineers (Cape Town), Melis and Du Plessis Consulting Engineers, SMEC South Africa (Cape Town), Airports Company SA (Cape Town), Peregrine Geoconsultants (Pretoria), ASLA Group (Cape Town), and the Geotechnical Engineering Division of the University of Cape Town. Special thanks to John Yates and Jurgens Schoeman from Core Geotechnical Consultants for allowing me to perform my investigations alongside theirs, and for Jurgens' assistance on-site.

The piezocone penetrometer testing was made possible by Prof. Peter Day and Jones & Wagener (Pty) Limited and the Geo Group - thank you for this opportunity. I would also like to express my sincere gratitude to Prof. Gerhard Heymann and CSW Soil Engineering for funding and performing the CSW tests.

I wish to thank Colin Isaacs, Ayyoob Soloman and Kintu Sebuyira who assisting in the laboratory and on-site.

Lastly, I would like to thank Danie Smuts and my mother, Marianne, for proofreading the thesis.

## Contents

Declaration.....	ii
Abstract.....	iii
Opsomming.....	v
Acknowledgements.....	ix
Contents.....	x
List of Figures.....	xv
List of Tables.....	xix
List of symbols and abbreviations.....	xxi
1. Introduction.....	1
1.1 Background to the study.....	1
1.2 Problem statement.....	2
1.3 Aim and objectives.....	3
1.4 Contribution of the research.....	4
1.5 Research limitations.....	4
1.6 Thesis outline.....	5
2. Literature Review.....	6
2.1 Introduction.....	6
2.2 The Cape Flats.....	6
2.2.1 Introduction.....	6
2.2.1.1 Locality.....	6
2.2.1.2 Background and development.....	7
2.2.2 Physiography of the Cape Flats.....	8
2.2.2.1 Topography.....	8
2.2.2.2 Drainage and groundwater.....	8
2.2.2.3 Geomorphological history.....	10
2.2.2.4 Climate and rainfall.....	11
2.2.3 Geology of the Cape Flats.....	11
2.2.3.1 Introduction.....	11
2.2.3.2 Stratigraphy.....	12
2.2.3.3 Seismicity.....	14
2.3 Geotechnical and engineering geological characterisation of soils.....	14
2.3.1 Introduction.....	14
2.3.2 Engineering geology of the Cape Flats.....	14

2.4 The geotechnical site investigation.....	18
2.5 The geotechnical properties of cohesionless soils.....	25
2.5.1 Introduction .....	25
2.5.2 Grading properties .....	26
2.5.3 Atterberg limits .....	28
2.5.4 Maximum dry density and optimum moisture content .....	30
2.5.5 California Bearing Ratio .....	32
2.5.6 Minimum and maximum index densities and relative density.....	34
2.5.7 Corrosivity .....	36
2.5.8 Erodibility .....	39
2.5.9 Specific gravity .....	41
2.5.10 In-situ moisture content .....	42
2.5.11 In-situ density.....	44
2.5.12 Collapse Settlement .....	45
2.5.13 Hydraulic conductivity .....	48
2.5.14 Shear strength.....	52
3.5.14.1 Critical state soil concept.....	55
2.5.15 Soil liquefaction.....	57
2.5.16 Compressibility.....	63
2.5.16.1 Soil elastic modulus .....	65
2.5.16.2 Calculation of resilient modulus .....	68
2.5.16.3 Small-strain elastic modulus .....	71
2.6 Aeolian deposits of the interior of Southern Africa.....	81
2.7 Evaluation of literature themes .....	84
3. Methodology.....	85
3.1 Introduction .....	85
3.2 Method overview.....	85
3.3 Data collection .....	86
3.3.1 Existing data .....	86
3.3.2 Additional data.....	87
3.3.2.1 Fieldwork.....	88
3.3.2.2 Laboratory testing methods .....	98
3.4 Data capturing.....	114
3.5 Data processing.....	116

3.5.1 Introduction .....	116
3.5.2 Grading properties .....	116
3.5.3 Material classification .....	118
3.5.4 California Bearing Ratio (CBR).....	118
3.5.5 Corrosivity .....	119
3.5.6 Erodibility .....	121
3.5.7 Collapsibility .....	124
3.5.8 Hydraulic conductivity .....	127
3.5.9 Shear strength.....	132
3.5.10 Dilative/contractive behaviour (liquefaction potential) .....	136
3.5.11 Compressibility.....	141
4. Results and Discussion .....	143
4.1 Introduction .....	143
4.2 Grading results .....	143
4.2.1 Overview .....	143
4.2.2 Texture of Cape Flats sand.....	144
4.2.3 Soil gradation coefficients.....	150
4.2.4 Other grading-related properties .....	151
4.3 Groundwater table.....	153
4.4 Plasticity properties .....	155
4.5 Maximum dry density and optimum moisture content .....	158
4.6 Soil classification .....	164
4.7 California Bearing Ratio .....	167
4.7.1 Laboratory soaked CBR .....	167
4.7.2 In-situ CBR (DCP CBR).....	172
4.8 Minimum index density .....	175
4.9 Corrosivity .....	177
4.9.1 Corrosion influencing factors.....	177
4.9.1.1 pH.....	177
4.9.1.2 Resistivity .....	179
4.9.2 Corrosion indices and classes .....	180
4.10 Erodibility .....	182
4.10.1 Erosion hazard potential.....	182
4.10.2 Soil erodibility factor.....	183

4.10.3 Erosion of unpaved gravel wearing course.....	185
4.11 Specific gravity .....	187
4.12 In-situ density and moisture content.....	188
4.12.1 Field measurements.....	188
4.12.2 Laboratory moisture content test results .....	188
4.13 Collapse settlement .....	191
4.13.1 Empirical methods .....	191
4.13.2 Collapse potential tests.....	192
4.13.3 Summary .....	194
4.14 Hydraulic conductivity .....	195
4.15 Shear strength.....	197
4.15.1 Shear strength of compacted sands .....	197
4.15.1.1 Monotonic triaxial compression tests .....	197
4.15.1.2 Direct shear tests .....	199
4.15.2 Shear strength of reconstituted sands .....	200
4.15.3 Transformation models.....	201
4.15.3.1 SPT-based methods .....	201
4.15.3.2 CPT/CPTu-based methods .....	203
4.16 Dilative/Contractive behaviour (Liquefaction potential).....	206
4.16.1 Cyclic liquefaction potential.....	207
4.16.2 Flow liquefaction potential .....	209
4.17 Compressibility.....	211
4.17.1 Soil elastic modulus.....	212
4.17.1.1 Monotonic triaxial tests .....	212
4.17.1.2 Transformation models.....	215
4.17.2 Resilient modulus.....	219
4.17.2.1 Modelling resilient deformation behaviour.....	220
4.17.2.2 Influence of compaction and moisture content on resilient response .....	223
4.17.3 Small-strain Stiffness.....	225
5. Settlement Analysis.....	231
5.1 Introduction .....	231
5.2 Settlement analysis methods.....	232
5.2.1 Non-linear stepwise method using small-strain stiffness data.....	232
5.2.1.1 Input data.....	233

Soil parameters .....	234
Foundation information.....	234
5.2.2 General elastic solution using SPT $N_{60}$ -E transformation models.....	235
5.2.2.1 Input data.....	236
5.3 Predicted settlements.....	237
5.3.1 Versak analysis results .....	237
5.3.2 Comparative analyses results .....	238
5.3.3 General comments.....	239
6. Conclusions, Summary of Properties and Recommendations.....	243
6.1 Introduction .....	243
6.2 Conclusions .....	244
6.2.1 Soil classification properties .....	244
6.2.2 Soil characterisation properties.....	246
6.2.3 Horizontal and vertical variation of soil properties .....	248
6.2.4 Soil properties for the various formations.....	248
6.2.5 Compressibility and foundation performance in the Cape Flats .....	259
6.3 Recommendations .....	260
6.3.1 Geotechnical Investigations.....	260
6.3.2 Further Research.....	260
References .....	262
Appendix A.....	278
Appendix B.....	280
Appendix C.....	283
Appendix D.....	298
Appendix E.....	305
Appendix F.....	309
Appendix G.....	312
Appendix H.....	335

## List of Figures

Figure 2-1: Locality of the Cape Flats (Hill and Theron, 1981) .....	7
Figure 2-2: Cape Flats draining system (Adelana, Xu and Vrbka, 2010) .....	9
Figure 2-3: Effects of rod friction in DPSH test results .....	21
Figure 2-4: a) $Q_t$ - $F_r$ SBTn chart and b) $Q_t$ - $B_q$ SBTn chart (Robertson and Cabal, 2012 after Robertson, 1990) .....	23
Figure 2-5: Particle size ranges for soil classification as per (a) American Standards ASTM D422:2007) and (b) British Standards (BS1377:1990) .....	26
Figure 2-6: Particle size distribution curves .....	27
Figure 2-7: Atterberg limits of fine-grained soils (modified from Das and Sobhan, 2018) .....	29
Figure 2-8: Dry density-moisture content relationship .....	31
Figure 2-9: CBR test procedure (Jenkins and Rudman, 2016) .....	33
Figure 2-10: Mechanisms of additional settlement due to soil fabric collapse (Schwartz, 1985). 46	
Figure 2-11: Mohr circles from monotonic triaxial test data (Jenkins and Rudman, 2016) .....	53
Figure 2-12: Shear strength characteristics of loose and dense sand (redrawn from Das and Sobhan, 2018) .....	54
Figure 2-13: CSL in (a) $q'$ - $p'$ space and (b) $v$ - $p'$ space .....	56
Figure 2-14: Behaviour of saturated sand in a loose (contractive) state during undrained shear (redrawn from Rauch, 1997) .....	57
Figure 2-15: Behaviour of saturated sand in a dense (dilative) state during undrained shear (redrawn from Rauch, 1997) .....	58
Figure 2-16: State diagram with triaxial stress paths (redrawn from Rauch, 1997) .....	58
Figure 2-17: Comparison of SPT-based liquefaction triggering curves (Idriss and Boulanger, 2010) .....	60
Figure 2-18: Behaviour of isotropic linear elastic material in (a) simple compression and (b) shear (Chen and Mizuno, 1990) .....	65
Figure 2-19: Loading during repeated load triaxial testing (Jenkins and Rudman, 2016) .....	69
Figure 2-20: $M_r$ - $\theta$ model for coarse granular material (Jenkins and Rudman, 2016) .....	70
Figure 2-21: $M_r$ - $\theta$ relationship for bitumen treated granular material (Jenkins and Rudman, 2016) .....	70
Figure 2-22: Non-linear behaviour of soil shear stiffness (Knappett and Craig, 2012) .....	71
Figure 2-23: Typical stiffness degradation curve (after Mair, 1993 from Archer, 2014) .....	72
Figure 2-24: Stiffness degradation functions (Heymann, 2012 as cited in Day, 2016) .....	72
Figure 2-25: Components of the continuous surface wave system (Heymann, 2007) .....	74
Figure 2-26: Influence of geological age on void ratio for sand and clay soils (Ohta and Goto, 1978 from Sykora, 1987) .....	76
Figure 2-27: Shear wave velocity versus void ratio for soils of different geological age (Fumal and Tinsley, 1985 as cited in Sykora, 1987) .....	77
Figure 2-28: Shear wave velocity versus SPT $N_{60}$ and $P_a/\sigma'_v$ (overburden correction term) for sand, silt and clay soils of different geological age (Bellana, 2009) .....	77
Figure 2-29: Existing laboratory data showing SPT blow count versus ( $n_{max} - n$ ) for different overburden values (Shibata, 1970 as cited in Sykora, 1987) .....	78
Figure 3-1: Flow chart of methodology .....	85
Figure 3-2: Mfuleni a) site view northwards and b) soil profile .....	89

Figure 3-3: Gatesville typical soil profile.....	90
Figure 3-4: Stockpiled sand at Bellville South .....	90
Figure 3-5: Piezocone penetrometer testing in the Cape Flats .....	91
Figure 3-6: SBT with depth at a) Capricorn and b) Airport Industria .....	92
Figure 3-7: Nuclear density gauge testing a) at Gatesville by b) lowering the ground level .....	93
Figure 3-8: Double ring infiltrometer test equipment (Eijkelkamp, 2018) .....	94
Figure 3-9: CSW testing at the Athlone WWTW .....	95
Figure 3-10: $V_s$ profile showing measurement uncertainty with depth .....	96
Figure 3-11: Minimum loose density testing .....	99
Figure 3-12: Permeability test, adapted for both constant and falling head tests (Hoffman, 2019) .....	102
Figure 3-13: Determination of $G_s$ with the water pycnometer .....	102
Figure 3-14: Triaxial test setup.....	104
Figure 3-15: Dry density - moisture content curve for Cape Flats sand from Mfuleni.....	105
Figure 3-16: Electronic pan mixer .....	105
Figure 3-17: Vibratory hammer.....	106
Figure 3-18: Split specimen upon opening of mould.....	106
Figure 3-19: Distribution of grain sizes in the unmodified and modified Cape Flats sand from Mfuleni.....	107
Figure 3-20: Membrane enclosing triaxial.....	108
Figure 3-21: Completed specimen setup .....	108
Figure 3-22: Triaxial specimen with LVDT's for dynamic testing .....	111
Figure 3-23: Soil erodibility nomograph (Wischmeier and Smith, 1987) .....	123
Figure 3-24: Performance categories for gravel wearing courses (after TRH20, 1990) .....	124
Figure 3-25: Interpretation of a collapse potential test result (Schwartz, 1985) .....	125
Figure 3-26: Interpretation of dissipation test curve from CPTu tests a) Airport CPTu 2 at 4.27m depth and b) Capricorn CPTu 2 at 9.1m depth .....	131
Figure 3-27: Relationship between cone resistance and drained friction angle for quartz sand (after Durgunoglu and Mitchell, 1975 from Meigh, 1987) .....	135
Figure 3-28: Liquefaction triggering curve for Cape Flats sands .....	138
Figure 3-29: CPT SBTn chart with contractive/dilative soil boundaries (Robertson, 2016) .....	140
Figure 3-30: Relationship between soil stiffness, strain level, and SPT N for sands and gravels (Stroud, 1989 from Clayton, 1993) .....	142
Figure 4-1: Typical Cape Flats PSD curve .....	143
Figure 4-2: Springfontyn Formation variation in soil texture with depth.....	145
Figure 4-3: Witzand Formation variation in soil texture with depth .....	146
Figure 4-4: Langebaan Formation variation in soil texture with depth.....	147
Figure 4-5: Comparison of a) $C_u$ and b) $C_z$ in the upper 2m of the Witzand, Springfontyn and Langebaan Formations.....	150
Figure 4-6: Groundwater levels in the Cape Flats from 2008 to 2018 .....	154
Figure 4-7: Fluctuation in groundwater level in a single Cape Flats borehole .....	155
Figure 4-8: Statistical summary of MDD in the shallow Cape Flats sands .....	158
Figure 4-9: Statistical summary of OMC in the shallow Cape Flats sands .....	159
Figure 4-10: MDD versus GM for the Cape Flats sands .....	162
Figure 4-11: OMC versus GM for the Cape Flats sand .....	163

Figure 4-12: Distribution of USCS classes in the Cape Flats in terms of a) number and b) percentage .....	164
Figure 4-13: Distribution of the TRH14 classes in the Cape Flats in terms of a) number and b) percentage .....	165
Figure 4-14: Distribution of AASHTO classes in the Cape Flats in terms of a) number and b) percentage .....	166
Figure 4-15: Soaked CBR data for the Springfontyn Formation sands .....	168
Figure 4-16: Soaked CBR data for the Witzand Formation sands.....	168
Figure 4-17: Soaked CBR data for the Langebaan Formation sands.....	169
Figure 4-18: CBR versus dry density and regression lines for GM values for the Springfontyn Formation sands .....	172
Figure 4-19: In-situ CBR summary for the Cape Flats sands .....	173
Figure 4-20: CT scan image of Mfuleni sand (Sitela, 2018).....	177
Figure 4-21: Distribution of acidity classes in the Cape Flats in terms of a) number and b) percentage .....	178
Figure 4-22: Distribution of corrosivity ratings based on soil resistivity in the Cape Flats in terms of a) number and b) percentage .....	179
Figure 4-23: Erosion hazard potential map for Region 8, including the Cape Flats (WRC, 2010).....	184
Figure 4-24: Performance of Cape Flats sand as unpaved gravel wearing course .....	186
Figure 4-25: Distribution of gravel wearing course performance in the Cape Flats in terms of a) number and b) percentage .....	186
Figure 4-26: In-situ moisture content summary for all formations.....	191
Figure 4-27: Collapse potential test results for Cape Flats sands.....	194
Figure 4-28: $\sigma_{1,f}$ and $\sigma_3$ relationship for Specimen 1 (CSIR, 2014 method) .....	198
Figure 4-29: Mohr circle plot for Specimen 1 .....	198
Figure 4-30: Comparison of peak friction angles from triaxial and direct shear testing on compacted sands .....	199
Figure 4-31: SPT derived $\phi'$ versus depth.....	203
Figure 4-32: SPT $N_{60}$ versus depth .....	203
Figure 4-33: CPT derived $\phi'$ versus depth.....	206
Figure 4-34: CPTu derived $\phi'$ profiles .....	206
Figure 4-35: Cyclic stress ratio plotted against clean sand equivalent SPT blow count for a design earthquake with $M = 6.0$ and $a_{max} = 0.15g$ .....	207
Figure 4-36: Liquefaction analysis in a borehole in Pinelands.....	208
Figure 4-37: Cyclic stress ratio plotted against clean sand equivalent SPT blow count for design earthquake with $M = 7.5$ and $a_{max} = 0.2g$ .....	208
Figure 4-38: SBTn charts showing dilative/contractive response of Cape Flats soils during shear .....	209
Figure 4-39: Contractive-dilative chart for a CPTu in Airport Industria .....	210
Figure 4-40: Stress-strain plot for $\rho_d = 1560\text{kg/m}^3$ , $w = 9\%$ specimens.....	212
Figure 4-41: Stress-strain plot for $\rho_d = 1560\text{kg/m}^3$ , $w = 12\%$ specimens.....	212
Figure 4-42: Stress-strain plot for $\rho_d = 1660\text{kg/m}^3$ , $w = 9\%$ specimens.....	213
Figure 4-43: Stress-strain plot for $\rho_d = 1660\text{kg/m}^3$ , $w = 12\%$ specimens.....	213
Figure 4-44: Elastic modulus versus confining pressure.....	214
Figure 4-45: Elastic modulus estimates for the Witzand Formation sands .....	216
Figure 4-46: Elastic modulus estimates for the Springfontyn Formation sands.....	216

Figure 4-47: Elastic modulus estimates for the Langebaan Formation sands .....	217
Figure 4-48: Typical graphs of E modulus versus depth in (a) Capricorn and (b) Airport Industria .....	219
Figure 4-49: $M_r$ - $\Theta$ model for $\rho_d = 1660\text{kg/m}^3$ , $w = 9\%$ specimen .....	221
Figure 4-50: $M_r$ - $\sigma_3$ - $\sigma_d$ model for $\rho_d = 1660\text{kg/m}^3$ , $w = 9\%$ specimen.....	221
Figure 4-51: $M_r$ - $\Theta$ model for $\rho_d = 1660\text{kg/m}^3$ , $w = 12\%$ specimen .....	222
Figure 4-52: $M_r$ - $\Theta$ model for $\rho_d = 1560\text{kg/m}^3$ , $w = 9\%$ specimen .....	222
Figure 4-53: $M_r$ - $\Theta$ model for $\rho_d = 1560\text{kg/m}^3$ , $w = 12\%$ specimen .....	223
Figure 4-54: $M_r$ - $\Theta$ model lines showing influence of moisture and density on resilient response .....	224
Figure 4-55: Influence of moisture content and compaction on resilient stiffness .....	224
Figure 4-56: $E_0$ -depth profiles at the a) Cape Flats and Athlone WWTW's and b) Atlantis.....	226
Figure 4-57: a) $V_s$ versus $N_{60}$ with $P_a/\sigma_v'$ trendlines and b) $V_s$ versus $P_a/\sigma_v'$ with $N_{60}$ trendlines .	228
Figure 4-58: Atlantis soils regression results with a) $V_s$ versus $N_{60}$ with $P_a/\sigma_v'$ trendlines and b) $V_s$ versus $P_a/\sigma_v'$ with $N_{60}$ trendlines .....	228
Figure 4-59: Regression residuals versus a) $N_{60}$ and b) $P_a/\sigma_v'$ for all data pairs.....	229
Figure 4-60: Regression residuals versus a) $N_{60}$ and b) $P_a/\sigma_v'$ for Atlantis data.....	229
Figure 4-61: Distribution of regression errors based on a) all data and b) Atlantis data .....	230
Figure 5-1: Softening functions proposed by Archer and Heymann (2015) .....	233
Figure 5-2: SPT $(N_1)_{60}$ profiles.....	235
Figure 5-3: $G_o$ profiles (solid line: WT = 1.5m, dotted line: no WT) .....	235
Figure 5-4: Settlement of square and strip footings at 1m in loose sand.....	240
Figure 5-5: Settlement of square and strip footings at 2m in loose sand .....	240
Figure 5-6: Settlement of square and strip footings at 1m in med dense sand.....	240
Figure 5-7: Settlement of square and strip footings at 2m in med dense sand .....	240
Figure 5-8: Settlement of square and strip footings at 1m in dense sand.....	241
Figure 5-9: Settlement of square and strip footings at 2m in dense sand .....	241
Figure 5-10: Settlement comparison in loose sand (B = 2m and WT = 1.5m).....	242
Figure 5-11: Settlement comparison in medium dense sand (B = 2m and WT = 1.5m).....	242
Figure 5-12: Settlement comparison in dense sand (B = 2m and WT = 1.5m) .....	242

## List of Tables

Table 2-1: Lithology of the Cenozoic Formations of the Cape Flats (after Theron et al., 1992 and Johnson, Anhaeusser and Thomas, 2006) .....	12
Table 2-2: Cape Flats soil properties (compiled from Amdurer, 1956) .....	16
Table 2-3: Summarised soil properties of Cape Flats sediment (compiled from Brink, 1985) .....	17
Table 2-4: Relative density of sandy soils with corresponding SPT N-values (composite from Jennings, Brink and Williams, 1973 and Brink, Partridge and Williams, 1982) .....	20
Table 2-5: Soil behaviour types associated with SBTn chart zones and index $I_c$ (Robertson and Cabal, 2012 after Robertson, 2010a) .....	24
Table 2-6: Geotechnical parameters required for soil classification and characterisation (modified from SAICE, 2010) .....	26
Table 2-7: Grain sizes in Springfontyn Formation sands from Philippi (compiled from Hill and Theron, 1981) .....	28
Table 2-8: Void ratios of different soil types (after Knappett and Craig, 2012) .....	35
Table 2-9: Corrosivity rating based on soil resistivity (Roberge, 2008) .....	38
Table 2-10: Groundwater chemistry results from the Cape Town International Airport (GEOSS, 2014) .....	39
Table 2-11: Typical densities of soils (after Head, 1992) .....	45
Table 2-12: Hydraulic conductivity values for a series of soils in m/s (Knappett and Craig, 2012) .....	49
Table 2-13: Permeability of the Cape Flats sands (after Stapelberg, 2009) .....	52
Table 2-14: Existing correlations between soil elastic modulus and SPT blow count for coarse-grained soils (after Das and Sivakugan, 2007) .....	67
Table 2-15: Existing correlations between drained elastic modulus and cone penetration resistance for granular soils .....	68
Table 2-16: Existing $V_s$ -SPT N correlations (modified from Bellana, 2009 and Wair, DeJong and Shantz, 2012) .....	74
Table 2-17: Regression equations for Holocene sands grouped by fines content (Andrus, Piratheepan, Juang, 2007) .....	80
Table 2-18: Engineering properties of Kalahari sands (compiled after Schwartz and Yates, 1980 and Brink, 1985) .....	83
Table 3-1: Soil and groundwater sampling details .....	88
Table 3-2: ASTM particle size classification (compiled from ASTM D422, 2007) .....	98
Table 3-3: Chemical tests for corrosion potential .....	100
Table 3-4: Triaxial test output data .....	110
Table 3-5: Dynamic triaxial testing loading schedule .....	112
Table 3-6: Typical grading test result .....	117
Table 3-7: Calculation of indices $N_1$ to $N_7$ for the determination of N, LCSi and SCSi (Basson, 1989) .....	120
Table 3-8: ACEC classification for natural ground conditions (BRE, 2005a) .....	121
Table 3-9: Evaluation of collapse potential values (Schwartz, 1985 after Jennings, 1974) .....	125
Table 3-10: Evaluation of $K_D$ (Howayek et al., 2011) .....	126
Table 3-11: CPTu dissipation test information .....	128
Table 3-12: Summary of calculated parameter values for determination of $k_h$ .....	132
Table 4-1: Extract from grading summary table in Appendix G .....	144

Table 4-2: Extract from gradation summary in Appendix G .....	150
Table 4-3: Grading modulus of Cape Flats sand .....	152
Table 4-4: Plasticity properties of clayey Cape Flats sands exhibiting non-zero plasticity indices .....	156
Table 4-5: Extract from compaction summary table in Appendix G.....	158
Table 4-6: Extract from CBR summary table in Appendix G .....	168
Table 4-7: CBR prediction equations .....	171
Table 4-8: Minimum index density test results for Cape Flats sand.....	175
Table 4-9: Corrosion indices for metal and concrete .....	181
Table 4-10: Erodibility results based on the soil nomograph method .....	184
Table 4-11: Summarised natural moisture content results .....	189
Table 4-12: Summary of collapse potential test results on Cape Flats sands.....	193
Table 4-13: Hydraulic conductivity test results.....	195
Table 4-14: Triaxial test results .....	197
Table 4-15: Summary of direct shear test results .....	200
Table 4-16: Comparison of $\phi'$ values from SPT based methods.....	202
Table 4-17: Comparison of $\phi'$ values from CPTu data (Capricorn site) .....	204
Table 4-18: Regression equations for predicting the shear wave velocity (m/s) of Cape Flats sand .....	227
Table 5-1: Softening function variables .....	233
Table 5-2: Variables of analysis (non-linear stepwise method).....	235
Table 5-3: Variables of analysis (general elastic solution) .....	237
Table 6-1: Summary of soil properties in the Witzand Formation per USCS class .....	249
Table 6-2: Summary of soil properties in the Springfontyn Formation per USCS class.....	253
Table 6-3: Summary of soil properties in the Langebaan Formation per USCS class .....	257

## List of symbols and abbreviations

### Symbols

$\phi$	Friction angle (°)
$\phi'$	Effective friction angle (°)
$\phi_{\max}$	Peak friction angle (°)
$\phi_{cv}$	Critical state friction angle (°)
$c$	Cohesion (kPa)
$c'$	Effective cohesion (kPa)
$c_{\max}$	Peak cohesion (kPa)
$\gamma$	Bulk unit weight (kN/m <sup>3</sup> ) /shear strain (%)
$\gamma_{d\max}$	Maximum dry unit weight (kN/m <sup>3</sup> )
$\rho$	Bulk density (kg/m <sup>3</sup> )
$\rho_d$	Dry density (kg/m <sup>3</sup> )
$\rho_{\text{sat}}$	Saturated density (kg/m <sup>3</sup> )
$\rho_{d\min}$	Minimum dry density (kg/m <sup>3</sup> )
$\rho_{d\max}$	Maximum dry density (kg/m <sup>3</sup> )
$\sigma$	Total normal stress (kPa)
$\sigma'$	Effective normal stress (kPa)
$\sigma'_{v0}$	Effective overburden pressure (kPa)
$\Delta\sigma'_v$	Vertical stress increment (kPa)
$\sigma_1$	Major principle stress (kPa)
$\sigma_{1,f}$	Major principle stress at failure (kPa)
$\sigma_2$	Intermediate principle stress (kPa)
$\sigma_3$	Minor principle stress/confining pressure (kPa)
$\sigma_d$	Principle stress difference/deviator stress (kPa)
$\Theta$	Bulk stress ( $\sigma_1 + \sigma_2 + \sigma_3$ ) (kPa)
$\nu$	Poisson's ratio
$a_{\max}/PGA$	Peak horizontal ground acceleration (g or m/s <sup>2</sup> )
$B$	Footing width (m)
$C_u$	Coefficient of uniformity
$C_z$	Coefficient of curvature
$D$	Footing depth (m)
$D_{10}$	Effective particle size (mm)
$D_{30}$	Size such that 30% of particles are smaller than that size (mm)

$D_{60}$	Size such that 60% of particles are smaller than that size (mm)
$D_{50}$	Median particle size (mm)
DN	DCP number (mm/blow)
$D_r$	Relative density/density index (%)
E	Soil elastic modulus (MPa)
$E_0$	Small-strain soil elastic modulus (MPa)
$e/e_0$	Void ratio (in-situ)
$e_{max}$	Maximum void ratio
$e_{min}$	Minimum void ratio
$F_D$	Depth correction factor (Fox, 1948)
$F_R$	Rigidity correction factor
$F_r$	Friction ratio (%)
$f_s$	Sleeve friction (kPa)
g	Gravitational acceleration ( $9.8\text{m/s}^2$ )
G	Shear modulus (MPa)
$G_0$	Small-strain shear modulus (MPa)
Gc	Grading coefficient
$G_s$	Specific gravity
$I_c$	Soil behaviour type index
k	Coefficient of permeability (m/s)
K	Soil erodibility factor
$K_D$	Liquidity index
M	Constrained soil modulus (MPa) / Design earthquake moment magnitude
$M_r$	Resilient modulus (MPa)
N	SPT blow count (uncorrected) / aggressiveness index (Basson, 1989)
$N_{60}$	SPT blow count corrected to 60% of the hammer energy
$(N_1)_{60}$	SPT blow count corrected for energy and overburden pressure
$(N_1)_{60cs}$	Clean sand equivalent SPT blow count
$P_a$	Atmospheric pressure (kPa)
$q_c$	Cone tip resistance (MPa)
$q_t$	Cone tip resistance corrected for pore pressure (MPa)
$Q_t$	Normalised cone resistance (MPa)
$Q_{tn}$	Normalised cone resistance - with stress exponent 'n'(MPa)
$q_{net}$	Net bearing pressure (kPa)

$q_{ult}$	Ultimate bearing capacity (kPa)
$S$	Total settlement (mm)
$Sp$	Shrinkage product
$S_r$	Degree of saturation (%)
$u_2$	Pore water pressure (measured behind the cone) (kPa)
$V_r$	Raleigh wave velocity (m/s)
$V_s$	Shear wave velocity (m/s)
$V_{s1}$	Shear wave velocity corrected for overburden pressure (m/s)
$w/w_n$	Natural moisture content (%)

### Abbreviations

AASHTO	American Association of State Highway and Transportation Officials
ACEC	Aggressive chemical environment for concrete
ASTM	American Society for Testing and Materials
CBR	California Bearing Ratio
CD	Contractive-dilative
CP	Collapse potential
CPT	Cone penetration test
CPTu	Piezocone penetrometer test
CRR	Cyclic resistance ratio
CSR	Cyclic stress ratio
CSL	Critical state line
CSW	Continuous surface wave
CTSDF	Cape Town spatial development framework
DCP	Dynamic cone penetrometer
DPSH	Dynamic probe super heavy
DSR	Deviator stress ratio
EC	Electrical conductivity
EI	Erosion index
FC	Fines content
FoS	Factor of safety
GM	Grading modulus
GR	Grading ratio
LCSI	Leaching-corrosion sub-index

LL	Liquid limit
LS	Linear shrinkage
LSI	Langelier Saturation Index
LVDT	Linear variable differential transducers
MASW	Multi-channel analysis of surface waves
MDD	Maximum dry density
MMS	Modified Mercalli Scale
Mod	Modified
MSF	Magnitude scaling factor
NGA	National Groundwater Archive
ngl	Natural ground level
NP	Non-plastic
OCR	Over-consolidation ratio
OMC	Optimum moisture content
PD	Permanent deformation
PI	Plasticity index
PL	Plastic limit
PSD	Particle size distribution
RUSLE	Revised Universal Soil Loss Equation
SANS	South African National Standard
SBT	Soil behaviour type
SBT <sub>n</sub>	Normalised soil behaviour type
SCSI	Spalling-corrosion sub-index
SP	Slightly plastic
SPT	Standard penetration test
TMH	Technical Methods for Highways
TP	Test pit
TRH	Technical Recommendations for Highways
USCS	Unified Soil Classification System
WT	Water table
WWTW	Wastewater treatment works

# 1. Introduction

## 1.1 Background to the study

The low-lying, sand-covered area between the Cape Peninsula and the South-Western Cape mainland is known as the Cape Flats (Hill and Theron, 1981). This expansive area of the Cape Town Metropole, covering about 460 km<sup>2</sup>, is home to a substantial portion of the population of the greater Cape Town area. The terrain is flat, densely inhabited and typically characterised by suburban townships and informal settlements.

Rapid on-going civil infrastructure development is taking place within the boundaries of the Cape Flats to improve existing infrastructure, develop new facilities and, as such, uplifting the local communities. The planning, design and construction of educational, community and public transport facilities and housing developments are some of the recent and future envisaged improvement projects. The statement by Charles E Kellog: *“Civilisation has its roots in the soil”* has application in soils engineering, highlighting the importance of the subsoil as founding material for all engineering structures. A knowledge of the subsoil conditions; that is the geotechnical properties and engineering behaviour of geo-materials, is essential for design of suitable foundations for proposed structures and earthworks associated with such developments. During the early planning stages of a project, when assumptions must be made regarding investigation and construction methods best suited to the project, a knowledge of general characterisation can also be advantageous. To achieve this, invasive investigative measures are required to obtain data on the physical properties of soil and/or rock underlying the respective site. Geotechnical practitioners have undertaken many such investigations within the Cape Flats area over the years, however, the information has mostly remained unexplored, unpublished and in the possession of the practitioners and their clients. Much of the scientific research to date has focused on describing and understanding the geological background and setting of the Cape Flats and, in more recent time, upon the geohydrological characteristics, with specific reference to the Cape Flats aquifer. The details and full description of the geology of the Cape Flats has been reported, amongst others, by Rogers (1980), Theron, (1984) and Theron et al. (1992). Recent studies dedicated to the Cape Flats aquifer have been undertaken by Adelana, Xu and Vrbka (2010) and Hay et al. (2015).

The importance of characterising soil and rock, in terms of their engineering properties and engineering geological characteristics, has been emphasised by various researchers. This is especially important for sites where problem soils are likely to be encountered. Some of the more recent studies and academic dissertations focusing on comprehensively describing and understanding the response of geomaterials include Vermaak (2000), Viana da Fonseca (2003), Lunne, Long and Forsberg (2003), Meisina (2006) and Di Buo et al. (2019). With particular reference to the Cape Flats, highly compressible and potentially collapsible soils are expected to occur at shallow depths across the area.

The wealth of geotechnical data on the upper Quaternary sands of the Cape Flats accumulated over the last few decades by geotechnical practitioners allows the author to collect and analyse the existing data, and present the first substantial contribution to geotechnical classification and characterisation of the sand deposits underlying the ever developing Cape Flats area.

## 1.2 Problem statement

Literature on the geotechnical and engineering geological properties of the upper Quaternary age sands of the Cape Flats is limited. As mentioned in Section 1.1, many geotechnical investigations have been undertaken in the area. However, the valuable geotechnical data obtained has largely remained unexplored and unpublished. An in-depth search of existing literature revealed research contributions of an engineering geological nature by Amdurer (1956), Brink (1985) and Stapelberg (2009). In addition, a number of other studies have been undertaken, involving the upper sands of the Cape Flats, but these focus mainly on specific aspects such as liquefaction potential (Parker, 1991 and Schoeman, 2018), groundwater in the Cape Flats aquifer (Henzen, 1973 and Adelana, Xu and Vrbka, 2010) and the use of geotextiles in the sands (Kalumba, 1998). Most of these studies involved a basic characterisation of the specific study site in terms of its geotechnical properties.

The following broad description is often applied to the Cape Flats sands: Light coloured, poorly graded (uniform), fine and medium quartzitic aeolian sand; assigned the group symbol 'SP' based on the Unified Soil Classification System. This description provides an indication of the basic properties of the material underlying the Cape Flats and creates the impression of a uniform deposit of mainly sandy soils. However, these soils have been found to be highly variable, with a wide range of values assigned to many material properties. Some of these properties were investigated to limited extent by Amdurer (1956), Brink (1985) and Stapelberg (2009). The very limited research into the physical characteristics of the different formations of Cape Flats sands has created a shortcoming in detailed knowledge of soil parameters facilitating material characterisation, such as compressibility and shear strength, as well as of geotechnical parameters enabling soil classification, such as index properties and compaction characteristics. As a result of the geographical and investigative limits associated with the abovementioned prior research, the analysis of large quantities and a wide range of geotechnical data, accurately representing the geotechnical and engineering geological nature of the entire Cape Flats area, has not been possible. Furthermore, statistical analysis showing significant outcomes and distinctive trends - including vertical and horizontal (intra-formation) variations - distributions and parameter correlations, and the resultant practical importance have not emerged.

The compressibility characteristics of Cape Flats soils is of particular importance in the current research, as the design of structures in the study area is often governed by the compressibility of the upper sand horizons, as opposed to their bearing capacity. Bearing capacity is only of concern for shallow foundations of limited size with a shallow water table. Very loose and loose near-surface sands will be highly compressible and susceptible to excessive settlement when loaded. In addition, differential settlements may be large where the consistency of the sands below different footings of the same structure varies substantially; for example, compressible sands (possibly with intermittent highly compressible peaty layers in the Springfontyn Formation) and hard calcretised horizons. For this reason, focus is placed on compressibility and material stiffness under static forces and repeated loading, using mathematical models to characterise the stiffness behaviour of the sands.

### 1.3 Aim and objectives

The aim of the research is to classify and characterise the sands of the Witzand, Springfontyn and Langebaan Formations from the Cape Flats. Classification is undertaken according to various standard classification systems based on grading properties, Atterberg limits, maximum dry density and optimum moisture content, minimum dry density, California Bearing Ratio (CBR), erodibility and corrosivity. Characterisation is based on the geotechnical properties of the sands, including in-situ density, moisture content, specific gravity, compressibility, shear strength, permeability and volumetric behaviour during shear including liquefaction potential. Vertical and horizontal (inter-formation) variation of these properties are poorly understood, as well as the compressibility of near surface deposits for foundation design. These aspects form the basis of the current research.

The following supporting objectives are addressed with the purpose of achieving the abovementioned primary aim:

- Collecting geotechnical data from previous investigations in the study area, primarily in-situ and laboratory test results, to generate a database of soil parameters. This involves processing of raw data to acquire soil classification and characterisation parameters.
- Applying methods of investigation and testing not traditionally used in the area by way of fieldwork and laboratory testing, including but not limited to:
  - Ground stiffness measurement through the continuous surface wave (CSW) test to obtain representative shear wave velocity ( $V_s$ ) profiles in the Cape Flats sands and enable statistical correlation between  $V_s$  and SPT blow counts.
  - Piezocone penetrometer (CPTu) testing, primarily to evaluate the volumetric response of the Cape Flats sands during shear to provide an indication of the potential of these soils to liquefy during static or cyclic loading.
  - Double ring infiltrometer testing to determine the infiltration capacity of the shallow Cape Flats sands.
  - Monotonic and repeated load triaxial tests on reconstituted Cape Flats sand to determine the peak shear strength and resilient modulus ( $M_r$ ) of compacted layerworks in road construction to ultimately produce  $M_r$  predictive models.
  - Laboratory test methods rarely performed on Cape Flats sands such as minimum index density and collapse potential tests.
  - Monitoring the long-term changes in groundwater levels in the Cape Flats through National Groundwater Archive (NGA) records.
- Analysing the data, involving descriptive statistics and regression techniques to assess inter- and intra-formation variation and trends, and to find statistically significant relationships between the studied parameters, allowing the influence of properties such as grading and penetration resistance on the parameters such as CBR and  $V_s$  to emerge.
- Performing non-linear stepwise settlement analyses to predict foundation settlement in Cape Flats sands using small-strain stiffness data from a  $V_s$ - $N_{60}$  model for Cape Flats sands proposed by the candidate.

## 1.4 Contribution of the research

This research represents the first contribution towards comprehensively describing, classifying and characterising the Quaternary-aged sands of the Cape Flats area in terms of their physical properties and engineering behaviour, by combining, analysing and interpreting the wealth of geotechnical information from previous and new soil investigations undertaken in the area. The addition of experimental values from the laboratory tests provide comparison with empirically obtained parameter values. Knowledge of the likely classification and characterisation of the sands from the various sand formations on the Cape Flats, will enable early prediction of the likely engineering behaviour of the sands during the planning stages of construction projects, enabling informed decision making regarding investigation and construction methods most suitable to the project.

The geotechnical properties that characterise the distinctive sand formations are statistically analysed to reveal underlying patterns, distinctive trends, distributions and correlations, and the resultant practical importance and probable implications are explored. Focus is placed upon soil compressibility and determining relationships between the soil parameters specifically for the sands of the Cape Flats, and any inter-formation variation in such relationships. Correlations are developed between SPT N-values and shear wave velocity for the upper sand deposits of the Cape Flats to facilitate better settlement predictions. Such predictions have the advantage of considering non-linear stress-strain behaviour of soil and the degradation of stiffness with increasing strain. Settlement analysis using small-strain stiffness data from these  $V_s$ - $N_{60}$  models are used to estimate the expected settlement of a series of shallow foundations on Cape Flats sand.

## 1.5 Research limitations

The main limitations of the research can be summarised as follows:

- The research deals with the recent (upper) aeolian deposits which typically cover the surface of the study area. It includes the largely cohesionless or slightly cohesive sands and silty and/or clayey sands from the Witzand, Springfontyn and Langebaan Formations. The geotechnical properties and engineering behaviour of sporadic cohesive soil horizons (alluvial, lacustrine and estuarine deposits) in the Springfontyn Formation, the littoral sand of the older Velddrif Formation, and the residual Malmesbury soils from the underlying bedrock were not investigated.
- Much of the data used in this research comes from existing site investigation reports. The information obtained reflects traditional methods of investigation commonly employed in the area, which tend to be limited. Data from depths exceeding 3m is typically sparse (aside from penetration test results). There are areas with concentrated data, and others with no or limited data.
- To compare experimental and theoretical parameter values and to establish interrelationships between soil properties, multiple investigation methods, i.e. in-situ tests and/or laboratory tests (from sampled soils) should be available for a site. The availability of overlapping data was limited.

- Many of the additional investigations undertaken by the candidate were sponsored and were typically undertaken alongside planned investigations by geotechnical consultants to facilitate access to sites and reduce costs. This placed limitations on the fieldwork in particular, which was restricted to sites on the Witzand and Springfontyn Formations.
- The study is also limited by the quality of data obtained from external sources, ultimately influencing the accuracy of the data and the assessment results.

## 1.6 Thesis outline

The thesis consists of six chapters. An overview of each chapter is given below.

**Chapter 1: Introduction.** This chapter introduces the research topic, focussing on the background of the study, the research problem and the unique research contribution. The aims and objectives are discussed, and the limitations identified.

**Chapter 2: Literature review.** An overview and evaluation of significant findings relevant to the field of research are given in this chapter. The literature themes contained within the chapter include: (1) the Cape Flats: an overview of the physiography, geology and engineering geological and geotechnical properties, (2) the geotechnical investigation, (3) the geotechnical properties of sandy soils enabling material classification and characterisation, with specific reference to the windblown Cape Flats sands, and (4) the geotechnical properties of aeolian deposits of other parts of South Africa and Africa.

**Chapter 3: Methodology.** This chapter presents the methods used to achieve the objectives set out in Section 1.3. It discusses the collection of existing geotechnical data from geotechnical and civil engineering consultants, contractors and laboratories, including the type, quantity, distribution and quality of the data. The field and laboratory methods undertaken to obtain experimental data are also described. Data processing methods are described in this chapter, involving sorting and input of raw data, followed by the determination or estimation of soil parameters from in-situ and laboratory results using established methods and transformation models.

**Chapter 4: Results and discussion.** The results associated with the classification and characterisation of the Cape Flats sands are presented, explained and evaluated in this Chapter. The completed data sets, obtained from the collection, sorting, input and processing of pertinent geotechnical data are statistically analysed, and the outcomes are presented as graphs, tables and equations. The results are contextualised within previous research and theory, and the implications of the results discussed.

**Chapter 5: Elastic settlement analysis.** In this chapter, the settlement methodology is discussed, including the procedure followed to obtain the input data. The settlement prediction results for shallow foundations on Cape Flats sands are presented in graph form and the outcomes discussed.

**Chapter 6: Conclusions, summary of properties and recommendations.** The important aspects discussed in detail in Chapters 4 and 5 are highlighted to emphasise the findings of the research. Recommendations are also made about the research outcomes and possible future research.

## 2. Literature Review

### 2.1 Introduction

The literature review provides an overview and evaluation of substantive findings pertinent to the field of research. The review aims to position the current research focus within the context of the wider research field, and to identify the research gap within the addressed literature. The relevant literature themes contained within the current chapter include: (1) the Cape Flats - an overview of its physiography, geology and engineering geological and geotechnical properties, (2) geotechnical investigations, with specific focus on in-situ penetration testing, (3) the geotechnical properties of non-cohesive soils used for material classification and characterisation, with specific reference to the aeolian sands of the Cape Flats, and (4) the geotechnical properties of aeolian deposits of other parts of South Africa and Africa.

Each of the classification and characterisation parameters listed in Section 1.3 of Chapter 1 is dealt with, focussing on the laboratory, field and empirical methods by which they are determined, and current knowledge, inclusive of pertinent published research relating to each soil parameter and, more specifically, the findings of investigational work within the study area. Focus is placed on soil compressibility, with elastic settlement prediction using small-strain Young's modulus and the characterisation of pavement materials based on resilient modulus, forming central themes.

### 2.2 The Cape Flats

#### 2.2.1 Introduction

##### 2.2.1.1 Locality

Hill and Theron (1981) described the Cape Flats as a low-lying sand-covered expanse, linking the south western Cape mainland with the mountainous Cape Peninsula. More specifically, it can be defined as the area bounded by the Muizenberg-Cape Town and the Cape Town-Bellville-Eerste River railway lines as shown in Figure 2-1 (Hill and Theron, 1981). Taylor (1972) defined the area more loosely as that bounded by the mountains of the Cape Peninsula to the west, Tygerberg and Bottelary Hills to the north and north east, the Eerste River to the east and the False Bay coast to the south. These boundaries will be used as a guide in the current research.

Within this area of approximately 460 square kilometres, the whitish transported sands are referred to as the upper Quaternary sands of the Cape Flats. The same transported sand deposits extend northwards along the west coast through Bloubergstrand to Atlantis; however, these sand-covered areas do not lie within the geographical boundaries of the Cape Flats and will typically not form part of the area considered in this research.

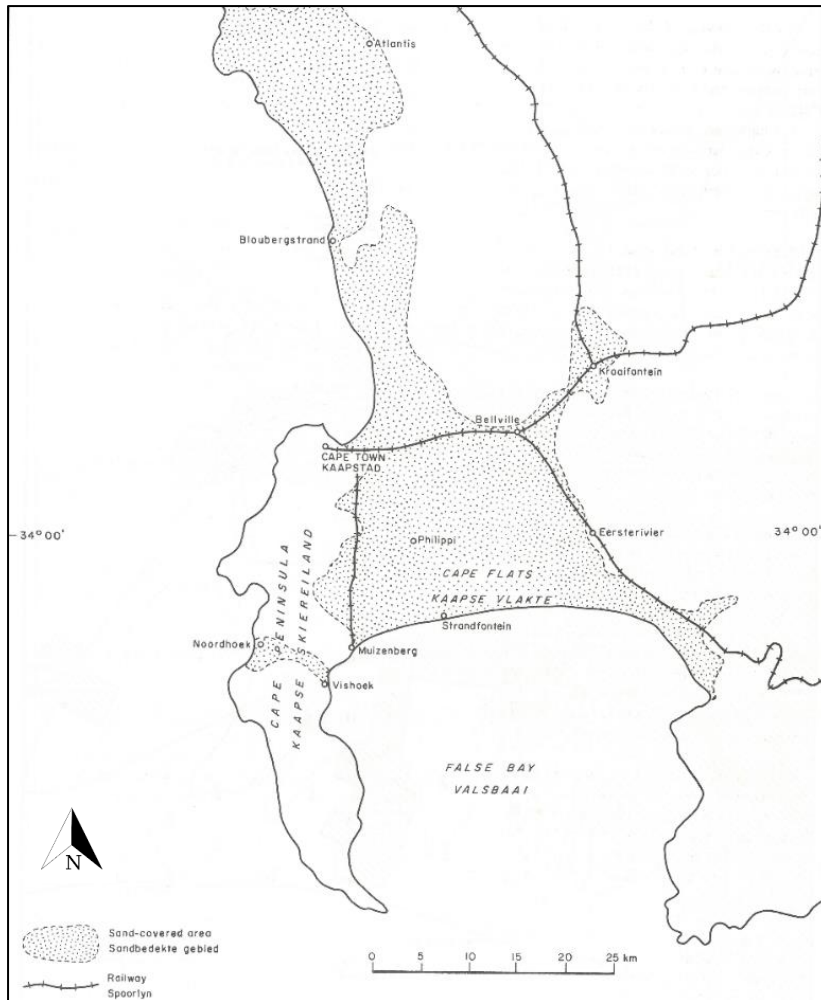


**Figure 2-1: Locality of the Cape Flats (Hill and Theron, 1981)**

### 2.2.1.2 Background and development

The Cape Flats, which is located on the outskirts of the city of Cape Town, consists of many densely populated townships comprising an amalgamation of formal and informal housing. Some of the well-known townships of the Cape Flats include Mitchells Plain, Khayelitsha, Gugulethu and Hanover Park. Poor living conditions are the norm in the informal settlements of the Cape Flats, and dwellings are often erected by the residents without official approval; typically using non-conventional building materials. As a result of inadequate infrastructure and general lack of basic services, many of these dwellings are unsafe and unsuitable for occupation. The formal dwellings of the suburban townships are often poorly built and lack proper maintenance. The City of Cape Town has also identified several areas in the Cape Flats which lack public facilities such as community centres, libraries, schools, hospitals, district parks and sports facilities (CoCT, 2012b).

The City of Cape Town has developed a city-wide Cape Town spatial development framework (CTSDF) in which the long-term plan to manage the spatial growth and development of the greater Cape Town area is stipulated (CoCT, 2012a). The CTSDF informs a few local area plans (district plans), developed for each of the planning districts of the city. Of the eight district plans compiled by the City of Cape Town, the Cape Flats district is considered most in need of regeneration, economic development, the provision of services, and the provision of adequate housing and effective transportation systems (CoCT, 2011).

The CTSDf represents a long-term development plan for the Cape Town districts, thus indicating on-going civil development in the study area. Characterisation of the soils in the area, together with knowledge of the state of the soil, along with specific soil parameters such as strength and compressibility, will aid in the design of suitable foundations, excavations and pavements associated with the planned developments.

## **2.2.2 Physiography of the Cape Flats**

### *2.2.2.1 Topography*

The topography of the Cape Flats is typical of a coastal plain; that is, flat and low lying. The area is characterised by a dune system, which is poorly defined in some areas. Taylor (1972) describes the topography as a belt of foredunes facing the coast and long sand ridges extending inland in a predominantly south easterly direction. The average elevation of this low relief area is approximately 30 metres above mean sea level (m amsl) with the highest sand dunes reaching about 65 m amsl (Adelana, Xu and Vrbka, 2010). In several dune depressions, saturated soils and shallow inundation lead to the formation of flat, marshy areas known as wetlands. These conditions are exacerbated by the absence of prominent drainage lines in the Cape Flats. The long sandy beaches and low limestone cliffs along the False Bay coast are pronounced topographic features of the area.

### *2.2.2.2 Drainage and groundwater*

The drainage of surface water in the Cape Flats takes place through the Eerste River, Kuils River, Sout River, Diep River and open bodies of water such as the Zeekoevlei (Adelana, Xu and Vrbka, 2010), as shown in Figure 2-2. The Kuils and Eerste Rivers both flow southwards, joining in the vicinity of Macassar and then draining into False Bay. Drainage into False Bay also takes place via Zeekoevlei, which collects water from southwards flowing rivers draining the western parts of the Cape Flats. In the north-western parts of the Cape Flats, there are several tributaries of the Salt River which flow northwards, merging with the parent river and then draining into Table Bay (CoCT, 2011). The Diep River also drains into Table Bay.

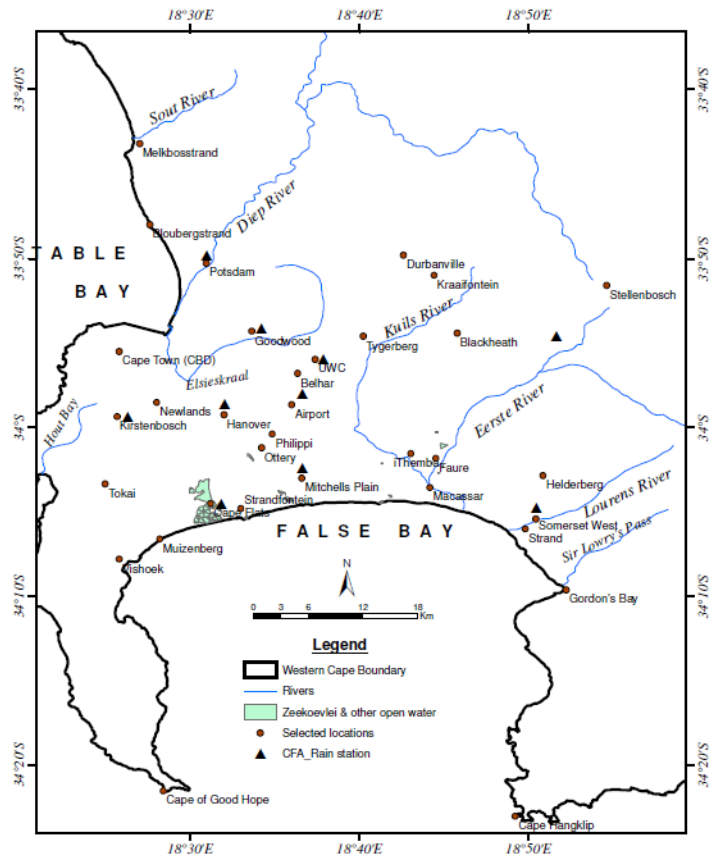


**Figure 2-2: Cape Flats draining system (Adelana, Xu and Vrbka, 2010)**

The Cape Flats is located on a predominantly unconfined sandy aquifer known as the Cape Flats aquifer. The porous and permeable sands of the Elandsfontein, Witzand and Springfontyn Formations form a large water storage unit (Hay et al., 2015). The Cape Flats aquifer extends from the False Bay coastline northwards to the Tygerberg Hills in the north east and Milnerton in the north west. According to Hay et al. (2015), cross-sections show that the sands of the Cape Flats aquifer extend to a maximum depth of approximately 55 metres.

The Cape Flats aquifer has been investigated extensively by various researchers, including Henzen (1973), Gerber (1981), Giljam (2002), Adelana and Xu (2006, 2008), Adelana, Xu and Vrbka (2010) and Hay et al. (2015). These authors focused on aspects such as urban aquifer management, groundwater contamination in the Cape Flats aquifer, and the development of a conceptual hydrogeological model to explain groundwater flow and recharge mechanisms in the Cape Flats. In addition, Henzen (1973) investigated the economic feasibility of large-scale purification of sewage effluent to be stored, and abstracted from, the sand formations of the Cape Flats. The recent water crises in Cape Town, brought on by drought, increase in the demand for drinking and industrial water, and the reduction of surface water resources, has created the need for abstraction of groundwater from underground resources such as the Cape Flats aquifer. A geophysical survey of the area identified target areas for borehole installation and water abstraction. However, the typically poor water quality coupled with low yield from potable water sources, led to the abandonment of the abstraction project.

According to Hay et al. (2015) groundwater typically flows from the raised basement in the northeast Cape Flats, towards Table Bay to the northwest and False Bay to the south. Groundwater levels in the Cape Flats vary with the topography, however, the typically low relief terrain causes rainfall to drain slowly off the land, resulting in a shallow water table (DWAF, 2008). To monitor the fluctuations in ground water levels, as well as the quality of the water for abstraction purposes, various institutions, departments and consultants have installed monitoring wells in the Cape Flats. The City of Cape Town's Department of Water and Sanitation has installed many wells on monitoring sites within the study area (and across the Western Cape), called Geosites. The measurement of groundwater levels and water quality in these wells provides valuable data that is subsequently captured in the National Groundwater Archive (NGA). Existing literature indicates that groundwater levels vary in accordance with seasonal changes, the undulating topography and less permeable or impermeable layers and lenses of pedogenic material or clay, causing perched water tables. Groundwater can occur at, or close to the surface, especially during the wetter winter months.

### *2.2.2.3 Geomorphological history*

It is postulated that the south western Cape mainland and the present Cape Peninsula were formerly separated by a sea-strait. According to Walker (1952) (as cited in Schalke, 1973), the closure of this so-called 'Cape Strait', occurred by the lowering of the sea-level and a likely rise of the basement, which resulted in the formation of the Cape Flats. The coastal elevation is thought to have occurred approximately one hundred and seventy-five thousand years ago. According to Barwis and Tankard (1983), the Quaternary-aged sands of the Cape Flats accumulated in reaction to global fluctuations in the sea level and local climate changes. Schalke (1973) highlights evidence of such past fluctuations in sea level, which were found in the form of raised beaches along the Cape Peninsula coastline and on sites where coastal cliffs are present. At Swartklip, along the False Bay coast, a 50 metres thick Late Pleistocene succession of poorly cemented sandstone provides such evidence. Based on faunal evidence and the general physical characteristics and sedimentary structures, four distinct facies were identified, namely estuarine, beach, washover fan and aeolian (Barwis and Tankard, 1983). The whole facies succession was deposited during two sea-level peaks and the successive withdrawals during the most recent interglacial period (Barwis and Tankard, 1983). According to Schalke (1973), evidence of remnant warm and cool water fauna was found within these ancient beaches. The existence of considerably warmer conditions during the formation of the raised beaches is supported by the presence of numerous warm water species. Krige (1927) explains the presence of these fossils by postulating that the 'Cape-Strait' could have been a passage for the warm Agulhas current and accompanying fauna.

Based on the geomorphological history of the Cape Flats, the stress history of the windblown sands relevant to the current study probably reflects that of normally consolidated deposits. Notwithstanding this, the continuous migration of the dune sand across the low-gradient landscape during summer months (by the dominant south easterly winds), together with removal of dune sands for mining purposes, will result in over-consolidation in some areas. In addition, changes in the ground water level will also cause light over-consolidation. It is thus anticipated that both normally and probably slightly over-consolidated deposits will occur in the study area. This aspect will be further investigated in subsequent chapters.

#### 2.2.2.4 Climate and rainfall

The Cape Flats experiences dry and warm summers (from October to April) and mostly wet and cool winters (from May to September), which is typical of the semi-arid Mediterranean climate which prevails on this coastal plain. Seasonal fluctuations are strongly influenced by the ocean currents and water temperatures. Annual precipitation in the area generally varies between 400 millimetres and 800 millimetres with a dry spell from November to March (Adelana, Xu and Vrbka, 2010). Periods of intense and prolonged rainfall often occur during the winter months, making the low-lying area prone to flooding. Strong winds are characteristic of the area. South-easterly winds prevail in summer whereas north westerly winds are dominant during winter. The orientation of the sand dunes in the Cape Flats indicates a dominant south easterly wind.

The Weinert N-value (Weinert, 1980), which describes the climatic environment of an area, has been determined to be 5.8 at the Cape Town International Airport, which is situated on the Cape Flats (Stapelberg, 2009). This value – which represents a dry climate – is influenced by the high evaporation rates during summer months, and points to dominating physical weathering (disintegration) processes in the study area. The Weinert N-value for the area will be less than 5 (representing a semi-dry climate), when the annual rainfall is at the upper end of the above given range.

### 2.2.3 Geology of the Cape Flats

#### 2.2.3.1 Introduction

On the Cape Flats, sediments of Quaternary age overlie Neogene deposits, which in turn rest on basement rocks composed of Precambrian and Paleozoic rocks. The Quaternary deposits, divided into the Holocene and Pleistocene epochs, are mainly aeolian sands and calcarenites of the more recent Witzand, Springfontyn and Langebaan Formations, but with minor littoral sand and calcrete-capped coquina of the older Velddrif Formation. This research is concerned with the recent aeolian deposits which typically cover the surface of the study area. The distribution of the Neogene deposits which occur below the present sea level is determined by the topographic profile of the underlying bedrock, which seldom lies at depths greater than fifty metres below the present sea level (Theron et al., 1992). The deep-seated basement rocks underlying the Quaternary and Neogene deposits comprise the Cape Granite suite in the extreme west and metasediments of the Malmesbury Group (Hill and Theron, 1981). Small outcrops of these Precambrian and Palaeozoic rocks have been identified in several localities. The formations of the Quaternary and Neogene periods of the Cenozoic Era are shown in Table 2-1. A review of existing literature revealed slight variations in the geological age of the sand deposits. The geological ages given in Table 2-1 should therefore be viewed only as a guide.

The Geological Survey of South Africa (now the Council for Geoscience) has produced a geological map of the area at 1:250 000 scale (map sheet 3318 Cape Town), which was compiled from four 1:50 000 scale maps covering the Cape Flats area (map sheets 3318 CD, 3318 DC, 3418 AB and AD and 3418BA). The portion of the 1:250 000 scale geological map covering the Cape Flats is shown as Figure A1 in Appendix A. The geology of the Cape Flats has been described by Theron (1984) and Theron et al. (1992) in the explanations accompanying the abovementioned geological maps. Several cross-sections illustrating the general geological profile underlying the Cape Flats, were put forth by Adelana, Xu and Vrbka (2010). In this regard, a simplified geological map of the area and geological cross sections shows predominantly sand with layers and lenses of clayey sand, clay, peat and argillaceous sand, calcrete, and gravel and stone, all overlying Malmesbury shale

(refer to Adelana, Xu and Vrbka, 2010). Amdurer (1956) highlights the variability of the geo-materials, both in vertical and horizontal directions. Nevertheless, a typical profile includes aeolian sands and/or silty sands with intermittent clay, silt and peat mixed in varying proportions (e.g. silty clay, sandy clay and peaty clayey silt), often with a small sand fraction. In the southern and eastern parts of the Cape Flats, hardpan calcrete occurs at shallow depth often underlain by nodular powdery calcrete and calcareous sand.

**Table 2-1: Lithology of the Cenozoic Formations of the Cape Flats (after Theron et al., 1992 and Johnson, Anhaeusser and Thomas, 2006)**

Group	Formation	Lithology	Age	
Sandveld	Witzand	Aeolian, calcareous, quartzose sand	Holocene (0.01 Ma to present)	Quaternary
	Springfontyn	Aeolian, quartzose sand with intermittent clay and peaty layers	Pleistocene (2.6 – 0.01 Ma)	
	Langebaan	Aeolian, calcrete-capped calcareous sandstone		
	Velddrif	Littoral, calcrete-capped coquina		

### 2.2.3.2 Stratigraphy

The 1:250 000 geological map of the area (3318 Cape Town) indicates the presence of unconsolidated white sand with shells and pebbles or light grey to pale red sandy soils - part of the Witzand and Springfontyn Formations respectively - over most of the Cape Flats area. Elongated zones of limestone and calcrete and calcified parabolic dune sand of the Langebaan Formation are exposed at the surface to the south and south east. These stratigraphic units are described fully below. The exposure of the partially consolidated sediments of the Velddrif Formation is limited to a small area in Swartklip on the northern False Bay shore and, as such, description of this stratigraphic unit will not be included below.

The **Witzand Formation** forms the youngest and uppermost stratigraphic unit of the Sandveld Group (Theron et al., 1992). These unconsolidated and light-coloured sands cover a large portion of southern and central Cape Flats, extending approximately eighteen kilometres inland from the False Bay coast towards Bellville. These sands are typically partly vegetated and are described as fine to medium grained calcareous coastal dune sand with shells and pebbles (Theron, 1984). The dune sands are the result of the most recent phase of aeolian activity in the Sandveld Group, and a deflation product of modern beaches (Theron et al., 1992). The south easterly winds are the responsible transportation agent. Within the outer limits of the Cape Flats, the Witzand sands are underlain either by the unconsolidated sand of the Springfontyn Formation or the calcarenites of the Langebaan Formation.

The **Springfontyn Formation** consists of light grey to pale red unconsolidated quartzose sand with intermittent peaty layers (Rogers, 1980). It covers a large portion of the Cape Flats including the entire north western part and a corridor along the eastern boundary. Over large portions of the remainder of the area, it underlies the Witzand Formation. The clean quartzose sands of the Philippi member and the more inland, peaty sands of the Epping member can be distinguished

within the Springfontyn Formation (Theron, 1984). The sands are fine and medium grained, uniformly graded and typically structureless, although rare crossbedding has been identified (Theron et al., 1992). Clayey layers, conglomerate lenses and thin layers of ferricrete are present in places. Shell fragments and shark teeth have also been found sporadically at depth in borehole cores from this formation (Theron et al., 1992). Where iron is present in the soil, a pale red colour is observed. In areas where the sands are largely derived from granite bedrock, feldspar grains are present in addition to quartz. A typical profile from the Springfontyn Formation is given by Brink (1985) as: Loose becoming medium dense sands to about 5m depth, underlain by dense and very dense sands with intermittent sandy clay layers to about 10m, containing shell fragments. Below the sandy soils, there are soft to firm peaty, silty and clayey sand and clayey silt to the maximum profile depth of 12.5m.

Rogers (1980) suggests that the similarity in the distribution of grain sizes in the sand of the Springfontyn Formation and the overlying aeolian dune sand of the Witzand Formation is indicative that the lower formation is also fundamentally of aeolian origin. A maximum thickness of 32 metres has been recorded for the Springfontyn Formation on the Cape Flats in the vicinity of Philippi (Theron et al., 1992). In this area, particularly the western and northern parts of the area around Philippi, high-grade silica sand is exploited for glass-making purposes. In this regard, Hill and Theron (1981) presented the results of an investigation into these sands undertaken in 1981 by the Geological Survey of South Africa.

The sediments of the **Langebaan Formation** vary from massive, grey sandy limestone to layered sandy calcrete and calcareous sand with shells (Theron, 1984). The calcareous deposits of this formation are medium and coarse grained and poorly graded (Roberts, 2001 and Franceschini, 2003). Calcretised dunes of this middle to late Pleistocene formation, called the Wolfgat member, are prominent along the southern Cape Flats with maximum development between Strandfontein and Macassar (Theron et al., 1992). Massive sandy limestones outcrop in elongated zones parallel to the prevailing south easterly wind in this area. Approximately ninety percent of the surface exposures of this formation comprise massive sandy limestone, whereas the calcareous sand is limited to a few sites in the vicinity of Swartklip (Theron, 1984). Over an extensive area of the Cape Flats, a hard, irregular bank of limestone is covered by aeolian sands of varying thickness. Theron (1984) and Theron et al. (1992) highlight the complex geological history of this formation, involving alternating dune formation and beach deposition over a long period. The sediments of this formation consist of an upper, hard calcretised layer overlying yellow soft sandy calcrete which in turn overlies calcareous sand, the lime content gradually decreasing with depth. The calcareous strata, in which bedding and/or cross bedding is rarely seen, is generally only a few metres thick, with boreholes and old test pits at Mitchells Plain revealing a unique thickness in excess of ten metres. According to Johnson, Anhaeusser and Thomas (2006), the calcareous deposits often contain microfossils and terrestrial gastropods.

Within the Cape Flats area, greywacke, phyllite and quartzitic sandstone of the **Tygerberg Formation** (Malmesbury Group) are mapped at the surface in two confined areas in the vicinity of Silversands and Eerste River (towards the eastern boundary of the Cape Flats).

### 2.2.3.3 Seismicity

An intraplate fault, known as the Milnerton fault, extends across the Cape Flats in a north westerly to south easterly direction and exposes the area to a possible seismic event. Movement along this fault line has been the cause of a few earthquakes (predominantly in the 19<sup>th</sup> century), including the large event in 1809 in Cape Town measuring 6.3 on the Richter scale (de la Harpe, 2015). A peak ground acceleration (PGA) of 0.15 g (where g = gravitational acceleration) with a 10% probability of exceedance in fifty years has been assigned to the Cape Flats area (SANS 10160-4:2010).

## 2.3 Geotechnical and engineering geological characterisation of soils

### 2.3.1 Introduction

Many researches have emphasised the importance of characterising geomaterials in terms of their engineering properties and engineering geological characteristics (often referred to as benchmarking). This is especially important for sites earmarked for civil engineering development, particularly where problem soils are expected to be encountered. Some of the more recent research publications and academic dissertations focusing on describing and understanding the response of geomaterials include works by Meriggi, Paronuzzi and Simeoni (2000), Vermaak (2000), Viana da Fonseca (2003), Jamiolkowski and Presti (2003), Lunne, Long and Forsberg (2003), Meisina (2006), and Di Buo et al. (2019).

Most benchmarking studies are focused on clay soils - often associated with a specific geotechnical issue, such as landslides. The importance of describing and understanding the geotechnical properties and engineering behavior of non-cohesive soils should however not be overlooked. According to Bruand, Hartmann and Lesturgez (2005), analysis of existing literature indicates that the physical properties of sandy soils are “far from simple” and cannot be narrowed to the general definition, that is, weak or no structure, high permeability, poor water retaining properties and easier to compact. Compressibility characteristics of sandy soils are directly linked to settlement response and thus a vital design consideration. The importance of determining the often-variable nature of sandy soils by describing and understanding fundamental properties such as compressibility is thus apparent.

In the South African context, the most comprehensive information on the properties of soils from various geological formations is contained in the four volumes of *Engineering Geology of Southern Africa* by A.B.A Brink, published between 1979 and 1985. The engineering and geological characteristics of various soil types are presented in these landmark books. Although considerable attention is paid to residual soils derived from the formations such as the Basement granites, the Malmani dolomites and the Ventersdorp lavas, only a brief explanation of the engineering geological nature of the Cape Flats sands is given by Brink (1985), as described in Section 2.3.2 below.

### 2.3.2 Engineering geology of the Cape Flats

As mentioned in Section 1.2 of Chapter 1, limited published literature is available pertaining to the geotechnical and engineering geological properties of the Quaternary age sand deposits of the Cape Flats. Countless geotechnical investigations have been undertaken in the area; however, the valuable geotechnical data has largely remained unexplored and unpublished. An extensive search of existing literature revealed notable research contributions by Amdurer (1956), Brink

(1985) and Stapelberg (2009). Other studies have also been undertaken, involving the upper sands of the Cape Flats, but these focus mainly on specific aspects such as liquefaction risk (Parker, 1991 and Schoeman, 2018), groundwater in the Cape Flats aquifer (Henzen, 1973 and Adelana, Xu and Vrbka, 2010) and the use of geotextiles in the sands (Kalumba, 1998). Most of these studies involved a basic characterisation of the specific study site in terms of its geotechnical properties. This information will be included in the current research. A review of the existing literature has revealed the following generic description for the sands of the Cape Flats:

*Light coloured, poorly graded (uniform), fine and medium quartzitic aeolian sand; assigned the group symbol 'SP' based on the Unified Soil Classification System.*

Despite this simple generic description, these soils have been found to be highly variable, with a wide range of values assigned to many material properties. Some of these properties were investigated to limited extent by Amdurer (1956), Brink (1985) and Stapelberg (2009).

The engineering geology of a portion of the Cape Flats was investigated by Amdurer in 1956. The investigations, undertaken in the northern portion of the Cape Flats, comprised a series of boreholes and in-situ penetration tests spaced approximately one kilometre apart, resulting in approximately eighty testing and sampling locations. The research by Amdurer focused on the shear strength of the cohesive soils (alluvial, lacustrine and estuarine deposits) found interlayered with the sandy horizons and the residual Malmesbury soils (organic clay, sandy clay and plastic clay), the compaction characteristics and consistency of the sandy soils, and the limits of consistency of a range of soils from the study area. The findings of these research subjects are summarised in Table 2-2.

Amdurer also explored the genesis of the major soil components, that is the sand, silt and clay present in the study area. The influence of the attributes of these components, including grading and sorting, shape and roundness and mineralogy, on soil strength and stability was also unfolded. Combining the results of laboratory work, engineering, geological and pedological consideration and field observations, an attempt was made to reconstruct the depositional history of these soils.

Amdurer's investigation revealed a consistent pattern of interstratified bands and lenses of sand, clay and silt, in varying proportions, from ground surface to varying depths but typically not greater than 15 metres. Weathered Malmesbury Group sediments in the form of bedded clays, were encountered below the transported horizons. Layers and lenses of organic matter occur regularly, especially in the proximity of clay layers, forming black, plastic, sulphurous smelling material. Amdurer (1956) suggested that these sand, clay and silt layers originated through agencies of continental erosion in the form of strong prevailing winds alternating with torrential winter rains. According to Amdurer (1956), the borehole profiles reflect seasonal changes in topography, resulting from these dynamic forces. The variation and disparity in the engineering properties of macroscopically similar soils, as seen in the test results summarised in Table 2-2, was attributed to these forces.

Table 2-2: Cape Flats soil properties (compiled from Amdurer, 1956)

Soil property	Soil type Investigated *	Testing method	Result	Comments
Shear strength	Clays: Organic clay, plastic clay, silty clay, sandy clay [65 No.]	Unconfined compression tests; triaxial compression tests	<u>Unconfined compressive strength</u> ( $q_u$ ): Mean = 43 MPa Median = 40 MPa Maximum = 93 MPa Minimum = 10 MPa	Shape of frequency distribution graph suggests variation is inherent in material
			<u>Shear strength parameters</u> $\phi$ = Between 10° and 25° (average = 14°). $c$ = Between 16kPa and 152kPa (average = 82 kPa).	Residual Malmesbury soils tested. Variation in results possibly explained by attitude of residual bedding planes i.e. anisotropy
Compacted density	Sands and silty sands [±27 No.]	Modified Proctor test; Modified AASHO (now AASHTO) compaction tests	<u>Modified Proctor</u> Maximum dry density (MDD): Varies between ±1620 kg/m <sup>3</sup> and 1880 kg/m <sup>3</sup> ; Optimum moisture content: Between 7% and 11.5% <u>Modified AASHO</u> Maximum dry density (MDD): Varies between ±1630 kg/m <sup>3</sup> and 1890 kg/m <sup>3</sup> ; Optimum moisture content: Between 7% and 11.5%	Dry density-moisture content curves from Proctor tests are dissimilar and follow no overall pattern. Results variable for seemingly similar material
			California Bearing Ratio (CBR) tests on two samples, identical at the upper and lower ends of grading curve, only different proportions of fine and very fine sand	<u>CBR tests</u> <b>Sample 1:</b> CBR 61 (at MDD = 1720 kg/m <sup>3</sup> and OMC = 9.7%) <b>Sample 2:</b> CBR 94 (at MDD = 1897 kg/m <sup>3</sup> and OMC = 8.6%)
Resistance to penetration (consistency)	Sandy soils [4 testing locations]	Dutch probe (cone penetration test); drop-penetration test using a dry spoon sampler	<u>Depth penetration resistance plots</u> display variation and trend reversal within consistent stratum of sand, clayey sand, etc. (no change by soil type)	Result can be explained by changes in soil material densities, resulting from conditions of sedimentation
Atterberg limits	Not specified (inferred to be mostly cohesive layers and lenses within aeolian sand deposits) [129]	Liquid limit: Method by Casagrande (1932)	<u>Liquid limit</u> : Varies from ±20% to 78%	Materials vary greatly as to quantity of water which can be retained before rendered liquid. Results are grouped around Casagrande "A" line.
		Plastic limit: Method by Amdurer (1956)	<u>Plasticity index</u> : Varies from ±4% to 60%.	
		Linear shrinkage: Standard test method described in ASTM D427	<u>Linear shrinkage</u> : Varies from ±1% to 16%; 55% of samples tested had shrinkages of 6% to 8%.	

\* Number of samples/testing locations in [brackets]

Approximately thirty years after Amdurer studied the engineering geology of the northern portion of the Cape Flats, Brink (1985) provided a brief description of the engineering geological nature of the Wolfgat, and Philippi and Epping members of the Langebaan and Springfontyn Formations respectively. According to Brink, the shelly and frequently slightly calcified sands of the Wolfgat member typically present with higher consistencies than the Philippi and Epping members. A complete summary of the soil parameters and additional information given by Brink (1985), is presented in Table 2-3. This table includes geotechnical data obtained from the foundation investigation for the Tygerberg hospital (referred to as the Tiervlei hospital) in Parow, situated close to the northern boundary of the Cape Flats.

**Table 2-3: Summarised soil properties of Cape Flats sediment (compiled from Brink, 1985)**

Stratigraphic unit		Soil parameters			Ground water level	Additional comments
		Soil consistency		Shear strength		
		SPT N-value	CPT point resistance			
Wolfgat Member, Langebaan Formation		25 (mean)	15 MPa (mean)	-	Minimum 1–2m below surface in interdune areas; varies with surface topography.	SPT N-value may exceed 60 in places CPT point resistance may exceed 50MPa
Epping Member, Springfontyn Formation	Sand horizons	10–20	<20 MPa	-	Within 3m of surface	<u>Upper 6–11m:</u> Sands with peaty or clayey layers
	Clayey/organic horizons	1–10	<6 MPa	±105 kPa	-	<u>Lower 12–15m:</u> Clay with sandy interbeds

The engineering geology of Bellville and its surrounding areas (including the northern portion of the Cape Flats) was investigated by Stapelberg of the Council for Geoscience in 2009. The focus of the investigation was to determine the geotechnical properties influencing suburban development; highlighting the resulting cost implication of intersecting potentially problematic properties or soil types. The major factors affecting development included slope instability/erosion, excavatability of ground, variable fill, flood risk, shallow water tables, permeability, compressibility, aggressive soil and collapse potential. Stapelberg (2009) focussed on civil engineering development potential and terrain evaluation and, as such, mostly descriptive information is provided as well as a severity class assigned to give an indication of possible geotechnical issues, their extent and the cost implications. The approximately forty data points from the investigated Cape Flats region, together with geotechnical data from previous work in the Cape Flats, revealed mostly sands and silty sands of aeolian origin (iron-rich or calcareous in places) described in the following manner:

- Mostly semi-pervious ( $k = 10^{-4}$  to  $3 \times 10^{-7}$  m/s).
- Typically, not collapsible or possibly collapsible, except for the calcareous soil horizons from the Langebaan Formation which are prone to collapse settlement.
- Variable in susceptibility to excessive settlement (consolidation).
- Mostly low erosion potential.
- Springfontyn Formation soils are moderately acidic and moderately corrosive.
- Grading modulus ranging from 0.85 to 1.36 and fineness modulus ranging from 0.85 to 1.75.

An engineering geological map (3318DC Bellville 2008, 1:50 000 Geotechnical Series) indicating the geotechnical restrictions and delineating development potential, was compiled based on the Stapelberg's work, existing geological maps and unpublished field maps. In addition, an accompanying explanation entitled 'The Engineering Geology of Bellville and Environs, Western Cape, South Africa' was produced by the Council for Geoscience.

The engineering geology of the Melkbosstrand area was similarly investigated by Stapelberg of the Council for Geoscience in 2005 and an engineering geological map (3318CB Melkbosstrand 2005, 1:50 000 Geotechnical Series) with an accompanying explanation entitled 'The engineering geology of the Melkbosstrand area' was produced. As mentioned in Section 2.2.1.1, the same transported sand deposits on the Cape Flats extend northwards along the west coast through Bloubergstrand and Melkbosstrand to Atlantis. These northern sand covered areas are located outside the geographical boundaries of the Cape Flats, which is the delineated study area.

## 2.4 The geotechnical site investigation

The first step in characterising subsurface materials for engineering purposes involves a geotechnical site investigation. The Geotechnical Division of The South African Institution of Civil Engineering (SAICE) has compiled a Site Investigation Code of Practice, establishing a standard of acceptable engineering practice for the planning, design and execution of geotechnical site investigations in South Africa. This Code of Practice, issued in 2010, describes the aim of the geotechnical site investigation as follows: "to characterise the nature and distribution of the geotechnical properties of the site to permit the acceptable design, construction and operation of the proposed works".

A detailed geotechnical investigation generally commences with a desk study of available geological and topographic maps and aerial photographs, and any other information pertaining to the specific site. This is often followed by a reconnaissance of the site to corroborate the findings of the desk study, to assist in planning field investigations and identify potential geotechnical constraints on future development. The desk study and reconnaissance are followed by a field investigation phase which comprises the description of the soil and/or rock profile in test pits or boreholes, in-situ testing to measure geotechnical parameters either directly or empirically, and recovery of representative disturbed and undisturbed soil samples for laboratory testing. The results of these investigations and tests enable material classification and/or characterisation and provide insight into the nature and engineering behaviour of the soils.

The importance of a systematic and detailed description of the soil profile cannot be overestimated as it forms the basis of the geotechnical site investigation. Soil profiling involves detailed examination of the sidewalls of trial holes or core samples extracted from boreholes to describe each distinctive layer in the vertical succession separately and consistently. These soil profiles or borehole logs give basic information to enable an approximate quantitative assessment of the engineering properties of the site soils. Jennings, Brink and Williams (1973) (a revision of the original soil profiling guide in South Africa published by Jennings and Brink in 1961) and Brink and Bruin (1990) establish requirements for describing soil profiles in Southern Africa in terms of six descriptors, namely moisture content, colour, consistency, structure, soil type and origin (MCCSSO in short). The consistency of the soil layers in a vertical profile is considered central to the description as it provides a measure of the strength and stiffness of the soil. To determine the consistency of subsurface cohesionless soils, penetrometers are considered valuable tools (Byrne and Berry, 2008). Numerous empirical correlations have been developed for the determination of soil properties from penetration test results including shear strength and stiffness (compressibility). Current practice relies on standard penetration tests (SPT) and cone penetration tests (CPT or CPTu) to estimate various soil parameters such as the Young's modulus, angle of internal friction, undrained shear strength of clays, relative density, state parameters and liquefaction potential. In addition, dynamic cone penetrometer (DCP) test results are used to measure the in-situ California Bearing Ratio (CBR) of road layerworks. An overview of these penetration tests is given below as these tests are used extensively in the current study to characterise the Cape Flats soils.

### **Standard penetration test (SPT)**

According to Byrne and Berry (2008), the SPT method currently used was developed during the 1920's and 1930's. In 1993, CIRIA produced a comprehensive Funders Report prepared by C.R.I Clayton from the University of Surrey, entitled "The Standard Penetration Test (SPT): Methods and Use". This report provides in-depth guidance on the use of the SPT in geotechnical engineering. Clayton (1993) explains that the test procedure comprises driving a split-spoon sampler (with a standard outside diameter of 50 mm) into the soil at the base of a borehole by repeatedly dropping a 63.5 kg hammer over a free-fall distance of 760 mm. The number of blows required to drive the sampler through the last four of six 75 mm increments (i.e. through the final 300mm of a total 450 mm penetration) is then recorded as the SPT N-value. The upper 150 mm (first two 75mm increments) is considered disturbed material and, as such, these blow counts are discarded. Refusal is recorded (and the test terminated) where the blow count exceeds 50 blows per 150 mm penetration (SAICE, 2010).

According to Das (2008) there are several factors, including SPT hammer efficiency, that affect the SPT N-value at a specific depth for similar soil profiles. To determine the hammer efficiency, otherwise known as the drill system dependent energy ratio ( $E_r$ ), Equation 2-1 is used (Bowles, 1997). The calculated energy ratio is subsequently referenced to a standard energy ratio, typically taken as 60%, to obtain to a corrected value known as the  $N_{60}$  value.

$$E_r (\%) = \frac{\text{Actual hammer energy to sampler}}{\text{Input energy}} \times 100 \quad \text{Equation 2-1}$$

In South Africa, the actual hammer energy to the sampler is not normally determined and, as such, the energy ratio is unknown. Typical practice in South Africa is to assume that the automatic trip hammers commonly used in the country have an energy ratio of approximately 60% and that the measured N-value is representative of the  $N_{60}$  value. In line with these assumptions, measured SPT N-values used in the current research study are considered to be  $N_{60}$  values. Additional corrections include those for drill rod length, borehole diameter and sampling method (Clayton, 1993 and Bowles, 1997). For certain empirical correlations in granular soils, the corrected blow counts are additionally normalised to allow for the effective overburden pressure ( $\sigma'_{v0}$ ) at the test depth to avoid minor changes in constitutive properties being overlooked. In such cases, the  $N_{60}$  value is adjusted to correspond to a standard overburden pressure. The normalised blow count,  $(N_1)_{60}$  is given by (Liao and Whitman, 1986):

$$(N_1)_{60} = \left( \frac{p_a}{\sigma'_{v0}} \right)^n \cdot N_{60} \quad \text{Equation 2-2}$$

Where:

$p_a$  = Atmospheric pressure (kPa)

$\sigma'_{v0}$  = Effective overburden pressure (kPa)

$n \sim 0.5$  (variation of 'n' with soil cementation, age and plasticity occurs)

The relationship between the corrected SPT  $(N_1)_{60}$ -value and the relative density ( $D_r$ ) of granular materials, as given by Byrne and Berry (2008) (presumably based on Cubrinovski and Ishihara, 1999), is:

$$D_r (\%) = 100 \sqrt{\frac{(N_1)_{60}}{60}} \quad \text{Equation 2-3}$$

The consistency of granular soils in terms of relative density is shown in Table 2-4. SPT-based classifications are also given by Clayton (1993), differing slightly from the ranges given in Table 2-4.

**Table 2-4: Relative density of sandy soils with corresponding SPT N-values (composite from Jennings, Brink and Williams, 1973 and Brink, Partridge and Williams, 1982)**

Relative density description	Relative density, $D_r$ (%)	Saturated SPT N-value (blows per 300 mm)
Very loose	0 – 20	< 4
Loose	20 – 40	4 – 10
Medium dense	40 – 60	10 – 30
Dense	60 – 80	30 – 50
Very dense	80 - 100	>50

In addition to soil classification, principle uses of the SPT include the determination of geotechnical design parameters, and for direct design. The predictive methods utilised in the current research are discussed in Chapter 3.

For the current study, the SPT was preferred to the dynamic probe super heavy (DPSH) test, which is widely used to provide an empirical indication of soil consistency (Byrne and Berry, 2008). The test comprises a 60° disposable cone, 50 mm in diameter, placed onto the base of a rod that is driven into the ground by dropping a 63.5 kg hammer through a free-fall distance of 762 mm. The number of blows required to drive the cone through each consecutive 300 mm of penetration is continuously recorded until refusal is reached. No soil sample is obtained during the test. The DPSH blow counts are often converted to equivalent SPT N values, to be used in design applications. Notwithstanding this, rod friction is a major factor to be considered when interpreting dynamic probing resistance values. MacRobert (2009) explains that as the probe is uninterruptedly hammered into the ground, the skin friction acting on the rods has a significant effect on the penetration resistance. Skin friction is created when soil meets the driving rods, resulting from the collapse of the annulus around the rod arising from the difference in cone- and rod- diameter). According to MacRobert (2009), rod friction associated with the DPSH test increases linearly with depth below the water table. The effect of rod friction is illustrated in Figure 2-3, in which the penetration results from DPSH tests and SPT's, carried out at the same site in the Cape Flats, are plotted. The water table occurs between 1.5m and 2.5m below ground level at the site. In the figure, the effects of rod friction on the DPSH n-values can be seen. The DPSH penetration values rapidly increases with depth to approximately 5 m, at which refusal occurs. The two SPT's (shown in red), however, extend much deeper without refusal being recorded. These falsely high DPSH penetration values incorrectly over-predict the soil consistency.

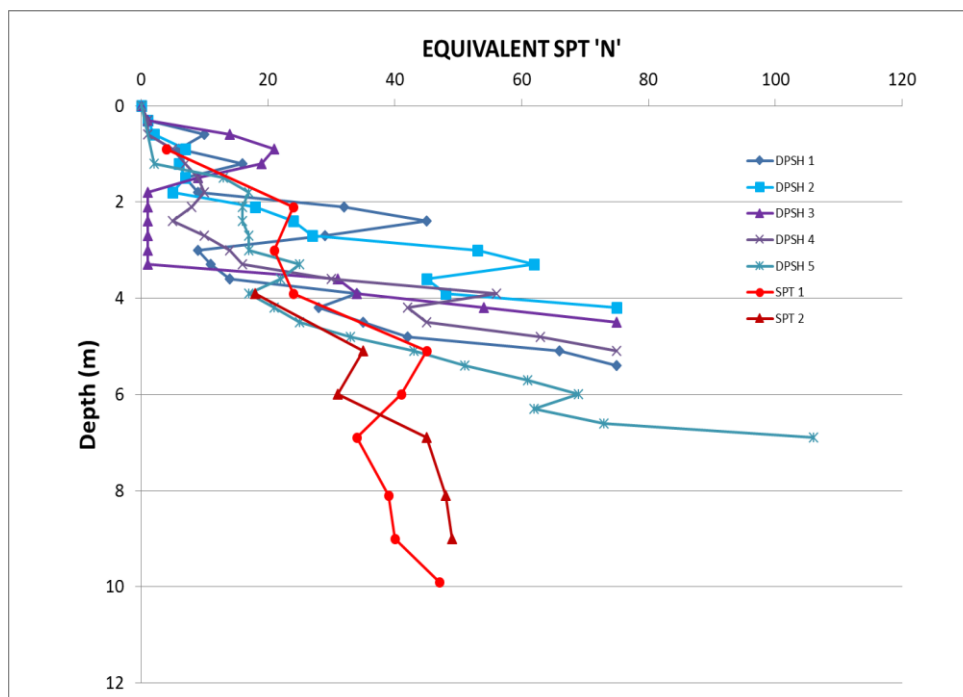


Figure 2-3: Effects of rod friction in DPSH test results

### Cone penetration test (CPT)

The CPT, which was initially developed in the Netherlands in the 1930's, is widely used in the field of geotechnical engineering to evaluate subsurface stratigraphy and infer soil properties. A summary of the historical development of the CPT is provided by Meigh (1987) and Robertson and Cabal (2012). The test comprises a probe with a 60° cone and a tubular friction sleeve which

is hydraulically pushed into the ground at a constant rate of 20 mm per second (SAICE, 2010). The force needed to advance the cone,  $Q_c$ , is recorded and divided by the cone area,  $A_c$ , to produce the tip resistance,  $q_c$  in MPa. In addition, the force on the friction sleeve,  $F_s$ , is divided by the surface area of the sleeve,  $A_s$ , to give the sleeve friction,  $f_s$  (Robertson and Cabal, 2012). Continuous measurements of cone resistance and sleeve friction are made with depth as the test progresses. In South Africa, the electric CPT is used in accordance with ASTM D5778 (2020).

The use and interpretation of the cone penetrometer test were detailed by Robertson and Campanella (1983) and Campanella et al. (1985), in which the latest advancements in the use and understanding of the CPT were highlighted. Furthermore, Meigh (1987) compiled a comprehensive CIRIA Ground Engineering Report detailing the use of the CPT (including its enhancements) and the interpretation of its results and their use in design. More recently, Robertson and Cabal (2012) put forth the '5<sup>th</sup> Guide to Cone Penetration Testing for Geotechnical Engineering', which focusses on the successful application of the CPT in the field of geotechnical engineering. This guide serves as an update to Lunne, Robertson and Powell's book entitled 'CPT in Geotechnical Practice', published fifteen years prior to Robertson and Cabal's guide.

The relationship between cone resistance and relative density for sands is given in Robertson and Cabal (2012) as:

$$D_r (\%) = 100 \cdot \left(\frac{1}{C_2}\right) \ln \left(\frac{Q_{cn}}{C_0}\right) \quad \text{Equation 2-4}$$

Where:

$$Q_{cn} = \frac{q_c/P_a}{(\sigma'_{vo}/P_a)^{0.5}} \quad \text{Equation 2-5}$$

And where:

$q_c$  = Measured cone resistance (MPa) (more recently,  $q_t$ )

$q_t$  = Cone resistance corrected for water effects (MPa)

$P_a$  = Reference pressure of 100kPa, in the same units as  $q_c$  and  $\sigma'_{vo}$

$\sigma'_{vo}$  = Current in-situ vertical effective stress (MPa)

For moderately compressible, normally consolidated, unaged and uncemented, predominantly quartz sand, the constants are  $C_0 = 15.7$  and  $C_2 = 2.41$ .

Approximate relationships between cone tip resistance and relative density (as a function of in-situ effective normal stress) for both normally and over-consolidated non-cohesive soils have also been given by Bowles (1997). According to Meigh (1978), calibration chamber tests have provided most of the knowledge pertaining to the relationship between relative density and cone resistance. One such relationship for uncemented, normally consolidated quartz sand, in which the values were derived from calibration chamber tests, can be viewed in Meigh (1978).

A major advancement with regards to the electric cone penetrometer is the addition of a porous disc and a pore pressure transducer behind the cone tip. This improved apparatus, named the piezocone or CPTu, allows for the pore pressure response at the porous disc position to be recorded during penetration testing (SAICE, 2010). Furthermore, at any time during the test, a dissipation test can be performed during which advancement of the cone is paused and the rate of dissipation of excess pore pressure generated around the cone is measured. If the dissipation

period is continued until all excess pore water pressure has dissipated and equilibrium is reached, the position of the water table can be determined. In 1983, Jones and Rust presented a detailed overview of the apparatus, its use and interpretation in a symposium article entitled: "Piezometer probe (CUPT) for subsoil identification". Further investigation by Jones and Rust (1995) into the long-term performance of road embankments constructed over alluvium in South Africa, found that long term settlement within these embankments can be accurately predicted from piezocone test data.

A major application of the CPT and CPTu is soil profiling and soil type classification. A CPT soil classification chart, known as the soil behaviour type (SBT) chart, is created by plotting the cone resistance,  $q_c$ , on the vertical axis and the friction ratio,  $F_r$  (the ratio of the sleeve friction to the tip resistance), on the horizontal axis. The chart area is divided into zones of soil type based on its behaviour, that is, its mechanical properties. To account for the effects of overburden pressure, the penetration resistance and sleeve friction require normalisation. A CPT soil behaviour type chart based on normalised values of cone resistance,  $Q_t$ , and friction ratio,  $F_r$ , (known as the SBTn chart) has been proposed by Robertson (1990). The complete SBTn chart suggested by Robertson (1990) includes an additional chart based on the normalised values of cone resistance and the pore pressure ratio,  $B_q$ , whereby the soil behaviour type can similarly be identified. The normalised CPT soil behaviour type charts are shown in Figure 2-4 below. The soil behaviour type associated with the number in each delineated zone is given in Table 2-5. The boundaries of soil behaviour types can also be given in terms of an index,  $I_c$ , known as the soil behaviour type index. The indices for zones 2 to 7 are given in Table 2-5 (SBT index does not apply to zones 1, 8 and 9).

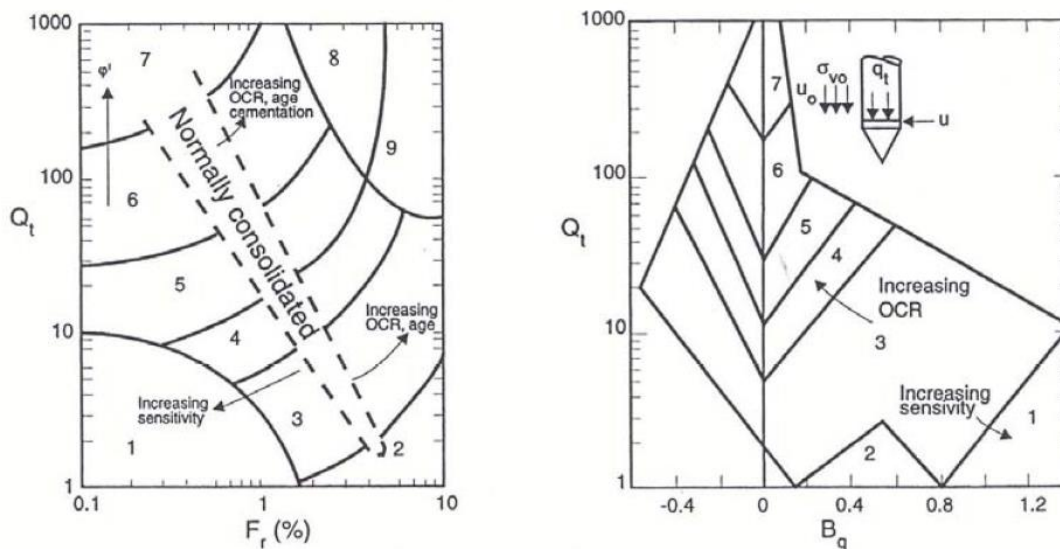


Figure 2-4: a)  $Q_t$ - $F_r$  SBTn chart and b)  $Q_t$ - $B_q$  SBTn chart (Robertson and Cabal, 2012 after Robertson, 1990)

**Table 2-5: Soil behaviour types associated with SBTn chart zones and index  $I_c$  (Robertson and Cabal, 2012 after Robertson, 2010a)**

Zone	Soil Behavior Type	$I_c$
1	Sensitive, fine grained	N/A
2	Organic soils – clay	> 3.6
3	Clays – silty clay to clay	2.95 – 3.6
4	Silt mixtures – clayey silt to silty clay	2.60 – 2.95
5	Sand mixtures – silty sand to sandy silt	2.05 – 2.6
6	Sands – clean sand to silty sand	1.31 – 2.05
7	Gravelly sand to dense sand	< 1.31
8	Very stiff sand to clayey sand*	N/A
9	Very stiff, fine grained*	N/A

Numerous transformation models have been proposed whereby soil parameters can be estimated based on CPT cone resistance. Additionally, direct design methods based on the CPT have also been developed to calculate the settlement of footings in sand and the ultimate bearing capacity of piles. According to Meigh (1978), the data from CPT and CPTu tests are primarily used to assess the angle of shearing resistance and the deformation characteristics of cohesionless soils. The transformation models utilised in the current research are discussed in Chapter 3.

#### **Dynamic cone penetrometer test**

In Southern Africa, the dynamic cone penetrometer (DCP) test is used as a crude measure of soil consistency over the depth of a soil profile. The test involves driving a 20mm diameter 60° cone, attached to a 16 mm diameter rod into the ground by dropping an 8 kg weight through 575 mm. The penetration resistance is subsequently recorded in millimetres per blow. According to Byrne and Berry (2008), the test was originally designed to rapidly determine the in-situ California Bearing Ratio of road pavements. Since then, various models have been developed to estimate CBR from DCP penetration rate for different material types (Paige-Green and Du Plessis, 2009 and Gill, Jha and Choudhary, 2010). The DCP results have also been correlated with geotechnical parameters such as the unconfined compressive strength, soil elastic modulus, shear strength, and standard penetration resistance. The results are also erroneously used to estimate the bearing capacity of the soil. The test is limited by a test depth of 2 m and the inability of the equipment to penetrate hard layers or lenses, as well as other obstructions such as gravel and boulders (Byrne and Berry, 2008). When the DCP is applied in harder materials (CBR > 15), side friction on the rod may influence the results (Paige-Green and Du Plessis, 2009). In the current study, DCP penetration resistance will only be used as originally intended for the estimation of in-situ CBR values, and as an add-on to laboratory-derived CBR values.

An overall increase in penetration resistance with depth is commonly observed for Cape Flats soil profiles, mainly due to rod friction. Nonetheless, changes in soil density arising from cementation and soft clay or peat layers for instance, will result in departures from this trend. Increased consistency, indicated by reduced penetration per blow or refusal, is likely in the deposits of the Langebaan Formations, and to a lesser extent in the Witzand Formation (compared to the Springfontyn Formation), due to the presence of calcretised strata.

## 2.5 The geotechnical properties of cohesionless soils

### 2.5.1 Introduction

The geotechnical parameters commonly used for material classification and characterisation are given in Table 2-6 below.

According to SAICE (2010), the aim of material classification is to group representative site soils into standard classes with comparable engineering properties and behaviour. In this way, the engineering behaviour of a soil can be predicted to some extent by knowing to which standard class the specific material belongs. Currently, there are several classification systems used by South African engineers, including the Unified Soil Classification System (USCS), the AASHTO Soil Classification System, and the TRH14 classification system. The USCS, which is widely used in engineering and geology disciplines, groups material binomially according to its governing grain size (gravel and sand or silt and clay) and the degree of particle sorting or plasticity respectively (Jenkins and Rudman, 2016). The AASHTO system, used as a guide for the selection of soils and soil-aggregate mixtures in road construction, groups material into primary and secondary classes based on gradation and plasticity. In the TRH14 system, pavement materials are categorised as G1 to G10 based on their grading, Atterberg limits, CBR and swell properties. The three soil classification systems are given in Appendix B.

Material characterisation involves the determination of material properties from in-situ testing or laboratory tests typically on undisturbed representative soil samples. Determination of the specific gravity, bulk density, in-situ moisture content, hydraulic conductivity and the collapse potential allows the in-situ state of the soil to be studied (SAICE, 2010). Of importance in the proposed study, is the in-situ moisture content and seasonal fluctuations in groundwater levels in the Cape Flats and their effect on soil parameters and engineering behaviour. The specific material properties of shear strength and compressibility are utilised in design calculations. Additionally, the tendency of the soil to dilate or contract during shearing can be used as an indication of the liquefaction potential of the material. Knowledge of the general characterisation of the soils on the Cape Flats can be beneficial during the early planning stages of a project where assumptions must be made regarding investigation and construction methods best suited to the project.

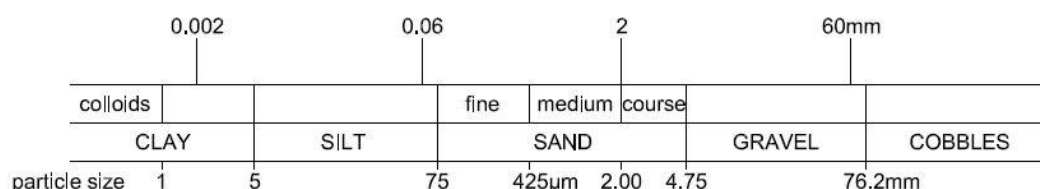
The geotechnical parameters commonly used for material classification and characterisation are listed in Table 2-6. This is followed by a discussion of each parameter (in the order given in Table 2-6) to provide the necessary contextual information, an overview of previous research findings, and anticipated classification and characterisation outcomes pertaining to the Cape Flats soils.

**Table 2-6: Geotechnical parameters required for soil classification and characterisation (modified from SAICE, 2010)**

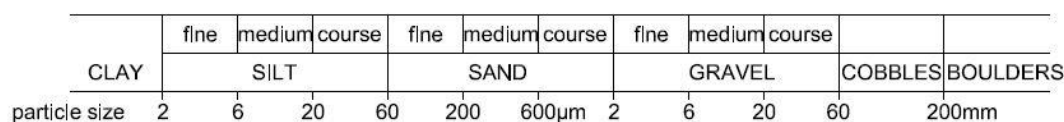
Geotechnical parameter	
Grading properties	Classification
Atterberg Limits	
Maximum dry density and optimum moisture content	
California Bearing Ratio	
Minimum and maximum index densities and relative density	
Corrosivity	
Erodibility	
Specific gravity	Characterisation
In-situ moisture content	
In-situ density (bulk density)	
Collapsibility	
Permeability	
Shear strength	
Compressibility	
Dilatative / contractive behaviour during shear (liquefaction potential)	Additional characterisation

### 2.5.2 Grading properties

The range in the size of particles present in a soil, expressed as a percentage of the total dry weight, is used to compile a particle size distribution (PSD) curve, often referred to as a grading curve. Full details of the determination of grading properties by sieving and hydrometer analysis are stated in ASTM D6913 and D7928 (2017). Particle size ranges for classification, based on ASTM and BS designations, are given in Figure 2-5. Grain sizes of the Cape Flats sands will be grouped based on the ASTM values.



(a) U.S.A. ASTM D422



(a) Great Britain BS1377:1975

**Figure 2-5: Particle size ranges for soil classification as per (a) American Standards ASTM D422:2007) and (b) British Standards (BS1377:1990)**

Grain size distribution results are normally presented graphically to illustrate the range of particle sizes present in the soil as well as the type of distribution of various-size particles (Das and Sobhan, 2018). PSD curves for a well graded soil and poorly graded soils (uniformly graded and gap graded)

are shown in Figure 2-6. From the PSD curves, the coefficient of uniformity ( $C_u$ ) and the coefficient of curvature ( $C_z$ ), representing the slope and shape of the curve respectively, can be determined (refer to Das and Sobhan, 2018). Classification of a soil as “well graded” requires a value of  $C_u$  exceeding 6, and a  $C_z$  value between 1 and 3 (Knappett and Craig, 2012). The properties of coarse-grained materials can also be assessed in terms of their quality as road building material by the grading and fineness moduli and the grading coefficient (all calculated from the grading results), as well as the shrinkage product, calculated from the grading results and linear shrinkage.

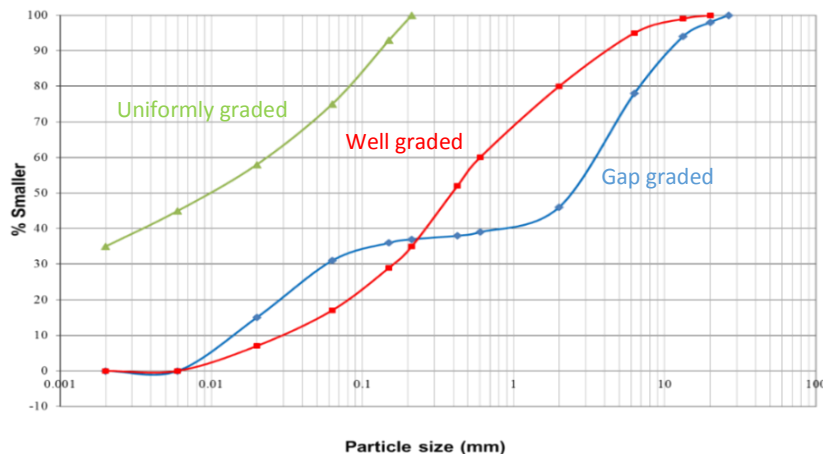


**Figure 2-6: Particle size distribution curves**

The grading of a soil provides a primary classification of the soil and an indication of its likely engineering properties. The physical behaviour of coarse-grained, typically cohesionless, soils can be determined to a large extent by their particle size distribution. For this reason, soil gradation is considered a basic and fundamental property to estimate characteristics of coarse-grained soils such as density, permeability, shear strength, and their consolidation and compaction properties. The presence of even a small amount of soil fines, particularly colloidal clays, will affect the water holding capacity of the soil, as well as the packing efficiency, which in turn influences the above-mentioned soil characteristics.

Existing literature describes the windblown deposits of the Cape Flats as predominantly fine and medium grained sand, mostly with a minor fines content, particularly plastic fines (Theron et al., 1992 and Stapelberg, 2009). Increased fines and peat are associated with lacustrine, estuarine and alluvial deposits occurring intermittently with the aeolian sands in the Springfontyn Formation. The grain size of organic particles in peat ranges from 0.0001 mm to greater than 2 mm (Mitchell, 1993). The presence of coarse sand and calcrete gravel, particularly in the Langebaan Formation, is highlighted by Roberts (2001) and Stapelberg (2009). Strongly bimodal grain size distributions (poorly graded sands) are characteristic. An increase in grain size with depth has been documented for the sands of the Springfontyn Formation (Hill and Theron, 1981). The uniform and coarse-grained nature of the soils from the Witzand, Springfontyn and Langebaan Formation (predominance of fine and medium sized sand grains) will govern the engineering properties of the Cape Flats soils. The presence of plastic soil fines and cohesion (also arising from organic matter) in some windblown sands will alter its projected engineering behaviour, likely dominated by physical and physiochemical interactions. Although typically

structureless, the development of a honeycombed structure (where clays are maintained at particle contacts) or preferred orientation of elongated grains, is possible.

The silica sands in the vicinity of Philippi on the Cape Flats, which are exploited for glass-making purposes, were investigated by the Geological Survey of South Africa in 1981. The grain size characteristics, chemical composition and mineralogy of the Springfontyn Formation sands in the area were studied to assess their suitability as a glass-sand source (Hill and Theron, 1981). As part of their study, the distribution of particle sizes in soils sampled from a 50m deep borehole were determined, illustrative of the typical sand succession in the area. The results are tabulated below, showing the average percentage fine, medium and coarse-grained sand in each of the provided depth intervals. A marked increase in medium sand size grains is observed between 40m and 50m depth.

**Table 2-7: Grain sizes in Springfontyn Formation sands from Philippi (compiled from Hill and Theron, 1981)**

Depth interval	Percentage by mass of particles in size range (from average distribution curve)			Number of samples from each depth interval
	Fine sand (0.075-0.425mm)	Medium sand (0.425 – 2.0mm)	Coarse sand (2.0 – 4.75mm)	
0 to 8m	50%	49%	1%	7
8 to 15m	75%	24%	1%	12
15 to 30m	80%	19%	1%	17
30 to 40m	80%	19%	1%	19
40 to 50m	28%	69%	3%	15

The distribution of grain sizes in a sand sample from the Philippi area was also determined as part of a liquefaction study by Neal (2011). The results, which showed the sand to be fine grained and uniformly graded, ( $C_u = 1.95$  and  $C_z = 1.25$ ), confirmed the findings of Hill and Theron and the textural descriptions given in literature.

Existing literature contributes either generalised descriptions of particle size and gradation, or investigative results demonstrating the particle characteristics in small and isolated study areas. The engineering behaviour of the Cape Flats soils will be dominated by the presence of sand sized grain fractions, nonetheless, variation in grading properties, both vertically and laterally (interformation) is anticipated. The presence and proportion of fines will exert considerable influence on soil properties such as permeability, shear strength, compressibility and collapse potential. The results associated with the characterisation parameters will therefore be interpreted in relation to the revealed gradings.

### 2.5.3 Atterberg limits

Water is strongly attracted to the surfaces of clay minerals, giving rise to soil plasticity (allowing remoulding of soil without cracking or crumbling). An increase in clay content is generally associated with higher plasticity and cohesion (Mitchell, 1993). The Atterberg limits, corresponding to the water content values at which the soil changes from one phase to another, are shown in Figure 2-7. The stress-strain diagrams at different states are also shown in the figure. The range of water content over which the soil will display plastic behaviour, known as the plasticity index (PI), is fundamental in the classification of soil fines. In this regard, the Unified plasticity chart (associated with the Unified Soil Classification System and adapted from

Casagrande's plasticity chart), allows distinction of soil fines based on liquid limit – PI data points. The type and amount of clay minerals in a soil will affect the plasticity values, with minor amounts of some clays (e.g. montmorillonite) associated with significantly higher PI's compared to similar amounts of other clay types (e.g. kaolinite). The activity of a clay soil (potential to undergo volume change with a change in soil moisture) is illustrated by the gradient of the mostly straight-line clay content – PI plot.

The procedures for determining the liquid and plastic limits, specifically for engineering purposes, are specified in ASTM D4318 (2017), whereas the shrinkage limit test procedure is given by ASTM D4943 (2018).

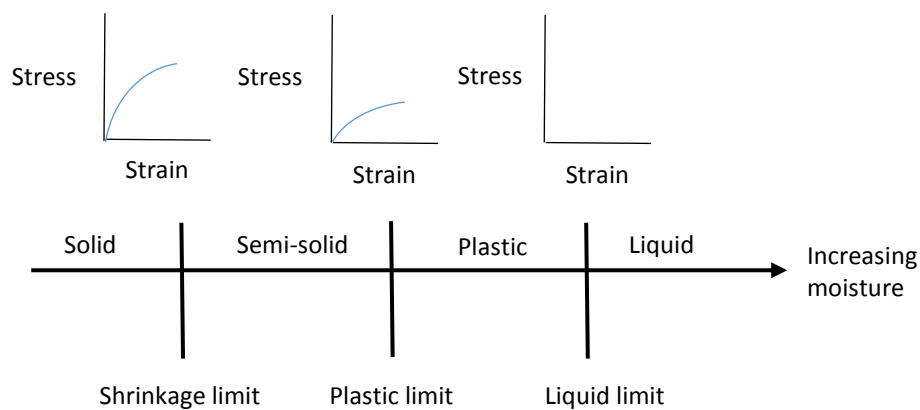


**Figure 2-7: Atterberg limits of fine-grained soils (modified from Das and Sobhan, 2018)**

The Atterberg limits are strongly related to the clay content and the clay mineral type present in the soil, and therefore considered useful in the differentiation between plastic and non-plastic fines, that is, clays and silts. Sands and gravel - including composites with slight fines contents - are non-plastic or occasionally slightly plastic in nature. The liquid limit of these coarse soils is difficult to determine (unable to establish using the Casagrande cup), and the plastic limit and linear shrinkage are equal to zero. The aeolian sands of the Cape Flats often include some soil fines, although mostly minor, and the sands are therefore unlikely to have measurable PI. The presence of inert clay minerals, such as kaolinite, will render low plasticity values, even in increased quantities. Layers and lenses of clay, silt and peat - mixed in varying proportions and often with a sand fraction - are frequently present within the thick sand successions of the Springfontyn Formation. Significant plasticity is likely to be associated with these deposits. The organic matter making up a significant proportion of the peaty soils may account for high plasticity as a result of its water holding capacity.

Limited information is available regarding the mineralogy of the Cape Flats sands. According to Amdurer (1956), the sands from the study area mostly comprise quartz, with lesser feldspar and kaolinite. No distinction is made between the mineralogy of the different sand types. The sand-size particles consist of quartz, whereas the coarse silt size fraction is presumably quartz and feldspar. Both quartz and feldspar are common in the bedrock underlying the Quaternary sands, a source material of these sands. Kaolinite, which weathers from feldspar, is possibly dominant in the fine silt and clay size fractions in the study area, although the presence of other common clay

minerals such as illite and montmorillonite is possible. The Atterberg limits of sands with appreciable fines contents will be determined by the clay mineral type present in the soil. The link between soil mineralogy and engineering behaviour will be explored in Chapter 4.

Amdurer (1956) determined the Atterberg limits of soils from the Cape Flats; presumed to be mostly cohesive transported (other than aeolian) layers and residual shale soils. These transported soils occur sporadically within the windblown sands of the Springfontyn Formation. The liquid limits of these soils vary significantly, from 20% to 78% and the plasticity indices range from 4% to 60%. Fifty five percent of the samples displayed shrinkages between 6% and 8%. The current study focusses on the sand-dominated windblown soils of the Cape Flats, rather than the fine-grained, plastic materials studied by Amdurer. Stapelberg (2009), confirmed the presence of typically non-plastic sands and slightly silty and/or clayey sands in the northern Cape Flats. A few samples displayed plasticity, with PI's varying between 7% and 15% (average of 10%).

Soil parameters, such as the angle of shearing resistance, compressibility and permeability are influenced by the presence and type of clay minerals and soil PI. For fine-grained soils, these parameters can be estimated from plasticity values using relationships such as those given by Skempton (1944), Bjerrum and Simons (1960), Brooker and Ireland (1965), Terzaghi and Peck (1967), Kulhawy and Mayne (1990) and Terzaghi, Peck and Mesri (1996). The early work up to 1967, could not be obtained, and are cited from Bowles (1997) and Vinod and Bindu (2010). By contrast, for non-cohesive soils with no or slight plasticity, estimation of the friction angle is based on relative density, unit weight, SPT blow count or CPT cone tip resistance (Ching et al., 2017); compressibility represented by the soil's elastic modulus, based on penetration resistances recorded by the SPT and the CPT; and permeability indirectly estimated from grading characteristics.

#### **2.5.4 Maximum dry density and optimum moisture content**

Several engineering structures, such as roads, retaining walls and earth fill dams require the placement of fill material which is compacted to improve its strength and stiffness. The degree of compaction of fills is often expressed as percentage of the maximum dry density (MDD) at optimum moisture content (OMC). When a soil is dry of optimum moisture content, the capillary tension in the pore water impedes the rearrangement of the soil grains into a denser state of packing (Das and Sobhan, 2018). When the soil is wet of optimum moisture, water will occupy the pore space, again impeding proper compaction. On-site determination of compacted dry density can be achieved by means of the sand cone method (ASTM D1556:2015), the rubber balloon method (ASTM D2167:2015) or using nuclear density meters.

The standard or modified Proctor test, the Modified AASHTO test or the vibrating hammer test are standard test methods to determine maximum dry density in the laboratory. The procedures and equipment details for the compaction tests are given in ASTM D698 (2012), D1557 (2012) and D7382 (2020). A typical dry density - water content curve is shown in Figure 2-8, illustrating the point of MDD and OMC.

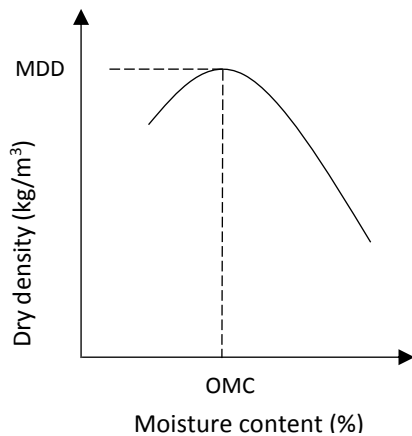


**Figure 2-8: Dry density-moisture content relationship**

In addition to moisture content and compaction energy, maximum dry density (minimum void ratio) is also influenced by grain characteristics such as the size and shape of the soil particles and the soil particle size distribution (Das and Sobhan, 2018). Coarse grained soils typically exhibit higher MDDs than fine grained soils and the MDD is achieved at lower moisture contents. Fine grained soils lack the range of sizes required to reduce the void space to a similar extent. Furthermore, fine grained soils typically hold a film of water around the individual grains, making it more difficult for particles to pack closely together. Even in predominantly coarse-grained soils, gradation has a significant influence on the compaction characteristics. Coarse grained soils with larger values of  $C_u$  will achieve higher MDDs due to the smaller particles filling the voids between larger grains. Compaction of poorly graded soils with uniform particle sizes will result in more air-filled voids after compaction and a lower dry density. The latter scenario is expected for the typically uniformly graded sands of the Cape Flats. The sands from the Springfontyn and Langebaan Formations are expected to achieve slightly higher MDDs at lower OMCs (when compared to the Witzand Formation sands), due to the somewhat higher fines content and lower degree of uniformity presumably associated with Springfontyn Formation sands and the typically larger particle size of the sands from the Langebaan Formation. If organic matter in the Springfontyn Formation is included in the material being compacted, the maximum dry density will decrease, and the OMC will increase. According to Mitchell (1993), a significant reduction in compacted density is noted in both natural soils and soil-peat mixtures as the organic matter content is raised. The amount of fines in the sands of the Cape Flats will have a pronounced effect on the dry density by filling pore space and lowering the void ratio. However, a fines content in excess of 40% is associated with decreased soil compaction (Das and Sobhan, 2018). The shape of aeolian sand particles is typically described as rounded or sub-rounded due to abrasion during transportation (Novak-Szabo et al., 2018). Increased roundness is associated with increased travel distances. Fragmentation of colliding grains create angular and sub-angular particle shapes. The shapes of windblown sand particles in the study area – transported by the prevailing south easterly winds - are therefore likely to vary (based on transportation distance), but mostly rounded and sub-rounded. An increase in grain angularity is also typically associated with a decrease in grain size. Amdurer (1956) investigated the shape of coarse and fine-grained sands from the Cape Flats, using a visual method proposed by Pettijohn (1948) (refer to Amdurer, 1956). It was found that the coarse sands (0.5mm to 1mm) are rounded and sub-rounded in shape, and the fine sands (0.05mm to 0.1mm) sub-rounded. The presumed rounded and sub-rounded shape

of sand grains in the study area should allow denser packing compared to similarly graded soils with angular particle shapes.

Amdurer (1956) studied the compaction characteristics of the aeolian sands and silty sands of the northern Cape Flats. Modified Proctor compaction tests and modified AASHTO (now modified AASHTO) compaction tests were carried out on 23 soils sampled from the area. It should be noted that the procedures followed in the execution of the modified compaction tests were not specified. The Proctor tests revealed MDD values between approximately 1620 kg/m<sup>3</sup> and 1880 kg/m<sup>3</sup>, with the associated OMC's ranging from 7% to 11.4%. The modified AASHTO tests produced MDD values between approximately 1630 kg/m<sup>3</sup> and 1890 kg/m<sup>3</sup>, with the OMC varying between 7% and 11.5%. The range of values obtained for each test method can be ascribed to variabilities in the soil texture (in particular, the fines content) and the distribution of grain sizes. The higher compaction energy associated with the modified AASHTO test did not significantly affect the obtained MDDs and OMCs. This suggests that grading, rather than compactive effort, dictates the density that can be achieved by compaction. The soil type or gradation associated with each test was not specified by Amdurer, nor the soil sampling locations and, as such, limited interpretation of the findings is possible.

Numerous authors have produced transformation models to estimate MDD and OMC based on soil classification properties (Korfiatis and Manikopoulos, 1982; Gomaa and Abdel-rahman, 2007 and Metcalf and Romanoschi, 2009). The compaction characteristics are often presented as a function of one or more of the following independent variables: plastic limit, plasticity index (PI), linear shrinkage, percentage passing particular sieve sizes (e.g. P<sub>0.075</sub> and P<sub>0.425</sub>), plasticity modulus (PI x P<sub>0.425</sub>), grading coefficient [ $P_{4.75} \times (P_{26} - P_2) / 100$ ] and grading ratio (P<sub>0.075</sub>/P<sub>0.425</sub>). Moderate to strong correlations are typically attained in the prediction of MDD and OMC from these basic soil properties. Interested readers can refer to the abovementioned published works for the respective predictive equations.

Where the windblown sandy soils of the Cape Flats are used as engineered fill, or where the upper unconsolidated and potentially highly compressible in-situ soils are used as a founding stratum, compaction of the sands to an appropriate specification is required. From the above it is clear that the distribution of grain sizes in the Cape Flats sands will have a significant influence on the attainable degree of compaction. The compaction characteristics of the soils from the study area will therefore be explored in relation to the particle characteristics.

### **2.5.5 California Bearing Ratio**

The California Bearing Ratio (CBR), which is an index that compares the resistance to penetration provided by a compacted soil mass to that of a standard reference material (high quality California gravel), is an indirect measure of soil strength under a single load (SAPEM, 2014). The test involves measuring the load required to penetrate a soil at a rate of 1.25mm per minute with a standard circular plunger. The CBR of a material is often determined at modified AASHTO maximum dry density, and at 98%, 97%, 95%, 93% and 90% of maximum dry density. The procedure for calculating the CBR is shown in Figure 2-9. The equipment and procedure details for this standard test method are stipulated in ASTM D1883 (2016). Note that this test is carried out on samples that have been soaked for four days prior to testing.

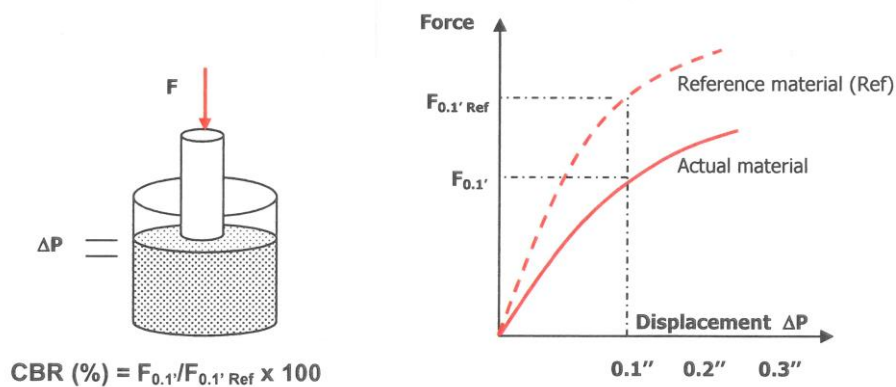


**Figure 2-9: CBR test procedure (Jenkins and Rudman, 2016)**

According to Breytenbach (2009), the strength of a soil (reflected by its CBR value), is owed to particle friction and interlocking – a function of grading, particle shape and compaction (density) - and soil cohesion – a function of moisture content, plasticity (in cohesive soils), and grading. The process of determining CBR has been described as time consuming and requiring large quantities of material. For this reason, numerous researchers have attempted to produce transformation models incorporating CBR and soil parameters based on the abovementioned strength components. Such parameters include the grading modulus (the sum of the total percentage of the sample retained on the 2mm, 0.425mm and 0.075mm sieves, divided by 100), maximum dry density, bearing capacity, optimum moisture content, plastic limit, liquid limit and plasticity index. In this regard, attempts to correlate CBR and index test parameters have been made, amongst others, by Kley (1955), Wermers (1963), Lawrance and Toole (1984), Netterberg and Paige-Green (1988), Stephens (1988), Gawith and Perrin (1988) and, more recently by Breytenbach (2009) for natural road construction materials in South Africa. The early work up to 1988, could not be obtained, and are cited from Breytenbach (2009). According to Breytenbach, many of these relationships were derived in countries other than South Africa with different material and climatic conditions. Breytenbach highlights the inaccuracy of some of these predictive models, including his own, probably due to the number of factors influencing the CBR and data variability ascribed to poor test repeatability. Nonetheless, his study revealed plasticity index, linear shrinkage and grading modulus to be the best predictors of CBR.

Various models have also been developed to estimate CBR from DCP penetration rate (mm/blow) for different material types. It is the power model (or log-log equation) that most often provides the best fit to data. CBR-DCP predictive models have been produced, for example, by Sampson (1984), Harison (1986), TRL (1993), Paige-Green and Du Plessis (2009) and Gill, Jha and Choudhary (2010). When applying these predictive methods, the in-situ moisture content and density at which the DCP test was conducted - which will influence the DCP CBR value - should be noted. Furthermore, the importance of assessing the results together with the material properties, such as the maximum particle size, grading and plasticity should not be overlooked (Paige-Green and Du Plessis, 2009). The possible influence of skin friction on DCP penetration resistance should also be considered.

The soaked CBR of the Cape Flats sand will be a function of density (compaction). Notwithstanding this, the grading properties of the sands will have a significant effect on the interlocking of the particles. In this regard, the combined effects of particle size and distribution, fines content and particle shape will account for differing CBR values at a given compaction level. Rarely, the component of cohesion will influence CBR of the Cape Flats sands, likely only in cohesive soils from the Springfontyn Formation. In-situ CBR (DCP CBR values), will be influenced by calcretisation in the Langebaan and Witzand Formation, with slow penetration or refusal of the DCP probe. Refusal on nodular calcrete gravel or other large diameter particles can result in overestimation of soil strength. Penetration resistance and DCP CBR will vary with the natural moisture content, with apparent strength reduction below the often-shallow water table.

As part of the research conducted by Amdurer (1956) in the Cape Flats, two CBR tests were performed on slightly silty sands from the area. Grading analyses were also performed on the two soils, which showed identical upper and lower particle size percentages, with a difference only in the intermediate sizes: fine sand (taken as 0.105 to 0.25 mm) and very fine sand (taken as 0.056 to 0.105 mm). The finer of the two soils (very fine sand > fine sand) had an MDD of 1720 kg/m<sup>3</sup> at an OMC of 9.7% and a CBR of 61%, whereas the coarser sample had an MDD of 1897 kg/m<sup>3</sup> at an OMC of 8.6% and a CBR of 94%. The difference in the density values (influencing the CBR) was ascribed to the disparity in the average particle size. Amdurer argued that the smaller the particle size, the greater the area of particle surfaces; and, because the particle surface area directly determines the amount of water that can be absorbed, its presence in the finer grained soil would lead to more voids being filled with water as opposed to mineral particles. The significantly higher CBR value obtained for the coarser soil can partly be ascribed to its density and moisture content. However, other factors such as inter-particle friction, particle shape, maximum particle size and the packing arrangement of the soil grains will additionally influence the strength of the material, which is reflected in the CBR.

TRH 14 (1985) "Guidelines for Road Construction Material" and COLTO's Standard Specifications for Road and Bridge Works for State Road Authorities (COLTO, 1998) define a series of material classes for untreated road pavement layers ranging from graded crushed stone to gravel-soil mixtures (categorised as G1 to G10 materials). These specifications stipulate minimum CBR values at prescribed compacted densities for the various material classes, emphasising the importance of CBR in the categorisation of pavement layer materials. Many of the methods used to design flexible pavements make use of the California Bearing Ratio of the various pavement layers. To evaluate the strength of the Cape Flats sands, providing an input parameter for material classification and design methods, both the laboratory-derived soaked CBR and in-situ CBR of the sands will be investigated.

### **2.5.6 Minimum and maximum index densities and relative density**

The minimum index density is defined as the density achieved when dry soil particles are packed at the loosest state that can be sustained (Head, 1992). This minimum dry density ( $\rho_{dmin}$ ) corresponds to the maximum void ratio ( $e_{max}$ ). The minimum density of cohesionless, free draining soils can be determined by means of the funnel method or the double tube method, using the procedures described in ASTM Designation D4254 (2016) Methods A and B respectively. Other methods include the inverted container method, the shaken container method and the trapdoor method. According to Germaine and Germaine (2009), caution should be exercised when the minimum density of fine sands (such as the Cape Flats sands) is determined, as the repulsive

forces acting between the grains of fine-grained sands, can result in an over-estimation of the maximum void ratio. The maximum index density ( $\rho_{dmax}$ ), which corresponds to the minimum void ratio ( $e_{min}$ ) can be determined using a vibratory table as stipulated in ASTM D4253 (2016). This standard method allows the densest state of compactness to be achieved, minimising particle segregation and breakdown.

Relative density ( $D_r$ ) is generally used to describe the in-situ denseness or looseness of cohesionless soils, and it can be defined in terms of the minimum and maximum void ratios, and the in-situ void ratio ( $e$ ), as shown in Equation 2-6 (Bowles, 1997). Where the minimum loose density is achieved, the relative density of the soil is equal to zero and the soil is described as very loose.

$$D_r (\%) = \frac{e_{max} - e}{e_{max} - e_{min}} \cdot 100 \quad \text{Equation 2-6}$$

The minimum and maximum index densities (or maximum and minimum void ratios) of coarse grained soils are influenced by several factors, including particle size and shape, the nature of the particle size distribution curve (gradation) and the amount of fines (Das and Sobhan, 2018). Youd (1973) (refer to Das and Sobhan, 2018), studied the variation of  $e_{max}$  and  $e_{min}$  with particle shape or angularity and the coefficient of uniformity ( $C_u$ ). His findings showed that, for a given angularity value, the minimum and maximum void ratios decrease with an increase in  $C_u$ . Therefore, as the range of particle sizes in the soil increases, representing a well graded soil, the particles arrange in a denser state of packing and the void ratio decreases. Furthermore, for a particular value of  $C_u$ , the void ratios decrease, and the density increase as the particles become increasingly more rounded. This can be ascribed to sharp and irregular particle edges preventing proper densification in the case of angular grains. Research by Lade, Liggio and Yamamuro (1998) has shown that, for sands mixed with various proportions of soil fines (by volume), an increase in the volume of fines from zero to approximately 30%, is accompanied by a decrease in the maximum and minimum void ratios.  $e_{max}$  and  $e_{min}$  values typically associated with different soil types are given in Table 2-8. From the above, it is evident that the minimum loose density of the Cape Flats sands will be influenced by the uniform particle size, presumed rounded and sub-rounded shape, and the typical lack in soil fines. The combined influence of these particle features will determine the  $e_{max}$  values associated with the sands from the Witzand, Springfontyn and Langebaan Formations. The minimum density results obtained for the Cape Flats sand will be interpreted in relation to the particle characteristics.

**Table 2-8: Void ratios of different soil types (after Knappett and Craig, 2012)**

Soil type	Unit weight $\gamma_{sat}$ (kN/m <sup>3</sup> )	Minimum void ratio ( $e_{min}$ )	Maximum void ratio ( $e_{max}$ )	Water content %
Sand and gravel	16-22	0.44-0.8	0.2-0.5	0-25
Silt	16-20	0.68-0.86	0.49-0.68	10-30
Stiff clay	19-23	N/A	N/A	10-20/20-40
Soft clay	17-20	N/A	N/A	20-40/50-90
Peat	10-14	N/A	N/A	>100

Neal (2011) investigated the dry density, void ratio and relative density of the windblown dune sands of Big Bay along the Cape West Coast. These unconsolidated dune sands belong to the Witzand Formation and extends northwards to Atlantis. The void ratios and relative densities of the sands, although not located within the geographical boundary of the Cape Flats, provide an indication of the values of these parameters in similar dune sands of the study area. Neal determined the minimum density of the Big Bay sands in accordance with ASTM method D4253 and the maximum dry density using a Marshall Hammer and vibratory table. The maximum void ratio of the Big Bay dune sands was found to vary between 0.798 and 0.808 (mean value of 0.804), the minimum void ratio between 0.538 and 0.564 (mean value of 0.549), and the in-situ void ratio varied from 0.576 to 0.595 (mean value of 0.589). The relative density of the same sands ranged from 78.8% to 93.2% which relates to dense and very dense sand. Sampling and testing depths were not specified by Neal.

### **2.5.7 Corrosivity**

During its service life, reinforced concrete foundations can be exposed to aggressive ground and groundwater. In addition, buried metal work, such as steel and cast-iron pipes and steel sheet piling and steel piles, are also affected by the aggressive chemical environment. Basson (1989) describes the more susceptible components of concrete as the cementitious binder - due to its greater chemical reactivity - as well as the steel reinforcement when exposed by deterioration of the surrounding concrete. According to Basson (1989), it is the ability of water to dissolve salts and then dissociate solution products – which subsequently contributes to ion-exchange and ion-addition reactions - that contributes most to high corrosivity. The materials present in cement are all soluble in water (although not to the same extent) and it is the rate of dissolution of these materials, which is influenced by the concentration gradient between solid and liquid phases and the acidity of the water, that determines the corrosivity (Basson, 1989). The corrosion rate is also influenced by factors such as the water temperature, the movement of water in relation to the concrete, the volatility of the reaction products, the potential for ion penetration into the concrete, and the occurrence of dissolved gases such as oxygen and carbon dioxide (Basson, 1989). The aggressive chemical agents generally present in natural ground and groundwater include sulfides and sulfates, magnesium, calcium, sodium, potassium, ammonium and chloride ions, and acids such as sulfuric acid, humic acid and carbonic acid (BRE, 2005a).

Basson (1989) developed the concept of an aggressiveness index to quantify the extent to which concrete is likely to be corroded by water. The water properties required to determine the aggressiveness index include pH, calcium carbonate saturated pH, calcium hardness, total ammonium-ion content, magnesium-ion content, total sulphate-ion content, chloride-ion content and total dissolved solids. The standard methods of analysis are given in Basson (1989). In the case of special conditions such as waters from hot springs, Basson makes provision for additional tests.

An alternative procedure for classifying aggressive ground conditions has also been published by the Building Research Establishment (BRE) in the United Kingdom in Special Digest 1: 2005 Part C (BRE, 2005a). The procedure is based on the aggressive chemical environment for concrete (ACEC) Class, which is assigned to the ground. The ACEC class considers the type of site (natural ground condition or brownfield locations), the sulfate concentration (an aggressive chemical agent), and the acidity and mobility of the groundwater. In addition to sulfates present in soil and/or groundwater, oxidation of sulfides can also form sulfate in the presence of mobile waters.

The ACEC class is used to prescribe concrete quality in terms of a design chemical class (BRE, 2005b).

To determine the corrosion impact of water on metal components, the Langelier Saturation Index is seen as a valuable indicator. It provides a measure of the ability of a solution to dissolve or deposit calcium carbonate (Roberge, 2007). When deposited, the calcium carbonate forms a covering which protects metallic surfaces from contact with water. When in excess, however, the protective film can damage systems. The index is calculated using the measured pH of the water, and from calcium carbonate-saturated pH, which in turn is calculated from the alkalinity, calcium hardness, total dissolved solids and water temperature. A value close to zero indicates a non-scaling and non-etching fluid, it thus being non-corrosive. If the water is under-saturated with calcium carbonate – producing a negative Langelier Index - the water will be corrosive, whereas a positive Index value – indicating over-saturation - would result in the formation of scales.

The aggressiveness of the soils and groundwater of the Cape Flats is influenced by a complex set of variables. Electrochemical corrosion reactions are supported by water and, as such, buried concrete and metals will be prone to corrosion below the groundwater table, which can be intersected at shallow depths in the Cape Flats, especially during winter months. The presumed permeable nature of the sands from the Cape Flats will provide minimal resistance to the movement of water and thus any corrosion products would be removed, and dissolved chemicals present in the groundwater would be replenished at the reaction surfaces, leading to increased rates of chemical attack on concrete. Where the sands below the water table are alkaline or neutral in nature, the combination of anaerobic conditions and the lack of acidity will require the presence of certain microbes to support corrosion (Roberge, 2008). Rapid oxygen transport in the moist sands above the water table will result in an increased rate of corrosion. Varying quantities of crushed shell matter are present in the Cape Flats sands. The shell matter increases the calcium carbonate content which, in turn, raises the soil pH. Soils and groundwater that are highly alkaline ( $\text{pH} > 8$ ) present an increased risk to corrode buried metals (Clayton, 2013). The presence of high acidity in soil and groundwater ( $\text{pH} < 4$ ) is also considered a corrosive condition for steel, cast iron and zinc coatings (Clayton, 2013). According to Basson (1989), materials typically found in concrete are more soluble in acidic waters with pH values below seven, than in alkaline waters with pH values above seven. According to Roberge (2008), acidic soils are typically produced by processes such as mineral leaching, decomposition of acidic plants (e.g., coniferous tree needles), acid rain, and certain forms of microbiological activity. In the Springfontyn Formation, the water from peat deposits may be highly acidic and aggressive to concrete (Brink, 1985). The major components of salts in seawater are chloride ions, and it is the presence of these ions in the aeolian and marine sands and groundwater of the Cape Flats that promote corrosion of reinforcing steel in concrete. Chloride ions can also be introduced by contaminants in the concrete mixture (Alao, 2015). In marine environments, air-borne chlorides are also responsible for corrosion of reinforcement in reinforced concrete structures. The permeability of the concrete determines the entry of chloride ions into the concrete, disintegrating the protecting film on the steel, thus leading to corrosion of the inner support (Alao, 2015). In the case of plain concrete, chloride ions present no risk.

The rate of corrosion of buried concrete and metals has been found to be influenced by the electrical conductivity of the soil. If the ionic current flow is strongly resisted (i.e. high electrical resistivity), the corrosion reactions will be slowed down (Roberge, 2008). An increase in soil moisture or soluble salts content is typically accompanied by an increase in the electrical conductivity. The pH and electrical conductivity of a soil is often determined to provide an initial indication of corrosion potential. The amount of acidity (pH <7) and alkalinity (pH >7) influences corrosion susceptibility and rates. According to Clayton (2013), highly acidic (pH <4.5) and highly alkaline (8 < pH < 10.5) solutions and soils have increased metal corrosion rates, whereas cementitious binders in concrete are more soluble in acidic environments (pH <5).

Stapelberg (2009), determined the pH and electrical conductivity of the Springfontyn Formation sands and, based on the property value classes given by MacVicar (1991) (as cited in Stapelberg, 2009) and Roberge (2008) for pH and resistivity respectively, the sands can be described as moderately acidic and moderately corrosive. The corrosion ratings for different resistivity ranges are given in Table 2-9.

**Table 2-9: Corrosivity rating based on soil resistivity (Roberge, 2008)**

Soil resistivity (ohm-cm)	Corrosivity
>20,000	Basically, non-corrosive
10,000 – 20,000	Mildly corrosive
5,000 – 10,000	Moderately corrosive
3,000 – 5,000	Corrosive
1,000 – 3,000	Highly corrosive
<1,000	Extremely corrosive

Geohydrological and Spatial Solutions International (Pty) Ltd (GEOSS) carried out a groundwater specialist study at the Cape Town International Airport in 2014, which has been made available to the public (GEOSS, 2014). The study aimed to describe and map the existing ground water resources in the study area, and to identify and assess the potential impact of the runway re-alignment project on the groundwater resources. The influence of groundwater on the proposed project was also assessed. GEOSS made use of existing groundwater data as well as data from their own investigative work. Existing ground water quality data obtained by GEOSS from the National Groundwater Archive revealed soil pH values between 7.2 and 7.7 (average pH of 7.43) for the shallow groundwater at the airport site. The soil pH and electrical conductivity was also measured at 32 groundwater monitoring localities, installed by the Airports Company of South Africa for on-going water monitoring. The results revealed pH values ranging from 5.1 to 8.02 and electrical conductivities ranging from 54.5 mS/m to 126.6 mS/m. In addition, GEOSS conducted their own investigation comprising ground water sampling from two sites in the study area. The ground water chemistry results are presented in Table 2-10. From the results, the ACEC class (BRE, 2005a) could be determined by the candidate, revealing classes AC-1 and AC-2 for BH 1 and 2 respectively. These classes represent non-aggressive and slightly aggressive waters.

**Table 2-10: Groundwater chemistry results from the Cape Town International Airport (GEOSS, 2014)**

BH	pH	EC mS/m	TDS mg/l	Sodium as Na mg/l	Magnesium as Mg mg/l	Calcium as Ca mg/l	Potassium as K mg/l	Chloride mg/l	Nitrate mg/l	Sulphate as SO <sub>4</sub> mg/l	Alkalinity as CaCO <sub>3</sub> mg/l	Iron as Fe mg/l	Manganese as Mn mg/l
1	7.2	464	2746	747	72	210	25	1220	17	147	452	0.01	<0.01
2	7.7	518	4416	1290	229	254	37	2200	2.8	671	505	0.05	0.01

The GEOSS groundwater specialist study report indicates the presence of zones of saline water in the study area, which occur at varying depths in the Cape Flats due to the varied depositional history of the geological formations. Other high salinity areas also arise during summer when evaporation rates increase. According to Rhoades, Chanduvi and Lesch (1999), soil salinity refers to the presence of soluble and readily dissolvable salts in the soil. Aside from measuring soil salinity in terms of the total concentration of these soluble salts, it can also be quantified in terms of electrical conductivity. In this regard, the local groundwater quality at the airport study site, as showed by the total dissolved solids, are specified by The Department of Water Affairs and Forestry, and ranges from 500 mg/l to 2 000 mg/l, which corresponds to an electrical conductivity of 70 mS/m to 300 mS/m (DWAf, 2000 as cited in GEOSS, 2014). Notwithstanding this, the analytical test results obtained for the two groundwater samples from the airport study area presented in Table 2-10, reveals higher total dissolved solid concentrations of 2746 mg/l and 4416 mg/l. The salinity of these groundwater samples was determined to be 2400 mg/l and 3510 mg/l, and the corresponding electrical conductivities are 464 mS/m and 518 mS/m.

To ensure durable reinforced concrete structures, South African National Standard (SANS) 10100-2 (Draft 2013) defines corrosion exposure conditions in a quantitative manner, using the expressions mild, moderate, severe, very severe and extreme to propose the minimum cover to reinforcing steel. A study of the aggressiveness of the soil and groundwater from the Cape Flats will aid this design consideration.

### 2.5.8 Erodibility

The soil erosion hazard depends on several factors including soil erodibility, rainfall erosivity, topography, and vegetation cover (Wischmeier and Smith, 1978). Soil erodibility, which describes the susceptibility of a soil to be eroded, depends on a few soil properties, such as texture, soil accumulation, shearing resistance (incorporating particle shape), infiltration capacity, permeability and organic and chemical content (Ezeabasili, Okoro and Emengini, 2014). Soil erodibility accounts for the influence or response of soil properties on soil loss during periods of rainfall and it is represented by the soil erodibility factor – known as the K-factor - which provides a measurable description of the exposure of a soil to erosion (WRC, 2010). The K-factor can be estimated using the soil erodibility nomograph, which is based on soil texture and structure, organic material content and permeability (Wischmeier and Smith, 1978). To assist with the determination of the soil erodibility factor, Wischmeier and Smith (1978) developed the classical K-factor equation. According to Auerswald et al. (2014) the nomograph does not completely correspond with the K-factor equation. Consequently, Auerswald et al. (2014) developed a series of equations that fully agrees with the nomograph.

The Institute for Soil, Climate and Water (ISCW) at the Agricultural Research Council (ARC) has developed a spatial modelling framework to predict water erosion on a national scale for South Africa (Le Roux et al., 2006). The method is based on the Revised Universal Soil Loss Equation (RUSLE) which separates the erosion influences into five groupings or erosion factors, namely climate (rainfall erosivity, R), soil profile (soil erodibility, K), relief (slope length, L, and slope gradient, S), vegetation and land use (vegetation cover factor, C), and land management practices (supporting practice, P). To estimate soil erodibility using the abovementioned nomograph method, data on the soil profile, organic matter content, soil structure and permeability is needed. The unavailability of this soil data, lead to an alternative approach, using soil attribute polygon data, to estimate K-values at a national scale. Soil maps were utilised to acquire soil erodibility ratings for the individual soil series of the Binomial Soil Classification System of South Africa. The erodibility values were then related to corresponding soil series to be shown spatially on 1:50 000 scale maps. The product of the factors (i.e. R, K, LS, C and P values) gives the expected soil loss (A) in t/ha/yr (Renard et al., 1994 as cited in WRC, 2010). By combining the rainfall erosivity (R), soil erodibility (K), and slope length and gradient, LS, Le Roux et al. (2006) produced a potential soil erosion risk map of South Africa and Le Roux et al. (2008) produced an actual water erosion prediction map of South Africa indicating soil loss in t/ha/yr. The water erosion map of Le Roux et al. (2008) was subsequently modified and improved by replacing the topography factor (LS) map and the vegetation cover factor (C) map. The improved map identifies ten erosion hazard classes, ranging from 1 (very low erosion hazard) to 10 (very high erosion hazard).

The Water Research Commission (WRC) carried out the revision of the sediment yield map of Southern Africa in 2010 (WRC, 2010). As stated in WRC (2010) sediment transport is influenced by sediment availability and, in turn, sediment availability is influenced by the soil erosion hazard. As such, the importance of establishing the relationship between soil erosion and observed sediment yield is evident. Firstly, the WRC delineated ten homogeneous sediment yield regions within South Africa, using GIS. Using improved input data, the WRC calculated the four main factors of rainfall erosivity, soil erodibility, topography and land cover from new maps created in a GIS framework. Using statistical procedures in ARC/INFO (i.e. focal statistics set as the sum of a circle with a radius of forty cells), erosion hazard classes were obtained. These classes were grouped in terms of an index scale, ranging from one (very low erosion hazard) to ten (extremely high erosion hazard) for the entire country. Electronic copies of erosion hazard potential maps were ultimately produced for each of the sediment yield regions, also delineating catchment boundaries. From these maps, the proportion of the area covered by specific hazard classes per catchment were estimated, and a weighted average determined to give a dominant erosion index value for each catchment. The assigned erosion index ultimately identifies the soil erosion risk in the area.

The suitability of wearing course gravels for the construction of unpaved roads, including their potential for erosion, can be evaluated using the classification system in the Technical Recommendation for Highways (TRH) 20 (1990). The system is based on the relationship between the shrinkage product,  $S_p$  (linear shrinkage x percent passing 0.425mm sieve), the grading coefficient,  $G_c$  [(percent passing 26.5mm sieve - percent passing 2mm sieve) x percent passing 4.75mm sieve/100], and the performance of unpaved wearing course gravels. Materials are classed into one of five groups, namely (TRH 20, 1990): “erodible”, “slippery”, “good” (or ideal), “ravels”, and “ravels and corrugates”. “Erodible” materials are typically fine grained with  $G_c < 16$ . Although susceptible to water erosion, the erodible surfacing is typically considered acceptable

based on its performance but requiring recurrent maintenance. When the shrinkage product of a material exceeds 365, it will become “slippery” when moisture is introduced. Poorly graded materials lacking intermediate grain sizes and cohesion are typically categorised into the “ravels” category and will generate loose gravel under road traffic. Materials placed in the “ravels and corrugates” group have shrinkage product values of less than 100. These materials are prone to form undulations and loose material, increasing the roughness of road surfaces. “Good” or ideal materials will perform well on condition that the maximum particle size recommendations are followed.

As stated before, typical Cape Flats soils can be described as fine and medium sand with minor fines (silt and/or clay). Layers of clay and peat in the Springfontyn Formation, and calcretisation in the Langebaan and Witzand Formations, are characteristic of many profile descriptions. Murray (1976) investigated the erodibility of uniform coarse sand mixed with varying proportions of clayey silt (sampled from Colombia, South America) which is comparable to the typical Cape Flats profile. To investigate the influence of the fines content on the erodibility of the sands, an artificial channel conveying water, termed a flume, was constructed and the various mixtures exposed to the erosive action of water. The depth and flow rates of the water, and time rate of erosion, were recorded. Murray (1976) found the existence of a power law relationship between the sediment transport rate and the bed shear stress, and concluded that the bed shear stress needed to transport a particular rate of sediment increased as the amount of clay and silt in the soil bed increased. Better particle packing associated with increased fine contents, and cohesion provided by clay minerals, can possibly explain the findings.

Various researchers have determined the erodibility factor for soils with textures like those found in the Cape Flats study area, using the nomograph method or K-factor equation put forth by Wischmeier and Smith (1978). In this regard, Kusumandari (2013) determined the soil texture, structure, permeability and organic matter content of sands with varying silt and clay contents from 11 sites in Yogyakarta City in Indonesia, from which the soil erodibility was calculated. The K-factors varied from 0.16 to 0.29, indicating low to moderate soil erodibility. The result was attributed to the predominance of larger sand size particles requiring more energy to transport, the relatively high permeability promoting infiltration and organic matter cementing soil particles.

Based on research undertaken on sandy soils like the Cape Flats sands by authors such as Murray (1976) and Kusumandari (2013), the erodibility of the Cape Flats sands is anticipated to be low. An additional influencing factor on erodibility, is particle shape, which is excluded from the above-given soil erosion prediction methods and often ignored in the evaluation of soil erodibility (Guo, Yang, and Yu, 2017). The erodibility results obtained for the Cape Flats sands will be interpreted alongside all influencing particle characteristics.

### **2.5.9 Specific gravity**

Specific gravity ( $G_s$ ) is defined as the ratio of the mass of solid soil particles to the mass of water displaced by the dry soil (Head, 1992). The specific gravity of soils is required for several calculations in soil mechanics and particularly the phase relationships of soils, including void ratio, porosity, degree of saturation, density and unit weight. It can be determined in the laboratory by means of a water pycnometer, as stipulated in ASTM D854 (2002). The specific gravity of most soils varies within narrow limits, and for sands (constituting mainly quartz grains), it typically ranges between 2.65 and 2.68. According to Bowles (1997), the determination of the specific

gravity is moderately difficult, and the results can potentially be compromised by the presence of entrapped air in the specimen. When the specific gravity of a soil is unknown or is not accurately determined in the laboratory, a value of  $G_s = 2.67$  is often assumed for cohesionless soils.

Prasad and Pandey (2013) investigated the effect of fines content on specific gravity by creating sand-fines mixtures at different percentages of fines. The specific gravity of these mixtures was determined by the pycnometer method. The results show an initial decrease in  $G_s$  with increasing fines content to a maximum fines content of 30%, where after the  $G_s$  increases. The initial decrease in specific gravity is uncharacteristic as most clay minerals are typically denser than minerals making up the coarser size fractions of a soil (e.g. quartz and feldspar). An overall higher specific gravity of the mixture is expected as the fines content increases (particularly clay fines). Possible explanations for the atypical result are not provided by the authors, but likely explained by the mineralogy of the soil framework (possibly slight differences between samples) or methodological issues.

The specific gravity of the Cape Flats sands is anticipated to generally vary between 2.65 and 2.67 – ascribed to the predominance of quartz sand. The presence of denser clay minerals such as illite and montmorillonite, or iron-rich laterite (scarce, but observed in some profiles), will increase the average  $G_s$  for the combined soil particles. The clay mineral kaolinite has a specific gravity of 2.6 (Das and Sobhan, 2018), and will lower the overall  $G_s$  of the soil when present in appreciable amounts. Lower values of  $G_s$  will also be associated with sands containing organic matter, lowering the value of  $G_s$  through the presence of cellulose and lignin. According to Mitchell (1993), a significant reduction in specific gravity occurs with an increase in organic matter.

#### **2.5.10 In-situ moisture content**

The moisture in pore spaces between solid soil particles at the time of sampling is a key index property providing valuable material property information. Determination of moisture content is undertaken in the laboratory by following the oven-drying method presented in ASTM D2216 (2019), or it can be assessed qualitatively during in-situ soil profiling.

The moisture held within a soil depends on the particle sizes. Sands typically compact to higher in-situ densities than silts and clays, and if the  $G_s$  is the same, the void ratio will be lower for the sand (compared to silt and clay), resulting in reduced water holding capacity. In addition, sand particles do not retain or bind water (due to their smaller surface area) and drainage from the soil will be rapid, thus resulting in a lower water content. The maximum and minimum water contents of sandy soils (such as the Cape Flats sands), are therefore typically lower than for clay soil. The in-situ moisture content of the Cape Flats sands will additionally be influenced by the soil structure (often structureless), density, temperature, presence of organic matter, and the position of the water table which is influenced by the topography and the season of sampling. The in-situ moisture content and seasonal fluctuations in groundwater levels in the Cape Flats, and its effect on the soil parameters and engineering behaviour is of importance. Changes in the soil moisture will influence the consistency, compressibility and shear strength as well as the bulk density and corrosivity of the soil. In addition, the natural moisture content of the soil will provide an indication of the water requirements for compaction.

The influence of soil moisture on the compressibility of granular soils has been investigated by various researchers. In this regard, Wils, Van Impe and Haegeman (2015) investigated the effect of water on the compression behaviour of calcareous sand (crushable) and silica sand (non-crushable). The study involved the execution of one-dimensional consolidometer tests on dry and wet specimens where pressures were increased to 8.6 MPa. It was found that the crushability of the soil grains and the one-dimensional volume reduction are higher for the wet calcareous sand. The crushability of the sand was determined by means of sieve analysis before and after the oedometer testing and Hardin's relative breakage factor. According to Wils, Van Impe and Haegeman (2015), water accelerates the crushing of soil grains due to its high polarity, low viscosity and small molar volume, which results in surface energy reduction inside particle cracks which are formed under high stresses. The influence of negative pore water pressure on the compression behaviour of sands was also highlighted by Wils, Van Impe and Haegeman (2015), stating that the presence of suction in a partially saturated soil will reduce its compressibility, with its effects decreasing as the water content increases. For the non-crushable silica sand, tested in the same manner with the same stress range, it was found that the one-dimensional compression is equal for the wet and dry specimens. This is attributed to the absence of accelerated crushing of wet particles in these sands, which come into play after a certain threshold stress has been reached. Similar findings were obtained by Ham et al. (2010) based on the outcomes of dry and wet oedometer tests on residual granite and quartz rich silica sand.

The shear strength of sands is largely due to frictional resistance between touching sand grains. With increasing moisture content, the sliding friction (which contributes to the frictional resistance) is significantly reduced, due to the lubricating effect of the water. In addition, apparent cohesion between soil particles in a partially saturated soil also influences the shear strength. According to Mitchell (1993) it is the combination of water attraction to the surfaces of soil grains and surface tension that lead to the frictional strength generated by negative pore water pressure. As the soil moisture content increases, the soil suction decreases, the effective stress decreases thereby reducing the soil shear strength. A study by Farouk, Lamboj and Kos (2004) investigated the influence of matric suction on the shear strength characteristics of unsaturated siliceous sands, confirming the effect of negative pore water pressure on shear strength, achieving maximum effect at a specific value of matric suction, beyond which the increase in strength declines.

One of the main factors influencing the resistance to penetration during penetration testing in granular soils (causing dynamic failure), is the effective angle of friction (Clayton, 1993). The relationship between drained friction angle and SPT blow count given by Peck, Hanson and Thorburn (1974) indicates an approximately linear relationship between the two parameters. A more complex influence of friction angle on penetration resistance was however highlighted by Clayton (1993). Notwithstanding this, the influence of soil water content on the shear strength of granular soils and, in turn, its influence on soil penetration resistance is apparent and should be considered in the interpretation of penetration test results.

Additional influences on soil strength and stiffness such as grading, particle shape, and compaction will be considered in subsequent sections of the chapter.

### 2.5.11 In-situ density

In-situ density is expressed in terms of the dry density or bulk density of the soil. Dry density is the mass of the dry soil per unit volume. Bulk density is total mass of soil, including soil and water, per unit volume. The saturated density is a special case of bulk density where the voids in the soil are completely filled with water.

The in-situ density can be determined in the field by means of the sand cone method (ASTM D1556:2015), the rubber balloon method (ASTM D2167:2015), and the core cutter method (IS 27270-Part-29:2007). Nuclear density meters, such as the Troxler density gauge, provide immediate measures of bulk density and moisture content from which the dry density can be obtained. The accuracy of measurements, particularly the moisture content, has been questioned and often calibration with other methods is deemed necessary before the results of nuclear density gauges are accepted as a control procedure (Byrne and Berry, 2008). The bulk density of soils can also be determined from laboratory tests carried out on undisturbed soil samples. Moisture content can be determined from either undisturbed or disturbed samples by oven drying the soil in the laboratory.

The in-situ bulk density is used in the calculation of vertical loads on buried structures, bearing capacity, slope stability and earth pressure. The in-situ dry density is used to determine the void ratio and porosity of the soil, its relative density and degree of compaction. The shear strength of a soil, and whether it will dilate or contract during shear, is related to dry density of the soil via the void ratio. Some existing empirical methods rely on in-situ density or in-situ void ratio to estimate soil permeability and collapse potential.

From the above it is evident that any factor that influences void space will affect the in-situ density, which includes soil texture, gradation, particle shape, structure and organic content. Sandy soils (such as the Cape Flats sands) typically have higher densities than fine textured soils such as silts and clays due to the total pore space being less in sands. An increase in aggregation and soil fines, leading to the formation of micropores, lowers bulk density. The uniform gradation of the Cape Flats sands, and the presence of organic matter - in surficial soils and occurring intermittently within the Springfontyn Formation - will lower soil density. Peaty layers of low density will be associated with lower strength and increased compressibility. The calcretised (cemented) nature of the deposits from the Langebaan Formation, and the presence of cementation in some Witzand Formation sands (calcium carbonate bonds) will result in a higher bulk density. An increase in density with depth is expected as subsurface deposits are more consolidated, and as bulk density rises with increasing soil moisture content. Typical bulk and dry densities of soils are given in Table 2-11, reflecting the influences of grading, particle packing and organic matter.

Neal (2011) determined the in-situ density of the windblown sands of Melkbosstrand which belong to the Witzand Formation. Shelby tubes were inserted into the sidewalls and base of test pits to extract undisturbed samples. In the laboratory, the mass of each tube with the sand, and the empty tube were determined, and the difference between the obtained masses divided by the volume of the tube. The in-situ bulk density of the windblown sands was found to range from approximately 1700 kg/m<sup>3</sup> in the upper part of the soil profile, to approximately 1830 kg/m<sup>3</sup> in the lower part of the soil profile (at approximately 1.2 m depth).

**Table 2-11: Typical densities of soils (after Head, 1992)**

Soil type	Bulk density ( $\rho$ ) (kg/m <sup>3</sup> )	Dry density ( $\rho_d$ ) (kg/m <sup>3</sup> )
Dry, loose uniform sand	1360	1360
Well-graded sand	1950	1810
Soft clay	1670	1070
Firm clay	1960	1610
Peat	980	310

Measurements of field densities from current and past investigations will be considered and applied to the determination of relative density, and to existing predictive equations to estimate permeability and collapse potential in the study area.

### 2.5.12 Collapse Settlement

Collapse settlement of South African soils, i.e. sudden, large settlement of soils on wetting, was identified as early as 1948. According to Schwartz (1985), less than a decade thereafter, the settlement of portions of a building near Witbank again drew attention to this phenomenon which motivated a research project on these soils at the University of the Witwatersrand. Schwartz explains that research by Knight (1961) in this regard, led to the development of a theory explaining the mechanism of collapse, as well as an identification procedure based on a laboratory test method. In 1985, a paper by Schwartz published in the *Civil Engineer in South Africa*, provided a thorough review of the latest engineering practice with regards to collapsible soils in South Africa. The methods of identifying and quantifying collapse settlement, as well as potential engineering solutions presented in this article, have remained relevant and this paper is still regarded as the state of the art on collapse settlement.

Collapse settlement is the result of large decreases in the bulk volume of a soil when it becomes saturated when under load. Occasionally soils will also collapse under their own weight. Brink, Partridge and Williams (1982) stated that collapse settlement may occur in any open textured soil comprising predominantly silt and sand-sized particles and possessing a high void ratio. These soils have a high apparent strength at low moisture content, owing to coatings of clay minerals around larger grains, which form "bridges" at the contacts between the larger particles or the presence of cementing agents such as CaCO<sub>3</sub> and Fe<sub>2</sub>O<sub>3</sub>. When these soils become saturated, however, the bridging matter loses its strength and stiffness, leading to rearrangement of the grains, a large reduction in void ratio and surface settlement (Schwartz, 1985). Differential settlement and distortion are the result. The settlement of a collapsing soil occurs rapidly and coincides with the intake of moisture by the soil. Schwartz suggests that the rate of collapse is dependent upon the rate at which the soil mass can be saturated by water from the surrounding environment. This process can be distinguished from consolidation settlement, where the decrease in void ratio is the result of the time-dependent expulsion of pore water from a saturated soil. The basic concept of collapse settlement is illustrated in Figure 2-10.

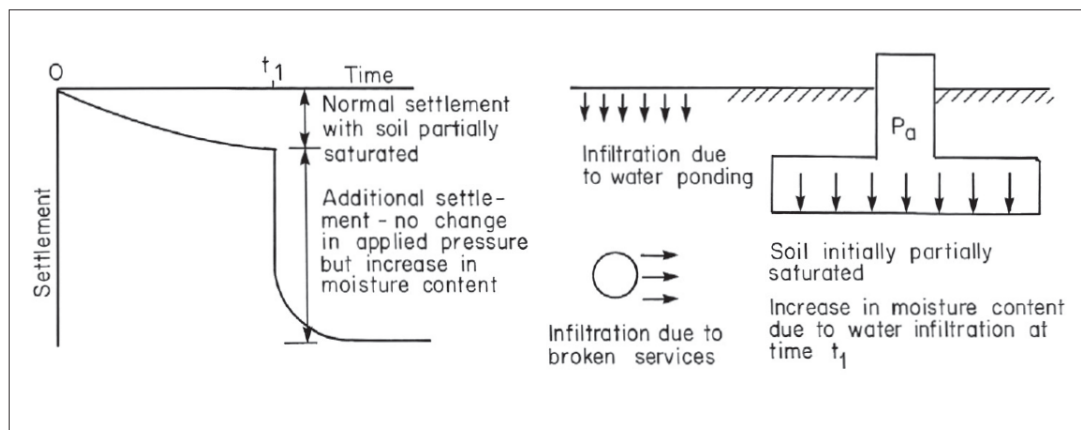


**Figure 2-10: Mechanisms of additional settlement due to soil fabric collapse (Schwartz, 1985)**

Collapse settlement is most severe in soils which have low moisture content at the time of load application. At higher initial moisture contents, the proportion of normal settlement (see Figure 2-10) increases and the collapse settlement on further wetting is reduced.

Collapse settlement can occur in a wide range of soils, including transported soils such as hillwash, gullywash, aeolian and littoral deposits, residual soils, and poorly-compacted fill material. In a South African context, the residual granite soils of the Basement Complex, and, to a lesser extent of the Cape Granite Suite, have been responsible for extensive foundation problems associated with the collapse phenomenon. In these soils, the collapsible fabric comprises a framework of sand grains (unaltered quartz) and mica, and colloidal kaolinite from feldspars, which have been largely removed in suspension by percolating ground water, leaving behind a honeycomb-like structure. Occurrences of collapse settlement have also been reported for the residual red sands from the Berea Formation on the east coast of South Africa.

Notwithstanding the above, most naturally occurring collapsible soils are wind-blown in origin and comprising largely sand and silt sized particles, with some clay (Brink and Banley, 1961, as cited in Houston, Houston and Spadola, 1988). These soils are mostly non-cohesive or possess slight cohesion and plasticity and are prone to large decreases in volume due to their ample void space (low density). In addition to clay fines (or to a lesser extent, silt), which covers particles and forms a bridging material, calcium carbonate or iron oxide may act as a cementing substance. It has been found that collapse potential [defined by Jennings (1974) as the percentage reduction in height of a sample when soaked under an applied load of 200kPa] increases as clay content decreases, nonetheless, pure sands have rarely shown to be collapsible. The wind-blown deposits covering the Cape Flats comprise mostly uniformly graded fine and medium sands with subordinate silt and/or clay sized particles. Pure sands with no fines or sands with minor fines (especially plastic fines) are characteristic of many areas, particularly in the Witzand Formation. Chemical cementing agents in the form of calcium carbonate in the Langebaan Formation or iron oxide (presenting as ferricrete) are likely to form. The deposits are geologically young, increasing the likelihood of collapse settlement. It is thus evident that the Cape Flats sands are potentially vulnerable to collapsible settlement. The near surface soils are particularly susceptible to collapse due to capillary tension causing soil moisture (from precipitation) to draw into small spaces at inter-particle contacts. This water contains soluble salts, clay colloids and silt particles, which ultimately acts as a binder at particle contacts. Upon drying, the soil possesses high strength at

the low moisture condition; however, inundation will result in collapse of the unstable framework. Notwithstanding this, the typically shallow water table in the low-lying area will reduce the potential for collapse settlement as saturated soils below the water table cannot collapse (Schwartz, 1985). Stapelberg (2009) described the Cape Flats sands as “not collapsible or possibly collapsible, except for the calcareous soil horizons from the Langebaan Formation which are prone to collapse settlement”. His findings are based on a limited number of collapse potential tests undertaken in the northern portions of the study area.

According to Byrne and Berry (2008) the identification and quantification of collapse settlement needs comprehensive field identification in addition to laboratory or in-situ testing. Firstly, the soil profile should be recorded accurately, with a focus on moisture content, consistency and soil structure, and all existing structures should be inspected for evidence of cracks and distortion. Simple in-situ tests such as the ‘sausage’ test or test pit backfilling can give an indication of a collapsible grain structure when noteworthy volume reduction occurs upon wetting.

Collapsible soils may be identified using criteria proposed in literature, based on the results of simple laboratory or field tests. These methods are empirical and mostly based on the particle size distribution, Atterberg limits, natural water content, dry density, void ratio and degree of saturation. Schwartz (1985) suggests typical dry densities of collapsible soils to be from 900 to 1600 kg/m<sup>3</sup>, although collapse cannot be excluded at dry density values exceeding this upper limit. Brink (1985) provided a relationship between the collapse potential index and dry unit weight for aeolian sands (refer to Section 3.5.7 in Chapter 3). This method relies solely on dry density, having found that windblown soils with a dry density exceeding 1672 kg/m<sup>3</sup> generally does not collapse. Based on the obtained percentage of collapse settlement, the severity of the problem can be identified. Prikloński (1952) (refer to Howayek et al., 2011) published a criterion for collapse potential based on the liquidity index [(natural moisture content,  $w_n$  - plastic limit, PL) / plasticity index, PI]. The method is based on the susceptibility of the soil to water infiltration and the plasticity. A very dry soil, with  $PL > W_n$ , is considered potentially highly collapsible. The potential of a soil to collapse (based on the criterion) will however change in relation to the in-situ moisture content. When  $W_n > PL$ , the PI (relative to the moisture condition) separates non collapsible soils from swelling soils. This criterion cannot be applied to non-plastic soils. The presence of non-colloidal bridging matter such as salts can, however, lead to the formation of a collapsible fabric in non-plastic soils. A comprehensive list of existing criteria is given in Howayek et al. (2011).

The degree of collapse can be determined in the laboratory by means of the triaxial test as well as test methods based on the consolidometer, namely the double-oedometer test, the single oedometer test and the collapse potential test. The test, and interpretation procedures associated with each of these methods, are given in Schwartz (1985). It is important to note that the accuracy of the results produced by the abovementioned laboratory methods is dependent on the tests being carried out on undisturbed and representative soil samples. According to Reznik (1993), even the most sophisticated laboratory test does not duplicate the mechanism of the base-foundation interaction. Reznik explains that the use of plate load test results allows minimisation of the effects of the ‘scale’ factor and sample disturbance. During the test, the soil below the plate is saturated at various pressures to evaluate the collapse settlement. By assuming the plate represents a circular rigid loaded area on a semi-infinite mass, it is possible to calculate the soil elastic modulus before and after saturation (Schwartz, 1985).

Rust, Heymann and Jones (2005) investigated the collapsible red sands from Mozal, Mozambique (forming part of the Berea Formation). Although residual in nature, these soils have many similarities with the sandy soils of the Cape Flats. The red sands have an average dry density of  $1650 \text{ kg/m}^3$ , the clay content varies from less than 5% to more than 40%, and the moisture content is mostly between 4% and 6%. The focus of the research was to identify appropriate testing methods to determine the probable magnitude of collapse settlement in the sands, which occur from northern Mozambique to the south coast of KwaZulu-Natal. It is the unlikely findings of an initial investigation, comprising collapse potential tests and extensive pile testing, that lead to the research focussing on unconventional testing techniques. Collapse potentials up to 12% were noted with significant scatter in the results. According to Schwartz's (1985) classification of the severity of collapse (based on the original classification by Jennings, 1974) (refer to Table 3.9 in Chapter 3), "severe trouble" is indicated based on this maximum value of collapse potential. Empirical methods, such as the Brink (1985) criterion on the other hand, indicated a low potential for collapse. The authors carried out triaxial collapse tests, one-dimensional incremental collapse tests, and pore fluid suction pressure measurements. The results from these unconventional tests did not agree well with the initial test findings, highlighting potential issues with the preparation of samples and testing procedure of the collapse potential test. The Mozal red sands were ultimately found to be moderately collapsible soils. The authors conclude that if critical foundation design decisions are to be made, based on the collapsibility of the soils, careful oedometer testing should be carried out along with triaxial tests. The research highlights the importance of careful sampling and preparation of sand specimens, and confirmative triaxial testing, particularly where scatter in results are noted or where disagreement with empirical methods occurs.

### **2.5.13 Hydraulic conductivity**

The ability of a material to transmit water is defined by its hydraulic conductivity and is measured in terms of the coefficient of permeability. Soil permeability influences, amongst other things (i) the rate of consolidation of a saturated soil (with a change in effective stress), (ii) the stability of slopes and retaining structures (via the phreatic surface), and (iii) the design of earth dams and soil filters (Mitchell, 1993). The hydraulic conductivity of soils depends on a few factors, namely: distribution of particle and pore sizes, void ratio, degree of soil saturation, roughness of mineral particles, soil structure and fluid viscosity (Das and Sobhan, 2018). Knappett and Craig (2012) explain the influences of grain and pore characteristics on permeability as follows: Typically, the smaller the particles and thus the average pore size, the lower the soil permeability. In well graded soils smaller particles fill the void spaces between larger grains, thus reducing the size and interconnectedness of pores and increasing the soil density. As the soil becomes denser and the void ratio decreases, the coefficient of permeability will too decrease. In uniform soils, the sharp and irregular edges of angular grains will hinder proper densification, showing the influence of particle shape on void ratio and thus hydraulic conductivity. In a soil consisting of more- and less-permeable layers, the overall permeability will be higher in the direction parallel to the layering than perpendicular to the layering. In fine grained soils, the presence of fissures will result in a significant increase in permeability due to preferential flow along the discontinuities. The hydraulic conductivity also depends on the water temperature, which affects the viscosity of water.

From the above, it is evident that different soil types have an inherent permeability associated with them. Coefficient of permeability ( $k$ ) values for a range of soils, from clean gravels to unfissured clays, is given in Table 2-12. The values of  $k$  are lower for unsaturated soils and rise rapidly as the degree of saturation increases.

**Table 2-12: Hydraulic conductivity values for a series of soils in m/s (Knappett and Craig, 2012)**

1	$10^{-1}$	$10^{-2}$	$10^{-3}$	$10^{-4}$	$10^{-5}$	$10^{-6}$	$10^{-7}$	$10^{-8}$	$10^{-9}$	$10^{-10}$
Desiccated and fissured clays ( $10^{-2}$ - $10^{-7}$ )										
Clean gravels		Clean sands and sand - gravel mixtures			Very fine sands, silts and clay-silt laminate			Unfissured clays and clay- silts (>20% clay)		

Soil permeability can be determined in the laboratory from either remoulded or undisturbed specimens, using the constant-head or falling-head permeability tests, or by means of a Rowe Cell consolidation test (allowing both horizontal and vertical permeability determination of large diameter specimens). According to Head (1992), the differentiation between coarse- and fine-grained soils suitable for constant- and falling-head testing respectively, is at  $10^{-5}$  m/s. In the case of fine-grained soils presenting with discontinuities, disturbance during sampling will impact laboratory findings. The findings for structureless (intact) coarse grained soils from the study area will not be affected by the sampling method.

On-site measurement of hydraulic conductivity can be made by means of the well pumping test, involving incessant pumping from a well, and the lugeon test performed in soil and rock through boreholes. These tests can be costly. More often, a standpipe permeameter is simply used for the field determination of permeability. The use of the piezocone penetrometer test (CPTu) also allows determination of the  $k$  value. This method is based either on the estimated soil type or on the rate of pore water pressure dissipation during CPTu dissipation tests (Robertson and Cabal, 2012). A relationship between soil permeability and soil behaviour type (SBT) index,  $I_c$ , has been established by Robertson (2010b). This relationship only applies to soils allocated to SBT 2 to SBT 7 (i.e. excluding zones one, eight and nine). Robertson (2010b) however highlights the dependence of the normalised CPT parameters on various soil variables and states that the suggested relationship is approximate and should be used as a guide only. Improved estimates of permeability can be obtained from CPTu dissipation tests. During a dissipation test, penetration of the cone is paused and the rate of dissipation of excess pore pressure generated around the cone is measured. The pore pressures are subsequently plotted as a function of square root of time. The rate of dissipation of pore pressure is controlled by the coefficient of consolidation in the horizontal direction which, in turn, is a function of soil permeability in that direction and the constrained soil modulus (compressibility). To determine the soil permeability from the dissipation test results, the coefficient of consolidation is calculated as a function of time for 50% dissipation, and the constrained soil modulus is determined from the CPT corrected total cone resistance,  $q_t$ , the overburden pressure,  $\sigma'_{vo}$ , and a value,  $\alpha_M$ , dependent upon SBT index,  $I_c$ .

Measurement of infiltration rates can also be made on-site by means of the double ring infiltrometer test. The attained rates depend on the soils' permeability and frequently serve as input in the design of soakaways or stormwater drainage systems for residential erven and sports fields, amongst other applications. Some of the factors affecting infiltration rate includes the

degree of saturation of the soil, structure and layering, and the state of the ground surface (e.g. vegetated).

Extensive research has been performed to establish a relation between soil permeability and particle characteristics. In this regard, empirical relationships based on grain size and distribution, have been presented, amongst others, by Hazen (1930), the US Department of Navy (1986), Krumbein and Monk (1942), Masch and Denny (1966), and Chapuis (2004). The original work of these authors (excluding Chapuis, 2004) could not be obtained and are cited from Das and Sobhan (2018) and Shipeng et al. (2015). The more recent relationship given by Chapuis (2004) for granular soils without plasticity, relies on the effective particle size ( $D_{10}$ ) and soil density. A hydraulically based method, relating the coefficient of permeability to granular soil properties, was put forward by Joseph Kozeny and Philip C. Carman. The well-known Kozeny-Carman equation stems from the initial work of Kozeny in 1927, in which a porous medium was considered as a bundle of capillary tubes. The relationship produced by Kozeny was subsequently modified by Carman (1956) (as cited in Chapuis and Aubertin, 2003). The equation has taken on many forms over time and, in 2003, Carrier suggested further but minor modification to increase its practicality. The relation, which is based on grading, particle shape and void ratio, provides fairly accurate estimates of permeability (Das and Sobhan, 2018). Nonetheless, the Kozeny-Carman equation is constrained by a number of limitations (Carrier, 2003): It is unsuitable for clayey soils and gravels, soils with platy particles, and soils in which the particle size distribution has an extended and flat 'tail' in the fine fraction. The equation also does not explicitly account for anisotropy.

The influence of the shapes of individual grains is accounted for in most empirical and semi-empirical relationships. According to Goktepe and Sezer (2011), particle shape is one of the most important influences to consider when assessing the behaviour of coarse-grained soils. Much research has been carried out into the significance of grain shape and its role in determining soil permeability (Mavis and Wilsey, 1936, Goktepe and Sezer, 2011, and Cabalar and Akbulut, 2016). Cabalar and Akbulut (2016) estimated the hydraulic conductivity of sands with different gradation and grain shape and later compared these values to hydraulic conductivities estimated using existing empirical equations. The sphericity and roundness of two different sand types were determined and found to be rounded and very angular respectively. Both sand types were then artificially graded into sixteen grain-size fractions each and the coefficient of permeability of these fractions determined in a constant head permeability test, at relative densities of about 40% and a temperature of  $22 \pm 2^\circ\text{C}$ . It was found that the samples with rounded particles consistently have lower values of hydraulic conductivity compared to the samples with angular grains, which can be ascribed to the shape characteristics resulting in different void ratios. Sphericity is thought to have a less pronounced effect on permeability. In addition, the grading characteristics were found to have a significant effect on the hydraulic conductivity. The best correlation with the measured values were given by the empirical formulas of Slichter (1898) and Terzaghi (refer to Odong, 2007). The relation given by Chapuis (2004) also produced reasonable estimates.

Conversely, Goktepe and Sezer (2011) found that, for uniform soil, soil pores are better filled, and soil density increased as the irregularity of the grains increases. This result was obtained at several compacted densities. To form an association between defined particle shape parameters (roundness, regularity and sphericity) and the relative density values, goodness-of-fit tests were conducted. Anderson-Darling tests were used to determine whether the data is drawn from a

predefined probability distribution, which showed an overall best fit to a log-normal distribution. Uncertainties in the statistical evaluation were however highlighted, as well as the possibility of questionable relationships between the means of the shape parameters and their statistical identifiers, and the relative densities obtained. These findings contradict the conclusions made by Cabalar and Akbulut (2016). Furthermore, extensive studies by Youd (1973) (refer to Das and Sobhan, 2018) showed maximum and minimum void ratios to increase as particle roundness decreases (for uniform soils). This aspect will be considered in the interpretation of the hydraulic conductivity of the Cape Flats sands.

Based on existing knowledge for the Cape Flats sand, some early assumptions can be made with regards to permeability. The permeability of the sands is a function of the void ratio, which is ultimately influenced by the grain sizes in the soil, the distribution of these sizes, particle shape, organic matter content and soil compaction. Other influential factors include the degree of saturation, soil structure and fluid viscosity. The permeability of the Cape Flats sands at any given location and depth will be a function of the combined effects of these influences. The deposits that underlie the study area comprise mainly fine and medium sand with subordinate silt and/or clay. Clean sands and silty sands predominate, with minor plastic fines, particularly in the Witzand and Langebaan Formations. Fine sands ranging in size from 0.075mm to 0.425mm predominate, dictating pore size and water flow. The proportion of fines will exert considerable influence on permeability, and in the Springfontyn Formation where higher fines contents are often associated with the aeolian sands and intermittent clayey layers of lacustrine, estuarine and alluvial origin occur, soil permeability will decrease. The soil fines will fill void spaces, decreasing the void ratio and raising the value of  $C_u$ . According to Roberts (2001), the sands from the Langebaan Formation are typically medium to coarse grained containing calcrete gravel. Increased flow rates will therefore likely be associated with the calcareous sands of the Langebaan Formation. Notwithstanding this, substantially decreased flow rates will be experienced in the hardpan calcrete and cemented dunes of calcarenite rock in this formation. Existing literature mostly associates rounded and sub-rounded grain shapes with windblown sands, which will result in less void space and lower permeability compared to angular particle shapes in the uniform sands. Notwithstanding this, grain shape varies as a function of transportation distance and is likely to show some variation across the study area. The presence of peaty layers and lenses in the Springfontyn Formation will typically decrease hydraulic conductivity in these zones. The soils from the Springfontyn and Langebaan Formations (and to a lesser extent the Witzand Formation), have a degree of anisotropy due to the presence of limestone, calcrete, clay and peat layers, which will result in dissimilar flow rates in the horizontal and vertical directions. A decrease in void ratio is expected to occur with depth, as bulk density rises with densification. Based on the above, it is expected that the  $k$  values of the windblown sands will mostly range between  $10^{-2}$  and  $10^{-6}$  m/s (refer to Table 2-12).

Stapelberg (2009) determined the permeability of the Cape Flats soils by (i) carrying out soil permeability testing in the field using a standpipe permeameter and (ii) performing constant-head permeability tests in a laboratory. Forty-seven permeability values were obtained for the aeolian sands from the northern portions of the study area. The permeability values obtained for the sands of the Witzand, Springfontyn and Langebaan Formations are shown in Table 2-13. The aeolian sand were determined to be mostly semi-pervious ( $10^{-4}$  to  $3 \times 10^{-7}$  m/s).

**Table 2-13: Permeability of the Cape Flats sands (after Stapelberg,2009)**

Formation	Permeability (m/s)		
	Number of values	Range	Average
Witzand	3	$6.4 \times 10^{-5} - 9.9 \times 10^{-5}$	$8.73 \times 10^{-5}$
Springfontyn	36	$< 4 \times 10^{-8} - 1.0 \times 10^{-4}$	$4.15 \times 10^{-5}$
Langebaan	8	$< 4 \times 10^{-8} - 5.84 \times 10^{-4}$	$1.03 \times 10^{-4}$

The narrow range of permeability values obtained for the Witzand Formation sands agrees with the initial assumptions made with regards to the typical lack of anisotropy in this formation. Permeabilities in the other formations span a much larger range of k values, possibly illustrating the presence of layering (intermittent cohesive layers), structure, organic matter, calcretisation etc. Nonetheless, the fewer number of values applicable to the Witzand sands, could introduce bias.

Adelana, Xu and Vrbka (2010) conducted two well pumping tests on the Cape Flats aquifer. The transmissivity values for the aquifer were determined to be 32 m<sup>2</sup> per day and 620 m<sup>2</sup> per day. These values provide an indication of the rate at which groundwater is transmitted horizontally through the aquifer and are directly related to horizontal hydraulic conductivity. The permeability of the Cape Flats sands has also been evaluated by Gerber (1981) (refer to Adelana, Xu and Shafick, 2006). According to Gerber (1981), hydraulic conductivities of 30 to 40 m/day ( $3.5 \times 10^{-4}$  to  $4.6 \times 10^{-4}$  m/s) and 15 to 50 m/day ( $1.7 \times 10^{-4}$  to  $5.8 \times 10^{-4}$  m/s) can be expected centrally and in the eastern portions of the aquifer respectively (Adelana, Xu and Shafick, 2006). In the same study, transmissivity values were found to vary between < 50 m<sup>2</sup> per day and 600 m<sup>2</sup> per day. From the work of Gerber (1981) a transmissivity map has been created for the Cape Flats (Adelana, Xu and Vrbka, 2010).

The permeability of the Cape Flats sands will be evaluated based on field, laboratory and empirical methods to explore the previously mentioned assumptions. This includes the study of inter-formation variation in permeability, as well as the influence of factors such as grain shape and gradation on the k values. Furthermore, the infiltration capacity of the Cape Flats sands will be investigated based on the results of double ring infiltrometer tests. The chosen methods will be justified and discussed in Section 3.5.8 from Chapter 3.

#### 2.5.14 Shear strength

Shear strength is a governing influence in all aspects of soil stability such as bearing capacity, lateral earth support and slope stability. When a soil fails in shear, sliding between soil particles results in movement of a portion of the soil relative to the rest of the soil mass. The shear strength of a soil arises from particle friction and interlock, as well as from cohesive forces between grains. In the absence of electrostatic forces or cementation between soil particles providing cohesive strength, the shear strength of cohesionless soils is approximated by the following linear relationship, expressed in terms of effective stress:

$$\tau_f = \sigma' \tan \varphi' \quad \text{Equation 2-7}$$

Where:

$\phi'$  = Drained friction angle ( $^{\circ}$ )

Drained shear strength can be determined in the laboratory from drained direct shear and triaxial testing and undrained triaxial testing with pore water pressure measurement. These tests methods are stipulated in ASTM D3080 (2011), ASTM D4767 (2020), ASTM D2850 (2015), and ASTM D7181 (2020). The triaxial test is typically considered superior as it is suitable for all soil types and drainage conditions can be controlled (Knappett and Craig, 2012). A brief overview of the use and interpretation of the triaxial test is given below.

Monotonic triaxial compression tests are widely used to determine the Mohr-Coulomb failure parameters of cohesion ( $c$  or  $c'$ ) and friction angle ( $\phi$  or  $\phi'$ ). To characterise the failure behaviour of a coarse-grained soil, a representative cylindrical specimen is loaded under steadily increasing vertical stress up to failure at a constant confining pressure. The major principal stress ( $\sigma_1$ ) at failure is determined at a minimum of three different confining pressures ( $\sigma_3$ ) and the Mohr circles drawn, illustrating the stress conditions at failure. A straight line is drawn tangential to the circles to obtain the Mohr Coulomb failure envelope. The slope of the envelope gives the friction angle, and the intercept with the y-axis gives the cohesion value. When drainage of a saturated specimen is allowed during testing, or where pore water pressure is measured during undrained testing, the effective stress parameters of  $c'$  and  $\phi'$  can be calculated by plotting the Mohr circles in terms of  $\sigma_1'$  and  $\sigma_3'$ . When the soil is partially saturated, the effective stress will be influenced by soil suction and only the total stress parameters of  $c$  and  $\phi$  will be known. The Mohr Coulomb representation (in terms of total normal stress) for two triaxial compression tests (annotated 'L' and 'H' for low and high stress respectively) are shown in Figure 2-11.

Several transformation models exist in literature whereby the effective friction angle of granular soils can be estimated from relative density (Bolton, 1986 and Salgado et al., 2000 as cited in Ching et al., 2017), SPT blow count (Peck, Hansen and Thorburn, 1974, Mitchell, Guzikowski and Villet, 1978, Hatanaka and Uchida, 1996, and Chen, 2004), or CPT tip resistance (ESOPT, 1974, Durgunoglu and Mitchell, 1975 as cited in Meigh, 1987, Schmertmann, 1978, Robertson and Campanella, 1983, and Kulhawy and Mayne, 1990).

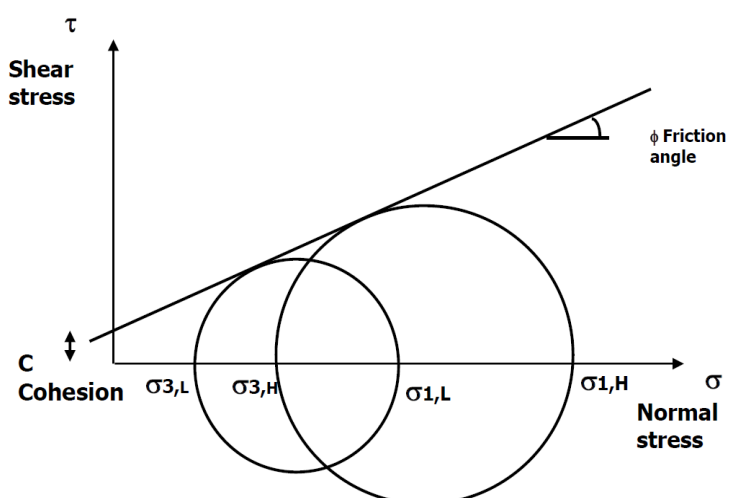
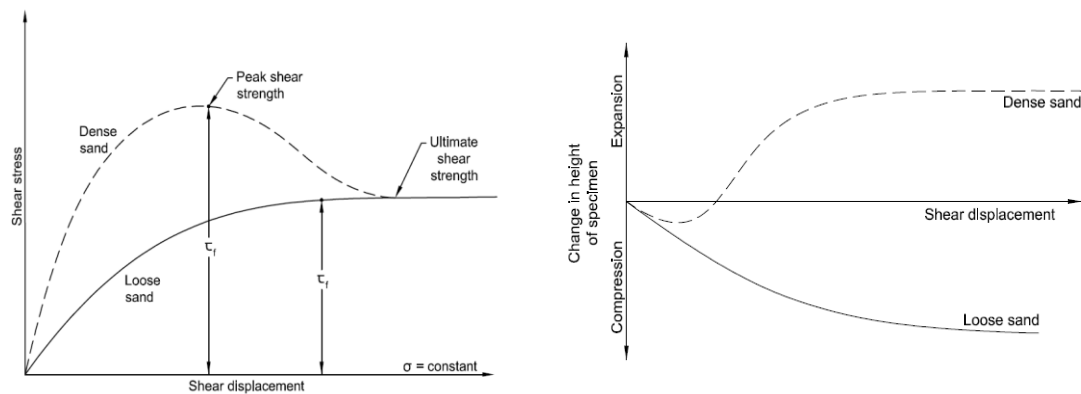


Figure 2-11: Mohr circles from monotonic triaxial test data (Jenkins and Rudman, 2016)

The effective friction angle of a soil is the result of the combined effects of inter-grain sliding friction (strength from frictional resistance), interlocking friction (strength developed by energy needed to cause dilation) and rolling friction (strength developed by energy needed to rearrange grains) (Mitchell, 1993 and Kara, Meghachou and Aboubekr, 2013). These strength components are influenced by relative density, gradation, particle size and shape, and confining pressure.

The stress-strain curves of initially loose and dense soils from a direct shear test are shown in Figure 2-12. The concept of soil dilation is also shown whereby grain interlock in a dense soil - producing the peak stress value shown in the figure – must be overcome by movement of grains up and over one another, causing volume increase. Once the interlocking is overcome, the shear resistance decreases, and the ultimate shear strength value is reached where no further change in soil volume occurs. At this point, the critical state of the soil is reached. Plotting the ultimate values of shear stress against the normal stresses reveals the critical state line (CSL). At the critical state, all cohesion has been lost and the CSL passes through the origin. The resistance of the volume change contributes significantly to the friction angle.



**Figure 2-12: Shear strength characteristics of loose and dense sand (redrawn from Das and Sobhan, 2018)**

The effects of relative density on friction angle have been investigated, amongst others, by Cerato and Lutenegro (2006) and Sivadas and Lee (2008). These studies, making use of the direct shear and direct simple shear test methods, showed that an increase in relative density (decrease in void ratio) typically implies an increase in grain to grain contact areas, and thus resistance to shear.

Typically, an increase in the particle size and the distribution of particle sizes in a coarse-grained soil will be associated with an increase in sliding, interlocking and rolling friction, and thus shear strength. An increase in particle surface roughness and angularity will also increase the sliding and interlocking friction. The effects of particle size and gradation on the shear strength of granular materials have been studied by various researchers including Yasin and Safiullah (2003), Bareither et al. (2008), Latha and Sitharam (2008), Wanasinghe and Suzuki (2012), Kara, Meghachou and Aboubekr (2013), Alias, Kasa and Taha (2014) and Mehta and Gandhi (2016). Although contradictory findings regarding the influence of particle size and gradation on strength exist in the literature, the findings typically illustrate the dependence of the effective friction angle on both particle size and gradation. Multivariate regression analysis was used by Bareither et al. (2008) to develop a model to predict the effective friction angle of compacted sands based on the

effective particle size ( $D_{10}$  in mm), particle shape and maximum dry unit weight ( $\gamma_{dmax}$  in  $\text{kN/m}^3$ ). The relationship obtained by Bareither et al. (2008) is given as follows:

$$\varphi' = 1.89 + 20.56 \times D_{10} + 2.35 \times \gamma_{dmax} - 24.10 \times R_s \quad \text{Equation 2-8}$$

Where:

$R_s$  = Weighted average Krumbein roundness.

Interlocking friction, which provides the main contribution to the strength of coarse-grained soils, is the result of physical resistance to relative particle translation. The interlocking between particles is greatest in dense, well graded soils with angular particle shapes. The uniformly graded sands of the Cape Flats will lead to lower densities and less particle interlocking compared to well graded sands. The presumed rounded and sub-rounded particle shapes will further reduce the frictional resistance. Notwithstanding this, the presence of cementing agents in the sands from the Witzand and Langebaan Formations, will increase the cohesive component, resulting in increased shear strengths in these sediments. Apparent cohesion, arising from negative pore water pressures, will exist in the partially saturated sands above the water table. Decreased friction between grains is expected in clay soils and peat from the Springfontyn Formation. Electrostatic forces between clay minerals will contribute true friction in the cohesive soils. In this regard, Amdurer (1956) determined the strength of 65 specimens of organic clay, plastic clay, and silty and sandy clay, representing transported and residual Malmesbury shale deposits from the Cape Flats. Triaxial compression testing showed variation in friction angles from  $10^\circ$  to  $25^\circ$  (average of  $14^\circ$ ), and cohesion values between 16kPa and 152kPa. The variation was ascribed to anisotropy arising from bedding planes. The current research will focus on the shear strength of the typically cohesionless windblown sands of the study area.

Neal (2011) investigated the characteristics of the windblown sands of the Witzand Formation, near Melkbosstrand, to explore the possibility of liquefaction in these sands and to establish a correlation with settlement, using the flat plate dilatometer. As part of the study, drained direct shear tests were undertaken on uniformly graded fine-grained sand specimens from the study site to determine their effective friction angle. Peak friction angles were found to range between  $37.9^\circ$  and  $44.5^\circ$  for the very loose to medium dense sands (consistency descriptions are from the dry densities attained in the laboratory), with the average friction angle determined to be  $41.7^\circ$ . These values are considered high when compared to the typical friction angles of sands (Byrne and Berry, 2008 and Das and Sobhan, 2018). Kalumba (1998) obtained a peak friction angle of  $36^\circ$  for loosely compacted ( $\rho_d = 1520 \text{ kg/m}^3$ ) fine sands from the Cape Flats during his investigation of the effect of grading and grain size on the friction characteristics of a sand/geotextile interface.

#### 3.5.14.1 Critical state soil concept

The central idea of the critical state concept, which applies to both fine and coarse-grained soils, is the notion that if these geo-materials are continuously distorted, a critical state is reached where no further change in volume or effective stress occurs and the soil flows as a frictional fluid (Schofield and Wroth, 1968). The critical state is determined by Equations 2-9 and 2-10, as presented by Schofield and Wroth (1968), which can be explained graphically by means of Figure 2-13a and b respectively.

$$q' = Mp' \quad \text{Equation 2-9}$$

$$T = v + \lambda \ln p'$$

Equation 2-10

Where:

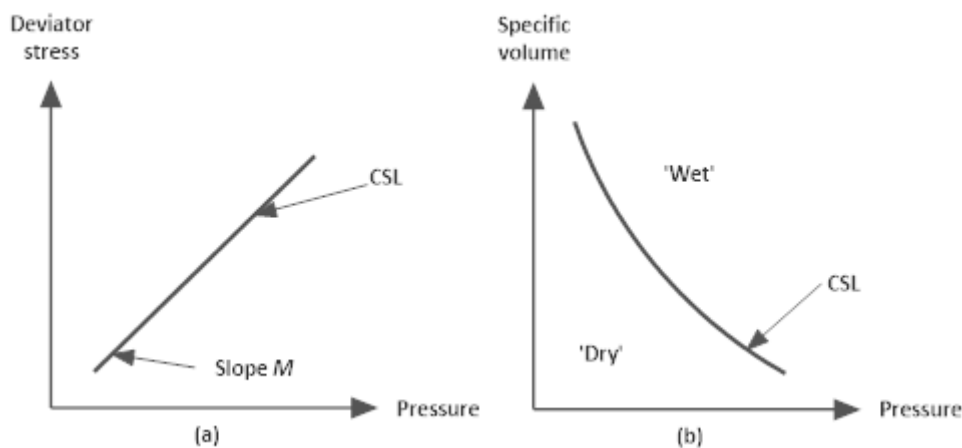
$q'$  = Deviator stress ( $\sigma'_1 - \sigma'_3$  in the triaxial compression test)

$M$  = Frictional constant (gradient of failure envelope)

$v$  = Specific volume ( $1 + e$ )

$T$  and  $\lambda$  = Basic soil-material properties

$p'$  = Average effective principle stress ( $\frac{\sigma'_1 + 2\sigma'_3}{3}$  in the triaxial compression test)



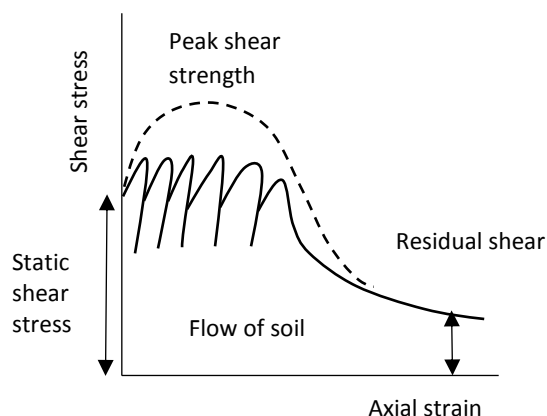
**Figure 2-13: CSL in (a)  $q'$ - $p'$  space and (b)  $v$ - $p'$  space**

Figure 2-13a shows the combination of deviator stress and effective pressure required to keep the soil flowing, which defines the CSL with slope  $M$ . This straight line through the origin connects failure data points in the  $p'$ - $q'$  plane from drained and undrained triaxial tests (Atkinson and Bransby, 1978). In Figure 2-13b, the CSL is represented in the volume - effective pressure space, thus illustrating the specific volume of the soil at the critical state. In Equation 2-10,  $T$  - which is the value of  $v$  associated with  $p' = 1.0$  kPa on the CSL - fixes the position of the CSL in the  $v$ - $\ln p'$  plane (Atkinson and Bransby, 1978). Collectively, Equations 2-9 and 2-10 determines the position of the critical state line in the  $q'$ - $p'$ - $v$  space.

Schofield and Wroth (1968) highlight the fact that remoulded soil specimens can be obtained in a wide range of states due to variable loading and unloading sequences. This creates uncertainty with regards to a materials' behaviour during shear and after yielding has occurred. A solution to the abovementioned problem is to examine the ultimate completely remoulded condition of the soil. The critical state line then becomes the point of reference (Schofield and Wroth, 1968). The volumetric response of soils during shear is revealed by the position of  $v$ - $p'$  data points (for soils at different states), plotting either above or below the CSL in Figure 2-13b. Combinations of  $v$ - $p'$  plotting above the CSL (loose state) are illustrative of a contractive soil, whereas points plotting below the CSL (dense state) show a dilative soil response. The change in volume of soils during shear provides an indication of the potential of the specific material to liquefy under static and dynamic shear loading. The following section provides an overview of soil liquefaction and empirical methods for liquefaction assessment.

### 2.5.15 Soil liquefaction

Liquefaction is said to occur when a saturated, non-cohesive soil mass loses its shear resistance due to an increase in pore water pressure during monotonic, cyclic, or shock loading. Liquefaction results from the tendency of loose, saturated sandy soils to contract under static and shear loads (Rauch, 1997). When sheared, the soil particles rearrange into a denser state of packing, thus decreasing the soil volume which, in turn, causes an increase in pore water pressure. The pore water pressure is unable to dissipate during the undrained conditions, and stresses are subsequently transferred from the soil framework to the water occupying the soil pores. The inter-particle forces become zero and the shear strength of the soil is lost, causing it to liquefy (existing in a liquid state). The response of a contractive saturated sand during undrained shear is shown in Figure 2-14.



**Figure 2-14: Behaviour of saturated sand in a loose (contractive) state during undrained shear (redrawn from Rauch, 1997)**

From the figure it is evident that a peak strength value is reached during static shear, after which the soil softens to its residual shear strength. Flow liquefaction occurs where the static shear stress becomes greater than the residual shear strength (Rauch, 1997). Figure 2-14 also illustrates the response of the soil during cyclic loading. During each load cycle, pore water pressure accumulates (if drainage is not allowed), resulting in the shear strength dropping below the static driving stress. The result is the occurrence of liquefaction flow failure in the loose, contractive soils.

During undrained cyclic shear (with cycles of small shear strains), dense, saturated sands have the tendency to gradually soften as excess pore water pressures are generated. However, when these soils are subsequently monotonically loaded without pore water drainage, dilation of the soil occurs as the particles move up and over each other, resulting in a decrease in pore water pressure and an increased shear resistance (Rauch, 1997). This behaviour of dense, saturated sands is described as cyclic mobility and often referred to as 'limited liquefaction'.

In addition, Rauch (1997) explains that a soil which normally tends to dilate during undrained, monotonic shear (dense sand) may temporarily lose its shear resistance when the effective stress becomes zero; thus, leading to substantial deformations. This occurrence, described by the term cyclic liquefaction, ensues when cyclic shear stresses become larger than the initial, static shear stress, producing a reversal in the direction of shear stress (stress path passes through a state of

zero shear stress). Deformations will however stabilise when the cyclic loading ends. The tendency of a dense dilative soil to produce an increase in shear strength when monotonically sheared, is shown in Figure 2-15. When the same soil is cyclically sheared, pore water pressures build up during each cycle leads to soil deformation. However, when cyclic loading ends, the soil will dilate and develop negative pore water pressures, which leads to an increase in effective stress and shear strength.

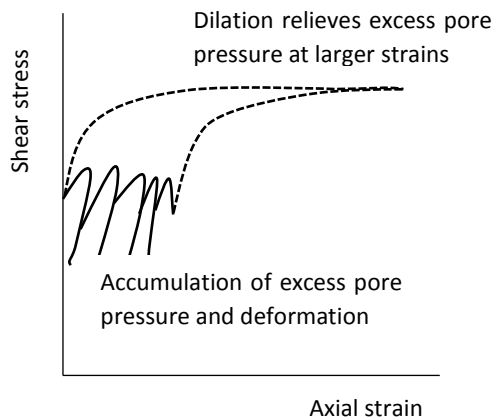


**Figure 2-15: Behaviour of saturated sand in a dense (dilative) state during undrained shear (redrawn from Rauch, 1997)**

As discussed in Section 2.5.14.1, the volumetric response of a soil during shear can provide an indication of the liquefaction potential of the soil. Figure 2-16 below illustrates the CSL in the void ratio ( $e$ ) - effective stress ( $\sigma'_3$ ) space and the volume and effective stress changes observed during drained and undrained monotonic shear tests, initially from different states.

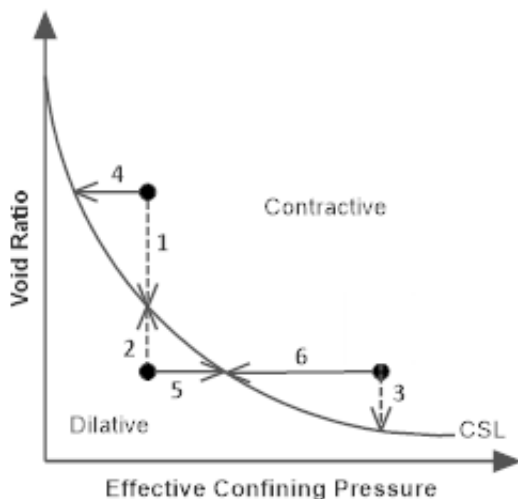


**Figure 2-16: State diagram with triaxial stress paths (redrawn from Rauch, 1997)**

From the three drained tests undertaken (1-3), it is evident that tests 1 and 3 illustrate the shear of contractive soils (plotting above the CSL), whereas a dilative soil (plotting below the CSL) is depicted by test 2. At a particular confining pressure, the same ultimate shear strength will be attained irrespective of the initial void ratio (see tests 1 and 2), whereas an increase in confining pressure for soils with identical initial void ratios, will result in higher ultimate strengths (see tests

2 and 3). The results of the undrained monotonic tests (4-6) show that excess pore water pressures developed when the contractive soils (tests 4 and 6) were sheared, leading to a decrease in effective stress. Conversely, an increase in effective stress due to the dilatant behaviour of the sample from test 5, was noted.

With increased deviation between the initial void ratio and the critical void ratio ( $e_c$ ) – the void ratio at the critical state – larger volume changes (contraction or dilation) will occur. Been and Jefferies (1985) defined the state parameter ( $\Psi$ ), to characterise the volumetric change, defined as the initial void ratio minus the critical void ratio at the same average effective stress. The state parameter accordingly provides an indication of the flow liquefaction potential (dilative/contractive response).

The liquefaction characteristics of a soil is not only affected by the initial density and effective confining stress, but also by factors such as particle cementation, soil fabric, and aging, which will prevent movement and rearrangement of the soil particles and thus increase liquefaction resistance (Rauch, 1997). In addition, factors such as stress history, frictional resistance (which increases with effective confining stress), plasticity, permeability, and characteristics of soil grains such as grain size, shape and size distribution, also influences liquefaction potential. When evaluating the susceptibility of a soil to liquefaction, a distinction needs to be made between cyclic liquefaction and liquefaction resulting from strain softening with a subsequent loss of shear strength. The methods for assessing both cyclic and flow liquefaction potential in the Cape Flats are presented below.

To evaluate cyclic liquefaction for level ground sites, Robertson and Cabal (2012) proposed the following sequence for assessment:

- Estimate susceptibility to cyclic liquefaction
- Estimate triggering of cyclic liquefaction
- Assess post-earthquake deformations

According to Robertson and Cabal (2012), a sand-like soil is susceptible to cyclic liquefaction when its plasticity index (PI) is less than 10, its liquid limit ( $w_L$ ) is less than 37 and its natural moisture content is greater than  $0.85 \times w_L$ . Other criteria defining potentially liquefiable soils have been put forward by Idriss and Boulanger (2004), Seed et al. (2003) and Bray and Sancio (2006) (refer to Robertson and Cabal, 2012).

The trigger for cyclic liquefaction in a given soil deposit is often assessed using empirical methods based on in-situ penetration tests. To develop such an empirical method, sites possibly subjected to earthquake induced liquefaction in the past, are investigated to determine whether liquefaction occurred, and to measure the in-situ soil strength. The shear stresses induced in the ground by the earthquake are also estimated. By separating conditions where a soil liquefied from those where liquefaction did not occur, a liquefaction assessment criterion is formulated (Rauch, 1997). Penetration test methods are widely used to evaluate liquefaction potential, since the same factors that contribute to cyclic shear strength, increase the resistance to ground penetration (Rauch, 1997). According to Robertson and Cabal (2012), most of the existing work involving cyclic liquefaction, has been for earthquakes. To evaluate the cyclic liquefaction potential of saturated cohesionless soils during earthquakes, SPT-based correlations are the oldest and most widely used methods. Notwithstanding this, the cone penetration test has

become increasingly popular in estimating cyclic liquefaction potential and the works by Robertson and Wride (1998) and Robertson (2010c) are particularly significant in this regard. To estimate the potential for cyclic liquefaction for level ground sites due to an earthquake, the cyclic stress ratio (CSR) profile produced by the design earthquake, demonstrating the seismic demand of a soil layer, and the cyclic resistance ratio (CRR) of the ground, which provides a measure of the soils' resistance to liquefy, should be known. The CSR is calculated from the maximum horizontal surface acceleration ( $a_{max}$ ) produced by the earthquake, whereas the CRR depends upon penetration resistance data. When the CRR exceeds the CSR induced by the earthquake ground motions, the soil is considered resistant to cyclic liquefaction. Most empirical liquefaction assessment methods are based on the cyclic resistance ratio and a standardised SPT blow count. One of the most widely used SPT-based correlations is the deterministic relationship presented by Seed et al. (1984, 1985) (refer to Seed et al., 2003). This familiar method has been the standard for many years with only slight amendment at low CSR suggested by the NCEER Working Group (NCEER, 1997). Since the publication of this earlier method, SPT-based correlations have been produced by numerous authors including Liao et al. (1988, 1998), Youd and Noble (1997), and Toprak et al. (1999) (as cited in Seed et al., 2003). The low data quality and overall uncertainty related to these methods are however highlighted. More recently, Cetin et al. (2004) and Idriss and Boulanger (2004, 2008) put forward similar relationships between CRR and equivalent clean sand corrected SPT blow count  $[(N_1)_{60cs}]$ . The three liquefaction triggering curves are shown in Figure 2-17.

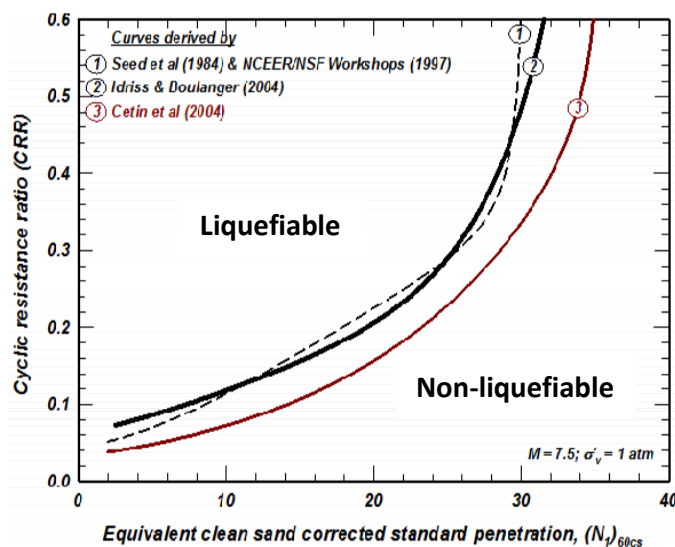


**Figure 2-17: Comparison of SPT-based liquefaction triggering curves (Idriss and Boulanger, 2010)**

Comparison of the liquefaction triggering curves reveals slight differentiation, with the Cetin et al. (2004) curve positioned lower than those proposed by the other authors. A review of SPT-based liquefaction triggering procedures for cohesionless soils was undertaken by Idriss and Boulanger (2010) during which the database of case histories was re-examined and updated. The review found that the lower position of the Cetin et al. (2004) curve was mainly due to their interpretations of several important case histories at a specific range of effective stresses. In their report, Idriss and Boulanger (2010) concluded that the modified Seed et al. (1984) and Idriss and Boulanger (2004, 2008) procedures are considered realistic to a depth of 12 meters (case histories

apply to these depth) and that the Idriss-Boulanger method is well supported by existing data for extrapolation to even greater depths.

The  $CRR-(N_1)_{60cs}$  curves presented in Figure 2-17 represent the boundaries between the no-liquefaction case histories and the liquefaction case histories. Where  $CSR-(N_1)_{60cs}$  data pairs plot above the curve, cyclic liquefaction can be triggered during an earthquake. The SPT blow count values which form the basis of this method should be corrected to an equivalent 60% hammer efficiency and normalised for overburden pressure, that is, the  $(N_1)_{60}$  values determined, and then adjusted to an equivalent clean sand value.

Post-earthquake settlement and lateral deformation can be estimated using empirical methods. Robertson and Cabal (2012) highlight the importance of engineering judgement in this regard, to ensure that the consequences of the calculated vertical settlement and lateral deformation consider aspects such as soil variability, site geometry and thickness of liquefied strata.

To evaluate susceptibility to flow liquefaction, the potential for a soil to strain soften in undrained shear, should be evaluated. According to Robertson (2010c), experience indicates that very loose sands are prone to abrupt strength loss at small shear strains and, as such, the identification of very loose coarse-grained soils is considered the core component in exposing soils susceptible to flow liquefaction. Robertson (2016) created a CPT-based normalised soil behaviour type (SBT<sub>n</sub>) chart (plotting normalised cone resistance,  $Q_{tn}$  against normalised friction ratio,  $F_r$ ), whereby an approximate boundary between dilative and contractive soil response is given. This boundary separates dense, dilative soils in which deformations occur only during cyclic loading. The CPT-based chart with delineated zones and associated soil behaviour types is given in Chapter 3.

According to Rauch (1997), liquefaction is mostly seen in shallow, loose, saturated sand and silt deposits that is exposed to strong earthquake shaking. Round particle shapes of similar size are especially prone to liquefaction. It is the more stable interlocking of well-graded sands with angular particle shapes that increases its resistance to liquefaction. Liquefaction is additionally associated with recent deposits in which particle movement is not hindered by age related cementation. The presence of clay minerals with cohesion will prevent rearrangement of grains into denser arrangements and causing an increase on pore water pressure, thus preventing soil liquefaction. Conversely, soils with non-plastic fines (silts) will not hinder particle movement, enabling an increase in pore water pressure during shear. Additionally, the presence of large proportions of non-plastic fines in a soil, resulting in lower permeability, will impede drainage of excess pore water pressure, making the soil more likely to liquefy (Rauch, 1997).

The recent windblown sands and silty sands of the Witzand and Springfontyn Formations of the Cape Flats are typically described as unconsolidated and fine and medium grained. The uniform gradation, presumed rounded and sub-rounded particle shape, and loose particle packing without cementation, make these soils potentially prone to liquefaction. In addition, shallow groundwater often occurs widespread across the Cape Flats, especially during the wet winter months, making the sediments susceptible to the accumulation of excess pore water pressures during seismic shearing. Conversely, the consolidated sand of the Langebaan Formation, comprising calcretised layers, will provide significant resistance to grain movement, and thus liquefaction, during shearing.

Although the Western Cape Province of South Africa, and specifically Cape Town is not located close to a plate boundary, intraplate fault lines present local weaknesses in the earth's crust, which are vulnerable to slip in the case of accumulation of sufficient regional tectonic strain. An intraplate fault line, known as the Milnerton fault, extends beneath the Cape Flats in a north westerly to south easterly direction. Seismic activity associated with this intraplate fault is considered responsible for the largest earthquake experienced by the City of Cape Town in 1809. During this event, observations of muddy water squirting out of fountains were made, possibly providing evidence of soil liquefaction induced by earthquake vibrations (De la Harpe, 2015). In 2003, the Council for Geoscience produced a seismic hazard map, showing peak ground accelerations for the whole of South Africa (De la Harpe, 2015 and SANS10160-4, 2010). According to this map, a peak acceleration of  $1.47 \text{ m/s}^2$  - with a 10% probability of exceedance in 50 years - is applicable to the Cape Town area. The Council for Geoscience also produced a seismic intensities map of South Africa, showing probabilistic Modified Mercalli Scale (MMS) intensities with a 10% chance of exceedance in 50 years (based on seismological data from 1620 to 1989) (Brandt, 2011). Seismic intensity class VI was assigned to the study area.

The liquefaction potential of the Cape Flats sands has been investigated by Parker (1991), and more recently by Schoeman (2018). Parker (1991) aimed to determine the cyclic liquefaction potential of five sites located in the Cape Flats, by making use of methods based on the field performance of liquefiable soils in previous earthquakes, as well as from laboratory testing methods. Empirical liquefaction criteria put forward by Seed, Idriss and Arango (1983) and Seed and Idriss (1971) - based on SPT blow count - and by Robertson and Campanella (1985) - based on CPT tip resistance - were utilised by Parker. In addition, a method proposed by Nishiyama et al. (1977) was also employed. According to the analyses, there is a possibility of cyclic liquefaction at four of the five investigated sites ( $\text{CSR} > \text{CRR}$ ). Contradictory results were however obtained for the SPT and CPT-based methods in several cases. The results from the in-situ correlations were confirmed by means of triaxial compression tests. The triaxial results showed that if the cyclic loading is large enough to cause a shear stress equal to 81kPa, cyclic mobility (known as 'limited liquefaction') would likely occur in the tested soils. Furthermore, the possibility of liquefaction was confirmed in a few of the cyclic triaxial tests. Parker concluded that SPT-based methods are most effective in determining the liquefaction potential of a soil deposit, and that these should be used in combination with cyclic triaxial tests to determine the liquefaction characteristics of a soil.

Schoeman (2018) constructed a vibratory table to simulate dynamic loading caused by an earthquake to investigate the potential of sandy soils to liquefy. The soil was compacted into a 40 litre plastic container mounted on the vibratory table, saturated and a brick placed on the soil surface. Vibrations were subsequently produced by means of an electric motor, and the acceleration forces measured. The time taken for liquefaction to occur - reflected by the submergence of the brick into the sand - was subsequently recorded. By varying the compacted density and grading properties of the sand, as well as the induced accelerations, the influence of each of these factors on liquefaction was studied. Experimental results confirmed the occurrence of liquefaction in many tests. An increase in soil density through compaction consistently increased the resistance to liquefaction. Soil was compacted to between  $1500 \text{ kg/m}^3$  and  $2000 \text{ kg/m}^3$ . Where soils were compacted to similar densities, an increase in the induced accelerations from 0.15 g to 0.25 g lead to liquefaction occurring more rapidly. The results additionally showed that gradation has a significant influence on the susceptibility of the soil to liquefy during cyclic

shear. In this regard, the liquefaction results obtained for both fine sand and medium sand subjected to identical accelerations and compacted to comparable densities, showed that the fine sand is more resistant to liquefaction than the medium sand. Schoeman (2018) ascribed the result to the smaller soil grains and void spaces, allowing less settlement and water ingress. Notwithstanding this, the smaller pore sizes will lower flow rates, supporting the build-up of excess pore water pressure and strength loss. The poorly graded sands showed increased susceptibility to liquefaction compared to the prepared well graded sands with stable interlocking (keeping other variables constant).

### **2.5.16 Compressibility**

Soils are compressible in nature and when a load is placed upon a soil, the stresses below the foundation level are increased, causing a decrease in the soil volume. The magnitude of this compression is reflected in the settlement of the foundation. The compression is caused by the deformation and rearrangement of soil grains, as well as the expulsion of water or air from soil pores (Das and Sobhan, 2018). In addition to vertical compression, lateral movement of the soils below a loaded area also contributes to settlement.

According to Das (2000) settlement can be divided into three broad categories; namely elastic settlement, consolidation settlement and secondary settlement (creep). The amount of settlement expected to occur depends on the stresses imposed on the soil (from structural loading) and the stress-strain properties of the soil. Consolidation settlement is observed in saturated cohesive soils and is the result of a gradual decrease in volume, as water is expelled from void spaces (primary consolidation settlement) and the plastic adjustment of soil fabrics (secondary consolidation settlement). Granular soils are typically highly permeable, and water rapidly flows from void spaces. In these soils, which occur widespread across the Cape Flats, the dissipation of excess pore water pressure occurs so rapidly that immediate and consolidation settlement are indistinguishable and are determined by the elastic deformation of the soil.

As stated by Simons and Menzies (1975), accurate prediction of the settlement of structures founded on granular soils is of considerable importance as it is the settlement, rather than the bearing capacity that typically governs the allowable pressure which may be applied to a foundation. In the study area, differential settlement may be large where the density index of the sands below footings of the same structure vary substantially; for example, compressible sands (possibly with intermittent highly compressible peaty layers in the Springfontyn Formation) and hard calcretised horizons. Only in instances where shallow footings, which are less than 1.5m wide, are founded in loose soils with a shallow water table, will bearing capacity failure become more critical than settlement.

In 1986, Douglas identified in excess of 40 methods by which settlement in granular soils can be estimated (Das and Sivakugan, 2007). According to Das and Sivakugan, all these methods incorporate the three most significant factors influencing settlement in coarse-grained materials, namely applied stress, soil stiffness and foundation width. Because of the difficulties related to obtaining undisturbed samples of granular soils, most of these methods are based on the results of in-situ tests such as the plate load test, SPT and CPT. According to Lutenegeger and DeGroot (1995), in-situ test results can be used to directly estimate settlement by means of empirical correlation or used to estimate the soil stiffness based on the elastic theory. Some of the settlement prediction methods which have been widely used over the past 30 years or more, and

based on the results of the in-situ tests described above, include the methods by Terzaghi and Peck (1948), Meyerhof (1965 and 1974), Peck and Bazaraa (1969), Burland and Burbidge (1985), Schmertmann (1970) and Schmertman et al. (1978). Interested readers can refer to Simons and Menzies (1975), Lutenegeger and DeGroot (1995), and Das and Sivakugan (2007) where the abovementioned methods are presented and discussed in detail.

Settlement prediction methods based on the elastic theory, requiring the elastic soil modulus (or Young's modulus,  $E$ ) as input parameter, are considered particularly valuable in the estimation of immediate soil settlement. According to Das and Sivakugan (2007), inaccurate settlement predictions for shallow foundations are mostly the result of imprecise stiffness moduli used in calculations. The accuracy of settlement prediction also depends on the selected method of analysis. Various elastic theory-based methods have been proposed, including the methods by Berardi and Lancellotta (1991), Mayne and Poulos (1999), Moxhay et al. (2008), Das (2011) and Yongqing (2011). Investigation of existing methods revealed the requirement of  $E_0$  (small-strain stiffness) - rather than  $E$  - as input parameter in recent methods. Archer and Heymann (2015), ascribe this shift to the use of seismic techniques to determine soil stiffness. Detailed descriptions of the elastic theory-based methods can be found in Archer (2014).

Tan and Duncan (1991) (as cited in Das and Sivakugan, 2007) evaluated twelve state-of-the-art settlement prediction methods in terms of reliability and accuracy, by comparing calculated and measured settlement data from footings founded on sands. It was found that the methods by Terzaghi and Peck (1948) and Schmertmann (1970) seem to have high reliability (consistency of outcomes), but poor accuracy (closeness to the actual value), whereas the methods proposed by Burland and Burbidge (1985) and Berardi and Lancellotta (1991) are deemed relatively accurate, but with low reliability.

Recently, an alternative approach to settlement prediction in sands has been proposed, based on the characteristic stress versus normalised displacement concept originally recommended by Fellenius and Altaee (1994) (as cited in Mayne, Uzielli and Illingworth, 2012). By carrying out full-scale load tests on 31 large footings, placed on various quartz-silica sand sites, Mayne, Uzielli and Illingworth (2012) developed methods whereby the elastic soil modulus and footing settlement can be obtained directly from CPT tip resistance. Post-processing of the data revealed that the applied footing stress ( $q$ ) versus displacement ( $s/B$ ) curves for all sands are unified when the foundation stress is normalised by the tip resistance ( $q_c$ ). Equivalent elastic moduli for the various footings were also back figured from the test data. The obtained relationships are given in Mayne, Uzielli and Illingworth (2012).

Besides the abovementioned scenario, in which the foundation is subjected to static forces from dead or permanent loads, some structures can also be subjected to dynamic and repeated loads as in the case of pavements, railroads and machine foundations. The loading on pavements comprise a large number of fairly small magnitude loads caused by traffic, resulting in an accumulation of small amounts of unrecoverable strain and gradual pavement deterioration. The design of flexible pavement systems is based on the analysis of stresses and strains in the pavement structure using linear elastic multi-layer models (Jenkins and Rudman, 2016). To create reliable designs that provide a good approximation of pavement performance, a knowledge of the shear strength, resilient modulus and permanent deformation is required. The resilient modulus, which is a measure of material stiffness under repeated loading, provides an indication

of the elastic response of the granular pavement materials. It should be noted that the stiffness is dependent upon the actual stress-state of the material of the pavement layer and therefore varies with the change in the stress state (Jenkins and Rudman, 2016). The permanent deformation (rutting) of granular materials constituting one of the common failure modes considered in the design of pavements, will also be affected by the soil stiffness. The resilient modulus is therefore an input parameter to the mechanistic-empirical pavement design method.

The important design parameters of elastic modulus, small-strain elastic modulus and resilient modulus can be determined from various laboratory and field methods, as well as from correlations with in-situ penetration test results. Each of these parameters is discussed in detail below, together with the methods to determine the parameters. Relevant published research pertaining to the design parameters is presented, with a focus on small-strain stiffness and previous studies relating shear wave velocity (related to  $E_0$ ) and standard penetration test blow count.

### 2.5.16.1 Soil elastic modulus

The stress-strain behaviour of soils is highly complex and, as such, simplifications and idealisations are used to produce basic mathematical models that can represent the properties of soils which are vital to the considered geotechnical problem. Various soil models have been created to describe the stress-strain and failure behaviour of soils, including the elastic-perfectly plastic model, the rigid-perfectly plastic model, the elastic-strain hardening plastic model, and the elastic-strain softening plastic model. Detailed descriptions of the deformation theory of plasticity and the flow theory of plasticity for perfectly plastic materials, as well as the basic concepts of plasticity for strain hardening materials can be studied in Chen and Mizuno (1990). The linear elastic model (generalised Hooke's law) gives a unique relation between state of stress and strain (one to one coordination), of which the gradient represents the material's response to the applied stress. If the stress applied to the soil is removed, the material returns to its original shape. The behaviour of isotropic linear elastic materials during simple compression and shear is illustrated in Figure 2-18.

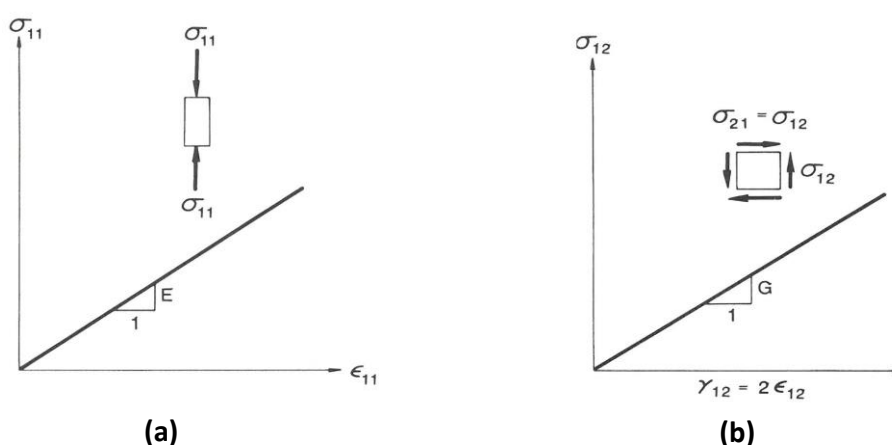


**Figure 2-18: Behaviour of isotropic linear elastic material in (a) simple compression and (b) shear (Chen and Mizuno, 1990)**

For a linearly elastic constitutive model, the stress-strain relationship during simple compression (characterised by a straight line) is given by Hooke's Law, in which

$$\varepsilon_x = \frac{1}{E} (\sigma'_x - \nu\sigma'_z) \quad \text{Equation 2-11}$$

$$\varepsilon_z = \frac{1}{E} (\sigma'_z - \nu\sigma'_x) \quad \text{Equation 2-12}$$

Where:

$\varepsilon_x$  and  $\varepsilon_z$  = Soil strains in the  $x$  and  $z$ -directions

$E$  = Soil elastic modulus (normal stress - strain relationship)

$\sigma_x$  and  $\sigma_z$  = Normal stress components in the  $x$ - and  $z$ -directions

$\nu$  = Poisson's ratio

The soil elastic modulus describes the material's response to axial stress in the direction of the stress. From Figure 2-18b the gradient of the straight line - the linear stress-strain relationship during shear - represents the shear modulus. In the case of an isotropically elastic material, the relationship between the elastic modulus ( $E$ ), the shear modulus ( $G$ ) and Poisson's ratio ( $\nu$ ) is as follows:

$$E = G [2(1 + \nu)] \quad \text{Equation 2-13}$$

The soil elastic modulus is not a material constant, but in fact, a non-linear function of strain and effective stress (Knappett and Craig, 2012). Likewise, the shear modulus is a non-linear function of shear strain and effective confining pressure. At very small strain values, the elastic and shear moduli have maximum values,  $E_0$  and  $G_0$  respectively. Clayton and Heymann (2001) studied the stress-strain behaviour of clays in the triaxial apparatus, noting constant stiffnesses up to shear strain levels of approximately 0.001%. It is assumed that the soil behaves elastically below these strain values. As the strain increases beyond this approximate value, soil stiffness decreases with increasing strain - the soil behaving in a non-linear manner. The concept of stiffness degradation will be discussed in further detail in Section 2.5.16.3.

As previously discussed, the elastic modulus is frequently used to estimate the settlement of soils and in elastic deformation analysis. Elastic modulus values are often obtained from existing empirical correlations relating penetration resistance to the stiffness of the soil. Alternatively, laboratory methods such as the monotonic triaxial test and oedometer test, or field methods such as the plate load test, pressuremeter test or dilatometer test can provide a more precise determination of the material stiffness. Strain levels exceeding 0.002% are induced by all these test methods, thus producing larger strain stiffness values.

Empirically correlated modulus values have been presented by various researchers undertaking experimental studies relating the stress-strain modulus and SPT blow count or cone penetration resistance. Standard penetration test correlations by Stroud (1989) and Webb (1969) are currently widely used for granular materials in the Southern African region. Webb put forward empirical relationships between the elastic modulus of estuarine sands on the Natal coast from helical plate load tests, and standard penetration resistance. The relationships are given by the following equations (Webb, 1969):

$$E = 0.537(N_{60} + 15) [MPa] \quad \text{Equation 2-14}$$

Equation 2-14 applies to fine and medium saturated sands.

$$E = 0.358(N_{60} + 5) \text{ [MPa]}$$

Equation 2-15

Equation 2-15 applies to clayey sands with PI < 15%.

Stroud's method is generally preferred as it recognises the importance of strain. The method of plotting the degree of loading (represented by the ultimate bearing capacity divided by the net bearing pressure below a foundation  $q_{\text{net}}/q_{\text{ult}}$ ) against  $E/N_{60}$  ratio, for normally and over-consolidated coarse-grained soils, allows estimation of soil stiffness at different strain levels based on SPT blow count. As  $q_{\text{net}}/q_{\text{ult}}$  increases, the factor of safety decreases, and soil stiffness reduces. The relationship is shown in Figure 3-30 in Chapter 3. The influence of stress history on soil compressibility is also recognised. The looser normally consolidated soils consistently display lower stiffnesses (at the same strain level) reaching a peak value at  $E/N_{60} \approx 2$ . The dense over-consolidated soils display greater stiffness, increasing sharply below a  $q_{\text{net}}/q_{\text{ult}}$  ratio of 0.1 (at lower strains) to values of  $E/N_{60}$  of 16 at very low values of  $q_{\text{net}}/q_{\text{ult}}$ .

Based on the geomorphological history of the Cape Flats (land and sea level changes), the stress history of the windblown sands relevant to the current study probably reflects that of normally consolidated deposits. Notwithstanding this, the continuous mobilisation of the dune sand across the low-gradient landscape during summer months (by the dominant south easterly winds), fluctuations in groundwater level, together with removal of dune sands for mining purposes, will result in over-consolidation in some areas. The presence of both normally and over-consolidated deposits is therefore anticipated in the study area.

Some of the other existing empirical correlations relating energy corrected SPT blow count to the modulus of elasticity, as summarised by Das and Sivakugan (2007), are included in Table 2-14. Clayton (1993) highlights the inconsistencies observed when comparing the range of relationships obtained and owes this to the strain dependency of stiffness being overlooked when determining stiffness in the laboratory.

**Table 2-14: Existing correlations between soil elastic modulus and SPT blow count for coarse-grained soils (after Das and Sivakugan, 2007)**

Author	Formulation	Soil type
Ferrent (1963)	$\frac{E}{P_a} = 7.5(1 - \nu^2)N_{60}$ [kPa]	Sand
Schultze and Melzer (1965)	$E = \left(246.2 \log N_{60} - 263.4 \frac{\sigma'_0}{P_a} + 375.6 \pm 57.6\right) \left(\frac{\sigma'_0}{P_a}\right)^{0.522}$ [kPa] for $0 \leq \frac{\sigma'_0}{P_a} \leq 1.2$	Dry sand
Begemann (1974)	$\frac{E}{P_a} = 40 + C(N_{60} - 6)$ for $N_{60} > 15$ [kPa]	C = 3 for silt with sand; 12 for gravel with sand Silt with sand to gravel with sand
	$\frac{E}{P_a} = 40 + C(N_{60} + 6)$ for $N_{60} < 15$ [kPa]	
Trofimenkov (1974)	$\frac{E}{P_a} = (350 \text{ to } 500) \log N_{60}$ [kPa]	Sand
Kulhawy and Mayne (1990)	$\frac{E}{P_a} = \alpha N_{60}$ [kPa]	$\alpha = 5$ for sand with fines; $\alpha = 10$ for clean, normally consolidated sand; $\alpha = 15$ for clean over-consolidated sands Sand

Numerous empirical correlations have emerged, whereby the drained soil modulus is represented as a function of cone penetration resistance. Some of these existing correlations for coarse-grained soils, used in routine design, are given in Table 2-15. The CPT-based relationships put forward by Webb (1974) also emanates from the before-mentioned research carried out on the estuarine sands from the Natal coast. A useful guide for estimating the modulus of elasticity of young, uncemented silica sand is given by Robertson and Cabal (2012). The correlation is applicable to a strain level of 0.1%.

**Table 2-15: Existing correlations between drained elastic modulus and cone penetration resistance for granular soils**

Author	Source	Formulation (MPa)	Soil type
De Beer (1965)	Byrne and Berry (2008)	$E_s = 1.5q_c$ [MPa]	Sand
Schultze and Melzer (1965)	Das and Sivakugan (2007)	$E = \left(301.1 \log q_c - 382.3 \frac{\sigma'_0}{P_a} + 60.3 \pm 50.3\right) \left(\frac{\sigma'_0}{P_a}\right)^{0.522}$ [MPa] for $0 \leq \frac{\sigma'_0}{P_a} \leq 0.8$	Dry sand
Webb (1974)	Webb (1974)	$E = \frac{5}{2} (q_c + 3.2)$ [MPa]	Saturated fine to medium estuarine and alluvial normally consolidated sands
		$E = \frac{5}{3} (q_c + 1.6)$ [MPa]	Estuarine and alluvial normally consolidated clayey sands with plasticity index less than 15%
Schmertmann (1970)	Das and Sivakugan (2007)	$E_s = 2q_c$ [MPa]	Sand
Schmertmann et al. (1978)	Knappett and Craig (2012)	$E_s = 2.5q_c$ (For square foundations) [MPa]	Normally consolidated sand (Values should be doubled for over-consolidated sands)
		$E_s = 3.5q_c$ (For strip foundations) [MPa]	
Robertson (2009)	Robertson (2009)	$E = \alpha_E (q_t - \sigma_{vo})$ Where $\alpha_E = 0.015 [10^{(0.55I_c + 1.68)}]$ [MPa]	Young, uncemented silica sands

### 2.5.16.2 Calculation of resilient modulus

The resilient modulus ( $M_r$ ), which provides an indication of the elastic response of the soil under repeated loading, and an input parameter to the pavement design method, can be determined by conducting repeated load or dynamic triaxial tests on material specimens at various combinations of applied loading and confinement (Jenkins and Rudman, 2016).

For coarse soils, the resilient modulus is primarily influenced by density (compaction), moisture content and stress state and, as such, representative cylindrical soil samples are prepared at varying combinations of moisture content and density. The stress dependent resilient deformation behaviour of the material is studied by subjecting the specimens to cyclic axial stress at a particular and constant confining pressure. Each sample is subjected to several deviator stress

to confining stress ratios at different confining pressures. 100 load repetitions are performed (at each stress level), using a haversine shaped load pulse, of which each repetition (loading and unloading) lasts one second (CSIR, 2014). The loading configuration for the repeated load test is shown in Figure 2-19.

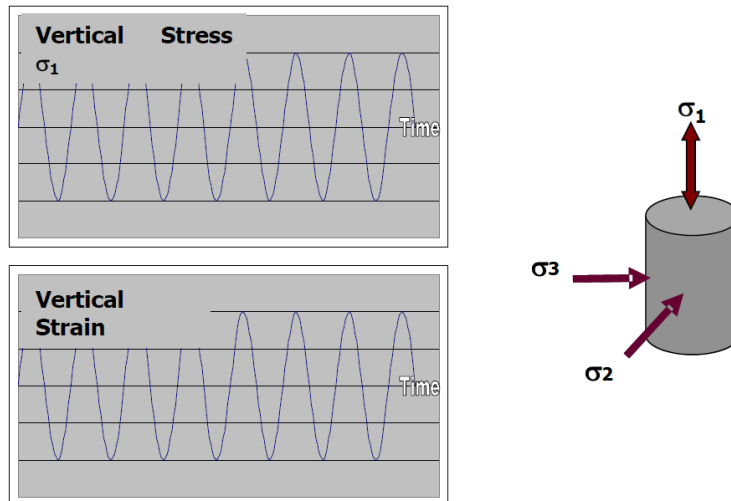


**Figure 2-19: Loading during repeated load triaxial testing (Jenkins and Rudman, 2016)**

The applied stress and the resulting axial strain are recorded for the last five loading cycles in each stress sequence and the resilient modulus calculated. The sum of the principle stresses ( $\Theta$ ) is then plotted against the resilient modulus for the different deviatoric stress to confining stress combinations on a log-log graph. For coarse grained granular materials, the resilient modulus is considered a stress dependent parameter, that is, the stiffness of the material increases as the bulk stress increases. The following simple power model, known as the  $M_r$ - $\Theta$  model, can be applied in the case of granular materials:

$$M_r = k_1 \theta^{k_2} \quad (MPa) \quad \text{Equation 2-16}$$

Where:

$\theta$  = Bulk stress ( $\sigma_1 + \sigma_2 + \sigma_3$ ) (kPa)

$k_1$  and  $k_2$  = Material coefficients

The  $M_r$ - $\theta$  model for coarse granular materials is illustrated in Figure 2-20.

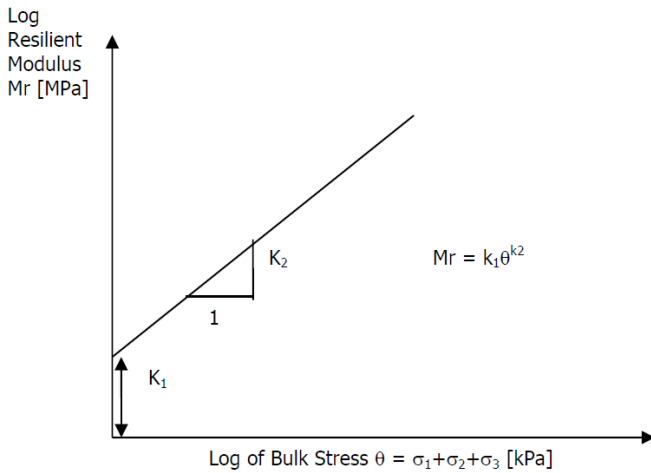


**Figure 2-20:  $M_r$ - $\theta$  model for coarse granular material (Jenkins and Rudman, 2016)**

The relationship between resilient modulus and bulk stress produced by triaxial tests on a 2% foamed bitumen sample - in which the confining pressure was kept constant and the vertical applied pressure increased - is shown in Figure 2-21. An increase in the value of  $M_r$  is seen as the confining pressure is increased. A slight initial increase in  $M_r$  with increasing applied pressure, followed by stabilisation or slight decrease, is noted at each confining pressure. It is evident that the straight-line relationship illustrated in Figure 2-20 does not simulate the results entirely accurately, however, it follows the trend and depicts the stress dependency of the modulus. Other mathematical models have also been developed to describe the stress dependency of the resilient response of materials (Van Niekerk, 2002). Some of these models will be discussed in Chapter 3 and the models selected for the current study identified.

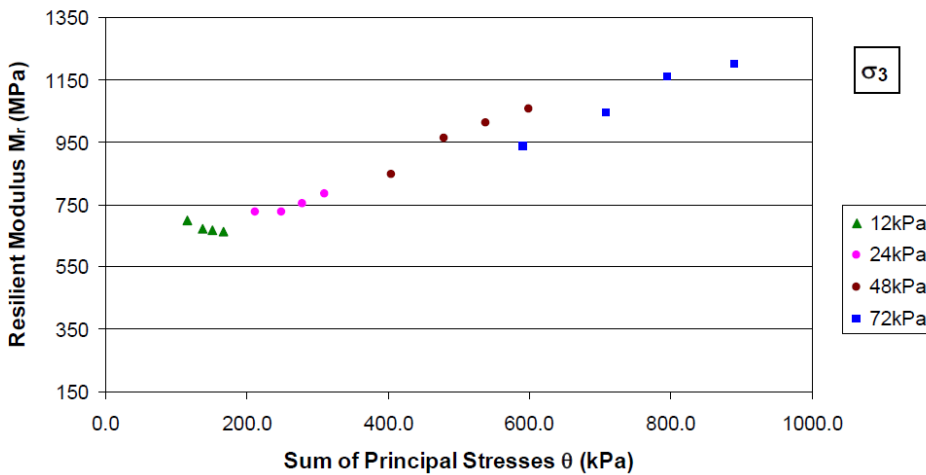


**Figure 2-21:  $M_r$ - $\theta$  relationship for bitumen treated granular material (Jenkins and Rudman, 2016)**

In addition to the cyclic loading resilient deformation test, cyclic loading permanent deformation tests can be performed to predict the long-term dynamic response of granular material. Each test is carried out at a different ratio of applied deviator stress to deviator stress at failure (known as the deviator stress ratio) and requires a new sample. The sample is loaded cyclically up to a million repetitions and the permanent deformation, or plastic strain, of the specimen monitored (Jenkins

and Rudman, 2016). Permanent deformation (PD) can be modelled in terms of two criteria, namely the number of load applications and the stress condition (Bredenkamp, 2018). In this regard, models for PD related to load cycles have been presented, amongst others, by Barksdale (1972), Wolff and Visser (1994), and Huurman (1997), and models related to stress condition have been produced by Barksdale (1972), Paute (1996) and Lekarp and Dawson (1998) (refer to Bredenkamp, 2018).

### 2.5.16.3 Small-strain elastic modulus

As emphasised by Knappett and Craig (2012), soils are typically non-homogeneous and anisotropic and exhibit non-linear stress-strain curves. These relationships are reliant on stress history and the stress path followed and, as such, complicates soil behaviour modelling. As previously mentioned, elastic settlement prediction for foundation design purposes relies largely upon the estimation of soil stiffness. This non-linear stress-strain behaviour of soil implies that the elastic modulus of a soil does not have a unique value. According to Yongqing (2011), an improvement in the understanding of the strain dependency of stiffness in recent years has enabled engineers to derive more consistent and reliable moduli for design. The soil elastic modulus can be obtained from the shear modulus. For this reason, the concept of stiffness degradation will be discussed in terms of shear stiffness. The non-linear behaviour of shear stiffness is shown in Figure 2-22.

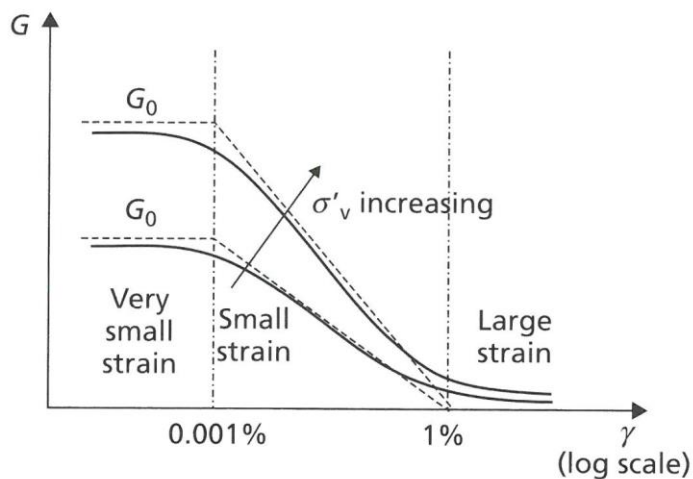


**Figure 2-22: Non-linear behaviour of soil shear stiffness (Knappett and Craig, 2012)**

From the figure it is evident that at very small strain, the shear stiffness value is at its maximum, defined as the small-strain shear stiffness ( $G_0$ ). Similarly, at very small values of normal strain, the small-strain elastic modulus ( $E_0$ ) is recorded. Stiffness moduli can also be expressed in other terms, such as the secant modulus and the tangent modulus. Convergence of the moduli occur at very small strains (Yongqing, 2011). As strain values increase beyond the threshold shear strain of about 0,001% (maximum of 0,002% recorded), stiffness decreases in a non-linear manner. The large stiffness values observed at very small strains are often not applicable to practical engineering problems in which larger strains are induced (Archer, 2014). As such, a knowledge of the small strain stiffness, as well as the stiffness degradation data, is essential for accurate prediction of ground movement. The non-linear stiffness behaviour of soil is illustrated in Figure 2-23 by means of a typical stiffness reduction- or softening curve. The modulus reduction curve is normally plotted as stiffness ( $G/G_0$ ) against shear strain. Shear moduli associated with specific geotechnical applications (strain ranges) are shown in Figure 2-23.

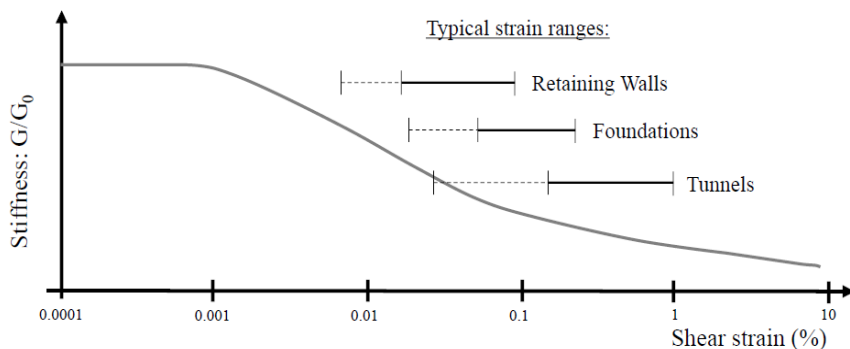


**Figure 2-23: Typical stiffness degradation curve (after Mair, 1993 from Archer, 2014)**

According to Yongqing (2011), the stiffness degradation curve is influenced by factors such as stress state, strain level, stress and strain history, density index, rate of shearing and secondary settlement. In addition, Yongqing observed a difference in the modulus degradation curves obtained from strain-rate controlled triaxial tests and torsional shear tests.

Various authors have developed mathematical equations to represent the modulus reduction curve, based on either strength or stiffness parameters. Archer (2014) lists a number of these softening equations based on strength parameters, including equations by Ramberg and Osgood (1943), Hardin and Drnevich (1972), Prevast and Keane (1990), Mayne (1995), Puzrin and Burland (1996, 1990) and Shibuya et al. (1997). According to Archer (2014), the use of these reduction curves necessitates laboratory or field tests which, in many cases, are impractical. Alternatively, the reduction curves based on stiffness parameters only require a knowledge of the small-strain stiffness and existing strain levels. In this regard, the relationships presented by Rollins et al. (1998), Bolton and Whittle (1999), Atkinson (2000), Clayton and Heymann (2001), Oztoprak and Bolton (2013), and Archer and Heymann (2015), are useful. The stiffness reduction curves proposed by Rollins et al. (1998) and Clayton and Heymann (2001), together with their respective softening equations, are presented in Figure 2-24.

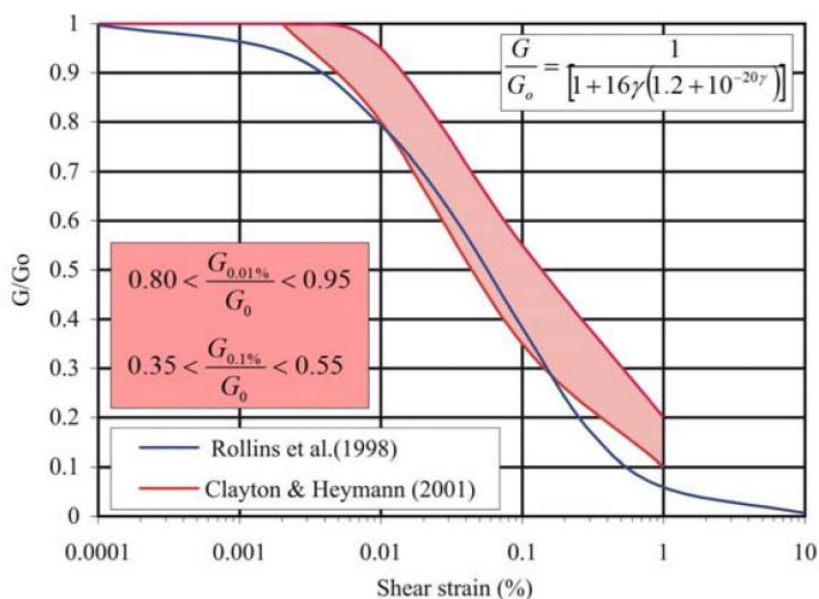


**Figure 2-24: Stiffness degradation functions (Heymann, 2012 as cited in Day, 2016)**

Stiffness reduction functions were also developed by Archer and Heymann (2015) for loose ( $D_r = 20\%$ ), medium dense ( $D_r = 50\%$ ) and dense ( $D_r = 80\%$ ) sands, using a hyperbolic relationship. Centrifuge modelling was used in the development of these functions. Archer and Heymann highlight the increased divergence between measured and predicted reduction curves with an increase in density index. The variables of the fractional formulas and the associated softening curves are given in Chapter 5 and are utilised in the calculation of immediate settlement in the Cape Flats.

Small-strain shear stiffness can be measured in the laboratory by means of bender element testing, resonant column testing and advanced triaxial testing, or in the field, using seismic techniques such as continuous surface wave (CSW) testing, multi-channel analysis of surface waves (MASW) and downhole- or crosshole-geophysics. These methods involve the determination of the wave velocity to calculate small-strain shear stiffness, provided the soil bulk density is known (Archer, 2014).

Small-strain stiffness values obtained by means of seismic geophysical techniques, such as in-situ continuous surface wave (CSW) testing, are now recognised as reliable in the determination of ground stiffness and are becoming more common. The large stiffness values observed at the very small strains obtained using geophysical techniques can be adjusted for actual strain levels applicable to the specific engineering problem. To determine the strain-dependent elastic modulus and subsequently the anticipated foundation settlement, using only small-strain stiffness data, various methods including the non-linear stepwise method can be employed (Moxhay et al., 2008 and Archer and Heymann, 2015). Due to the affordability, rapid execution and non-intrusive and non-destructive nature of the continuous surface wave test (Heymann, 2007), it is a preferred seismic method; providing a practical solution to the ongoing difficulties experienced with accurately calculating the settlement below shallow foundation in sand covered areas such as the Cape flats.

Heymann (2007) gives an in-depth description of the continuous surface wave (CSW) test including its execution, the examination of obtained data and the interpretation of test results. The test is based on the measurement of the velocity of stress waves as they propagate through the ground. According to Heymann, seismic energy is produced during the test using a shaker at ground level which generates primary and secondary body waves known as compression waves and shear waves respectively, as well as surface waves (comprising Love and Raleigh waves). Raleigh waves are preferred for seismic surveys, as the majority of the energy directed at the ground surface, produces these waves and they weaken slowly with increasing distance from the source (Heymann, 2007). When a vertical sinusoidal force is applied to the ground (covering a range of frequencies), a complete profile of Raleigh wave velocities can be attained. Geophones placed at the soil surface, spaced at equal intervals, or varied based on surface wave wavelength, picks-up the Raleigh waves. The components of the CSW testing system are shown in Figure 2-25.

From the known Raleigh wave velocities (and Poisson's ratio), the shear wave velocities can be determined. The accuracy of wave velocity measurements decreases with depth as the source and geophones are placed at the soil surface. Inversion analysis is used to interpret the data by revealing the  $V_s$  profile best fitting the measured data. The small-strain shear stiffness ( $G_0$ ) of the

ground profile can, in turn, be calculated from the shear wave velocity ( $V_s$ ) and the bulk density ( $\rho$ ) (refer to Section 3.3.2.1: Continuous surface wave (CSW) tests in Chapter 3 for the formulas).

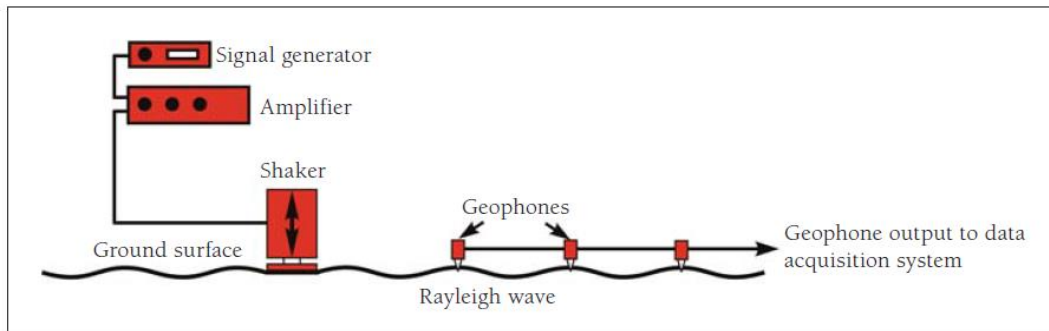


**Figure 2-25: Components of the continuous surface wave system (Heymann, 2007)**

Determination of  $V_s$  from in-situ testing such as CSW testing is favoured, nevertheless, it is often not viable to measure  $V_s$  at all locations (Andrus, Piratheepan and Juang, 2007). In the past 40 years, many researchers have therefore aimed to create statistically generated regression equations, representing shear wave velocity ( $V_s$ ) as a function of penetration resistance. Particular attention has been paid to the standard penetration test (SPT), as it is the penetration test method which has historically been the most widely used (Clayton, 1993). The influence of variables, such as depth (overburden pressure), soil type, geological epoch, fines content, coefficient of uniformity and median particle size, have been included in the regression of  $V_s$  and SPT  $N$  to ultimately accurately predict stiffness for the estimation of settlement. A summary of several existing correlations between  $V_s$  and SPT  $N$  for sands, gravels and soil mixtures is presented in Table 2-16. The information listed in the table illustrates the significant variations in the experimental findings of researchers over the past four decades.

**Table 2-16: Existing  $V_s$ -SPT  $N$  correlations (modified from Bellana, 2009 and Wair, DeJong and Shantz, 2012)**

Author(s)	All soils	Sand	Gravel
Kanai (1966)	$V_s = 19 N^{0.6}$	-	-
Shibata (1970)	-	$V_s = 31.7N^{0.54}$	-
Ohba and Toriuma (1970)	$V_s = 85.3N^{0.31}$	-	-
Fujiwara (1972)	$V_s = 92.1N^{0.337}$	-	-
Ohta et al. (1972)	-	$V_s = 87.2N^{0.36}$	-
Ohsaki and Iwasaki (1973)	$V_s = 81.4 N^{0.39}$	-	-
Imai and Yoshimura (1975)	$V_s = 76 N^{0.33}$	-	-
Imai et al. (1975)	$V_s = 89.9 N^{0.31}$	-	-
Imai (1977)	$V_s = 91 N^{0.337}$	$V_s = 80.6 N^{0.331}$	-
Ohta and Goto (1978)	$V_s = 85.35N^{0.348}$	-	$V_s = 104.6 N^{0.34}$
Seed and Idriss (1981)	$V_s = 61.4 N^{0.5}$	-	-
Imai and Tonouchi (1982)	$V_s = 96.9 N^{0.314}$	-	$V_s = 75.4 N^{0.35}$

Author(s)	All soils	Sand	Gravel
Sykora and Stokoe (1983)	-	$V_s = 100.5N^{0.29}$	-
Jinan (1987)	$V_s = 116.1 (N + 0.3185)^{0.202}$	-	-
Okamoto et al. (1989)	-	$V_s = 125 N^{0.3}$	-
Lee (1990)	-	$V_s = 57.4 N^{0.49}$	-
Dickenson (1994)	-	$V_s = 88.4(N+1)^{0.3}$	-
Lum and Yan (1994)	-	-	$V_s = 116 (N_{60})^{-27}$
Athanasopoulos (1995)	$V_s = 107.6N^{0.36}$	-	-
Sisman (1995)	$V_s = 32.8 N^{0.51}$	-	-
Iyisan (1996)	$V_s = 51.5 N^{0.516}$	-	-
Jafari et al. (1997)	$V_s = 22 N^{0.85}$	-	-
Rollins et al. (1998)	-	-	$V_s = 63 (N_{60})^{0.43}$ $V_s = 132(N_{60})^{0.32}$
Pitilakis et al. (1999)	-	$V_s = 145(N_{60})^{0.178}$	-
Kiku et al. (2001)	$V_s = 68.3 N^{0.292}$	-	-
Hasancebi and Ulusay (2006)	$V_s = 104.79 (N_{60})^{0.26}$	$V_s = 131(N_{60})^{0.205}$	-
Dikmen (2009)	$V_s = 58 N^{0.39}$	$V_s = 73 N^{0.33}$	-

The substantial differences observed in the correlations obtained via regression analyses by the respective investigators can be attributed to the following (Bellana, 2009):

- **Measurement of shear wave velocity.** Several different methods were used to measure shear wave velocity, such as seismic CPT, cross-hole and down-hole seismic methods, seismic refraction, spectral analysis of surface waves (SASW) and suspension logging. For each of these methods, the shear wave velocity measurements vary in terms of the resolution provided at various depths in the soil profile.
- **Correction of SPT N-values.** The N-values listed in Table 2-16 are inconsistently corrected for hammer energy, rod length and sampler inside diameter. In addition, the N-values are generally not corrected for overburden pressure. Bellana (2009) highlights the fact that shear wave velocity and SPT blow count normalise in a different way with overburden pressure and that regressions excluding the influence of test depth (i.e.  $V_s$  versus N) will introduce significant bias. This aspect will be discussed in more detail in subsequent sections.
- **Geological differences.** According to Wair, DeJong and Shantz (2012) the stiffness and compressibility of soils and rock are affected by geological processes such as sedimentation, glaciation and uplift (loading and unloading cycles). Other processes such as cementation, chemical reactions and fluctuations in groundwater also influence the estimation of soil stiffness. Geological age (associated with soil cementation) affects soil stiffness by altering the void ratio.  $V_s$  (and subsequently  $G_0$ ) has been found to be directly related to void ratio, thus proving the relationship between geological age and soil stiffness. The influence of geological age on void ratio, and in turn, on shear wave velocity, has been investigated by Ohta and Goto

(1978), Fumal (1978), Sykora and Stokoe (1983), Fumal and Tinsley (1985), and Bellana (2009). An overview of their findings is given below. The original work of the earlier studies (1978 to 1985) could not be obtained and are cited from Sykora (1987).

In 1978, Yutaka Ohta and Noritoshi Goto from Hokkaido University in Japan published their findings on the influence of geological age on the void ratio of geo-materials. A summary of the results for clays and sands are shown in Figure 2-26. For sand deposits, a slight decrease in void ratio with geological age in the younger alluvium and diluvium, can be seen. Void ratio decreases more steeply with geological age in the tertiary aged (and older) sand deposits. It is also evident that void ratio decreases more rapidly and linearly with geological age in the clay soils, compared to the sands. Ohta and Goto (1978) determined the ratio of shear wave velocity of diluvial sands to that of alluvial sands to be 1.44, however, they concluded that the difference in shear wave velocity between the deposits cannot solely be attributed to void ratio.

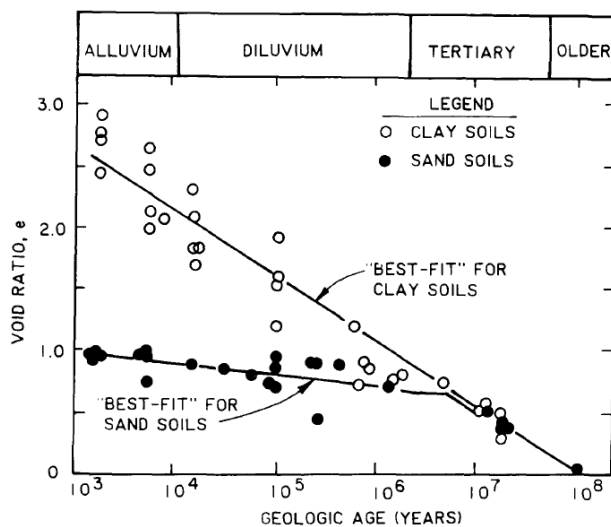


**Figure 2-26: Influence of geological age on void ratio for sand and clay soils (Ohta and Goto, 1978 from Sykora, 1987)**

The relationship between shear wave velocity and void ratio has been investigated by Fumal (1978) and Fumal and Tinsley (1985). For their studies, in-situ measurements of shear wave velocity were made in California sands, and the void ratio of representative field specimens was determined. Fumal and Tinsley (1985) found that shear wave velocity is highly dependent on void ratio, particularly at void ratios below 0.6. Their findings, which suggest that Pleistocene-age soils have a higher dependence of shear wave velocity on void ratio than Holocene-age soils, are summarised in Figure 2-27.

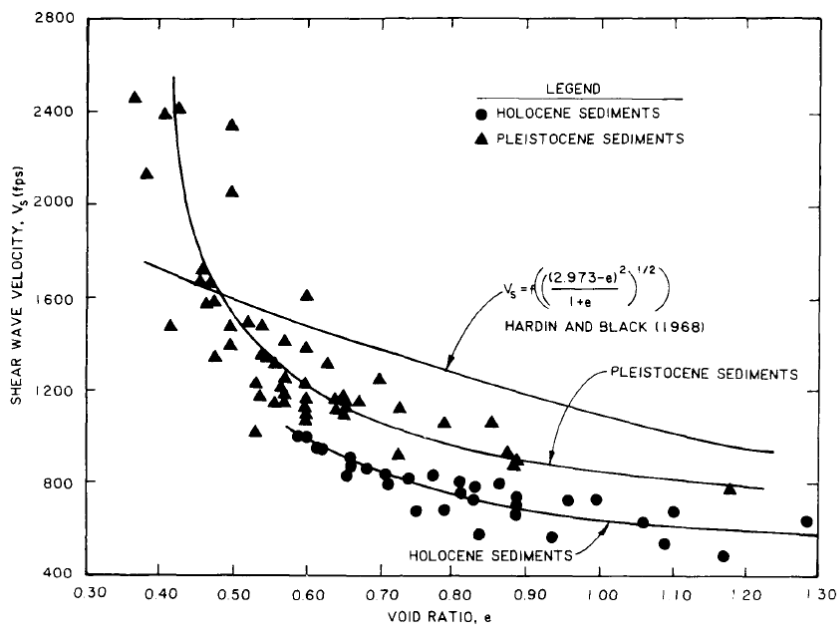


**Figure 2-27: Shear wave velocity versus void ratio for soils of different geological age (Fumal and Tinsley, 1985 as cited in Sykora, 1987)**

The influence of surface geology on  $V_s$  was studied by Bellana (2009). The results of the analyses are presented in Figure 2-28, in which the non-dependency on surface geology is evident. This result is consistent with selected previous studies, in which it was found that the surface geology and type of soil present are not predictive of shear wave velocity (e.g. Sykora and Stokoe, 1983). Nonetheless, Bellana noted that the  $V_s$ - $N_{60}$  data pairs were obtained from a range of depths where vertical changes in geological age occur, thus providing a possible explanation for the findings.

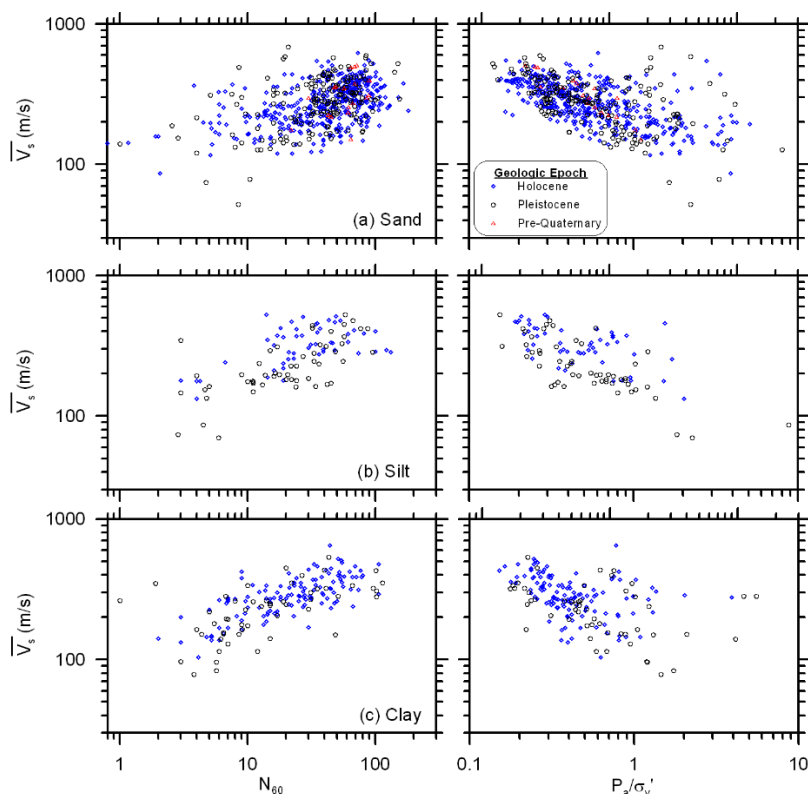


**Figure 2-28: Shear wave velocity versus SPT  $N_{60}$  and  $P_a/\sigma'_v$  (overburden correction term) for sand, silt and clay soils of different geological age (Bellana, 2009)**

The earliest correlations between  $V_s$  and SPT N were presented by researchers from Japan. Sykora (1987) provides an overview of a number of these studies. In this regard, the research carried out by Shibata (1970) and Ohsaki and Iwasaki (1973) is discussed below. It should be noted that the SPT blow counts utilised in these initial studies were not corrected for overburden, hammer energy, rod length, or sampler inside diameter.

To obtain a correlation between  $V_s$  and SPT N, Shibata (1970) analysed results from several researchers in which the factors influencing  $V_s$  were studied. Shibata aimed to address the effect of density (for sands) and effective overburden pressure on  $V_s$  and SPT N. Combining the research of various authors, Shibata found that the log N-log  $\sigma_v$  relationship is linear for any specific relative density, with a slope of almost 0.5, and that the log N-log  $D_r$  relationship is linear for any specific effective overburden stress, with a slope of almost 2.0. Shibata also studied soil porosity ( $n$ ) and concluded that SPT N is a linear function of  $(n_{max}-n)$  for a specific overburden pressure. In Figure 2-29, the existing laboratory data used by Shibata are plotted to display the linear relationship between SPT N and  $(n_{max}-n)$ . The following equation was subsequently obtained:

$$SPT\ N = A(n_{max} - n)\sigma_v^{-0.5} \quad (\text{blows/ft}) \quad \text{Equation 2-17}$$

A = constant between 57 and 61  
 $\sigma'_v$  = Effective stress (PSI)

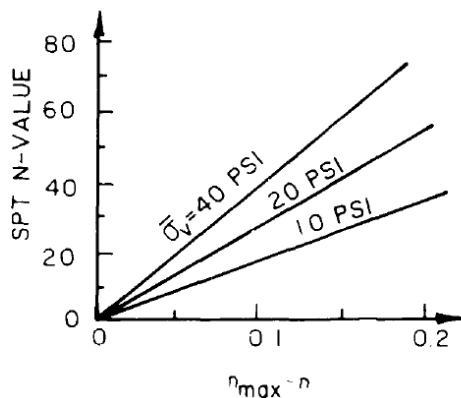


**Figure 2-29: Existing laboratory data showing SPT blow count versus  $(n_{max} - n)$  for different overburden values (Shibata, 1970 as cited in Sykora, 1987)**

By linking the work of selected researchers, Shibata found that  $V_s$  could be expressed as a function of SPT N, porosity and effective overburden pressure. Then, combining Equation 2-17, and Equation 2-18 presented by Toki (1969) (refer to Sykora, 1987), Shibata subsequently developed Equation 2-19 which is independent of effective overburden pressure and porosity, but dependent on soil type (only relevant for sands).

$$V_s^2 = A'(n_{max} - n)\sigma_v^{-0.5} \quad (\text{ft}^2/\text{s}^2) \quad \text{Equation 2-18}$$

Where  $A' = 5.7 \times 10^5$

$$V_s = 104N^{0.5} \quad (\text{ft/s}) \quad \text{or} \quad V_s = 31.7N^{0.5} \quad (\text{m/s}) \quad \text{Equation 2-19}$$

Ohsaki and Iwasaki (1973) focussed on finding a basic connection between shear modulus ( $G$ ) and uncorrected SPT  $N$  for a combination of soils, by undertaking statistical analyses on more than 200 data sets.  $V_s$  was determined mainly by means of the down-hole seismic method. Based on the accumulated data, Ohsaki and Iwasaki developed Equation 2-20 from which Equation 2-21 was obtained assuming the unit weight of the soil to be 112.4 pcf (1800 kg/m<sup>3</sup>) (typical value for soils in Japan).

$$G = 11.9N^{0.78} \quad (\text{MPa}) \quad \text{Equation 2-20}$$

$$V_s = 81.4N^{0.39} \quad (\text{m/s}) \quad \text{Equation 2-21}$$

Ohsaki and Iwasaki also performed statistical analyses on subsections of their data records by separating the information into sets, based on geological epoch and soil type and found that the most precise relationship between shear modulus and SPT  $N$  is independent of geological age and soil texture. Notwithstanding this, only independent use of either variable was utilised in the regression.

Since these earliest publications, a significant number of other correlations between  $V_s$  and SPT  $N$  have been published for different soil types worldwide. Some of the more recent works are briefly summarised below.

Rollins et al. (1998) combined existing investigation results to establish a strong correlation between  $V_s$  and SPT  $N_{60}$  (from Becker penetration tests) for Holocene and Pleistocene gravels. Rollins et al. found that correlations with  $N_{60}$  is more favourable than correlations with  $(N_1)_{60}$ , therefore an average  $N_{60}$  value was used within a region of constant shear wave velocity. A data set comprising of 186 points from seven sites was used to obtain the following regression equation for Holocene deposits (with  $R^2 = 0.59$ ):

$$V_s = 63(N_{60})^{0.43} \quad (\text{m/s}) \quad \text{Equation 2-22}$$

105 data points from 5 sites were used to produce the following equation for Pleistocene gravels ( $R^2 = 0.48$ ):

$$V_s = 132(N_{60})^{0.32} \quad (\text{m/s}) \quad \text{Equation 2-23}$$

Rollins et al. found that the curve derived for the Holocene gravels is about 40 – 70% lower than that for the Pleistocene gravels. In addition, it was noted that the estimation of shear wave velocity can become slightly more accurate by incorporating the vertical effective stress as a separate term in the regression. In this regard, the best-fit equations for Holocene and Pleistocene aged gravels are given by Equations 2-24 and 2-25 respectively.

$$V_s = 53(N_{60})^{0.19} \cdot (\sigma'_0)^{0.18} \quad (\text{m/s}) \text{ (Holocene)} \quad \text{Equation 2-24}$$

$$V_s = 115(N_{60})^{0.17} \cdot (\sigma'_0)^{0.12} \quad (\text{m/s}) \text{ (Pleistocene)} \quad \text{Equation 2-25}$$

Rollins et al. established that the  $V_s$  values obtained by the  $V_s$ - $N_{60}$  models are within approximately  $\pm 30\%$  of the measured  $V_s$  values. From the results presented by Rollins et al. it was concluded that  $V_s$  estimates for the Pleistocene sediments are notably higher than those calculated for the

Holocene sediments when compared at a specific SPT N value. In this regard, Rollins et al. recommends that these Quaternary deposits be divided, based on geological age before individual correlations are obtained.

The main aim of the research carried out by Andrus, Piratheepan and Juang (2007) was to improve on the existing relations between  $V_s$  and penetration resistance from CPT and SPT test data for the evaluation of ground shaking and liquefaction risk. The section below will focus on their findings, specifically concerning the  $V_s$ -N relationships obtained for the Holocene sandy deposits from California, Japan and Canada.

As part of the research project, sixty-three  $V_s$ -N data pairs from existing reports and published literature were used. Most of the shear wave velocity measurements were made via crosshole, downhole or seismic CPT methods. Andrus, Piratheepan and Juang (2007) considered  $V_s$ ,  $V_{s1}$  ( $V_s$  corrected for overburden),  $N_{60}$ ,  $(N_1)_{60}$ , depth (D), amount of fines (FC), uniformity coefficient ( $C_u$ ) and median particle size ( $D_{50}$ ) in the regression analyses. By grouping the information by fines content and exploring with various variable combinations, several meaningful equations emerged (see Table 2-17). It is evident from the table that the uncorrected equations (based on  $V_s$  and  $N_{60}$ ) produce slightly improved fits as opposed to the stress corrected equations, in which the coefficient of determination ( $R^2$ ) of the regression is lower. Andrus, Piratheepan and Juang explains that this may be due to the additional independent variable of depth included in the uncorrected correlations.

**Table 2-17: Regression equations for Holocene sands grouped by fines content (Andrus, Piratheepan, Juang, 2007)**

Regression equations for predicting shear wave velocity (m/s)		Number of data pairs	Coefficient of determination ( $R^2$ )	Standard deviation error (m/s)
FC < 10%	$V_s = 66.7(N_{60})^{0.248}D^{0.138}$	25	0.823	14.8
FC = 10 – 35%	$V_s = 72.3(N_{60})^{0.228}D^{0.152}$	10	0.951	8.4
FC = 0 – 40%	$V_s = 72.9(N_{60})^{0.224}D^{0.130}$	39	0.788	15.5
FC < 10%	$V_{s1} = 95.5(N_1)_{60}^{0.226}$	28	0.688	17.5
FC = 10 – 35%	$V_{s1} = 103.4(N_1)_{60}^{0.205}$	13	0.878	11.7
FC = 0 – 40%	$V_{s1} = 101.8(N_1)_{60}^{0.205}$	45	0.719	16.7

The research undertaken by Bellana (2009) aimed to create statistically generated regression equations, representing  $V_s$  as a function of  $N_{60}$  and  $\sigma'_v$ . 918 data pairs of SPT  $N_{60}$  and  $V_s$  values were used in the regression analyses, where  $V_s$  measurements were acquired via suspension logging. Bellana (2009) explored the influence of overburden pressure in his comparative studies, which has been overlooked in numerous previous studies. As a result of the difficulties in accurately calculating  $V_{s1}$  and  $(N_1)_{60}$  from  $V_s$  and  $N_{60}$ , as explained by Bellana (2009), the overburden correction was not directly applied to  $V_s$  and  $N_{60}$ , but an independent  $\sigma'_v$  term was considered. Power regressions were performed separately for sand, silt and clay, producing statistically significant regression equations (refer to Bellana, 2009 for regression parameters).  $V_s$  was then plotted against N (with trendlines from various  $P_a/\sigma'_v$  values) and  $P_a/\sigma'_v$  (with trendlines through various N values) to reveal the influence of the variables on the relations.

Bellana (2009) found that, in the case of sands,  $V_s$  correlates better with  $P_a/\sigma'_v$  than  $N_{60}$ . For silts and clays on the other hand, a better correlation exists between  $V_s$  and  $N_{60}$ . As mentioned previously in this section of literature, Bellana also investigated the influence of surface geology on  $V_s$  and SPT N-values, however, no meaningful trends emerged.

## 2.6 Aeolian deposits of the interior of Southern Africa

According to Brink (1985), windblown sands cover approximately half of southern Africa. The uppermost aeolian formation of the Kalahari Group, known as the Gordonina Formation (and informally termed Kalahari sand) is present in the Northern Cape and found scattered within the North West Province, the Free State and parts of the semi-arid Karoo (Johnson, Anhaeusser and Thomas, 2006). Outside the boundaries of South Africa, these sands are widespread in Botswana, extending into eastern Namibia and western Zimbabwe (Brink, 1985). According to Baillieul (1975) (as cited in Brink, 1985), the Kalahari sands constitute the largest continuous sand body in the world. The distribution of the Kalahari sands can be viewed in map form in Johnson, Anhaeusser and Thomas (2006), showing the vast extent of the main sand body. In addition, the units of the Kalahari Group, comprising amongst others, pebble and boulder clasts of the Obobogorop Formation and calcretes of the Mokalanen Formation, can also be viewed in Johnson, Anhaeusser and Thomas (2006).

The engineering properties of the Kalahari sands have been studied and described by Schwartz and Yates (1980), Schwartz, Yates and Tromp (1981) and Brink (1985). The findings of their work are given below and compared to the Cape Flats sands where appropriate. The engineering properties are summarised in Table 2-18, for later comparison with the windblown sands from the study area.

Typical grading analysis reveals uniformly graded, fine and medium sands (Schwartz and Yates, 1980). According to Brink (1985), dominant particle size varies in dune areas in relation to changing wind velocities. Fines are typically concentrated in interdune areas. These fines fill spaces between larger grains and are thereby remaining protected from further wind transportation (Lancaster, 1984 as cited in Brink, 1985). The widespread distribution of these sands leads to variation in fines content through differences in climate and the role that this plays in the development of the soil profile. In the Welkom area, located close to the Weinert  $N = 5$  line, fines contents of the order of 40% have been noted (Brink, 1985). The sands are typically non-plastic or slightly plastic, although measurable plasticity indices can be found in sands with appreciable fines contents. Individual particle grains have been described as rounded (Johnson, Anhaeusser and Thomas, 2006). The above description aligns closely with the typical broad textural description applied to the Cape Flats sands.

The predominantly fine sands with varying fines contents typically have relatively low permeability and, together with the low rainfall prevalent in most of their occurrences in southern Africa, this impedes recharge of the underlying aquifer where thick sand successions occur (Brink, 1985). Conversely, it is estimated that approximately 15% to 37% of the annual precipitation in the Cape Flats area recharges groundwater in the Cape Flats aquifer (GEOSS, 2014).

In the upper 3m of the Kalahari sands, the in-situ dry density has been found to vary between  $1550\text{kg/m}^3$  and  $1675\text{kg/m}^3$ , with the in-situ moisture content ranging from 2.5% to 5% (Schwartz, Yates and Tromp, 1981). In the Cape Flats, a larger range in in-situ density is anticipated in the

shallow soil profile, with the calcretised sands from the Witzand and Langebaan Formations most likely associated with higher bulk densities. The typically shallow water table in the study area will also result in higher in-situ moisture contents.

Compaction of disturbed bulk samples of Kalahari sands using modified AASHTO compaction produces an average maximum dry density of  $1841\text{kg/m}^3$  with an average optimum moisture content of 9.1% (Schwartz and Yates, 1980). Viewing the Kalahari sands under the microscope reveals that the quartz sands are covered with yellow isotropic material, forming a bridging material between adjacent sand grains (Schwartz and Yates, 1980). These bridges were found to be from clay-sized particles of ferric oxides (providing the yellow colour) and kaolinite. The bridging material will influence in-situ compaction, requiring the addition of water or mechanical breakdown to achieve proper compaction. Average California Bearing Ratio values of 50% and 20% at densities of 100% and 95% of modified AASHTO compaction effort have been found (Schwartz and Yates, 1980).

In a partially saturated condition, Kalahari sands have relatively high shear strengths due to negative pore water pressures (suction) and the kaolinite bridges. Upon saturation, this apparent strength will be lost. The results of drained saturated direct shear tests on Kalahari sands from Welkom and Jwaneng in south-eastern Botswana, reveals an effective cohesion of zero and effective friction angles between  $31^\circ$  and  $36^\circ$  (Brink, 1985). Using Terzaghi's local shear criteria and typical shear strength parameters, Schwartz and Yates (1980) obtained an ultimate bearing capacity of 300kPa for the Kalahari sands.

The presence of kaolinite bridging material may also give rise to a collapsible fabric. Even in its absence, iron oxides, calcium carbonates or other soluble salts may form bridges between quartz grains. Clayey and silty sands from Welkom were subjected to consolidometer testing to determine their collapse potential. A maximum collapse potential of 9.3% was obtained, described as "trouble" according to criteria given by Jennings (1974) (refer to Table 3-9 in Chapter 3). Notwithstanding this, sands with very low clay contents characteristic of some areas, are likely to be non-collapsible or slightly collapsible in nature (in the absence of strong chemical bonds). In addition, sands occurring within the zone of shallow groundwater fluctuation, usually lack a collapse fabric as the bridging material is leached away. Schwartz and Yates (1980) investigated the compressibility and collapse characteristics of the sands by performing plate bearing tests. The elastic modulus was calculated at in-situ moisture content and after saturation and showed to decrease from approximately 8MPa to 2MPa when saturated. The sands were saturated at pressures of 35kPa and 110kPa. At both these pressures, significant collapse settlement occurred. Test results also showed that differential settlements can be as high as 95% of the total settlement (average of 90%).

Considering the above, construction on or with the Kalahari sands necessitates consideration of the presence of a collapsible soil fabric. The collapsibility of Kalahari sands has been determined by means of on-site plate bearing tests as well as laboratory procedures such as double oedometer and collapse potential tests. Conventional penetration test procedures are considered unsuitable for the identification of collapsible soils. Densification or collapse of Kalahari sands supporting buildings, roads and airfields have been reported by various authors (Brink, 1985). Severe differential settlement can occur upon localised wetting. Flexible pavements may be affected by collapse settlement due to static and dynamic traffic loads.

In-situ densification of Kalahari sands with a collapsible fabric has been attempted using impact and vibratory rollers. In this regard, densities exceeding 100% of modified AASHTO MDD in the upper 1m of the soil profile, decreasing to 93% of MDD at 4m depth, have been recorded (Wolmarans and Clifford, 1975 as cited in Brink, 1985). Inconsistent outcomes have however been achieved using similar densification procedures in subsequent projects, particularly where the sands are dry and lightly cemented. In general, little to no improvement in in-situ density was noted below 1m depth following densification using various techniques (Brink, 1985). Stabilisation using bitumen has been found to improve the aeolian soils to subbase and base quality road building materials (Brink, 1985).

According to Brink (1985) the Kalahari sands are of major engineering importance, and the value of investigating their engineering properties is evident. The engineering properties of the Kalahari sands are summarised in Table 2-18.

**Table 2-18: Engineering properties of Kalahari sands (compiled after Schwartz and Yates, 1980 and Brink, 1985)**

Property	Value/description		
<b>Texture</b>	Fine and medium sand, uniformly graded. Maximum fines content up to 40% noted in the Welkom area.		
<b>Plasticity</b>	Generally non-plastic and slightly plastic.		
<b>Atterberg limits</b> (Soils from Welkom area in the Free State with fines contents up to 40%)	<b>LL (%)</b>	<b>PI (%)</b>	<b>LS (%)</b>
Range	0 - 34	0 – 19	0 – 9.3
Average	18.6	7.4	3.7
Number of tests	7	7	7
Standard deviation	13.4	7	3.3
<b>In-situ density (kg/m<sup>3</sup>) (upper 3m of soil profile)</b>			
Range	1550 – 1675. Density found to increase with depth.		
<b>In-situ moisture content (%)</b>			
Range	2.5 - 5		
<b>Maximum dry density (Modified AASHTO) (kg/m<sup>3</sup>)</b>			
Average	1841		
<b>Optimum moisture content (%)</b>			
Average	9.1		
<b>CBR (%)</b>	<b>100% of MDD</b>	<b>95% of MDD</b>	
Average	50	20	
<b>Shear strength</b>	<b>Friction angle (°)</b>	<b>Cohesion (kPa)</b>	
Range	31-36	0	
<b>Collapsibility</b>	Collapse potential test		Plate load test
Maximum	9.3%	Highly collapsible. A slight decrease in collapsibility from 2m depth.	
Elastic modulus	Decreases from approximately 8MPa to 2MPa when saturated at 35MPa and 110MPa during plate load testing (from in-situ moisture content).		

## 2.7 Evaluation of literature themes

Whilst investigating existing literature concerning the engineering geological and geotechnical properties of the Cape Flats, limited published works, including those by Amdurer (1956), Brink (1985) and Stapelberg (2009) were obtained. Summaries of their research findings are given in Section 2.3.2. The investigative work carried out by Amdurer (1956) and Stapelberg (2009) will supplement the proposed research. The significance of the outcome of the current research will not be influenced by these prior works.

Stapelberg (2009) focussed on civil development potential and, as such, only descriptive information is provided and a severity class assigned to give an indication of possible geotechnical issues, their extent and the cost implications. Apart from the determination of soil permeability by means of a standpipe permeameter, no other calculated or measured soil parameter values are given. By combining the findings of the investigative work, Stapelberg described the engineering geological nature of the Cape Flats sands in a broad sense. It should be noted that these findings are based on a limited number of investigative points concentrated in selected areas. Variations and nuances in soil parameters occur both in horizontal and vertical directions and over small distances (even within the bounds of the individual formations) and, as such, no typical soil profile exists.

The research carried out by Amdurer dates to 1956 and was largely dedicated to unfolding the geological processes functioning within the Cape Flats, as well as the geological implications of individual soil features. The soil properties considered in the engineering geological description of the soils included the shear strength, compaction characteristics, relative density and limits of consistency. The shear strength and limits of consistency of only the cohesive layers occurring intermittently with the sandy soils and the underlying residual Malmesbury soils were investigated, whereas the current research is concerned with the windblown sand horizons of the Cape Flats. In addition, the compaction characteristics and relative density were studied over a small area and including a limited number of data points.

Both studies only considered a portion of the Cape Flats, and not encompassing the extent of characterisation and classification intended for the current research. As a result of the geographical and investigative limits associated with prior research, the analysis of large quantities and a wide range of geotechnical data, accurately representing the nature of the Cape Flats soils, has not been possible. The extent of the current study will allow statistical analyses of data, revealing significant trends, including vertical and horizontal (intra-formation) variations in the study area. Regression analyses (multiple linear and non-linear) will be performed to produce predictive models, involving interrelated soil parameters to enable future prediction of classification and design parameters. The number of soil parameters included in the proposed study and the extent to which these parameters will be explored and analysed, is unique when considering prior research involving the Cape Flats sands.

The importance of investigating aeolian sands in general and the need for this particular research are also supported by extensive past research on the Kalahari sands which constitute the largest continuous sand body in the world.

## 3. Methodology

### 3.1 Introduction

In this chapter the methods used to achieve the objectives set out in Section 1.3 of Chapter 1 are presented. The collection of existing geotechnical data from geotechnical and civil engineering consultants, contractors and laboratories, is discussed, including the type, quantity, distribution and quality of the data. The field and laboratory methods undertaken to obtain experimental data, most often to supplement less investigated classification and characterisation parameters, will then be described, rounding out the data for processing. The processing methods are described in this chapter, involving sorting and input of raw data, followed by the determination or estimation of soil parameters from in-situ and laboratory results, using established methods and transformation models. Finally, output data analysis is performed to extract meaningful information for interpretation and discussion.

### 3.2 Method overview

The research methodology flow chart is given in Figure 3-1.

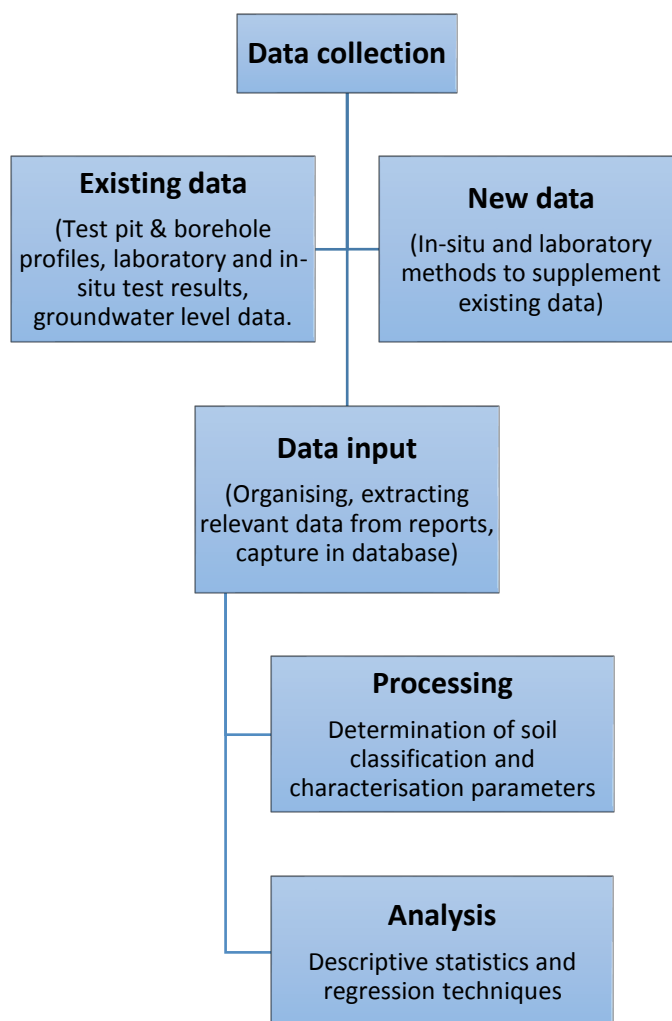


Figure 3-1: Flow chart of methodology

### 3.3 Data collection

#### 3.3.1 Existing data

The success of the current research project relies heavily upon the quantity and quality of geotechnical data obtained and, for this reason, the author approached reputable consultants, contractors and laboratories in the Cape Town area for data collection. Over the period extending from January 2016 to June 2019, investigative data was gathered from 14 geotechnical practises operational in the Cape Flats. In-situ and laboratory data from 155 site investigations undertaken within the boundaries of the study area - translating to 953 soil investigation points (i.e. test pits, boreholes, in-situ tests (not counting SPT's in a BH), and groundwater monitoring wells/sampling locations) - were collected and recorded. The obtained investigation reports date back to 1965. At each of the 953 soil investigation points, one or more of the following data types were obtained:

**Test pit or rotary cored borehole profiles.** The description of the soil profile forms the basis of any geotechnical investigation, and it encompasses the moisture content, colour, consistency, structure, soil type and origin (Jennings, Brink and Williams, 1973). In addition to the six basic descriptors, the position of a permanent or perched water table is also recorded, and any other pertinent information such as sidewall stability, refusal on hard horizons and the depths of sample collection or in-situ testing. The position of the test pit or borehole is typically given in the form of coordinates, with or without a collar elevation. The geological formation was often noted on the profile or log sheet. Where this was not the case, it was obtained from the relevant geological map using the given coordinates. Identifying the geological formation is key to the interpretation of the results, informing inter-formation variation. Springfontyn Formation deposits underlie the sands from Witzand Formation, and borehole logs were examined to identify and note any change in the soil formation with depth.

**In-situ test results.** The results from in-situ penetrometer, stiffness, infiltrometer, and density tests were collected. The penetration test results included SPT blow count data, CPT point and side friction resistance (from mechanical CPT's), and DCP penetration resistance. DCP data was only collected and recorded where the DCP profiles were available in electronic format. In this regard, the quantity of data gathered was considered sufficient for characterising in-situ soil strength and allowing comparison with laboratory-derived soaked CBR values. DPSH test results were excluded from processing and analysis as the influence of skin friction on the driving rods may lead to falsely high penetration readings (refer to Section 2.4 in Chapter 2). The results from plate load tests previously undertaken in the study area, encompassing plate bearing pressure and displacement, were collected, as well as infiltration rates from double ring infiltrometer tests and in-situ density values from density gauge readings.

**Laboratory test results.** The standard laboratory procedures from which soils data/properties were obtained, included index property tests (sieve and hydrometer analysis, and standard tests for the liquid, plastic and shrinkage limits, and natural moisture contents), moisture density relationship tests, California Bearing Ratio (CBR) tests, collapse potential tests, consolidated drained direct shear tests, soil chemical analysis, and tests to determine the specific gravity of the soil solids (water pycnometer). To perform these tests, representative disturbed or undisturbed samples were collected from the study area during the past investigations. In some cases, the

sampled material was remoulded to satisfy the specimen requirements for testing. All tests were performed in accordance with ASTM, TMH1 or SABS standards.

**Permanent of perched groundwater level.** In addition to the permanent and perched groundwater levels from the investigation reports, groundwater level data was also obtained from piezometers installed at the Cape Town International Airport (located in the study area) during a previous investigation and subsequently monitored over an extended period to determine the magnitude of seasonal groundwater fluctuations. Furthermore, groundwater level data was retrieved from the National Groundwater Archive (NGA) over the period January 2013 to December 2017. Since then, the archive has not been regularly updated. The data originated from monitoring wells installed by the City of Cape Town's Department of Water and Sanitation on sites within the Cape Flats. The NGA groundwater records are freely available to the public, which allowed the author to gather groundwater level data from 16 wells distributed over the study area.

To retrieve the groundwater level data from the NGA, the latitude and longitude coordinates demarcating the area of interest, first had to be specified. A list of the monitoring wells present in the specific area was then created, which was exported as a MS Excel spreadsheet. For each monitoring well, the following information was given: Data owner (Department of Water and Sanitation), borehole identifier/number and latitude and longitude coordinates. For many boreholes, no groundwater data existed for the selected time period or was inconsistently monitored (isolated groundwater level measurements or consistent measurements over a very short period). In a limited number of boreholes, water level measurements were made regularly over extended periods of time. The date and time of water level measurements were specified alongside the 71 measured levels from the 16 wells. It should be noted that the number of measurements and the monitoring period associated with each borehole varied significantly.

The locations of soil investigation points (test pits, boreholes, in-situ tests and water level monitoring/sampling locations), are given in Appendix C as Figures C1 to C14, each figure showing the distribution of points relating to a specific data type. These points include data obtained from experimental procedures during the current research. Reference to each figure will be made in the relevant section presented forthwith. A summary of the data collected from the external sources and current experimental procedures by the candidate is presented in Section 3.3.2. **The complete data set on which the characterisation of the Cape Flats is based is given in Section 3.4.**

### **3.3.2 Additional data**

Much of the data used in this research comes from existing site investigation reports and external sources as described in Section 3.3.1. The information obtained reflects traditional methods of investigation, commonly employed in the area, which tend to be limited. New or different methods of investigation and testing have been included in this research, by way of fieldwork or laboratory testing, carried out by the candidate. It should be noted that many of these additional investigations were sponsored and were typically undertaken alongside planned investigations by geotechnical consultants to facilitate access to sites and reduce costs. This placed limitations on the fieldwork in particular, which were restricted to sites on the Witzand and Springfontyn Formations.

### 3.3.2.1 Fieldwork

#### Soil and groundwater sampling

To supplement the existing data, samples of soil and groundwater for laboratory testing were taken from seven sites in the study area. The aim was to provide additional data where information on a specific classification or characterisation property was limited or absent (e.g. minimum density). The samples taken and the tests performed on the soils and groundwater from each of the sites, are given in Table 3-1. Selected photos from the investigated sites are shown in Figures 3-2 to 3-4.

**Table 3-1: Soil and groundwater sampling details**

Sampling site (date sampled)	Coordinates of site	Typical profile (Formation)	Sampling method and depth	Laboratory tests	Notes
Capricorn (May 2017)	<b>Latitude:</b> 34° 5'35.00"S <b>Longitude:</b> 18°29'29.97"E	No test pitting. From CPTu SBTn plot: Medium dense and dense, becoming very dense from approx. 5m, sand and silty sand to final test depth of 10m. (Witzand)	<b>Disturbed sample:</b> Approx. 10kg of surficial sands.	Sieve analysis	Grading results to enable estimation of permeability and collapse potential. Used in conjunction with in-situ density values.
Mfuleni (April 2018)	<b>Latitude:</b> 34° 0'18.52"S <b>Longitude:</b> 18°41'15.56"E	Slightly moist to very moist, light grey brown, medium dense and dense, structureless, slightly cemented fine sand to ≥2.5m. (Witzand)	<b>Disturbed sample:</b> Approx. 650kg between 0-2m depth. <b>Undisturbed samples:</b> 6 large block samples between 0-1m. <b>Groundwater:</b> One 5 litre container from 1m depth in TP.	Sieve analysis, constant head permeability, direct shear, funnel test, specific gravity test, modified AASHTO compaction, triaxial, collapse potential (on undisturbed sands), and chemical analysis (on groundwater).	For undisturbed sampling 300mm diam. PVC pipes were pushed into ground (excavator assistance). Samples collected from 0-0.3m, 0.3-0.6m and 0.6-0.9m at two positions
Blue Downs (May 2018)	<b>Latitude:</b> 34° 0'50.43"S <b>Longitude:</b> 18°42'45.35"E	Slightly moist, light grey, loose and medium dense, structureless, fine sand to 0.8 m depth underlain by residual Malmesbury shale. (Witzand)	<b>Disturbed sample:</b> Approx. 60kg between 0-0.8m.	Sieve analysis, constant head permeability, direct shear, funnel test, specific gravity test.	No groundwater table intersected.
Mitchells Plain (August 2018)	<b>Latitude:</b> 34°01'38.2"S <b>Longitude:</b> 18°34'39.0"E	Sandy fill to 0.9m underlain by light yellowish grey, medium dense to very dense, intact	<b>Disturbed sample:</b> Approx. 60kg between 0.9-1.3m.	Sieve analysis, constant head permeability, direct shear, funnel test, specific gravity test.	No groundwater table intersected.

		fine to coarse sand to $\geq 1.3\text{m}$ . (Witzand)			Refusal in dense sand with TLB.
Gatesville (October 2018)	<b>Latitude:</b> 33°58'52.2"S <b>Longitude:</b> 18°31'38.3"E	Sandy fill to an average depth of 0.7m, over light and dark grey brown and off-white loose to medium dense silty sand to $\geq 2.5\text{m}$ . (Springfontyn)	<b>Disturbed sample:</b> Approx. 100kg between 0.7-2.0m.	Sieve analysis, constant head permeability, direct shear, funnel test, specific gravity test.	No groundwater table intersected.
Bellville South (June 2019)	<b>Latitude:</b> 33°55'27.81"S <b>Longitude:</b> 18°39'43.26"E	Thin layer of sandy fill underlain by slightly moist to moist, light grey and creamy white, loose and medium dense slightly clayey sand to $\geq 2.5\text{m}$ . (Springfontyn)	<b>Disturbed sample:</b> Approx. 100kg between 0.5-2.0m.	Sieve analysis, constant head permeability, direct shear, funnel test, specific gravity test.	Perched groundwater at 2.5m.
Matroosfontein (August 2019)	<b>Latitude:</b> 33°57'23.3"S <b>Longitude:</b> 18°35'32.6"E	Moist, brown, very loose, intact fine and medium sand to about 1.2m, overlying moist to wet, cream or brown, loose to medium dense, intact fine and medium sand and silty sand to $\geq 2.4\text{m}$ . (Witzand)	<b>Disturbed sample:</b> Approx. 100kg between 0-1.5m.	Sieve analysis, constant head permeability, direct shear, funnel test, specific gravity test.	Water table intersected at about 2.0m depth.



(a)



(b)

Figure 3-2: Mfuleni a) site view northwards and b) soil profile



**Figure 3-3: Gatesville typical soil profile**



**Figure 3-4: Stockpiled sand at Bellville South**

### **In-situ testing**

Field measurements of penetration resistance, in-situ density, infiltration rates and ground stiffness were undertaken as described below.

#### **1) Piezocone penetrometer tests (CPTu)**

As part of the current research, and to aid characterisation of the Cape Flats sands, CPTu's were undertaken by Geomechanics (Pty) Ltd at two sites in the study area with an adaptable Pagani penetrometer TG73-200 (see Figure 3-5). Four tests were carried out during April 2017; two on a vacant parcel of land in Capricorn Business and Technology Park (Pty) in Muizenberg (tests Capricorn CPTu 1 and CPTu2) , and two on the premises of Geoscience laboratories (Pty) Ltd in Airport Industria (tests Airport CPTu 1 and CPTu 2). Both sites are underlain by Witzand Formation deposits, however, the Airport Industria site is near the boundary of the Springfontyn Formation and transition into these deposits may occur at the site. The test sites are shown in Figure C12 in Appendix C.

The CPT cone with porewater pressure sensor and friction sleeve, was advanced into the ground until refusal of the cone occurred between 9m and 11m depth below ground level on very dense sand and silty sand (as noted from SBT-depth and  $D_r$ -depth plots).

To determine the static pore water pressure around the cone (and subsequently the level of the water table), seven pore water pressure dissipation tests were undertaken at the four test positions, between depths of 4.27m and 10.0m. The test entailed a pause in penetration to allow the excess pore water pressure around the tip to dissipate until the equilibrium pore pressure

was reached. Ground water tables were found to vary between approximately 2.5m and 3.0m at the two sites.



**Figure 3-5: Piezocone penetrometer testing in the Cape Flats**

The raw in-situ test data of  $q_c$  (in MPa),  $f_s$  (in kPa) and  $u_2$  (in kPa) were imported into the CPTu interpretation software CPeT-IT (GeoLogismiki, 2014), from which basic output data was calculated (e.g. corrected cone resistance,  $q_t$ , friction ratio,  $F_r$ , and normalised CPT parameters). Various plots were generated from the basic data, including raw data plots, basic output data plots, normalised plots and SBT plots. From the SBT plots and SBT-depth profiles, the soil types at the sites were determined. The profiles comprised mainly sand and silty sand with thin clayey layers at the Airport Industria site (refer to Figure 3-6a and b). The CPeT-IT software allows for estimation of geotechnical parameters, using existing empirical relationships, water table depth and over-consolidation ratio (OCR). Estimated geotechnical parameters include Young's Modulus, friction angle, permeability ( $k$ ), and the constrained modulus, ultimately presented as a function of depth. For the current study, the CPTu data from the four sites were used to estimate the friction angle, stiffness ( $E$  and  $E_0$ ), and liquefaction potential (contractive/dilative behaviour) of the site soils. In addition, the porewater pressure dissipation test results were utilised to estimate soil permeability. The selected empirical correlations are discussed in the relevant sections of this chapter. Unfortunately, no other penetration test data, such as SPT blow counts, were available for the sites to draw comparisons and establish relationships between parameters.

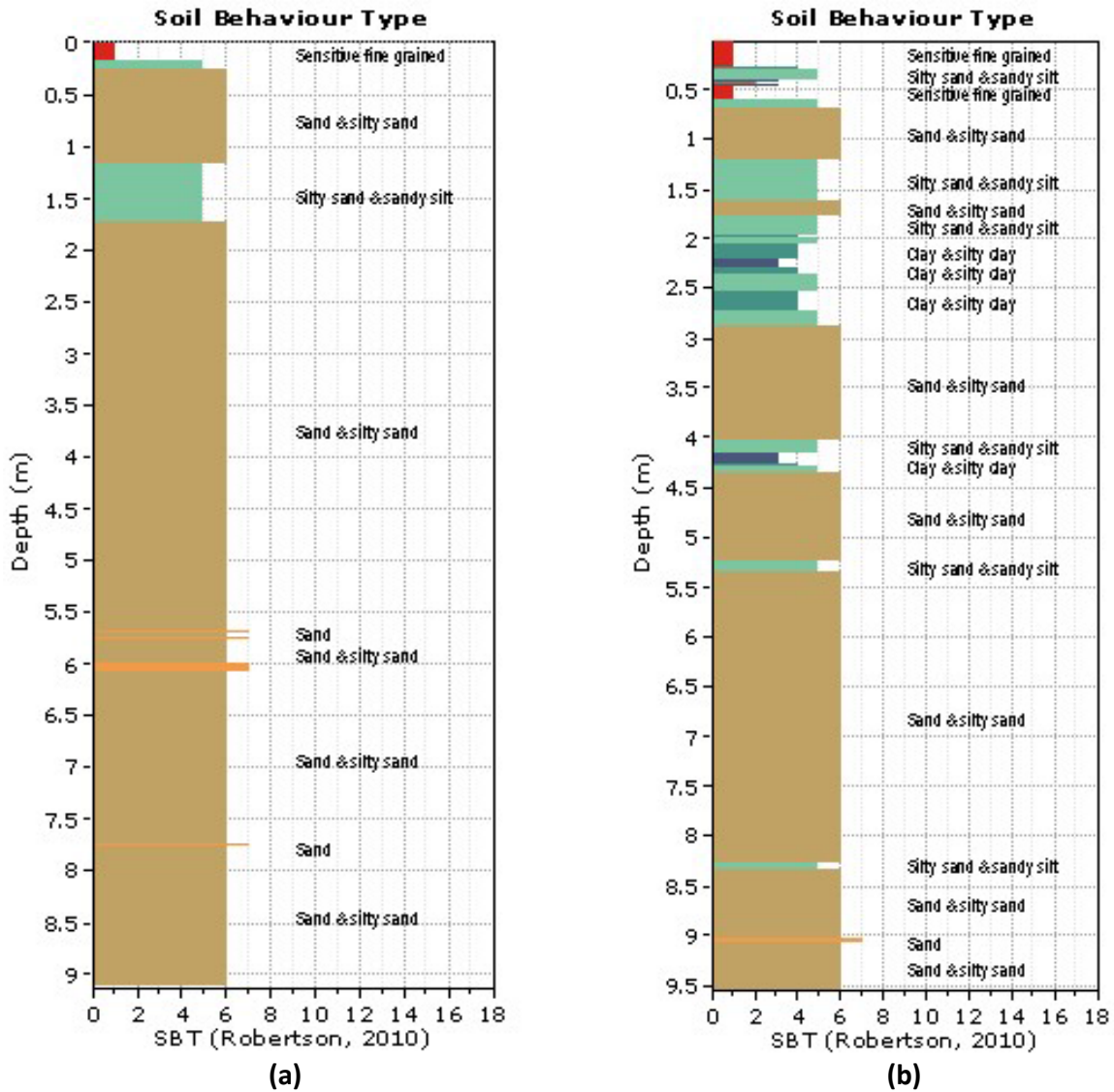


Figure 3-6: SBT with depth at a) Capricorn and b) Airport Industria

## 2) In-situ density tests

Field measurements of bulk density and moisture content (from which dry density is calculated) were undertaken at the Capricorn, Mfuleni and Gatesville sites, listed in Table 3-1. These values are additional to bulk density values from past investigations. In-situ density tests were undertaken with a nuclear density meter in accordance with TMH1 Method A10 (1986). The identified test positions were levelled, and a scraper used to create a smooth surface. The source rod was lowered 200mm into the ground and the test run. The direct transmission mode, whereby radiation is emitted from the source rod, was used to determine the wet density and moisture content. Eleven readings were taken at varying depths in the upper 1m of the profile at the three sites (see Figures 3-7a and b). Samples of sand were collected and sealed for moisture content determination in the laboratory to confirm the density values.



(a)



(b)

**Figure 3-7: Nuclear density gauge testing a) at Gatesville by b) lowering the ground level**

### 3) Double ring infiltrometer tests

The infiltration capacity of the shallow Witzand Formation soils from Capricorn (refer to Table 3-1), was determined by means of two double ring infiltrometer tests. The two tests were carried out approximately 30m apart after removal of the topsoil (about 0.2m). The tests were performed according to ASTM test designation D3385 (2018).

At each of three test sites a few metres apart (constituting one test), the inner and outer rings, similar to those shown in Figure 3-8, were placed on the prepared testing surfaces. The rings were driven approximately 50mm into the ground, using an impact absorbing hammer, first the inner ring and then the outer ring. The ring sets were placed a few metres apart, enabling simultaneous measurements and comparison of results. Both the inner and outer rings were filled with water to about 100mm, and continuously refilled to keep the water levels in the inner and outer ring the same. The time and water level in the inner rings were firstly noted, followed by continuous measurements of the drop in water level at set time intervals. Once constant infiltration rates were observed (within approximately 30 minutes), measurements were stopped. The infiltration capacity from each ring set was subsequently calculated, based on a reliable mean obtained from the last few readings. The near identical results from the ring sets were averaged, representing the infiltration rate (in m/s) at the testing locality.

These results will be used, together with infiltration rates from additional tests undertaken during a previous investigation in Bellville South to study the infiltration capacity of the Cape Flats soils.



**Figure 3-8: Double ring infiltrometer test equipment (Eijkelkamp, 2018)**

#### **4) Continuous surface wave (CSW) tests**

To allow the measurement of ground stiffness in the study area, CSW tests were undertaken by CSW Soil Engineering (Pty Ltd). The aim of the CSW testing was to obtain representative shear wave velocity ( $V_s$ ) profiles in the Cape Flats sands to enable statistical correlation between  $V_s$  and SPT blow counts. As such, two previously investigated terrains with known SPT resistance data, were chosen, namely the Athlone wastewater treatment works (WWTW), underlain by Springfontyn Formation deposits and the Cape Flats WWTW located on sands of the Witzand Formation. The latter site is in the False Bay nature reserve near Muizenberg. The site locations are shown in Figure C14 in Appendix C. Three tests were carried out at each site as follows: Firstly, borehole locations from past investigations were found on-site and appropriate CSW test areas selected in proximity. High and low frequency shakers were utilised as seismic sources, producing short and long Raleigh waves respectively (operating in the 15 to 200Hz and the 7 to 22Hz frequency ranges), that propagate through the soil. The Raleigh waves were detected by geophones, spaced equally in a line from the shaker on the ground surface. The output was recorded by a data acquisition system. The test setup is shown in Figure 3-9. A maximum depth of penetration of about 7m is possible with the high frequency shaker, and about 20m with the low frequency shaker.

Shear wave velocity profiles were obtained to depths of either 15m or 20m at the six test positions. At the Cape Flats WWTW, the profiles were entirely in aeolian deposits, described in the borehole logs as white, dark grey or brown, medium to coarse grained sand and silty sand with occasional clayey silt. Shell fragments were noted, and the absence of a water table documented. At the Athlone WWTW site, residual Malmesbury shale was intersected, varying in depth from 7m to 12m below ngl across the site. The residual deposits are overlain by aeolian sands described as mainly dark brown or grey, fine to medium grained silty sand and sandy silt with irregular layers of clayey sand and sandy clay. Organic matter was noted and the presence of gravel in places. The water table was encountered between 1.7m and 3.3m at this site.

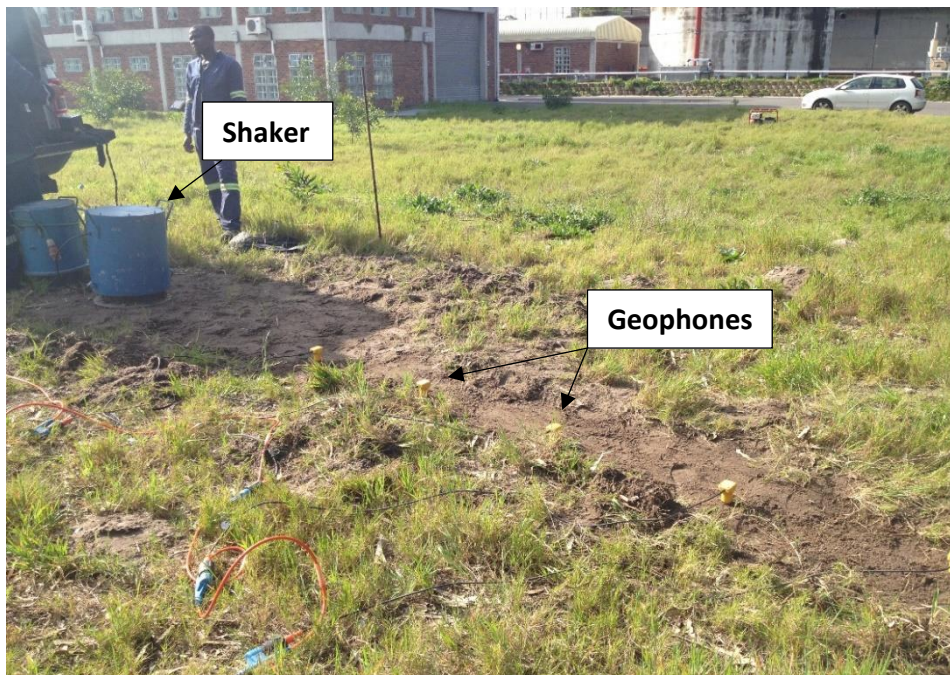


**Figure 3-9: CSW testing at the Athlone WWTW**

Shear wave velocity ( $V_s$ ) profiles derived from Raleigh wave velocity measurements were received by the author from CSW Soil Engineering (Pty) Ltd in an MS Excel spreadsheet. The Raleigh wave velocity ( $V_r$ ) measurements were converted to  $V_s$  by CSW Soil Engineering using Equation 3-1. Only measurements associated with the windblown sands were utilised to create the  $V_s$ -SPT N model for the Cape Flats.

$$\frac{V_r}{V_s} \cong \frac{0.874 + 1.117\nu}{1 + \nu} \quad \text{Equation 3-1}$$

Where:

$\nu$  =Poisson's ratio (varied between 0.2 and 0.5 during inversion analysis).

To interpret the CSW data, inversion analyses are undertaken to find the  $V_s$  profile that best fits the measured data. Software named Dinver from the Geopsy suite is used. The program varies  $\nu$  between 0.2 and 0.5 when using the optimization algorithm to select the best  $V_s$  profile. A typical result is shown in Figure 3-10, showing the best fit profile in blue and all other profiles in grey. Measurement uncertainty increases with depth, as seen by the increase in spread of the  $V_s$  profiles with depth. This aspect was considered during data interpretation.

The small-strain shear stiffnesses ( $G_0$ ) and the small-strain Young's Moduli ( $E_0$ ) of the ground profiles were calculated from  $V_s$  (in m/s) using Equations 3-2 and 3-3.

$$G_0 = \rho V_s^2 \quad (\text{in MPa}) \quad \text{Equation 3-2}$$

Where  $\rho$  = Bulk density ( $\text{kg/m}^3$ )

$$E_0 = 2(1 + \nu)G_0 \quad (\text{in MPa}) \quad \text{Equation 3-3}$$

Where  $\nu$  = Poisson's Ratio

With the aid of the SPT profiles, estimates of the bulk density and Poisson's ratio were made at the corresponding test depths. The stiffness profiles are not greatly affected by the estimations of density (Heymann, 2007) and Poisson's ratio, and the values used in the current study are considered adequate.

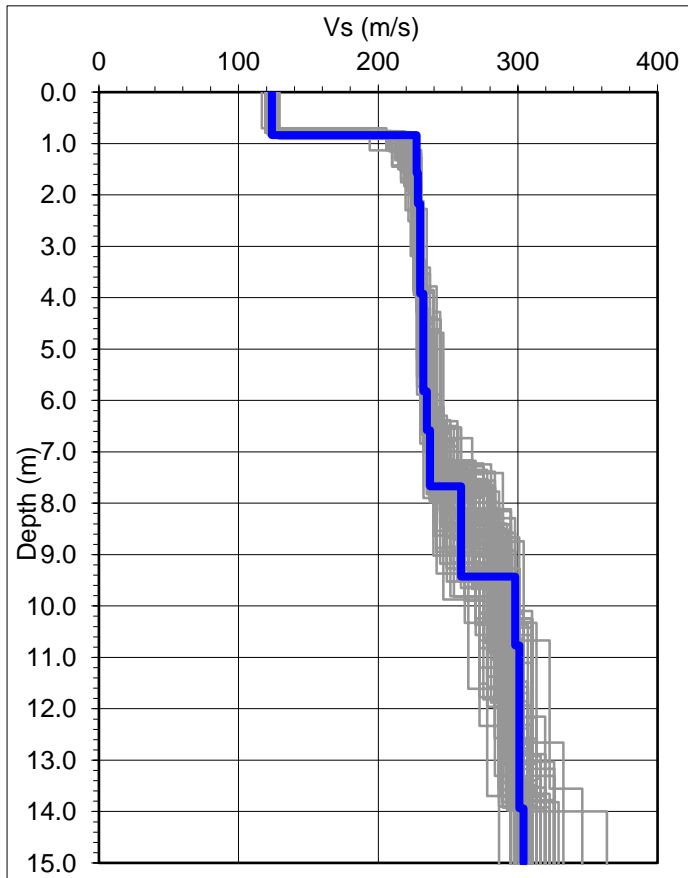


**Figure 3-10:  $V_s$  profile showing measurement uncertainty with depth**

Further development of the data set involved the selection of  $V_s$ -SPT N data pairs. SPT's were typically conducted every 1.5m (but spaced as close as 0.5m). Corresponding test profiles at each position were examined and pairs selected at overlapping testing depths or from interpolation between test depths. Measurements were excluded where an abrupt, large variation in stiffness was noted in one profile and missed in another due to test spacings, or where horizontal variation in the stratigraphy resulted in divergent profiles. Adjustments were made for elevation differences between CSW tests and adjacent boreholes where applicable. 48  $V_s$ -SPT N data pairs were obtained. The SPT N values for fine sand and silty sand below the water table were corrected using Equations 3-4a and b. Corrections were only made to penetration resistances from the Athlone WWTW where the water table was between 1.7m and 3.3m below surface.

$$N_{corrected} = 15 + \frac{1}{2}(N_{field} - 15) \text{ if } N_{field} > 15 \quad \text{Equation 3-4a}$$

$$N_{corrected} = 15 \text{ if } N_{field} < 15 \quad \text{Equation 3-4b}$$

Both SPT N and  $V_s$  were corrected for overburden pressure to obtain  $(N_1)_{60}$  and  $V_{s1}$  values using Equations 3-5 and 3-6. According to Bellana (2009), the empirical constants of 'n' and 'm', simply taken as 0.5 and 0.25 in Equations 3-5 and 3-6 respectively, vary with factors such as soil cementation, age and plasticity. Accordingly, inaccuracies may be introduced in the correction for overburden pressure in this manner. This aspect will be addressed further in Section 4.17.3 of Chapter 4. Due to the lack of information on the actual hammer energy supplied to the sampler by South African SPT equipment, it was not possible to correct the measured blow counts to  $N_{60}$  values. SPT N values were therefore taken as  $N_{60}$  values. Corrections for rod length, borehole diameter and sampling method were also not made.

$$(N_1)_{60} = \left(\frac{P_a}{\sigma'_v}\right)^n \cdot N_{60} \quad \text{Equation 3-5}$$

$$V_{s1} = \left(\frac{p_a}{\sigma'_v}\right)^m \cdot V_s \quad \text{Equation 3-6}$$

Where:

$P_a$  = Atmospheric pressure (kPa)

$\sigma'_v$  = Effective stress at test depth (kPa)

n = Constant set equal to 0.5 (see Bellana, 2009)

m = Constant set equal to 0.25 (see Bellana, 2009)

The Quaternary sands underlying the Cape Flats extend northwards along the West Coast to the small town of Atlantis (refer to Figure 2-1 in Chapter 2). Although beyond the geographical boundary of the Cape Flats, Atlantis is underlain by the same windblown sands that underlie large parts of the Cape Flats. Investigation involving CSW testing and SPT's was undertaken on a terrain in Atlantis in 2017, allowing additional  $V_s$ -SPT N data pairs to be generated for analysis. The location of the site is shown in Figure C14 in Appendix C. Obtained data included  $V_s$  profiles to 20m depth (spaced at irregular intervals) and SPT blow counts every 1m to a depth of 15m. The water table was recorded at depths ranging between 1.9m and 3.6m below ground surface. Thirty-two  $V_s$ -SPT N data pairs were obtained as described above, giving a total of 80 data pairs from the three sites. Sieve analyses carried out on samples obtained from boreholes at the Atlantis site, revealed fine and medium sands with fines contents ranging between 3% and 7%. This constitutes a typical Cape Flats sand grading result.

Statistical regression of the site investigation data generated equations expressing uncorrected shear wave velocity ( $V_s$ ) as a function of SPT blow counts ( $N_{60}$ ) and vertical effective stress ( $P_a/\sigma'_v$ ). Although bias with respect to overburden is possibly introduced in the correction of  $V_s$  and  $N_{60}$  to  $V_{s1}$  and  $(N_1)_{60}$  respectively, the stress corrected shear wave velocity and blow counts were also analysed to find the strongest relation and to reveal the most appropriate method of overburden correction. The functional form for the relations is  $V_s = A \cdot N_{60}^B$ , where the constants A and B are obtained by statistical regression of the set of information. This functional form is adopted in existing relations found in literature. The fines content, uniformity coefficient, and average particle size could not be analysed due to a lack of grading analyses. Shear wave velocity, rather

than small-strain stiffness,  $E_0$ , was preferred for regression analyses, as the calculation of  $E_0$  requires bulk density and Poisson's ratio with depth, which is likely to introduce additional uncertainty. In addition, estimates of  $V_s$  could simply be converted to  $E_0$  estimates where site specific information is available.

### 3.3.2.2 Laboratory testing methods

The laboratory tests performed on the soils sampled from the sites listed in Table 3-1 are discussed below. Laboratory procedures included grading analyses, funnel tests for minimum density, collapse potential tests, specific gravity determinations (water pycnometer), groundwater chemical analyses, constant head permeability tests, direct shear tests (on reconstituted soaked specimens), and direct shear and triaxial strength and resilient modulus tests on compacted sands.

#### 1) Mechanical analysis

The particle size distribution of the sands sampled from Capricorn, Mfuleni, Blue Downs, Gatesville, Bellville South, Mitchells Plain, and Matroosfontein in the Cape Flats were determined by means of sieve and hydrometer analyses. The results were added to the existing PSD data and were also used to enable estimation of soil characterisation properties, such as permeability.

The particle size analyses were undertaken in the geotechnical laboratory of the Civil Engineering Department of Stellenbosch University, using the methods given in the TMH1 (1986). Methods A1(a) and A1(b) were used for the wet and dry preparation and sieve analysis of the coarse soil fraction and method A6 was used for the hydrometer analysis. The percentage particles smaller than 63mm, 53mm, 37.5mm, 26.5mm, 19mm, 13.2mm, 4.75mm, 2.0mm, 0.425mm, 0.075mm, 0.05mm, and 0.005mm were subsequently calculated to determine the percentage of gravel, coarse, medium and fine sand, silt and clay in each soil. Particle size ranges for classification, based on ASTM D422, were used to finalise the soil texture descriptions. The ASTM grain size boundaries are shown in Table 3-2.

**Table 3-2: ASTM particle size classification (compiled from ASTM D422, 2007)**

Particle size	Size range (mm)
Gravel	>4.75
Coarse sand	2.0 – 4.75
Medium sand	0.425 – 2.0
Fine sand	0.075 – 0.425
Silt	0.005 – 0.075
Clay	<0.005

#### 2) Funnel test for minimum index density

The minimum loose density of the disturbed soils sampled from Mfuleni, Blue Downs, Gatesville, Bellville South, Mitchells Plain, and Matroosfontein were determined by means of the funnel test method, stipulated in Method A of ASTM D4254 (2016). Two tests were performed on each soil to check consistency. The test is not routinely performed (no other minimum density values were available for the Cape Flats sands) and, for this reason, a brief overview of the method is given.

For the specific material type (fine and medium sand with a maximum particle size smaller than 9.5mm) ASTM D 4254 Method A stipulates the following apparatus:

- A standard cylindrical metal mould with volume =  $2830\text{cm}^3$ . The inside diameter of the mould must be equal to 152.4mm and length equal to 155.24mm.
- A pouring device consisting out of a rigid container, having a volume of 1.25 to 2 times greater than the volume of the metal mould, and fitted with a 13mm diameter, 150mm long spout.

In accordance with the above specifications, a metal mould – having the dimensions and volume given above – was manufactured as well as a 200mm diameter, 160mm long rigid container with a volume of  $5026\text{cm}^3$  fitted with the specified spout (see Figure 3-11).

Sands from each location were oven-dried and placed as loosely as possible in the metal mould by pouring the soil in a continuous and steady stream from the spout. The pouring device was held in a near vertical position and the height of the container/spout slowly increased to keep the spout approximately 130mm above the soil surface, maintaining a constant free-fall height. The container was moved along a circular path, from the outside to the centre of the mould, to ensure uniform layer thicknesses. The mould was filled above the top of the mould, and the excess subsequently trimmed off with a straightedge in line with the top of the mould. The mass of the mould and the soil was then recorded, avoiding any disturbance of the soil, which may cause particle rearrangement. The mass of the empty mould (previously determined) was subtracted from the mass of the mould and the soil, and the minimum dry density calculated by dividing the mass of the dry soil by the volume of the mould. Execution of the test is shown in Figure 3-11.



**Figure 3-11: Minimum loose density testing**

### **3) Collapse potential test**

Twelve collapse potential tests were carried out on the undisturbed sandy soils sampled from the upper 1m of the profile from Mfuleni. Tests were undertaken in accordance with the guidelines set out in ASTM D5333 (2003). From the soils sampled as described in Table 3-1, specimens were

carefully cut into oedometer rings; two from each of the six undisturbed samples. The first set of six samples was saturated at 200kPa, and the second at 100kPa. The difficulty in obtaining undisturbed samples from the sands limited the number of tests undertaken on Cape Flats deposits. The presence of soil suction in the partially saturated samples enabled intact specimens to be transferred to the oedometer cell.

The void ratio at the end of each load increment was calculated and plotted against the corresponding effective stresses to give the compression and possibly the collapse of the sands. The change in void ratio ( $\Delta e$ ) at 200kPa was calculated and, together with the initial void ratios ( $e_0$ ), used to calculate the percentage collapse potential as shown in Equation 3-7. For specimens soaked at 100kPa, the collapse percentage was calculated using Equation 3-7. The e-log(p) curves associated with the collapse potential tests, are included in Appendix D.

$$CP (\%) = \frac{\Delta e}{1+e_0} \cdot 100 \quad \text{Equation 3-7}$$

#### 4) Groundwater chemical analysis

To determine the corrosion potential of groundwater in the study area, water and soil-water extract sampled from a test pit in Mfuleni (refer to Table 3-1), underwent chemical analysis at Bemlab (Pty) Ltd in Strand. The list of tests performed, and the methods/techniques followed, are given in Table 3-3. The obtained properties will be used to determine the Langelier Index, the aggressiveness index, the leaching-corrosion and spalling-corrosion sub-indices, and the aggressive chemical environment for concrete (ACEC) classification. From past investigations, chemical analysis results for groundwater, and pH and electrical conductivity values for numerous soils, will be utilised in the current research.

**Table 3-3: Chemical tests for corrosion potential**

<b>Water property</b>	<b>Test method/technique (SABS methods)</b>
pH at 25°	pH meter (3136)
Alkalinity as CaCO <sub>3</sub>	Titrimetric method (3137)
Calcium carbonate	Titrimetric method (3777)
Total ammonium-ion content	Auto analyser (3271)
Magnesium-ion content	ICP-OES (3132)
Sulphur	ICP-OES (3132)
Chloride-ion content	Titrimetric method (3138)
Calcium-ion content	ICP-OES (3132)
Total dissolved solids	EC meter (3135)
Water temperature	Thermometer
<b>Soil/water extract property</b>	<b>Test method/technique (SABS methods)</b>
pH	KCL method 3108
Electrical conductivity	EC meter (3135)
Phosphorus-ion content	ICP-OES, Bray I (3116)
Sodium-ion content	ICP-OES, Ammonium Acetate extraction (3113)
Potassium-ion content	ICP-OES, Ammonium Acetate extraction (3113)
Calcium-ion content	ICP-OES, Ammonium Acetate extraction (3113)
Magnesium-ion content	ICP-OES, Ammonium Acetate extraction (3113)
Iron-ion content	ICP-OES (3132)
Zinc-ion content	EDTA extraction method (3115)

Manganese-ion content	EDTA extraction method (3115)
Copper-ion content	EDTA extraction method (3115)
Boron-ion content	ICP-OES, hot water extraction method (3114)
Sulphate-ion content	ICP-OES, Calcium-phosphate extraction method (3119)

The calcium carbonate saturated pH ( $pH_s$ ) required for calculation of the Langelier Index, the aggressiveness index, and the leaching-corrosion sub index, was calculated by taking into consideration the water temperature, total dissolved solids, calcium hardness and total alkalinity.

### 5) Constant head permeability test

The sands from Mfuleni, Blue Downs, Gatesville, Bellville South, Mitchells Plain and Matroosfontein (refer to Table 3-1), were subjected to constant head permeability testing, performed at Geoscience laboratories (Pty) Ltd and in the geotechnical laboratory at Stellenbosch University, using the test method prescribed by Head (1992). A brief overview of the test procedure, which requires approximately 5.5kg of material, is given below.

The soils from the abovementioned localities are all cohesionless and were disturbed during the sampling process. As such, samples were recompacted in the laboratory to between  $1540 \text{ kg/m}^3$  and  $1727 \text{ kg/m}^3$ , using Modified AASHTO compaction effort. The length and diameter of the specimens were 125mm and 150mm respectively. Each compacted specimen (within the mould) was connected to a perforated base plate, and a geotextile layer and porous stone placed on top of the specimen, after which it was covered by the water inlet casing. The completed assemblage - known as the permeameter cell - was connected to the constant head water source and allowed to saturate. The test subsequently commenced, with water flowing through the cell, until a steady rate of flow was established. At this point, the time required for 500ml of water to pass through the specimen, and to be collected in a cylinder at the water outlet, was recorded. A head reading was noted from the standpipe and the hydraulic gradient ( $h/l$ ) calculated. The test was repeated four times by continuing water to flow through the sample to collect 500ml at a time. The coefficient of permeability ( $k$  in m/s) for each test was calculated, using Equation 3-8, and an average value of  $k$  determined. The test setup is shown in Figure 3-12.

$$k = \frac{ql}{Ah} \quad \text{Equation 3-8}$$

Where:

$q$  = Flow rate (ml/min, converted to  $\text{m}^3/\text{s}$ )

$l$  = Length of specimen (m)

$A$  = Area of cylindrical specimen ( $\text{m}^2$ )

$h$  = Head at top of specimen (zero at bottom) (m)

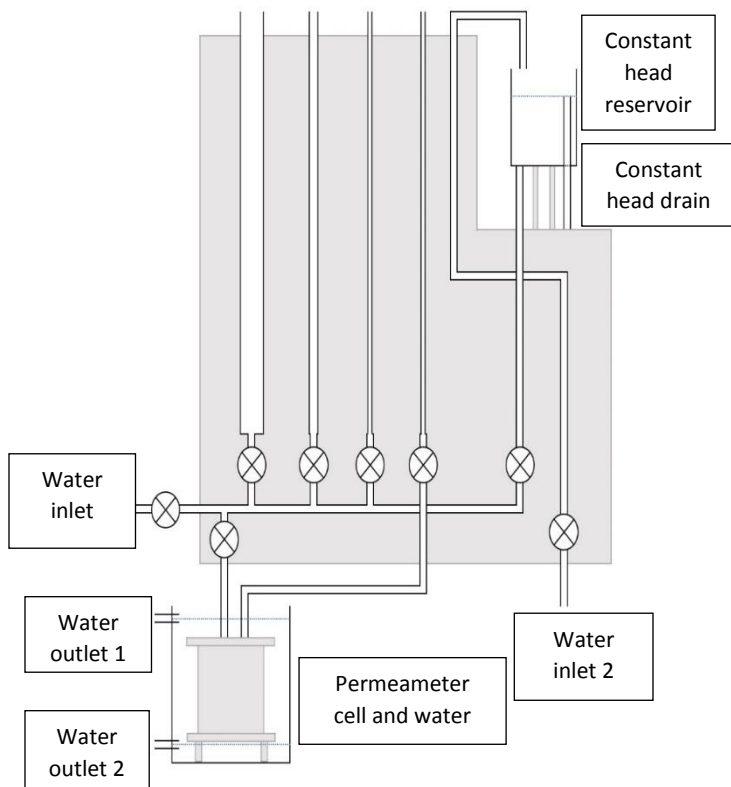


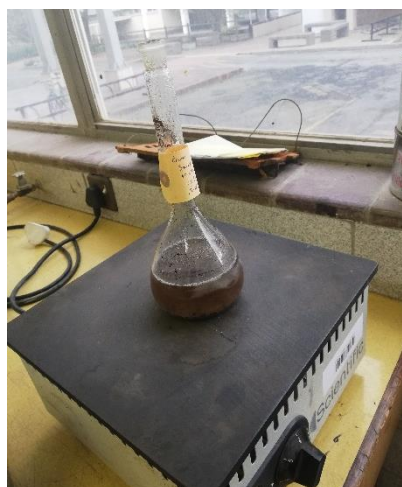
Figure 3-12: Permeability test, adapted for both constant and falling head tests (Hoffman, 2019)

## 6) Specific gravity test

The water pycnometer was used to determine the specific gravity of sands from Mfuleni, Blue Downs, Gatesville, Bellville South, Mitchells Plain and Matroosfontein, in accordance with Method B in ASTM D854 (2002) for oven-dried specimens. Two trials were performed on each soil type for accuracy. The pycnometer was first calibrated, as described in the ASTM standard, followed by the test procedure for particles <4.75mm. In Figure 3-13a the pycnometer with 100g sand and distilled water is shown, and in Figure 3-13b boiling of the mixture to remove entrapped air is illustrated.



(a)



(b)

Figure 3-13: Determination of  $G_s$  with the water pycnometer

## **7) Direct shear test on soaked reconstituted sands**

Direct shear tests were performed on reconstituted sands from Blue Downs, Gatesville, Bellville South, Mitchells Plain, and Matroosfontein (refer to Table 3-1). The direct shear tests were carried out in the geotechnical laboratory at Stellenbosch University, using the Digishear direct shear apparatus with a square shear box (60mm by 60mm by 20mm in size). Tests were undertaken in accordance with ASTM D3080 (2011).

Due to the cohesionless nature of the sands, specimens were created by placing the sand in three layers in the shear box and tamping each layer to achieve predetermined densities (between  $1535\text{kg/m}^3$  and  $1600\text{kg/m}^3$ ). Porous plates were positioned at the bottom and the top of the specimen. All specimens were soaked and consolidated prior to shearing. A shear force was applied at a strain rate of  $0.01\text{mm/min}$ , causing the top half of the sample to move relative to the stationary bottom half. The shear force and the corresponding shear movement were subsequently recorded. Three different vertical forces were applied to each soil type, exerting pressures of 50kPa, 100kPa, and 200kPa. The shear stress at failure was then plotted against the effective normal stress for each test and the failure envelope obtained by linear regression. The slope of the envelope revealed the drained friction angle, and the intercept with the y-axis the drained cohesion value. For dense dilative sands, the critical state friction angle was obtained from the critical state line by plotting the shear stress at the critical state against the effective normal stress. These direct shear test results add to existing results from past investigations (6 direct shear tests).

## **8) Triaxial strength and resilient modulus testing of compacted sands**

To perform static and dynamic triaxial tests, the draft version of the protocol developed by the Council for Scientific and Industrial Research (CSIR) for the determination of the resilient modulus of bound and unbound granular materials, was followed (CSIR, 2014). The Material Testing System (MTS 810, Model 318.10) of the pavement engineering laboratory at Stellenbosch University was used to perform the tests. The apparatus comprises a pressure chamber containing the specimen and the confining air, and a loading device providing static and repeated vertical loads. The MTS triaxial apparatus, and computer with data acquisition software, is shown in Figure 3-14.



**Figure 3-14: Triaxial test setup**

### **Specimen preparation**

The peak shear parameters and stiffness moduli of sands sampled from Mfuleni in the Cape Flats were determined by means of monotonic and dynamic triaxial tests. To determine the influence of density (compaction) and moisture content on the soil parameters, soil samples were compacted to two different densities, each density variation prepared at two moisture contents (optimum moisture content and 75% of optimum moisture content). Three replicas of each specimen type were produced for the monotonic triaxial tests (to test at three different confining pressures), resulting in a total of 12 specimens. The dynamic triaxial tests were undertaken on the same four soil types, with two replicas made of each allowing for test duplication.

The modified AASHTO compaction method was used to obtain the maximum dry density and optimum moisture content of the selected material, using Method A7 in TMH1 (1986). The procedure requires approximately 30 kg of representative air-dried material, divided into four portions of 7 kg, each portion compacted in 5 layers with 55 hammer blows at a different moisture content to obtain the moisture-density relationship of the material. The soil was compacted at moisture contents of 9%, 11%, 14%, 17% and 21%, and the corresponding dry densities were determined using Equation 3-9. The resulting graph of moisture content against dry density is shown in Figure 3-15, illustrating the determination of the maximum dry density (MDD) and the optimum moisture content (OMC). An MDD and OMC of 1556kg/m<sup>3</sup> and 12% respectively was achieved for the sand. The low dry density can be ascribed to the uniform grain size characteristic of the Cape Flats.

$$\rho_d = \frac{W}{d + 100} \times \frac{100}{V} \times 1000 \text{ (kg/m}^3\text{)} \quad \text{Equation 3-9}$$

Where:

W = Mass of wet material (g)

d = Moisture content (%)

V = Volume of mould (ml)

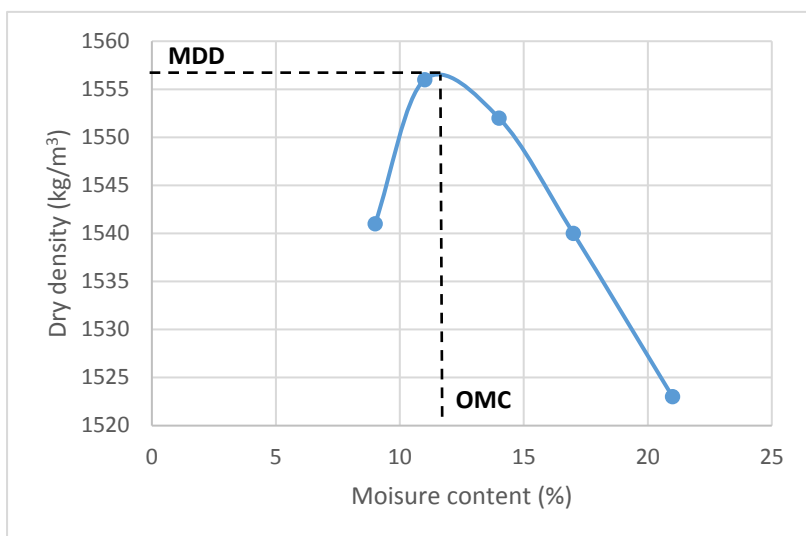


**Figure 3-15: Dry density - moisture content curve for Cape Flats sand from Mfuleni**

To create the compacted specimens for triaxial testing, the required mass of soil was determined from the volume of the compaction mould and the required dry density. An additional 1kg of sand was added for later determination of the hygroscopic moisture. Measured quantities of water were added to the soil and thoroughly mixed with an electronic pan mixer to achieve the predetermined moisture contents. Each specimens' material was subsequently divided into five equal portions and placed in plastic bags to prevent moisture loss.

To compact the soil specimens to the preselected dry densities of  $1556\text{kg/m}^3$  (Mod AASHTO MDD) and  $1630\text{kg/m}^3$  (105% of Mod AASHTO MDD) both at OMC and at 75% of OMC, the Wirtgen vibratory hammer was used. Higher compaction energy is associated with the vibratory hammer compared to the modified AASHTO method. Each of the five portions of material - prepared in the manner described above - was individually compacted to a height of 60mm in a split mould (152mm in diameter and 300mm in height). The subsequent removal of the specimens from the mould proved to be problematic due to the absence of plastic fines and thus cohesion in the sands. Attempts to open the split mould resulted in the specimen dividing longitudinally. The compaction process is shown in Figures 3-16 to 3-18.



**Figure 3-16: Electronic pan mixer**



**Figure 3-17: Vibratory hammer**



**Figure 3-18: Split specimen upon opening of mould**

To enable the extraction of intact samples from the compaction mould for triaxial testing, the addition of fines was considered essential. Based on the grading results of 260 soils previously sampled from the Cape Flats area, an average fines content of about 6% applies to the sandy soils from the area. For this reason, 6% fines (particles with diameter  $<0.075\text{mm}$ ) – sourced from Corobrick Clay in Eerste River – were added to the sand to provide the necessary cohesion. The sourced fines contain the inactive clay mineral kaolinite, providing large surface area particles for increased bonding. The fine material was dried, crushed by hand with a tamper fitted to a jackhammer to break down clayey clumps, and subsequently passed through the  $0.075\text{mm}$  sieve to separate the usable silt and clay particles from the larger sand grains.

Once the fines were prepared, the modified soil type was made, comprising 94% Mfuleni fine sand and 6% silt and clay. The PSD curves for the modified and unmodified material are shown in Figure 3-19. TRH 14 (1985) guidelines were used to categorise the modified material in terms of its suitability as a road construction material. In terms of surfacing, the altered Cape Flats soil did not meet the requirements for a sand seal or a second layer of a multiple surface treatment, the failing criteria being the excessive percentage of particles passing the  $0.15\text{mm}$  and  $0.3\text{mm}$  sieves (greater than 2% and 15% respectively). Based on grading alone a G7, G8, G9 or G10 category can apply to the material when used in the pavement structure. The altered sands do not meet the grading requirements to serve as fine aggregate in concrete pavements, as the fines content exceeds 5%. The suggested grading envelopes for gravel wearing course predicts poor performance of the modified sands in this regard.

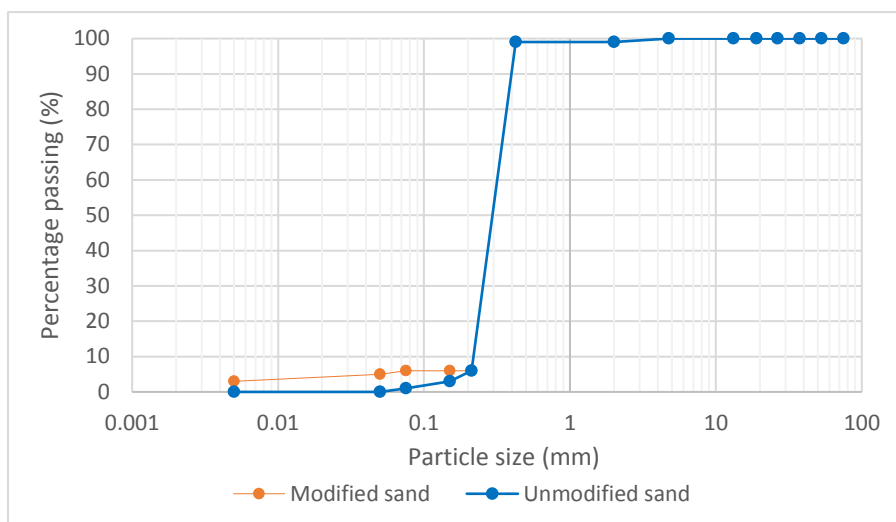


**Figure 3-19: Distribution of grain sizes in the unmodified and modified Cape Flats sand from Mfuleni**

The addition of the fines will alter the compaction properties of the material and, as such, the modified AASHTO test was repeated on the newly formed material in the manner previously described. The soil was compacted at moisture contents of 6%, 9%, 12%, and 15%, and the corresponding dry densities were determined. A Mod AASHTO MDD and OMC of 1660kg/m<sup>3</sup> and 11.6% (rounded to 12%) respectively was achieved for the modified sand.

As previously described, the required mass of soil to create the compacted specimens for triaxial testing, was determined from the volume of the compaction mould and the required dry density. Dry densities of 1660kg/m<sup>3</sup> (Mod AASHTO MDD) and 1560kg/m<sup>3</sup> (approximately 94% of Mod AASHTO MDD) were selected. Compaction with the vibratory hammer to MDD (>100% Mod AASHTO MDD) failed to produce a satisfactory gap between the two compacted densities. Approximately 9.0kg and 8.5kg of the sand were required to produce the higher and lower density specimens respectively. Measured quantities of water were added to the soil and thoroughly mixed to achieve the predetermined moisture contents of 12% (OMC) and 9% (75% of OMC). The soil was then compacted to the predetermined dry densities (at the appropriate water contents) with the Wirtgen vibratory hammer as described above. Upon extraction, intact specimens were removed for triaxial testing.

### **Specimen assembly in triaxial cell**

The specimen assembly procedure specified in the CSIR draft document of 2014 was followed, and it is summarised below.

The specimen was carefully covered by a rubber membrane (by means of a membrane dresser device) and placed in the centre of the triaxial cell base pedestal. Two O-rings were placed over the membrane onto the groove in the base pedestal to prevent entry of air between the sample and the membrane. The loading plate was placed on top of the specimen and the membrane pulled upwards and over the loading plate. Two O-rings were positioned over the membrane and onto the loading plate. The sample setup with membrane and O-rings positioned as described above, are shown in Figure 3-20.

The loading frame, cylindrical Perspex chamber and the lid loading unit were lubricated with grease to prevent air leakage during the test. The loading frame and chamber was placed over the sample, the lid positioned on top, and all the tie rods of the chamber components fastened. To ensure there are no leakages, the air supply hose was connected to the base plate and air supplied to the chamber. If air leakage can be heard, all seals should be checked, and the problem corrected. The base actuator was then set to a predetermined value to ensure consistency between tests. The top loading pin was lowered until light contact was made with the lid (seating load  $< 0.4\text{kN}$ ). The sample setup was now complete and monotonic triaxial testing could commence. The completed setup of the specimen in the MTS is shown in Figure 3-21.



**Figure 3-20: Membrane enclosing triaxial specimen as prescribed in CSIR (2014)**



**Figure 3-21: Completed specimen setup**

### **Monotonic testing**

The monotonic triaxial tests were performed to obtain the shear strength parameters of the material, and to determine the cyclic stresses to be applied during dynamic testing. In addition, elastic modulus values for the sands can be obtained from the resulting axial stress - axial strain curves.

Each of the four sample types (density and moisture content variants) were subjected to all-round pressures of 50kPa, 100kPa and 150kPa. The three same soil specimens (replicas) were prepared to near identical densities and moisture contents. Where failure load outliers were observed in the results, one or more of the tests was repeated to ensure accuracy. Each specimen was loaded at a constant displacement rate of 3mm per minute (strain rate of 1% per minute) up to failure at a constant confining pressure. The tests were stopped once the applied load had declined to 80% of the failure load, and the sample unloaded at a rate of 3mm per minute.

The major principle stress at failure was calculated for each soil specimen and the stress states at failure were subsequently represented by Mohr circles and the failure envelopes drawn. To obtain the shear strength parameters of the sand, the procedure specified in the CSIR draft document of

2014 was followed, as described below. It should be noted that, because the specimens were partially saturated during testing, soil suction was present, and the total normal stresses will not be equal to the effective normal stresses. The magnitude of the negative pore water pressure is unknown and therefore only the total stress parameters of  $c$  and  $\phi$  could be determined.

The deviator stress at failure,  $\sigma_{d,f}$ , was calculated for each soil specimen as follows:

$$\sigma_{d,f} = \frac{P_{d,f}}{A} \quad \text{Equation 3-10}$$

Where:

$P_{d,f}$  = Applied load at failure (in kN)

$A$  = Initial end area of the sample (in  $m^2$ )

The major principle stress at failure,  $\sigma_{1,f}$ , was subsequently calculated as the sum of the deviator stress at failure,  $\sigma_{d,f}$ , and the confining pressure,  $\sigma_3$ . The relationship between  $\sigma_{1,f}$  and  $\sigma_3$  was then determined by performing a linear regression analysis on the three pairs of  $\sigma_{1,f}$  and  $\sigma_3$  values. The obtained relationship is given in Equation 3-11.

$$\sigma_{1,f} = A \times \sigma_3 + B \quad \text{Equation 3-11}$$

Where:

$$A = \frac{1 + \sin\phi}{1 - \sin\phi}$$

$$B = \frac{2 \times c \cos\phi}{1 - \sin\phi}$$

The peak shear strength parameters of friction angle,  $\phi$ , and cohesion,  $c$ , were subsequently calculated for each of the four specimen types as follows:

$$\phi = \sin^{-1} \left( \frac{A-1}{A+1} \right) \quad \text{Equation 3-12}$$

$$c = \frac{B(1 - \sin\phi)}{2 \times \cos\phi} \quad \text{Equation 3-13}$$

The principle stresses were also plotted on a graph of normal stress against shear stress and Mohr circles drawn. The failure envelope was constructed as a tangent line to the three Mohr circles and the friction angle and cohesion obtained as the slope of the line and the y-intercept respectively. The shear strength parameters obtained through monotonic failure tests were compared to published values. The influence of the study variables, that is, moisture content and compaction, were also investigated. The critical strength parameters of  $\phi_{cv}$  and  $c_{cv}$  could not be determined, as the critical state was not reached in most of the tests. The intermediate parameters calculated in the manner described above are shown in Table 3-4.

**Table 3-4: Triaxial test output data**

Sample type: Dry density and moisture content	Confinement pressure (kPa)	Failure force, $P_{d,f}$ (kN)	Deviator stress at failure, $\sigma_{d,f}$ (kPa)	Major principle stress at failure, $\sigma_{1,f}$ (kPa)	Area of Specimen (m <sup>2</sup> )
$\rho_d = 1660 \text{ kg/m}^3$ and $w = 12\%$	50	5.46	301.1	351.1	0.018
	100	9.42	518.9	618.9	
	150	14.85	818.2	968.2	
$\rho_d = 1660 \text{ kg/m}^3$ and $w = 9\%$	50	4.48	246.7	296.7	
	100	8.72	280.4	580.4	
	150	13.43	739.9	889.9	
$\rho_d = 1560 \text{ kg/m}^3$ and $w = 12\%$	50	5.43	299.4	349.4	
	100	8.79	484.5	584.5	
	150	12.33	679.7	829.7	
$\rho_d = 1560 \text{ kg/m}^3$ and $w = 9\%$	50	4.28	236.0	286.0	
	100	6.11	336.7	436.7	
	150	9.15	504.2	654.2	

The elastic modulus values for the sands were determined as the gradient of the straight-line portion of the stress-strain curves.

The rubber membrane enclosing the triaxial test specimens, has in previous studies, been found to provide additional support to soil specimens, restricting deformation to some extent. During the current triaxial tests, the influence of the membrane on the failure force was evident. Where the membranes were reused, signs of stretching were noted, influencing the outcomes of results. Where outliers were found and the tests repeated with new membranes, higher values were consistently obtained when a new membrane was used. Results progressively became poorer (using the same soil sample) as the number of membrane-uses increased. For this reason, membranes were only reused once, before being discarded to minimise the variation in the support provided by the membrane. The rubber membranes were produced in the laboratory, and there was slight variation in membrane thicknesses.

The influence of the rubber membrane on the strength of test specimens has been studied by Henkel and Gilbert (1952), Baldi and Nova (1985), and Coetzee (2015). The study by Coetzee (2015), showed the friction angle of recycled concrete aggregate (RCA) specimens to increase from 47° to 53° when the membrane thickness was doubled. The correction factors proposed by the authors, applies to specific membrane types and thicknesses, and soil types. The supporting influence will, for example, be greater for the sands used during the current study than for the RCA tested by Coetzee (2015). To investigate the extent to which the obtained shear strength parameters and soil stiffness are influenced by the confining membrane, direct shear tests were carried out on each of the four sample types (density and moisture content variations). The acquired parameters were subsequently compared with those obtained through triaxial testing. The experimental procedures associated with the direct shear test are provided at the end of this section.

### **Dynamic testing**

Cyclic loading resilient deformation tests were undertaken on the same four sample types created for the monotonic failure tests to determine the stress dependent resilient deformation behaviour of the similar reconstituted sand samples. The same specimen preparation procedure followed for the constant load tests, was used for the dynamic load testing. A deformation measurement device was additionally assembled to enable on-specimen displacement measurement during the dynamic tests. Three vertical linear variable differential transducers (LVDT's) were placed at an offset of 120° around the circumference of the sample. The LVDT's are supported by two plastic placement rings positioned at 1/3 and 2/3 of the specimen height. The specimen with the LVDT's assembled is shown in Figure 3-22.



**Figure 3-22: Triaxial specimen with LVDT's for dynamic testing**

To determine the resilient modulus, repeated load tests must be performed at different magnitudes of stress and at different combinations of stress. The cyclic stress is specified as a percentage of the deviator stress at failure obtained from the static triaxial test. The specimens were subjected to stress ratios of 10%, 20%, 30% and 40%. The peak deviator stress ratio (DSR) was limited to 40% (as opposed to the DSR of 60% recommended in the CSIR draft protocol), owing to the lower strength of the natural sand compared to road construction materials. During the experimental program it was noted that the actual stresses (and thus the DSR's), were somewhat lower than the pre-determined DSR values. The actual DSR values ranged from 9% to a maximum of 35%. The DSR values were, however, reasonably consistent at each DSR level (typically not varying by more than 10%). The lower DSR values were due to characteristic impreciseness in pressure control at these lower values. This will, however, not influence the validity of the outcome and the resilient modulus ( $M_r$ )-bulk stress ( $\Theta = \sigma_1 + \sigma_2 + \sigma_3$ ) model.

The deviator stress at failure was obtained from Equation 3-10 for each of the static triaxial tests (performed at three confining pressures). The loading schedule adopted for the resilient modulus testing, is shown in Table 3-5.

**Table 3-5: Dynamic triaxial testing loading schedule**

Cycles	Stage	Confinement pressure (kPa)	Deviator stress ratio (DSR) (pre-entered)
0 - 100	Conditioning	100	15%
101 – 200			25%
201 – 300			35%
301 – 400	1	50	10%
401 – 500			20%
501 – 600			30%
601 – 700			40%
701 – 800	2	100	10%
801 – 900			20%
901 – 1000			30%
1001 – 1100			40%
1101 – 1200	3	150	10%
1201 – 1300			20%
1301 – 1400			30%
1401 - 1500			40%

As shown in Table 3-5, a conditioning phase was carried out prior to commencement of the dynamic testing. It comprised the application of repeated axial load (of three different magnitudes) at a confining pressure of 100kPa. The 100kPa confining pressure deviates from the 200kPa recommended in the CSIR draft protocol, to align with the average confining pressure in subsequent cycles of dynamic testing. During the conditioning stage, 300 cycles of loading and unloading, divided into three phases of 100 cycles each, were completed. A haversine shaped load pulse was used with a 0.1 second period of loading and unloading and a 0.9 second rest period. The conditioning phase helps to minimise the effects of imperfect contact between the system platens and the test specimen.

The method proposed by Van Niekerk (2002) was followed during dynamic testing, in which the Mr- $\theta$  test was performed under increasing confining stress levels. At each confining stress level (50kPa, 100kPa, and 150kPa) the cyclic deviator stress was increased in steps (refer to Table 3-5). One hundred load repetitions were applied at each DSR, each repetition lasting one second (as described in the conditioning phase). The axial force from the load cell, the confining pressure and the average axial deformation for each LVDT were recorded over the last five cycles of each loading sequence. A preload equal to 0.4kN was also applied to the specimen throughout the conditioning and testing phases to make sure the piston remains in contact with the top plate.

The calculation of the average axial deformation and the resilient axial strain per load cycle, and subsequently the resilient modulus, are given below. The complete loading regime (with actual load forces and deviator stress ratios) for the dynamic triaxial tests is given in Appendix E.

For each of the last five cycles in a loading sequence, the average axial deformation of the sample was obtained from the readings of the three LVDT's as follows:

$$\Delta\delta_{a(N)} = \frac{\sum_{j=1}^{j=3} LVDT_{j,max} - LVDT_{j,min}}{3} \quad \text{Equation 3-14}$$

Where:

LVDT  $j_{,max}$  = Maximum deformation reading for LVDT j

LVDT  $j_{,min}$  = Minimum deformation reading for LVDT j

The resilient vertical strain was then calculated for each load cycle using Equation 3-15.

$$\varepsilon_{a(N)} = \frac{\Delta\delta_{a(N)}}{L_g} \quad \text{Equation 3-15}$$

Where:

$L_g$  = Gauge length

For each cycle, the maximum deviator stress and the seating stress (applied to ensure contact of the piston with the top plate) were used to calculate the cyclic stress as follows:

$$\sigma_{cyclic(N)} = \sigma_{d(N)} = (\sigma_{max(N)} - \sigma_{contact(N)}) \quad \text{Equation 3-16}$$

Where:

$\sigma_{max(N)}$  = Maximum deviator stress

$\sigma_{contact(N)}$  = Seating stress

The resilient modulus was subsequently calculated for each of the five loading cycles using Equation 3-17.

$$M_{r(N)} = \frac{\sigma_{cyclic(N)}}{\varepsilon_{a(N)}} \quad \text{Equation 3-17}$$

The average resilient modulus value for the last five cycles in a loading sequence was calculated as follows:

$$M_r = \frac{\sum_{i=1}^{i=l} M_{r,j}}{l} \quad \text{Equation 3-18}$$

Where:

$l$  = Number of cycles (equal to five).

The results of the dynamic tests were examined by plotting the calculated resilient moduli values against the bulk stress, both on a logarithmic scale. Two mathematical models were fitted to the experimental data to find the most appropriate model, which shows a good correlation with the behaviour of the material. The following models were fitted to the data by means of non-linear regression analyses (Van Niekerk, 2002):

$$M_r = k_1 \left( \frac{\theta}{\theta_0} \right)^{k_2} \quad \text{Equation 3-19}$$

$$M_r = k_1 \left( \frac{\sigma_3}{\sigma_{3,0}} \right)^{k_2} \cdot \left( \frac{\sigma_d}{\sigma_{d,0}} \right)^{k_3} \quad \text{Equation 3-20}$$

Where:

$M_r$  = Resilient modulus (MPa)

$\theta$  = Bulk stress =  $\sigma_1 + \sigma_2 + \sigma_3$  (kPa)

$\sigma_3$  = Confining pressure (kPa)

$\sigma_d$  = Deviator stress (kPa)

$\theta_0, \sigma_{3,0}, \sigma_{d,0}$  = Reference stresses = 1 kPa

$k_1, k_2, k_3$  = Material coefficients

The abovementioned  $M_r$ - $\theta$  model (Eq. 3-19) and  $M_r$ - $\sigma_3$ - $\sigma_d$  model (Eq. 3-20) are relatively simple and extensively used to describe the stress dependence of  $M_r$ . The model parameters and  $R^2$  value for each relationship were derived and compared to select the most appropriate model. The effect of moisture content and compaction on the resilient stiffness was also considered.

### 9) Direct shear testing of compacted sands

Direct shear tests were carried out on the same four sample types (density and moisture content variations) prepared from the modified sands used for the triaxial testing to compare the peak shear parameters from the two tests. In this way, the influence of the confining membrane on the shear strength parameters obtained from the triaxial the tests can be examined. The direct shear tests were carried out in the geotechnical laboratory of Stellenbosch University, using the Digishear direct shear apparatus with a square shear box (60mm by 60mm by 20mm in size), in accordance with ASTM D3080 (2011).

To compact the modified Mfuleni sand specimens to the prescribed dry densities of 1660kg/m<sup>3</sup> and 1560kg/m<sup>3</sup>, both at OMC and at 75% of OMC, the Wirtgen vibratory hammer was used. Specimens were carefully cut from the compacted sands into a metal square sampler with the same dimensions as the shear box. The samples were transferred to the square shear box with porous plates positioned at the bottom and the top of the specimen. As for the conventional direct shear tests (refer to Section 3.3.2.2 (7)), a vertical force was applied to the sample via a loading plate and a shear force applied at a strain rate of 0.01mm/min. Again, three different vertical forces were applied to each soil type, exerting pressures of 50kPa, 100kPa, and 200kPa. For the partially saturated sands, the peak total stress parameters of  $\phi_{max}$  and  $c_{max}$  were obtained.

## 3.4 Data capturing

The 155 site investigation reports from previous investigations contained information from several investigation points, namely test pits, boreholes, in-situ tests, groundwater sampling locations and monitoring wells. In addition, the results from laboratory tests undertaken on sands sampled from the test pits and boreholes, were also contained in the reports. Information from soils laboratories comprised raw test data sheets.

The location of each of the investigation points retrieved from the investigation reports was plotted on a digital geological map of Cape Town (1:250 000 Cape Town sheet), constructed as an overlay in Google Earth. This allowed verification of the respective geological formations. The coordinates of the points were provided in most reports, however, in some reports only approximate localities were given. To account for changes in geological formation with depth, to ensure that the correct formation is paired with a particular result, profile descriptions were carefully examined and the changes in texture and origin noted. The geotechnical data was categorised and captured in MS Excel spreadsheets in the form in which it was obtained from the laboratory. Only results from tests undertaken in the windblown Cape Flats sands were included in the database. Data checks were done and outliers or unrealistic values, considered biased or simply incorrect, were discarded as described in the relevant sections of Chapter 4. The soil classification and characterisation properties were determined from the raw site and laboratory data (refer to Section 3.5).

With each in-situ and laboratory test result, the testing/sampling depth was recorded. The position of the permanent or perched groundwater table level at the time of the investigation (or the absence of groundwater) was also noted as well as the in-situ moisture contents. Changes in the soil moisture content will influence, amongst other things, the consistency, compressibility and shear strength of the soil, as well as the collapsibility and in-situ density. It is for this reason that the in-situ moisture content was recorded where available. Moisture content descriptions were either taken from soil profiles near in-situ test locations, or the laboratory derived values grouped with soils sampled near the in-situ tests.

When capturing penetrometer test data, penetration resistances associated with refusal of test on gravel (often calcrete gravel) are considered unrepresentative of the overall soil consistency and were discarded.

Taking into consideration all data collected, including past investigation outcomes and the above-discussed fieldwork and laboratory testing by the candidate, a summary of data available for processing and analysis is given as follows:

- **978** site investigation points (test pits, boreholes, in-situ tests (not including SPT's within a BH), and groundwater monitoring wells/sampling locations (**591** in the Witzand Formation, **289** in the Springfontyn Formation, and **98** in the Langebaan Formation).
- Number of boreholes: **178**.
- Number of test pits: **547**.
- Number of in-situ test results [SPT (individual tests counted), CPT/CPTu (profiles of test results counted), DCP, dry density, plate load, infiltrometer, CSW]: **1740**.
- Number of laboratory test results (full test sets, e.g. CBR at all compacted densities for a soil or set of Atterberg Limits): **1552**.
- Number of groundwater level measurements (including those from test pits): **471**.
- For the approx. **460km<sup>2</sup>** study area, there are approx. **2** site investigation points per sq.km, and **8** data points (in-situ, laboratory or groundwater level result) per sq.km.
- Areas with concentrated data include Blue Downs, Khayelitsha, Grassy Park, Airport Industria, Epping, and Bellville South,
- Areas with no or limited data include Mitchells Plain, Mountview, Pinelands, and Delft.

The number of values/results associated with each classification and characterisation property are specified in the individual sections that follow.

## **3.5 Data processing**

### **3.5.1 Introduction**

Data processing involved the application of various methods and transformation models to determine and/or estimate the soil classification and characterisation parameters from the raw data. Some of the properties, namely the plasticity properties, moisture content, specific gravity, maximum dry density and optimum moisture content, and minimum density, were obtained directly from laboratory testing, requiring no further data processing. Similarly, the results of in-situ density tests providing bulk density values, were extracted - as is - from investigation reports.

The remainder of the geotechnical parameters, namely the grading properties, CBR, corrosivity, erodibility, hydraulic conductivity, shear strength parameters, dilative/contractive behaviour, compressibility (soil elastic modulus), and collapsibility were determined or predicted from the results of in-situ or laboratory tests, using established methods and predictive models. The test methods associated with these parameters are the laboratory soaked CBR test, plate load test, direct shear and triaxial tests, constant head permeability test, and the collapse potential test.

Once all classification and characterisation parameters were determined, data analysis commenced, involving descriptive statistics to summarise and draw conclusions from the data, and regression techniques to find statistically significant relations between the studied parameters, allowing the influence of properties such as grading and penetration resistance on the selected dependent variables such as CBR and  $V_s$  to emerge.

The various methods and models used to determine the classification and characterisation parameters of the Cape Flats soils from the captured data, are described below.

### **3.5.2 Grading properties**

To allow determination of soil texture and gradation in the Cape Flats sands, and to aid classification according to the USCS, AASHTO, TRH14, and soil erodibility classification systems (refer to subsequent sections), the raw grading results obtained for 400 Cape Flats sand samples were processed as described below. The distribution of localities with known grading data is shown on Figure C1 in Appendix C.

The sieve and hydrometer analysis results were obtained in the form shown in Table 3-6, illustrating the percentage particles smaller than the corresponding sieve size given in the table. The sieve sizes depend on the grading test standard followed. From this, the percentage gravel, coarse sand, medium sand, fine sand, silt, and clay was calculated, based on ASTM size boundaries (refer to Figure 2.5 from Section 2.5.2). In the absence of hydrometer analysis results, the combined percentage clay and silt size particles was determined. Known sampling depths allowed changes in soil texture with depth to be studied (in addition to inter-formation variation). The vast majority of obtained grading data is for soils sampled from the upper 3m of the soil profile.

**Table 3-6: Typical grading test result**

Particle size (mm)	Percentage smaller	Particle size (mm)	Percentage smaller
75	100	2.36	100
63	100	2.0	100
53	100	1.18	99
37.5	100	0.6	68
26.5	100	0.425	51
19	100	0.3	42
13.2	100	0.15	14
9.5	100	0.075	2
6.7	100	0.05	2
4.75	100	0.005	0

PSD curves were drawn (plotting particle size - percentage smaller data points, connected with smooth lines) to study the distributions of grain sizes in the soils. To determine the coefficient of uniformity ( $C_u$ ) and the coefficient of curvature ( $C_z$ ), the  $D_{10}$ ,  $D_{30}$  and  $D_{60}$  particle sizes were read off the graphs. The equations for  $C_u$  and  $C_z$  are given below and the grading criteria, based on values of  $C_u$  and  $C_z$ , given in Section 2.5.2. The derived curve characteristics aided classification of the Cape Flats sands, and the interpretation of obtained design parameters.

$$C_u = \frac{D_{60}}{D_{10}} \quad \text{Equation 3-21}$$

$$C_z = \frac{D_{30}^2}{(D_{10} \times D_{60})} \quad \text{Equation 3-22}$$

The shrinkage product ( $Sp$ ) and the grading coefficient ( $Gc$ ) were also determined from the grading results for the assessment of the suitability of the Cape Flats sands as unpaved wearing course gravel. These material properties were calculated as follows:

$$Sp = LS \times \%P_{0.425} \quad \text{Equation 3-23}$$

Where:

LS = Linear shrinkage (obtained from the bar linear shrinkage test, Atterberg limits test procedures)

$\%P_{0.425}$  = Percentage by mass passing 0.425mm sieve

The sandy Cape Flats soils will typically display no reduction in length upon drying, resulting in a shrinkage product equal to zero (irrespective of grading). The lack of plastic fines and cohesion will markedly influence its suitability as a wearing course.

$$Gc = (\%P_{26.5} - \%P_{2.0}) \times \%P_{4.75} \div 100 \quad \text{Equation 3-24}$$

Where:

$\%P_{26.5}$ ,  $\%P_{2.0}$ ,  $\%P_{4.75}$  = Percentage particles passing the given sieve sizes

A lack of particle sizes greater than 2mm in diameter (coarse sand and gravel), will result in  $Gc$  being equal to zero.

The grading modulus (GM) was calculated from Equation 3-25, providing an indication of the coarseness of the material and its quality as a pavement layer material. The grading modulus was used to aid the interpretation of the compaction (MDD and OMC) and the CBR results.

$$GM = [(300 - (P_{2.0} + P_{0.425} + P_{0.075})) / 100] \quad \text{Equation 3-25}$$

Where:

%P<sub>2.0</sub>, %P<sub>0.425</sub>, %P<sub>0.075</sub> = Percentage particles passing the given sieve sizes

### 3.5.3 Material classification

The grain size characteristics, plasticity properties, bearing strength and swell potential of the Cape Flats sands were used to classify the soils according to three systems widely used by geotechnical and pavement engineers in Southern Africa, namely the Unified Soil Classification System (ASTM D2487, 2017), the AASHTO Soil Classification System (AASHTO M145-91, 2008), and the TRH14 classification system (TRH14, 1985). This will aid the understanding of the engineering behaviour of the material. To study the distribution of the classified soil types, the sampling locality and depth and the soil formation were noted with each result. In Figures C3 and C5 in Appendix C, the localities of the classified samples are shown.

The USCS and AASHTO classification systems group materials based on the particle sizes present in the soil, the distribution of these sizes, and the consistency limits of the soil fines. These classification systems are included as Figures B2 and B3 in Appendix B, from which the classification procedures can be construed. Both the AASHTO and TRH14 systems are used by pavement engineers to guide the selection of materials for road construction. In addition to grading characteristics and soil plasticity, the TRH14 system includes the CBR at various compaction levels and the maximum CBR swell in the classification. The TRH14 classification table is given in Appendix B (Figure B1). The soils from the study area fall within the gravel soil category (G7 to G10 quality materials) of the TRH14 system. For the G8 to G10 soils, no grading and Atterberg limits requirements apply, and only the CBR and CBR swell values were used to classify the material. In this regard, measured strengths at 93% of mod AASHTO maximum dry density were used. Less soils were classified according to the TRH14 system – compared to the other systems – because of the additional requirement of CBR and CBR swell values.

### 3.5.4 California Bearing Ratio (CBR)

Laboratory values of soaked CBR were obtained for 166 soils from past investigation reports, and in-situ CBR values were derived from 168 dynamic cone penetrometer (DCP) tests, undertaken on 33 sites across the Cape Flats to evaluate subgrade strength. All sampling and testing sites at which the CBR strength was determined, are shown in Figure C5 of Appendix C.

Laboratory derived CBR values are generally given at densities of 98%, 97%, 95%, 93%, and 90% mod AASHTO maximum dry density. All the samples on which CBR tests were conducted are from the shallow soil profile (surface to 3m depth).

The predictive model proposed by Paige-Green and Du Plessis (2009), presented as Equations 3-26a and b, was used to estimate field CBR (with depth) from cone penetration rate values (2986 DN values in total - in mm/blow). This method, based on research on South African soils, provides a good indication of field CBR, bearing in mind the material dependence of DCP outcomes (Paige-Green and Du Plessis, 2009). Only cone penetration resistances in the windblown sandy soils of

the Cape Flats were utilised. Maximum DCP test depths of the order of 4m below ground level were achieved. The DCP CBR was determined at the in-situ moisture content and density at the time of testing and, as such, the empirically obtained CBR values will be assessed in terms of these influences. The accompanying soil profiles were studied with the penetration results, providing insight into observed trends and outlier values. In addition to inter-formation variation in DCP CBR, the depth profiles enabled examination of vertical changes in in-situ CBR.

$$CBR = 410 \times DN^{-1.27} \quad \text{if } DN > 2\text{mm/blow} \quad \text{Equation 3-26a}$$

$$CBR = (66.66 \times DN^2) - (330 \times DN) + 563.33 \quad \text{if } DN \leq 2\text{mm/blow} \quad \text{Equation 3-26b}$$

### 3.5.5 Corrosivity

In addition to the 101 pH and 98 electrical conductivity values for soils and groundwater of the Cape Flats, from which an initial indication of corrosion potential (acidity/alkalinity and corrosion rate) can be obtained, the results from chemical analysis carried out on representative soils and groundwater from the study area, were also utilised to assess its aggressiveness to corrode buried concrete and metal. In this regard, the Langelier Saturation Index and the aggressiveness index, the leaching-corrosion and spalling-corrosion sub-indices, and the aggressive chemical environment for concrete (ACEC) class were determined from the laboratory results. The calculation procedures are given below, and the locations of sampled soils and groundwater which were assessed for its potential corrosivity are shown in Figure C6 of Appendix C.

#### Langelier Saturation Index (LSI)

To determine the aggressiveness of subsurface waters in the Cape Flats towards metallic components, the LSI of water sampled from a borehole and test pit in Macassar and Mfuleni respectively, was calculated as follows (Roberge, 2007):

$$LSI = pH(actual) - pH_s \quad \text{Equation 3-27}$$

$$\text{And } pH_s = (9.3 + A + B) - (C + D) \quad \text{Equation 3-28}$$

Where:

$$A = \frac{(\log_{10}[TDS]-1)}{10}$$

$$B = -13.12 \times \log_{10}(\text{°C} + 273) + 34.55$$

$$C = \log_{10}[Ca^{2+} \text{ as } CaCO_3] - 0.4$$

$$D = \log_{10}(\text{Alkalinity as } CaCO_3)$$

From the above it is evident that the total dissolved solids (TDS in mg/l), water temperature (°C), alkalinity (as CaCO<sub>3</sub> in mg/l) and calcium hardness (mg CaCO<sub>3</sub>/l), are required to calculate the calcium carbonate-saturated pH (pH<sub>s</sub>), and ultimately the LSI. If the LSI has a negative value (pH<sub>s</sub> > pH<sub>actual</sub>), the water will dissolve calcium carbonate and it is not scale forming (not protective). If the LSI has a positive value (pH<sub>s</sub> < pH<sub>actual</sub>), calcium carbonate precipitation can form a protective coating. An LSI value close to zero indicates borderline scale potential.

### **Aggressiveness indices (Basson, 1989)**

The aggressiveness of groundwater from Macassar and Mfueni in the study area towards buried concrete was assessed by means of the aggressiveness index (N), the leaching-corrosion sub-index (LCSI) and spalling-corrosion sub-index (SCSI), developed by Basson (1989). The required properties are shown in Table 3-7, determined by Bemlab as described in Section 3.3.2.2. The determination of indices  $N_1$  to  $N_7$  from the property values are also shown in the table, from which the N index, LCSI and SCSI were subsequently determined as follows:

$$N = N_1 + N_2 + N_3 + N_4 + N_5 + N_6 \quad \text{Equation 3-29}$$

$$LCSI = (N_1 + N_2 + N_3) \div 3 \quad \text{Equation 3-30}$$

$$SCSI = (N_4 + N_5 + N_6) \div 3 \quad \text{Equation 3-31}$$

The  $N_7$  index value, associated with the chloride ion content, is used to provide countermeasures against chloride corrosion (the minimum cover of concrete over the reinforcement) where embedded steel is present. The value of total dissolved solids ( $V_8$ ) is used when applying the optional corrections described below.

**Table 3-7: Calculation of indices  $N_1$  to  $N_7$  for the determination of N, LCSI and SCSI (Basson, 1989)**

Property	Units	Value	Formula	Index
pH	$1 \div \log H$	$V_1$	$200 \times (9.5 - V_1)$	$N_1$
$pH_s$	$1 \div \log H$	$V_2$	$-2\,000 \times (V_1 - V_2)$	$N_2$
Calcium hardness (as $CaCO_3$ )	mg/l	$V_3$	$2.2 \times (500 - V_3)$	$N_3$
Total ammonium ion ( $NH_4$ )	mg/l	$V_4$	$10 \times V_4$	$N_4$
Magnesium ion (Mg)	mg/l	$V_5$	$0.6 \times V_5$	$N_5$
Total sulphate ( $SO_4$ )	mg/l	$V_6$	$0.3 \times V_6$	$N_6$
Chloride ion (Cl)	mg/l	$V_7$	$0.2 \times V_7$	$N_7$
Total dissolved solids (TDS)	mg/l	$V_8$	-	-

The calculated N, LCSI and SCSI indices are applicable to standard temperature conditions (20°C) and laminar flow conditions. Optional corrections are provided for turbulent flow conditions, stagnant water conditions, cyclic wetting and drying conditions, and variations in the prevailing water temperature. A corrected final index (FI) can be calculated, and the aggressiveness assessed, following guidelines given by Basson (1989). These optional corrections were not applied in determining the aggressiveness of groundwater in the Cape Flats, and the abovementioned recommended guidelines were applied to the N index. Where the water was found to be aggressive, the dominant corrosion sub-index was also identified (leaching or spalling corrosion) to assist in the assessment of required countermeasures. The chloride ion content was considered in the assessment of chloride corrosion.

### **Aggressive chemical environment for concrete (ACEC) classification (BRE, 2005a)**

The aggressive chemical environment for concrete (ACEC) classification system was developed by the Building Research Establishment (BRE), and the latest version presented in Special Digest 1: 2005 Part C. For the current study, ACEC classes were determined for sites in Macassar, Mfuleni,

and Strandfontein, based on the results of chemical analysis undertaken on 16 groundwater specimens and one water-soil extract from the three localities. The classification system (applicable to the natural ground conditions at the investigated sites) is shown in Table 3-8. Firstly, the water-soluble sulfate content ( $\text{SO}_4$  in mg/l) of the ground and groundwaters was used to find the design sulphate class (DSC) associated with each location. Where both 2:1 water/soil extract and groundwater were sampled at a specific location, the highest of the two design sulfate classes was taken as the DSC for the location. Within the DSC, the mobility of the groundwater and the pH determined the ACEC class assigned to the ground. In this regard, mobile groundwater conditions – defined as water which is free to flow at a rate greater than  $10^{-7}\text{m/s}$  – were present at the sampling sites. The ACEC class determines the required concrete quality.

**Table 3-8: ACEC classification for natural ground conditions (BRE, 2005a)**

Design Sulfate Class for location	2:1 water/soil extract	Groundwater	Total potential sulfate	Groundwater		ACEC Class for location
				Static	Mobile	
	$\text{SO}_4$ mg/l	$\text{SO}_4$ mg/l	$\text{SO}_4$ %	pH	pH	
DS-1	<500	<400	<0.24	≥2.5		AC-1s
					≥5.5	AC-1 <sup>d</sup>
					2.5-5.5	AC-2z
DS-2	500-1 500	400-1 400	0.24-0.6	>3.5		AC-1s
					>5.5	AC-2
				2.5-3.5		AC-2s
					2.5-5.5	AC-3z
DS-3	1 600-3 000	1 500-3 000	0.7-1.2	>3.5		AC-2s
					>5.5	AC-3
				2.5-3.5		AC-3s
					2.5-5.5	AC-4
DS-4	3 100-6 000	3 100-6 000	1.3-2.4	>3.5		AC-3s
					>5.5	AC-4
				2.5-3.5		AC-4s
					2.5-5.5	AC-5
DS-5	>6 000	>6 000	>2.4	>3.5		AC-4s
				2.5-3.5	≥2.5	AC-5

### 3.5.6 Erodibility

The assessment of soil erodibility in the Cape Flats comprised the following three approaches:

- Assigning a dominant erosion index to the whole study area, providing an indication of the anticipated overall soil erosion risk (soil loss by water erosion), based on the erosion influences making up the Revised Universal Soil Loss Equation (RUSLE),
- Determination of the soil erodibility factor at several locations in the study area - including a range of soil textures – allowing the likely bounds of the K-factor in Cape Flats sands to be investigated,
- Evaluating the erodibility of the Cape Flats sands when used as gravel wearing course in unpaved roads, based on the grading results and bar linear shrinkage (using the TRH20 classification system).

### **Erosion hazard potential (WRC, 2010)**

Electronic copies of the erosion hazard potential maps produced by the Water Research Commission in 2010 were obtained from the Water Division of the Civil Engineering Department at Stellenbosch University for ten sediment yield regions in South Africa. The map containing the Cape Flats area, known as Region 8 of 10, was used to establish the erosion hazard and prediction of sediment yield in the study area. The catchment areas are also delineated on the map.

To determine the predominant erosion index of the study area, a pdf version of the Region 8 erosion hazard potential map was opened. The object data tool was selected, and the Model Tree opened. The required catchment was selected, and the catchment properties displayed. For each catchment, the proportion of the area (in square kilometres) covered by specific hazard classes was estimated and a weighted average determined to give a dominant erosion index value for the catchment. Varying portions of four catchment areas are located within the boundaries of the Cape Flats area. For this reason, the total sq.km area within the study boundaries, characterised by each erosion index class, was subsequently calculated and a dominant erosion index value assigned to the Cape Flats, revealing the general susceptibility of the sands to erosion by flowing water.

### **Soil erodibility factor (Wischmeier and Smith, 1978)**

The soil erodibility factor (K-factor), which provides an indication of the susceptibility of soil grains to detach and be transported by rainfall and runoff, was estimated for the soils from the Cape Flats, using the soil erodibility nomograph by Wischmeier and Smith (1978) shown in Figure 3-23. The nomograph was used in preference to the subsequently derived K-factor equations, based on the superior accuracy of the nomograph, especially for soils with high fine sand contents. The influencing factors of soil structure and permeability are incorporated as broad descriptive categories (based on property value ranges), which do not reflect the influence of slight changes in these properties on the K-value (most Cape Flats sands fall within a single category of permeability and structure). The organic matter content is unknown for the studied Cape Flats sands, and only soils with 0% organic matter (from profile texture description) were included in the evaluation. For these reasons, soil texture was the main factor separating erodibility factor values within the study area. The determination of individual K-factors for all soil samples with known grading data was considered unnecessary, bearing in mind the relatively narrow limits within which soil grading varies in the study area. As an alternative, ten soils with a range of textures were selected to illustrate the probable limits within which the K-factor is likely to vary (for the given permeability and structure class). The influence of substantial deviations in permeability, organic matter content and soil structure (from the norm) on the K-factor is discussed in the results section.

The K-factor was determined from the nomograph by following vertical and horizontal paths from left to right. First, the percentage silt and very fine sand (0.002-0.1mm) was marked on the left vertical axis. Then, straight lines were drawn to the percentage sand (0.1-2.0mm), percentage organic matter, soil structure class and permeability class - in this sequence. Finally, the K-factor was read from the vertical axis as shown in Figure 3-23. The percentage particles in the abovementioned size ranges were calculated from the grading results. The Cape Flats sands typically fall within soil structure class 1 (very fine granular soil with particle size <1mm) and permeability class 1 (rapid flow, sandy soils). Typically, the permeability class index is determined

by means of a cylinder infiltrometer test. For this study, infiltration and flow rates from past and current investigations were used to determine the permeability class. It should be noted that permeability results were only available for the sandy Cape Flats soils and, as such, the K-factor could not be calculated for calcretised or clayey soils, in which permeability will be significantly reduced. As mentioned above, hypothetical values will be derived based on anticipated permeability classes for these deposits. The ten soils for which the K-factor was determined, are from the Witzand, Springfontyn and Langebaan Formations. The obtained K-factor represents the rate of erosion (A) (in t/ha/year) per erosion index (EI) unit from a standard plot (221.3m long, 9% length wise slope).

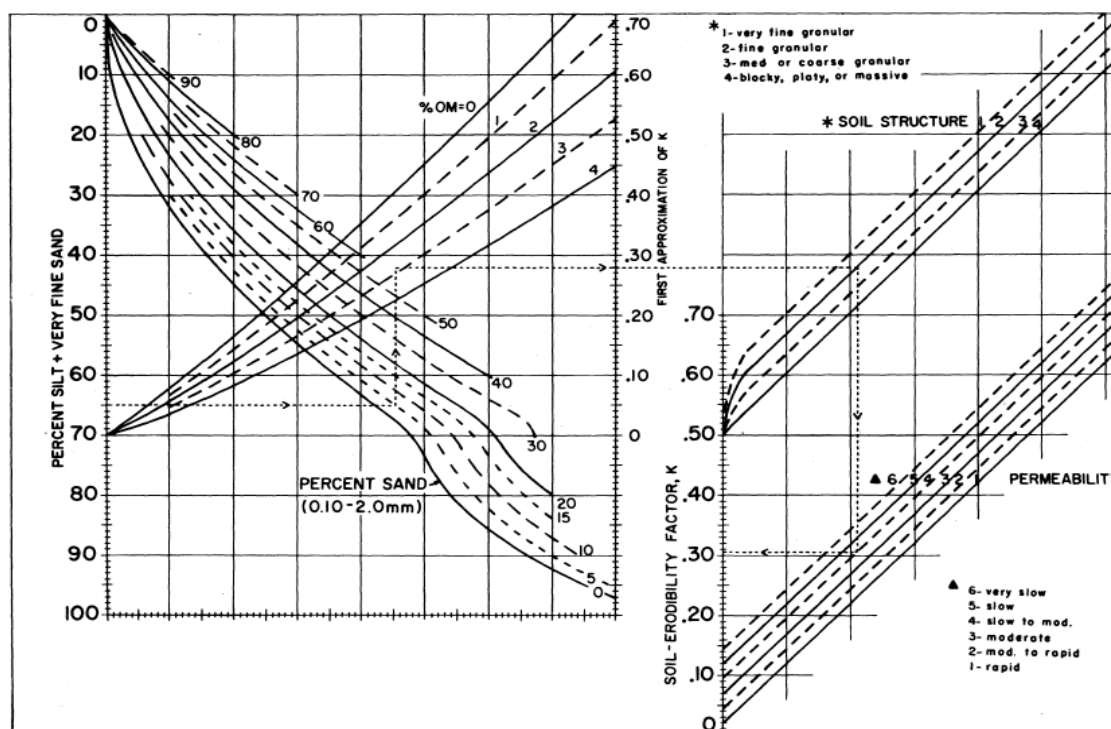
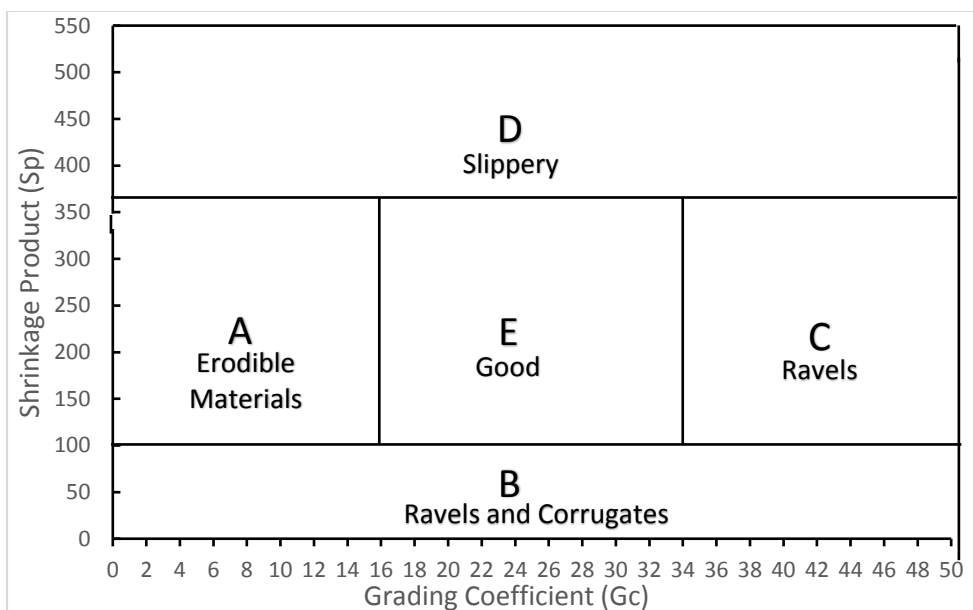


Figure 3-23: Soil erodibility nomograph (Wischmeier and Smith, 1987)

### Erosion of unpaved gravel wearing course (TRH20, 1990)

The erodibility of the Cape Flats sands, when utilised as a wearing course for unpaved roads, was evaluated using the system proposed in TRH20 (1990). The classification graph is presented in Figure 3-24. The  $S_p$  and  $G_c$  values calculated from the grading results (and bar linear shrinkage) as given in Section 3.5.2, were plotted on the graph to reveal the anticipated performance of the sands from the study area. The values  $S_p$  and  $G_c$  places the material in one of five categories namely: “erodible”, “slippery”, “ravels”, “ravels and corrugates”, and “good”. The suitability of the Cape Flats sands as gravel surfacing and its potential to erode with surface water flows will be governed by its grain sizes, gradation and fines content. The assessment of erodibility mostly applies to soils from the upper 3m of the soil profile. The results were separated by formation to compare the erodibility risk and the overall performance as gravel surfacing.

The localities where soils were sampled for erodibility assessment (including K-factor values and gravel wearing course suitability) are shown in Figure C7 in Appendix C.



**Figure 3-24: Performance categories for gravel wearing courses (after TRH20, 1990)**

### 3.5.7 Collapsibility

To investigate the potential of the windblown sands from the Cape Flats to undergo collapse settlement, the results from 21 collapse potential tests, undertaken on undisturbed sandy soils sampled from four sites, were studied. Except for one site underlain by Springfontyn Formation sands, all other sampled materials were sourced from the Witzand Formation. Twelve of the test results originate from oedometer tests carried out on soils from Mfuleni during the current research, as described in Section 3.3.2.2. The natural moisture contents of the specimens were well-maintained and noted, and the relative densities obtained from DCP test results and/or in-situ profile descriptions.

The void ratio at the end of each load increment in the oedometer test was plotted against the corresponding vertical stress to reveal the compressibility and collapse potential of the sands. The change in void ratio at either 100kPa or 200kPa was calculated (depending on point of saturation) and, together with the initial void ratios, used to calculate the percentage collapse (see Figure 3-25). The percentage collapse on wetting at an applied vertical stress of 200kPa is defined as the collapse potential of the soil (Schwartz, 1985). A description of the severity of the problems associated with collapse potential ranges is given in Table 3-9.

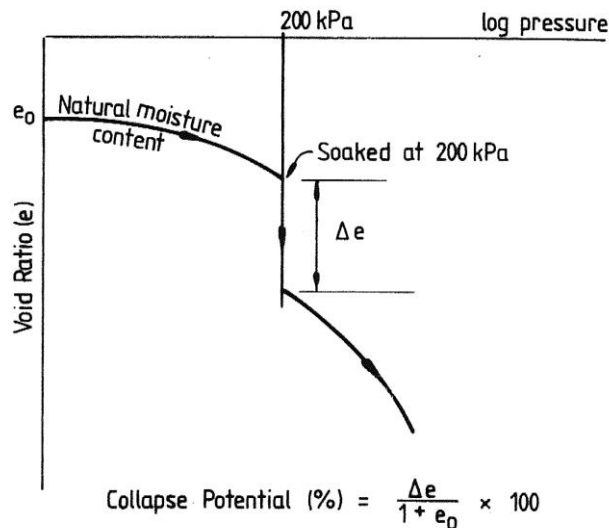


**Figure 3-25: Interpretation of a collapse potential test result (Schwartz, 1985)**

**Table 3-9: Evaluation of collapse potential values (Schwartz, 1985 after Jennings, 1974)**

CP (%)	Description of problem
0 - 1	No problem
1 - 5	Moderate trouble
5 - 10	Trouble
10 - 20	Severe trouble
>20	Very severe trouble

In addition to the laboratory test results, existing empirical criteria by Brink (1985) based on dry density, and Priklonski (1952) (as cited in Howayek et al., 2011) based on the liquidity index, were utilised to provide an approximation of the collapsibility of Cape Flats sands from 11 sites, and compared to the outcome of the collapse potential tests. These methods are based on the critical influences of density, moisture content and plasticity on collapsibility.

### **Brink (1985) empirical method**

Brink (1985) gives the following relationship between the collapse potential index (CP), and dry density ( $\rho_d$  in  $\text{kg/m}^3$ ) for aeolian sands:

$$CP = \frac{1672 - \rho_d}{22} \quad \text{Equation 3-32}$$

The guiding values given in Table 3-9 applies to the outcome of Equation 3-32.

This method relies only on dry density, having found that windblown soils with a dry density equal to or exceeding  $1672 \text{ kg/m}^3$  usually do not collapse. The texture and structure of the soil is not considered. Although dry density has been found to be a poor indicator of the likelihood and extent of collapse settlement, this method can provide an initial indication of the collapse potential of sandy soils such as the Cape Flats sands, and will be compared to the findings of the laboratory analyses. Field measurements of dry density from current and past investigations were used. In this regard, the nuclear density gauge was used to approximate the bulk density, natural moisture content, and dry density at 13 test positions spread across four sites as described in

Section 3.3.2.1. Two of these sites are underlain by Springfontyn Formation deposits and two by Witzand Formation deposits. Measurements were made at depths ranging from surface to 1m below ground. The calculated collapse potential thus reveals the possible degree of collapse in the upper metre of the Cape Flats soil profile at these localities (based simply on dry density).

### **Prikloński (1952) empirical method**

In 1952, Prikloński (refer to Howayek et al., 2011) published a classification of collapsible soils based on the liquidity index ( $K_D$ ). This method was additionally used to estimate the potential of the Cape Flats sands to collapse:

$$K_D = \frac{w_n - PL}{PI} \quad \text{Equation 3-33}$$

Where:

$w_n$  = Natural moisture content (%)

PL = Plastic limit (%)

PI = Plasticity index (%)

The relationship between severity of collapse and  $K_D$  is given in Table 3-10. A  $K_D$  value below zero reflects a very dry soil ( $PL > w_n$ ), possibly susceptible to severe collapse upon saturation. It is evident that a change in the natural moisture content (for the same soil) will influence the obtained value of  $K_D$  and thus the severity of the problem. The higher the moisture content, the more the soil will compress during the application of load and the less it will collapse on subsequent saturation. When  $w_n > PL$ , the PI value of the soil separates non collapsible soils from swelling soils.

**Table 3-10: Evaluation of  $K_D$  (Howayek et al., 2011)**

Liquidity index, $K_D$	Description of problem
<0	Highly collapsible
>0.5	Non-collapsible
>0	Swelling soils

The natural moisture content and plasticity properties of 11 samples of windblown sand from seven sites in the study area were used to calculate  $K_D$ . The non-plastic nature of the Cape Flats soils limited the number of usable results ( $K_D$  indeterminate for non-plastic soils). The soils were classed as either highly collapsible (where  $PL > w_n$ ), non-collapsible or swelling soils (high PI soils), based on Table 3-10.

The sites from which soils were sampled and/or in-situ density tests performed to determine the collapse potential are shown in Figure C10 in Appendix C. The collapse potential results will be interpreted alongside available grading results, soil moisture contents and CT scan images of the Cape Flats sands from a past investigation.

### 3.5.8 Hydraulic conductivity

The hydraulic conductivity (k) of the Cape Flats sands was investigated as follows:

- Constant head permeability tests on sands sampled from Mfuleni, Gatesville, Blue Downs, Mitchells Plain, Bellville South and Matroosfontein (refer to Section 3.3.2.2),
- Semi-empirical and empirical methods put forth by Carrier (2003) and Chapuis (2004), applied to in-situ density and grading test results on soils from the study area, and
- Piezocone (CPTu) dissipation tests in the areas of Capricorn and Airport Industria.

This section focusses on the semi-empirical and empirical methods and the CPTu dissipation test and interpretation procedures to obtain estimates of k.

Studies undertaken by Goktepe and Sezer (2011) and Elhakim (2016) showed that the empirical formulae given by Kozeny-Carman (including the modified version by Carrier, 2003) and Chapuis (2004) give reasonably accurate permeability values for fine and medium grained sands, which are characteristic of the Cape Flats area. An overestimation of permeability values can, however, be expected in calcretised layers in the study area. Elhakim's research findings showed that permeability values obtained from CPT results (from the SBT index,  $I_c$ ) were typically in agreement with field pump test and laboratory falling head test values. However, Robertson and Cabal (2012) highlights the impreciseness of permeability values estimated from  $I_c$ , instead favouring k values from pore pressure dissipation tests.

The sampling and testing sites with known k estimates (and the associated method of determining k) are shown in Figure C11 of Appendix C. At some locations more than one method was used to estimate soil permeability, thus enabling comparison of the results.

#### Semi-empirical and empirical methods

##### 1) Carrier (2003) method

The well-known Kozeny-Carman equation, with modification by Carrier (2003), is given as follows:

$$k \left( \frac{cm}{s} \right) = 1,99 \times 10^4 \left[ \frac{100 \%}{\sum \frac{f_i}{D_{li}^{0,404} \times D_{si}^{0,595}}} \right]^2 \left( \frac{1}{SF} \right)^2 \left( \frac{e^3}{1+e} \right) \quad \text{Equation 3-34}$$

Where:

$f_i$  = Fraction of particles between two sieve sizes (%)

$D_{li}$  = Larger sieve size, in cm

$D_{si}$  = Smaller sieve size, in cm

SF = Shape factor

e = In-situ void ratio

Equation 3-34 was used to estimate the hydraulic conductivity of soils from 13 locations spread across four sites in the study area. These sites are in Capricorn, Mfuleni, Gatesville and Bellville in the Cape Flats. Void ratios were calculated from in-situ dry densities obtained from nuclear density tests carried out in the upper 1m of the soil profile at these sites. The calculation of void ratio from density requires a value of  $G_s$  – which was taken as 2.67 – and the in-situ moisture content, measured on-site with the nuclear density gauge and confirmed in the laboratory by

oven drying. The shape factor, which depends on the angularity of the soil grains, ranges between 6 and 8. Windblown sands are frequently rounded and sub-rounded due to the strong action of wind rounding the soil grains during transportation. A shape factor of 6.6, suggested by Loudon (1952) (as cited in Carrier, 2003) for rounded grains, was selected. The effect of increasing grain angularity on the estimated  $k$  values was also considered.

## 2) Chapuis (2004) method

The empirical relationship for the coefficient of permeability of natural uniform sands without plasticity put forward by Chapuis (2004) is written as (Das and Sobhan, 2018):

$$k \left( \frac{cm}{s} \right) = 2.4622 \left[ D_{10}^2 \frac{e^3}{(1+e)} \right]^{0.7825} \quad \text{Equation 3-35}$$

Where:

$D_{10}$ : Effective size (mm)

The grading and in-situ density test data for the sites in Capricorn, Mflueni, Gatesville and Bellville, was also used to estimate  $k$  from the empirical relation by Chapuis (2004) given in Equation 3-35. The soils from these sites comprise uniform and non-plastic sandy soils, suitable for the above relation. The obtained permeabilities were subsequently compared to values obtained using Equation 3-34. Additionally,  $k$  values from both predictive methods were compared to the experimental  $k$  values (from the constant head permeability test).

### CPTu dissipation test method

Estimates of saturated soil permeability were also obtained from the results of seven CPTu pore water pressure (PWP) dissipation tests undertaken in Capricorn and Airport Industria in the Cape Flats. Two CPTu's were carried out at each of the sites as described in Section 3.3.2.1. The PWP dissipation test details are given in Table 3-11. The depth of the water table was calculated by dividing the equilibrium pore pressure by the unit weight of water to obtain the height of water above the test position; this value was then subtracted from the test depth to give the depth of the water table.

**Table 3-11: CPTu dissipation test information**

CPTu test	Dissipation test depth (m)	Equilibrium pore pressure (kPa)	Estimated depth of water table (m)	Water table assumed for test position (m)
Capricorn CPTu 1	10.0	70	2.9	2.9
Capricorn CPTu 2	5.98	33	2.6	2.6
	9.10	64	2.6	
Airport CPTu 1	5.13	27	2.4	2.45
	9.06	64	2.5	
Airport CPTu 2	4.27	17	2.5	2.6
	9.68	68	2.7	

The dissipation of pore pressure is controlled by the coefficient of consolidation in the horizontal direction ( $C_h$  in  $m^2/year$ ) which, in turn, is influenced by soil permeability ( $k_h$  in  $m/s$ ) in the same direction and the constrained soil modulus ( $M$  in  $MPa$ ), representing the soil compressibility. The calculation of soil permeability from the PWP dissipation test is based on the following equation (Robertson and Cabal, 2012):

$$K_h = (C_h \times \gamma_w) \div M \quad \text{Equation 3-36}$$

Where:

$\gamma_w$  = Unit weight of water,  $9.8kN/m^3$

To determine the value of  $K_h$  at the depths given in Table 3-11, using Equation 3-36, the following procedure was followed:

The raw CPTu field measurements of cone tip resistance ( $q_c$ ), sleeve friction ( $f_s$ ), and pore pressure during penetration ( $u$ ), contained in a text file, were imported into the CPeT-IT software developed by GeoLogismiki for interpreting CPTu data. The ground water level at the specific test position was entered, as well as the CPT parameters used to estimate the geotechnical parameters (e.g. Young's modulus, shear modulus, friction angle, undrained shear strength). The applicable CPT parameters were assigned the following values: Probe radius =  $0.0183m$ , cone area ratio =  $0.8$ , and soil unit weight =  $19kN/m^3$ . Basic output data was produced, and the soil parameters calculated using established empirical relationships.

The CPTu dissipation test results contained in an Excel file, comprising two data columns of time ( $t$ ) and pore pressure measured behind the cone ( $u_2$ ), were then imported into the CPeT-IT software. The ground water level entered for the associated CPTu was brought over to the dissipation data module. Each dissipation test result was presented on a plot of pore pressure (kPa) against square root of time (sec). To estimate the coefficient of permeability from the dissipation test result, the coefficient of consolidation in the horizontal direction and the constrained soil modulus are required (refer to Equation 3-35). The coefficient of consolidation was calculated by Houlsby and Teh's (1988) theory as follows:

$$C_h \left( \frac{m^2}{yr} \right) = \frac{(T_{50}) r^2 \sqrt{I_r}}{t_{50}} \quad \text{Equation 3-37}$$

Where:

$T_{50}$  = Theoretical time factor, equal to  $0.245$

$r$  = Probe radius, equal to  $0.0183m$

$t_{50}$  = Time corresponding to 50% consolidation

$I_r$  = Rigidity index, equal to the shear modulus ( $G$ ), divided by undrained shear strength of clay ( $S_u$ ).

The CPeT-IT software allows the user to either select the value of  $I_r$  calculated by the application in the abovementioned manner from the input parameters and basic output data, or to assign an independently determined value to the parameter. For the sandy soils of the study area, the undrained shear strength was determined to be zero and, as such, a default value of  $100$  was assigned to  $I_r$  by the program. The following equation given by Tomlinson (1994) was therefore used instead to determine the rigidity index:

$$I_r = \frac{E}{2(1+\nu)\sigma'_{vo}\tan\phi'} \quad \text{Equation 3-38}$$

Where:

$\sigma'_{vo}$  = Effective overburden stress (kPa)

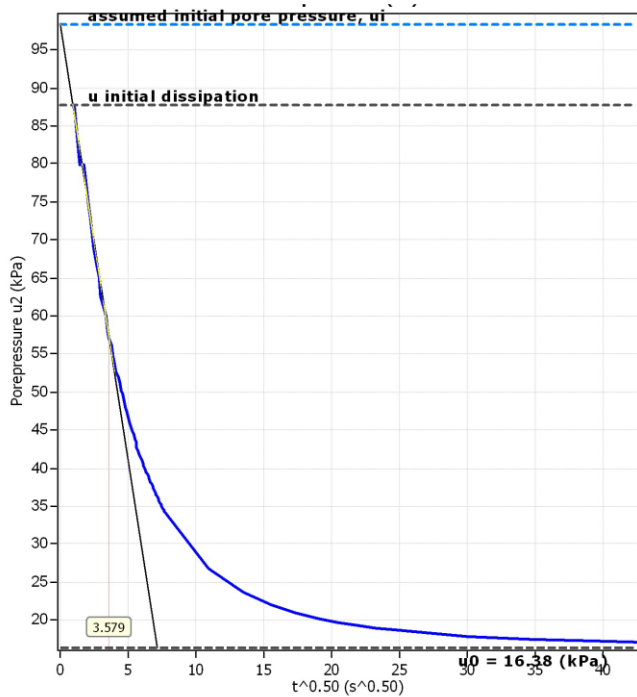
$\phi'$  = Drained friction angle, estimated from CPTu basic output data (°)

E = Deformation modulus, estimated from CPTu basic output data (MPa)

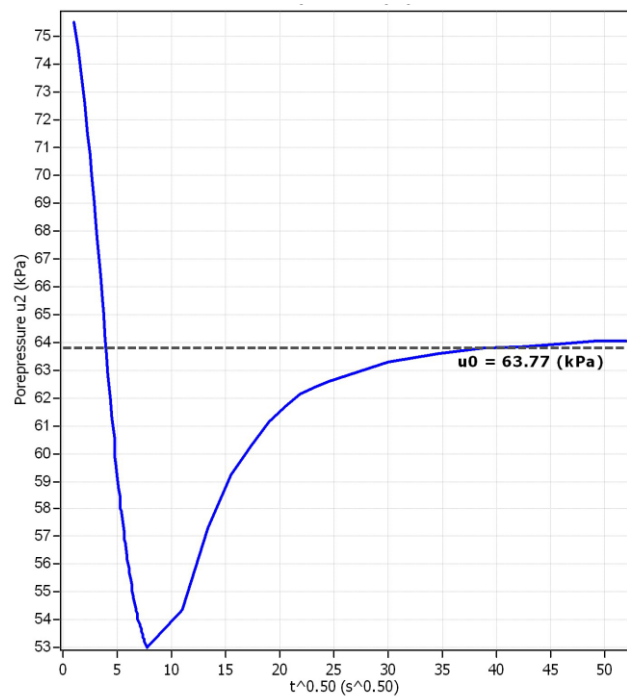
$\nu$  = Poisson's ratio, obtained from published figures

To determine the value of  $t_{50}$ , a graphical procedure suggested by Houlsby and Teh (1988) was used through the CPeT-IT software. The procedure entailed fitting a straight line over the linear portion of the square root time-pressure plot, where after the line was extended from time zero to the equilibrium pore pressure, and the  $t_{50}$  value calculated. The coefficient of consolidation was subsequently calculated. The graphical procedure followed to obtain  $t_{50}$  is illustrated in Figure 3-26a, in which a decrease in excess pore water pressure with time is seen.

The three PWP dissipation test results from Capricorn did not match theoretical models. A typical pore pressure-square root of time plot obtained from this site is shown in Figure 3-26b. The shape of the curve can be ascribed to a dilative response generating negative excess pore water pressure, which subsequently dissipate to equilibrium pore pressure by the influx of water. Dilative soils typically behave over-consolidated, i.e. an initial increase in pore pressure when penetration is stopped, followed by a decrease in pore pressure to the equilibrium value. The reverse dissipation data can possibly be ascribed to procedural problems such as unloading of push rods or a slight increase in down pressure from the rods (Vermeulen, personal communication 2018, June 7). When applying the before mentioned graphical interpretation procedure to the atypical result shown in Figure 3-26b, unrealistic values of  $t_{50}$  and  $C_h$  emerged. The corresponding permeability values obtained for the site sands were therefore discarded, and not included in later analysis.



(a)



(b)

**Figure 3-26: Interpretation of dissipation test curve from CPTu tests a) Airport CPTu 2 at 4.27m depth and b) Capricorn CPTu 2 at 9.1m depth**

The constrained soil modulus ( $M$ ), required for the determination of  $k_h$ , was calculated as follows (Robertson, 2009):

$$M \text{ (MPa)} = \alpha_M (q_t - \sigma_{vo}) \tag{Equation 3-39}$$

Where:

- $\alpha_M$  = Constrained modulus cone factor
- $q_t$  = Corrected total cone resistance (MPa)
- $\sigma_{vo}$  = Overburden pressure (MPa)

When SBT index  $I_c < 2.2$ :

$$\alpha_M = 0.0188 [10^{(0.55I_c + 1.68)}]$$

When SBT index  $I_c > 2.2$ :

- $\alpha_M = Q_{tn}$  (when  $Q_{tn} \leq 14$ )
- $\alpha_M = 14$  (when  $Q_{tn} > 14$ )

Where  $Q_{tn}$  = Normalised cone resistance (MPa)

The value of  $k_h$  was subsequently calculated at each of the CPTu dissipation test positions using Equation 3-36. A summary of the values of all input and intermediate parameters required to calculate  $k_h$  are given in Table 3-12. As previously mentioned, the values of  $t_{50}$  and  $C_h$ , and thus  $k_h$ , obtained for the dissipation tests associated with the tests from Capricorn, were discarded. The

permeability of the soils from Airport Industria will be interpreted with the soil density/relative density and texture data.

**Table 3-12: Summary of calculated parameter values for determination of  $k_h$**

CPTu test	Dissipation test depth (m)	Friction angle, $\phi'$ (°)	Elastic modulus, E (MPa)	Poisson's Ratio, $\nu$	Rigidity index, $I_r$	Time for 50% consolidation, $t_{50}$ (sec)	Coefficient of consolidation, $C_h$ ( $m^2/y$ )	Constrained Soil modulus, M (MPa)
Capricorn CPTu 1	10.0	42	129.4	0.35	42.2	193	87	162.1
Capricorn CPTu 2	5.98	45	127.4	0.4	54.2	182	104	159.7
	9.10	46	182	0.4	55	92	208	228.1
Airport CPTu 1	5.13	41	88.4	0.35	51	13	1402	110.8
	9.06	44	117.3	0.4	39	18	876	147
Airport CPTu 2	4.27	30	5	0.2	5.3	13	3 000	3.5
	9.68	44	134	0.4	41	12	1388	168

### 3.5.9 Shear strength

The shear strength parameters of the Cape Flats sands were obtained as follows:

- Experimentally from consolidated drained direct shear tests and monotonic loading triaxial tests, and
- Estimated from transformation models based on SPT and CPT data.

This section of the methodology focusses on the estimation of peak friction angles from SPT blow count and CPT cone resistance, using established empirical correlations.

Determination of the shear strength parameters from the abovementioned laboratory procedures are described in Section 3.3.2.2. The sites at which sands were sampled for laboratory determination of  $\phi'$  and  $c'$  are shown in Figure C12 in Appendix C. In addition, all CPT and CPTu positions, and boreholes with SPT's are shown in the Figure.

#### Standard penetration test (SPT) based models

It is common practice to estimate the shear strength of sand from the SPT and many graphs, tables and equations have been produced to relate SPT blow count and effective friction angle. The outcomes of these existing methods range from conservative to possibly overestimating soil strength. The selection of SPT-based transformation models for the current study was based on the proven accuracy and reliability of the specific method (from existing literature), as well as the ease with which the method could be applied to the large number of SPT blow count values from the study area. The SPT based methods selected for the study include those by Wolff (1989) (approximates graphical method by Peck, Hanson and Thorburn, 1974), Kulhawy and Mayne (1990), and Chen (2004). The obtained peak friction angles were assessed in terms of their agreement with experimentally obtained values, and only the  $\phi'$  values associated with the most accurate method were analysed and interpreted to characterise the Cape Flats sands in terms of shear strength.

### 1) Wolff (1989)

The well-known and widely used graphical method proposed by Peck, Hanson and Thorburn in 1974 was applied in the current study, but in the form given in Equation 3-40, produced by Wolff (1989) (refer to Hettiarachchi and Brown, 2009).

$$\phi' \approx 27.1 + 0.3(N_1)_{60} - 0.00054(N_1)_{60}^2 \quad \text{Equation 3-40}$$

Where  $(N_1)_{60}$  = SPT N-value corrected for overburden pressure and to 60% of the theoretical energy.

1526 SPT N-values were captured in the MS Excel database for the sands from the Cape Flats (from 178 boreholes). Refusal of the Raymond spoon, mostly on cemented layers and lenses, were recorded in places. As refusals are more of a reflection of the degree of cementing than of the shear strength of the sands, these results were omitted. To calculate the friction angles of the sands using Equation 3-40, the captured N-values first required correction for 60% energy and overburden pressure. As described in Section 2.4 from Chapter 2, all N values were assumed to be  $N_{60}$  values owing to the inability to estimate the hammer efficiency of SPT hammers commonly used in South Africa. Equation 2-2 from Chapter 2 was used to correct for overburden pressure to obtain  $(N_1)_{60}$ . To calculate  $(N_1)_{60}$ , the effective overburden pressure was required, calculated at SPT depths by applying the following property values:

$\gamma_{\text{sat}}$  = Saturated unit weight of soil below the water table, estimated as 21kN/m<sup>3</sup>

$\gamma$  = Bulk unit weight of soil above the water table, estimated as 19kN/m<sup>3</sup>

$\gamma_w$  = Unit weight of water (9.8kN/m<sup>3</sup>)

Where the depth of the groundwater table at an SPT location was unknown (and not indicated on the borehole log sheet), the position of the phreatic surface was assumed at 3.0m below natural ground level. Incorrectly estimating the depth of the water table above its actual position will result in an overestimate of the value of  $(N_1)_{60}$ . Estimates of  $\phi'$ , using the abovementioned relationship, are considered conservative, however, Clayton (1993) recommends its continued use in routine design.

### 2) Kulhawy and Mayne (1990)

The correlation produced by Kulhawy and Mayne (1990), is:

$$\phi' \approx \tan^{-1} \left\{ N_{60} / \left[ 12.2 + 20.3 \left( \frac{\sigma'_o}{P_a} \right) \right] \right\}^{0.34} \quad \text{Equation 3-41}$$

The relationship is dependent on vertical effective stress (incorporating a separate overburden pressure term into the equation) and should provide more accurate values of friction angle compared to the particularly conservative Wolff (1989) correlation.

### 3) Chen (2004)

More recently, Chen (2004) provided the transformation model presented as Equation 3-42 below. The captured SPT N-values were converted to  $(N_1)_{60}$  values as described above, and the drained friction angle calculated as follows:

$$\phi' \approx 27.5 + 9.2 \times \log_{10} [(N_1)_{60}] \quad \text{Equation 3-42}$$

The above described methodologies produced three sets of strength values for the same soil profiles from the study area. An evaluation of the accuracy of the derived friction angles, compared to experimental (direct shear)  $\phi'$  values, will be given in Chapter 4.

### **Cone penetration test (CPT) based models**

Numerous relationships, mostly presented in graph or equation form, have been published for assessing the drained friction angle from CPT tip resistance. As with the SPT-based methods, the selection of CPT-based transformation models for the current study was based on the accuracy and reliability of the specific method, as well as the ease with which the method could be applied to the large number of tip resistance ( $q_c$ ) values, obtained from 12 CPT's and four CPTu's undertaken by the candidate in the study area. From the CPTu's, continuous measurements of  $q_c$ , recorded every 1cm from surface to between 9.1m and 11.0m depth were obtained, whereas measurements of  $q_c$ , from surface to between 3m and 9m depth, were obtained from the CPT's for previous investigations.

Graphical CPT-based methods are particularly time-consuming and impracticable for large quantities of data. However, one such method given in Meigh (1987), based on a bearing capacity theory by Durgunoglu and Mitchell (1975), was selected to be applied at 0.5m intervals throughout the soil profiles. Transformation models published by Robertson and Campanella (1983) and Kulhawy and Mayne (1990) (refer to Robertson and Cabal, 2012) were also applied to estimate the shear strength of the Cape Flats sand. The three methods are discussed below.

#### **1) Durgunoglu and Mitchell (1975) (as cited in Meigh, 1987)**

The graphical method based on the theory of Durgunoglu and Mitchell (1975), is shown in Figure 3-27. The relationship is dependent on vertical effective stress and it applies to uncemented, normally consolidated quartz sand. It provides a reasonable lower bound value of  $\phi'$  for uniform quartz sand, becoming increasingly conservative as the soils become more compressible. The raw CPT and CPTu field measurement of cone resistance,  $q_c$ , recorded every half metre (or there about), was extracted from the data sheet containing all measurements of  $q_c$ . The cone resistance (in MPa) was subsequently plotted against the effective overburden stress (in  $\text{kN/m}^2$ ) calculated at the depth of the field measurement. As with the SPT-based methods, the groundwater table was estimated at a depth of 3m in cases where the water level could not be obtained from the penetration test data (e.g. CPT without pore pressure measurement). In some cases, the depth to groundwater could be estimated from nearby test pits or boreholes. Interpolation between diagonal lines of constant  $\phi'$  was required where data points placed between the lines, and the values were rounded to the nearest 0.5 degrees.

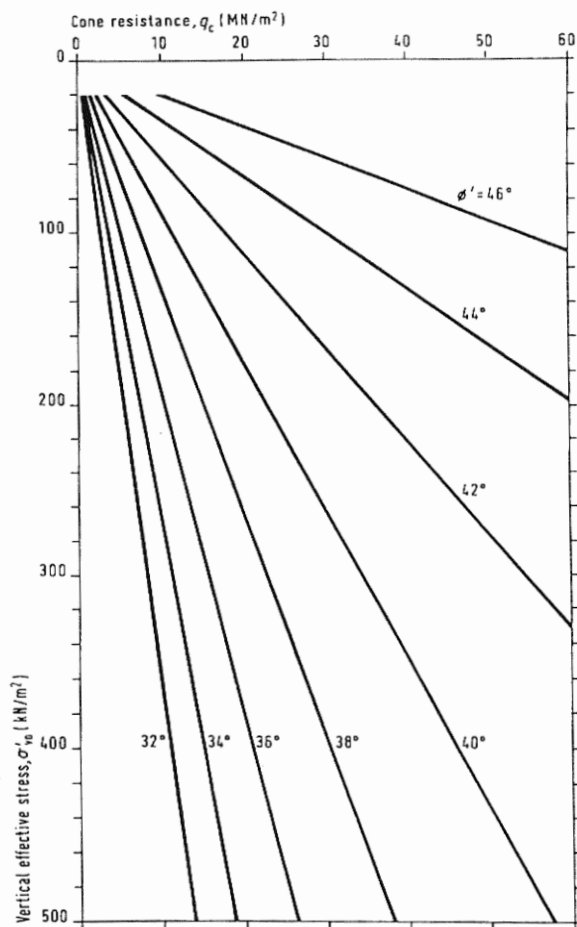


**Figure 3-27: Relationship between cone resistance and drained friction angle for quartz sand (after Durgunoglu and Mitchell, 1975 from Meigh, 1987)**

## 2) Robertson and Campanella (1983)

The correlation by Robertson and Campanella (1983), given by Equation 3-43, was used to estimate the peak angle of shearing resistance of uncemented, young quartz sands from the Cape Flats. Like the method proposed by Meigh (1987), highly compressible soils will produce low (conservative) estimates of the friction angle.

$$\varphi' = \tan^{-1} \left[ 0.1 + 0.38 \times \log_{10} \left( \frac{q_t}{\sigma'_{v0}} \right) \right] \quad \text{Equation 3-43}$$

Where:

$q_t$  = CPT corrected total cone resistance (in MPa) =  $q_c + u(1-a)$

Where:

$u$  = Pore pressure measured just behind cone (raw field measurement)

$a$  = Area ratio of tip equal to 0.8

The calculation of  $q_t$  requires the value of pore water pressure measured directly behind the cone. However, in the absence of pore pressure measurements (i.e. in the case of the CPT),  $q_t$  was set

equal to  $q_c$ . Equation 3-42 was therefore applied to both the CPTu and CPT results, producing a record of  $\phi'$  values with depth at the 16 test locations.

### 3) Kulhawy and Mayne (1990)

The correlation given by Equation 3-44 between drained friction angle and normalised cone resistance,  $Q_{tn}$ , which applies to clean, rounded, uncemented quartz sand, was published by Kulhawy and Mayne (1990) and evaluated with high quality field records by Robertson and Cabal (2012). Only the CPTu results were included, as the correction for pore pressure and the depth of the water table noticeably influences the outcome.

$$\phi' = 17.6 + 11 \log(Q_{tn}) \quad \text{Equation 3-44}$$

Where:

$$Q_{tn} = [(q_t - \sigma_{vo})/p_a](p_a/\sigma'_{vo})^n \quad \text{Equation 3-45}$$

Where:

$n$  = Stress exponent that varies with soil type

The stress exponent,  $n$ , was calculated from the soil behaviour type index,  $I_c$ , which in turn requires the value of  $Q_{tn}$  to be found. For this reason, an iteration process was followed to calculate the value of  $n$ . The normalised cone resistance, and subsequently the angle of internal friction, was calculated at 1cm intervals to the test refusal depths.

The methods proposed by Meigh (1987), Robertson and Campanella (1983), and Kulhawy and Mayne (1990) apply to uncemented sands. The CPT's and CPTu's were undertaken in sands from the Springfontyn and Witzand Formations respectively, which are typically uncemented, and therefore considered suitable for the above relations.

#### 3.5.10 Dilative/contractive behaviour (liquefaction potential)

The susceptibility of Cape Flats soil to undergo cyclic liquefaction, in which deformations occur only during cyclic loading, and flow liquefaction, in which there is a complete loss of shear strength (soil failure) due to pore pressure increase during static loading, was estimated following two approaches:

- Evaluation of the cyclic liquefaction potential of dense, dilative sands by means of an empirical SPT-based method put forward by Idriss and Boulanger (2004),
- Evaluating the volumetric response of the Cape Flats sands during shear (i.e. dilative or contractive) by means of a CPT-based method published by Robertson (2016), to determine whether flow liquefaction can occur (identification of loose, contractive soils).

The in-situ test locations (CPTu's and boreholes with SPT's) are shown in Figure C12 in Appendix C. The penetration test-based methods for assessing both cyclic- and flow liquefaction potential are presented below.

#### Evaluation of cyclic liquefaction

The susceptibility of a soil to undergo cyclic liquefaction can be estimated from its plasticity properties. The criteria's used to identify 'liquefaction prone' soils require the liquid limit value (Robertson and Cabal, 2012). The sandy soils of the study area are mostly non-plastic, thus,

making it difficult or impossible to determine the required liquid limit value. For this reason, liquefaction susceptibility criteria were not applied to the Cape Flats sands.

The cyclic liquefaction potential of the Cape Flats sands was studied in terms of the triggering of liquefaction. A semi-empirical SPT-based procedure proposed by Idriss and Boulanger (2004) was implemented in the current research. The selection of this method is motivated in Section 2.5.15 of Chapter 2. The prediction is based on two variables, namely the cyclic stress ratio (CSR) induced by earthquake ground motions, demonstrating the seismic demand of a soil layer, and the cyclic resistance ratio (CRR), which provides a measure of the soil's resistance to liquefaction. When the CRR is less than or equal to the CSR generated by the earthquake, liquefaction is expected to occur at the specific location. The factor of safety against liquefaction is given as:

$$FoS_{liq} = \frac{CRR}{CSR} \quad \text{Equation 3-46}$$

Where  $FoS_{liq} \leq 1$  indicates liquefaction, and  $FoS_{liq} > 1$  indicates no liquefaction.

Idriss and Boulanger developed a liquefaction triggering correlation by plotting clean-sand equivalent SPT  $(N_1)_{60}$  values  $[(N_1)_{60cs}]$  against corresponding cyclic resistance ratios (CRR) calculated at the depth of the SPT blow count value. This CRR- $(N_1)_{60cs}$  curve represents the boundary between liquefiable and non-liquefiable conditions (based on case histories). The cyclic stress ratio (CSR) is then determined at the SPT depths, and the CSR- $(N_1)_{60cs}$  data pairs plotted on the triggering curve to assess the soils' liquefaction potential. The Idriss and Boulanger (2004) boundary curve is expressed using Equations 3-47 to 3-49.

All the measured SPT N blow count values (considered  $N_{60}$  values in the current study) were first corrected for overburden stress at the test depths to give the  $(N_1)_{60}$  values. The clean-sand equivalent values of  $(N_1)_{60}$  were then calculated as follows (Idriss and Boulanger, 2004):

$$(N_1)_{60cs} = (N_1)_{60} + \Delta(N_1)_{60} \quad \text{Equation 3-47}$$

$$\Delta(N_1)_{60} = \exp\left(1.63 + \frac{9.7}{FC} - \left(\frac{15.7}{FC}\right)^2\right) \quad \text{Equation 3-48}$$

Where: FC = Fines content (percentage smaller than 0.075mm)

Where grading results were available at the SPT depths, the calculated fines contents were inserted into Equation 3-48. Where the actual fines content at an SPT depth was unknown, an average fines content value of 6.3%, calculated for the sands of the Cape Flats based on the results of particle size analyses, was entered.

The cyclic resistance ratio (CRR) was then calculated at each of the SPT depths from the clean-sand equivalent  $(N_1)_{60}$  values for a magnitude  $M = 7.5$  earthquake and an effective vertical stress of 1 atmosphere (101.3kPa), using Equation 3-49. A total of 1526 CRR- $(N_1)_{60cs}$  data pairs were produced from SPT data from 178 boreholes in the study area. These data pairs are shown graphically in Figure 3-28, revealing the Idriss and Boulanger (2004) liquefaction triggering curve.

$$CRR = \exp\left\{\left(\frac{(N_1)_{60cs}}{14.1}\right) + \left(\frac{(N_1)_{60cs}}{126}\right)^2 - \left(\frac{(N_1)_{60cs}}{23.6}\right)^3 + \left(\frac{(N_1)_{60cs}}{25.4}\right)^4 - 2.8\right\} \quad \text{Equation 3-49}$$

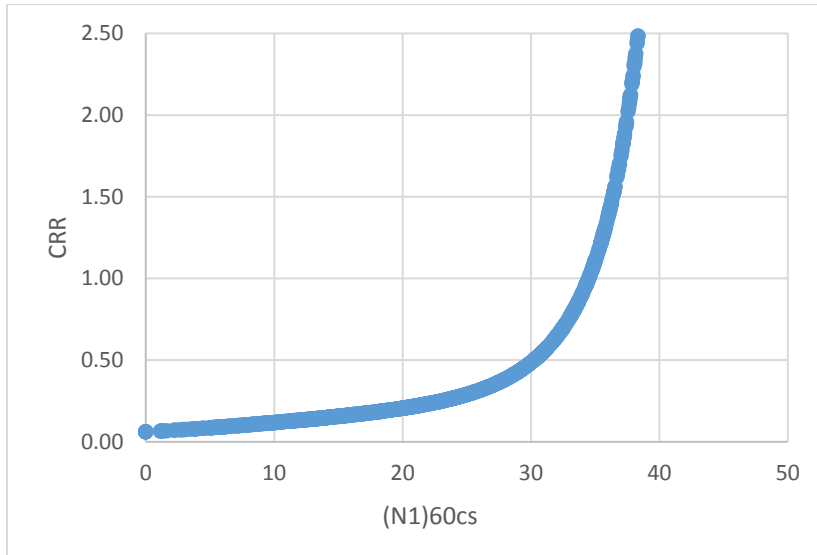


**Figure 3-28: Liquefaction triggering curve for Cape Flats sands**

To finally separate the liquefiable and non-liquefiable soils, the cyclic stress ratios induced by a design earthquake were calculated at the SPT depths as follows (Seed and Idriss, 1971) (refer to Idriss and Boulanger, 2004):

$$CSR = 0.65 \left( \frac{\sigma_{vo} a_{max}}{\sigma'_{vo}} \right) r_d \quad \text{Equation 3-50}$$

Where  $\sigma'_{vo}$  and  $\sigma_{vo}$  represent the effective and the total vertical stresses respectively. As before, the depth of the groundwater table was assumed at 3m in cases where the actual position of the phreatic surface was unknown at an SPT location.

$a_{max}$  = Maximum horizontal acceleration at the ground surface. This value was taken as 0.15g (1.471m/s<sup>2</sup>) for the Cape Flats area, representing the peak horizontal ground acceleration for the area with 10% chance of exceedance in 50 years (SANS 10160-4:2010).

$r_d$  = Stress reduction coefficient accounting for the flexibility of the soil column, obtained as follows:

$$\ln(r_d) = \alpha(z) + \beta(z)M \quad \text{Equation 3-51}$$

$$\alpha(z) = -1.012 - 1.126 \sin \left( \frac{z}{11.73} + 5.133 \right) \quad \text{Equation 3-52}$$

$$\beta(z) = 0.106 + 0.118 \sin \left( \frac{z}{11.28} + 5.142 \right) \quad \text{for depth } z \leq 34m \quad \text{Equation 3-53}$$

Where: M = Design earthquake moment magnitude = 6.0

The earthquake moment magnitude and the local Richter scale magnitude are, for all practical purposes, considered equal. The Richter scale magnitude was acquired from the Modified Mercalli Scale (MMS) intensity which was, in turn, obtained from a seismic intensities map of South Africa showing probabilistic MMS intensities with a 10% chance of exceedance in 50 years (Brandt, 2011 and de la Harpe, 2015).

The CSR requires adjustment for the equivalent number of stress cycles in different magnitude earthquakes. The CSR induced by an earthquake with magnitude  $M$ , is routinely adjusted to an equivalent CSR for an earthquake magnitude equal to 7.5 (Idriss and Boulanger, 2004), as follows:

$$(CSR)_{M=7.5} = \frac{CSR}{MSF} \quad \text{Equation 3-54}$$

Where:

MSF = Magnitude scaling factor, given by:

$$MSF = 6.9 \exp\left(\frac{-M}{4}\right) - 0.058 \quad \text{for } MSF \leq 1.8 \quad \text{Equation 3-55}$$

$M$  = Earthquake moment magnitude = 6.0, obtained as described above.

The cyclic stress ratios calculated at each of the SPT depths in the manner described above, was subsequently plotted against the clean-sand equivalent  $(N_1)_{60}$  values on the liquefaction triggering curve (Figure 3-28). A total of 1526 CSR- $(N_1)_{60cs}$  data pairs were included to assess the liquefaction potential of the Cape Flats sands.

To illustrate the occurrence and thicknesses of liquefiable soil layers, the CRR and CSR values were plotted relative to the SPT depths (with linear interpolation between points), providing continuous profiles of the factor of safety against liquefaction. Liquefaction can only occur below the water table and, as such, the indicated liquefiable zones may vary based on the depth of groundwater.

The evaluation of cyclic liquefaction in the Cape Flats was undertaken for a design earthquake with a moment magnitude of 6.0 and a peak ground acceleration (PGA) of 0.15g. The design earthquake compares to the magnitudes and horizontal ground accelerations recorded for historic seismic events associated with the intraplate fault line extending through the study area. To illustrate the effects of a larger magnitude earthquake producing higher PGA's, on the triggering of cyclic liquefaction in the study area, a design earthquake with moment magnitude  $M = 7.5$  and  $a_{max} = 0.2$  was applied in the calculation of the cyclic stress ratio.

### **Evaluation of flow liquefaction**

To evaluate the susceptibility of the Cape Flats sands to flow liquefaction, the potential for these soils to strain soften in undrained shear was evaluated. Robertson (2016) published a CPT-based normalised soil behaviour type (SBTn) chart, wherein an approximate boundary is drawn between dilative soils, in which deformations occur only during cyclic loading, and contractive soils (also known as strain softening soils), which are prone to strength loss (i.e. flow liquefaction). The proposed CPT SBTn chart serves as an updated version of the original SBTn chart produced by Robertson (1990). The basis for these modifications is discussed in Robertson (2016). The results from the four CPTu's undertaken by the candidate in the study area were applied to this CPT-based method.

The CPT SBTn chart, based on the CPT parameters of normalised cone resistance,  $Q_t$ , and friction ratio,  $F_r$ , is shown in Figure 3-29. The soil behaviour type associated with each of the delineated zones is provided with the figure. Note the transitional boundary between contractive and dilative soils and the zones marked 'TD' and 'TC', representing transitional areas, in which a soil can display behaviour somewhere between that of either sand-like or clay-like soil.

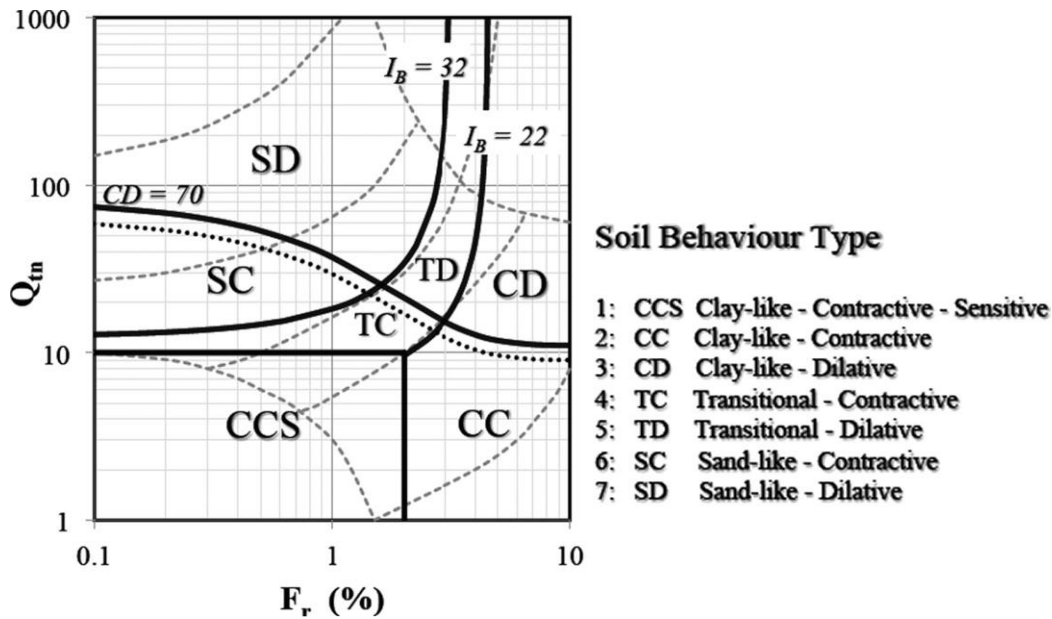


**Figure 3-29: CPT SBTn chart with contractive/dilative soil boundaries (Robertson, 2016)**

The CPT parameters of normalised cone resistance ( $Q_{tn}$ ), and normalised friction ratio ( $F_r$ ), were calculated from the raw CPT parameters of cone tip resistance ( $q_c$ ), sleeve friction ( $f_s$ ), and pore water pressure ( $u$ ), continuously recorded from surface to between 9.1m and 11.0m depth, using the following equations (Robertson, 2010):

$$F_r = [f_s \div (q_t - \sigma_{vo})]100\% \quad \text{Equation 3-56}$$

Where:

$q_t$  = Cone tip resistance corrected for pore pressure

The depth of the water table at each of the four CPT localities - required for the calculation of the total vertical stress - was calculated from the pore water pressure dissipation test results, as described in Section 3.5.8.

$$Q_{tn} = [(q_t - \sigma_{vo}) \div p_a](p_a \div \sigma'_{vo})^n \quad \text{Equation 3-57}$$

Where:

$p_a$  = Atmospheric pressure (101.3kPa), converted to same units as  $q_t$  and  $\sigma_v$

$n$  = Stress exponent varying with soil type, defined as:

$$n = 0.381(I_c) + 0.05(\sigma'_{vo} \div p_a) - 0.15 \quad \text{Equation 3-58}$$

Where:

$I_c$  = Soil behaviour type index, defined as:

$$I_c = [(3.47 - \log Q_{tn})^2 + (\log F_r + 1.22)^2]^{0.5} \quad \text{Equation 3-59}$$

To obtain the value of  $n$ , an iterative process involving equations 3-57 through 3-59, was followed.

As previously mentioned, soil liquefaction only occurs in cohesionless deposits and, as such, the identification of soil types at the CPT localities will provide an initial indication of the potential of the Cape Flats soils to liquefy. The normalised cone resistance and friction ratio values obtained with depth at the four piezocone penetrometer test positions in the manner described, were plotted on the SBTn chart. Both the soil behaviour types and the volumetric response of the site soils during shear were revealed. By plotting the normalised parameters on Figure 3-29, the depths and thicknesses of dilative and contractive soil zones in the profiles, are not discernible. For this reason, a contractive-dilative (CD) value was calculated using Equation 3-60 and plotted against depth to illustrate the volumetric behaviour during shear. When the value of CD exceeds 70, the soils are expected to be dilative at large shear strains, whereas CD values below 60 represent contractive soils. A transitional zone exists between CD values of 60 and 70, which was inserted on the graphs.

$$CD = (Q_{tn} - 11)(1 + 0.06F_r)^{17} \quad \text{Equation 3-60}$$

### 3.5.11 Compressibility

The stiffness of the Cape Flats sands was investigated as follows:

- Monotonic loading triaxial tests on representative soils from the study area to obtain the elastic modulus (E),
- Transformation models based on SPT blow count and CPT tip resistance to estimate the soil elastic modulus (E) with depth,
- Dynamic triaxial tests to obtain the resilient modulus ( $M_r$ ) and produce  $M_r$  predictive models,
- Continuous surface wave (CSW) tests to establish the shear wave velocity ( $V_s$ ) and small-strain stiffness ( $E_0$ ) with depth and produce  $V_s$  predictive models.

The sampling and in-situ test sites are shown in Figures C12 and C14 in Appendix C.

This section of the methodology focusses on the estimation of E by means of established empirical correlations. The determination of E and  $M_r$  from the results of static and dynamic triaxial tests, and  $V_s$  and  $E_0$  from CSW testing, were described in Sections 3.3.2.1 and 3.3.2.2.

#### **Standard penetration test (SPT) based method**

The SPT-based transformation model proposed by Stroud (1989) was applied in the current study. This method has been selected as it recognises the influence of strain on stiffness: decreasing soil stiffness with increasing strain. The method proposed by Stroud is shown in Figure 3-30, plotting the ratio  $E/N_{60}$  (in  $\text{MN/m}^2$ ) against degree of loading,  $q_{\text{net}}/q_{\text{ult}}$ .

Based on the geomorphological history of the Cape Flats (land and sea level changes), the stress history of the windblown sands seems to reflect that of normally consolidated deposits. Notwithstanding this, the continuous mobilisation of the dune sand across the low-gradient landscape during summer months (by the dominant south easterly winds), together with removal of dune sands for mining purposes, will result in over-consolidation in some areas. In this regard, the results from two consolidometer tests, undertaken on undisturbed sandy soil sampled from Blue Downs in the Cape Flats during a previous investigation, revealed over-consolidated sands with preconsolidation pressures of 40 and  $100\text{kN/m}^2$ . For these soils, sampled between 0.5m and 1.5m below ngl, over-consolidation ratios (OCR) of about 7 and 1.6 (with  $\gamma' = 19\text{kN/m}^2$ ) were

calculated. The presence of both normally and over-consolidated deposits are anticipated in the study area. The e-log(p) curves from the two consolidometer tests are included in Appendix F.

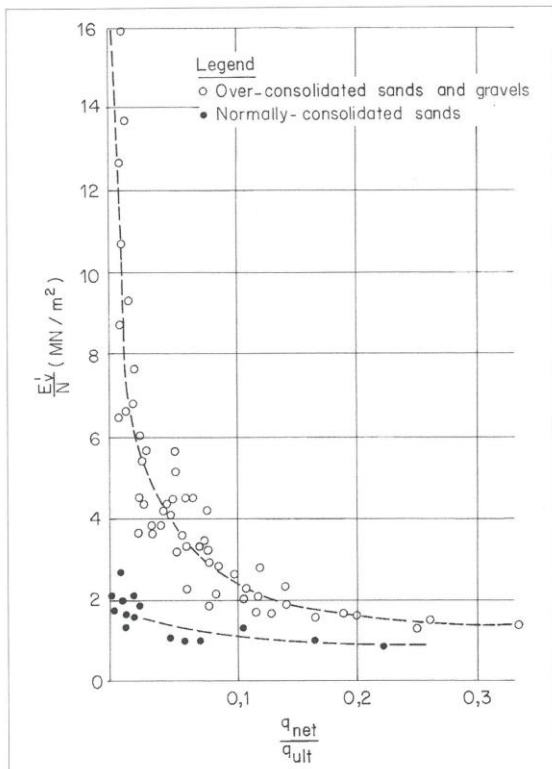


**Figure 3-30: Relationship between soil stiffness, strain level, and SPT N for sands and gravels (Stroud, 1989 from Clayton, 1993)**

The modulus of compressibility of the Cape Flats sands was determined for  $q_{net}/q_{ult}$  ratios (i.e. safety factors) 0.33 (FoS = 3), 0.14 (FoS = 7) and 0.05 (FoS = 20), corresponding to  $E/N_{60}$  ratios of 1.5, 2, and 4 respectively (over-consolidated sands curve), and 1, 1.1, and 1.5 (normally consolidated sands curve). Elastic moduli were calculated (for both normally and over-consolidated sands) from SPT data from 178 boreholes spread across the study area, providing an indication of soil compressibility with depth, and the influence of strain level on the stiffness of the Cape Flats sands.

### **Cone penetration test (CPT) based models**

The CPT-based method proposed by Robertson (2009), suitable to young, uncemented silica sand, and recognising the influence of strain on the elastic modulus, was applied in the current research. The relation is expressed as:

$$E = 0.047[1 - (q_{net} \div q_{ult})^{0.3}][10^{(0.55I_c + 1.68)}](q_t - \sigma_{vo}) \quad \text{Equation 3-61}$$

Porewater pressure measurements are required for correction of penetration resistances, as well as water table depth and, as such, only data from the four CPTu's undertaken in Capricorn and in the vicinity of the Cape Town International Airport were used. The elastic modulus was, once again, determined for  $q_{net}/q_{ult}$  ratios of 0.33, 0.14 and 0.05 corresponding to safety factors of 3, 7 and 20 respectively for comparison with the SPT-based findings.

## 4. Results and Discussion

### 4.1 Introduction

The results associated with the classification and characterisation of the Cape Flats sands are presented, explained and evaluated in this Chapter. The completed data sets, obtained from the collection, sorting, input and processing of pertinent geotechnical data as described in Chapter 3, are statistically analysed and the outcomes are presented as graphs, tables and equations for interpretation. The results are contextualised within previous research and theory, and the implications of the results discussed. The limitations of the research are highlighted.

Focus is placed on the soil compressibility and the development of transformation models by which the shear wave velocity (related to small-strain Young's modulus) can be predicted from the penetration resistance. The soundness and preciseness of the relations are evaluated, ensuring they are unbiased with respect to all variables.

The aim of this chapter is to comprehensively classify and characterise the aeolian sands of the Cape Flats, revealing underlying patterns and trends (inter- and intra-formation), and relationships between soil parameters, with the aim of understanding and predicting the engineering behavior of these sands.

### 4.2 Grading results

#### 4.2.1 Overview

A typical PSD curve for Cape Flats sand is shown in Figure 4-1 which illustrates the typical shape and slope of the curve. The steep curve reflects the predominance of particles with sizes between 0.6mm and 0.075mm. The typical fines content is around 5%. For this soil, the coefficient of uniformity ( $C_u$ ) is 2.9 and the coefficient of curvature ( $C_z$ ) is 1.1, both indication of a poorly (uniformly) graded soil. The predominance of fine sand size particles and uniform gradation of the sands contribute to higher void ratios (lower density), which will influence all aspects of the soils' engineering behaviour.

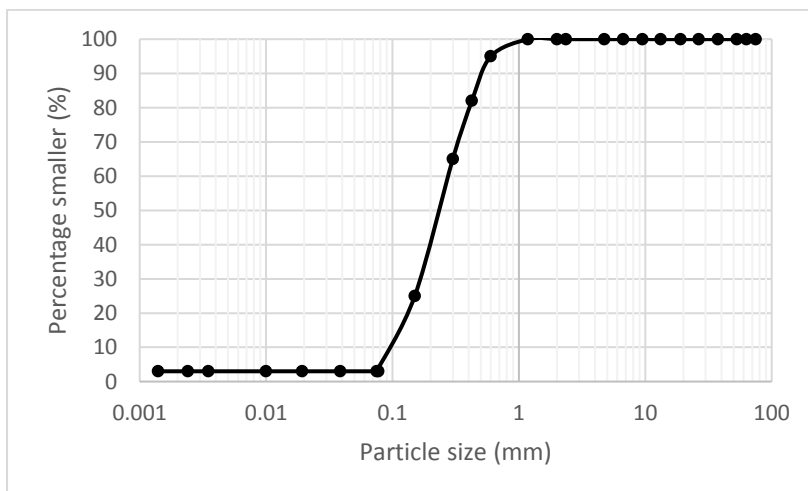


Figure 4-1: Typical Cape Flats PSD curve

### 4.2.2 Texture of Cape Flats sand

The texture of the Cape Flats sands, known from 400 grading results for windblown sands from test pits and boreholes, is presented in this section. The results of 235 hydrometer analyses were used to determine the clay and silt content of the sands. Sites with known grading data are shown on the map in Figure C1 in Appendix C. The sampling locations are distributed as follows: 247 (61%) in the Witzand Formation, 114 (29%) in the Springfontyn Formation and 39 (10%) in the Langebaan Formation. Size classification was based on the ranges specified in ASTM D422:2007 (refer to Section 2.5.2 in Chapter 2). Soil gradation, PSD curve characteristics and material properties are discussed in Sections 4.2.3 and 4.2.4.

An extract from the table summarising the statistical analysis of the particle size distribution is given in Table 4-1. The complete table is given in Appendix G (Table G1). The grading data was grouped into 1m depth intervals from ground surface to a maximum depth of 13m. Data from depths exceeding 3m is sparse. For each formation, the variation in soil texture with depth is shown by means of box and whiskers plots (see Figures 4-2 to 4-4). The 25<sup>th</sup> percentile (1<sup>st</sup> quartile), median (2<sup>nd</sup> quartile), and 75<sup>th</sup> percentile (3<sup>rd</sup> quartile) values are represented by the horizontal lines of the box. The vertical lines outside the box (whiskers) extend to the minimum and maximum values. The mean value is illustrated by the cross on the plot. Outlier values are plotted as individual points either above or below the maximum and minimum points. One-way analysis of variance (ANOVA) testing was also undertaken to assess the variance in particle size fractions between the formations. The research focusses on aeolian sands and, as such, all results are associated with these deposits.

**Table 4-1: Extract from grading summary table in Appendix G**

Springfontyn Formation						
Fine sand (0.075mm - 0.425mm)						
Depth range (m)	Maximum (%)	Minimum (%)	25 <sup>th</sup> /75 <sup>th</sup> percentile (%)	Average (%)	Standard deviation (%)	Number of values
0 - 1	93	11	65/84	71.3	13.5	66
1 - 2	100	28	61/85	70.5	15.5	64
2 - 3	86	44	62/79	68.6	12.0	16
3 - 4	82	77	-	79.5	3.5	2
Medium sand (0.425mm – 2mm)						
0 - 1	83	1	9/29	20.0	14.7	66
1 - 2	70	0	7/29	19.7	15.4	64
2 - 3	55	2	8/17	14.7	12.8	16

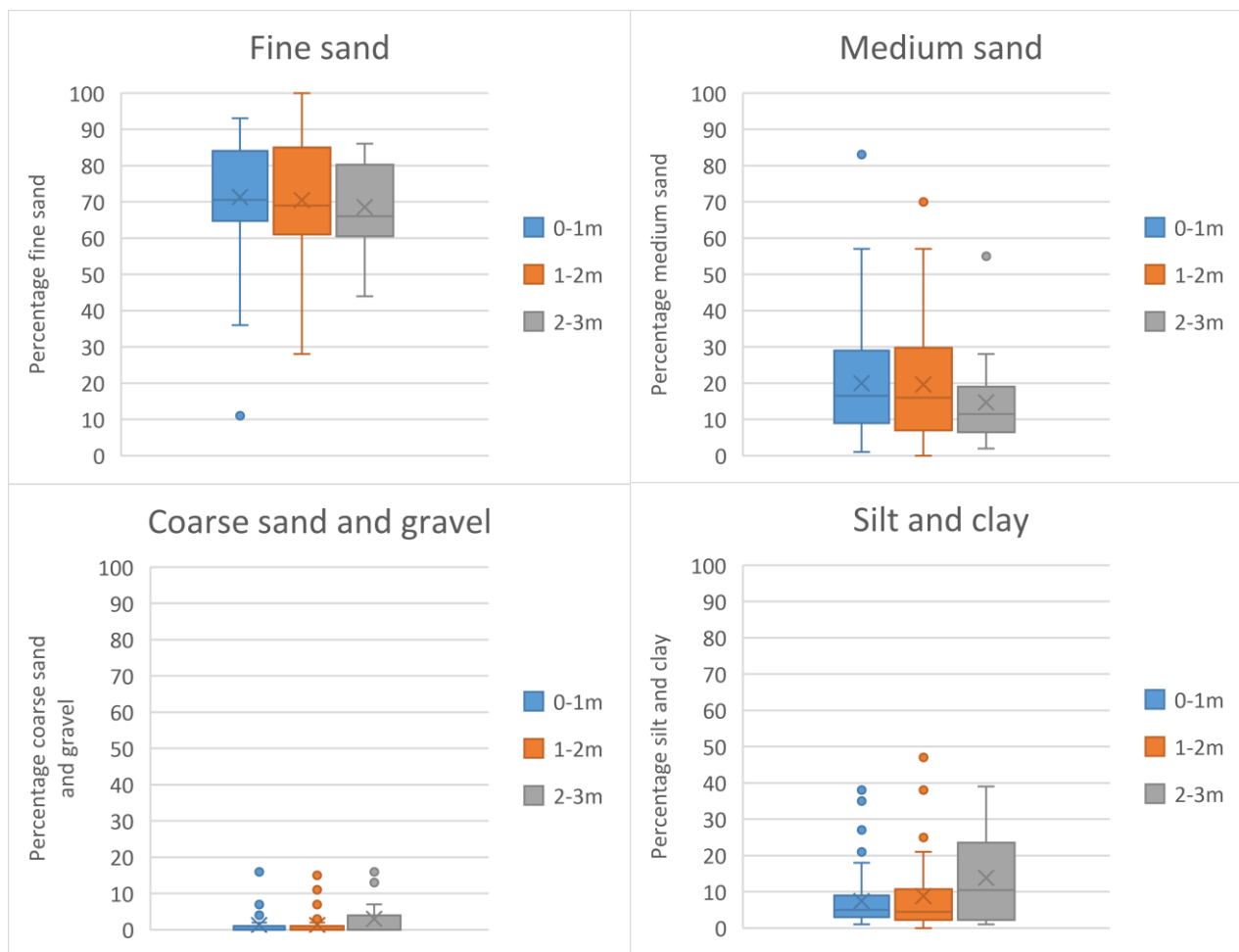


**Figure 4-2: Springfontyn Formation variation in soil texture with depth**

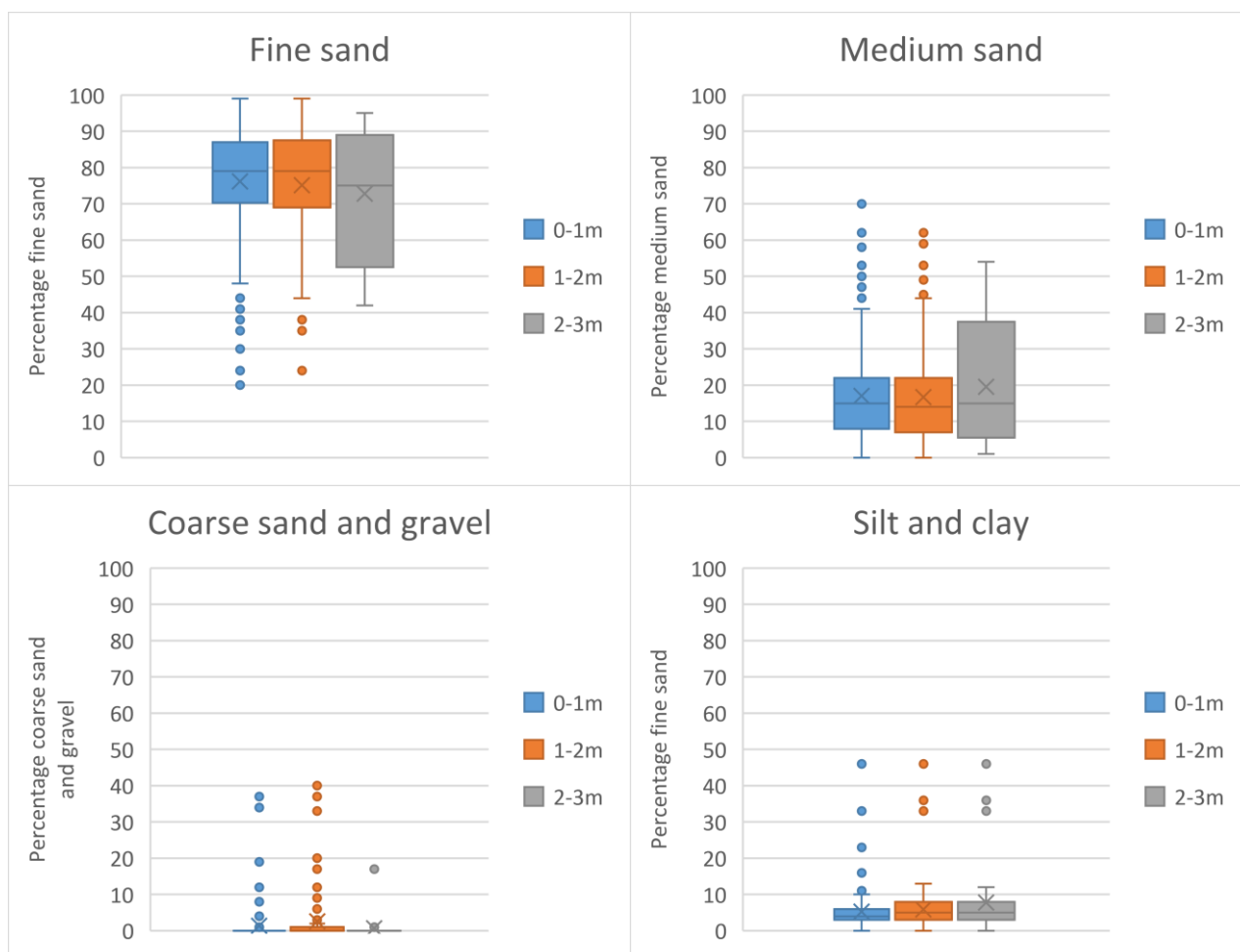


**Figure 4-3: Witzand Formation variation in soil texture with depth**

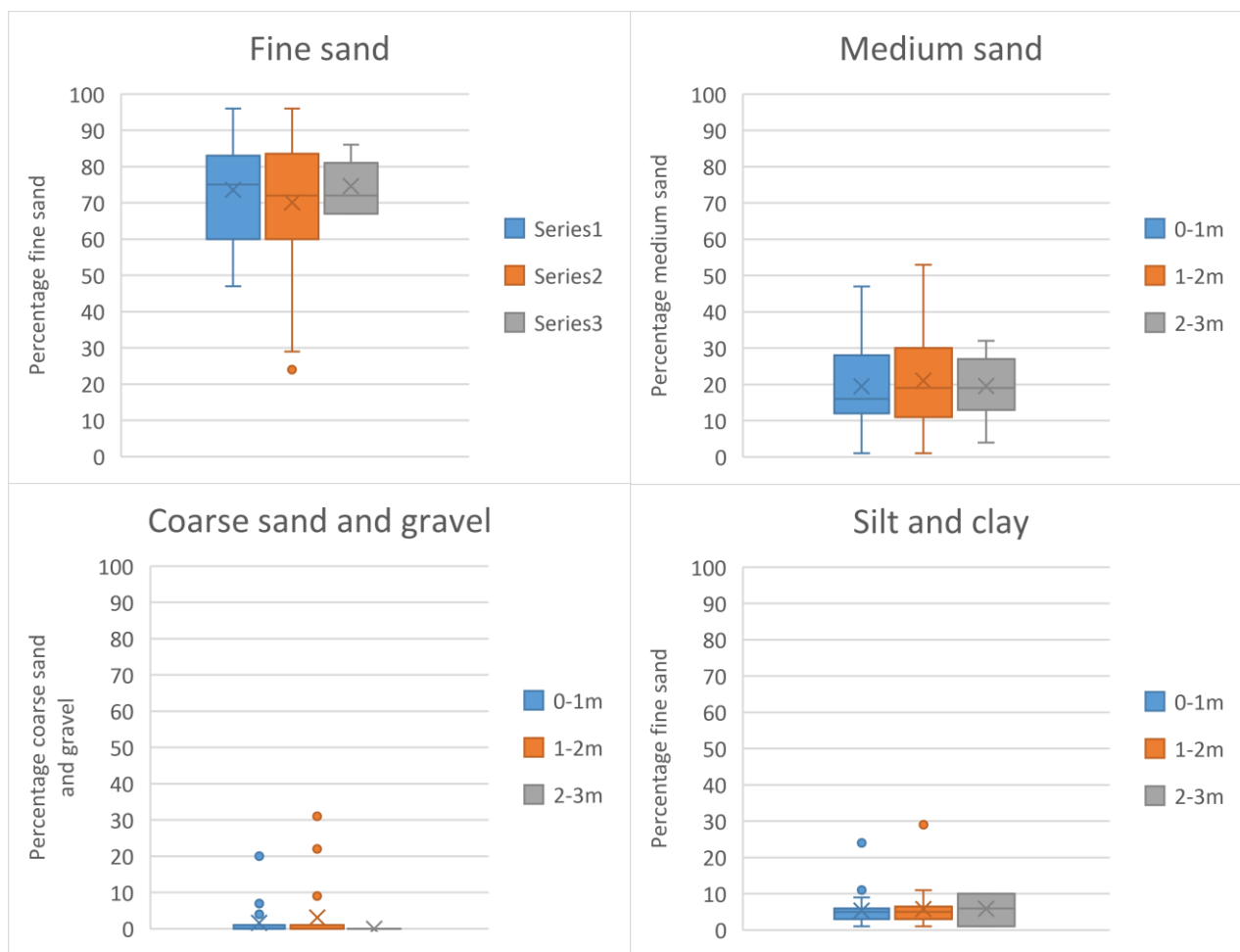


**Figure 4-4: Langebaan Formation variation in soil texture with depth**

The windblown deposits of the Witzand, Springfontyn and Langebaan Formations comprise predominantly sand size particles; typically, most in the fine sand range (0.425mm to 0.075mm). The average fine sand content in the upper 3m of the soil profile was found to be slightly higher in the Witzand Formation (approximately 75%), compared to the Springfontyn and Langebaan Formations with average fine sand contents of about 70% and 72% respectively. For all depth intervals but the 2-3m interval in the Langebaan Formation - for which insufficient grading data is available for reliable analysis - the quartile values of the Witzand Formation data set exceed the corresponding values from the Springfontyn and Langebaan Formations. A higher degree of uniformity is therefore indicated in the sands of the Witzand Formation. The findings indicate a slight decrease in the average fine sand content from surface to 3m depth in all formations (again excluding the 2-3m depth range in the Langebaan Formation); the trend confirmed by the gradual downwards shift in the boxplots. It is uncertain whether the observed trend represents the actual variation in texture with depth in the study area or whether the decrease in available data with depth influenced the outcome. ANOVA single-factor testing was undertaken to determine whether the fine sand contents (combined for the upper 3m) justly vary between the formations. Analysis shows that the calculated F-statistic (5.4) exceeds the F-critical value (3.0) for the alpha level selected (0.05), and therefore the null hypothesis can be rejected (P-value also less than 0.05). The t-test (two-sample assuming equal variances) shows that only the means of the fine

sand content data sets of the Springfontyn and Witzand Formations are significantly different from one another ( $P$  two-tail = 0.0015).

Medium sand size (0.425mm to 2mm) grains make up, on average, approximately 15% to 20% of the Cape Flats sands (in the investigated depth range). In the upper 2m of the soil profile, the average medium sand content was found to be slightly lower in the Witzand Formation (approximately 3% lower) compared to the Springfontyn and Langebaan Formations, with the upper two quartile values lower in this formation. In the 2-3m depth range in the Witzand Formation more soils with higher medium sand size fractions were sampled (compared to the upper 2m), corresponding to the lower fine sand content in this depth range. ANOVA testing reveals that, when comparing the means of the medium sand content data groups for the three formations, the difference between the formations is insignificant ( $F < F_{crit}$ ).

The investigated Cape Flats sands mostly have no or negligible fractions of coarse sand (2mm to 4.75mm) and gravel sized (>4.75mm) particles. The average percentage of particles in these size ranges, represented by the crosses on the plots is, in some instances, higher than the 75<sup>th</sup> percentile values. This is owed to the few soils possessing substantial coarse sand and/or gravel sized fractions (plotted as statistical outliers on the graphs), skewing the calculated averages. Soils with notable gravel fractions were found to be more prevalent in the Witzand and Langebaan Formations, mostly representing the presence of calcrete gravel and possibly marine pebbles and shells. As for the medium sand content, statistical comparison of gravel and coarse sand particle size data groups reveals an insignificant difference.

The average combined silt (0.005mm to 0.075mm) and clay (<0.005mm) content in the Cape Flats is typically less than 10%. The investigated sands from the Springfontyn Formation generally have higher silt and clay contents and less 'clean' sands compared to the Witzand and Langebaan Formations. The fine fraction (<0.075mm) of organic material in peat layers - noted in selected test pit and borehole profiles in the Springfontyn Formation - may also add to the fine contents. A slight increase in the average fines content (and the silt and clay contents individually) is noted from surface to 3m depth in all formations (excluding the 2-3m depth range in the Langebaan Formation); the trend confirmed by the gradual upwards shift in the boxplots. It is uncertain whether the observed trend represents the actual variation in texture with depth in the Cape Flats (likely due to illuviation), or whether the decrease in available data with depth influenced the outcome. In the Witzand Formation the sands were more often found to be silty than clayey (and plastic), whereas the opposite is true for the Springfontyn and Langebaan Formation deposits. It was noted that many profile descriptions overestimate the silt content. Laboratory tests on material described as a silty sand show silt contents mainly between 1% and 3%. ANOVA single-factor testing involving the combined silt and clay fractions shows that the calculated F-statistic (12.8) exceeds the F-critical value (3.0) for the alpha level selected (0.05), and therefore the null hypothesis can be rejected ( $P$ -value also less than 0.05). The t-test (two-sample assuming equal variances) showed that only the fines contents of the Witzand and Springfontyn Formations are significantly different from one another ( $P$  two-tail =  $1.7 \times 10^{-6}$ ).

Roberts (2001) and Franceschini (2003) described the sands from the Langebaan Formation as predominantly medium and coarse grained. From the results of 39 grading analyses of sands from 11 sites, the sands from this formation were found to be mostly fine and medium grained, with an average coarse sand content of less than 1%. Although unspecified, it is likely that prior classification was based on size boundaries from British Standards such as BS1377 (1990) rather than the ASTM D422 (2007) standard that was used by the candidate. Notwithstanding this, the fine, medium and coarse sand contents in the upper 3m in the Witzand, Springfontyn and Langebaan Formations were found to be comparable, particularly in the Springfontyn and Langebaan Formations. The few samples collected below a depth of 3m in the Langebaan Formation, similarly, did not reveal a coarser texture. The disparity in findings can possibly be ascribed to lateral variability in the Langebaan Formation, with coarser sands probably distinctive of some areas. To illustrate the influence of applying different classification standards when describing soil texture, the ASTM and BS standards were applied to the same grading result for the Langebaan Formation sand. For the particular grading, the silt and clay contents are similar using the ASTM and BS standard, however, fine sand contents of 58% (ASTM) and 20% (BS), medium sand contents of 39% (ASTM) and 56% (BS), and coarse sand contents of 0% (ASTM) and 21% (BS) were obtained, demonstrating the major difference in textural descriptions using the two standards.

The particle sizes present in a soil is largely determined by the mineralogy, which in the Cape Flats sands, is mostly quartz minerals with lesser feldspar and kaolinite (Amdurer, 1956). Quartz is the most common mineral in the sedimentary and igneous bedrock underlying the Quaternary sands, a source material of the windblown Cape Flats sand. The fine, medium and coarse sand size fractions consist of quartz (i.e. quartzose sands), whereas the coarse silt size fraction is presumably quartz and feldspar. Feldspar is also common in the abovementioned rock types, often weathering to kaolinite. The fine silt size fraction may comprise clay minerals such as kaolinite (in addition to feldspar). Amdurer (1956) identified kaolin clay in the study area, although other common clay minerals such as illite and montmorillonite may also be present. The clay content and Atterberg limits of cohesive soils sampled from the study area can give an indication of the clay mineral present. This aspect will be explored in Section 4.4. The predominance of fine, and to a lesser degree, medium sand size particles, the shape of these quartzose particles and the interparticle relation, will govern the engineering behaviour of the windblown deposits. The presence of soil fines (particularly plastic fines) will exert considerable influence on the soil parameters when present, through physical and physiochemical interactions. Soil texture will be considered in the evaluation of soil parameters discussed in subsequent sections.

Field descriptions of soil materials encountered in the Cape Flats were provided by Amdurer (1956). Apart from the windblown sands studied by the candidate, organic clay, plastic clay, silty clay, sandy clay, and peat were intersected during the fieldwork. These finer grained soils are mainly of marine, and presumably lacustrine, estuarine and alluvial origin. These deposits occurred sporadically with aeolian sands in the Springfontyn Formation.

### 4.2.3 Soil gradation coefficients

Grading coefficients were determined for 380 soils as described in Section 3.5.2. from Chapter 3. For some soils (20 of the 400) the effective size ( $D_{10}$ ), and thus the values of  $C_u$  and  $C_z$ , could not be calculated. In some cases, the long fines tails of PSD curves resulted in very large values of  $C_u$  and  $C_z$ , skewing the statistical parameters. For this reason, the Microsoft Excel outlier function was used to identify and exclude a small number of substantially higher or unusual values.

A summary of the results is presented in Table G2 in Appendix G, again grouped into 1m depth intervals to evaluate the variation in  $C_u$  and  $C_z$  with depth. An extract from Table G2 is given in Table 4-2. The findings do not reveal a notable variation in  $C_u$  and  $C_z$  between the 0-1m and 1-2m depth intervals. Below 2m depth, the representativeness of the results is uncertain as data become sparser. For each formation, the results for the upper 2m of the soil profile were combined and are shown graphically by means of box and whiskers plots in Figures 4-5a and 4-5b.

**Table 4-2: Extract from gradation summary in Appendix G**

Springfontyn Formation						
Coefficient of Uniformity, $C_u$						
Depth range (m)	Maximum	Minimum	25 <sup>th</sup> /75 <sup>th</sup> percentile	Average	Standard deviation	Number of values
0 - 1	24.4	2.0	2.5/3.4	4.6*	4.6	47
1 - 2	46.7	1.7	2.4/3.6	4.6*	7.0	47
2 - 3	46.7	2.3	2.9/5.5	7.6*	12.4	14
3 - 4	3.2	2.9	-	3.1	0.2	2
Coefficient of Curvature, $C_z$						
0 - 1	9.9	0.7	0.8/1.3	1.7*	2.1	47
1 - 2	13.4	0	0.9/1.2	1.6*	2.2	47
2 - 3	31.4	0.8	1.0/3.2	5.9*	9.6	14

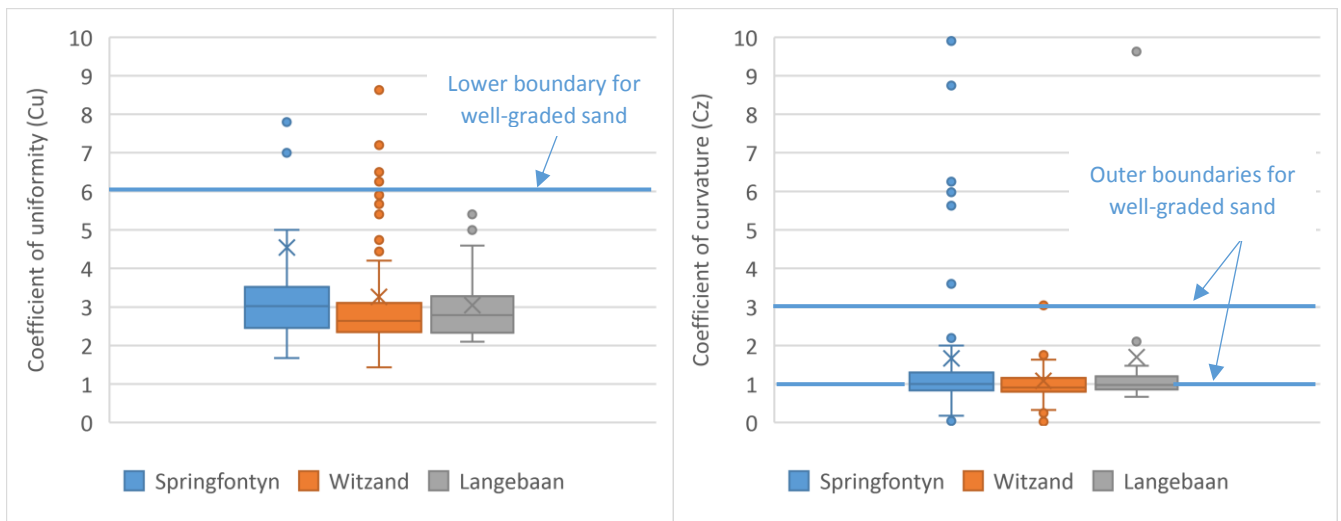


**Figure 4-5: Comparison of a)  $C_u$  and b)  $C_z$  in the upper 2m of the Witzand, Springfontyn and Langebaan Formations**

To ensure readable graphs, the upper range on the vertical axes of both plots was limited to 10. As a result, not all outlier values are shown on plots. The crosses on the plots (representing the average  $C_u$  and  $C_z$  values), are mostly above the 75<sup>th</sup> percentile lines. Outliers skewed these calculated averages, and an evaluation of  $C_u$  and  $C_z$  should therefore be based on the quartiles rather than the mean.

From the distribution of  $C_u$  and  $C_z$  values in Figures 4-5a and 4-5b, it is evident that the Cape Flats sands typically comprise soil particles within narrow size limits (uniform gradation). The predominance of fine, and to a lesser degree, medium sand size particles with minor fines will result in a steep PSD curve, characteristic of a uniformly graded soil (refer to Figure 4-1). In the Springfontyn Formation approximately 3% of the sampled soils satisfy the criteria for a well graded soil ( $C_u > 6$  and  $1 < C_z < 3$ ), whereas approximately 2% and 1% of the soils sampled from the Langebaan and Witzand Formations consist of particles in different size ranges. The well graded soils typically comprise a notable medium and/or coarse sand size fraction. No gap graded soils were identified.

When studying the quartiles of the data, it is noted that the degree of particle size uniformity is typically slightly lower in the Springfontyn Formation (compared to the Witzand and Langebaan Formations). The finding agrees with the grading results. ANOVA single-factor testing was undertaken to determine whether the  $C_u$  and  $C_z$  data sets both justly vary between the formations. Analysis shows that the calculated F-statistic (5.2) exceeds the F-critical value (3.0) for the alpha level selected (0.05), and therefore the null hypothesis can be rejected (P-value also less than 0.05). The t-test (two-sample assuming equal variances) shows that both the  $C_u$  and  $C_z$  data sets of the Springfontyn and Witzand Formations (with P two-tail = 0.0036 and 0.004 respectively), are significantly different from one another. There is no appreciable difference between the means of the data sets from the Witzand and Langebaan, and the Springfontyn and Langebaan Formations.

The variation in gradation with depth could not be assessed, as data values become sparser, and statistical outcomes more unreliable, with depth (refer to Table G2 in Appendix G).

#### **4.2.4 Other grading-related properties**

The shrinkage product (Sp) and grading coefficient (Gc) were calculated from the sieve analyses results and the bar linear shrinkage, as described in Section 3.5.2, mainly to assess the suitability of the site soils as unpaved gravel wearing course. In addition, the grading modulus (GM) was calculated from selected sieve analyses results to aid the interpretation of the compaction (MDD and OMC) and the CBR results. In some instances, the coefficients could not be calculated as the percentage particles passing certain required sieve sizes were not available. Sp and Gc were calculated for 338 soils and GM for 160 soils (for which compaction properties and CBR are known). A brief overview of the material properties is given below.

##### Shrinkage product and grading coefficient

The sandy Cape Flats soils will typically display no reduction in length upon drying, with the shrinkage product thus being equal to zero irrespective of grading. In addition, a characteristic lack of particle sizes greater than 2mm in diameter (coarse sand and gravel), will result in Gc being equal to zero. For each formation, the data was combined for discussion, extending to maximum

depths of 4m (Springfontyn Formation), 13m (Witzand Formation), and 9m (Langebaan Formation). It should be noted that, although included, limited data is available below 3m.

In the Springfontyn Formation, approximately 11% of the sampled soils (9 of 79) displayed shrinkage upon drying. For these soils, the values of  $S_p$  vary between 82 and 403 (average of 239). Textural descriptions for these soils include silty clayey sand and clayey sand. The incidence of soils with non-zero linear shrinkages, seems to increase with depth, agreeing with the grading results. In the Witzand Formation, about 4% of soils (9 of 220) shrink when dried. Values of  $S_p$  vary between 24 and 405 (average of 230). In the Langebaan Formation, approximately 2.5% (1 of 39) of the investigated soils has an  $S_p$  value greater than zero (equal to 116). Overall, these results are in line with the proportions of grain sizes present in the soils from each formation. A general lack of plastic fines and thus cohesion in the Cape Flats sands will lead to material loss under traffic. This aspect is discussed in greater detail in Section 4.10.3.

The grading coefficient ( $G_c$ ), which is a measure of the coarseness of the Cape Flats soils, was evaluated for the same depth ranges in which  $S_p$  was studied. In the Springfontyn Formation, approximately 60% of the investigated soils (47 of 79) contains no particles between 2mm and 26.5mm in size (coarse sand and fine and medium gravel), with  $G_c$  being equal to zero. This percentage increases to 80% in both the Witzand and Langebaan Formations, illustrating the increased prevalence of soils with grains all passing the 2mm opening sieve in these formations. Where particles between 2mm and 26.5mm make up a portion of the grading,  $G_c$  varies between 0.98 and 13.8 (average of 3.8) in the Springfontyn Formation. In the Witzand Formation  $G_c$  varies between 0.98 and 32 (average of 7.9). When compared to the Springfontyn Formation, the higher maximum and average  $G_c$  (and calculated interquartile range) agree with the higher gravel content noted in the Witzand formation (refer to Section 4.2.2). The value of  $G_c$  for soils with some grain sizes in the 2mm to 26.5mm range varies from 0.99 to 17.3 (average of 5.0) in the Langebaan Formation. Below 2m depth, the grading coefficient remains zero due to the absence of coarse sand and gravel sized particles.

For geo-material to be considered suitable as wearing course gravel for unpaved roads,  $G_c$  should fall between lower and upper limit values of 16 and 34 (TRH 20, 1990). Most of the investigated sands (>95%) do not meet this criterion, indicating an erosion risk. This erodibility of the Cape Flats sands, where utilised as gravel wearing course, is evaluated in Section 4.10.3.

#### Grading modulus

The grading modulus (GM) was calculated for sands sampled to a maximum depth of 9m, although data from depths exceeding 2m is sparse. A combined data set was analysed, as separation into depth intervals and/or formations, produced mostly insufficient data for analysis and potentially misleading outcomes. For the 160 soils sampled from the study area, the statistical summary values for the GM data set is shown in Table 4-3.

**Table 4-3: Grading modulus of Cape Flats sand**

Maximum	Minimum	25 <sup>th</sup> /75 <sup>th</sup> percentile	Average	Standard deviation	Number of values
1.92	0.57	1.04/1.27	1.2	0.2	160

The general lack of a coarse fraction in the Cape Flats sands is evident from the obtained GM summary values. At the upper end of the range of GM values, the soils contain between 30% and 40% gravel sized particles, fine, medium and coarse sands (combined approximately 60%) and a maximum fines content of 11%. GM values below 1 are associated with fine sands with combined silt and clay contents up to 47%. The TRH14 (1985) classification system for road construction materials stipulates minimum values of GM for natural gravels (G5 and G6 quality materials). Lower limits of 1.5 and 1.2 are specified for G5 and G6 materials respectively. From the given quartile values, it is evident that the investigated Cape Flats sands are typically worse than G6 quality based on GM alone. COLTO (1998) specifies a minimum GM of 0.75 for gravel soil (G7 to G10 materials). Only one soil sampled from Springfontyn Formation do not meet the GM requirement.

As previously mentioned, GM was primarily calculated to aid the interpretation of the compaction (MDD and OMC) and the CBR results (refer to Sections 4.5 and 4.7).

### **4.3 Groundwater table**

Groundwater level data from test pit and borehole profiles, monitoring well records, and the National Groundwater Archive (NGA), is presented and evaluated in this section. For each month of the year the documented water levels - within a ten-year period (2008 to 2018) - were combined and analysed. Four hundred and seventy-one (471) perched and permanent water table levels were grouped in this manner. The distribution of sites with groundwater level figures is shown in Figure C2 in Appendix C.

The groundwater data is summarised graphically in Figure 4-6, illustrating the average, maximum, and minimum water levels (in metres below ground level, m bgl) associated with each month of the year (in the period 2008 to 2018). Most groundwater levels were extracted from site investigation reports, where one or more measurements were taken at each site at the particular time of the year during which the fieldwork was carried out. Multiple measurements at different times of the year are scarce. This should be borne in mind when interpreting the summarised data, particularly the maximum and minimum groundwater levels. In most cases, temporary and permanent water tables could not be distinguished (based on the available information), and therefore no distinction is made in this regard in the provided summary.

The Cape Town area, including the Cape Flats (Cape Town area) is a winter rainfall region. This reflected in the average water levels shown in Figure 4-6. The average groundwater level varies between approximately 1.9m bgl and 2.2m bgl in the winter months, rising even closer to the surface in September. During the dry summer and early autumn, the average level of groundwater drops to between 2.6m bgl and 3.3m bgl. Significant variation in the depth to groundwater is expected in the study area (possibly over short distances), mainly influenced by the undulating topography and less permeable or impermeable layers and lenses of pedogenic material and clay forming perched groundwater tables. This is reflected in the range of levels observed for a particular month. The generally permeable sandy soils allow rapid infiltration with minimal runoff in open areas. Water will percolate through the void spaces, either accumulating on the impermeable strata or recharging the underlying aquifer. Ponding of water occurs on the coastal plain where the surficial soils become saturated.

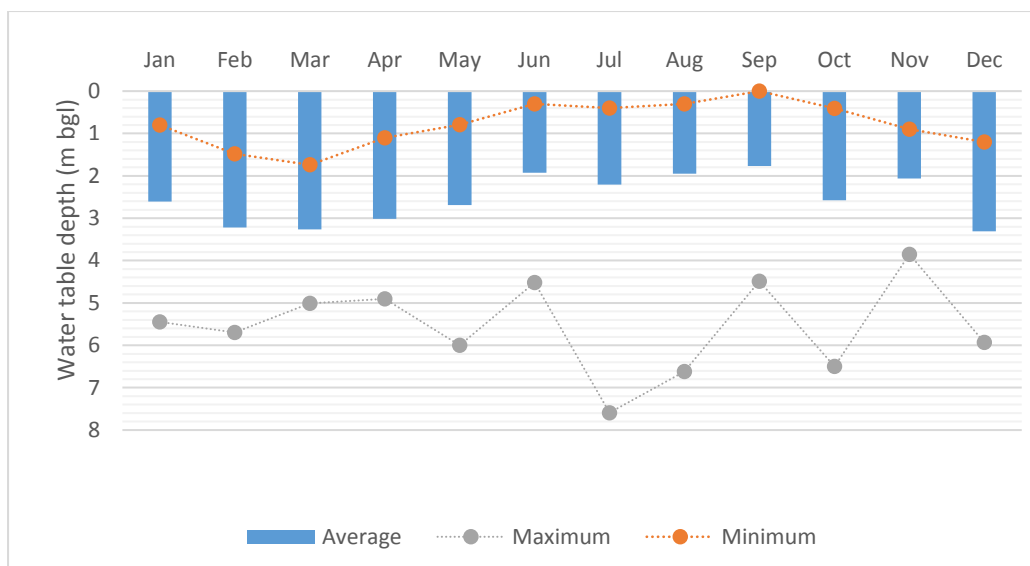


**Figure 4-6: Groundwater levels in the Cape Flats from 2008 to 2018**

To illustrate the effects of the drought conditions experienced from 2015 to 2018 on the groundwater level in the Cape Flats, the average water level during this period (per month) was compared to the years 2008 to 2014. In many cases, a notable drop in water level was noted after 2015. For the month of January, for instance, the average water level of 2.1m bgl calculated between 2008 and 2014 dropped to 4m bgl after 2015. Nonetheless, to accurately assess the fluctuation in water level over time, regular measurements should be made at the same site over a prolonged period. At two sites in the study area, groundwater levels in monitoring wells were studied over extended periods. These sites are located at the Cape Town International Airport and in Bellville (immediately north of the R102). At the latter site, measurements span the drought period.

The airport site is located in the northern part of the study area and is underlain by Witand deposits. In 2009, 11 boreholes were drilled to monitor the variation in groundwater levels across the site. Water levels were recorded on a monthly basis from January to October 2009. During this time, groundwater levels varied between 0.5m bgl and 4.5m bgl. At most monitoring positions, a similar trend was noted: a gradual decrease in groundwater level from January to March, where after it remained relatively constant until May. Groundwater then became notably shallower from May to June, remaining fairly constant from June to October. Groundwater levels varied quite significantly between the relatively closely spaced boreholes, likely owing to irregular calcrete layers and lenses typically noted in test pits and boreholes in the vicinity of the site. The largest seasonal fluctuation recorded in an individual borehole was 1.3m, the smallest fluctuation was 0.1m, and the average fluctuation between January and October per borehole was 0.6m.

At the Bellville site, fluctuations in groundwater in a single borehole, over a three-year period (2014 to 2016), were documented. The site is underlain by Springfontyn Formation deposits. No soil profile description is available. Measurements were separated per year and the respective curves – demonstrating the fluctuations arising from seasonal changes – are shown in Figure 4-7. The effects of the drought are visible at the site, with the depth to groundwater mostly increasing from 2014 to 2015/2016. Seasonal fluctuations at the site are substantial, varying between outer limits of 1.6m bgl and 5.8m bgl over the monitoring period.

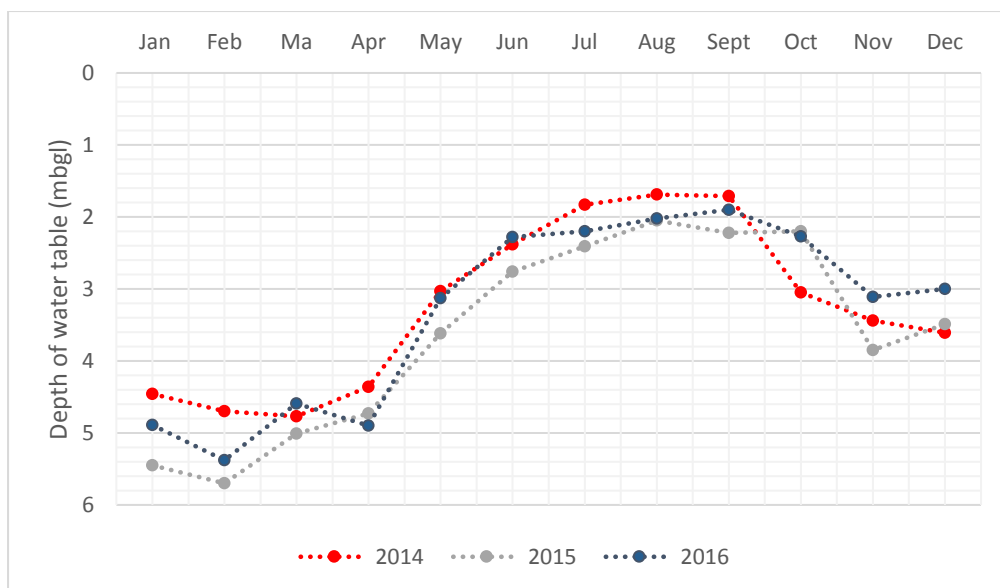


**Figure 4-7: Fluctuation in groundwater level in a single Cape Flats borehole**

Groundwater level measurements were obtained from 120 sites spread across the study area. Although an attempt was made to distinguish areas based on groundwater level data, the mostly isolated and sporadic measurements over the large geographical area and a wide time frame, prevented meaningful analysis. The depth to groundwater was taken into consideration in the interpretation of in-situ test results, as the saturated condition will have a pronounced effect on the shear strength (and penetration resistance) of the soil. The in-situ moisture content results are given in Section 4.12.

#### 4.4 Plasticity properties

The results of Atterberg limit determinations on 393 soil samples from the Witzand, Springfontyn and Langebaan Formations are presented in this section. The sites from which soils were sampled are shown on Figure C3 in Appendix C. The aeolian sands of the Cape Flats contain limited soil fines and are typically non-plastic or slightly plastic in nature. In this regard, clay content 75<sup>th</sup> percentile values are typically below 5% in the Witzand and Langebaan Formations and below 7% in the Springfontyn Formation. According to Amdurer (1956), mainly kaolinite (and trace illite), make up the clay mineral fraction in the Cape Flats deposits. The kaolinite clay minerals will produce low plasticity values, even in increased quantities, whereas illite will be associated with higher PI's.

##### Springfontyn Formation

In the Springfontyn Formation, 85% of the investigated soils (94 of 110) are non-plastic (NP), 5% are slightly plastic (SP) and 10% have measurable PI. These soils were all sampled from the upper 3m of the soil profile. The plasticity properties of the soils – all of windblown origin - are summarised in Table 4-4. The samples with measurable plasticity indices came predominantly from depths below 1.5m and showed PI values of 3% to 10% (average of 7.5%). The results were interpreted in relation to the clay contents (refer to Table 4-4), illustrating the relative high clay contents associated with the typically low PI values. When evaluating individual results, a positive, weak linear relationship between clay content and PI is identified. The slightly plastic (SP) soils in

this formation have clay contents ranging from approximately 5% to 19%, with a maximum linear shrinkage of 1.5% (no measurable PI). The plasticity properties associated with the Springfontyn Formation soils presented in Table 4-4, agrees well with the specified ranges for kaolinite clay (Mitchell, 1993).

#### Witzand Formation

In the Witzand Formation, 96% of the studied soils (234 of 244) are non-plastic, approximately 2.5% slightly plastic, and about 1.6% have a quantifiable plastic phase. The lower clay contents characteristically associated with the soils from this formation (compared to the Springfontyn Formation), are reflected in the ratio of soils with plasticity. When comparing the results from the two formations, it is noted that the plastic soils from the Witzand Formation have higher average, maximum and minimum values for all plasticity properties, despite the lower clay contents (refer to Table 4-4). When comparing individual clay content – PI pairs, similar clay contents consistently produce higher PI's in the Witzand Formation. This difference is likely ascribed to clay mineral type, with kaolinite likely being dominant in the Springfontyn Formation, and Illite (or potentially a smectite clay) presumably present in the Witzand Formation. A maximum PI-clay content ratio of 3 was calculated in the Witzand Formation, indicative of the aforementioned clay mineral types. The plastic soils from the Witzand Formation were sampled from clayey sand layers, up to 2m in thickness in the upper 3m of the soil profile.

#### Langebaan Formation

Only one of the 39 soils from the Langebaan Formation (sampled at a depth of 1.2m) possesses plasticity, with the remainder of soils being non-plastic (no slightly plastic soils). The plasticity properties of this sample which came from 1m to 2m depth are given in Table 4-4. The PI-clay ratio is similar to that of the Springfontyn Formation soils, suggesting the presence of a low plasticity clay such as kaolinite.

**Table 4-4: Plasticity properties of clayey Cape Flats sands exhibiting non-zero plasticity indices**

Springfontyn Formation					
Property	Maximum	Minimum	Average	Standard Deviation	Number of values
Liquid limit (%)	28	17	22.3	3.3	11
Plastic limit (%)	19	9	14.8	2.6	
Plasticity index (%)	10	3	7.5	2.3	
Linear shrinkage (%)	4.5	1	2.9	1.1	
Clay content (%)	30	9	21	7.2	
PI-clay ratio	0.67	0.21	0.37	0.13	
Witzand Formation					
Property	Maximum	Minimum	Average	Standard deviation	Number of values
Liquid limit (%)	36	19	25.8	7.2	4
Plastic limit (%)	27	10	16.5	7.3	
Plasticity index (%)	14	5	9.3	3.7	
Linear shrinkage (%)	5	2.5	4	1.1	
Clay content (%)	16	3	6.8	6.2	
PI-clay ratio	3	0.6	1.79	1.1	

Langebaan Formation					
Property	Value	Maximum	Minimum	Standard deviation	Number of values
Liquid limit (%)	20				1
Plastic limit (%)	15				
Plasticity index (%)	5				
Linear shrinkage (%)	2		N/A		
Clay content (%)	14				
PI-clay ratio	0.36				

The potential for swell and shrinkage is influenced by the clay content and the plasticity of the clay minerals. From the results tabulated above, particularly the PI-clay content ratio (known as the activity), the presence of low plasticity kaolinite, and potentially higher plasticity illite and/or smectite, is inferred. Based on the criteria of Van Der Merwe (1964) and Dakshanamurthy and Raman (1973), the above results show non-expansive soils. The former criterion is based on the PI of the whole sample and the clay content, and the latter on the PI and the liquid limit. Clayey sands containing increased quantities of illite and/or smectite clays will be prone to hydration expansion.

The above results agree with the range of PI values (7% to 15%) and the average PI of 10% given by Stapelberg (2009) for aeolian clayey sands from the Cape Flats. However, it must be noted that the values given in Table 4-4 are only for samples with non-zero plasticity indices. The bulk of the samples in the database were non-plastic.

The Atterberg limits of transported (mostly lacustrine and estuarine) and residual shale soils from a portion of the Cape Flats were studied by Amdurer (1956). These mostly clayey and plastic soils gave PI's ranging from 4% to 60% (25<sup>th</sup>/75<sup>th</sup> percentile values of 18%/33% respectively), and liquid limits between 20% and 78% (25<sup>th</sup>/75<sup>th</sup> percentile values of 37%/57% respectively). Linear shrinkage values mostly varied between the outer limits of about 4% and 10% (middle 50% between  $\pm 6\%$  and 8%). Many soils were also found to be potentially expansive based on the criteria used by Amdurer: Linear shrinkage > 8%, liquid limit > 30%, and plasticity index > 12%. The specific soil types (textures) or clay contents of the tested soils were not given by Amdurer.

The presence of clay minerals will have a considerable influence on the engineering properties of the sandy Cape Flats deposits. Clay particles cover larger sand grains, causing the grains to separate, and thereby dominating soil behaviour. Even in low quantities, the presence of high plasticity clay minerals will influence the engineering properties. An increase in the clay content will initially increase the maximum compacted density and decrease the OMC (up to a certain clay content), after which the maximum density will decrease and be attained at a higher OMC. An increase in clay content and plasticity is also associated with decreased permeability and frictional strength, and increased compressibility.

The criterion presented by Prikloński (1952) (refer to Howayek et al., 2011), to predict the collapse potential of soils, relies on the Atterberg limits. A low or intermediate clay content and PI are suggestive of potentially collapsible soils. Clean sands with no PI are typically non-collapsible. The collapsibility of the Cape Flats soils with plasticity properties will be evaluated - based on empirical criteria - in Section 4.13.1.

### 4.5 Maximum dry density and optimum moisture content

Soil compaction plays a key role in all facets of fill material behaviour, influencing amongst others, the stiffness, shear strength and permeability of a material. The maximum compacted densities (MDD) and optimum moisture contents (OMC) of 167 soils, sampled from the Witzand, Springfontyn and Langebaan Formations from the locations shown in Figure C4 in Appendix C, are summarised and discussed. A tabulated summary of the compaction data is given in Appendix G (Table G3), and an extract thereof shown in Table 4-5. The data was separated into 1m intervals from ground surface to a maximum depth of 4m, although less data was available below 2m. The research focusses on aeolian sands and, as such, all results are associated with these deposits. The obtained compaction results only included MDD and OMC values. Moisture-density curves were not evaluated as part of the research.

**Table 4-5: Extract from compaction summary table in Appendix G**

Springfontyn Formation						
Maximum dry density (kg/m <sup>3</sup> )						
Depth range (m)	Maximum	Minimum	25 <sup>th</sup> /75 <sup>th</sup> percentile	Average	Standard deviation	Number of values
0 - 1	1920	1606	1748/1819	1783	60.8	33
1 - 2	1888	1701	1729/1789	1768	48.4	19
2 - 3	N/A					1 (Value: 1797)
Optimum moisture content (%)						
0 - 1	12.6	7.8	8.9/11.2	10.2	1.4	33
1 - 2	12.2	7.2	9.5/11.6	10.5	1.4	19

Separating the data into 1m depth intervals does not reveal noteworthy variances or trends with depth, which can possibly be ascribed to the limited number of compaction test results per depth interval, diminishing the validity of comparison. As several particle characteristics (e.g. distribution of grain sizes, particle shape etc.) which influence MDD and OMC remain relatively constant with depth, clear trends with depth are unlikely to emerge. For this reason, the compaction test results from the upper 2m of the soil profile were combined, and a statistical summary of the MDD and OMC values are shown (per formation) in Figures 4-8 and 4-9.

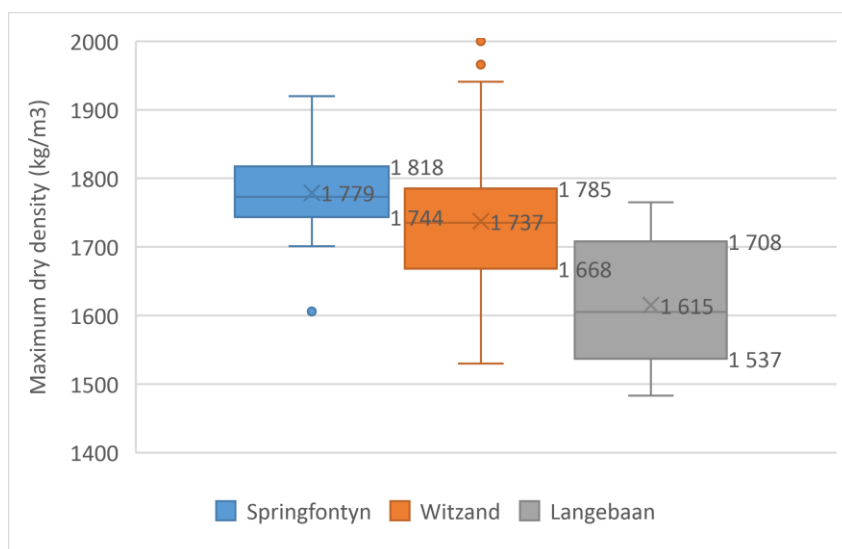


**Figure 4-8: Statistical summary of MDD in the shallow Cape Flats sands**

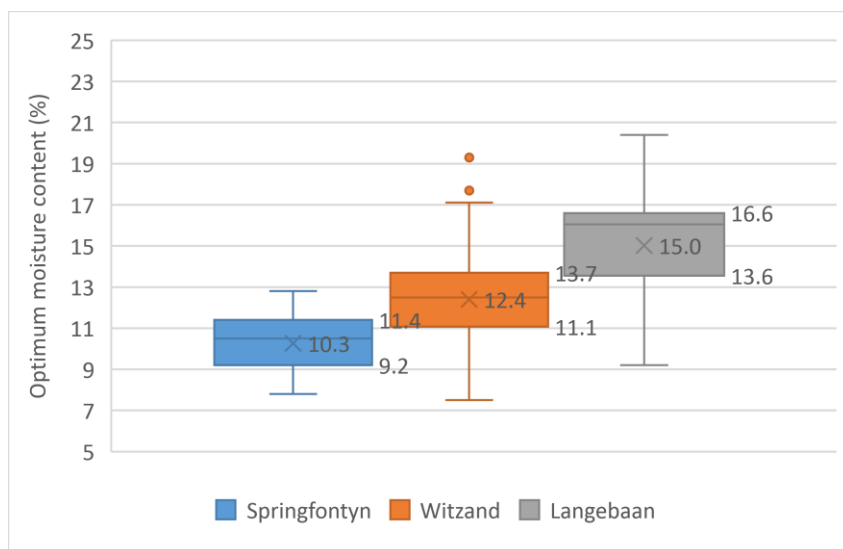


**Figure 4-9: Statistical summary of OMC in the shallow Cape Flats sands**

#### Springfontyn Formation

An average MDD of  $1779\text{kg/m}^3$  was obtained for the sands from the shallow soil profile (upper 2m) in the Springfontyn Formation. When compacted to its maximum density, the Cape Flats sands typically do not achieve densities as high as other soils. A slight decrease in the average and middle 50% of MDD values with depth is noted (refer to Table G3 in Appendix G), although the variance is rather insignificant and possibly biased by the fewer data values in the 1m to 2m depth interval. The range of MDDs achieved varies from  $1606\text{kg/m}^3$  to  $1920\text{kg/m}^3$ , with the lower value being identified as a statistical outlier (see Figure 4-8). This range of MDD values is mainly associated with the following obtained gradings: Clean fine and medium sand (containing both size ranges), and sand with varying proportions of soil fines (filling voids between larger quartz grains). In addition to the grain sizes, MDD is also influenced by the distribution of the grain sizes and the grain shapes. The middle 50% of values range between relatively narrow limits of  $1744\text{kg/m}^3$  and  $1818\text{kg/m}^3$ , ascribed to the similar soil types (textures) tested. A significant reduction in the obtained MDDs is anticipated for the peaty soil's characteristic of this formation (none observed in the accompanying profiles).

An average OMC of 10.3% was obtained for the Springfontyn Formation sands, varying between 7.8% and 12.8% respectively. The average in-situ moisture content in the upper 2m of the soil profile was found to be approximately 13%, with only 25% of values below 11.3% (refer to Section 4.12.2). The investigated soils are thus, on average, wet of optimum in the field. On average, the soil voids will contain more water than required for optimum compaction, making it more difficult to achieve the laboratory attained maximum dry densities.

#### Witzand Formation

The average MDD of the sands from the upper 2m in the Witzand Formation is  $1737\text{kg/m}^3$ . From Figure 4-8, lower compacted densities were achieved in the soils from the Witzand Formation compared to the Springfontyn Formation. This is reflected in the lower average, 25<sup>th</sup>, 50<sup>th</sup>, and 75<sup>th</sup> percentile values. In addition, ANOVA testing revealed that the variation between the means of the data sets from the Witzand and Springfontyn Formations are significant ( $F > F_{\text{crit}}$  and  $P \text{ two-tail} = 0.012$ ). This is mainly the result of the characteristically narrower range of particle sizes in

the Witzand Formation (lower average  $C_u$ ). The sands from the Witzand Formation were found to contain, on average, more fine sands and lower percentages of particles of other sizes, compared to the Springfontyn Formation. The larger range in MDD values (also noted in the standard deviations) in this formation can be ascribed to the presence of clean fine grained (uniform) sands producing very low densities, and a few soils with coarse sand and gravel fractions achieving compacted densities in the range of  $1900\text{kg/m}^3$  to  $2000\text{kg/m}^3$ . The larger interquartile range (compared to the Springfontyn Formation) is owed to the wider range of soil types (textures) tested. Variability between seemingly similar soils was also noted as well as inexplicable results (same gradings producing contrasting compactions). The controlling factor in these outcomes is rooted in the distribution of the grain sizes and the difference in average particle size. An increase in soil fineness is mostly associated with lower values of MDD. Variation in particle shape can also be a responsible factor.

The average OMC is 12.4%, higher than that for the Springfontyn Formation (confirmed to vary significantly through ANOVA testing). The average in-situ moisture content in the upper 2m of the Witzand Formation was found to be about 8.7%, with 75% of in-situ moisture contents below 12.1% (refer to Section 4.12.2). The investigated soils are thus mostly dry of OMC. On average, and at the determined moisture content, the lubrication between soil grains will be insufficient for grains to slide past each other to achieve the laboratory maximum dry densities. The summary values of compacted density and OMC show no noteworthy variation with depth (refer to Table G3 in Appendix G).

#### Langebaan Formation

Seventy-five percent of the soils from the Langebaan Formation achieved compacted densities of  $1708\text{kg/m}^3$  or less. A notable downwards shift in all statistical summary values for MDD is noted in comparison with the Springfontyn and Witzand Formations. A limited number of results were available for the soils from the Langebaan Formation (12 in total), possibly skewing the actual range of achievable densities. Notwithstanding this, the results mainly apply to fine sands, fine and medium sands and gravelly sands, and only some of the low densities could be explained based on the soils' grain size characteristics. ANOVA testing showed that, when comparing MDD data sets from the Langebaan Formation to the Witzand and Springfontyn Formations separately (in terms of their sample means and grand mean), that the former formation is significantly different from the latter two ( $P$  two-tail =  $7.1 \times 10^{-5}$  and  $1.2 \times 10^{-9}$ ).

The middle 50% of OMC values range between 13.6% and 16.6% (average of 15%), which is substantially higher than the moisture contents needed to achieve maximum compacted densities in the soils from the Springfontyn and Witzand Formations. ANOVA testing confirmed that the Langebaan Formation data set is significantly different (by comparison of means) from both the Witzand and Springfontyn Formation data sets. The average in-situ moisture content in the shallow Langebaan Formation soils was found to be approximately 6.8%, with the middle 50% of values ranging from 4.2% to 6.9%. The studied soils are therefore typically dry of OMC and will require wetting to achieve the benchmark densities. The summary values of compacted density and OMC show no noteworthy variation with depth (refer to Table G3 in Appendix G).

## General

Densities in excess of  $1850\text{kg/m}^3$  could seldom be reached in the soils from the Cape Flats sands with Modified AASHTO compaction effort. It is the predominance of fine sand sized particles (uniform gradation) that typically hinders proper densification. Compaction to higher densities was achieved in soils containing an appreciable fines content, in which the void space between the larger quartz grains is filled by soil fines, or where the sand fraction includes medium and/or coarse sand sized particles in addition to fine sand portion. Fines contents above 40% will however be associated with lower compacted densities (Das and Sobhan, 2018). Higher compaction densities were often associated with an increase in the range of particle sizes (wider PSD curve), although inconsistencies were noted in this regard. Other factors such as average particle size or particle shape are additional influences which could be responsible for these discrepancies. An increase in particle angularity (decrease in roundedness) will make the soil more difficult to compact. Variation in grain shape in the soils from the Cape Flats, which is a function of transportation distance, is likely (although probably dominated by rounded and sub-rounded grains) and will influence the attained densities to some extent.

Amdurer (1956) performed Proctor and Modified AASHTO compaction tests on 27 samples of sand and silty sand from the Cape Flats. The grading data for these soils and the sampling localities (from which the formation could be inferred) were mostly unavailable. Proctor densities ranging from  $1620\text{kg/m}^3$  to  $1880\text{kg/m}^3$  was achieved at optimum moisture contents of 7% to 11.4%. The Modified AASHTO MDD's varied from  $1630\text{kg/m}^3$  to  $1890\text{kg/m}^3$  at optimum moisture contents of 7% to 11.5%. An increase in compaction energy from Proctor to Modified AASHTO had minimal influence on the compacted densities. The variations noted for seemingly similar soils during the current research was also noted by Amdurer and ascribed to average grain size (fineness). The obtained densities and associated moisture contents are consistent with the compacted characteristics obtained during the current research.

The influence of particle size and gradation on MDD and OMC is evident (although complex), and an attempt was made to establish statistically significant relationships between grading and compaction properties. The aim was to explore the influencing factors of grading and gradation, and to ultimately create transformation models whereby MDD and OMC can be estimated - specifically for the Cape Flats sands - from the selected variables. In past studies, the grading coefficient  $[P_{4.75} \times (P_{26.0} - P_{2.0}) / 100]$ , the grading modulus  $[(300 - (P_{2.0} + P_{0.425} + P_{0.075})) / 100]$ , and the grading ratios  $(P_{0.075} / P_{0.425}$  and  $P_{0.425} / P_{2.36})$  were found to be relatively good/reliable predictors of MDD and OMC. In addition, the coefficients of uniformity and curvature have also been used to predict MDD and OMC. An attempt to include the latter two variables showed that unreliable outcomes are likely. In this regard, minor inaccuracies in the determination of the  $D_{10}$ ,  $D_{30}$  and  $D_{60}$  sizes (often arising from interpolation between sieve sizes on semi-log plots, and extrapolation of PSD curves with long fines 'tails') may affect the accuracy of the model, particularly for the closely spaced  $C_u$  and  $C_z$  values (often separated by the second decimal place) for the uniformly graded soils of the Cape Flats. Furthermore, it is unlikely that a strong correlation will be obtained between MDD and OMC and the very closely spaced  $C_u$  and  $C_z$  values for the similar soil textures. The coefficients were therefore excluded from the analysis. The compaction characteristics were presented as a function of the grading coefficient ( $G_c$ ), grading modulus (GM), and the grading ratios ( $GR_1$  and  $GR_2$ ), to find the predictive equation yielding the best fit to the data. For many soils,  $G_c$  was equal to zero and only 41 data pairs

incorporating the value of  $G_c$  could be analysed. One hundred and sixty data pairs including GM,  $GR_1$  (P0.075/P0.425) and  $GR_2$  (P0.425/P2.36) were used in the regression analyses. Results from the three formations were combined, as there are no clearly distinguishing factors, and separation of data will result in modelling with insufficient data.

Linear and non-linear regressions were performed. The power regression model gave the best fit. Regression analyses involving one independent variable (GM,  $G_c$ , P0.075/P0.425, or P0.425/P2.36), revealed the best correlations are between MDD and GM, and between OMC and GM. However, the coefficient of determination ( $R^2$ ) of 0.183 and 0.258 shows these correlations are weak. For instance, only 18.3% of the observed variation in MDD can be attributed to the approximate power relationship between MDD and GM. The best fit to the data yielded the power equations (sample regression lines) shown in Figures 4-10 and 4-11, with the standard form given as Equation 4-1. A standard error in MDD and OMC estimates of 85.94  $\text{kg/m}^3$  and 2.12% respectively, was obtained. The standard error bounds are shown on Figures 4-10 and 4-11, showing the average distance of data points from the regression line.

$$y = a \cdot x_1^{\beta_1} \times x_2^{\beta_2} \quad \text{Equation 4-1}$$

Where:

$a$  = Intercept

$x_1$  = First independent variable

$\beta_1$  = Regression coefficient for first independent variable

$x_2$  = Second independent variable

$\beta_2$  = Regression coefficient for second independent variable

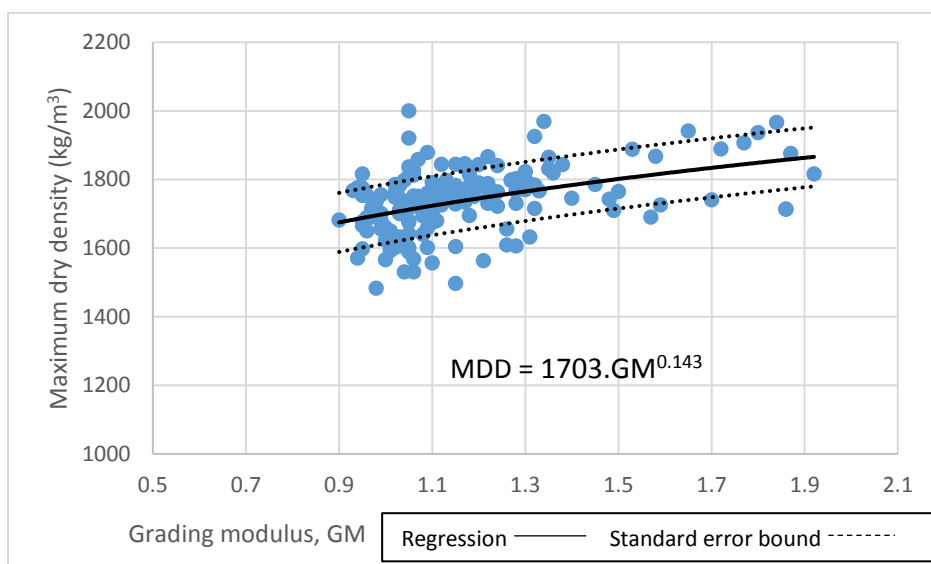


**Figure 4-10: MDD versus GM for the Cape Flats sands**

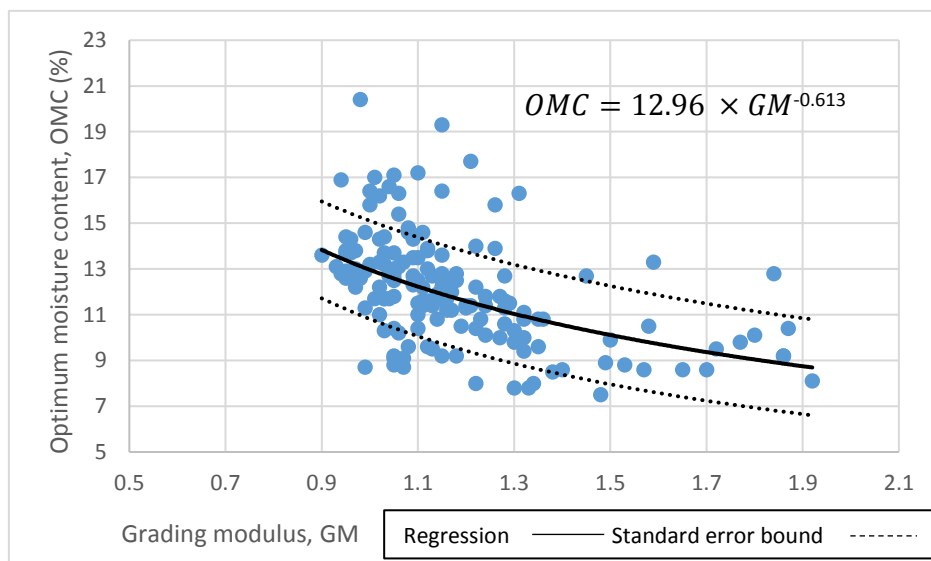


**Figure 4-11: OMC versus GM for the Cape Flats sand**

The differences between the natural logarithms of variables MDD and OMC and the natural logarithms of the predicted values, that is, the residuals, were calculated and studied. No unusual or highly influential observations were noted that could possibly suggest an improved fit to the data. The residuals of the regression of MDD and OMC also follow a normal distribution (presented as near linear plots).

Power regression analysis including multiple independent variables were also performed. Regression of a combination of the independent variables (GM, P0.075/P0.425 and P0.425/P2.36), were undertaken to develop prediction equations possibly superior to the simple regression (one explanatory variable) equations. The grading coefficient was excluded from the analysis due to the insufficient number of parameter values accessible for analysis. The grading modulus and P0.075/P0.425 proved the best combination of predictors of MDD with  $R^2$  equal to 0.325. The most accurate prediction of OMC, with an  $R^2$  value of 0.273, was obtained by incorporating all three independent variables (GM, P0.075/P0.425, and P0.425/P2.36). The standard errors decreased to  $78.25\text{kg/m}^3$  and 2.1%. The following best fit equations were obtained for the least squares lines:

$$MDD = 1837.4GM^{0.133} \times (P0.075/P0.425)^{0.026} \quad \text{Equation 4-2}$$

$$OMC = 12.6GM^{-0.453} \times (P0.075/P0.425)^{-0.013} \times (P0.425/P2.36)^{0.128} \quad \text{Equation 4-3}$$

An improved, but nevertheless still relatively weak relationship, is indicated between the compaction and grading characteristics. Plotting the regression residuals proved a reasonable distribution of errors and normal probability plots indicated near linear patterns. From the above analyses, it is advised that these equations are used cautiously and that MDD and OMC values should preferably be determined directly using the Modified AASHTO test.

## 4.6 Soil classification

The grain size distribution, plasticity index, CBR and CBR swell of the Cape Flats soils were used to classify the sands from the upper 4m of the profile according to the Unified Soil Classification System (USCS), the TRH14 Classification System and the AASHTO Soil Classification System. The sites from which soils were sampled for classification coincide with the sampling sites shown in Figure C3 (soils classified according to the AASHTO and USCS systems) and Figure C5 (soil classified according to TRH14 system) in Appendix C. The classification systems are included as Figures B1, B2 and B3 in Appendix B.

### Unified Soil Classification

The distribution of USCS classes assigned to 389 soils sampled from the Witzand, Springfontyn and Langebaan Formations are shown in the frequency bar charts in Figures 4-12a and 4-12b.

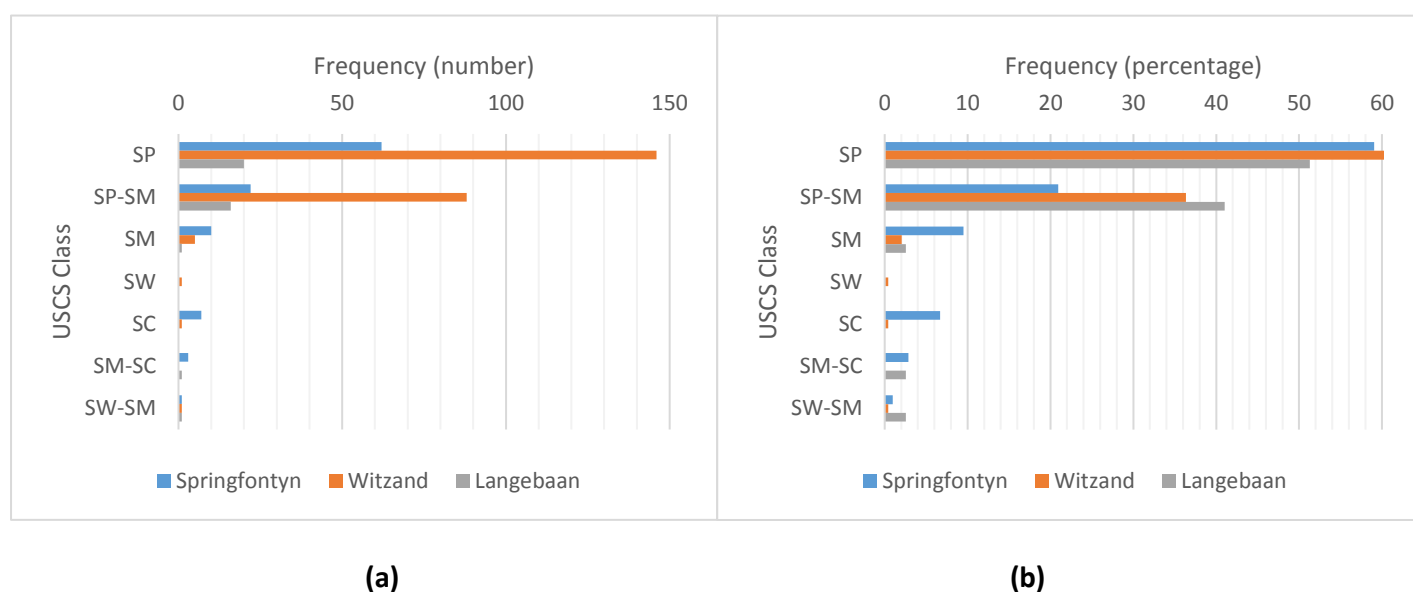


**Figure 4-12: Distribution of USCS classes in the Cape Flats in terms of a) number and b) percentage**

In the Witzand, Springfontyn and Langebaan Formations, between 51% and 60% of the sampled soils belong to group SP (poorly graded sand with less than 6% fines). The remainder of the soils (apart from one soil categorised as a well graded sand – with symbol SW), received a group symbol SM, SC, or SM-SC (silty and/or clayey sand) when the fines content exceeded 12%, or SP-SM or SW-SM (combination soils), when the fines content was between 6% and 12%; the assigned class depending on the gradation and type of soil fines (silt). From Figure 4-12 it is evident that only a few of the soils from the Witzand and Langebaan Formations comprise clay fines or an overall fines content in excess of 12%. Approximately 17% of the soils from the Springfontyn Formation were classified as SM or SC soils with more than 12% fines. With depth, an increase in the fines content was again observed in the Springfontyn Formation, demonstrated in the classification. In this regard, a decrease in SP soils from >60% to approximately 35% with depth (to a maximum depth of 3m), was accompanied by an increase in the number of SC, SM and SP-SM soils. The same trend, although less pronounced, was also noted in the Witzand Formation.

### TRH14 classification (for road layerworks)

Frequency bar charts showing the distribution of TRH14 classes in the Witzand, Springfontyn and Langebaan Formations, in terms of the number and percentage of each class per formation, are shown in Figures 4-13a and 4-13b. One hundred and fifty-two soils from the upper 2m of the soil profile in the Witzand and Springfontyn Formations, and from the upper 4m in the Langebaan Formation, were considered.

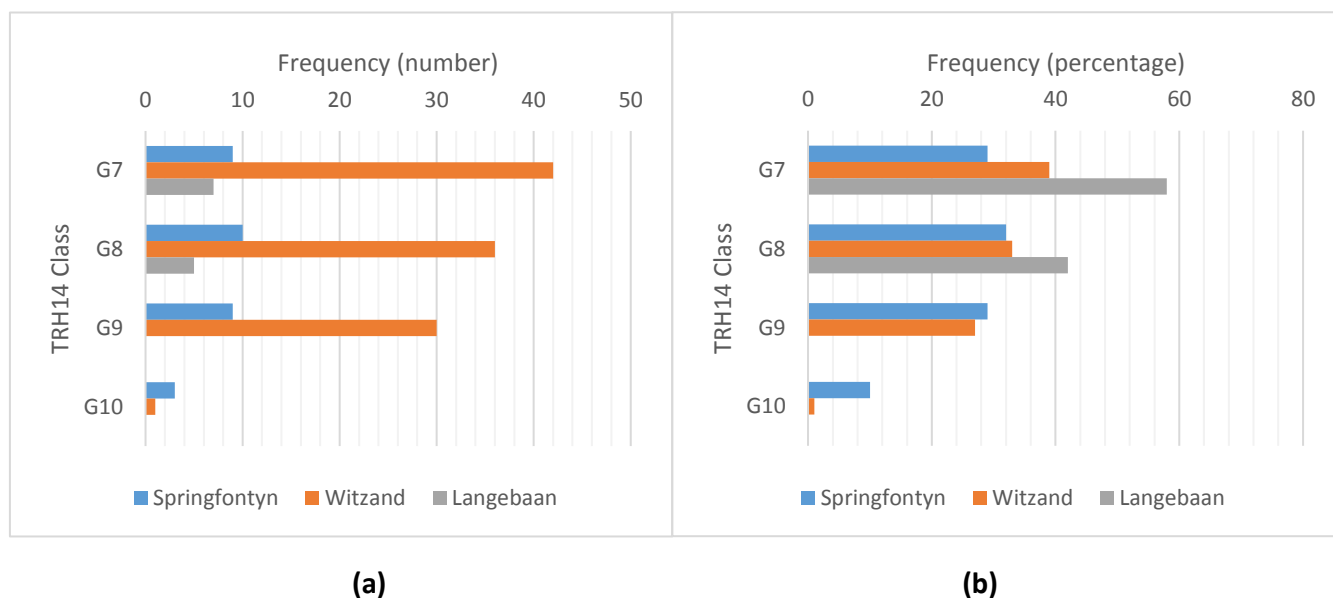


**Figure 4-13: Distribution of the TRH14 classes in the Cape Flats in terms of a) number and b) percentage**

All soils from the Cape Flats fall in the “gravel-soil” category (G7 to G10 quality materials). In keeping with the COLTO specification, the CBR at 93% Modified AASHTO MDD was selected for these classifications. The sands from the Springfontyn and Witzand Formations are distributed relatively equally between the G7, G8 and G9 classes. The Langebaan Formation sands are all G7 and G8 quality, possibly influenced by the limited number of soils classified. No noteworthy variation in soil classes with depth was observed.

G7, G8 and G9 material are suitable for use in the lower pavement layers or in the subgrade (Jenkins and Rudman, 2016). G7 material can be used in the upper selected layer, and G8 and G9 materials in the lower selected layer. The G10 quality soils can be used for the construction of embankment fills in the absence of more suitable material.

The general conclusion that can be drawn from this analysis is that the lower selected layer materials may be sourced from borrow pits in any of the three formations. Borrow pits in the Langebaan Formation are more likely to yield upper selected material than those in other formations.

The factors preventing a better classification were investigated. For G8, G9 and G10 materials, soils are classified on the basis of CBR and CBR swell alone. Classification as a G7 material or better is subject to additional criteria including PI, GM and maximum particle size. In most cases, the plasticity of the material is not a limiting factor and either the grading or CBR prevents classification as a G6 material. Although half of the samples from the Springfontyn and Langebaan

Formations and 25% of the samples from the Witzand formation meet the G6 grading requirements, the compliant samples fail to achieve the required CBR. Classification as G5 or G4 materials is prevented by both the grading and CBR requirements.

The above TRH14 classifications are based on the CBR at 93% Mod AASHTO MDD. However, most of the Cape Flats sands conform to the definition of a “sand” in SABS 1200M: Roads (General). As such, these materials would be compacted to 100% MDD when used in selected pavement layers. If the CBR at MDD is used in the classification, 90% of the samples from the Springfontyn Formation, 95% from the Witzand Formation and virtually all the samples from the Langebaan Formation would classify as G7 materials. 70% of the samples from the Springfontyn Formation, 50% from the Witzand Formation and 90% from the Langebaan Formation would meet the G6 CBR requirements but most would still fall short of a G6 classification based on grading. Although a few samples from all formations (3% - 17%) would meet the G5 CBR requirements, classification as a G5 material would be prevented by grading requirements.

AASHTO classification

The distribution of AASHTO classes assigned to 389 soils sampled from the Witzand, Springfontyn and Langebaan Formations are shown in the frequency bar charts in Figures 4-14a and 4-14b. Grading and Atterberg limits results for soils sampled between ground surface and maximum depths of 3m in the Springfontyn Formation and 4m in the Witzand and Langebaan Formations, were used to classify the soils.

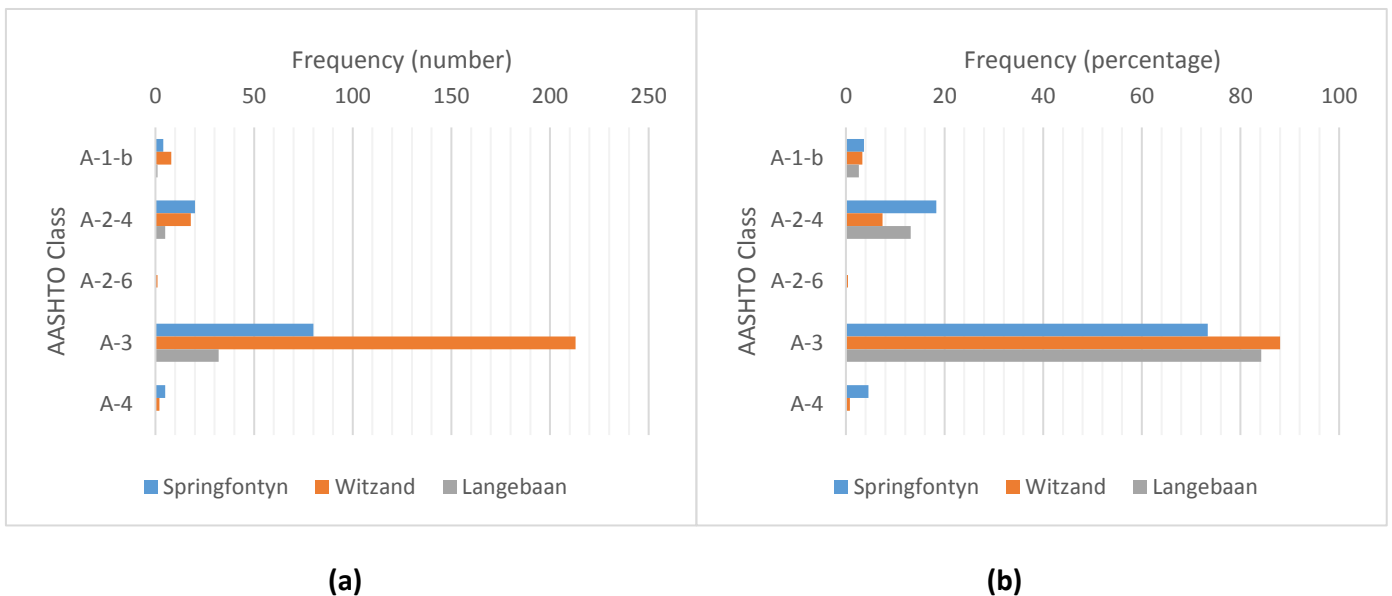


**Figure 4-14: Distribution of AASHTO classes in the Cape Flats in terms of a) number and b) percentage**

Most of the investigated soils from all three formations (between 73% and 88% of soils) are classified as A-3 materials, being non-plastic, fine sandy material with at least 51% of the particles passing the 0.425mm sieve and no more than 10% combined silt and clay sized grains. In the Springfontyn Formation, a higher percentage of the soils fell in groups A-2-4 and A-4 compared to the other formations (approximately 23% versus 8.5% and 13%). Class A-2-4 materials are described as silty or clayey gravel sand with a fines content (<0.075mm) between 11% and 35% and with plasticity index and liquid limit values not exceeding 10 and 40 respectively. A-4 group

materials are silty soils with more than 35% fines. This outcome was expected and agrees with the grading results presented in Section 4.2.2. In the Springfontyn Formation, a shift in the assigned soil class was noted with depth, as the percentage soils in class A-3 decreased and the percentage soils in class A-2-4 increased. Once more, this outcome supports the grading and plasticity property results, noting an increase in soil fines with depth. No noteworthy variation in the soil classes were noted with depth in the Witzand or Langebaan Formations. In the Witzand Formation, more than 80% of soils were allocated to class A-3 in all depth intervals. No distinction in the AASHTO soil class is made where the fines content is equal to or less than 10%. For this reason, slight increases in the fines content (with depth) won't necessarily reflect in the assigned AASHTO class.

The A-3, A-1-b, and A-2-4 classification of these soils indicates good to excellent subgrade materials.

## **4.7 California Bearing Ratio**

The California Bearing Ratio (CBR), which provides an indication of the strength of compacted soil, is one of the parameters used to categorise pavement layer materials according to the TRH14 and the COLTO (1998) material grading specifications, and is used in the design of flexible road pavements. This section of the results summarises and evaluates the outcomes of laboratory CBR tests (soaked) on 166 soils. One hundred and fifteen of these samples are from the Witzand Formation, 39 from the Springfontyn Formation and 12 from the Langebaan Formation. The results include CBR values at Modified AASHTO maximum dry density, and at 98%, 97%, 95%, 93%, and 90% of MDD. The soils sampled for CBR testing were all collected from the shallow soil profile (surface to 3m depth). In addition to the soaked CBR laboratory results, in-situ CBR values were derived from 168 DCP tests undertaken across the Cape Flats to evaluate subgrade strength, and to relate the in-situ CBR to material G-classes. The sampling and testing sites are shown in Figure C5 in Appendix C. The predictive model by Paige-Green and Du Plessis (2009) were used to estimate DCP CBR (refer to Section 3.5.4 from Chapter 3).

### **4.7.1 Laboratory soaked CBR**

A tabulated summary of the CBR data is given in Table G4 in Appendix G, and an extract in Table 4-6 below. The dry density (DD) corresponding to each compaction level was noted alongside the CBR value to study the relationship between the two soil properties. Note that both the CBR and dry density values in the table are maximum and minimum values and not corresponding values from individual samples. A statistical summary of the laboratory CBR results is shown in Figures 4-15, 4-16 and 4-17 for the Springfontyn, Witzand and Langebaan Formation soils respectively. The statistical outliers are not shown on the figures (as it affects the scale) but were included in the calculation of the statistical parameters. For the Langebaan Formation soils, no CBR data could be obtained at 97% of MDD.

**Table 4-6: Extract from CBR summary table in Appendix G**

Springfontyn Formation							
Compaction level	Property	Maximum	Minimum	25 <sup>th</sup> /75 <sup>th</sup> percentile	Average	Standard deviation	Number of values
MDD	CBR (%)	62	10	20/34	29	10.9	39
	DD (kg/m <sup>3</sup> )	1920	1606	1750/1814	1782	56.7	39
98% MDD	CBR	45	9	15/26	21.9	8	36
	DD	1850	1566	1712/1777	1738	61.3	36
97% MDD	CBR	22	9	13/18	15.1	3.8	11
	DD	1807	1558	1677/1759	1707	68	11

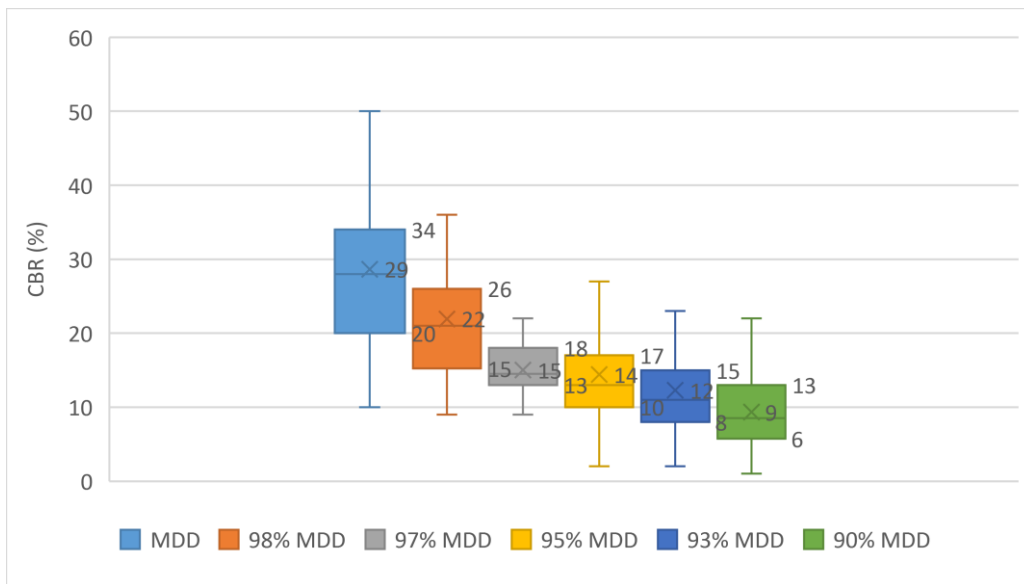


**Figure 4-15: Soaked CBR data for the Springfontyn Formation sands**

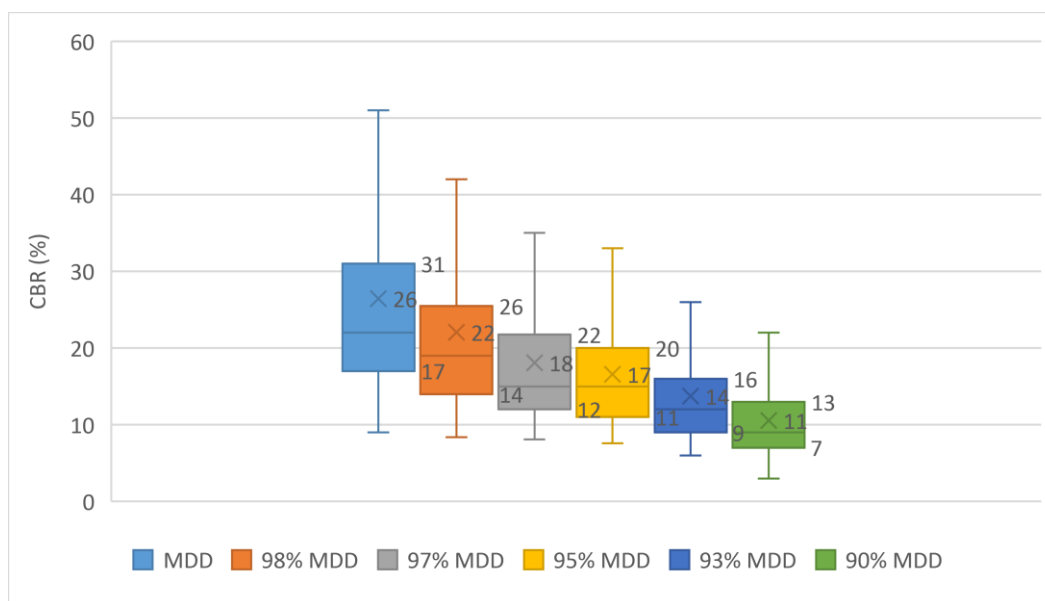


**Figure 4-16: Soaked CBR data for the Witzand Formation sands**

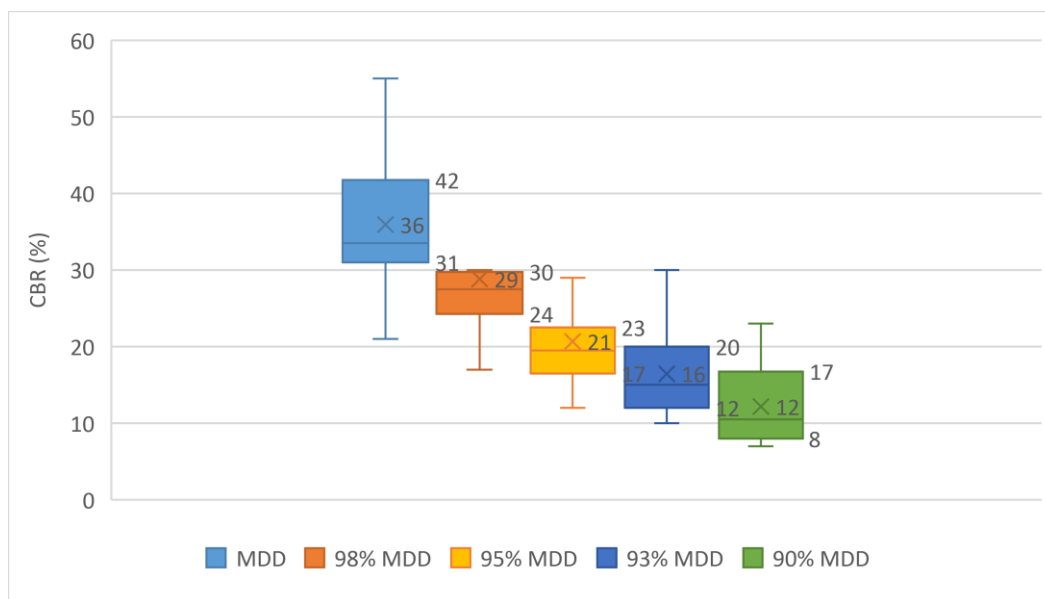


**Figure 4-17: Soaked CBR data for the Langebaan Formation sands**

Although it is evident from Figures 4-15, 4-16, and 4-17 that bearing strength decreases with decreasing compaction, it is unlikely that a strong relationship exists between individual CBR and dry density values. This is because both CBR and MDD (in terms of which degree of compaction is determined) are influenced by multiple factors, including interparticle friction, particle shape and grain size distribution in addition to degree of compaction.

From Table G4 in Appendix G it is evident that the highest average MDD was recorded in the Springfontyn Formation and the lowest average MDD in the Langebaan Formation sands. This corresponds to the compaction results presented in Section 4-5. Surprisingly, the CBR values show an opposite trend with the highest CBR values recorded in the Langebaan formation, followed by the Witzand formation. The quartiles reflect the same trend, illustrating that a few outliers are not responsible for skewed averages. When evaluating the spread in dry density data, the average, 25<sup>th</sup> percentile, 75<sup>th</sup> percentile and minimum dry density values are all lower in the Witzand Formation compared to the Springfontyn Formation soils. These statistical summary values are the lowest in the Langebaan Formation soils, although fewer values have possibly introduced bias. As explained in Section 4-5, a few soils with coarse sand and gravel fractions are responsible for denser states in the highest 25% of numbers (between 75<sup>th</sup> percentile and maximum). It is the variance in particle characteristics, such as particle shape, maximum particle size, packing arrangement and inter-particle friction in the soils from the different formations that is reflected in the CBR results. The higher CBR results obtained for the Langebaan and Witzand Formations can possibly be explained by the presence of angular micro shells increasing interlocking and friction and/or nodular calcrete affecting the maximum particle size.

To determine the statistical variation in CBR between the three formations, ANOVA testing was employed. For the analyses, CBR at 98%, 95%, 93% and 90% of MDD was selected. Analyses of the CBR data set at 98% of MDD revealed significant variation between the means of the data sets from the Langebaan and Witzand Formations and the Langebaan and Springfontyn Formations (P two-tail = 0.02 and 0.012 respectively). For the 95% of MDD data set, significant variation between the means of data from only the Witzand and Langebaan Formation was observed (P two-tail = 0.042). At 93% and 90% of MDD, the CBR data sets for the three formations cannot be

distinguished (i.e. are not statistically different) by ANOVA statistical testing. Overall, the variation in CBR between formations is not well defined and varies with compaction level. This outcome may change (and possibly become more distinct) with larger data sets.

The process of determining CBR has been described as time consuming and requiring large quantities of material and, as such, an attempt has been made to produce transformation models for the Cape Flats sands, whereby CBR can be estimated from dry density (DD) and the grading modulus (GM). According to Breytenbach (2009), grading characteristics largely determines particle interlock in coarse grained soils (affecting CBR). A comprehensive study by Breytenbach (2009) investigating the relationship between index testing and CBR, revealed GM to be one of the best predictors of CBR (together with plasticity index and linear shrinkage). From previous sections it is evident that compaction (dry density) influences strength significantly as it increases particle interlocking and particle packing.

CBR values were paired with the corresponding dry densities - determined at each percentage of MDD. The data pairs were considered separately for the three formations. Linear regression analyses were firstly performed with the single independent variable of dry density (in kg/m<sup>3</sup>), producing the results shown in Table 4-7 (regression numbers 1 to 3). Non-linear regression models were also applied, revealing similar results. The weak linear pattern, with R<sup>2</sup> values of 0.264 and 0.37 for the Springfontyn and Langebaan Formations respectively, and the near random pattern producing an R<sup>2</sup> value of 0.036 for the Witzand Formation, are not surprising, bearing in mind the number of factors influencing CBR. The sands were sampled over a large geographical area with inherent variability in particle characteristics, which would influence CBR. To potentially improve the fit of the data to a model, the grading modulus was included in the regression analysis. Analyses were conducted on three separate data sets (separating formations) and on a combined data set (combining formations), separating the data into compaction levels (MDD and 98%, 95%, 93%, and 90% of MDD). The results of all analyses are shown in Table 4-7. It should be noted that for the Langebaan Formation, no CBR-DD-GM sets were obtainable, thus only a single variable regression was performed for the soils from this formation. The linear regressions produced predictive equations of the following form:

$$Y = \beta_0 + \beta_1 \times X1 + \beta_2 \times X2 + \varepsilon \quad \text{Equation 4-4}$$

Where:

Y = Dependent variable

$\beta_0$  = Intercept

$\beta_1$  = Regression coefficient for first independent variable

X1 = First independent variable

$\beta_2$  = Regression coefficient for second independent variable

X2 = Second independent variable

$\varepsilon$  = Error term (Shown as standard error in table)

**Table 4-7: CBR prediction equations**

Regression number	Formation	Independent variable	Regression equation	Data pairs	R <sup>2</sup>	Standard Error (%)	Statistically significant (based only on p-value)
1	Springfontyn	DD	$CBR = 0.065DD - 93.42$	189	0.26	8.8	Yes
2	Witzand	DD	$CBR = 0.018DD - 11.39$	657	0.04	9.8	Yes
3	Langebaan	DD	$CBR = 0.065DD - 77.10$	59	0.37	8.8	Yes
4	Springfontyn	DD and GM	$CBR = 0.055DD + 9.86GM - 86.9$	70	0.37	7.2	Yes
5	Witzand	DD and GM	$CBR = 0.025DD - 5.47GM - 17.99$	473	0.06	9.7	Yes
6	All	MDD	$CBR = -0.024MDD + 67.22$	109	0.03	11.8	No
7	All	DD (at 98%MDD)	$CBR = -0.017DD + 51.03$	107	0.02	9.8	No
8	All	DD (at 95%MDD)	$CBR = -0.009DD + 30.80$	109	0.01	7.6	No
9	All	DD (at 93%MDD)	$CBR = -0.004DD + 20.28$	109	0.003	6.1	No
10	All	DD (at 90%MDD)	$CBR = -0.001DD + 12.29$	109	0.0003	5.0	No

From Table 4-7 it is evident that regression equations 3, 4, and 5 revealed the best fit of the data to the model. For the Springfontyn and Langebaan Formations, an R<sup>2</sup> value of 0.37 was obtained, with standard errors in CBR of 7.2% and 8.8%. For the Witzand Formation sands, a near random distribution of data points revealed an R<sup>2</sup> value of 0.06 and a standard error of nearly 10%. Evaluation of the data shows that 'goodness of fit' seems to decrease as the regression data (number of data pairs) increases. The poor outcomes can be ascribed to data variability arising both from material characteristics (wide range of soil types) and test repeatability. The influence of GM on CBR was shown by plotting the results for the Springfontyn Formation deposits in Figure 4-18 as CBR against dry density for different values of GM. From the figure it is evident that (for the sandy Cape Flats soils), soil coarseness exerts an influence on CBR, but is not the main determining factor. For example, considering a dry density of 1700kg/m<sup>3</sup>, an increase in GM from 1.0 to 1.4 relates to an increase in CBR from 16.5% to 20.4%, whereas the measured CBR values at a similar density varied from 2 to 33. CBR was found to be more strongly related to dry density than GM. Plotting the regression residuals proved a reasonable distribution of errors and normal probability plots indicated near linear patterns.

The relatively poor outcomes of the regression analysis could possibly be improved by creating data subsets, such as maximum particle shape, C<sub>u</sub> or USCS classes. There is insufficient data to justify such an approach.

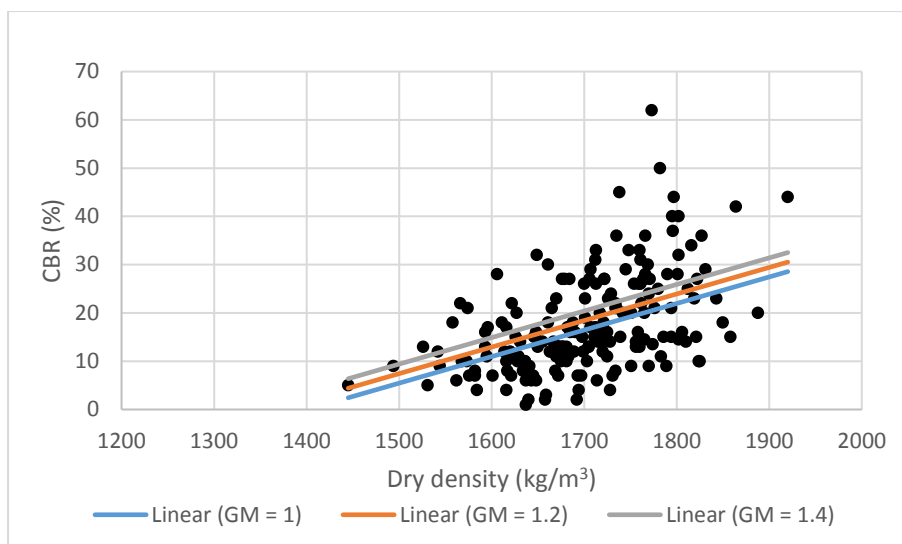


**Figure 4-18: CBR versus dry density and regression lines for GM values for the Springfontyn Formation sands**

#### 4.7.2 In-situ CBR (DCP CBR)

In-situ CBR values were derived from the results of 168 DCP tests undertaken on 33 sites to a maximum depth of about 4m below ground level in the study area. Summarising and interpreting the DCP CBR results provide an indication of subgrade strength of the in-situ soils, and material classification in accordance with TRH14 can be obtained from approximate correlations. The predictive model proposed by Paige-Green and Du Plessis (2009), presented as Equations 3-26a and 3-26b in Section 3.5.4, was used to estimate CBR from the cone penetration rate (DN in mm/blow). Sites with DCP data are shown in Figure C5 in Appendix C. Only cone penetration values recorded in the windblown sands of the Cape Flats were analysed. Accompanying soil profiles were used to identify layers of different origin.

The DCP CBR values were separated into 1m intervals for analysis to investigate possible variations with depth. Only data from the upper 2m in the Witzand and Springfontyn Formations, and from the upper metre in the Langebaan Formation could be included, as data is sparse below these depths. The results for all three formations are shown in Figure 4-19. It should be noted that there are multiple outlier values exceeding the maximum values on the plots, which are not shown, as they affect the scale and presentation of the graphs. The outlier values represent refusal in very dense sands or cemented sands (hardpan or nodular calcrete or silcrete) and possibly calcarenite banks. Layers of cemented soil and sandstone with thicknesses of 1m to 2m have been reported in the study area (GEOSS, 2014). Outlier values were included in the calculation of the statistical parameters. The results are interpreted with the aid of scatter plots of DCP CBR versus depth presented as Figures G1 to G3 in Appendix G. It is important to note that the DCP CBR was determined at the in-situ moisture content (and density) at the time of testing and that individual strength values will vary as the natural moisture content fluctuates.

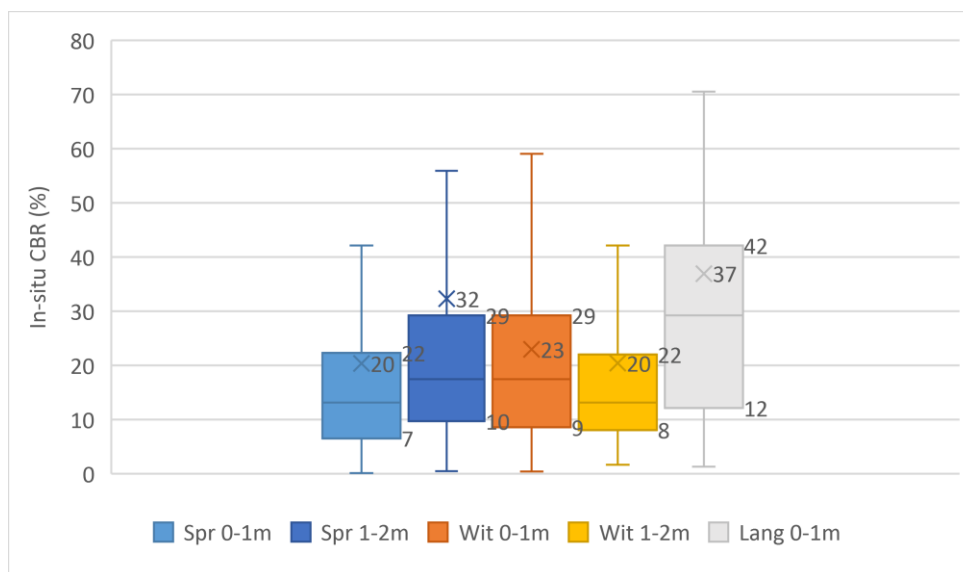


**Figure 4-19: In-situ CBR summary for the Cape Flats sands**

### Springfontyn Formation

Fifty DCP tests were performed in the soils from the Springfontyn Formation. From ground surface to 2.5m depth there is a gradually decreasing DN (and increasing DCP CBR) trend (refer to Figure G1 in Appendix G). This is probably the effect of skin friction on the rods, particularly in the harder materials where DCP CBR exceeds 15% and below the groundwater table (Paige-Green and Du Plessis, 2009 and MacRobert, 2009). The variation in density index noted in individual profiles mostly reflects changes in soil type, e.g. sands to clayey sands and moisture content. In most profiles a dense consistency ( $5 < DN < 12.5$ ; Byrne and Berry, 2008) was reached between 1.5m and 2m depth. Only a few DCP tests extended below 2.5 m depth, all producing DCP CBR values below 25%. The inclusion of outlier values caused by slow penetration through (or refusal on) very dense soils, influences the average CBR (plotting near 75<sup>th</sup> percentile values). The quartiles provide a good measure of the spread of the data. A gradual increase in soil moisture with depth was mostly noted from the accompanying soil profiles. The intersection of the water table was often associated with a sudden increase in DN (and decrease in DCP CBR), followed once again by a gradual decrease in DN with depth. The water table (presumably perched on impermeable layers/lenses) was intersected at approximately 80% of the DCP test positions at an average depth of 1.63m (obtained from accompanying test pit profiles).

From the inferred in-situ CBR's, material G-classes were estimated based on the relationship proposed by Paige-Green and Du Plessis (2009). The interpretation of the results depends on the moisture content of the penetrated soil. Approximately 75% of DCP CBR values are below 24% in the upper 2m. According to Paige-Green and Du Plessis, DCP CBRs of 24% and 20% below an unsurfaced area correspond to a soaked CBR of 3% in dry and wet climatic areas respectively. From this, it is inferred that most of the materials tested are G10 or worse quality soils (minimum soaked CBR of 3%). The largest portion of the remaining DCP CBR's categorise the soils as G9 material, with only a few soils of G7 and G8 quality. These estimated material classes are lower than those presented in Section 4.6. This could be due to the in-situ density being lower than that used in the TRH14 classification presented in Section 4.6.

### Witzand Formation

Ninety-nine DCP's were carried out in soils from the Witzand Formation. The soils are often loose and medium dense (and borderline dense) in the upper 2m of the soil profile (DN > 12mm/blow). At shallow depth (<1m), mostly thin horizons of very dense sand or cemented deposits were associated with slow penetration or refusal at some test positions. It is the DCP CBR values associated with these very dense/cemented layers that largely separates the spread of DCP CBR values in the 0-1m and 1-2m depth intervals, signifying the higher incidence of soils with very dense consistencies in the upper 1m of the soil profile. Perched water tables were intersected at about half of the DCP test positions in this formation at an average depth of 1.3m. As for the Springfontyn Formation soils, the majority of DCP CBR values are less than 24%, signifying the high proportion of G10 quality soils.

For the upper 1m of the soil profile, the results for the Witzand and Springfontyn Formations are similar, although there are more dense and very dense soils present in this upper zone in the Witzand Formation. Below this depth, the consistency and strength of the sands from the Springfontyn Formation were found to exceed that of the Witzand Formation.

### Langebaan Formation

In the Langebaan Formation, refusal of the DCP cone often occurred within the upper metre of the soil profile, presumably on calcretised sand. An average DCP CBR of 37% reflects the presence of these cemented layers and/or lenses. The middle 50% of the data ranges from 12% to 42%. A few DCP's extended beyond 1m depth in this formation, with no dense or impenetrable layers. The water table was not intersected at any of the DCP test positions in this formation. Approximately 25% of the data points are associated with G8 or better-quality soils, with the remainder indicative of soils of G9 and G10 quality.

### Factors influencing DCP CBR values

There are many factors influencing DCP cone penetration rate, including material composition, density, moisture condition and rod friction. At greater depths, vertical confinement plays a role. The limited number of DCP tests over the large extent of the study area will only provide an indication of soil consistency and in-situ CBR in the area. The DCP CBR was determined at the in-situ moisture content and density conditions at the time testing, and design CBR values should be evaluated at the moisture content and density representative of service life conditions.

The influence of soil moisture on the penetration resistances (and derived DCP CBRs) is significant. Soil moisture affects the sliding friction between soil particles and apparent cohesion in a partially saturated soil. The soil moisture content will vary depending on the time of year, and so also the achieved resistances and soil strengths. An assessment of the influence of soil moisture on DN and CBR was carried out by the candidate to possibly improve estimates of DCP CBR in the study area. The results from all formations were combined and the DCP CBR values grouped based on the season of testing (dry, intermediate and wet categories). The findings do not conclusively illustrate the influence of moisture content on DCP CBR, and the potentially misleading results are therefore omitted. Bearing in mind the limited number of DCP tests (varying per seasonal category) and range of factors influencing DCP CBR, the outcome was foreseeable.

## 4.8 Minimum index density

The minimum dry density ( $\rho_{dmin}$ ) of windblown sands from six sites in the Cape Flats was determined by means of the funnel test method stipulated in ASTM designation 4254, Method A. The coordinates of the sampling localities are given in Table 3-1 in Chapter 3 (refer to the site names in the table below). The sands were all sampled from the upper 2m of the soil profile. A summary of the results is given in Table 4-8. The influencing factors of grain size, distribution of grain sizes ( $C_u$ ), and fines content are included in the table.

The maximum index density ( $\rho_{dmax}$ ) was not determined experimentally but  $e_{min}$  was estimated from existing correlations proposed by Cubrinovski and Ishihara (2002) which estimates the difference between the maximum and minimum void ratios based on the mean grain size ( $D_{50}$ ).

**Table 4-8: Minimum index density test results for Cape Flats sand**

Sampling Site (depth in m)	Formation	Minimum density ( $\rho_{dmin}$ ) $kg/m^3$	$e_{max}$ ( $G_s = 2.66$ )	$e_{min}$ (estimate)	Grading*	$C_u$	$e_{max} - e_{min}$
Mfuleni (0 – 2m)	Witzand	1422	0.87	0.52	FS = 99% CS = 1%	1.43	0.35
Blue Downs (0 – 0.8m)		1466	0.81	0.48	FS = 92% MS = 2% CS = 1% Silt = 5%	2.61	0.33
Mitchells Plain (0.9 – 1.3m)		1492	0.78	0.46	FS = 24% MS = 53% CS = 10% Gravel = 9% Silt = 1% Clay = 3%	4.74	0.32
Matroosfontein (0-1.5m)		1475	0.80	0.48	FS = 79% MS = 17% Fines = 4%	2.89	0.32
Gatesville (0.7 – 2m)	Springfontyn	1590	0.67	0.39	FS = 56% MS = 41% Clay = 3%	3.14	0.28
Bellville South (0.5 – 2m)		1431	0.86	0.52	FS = 92% MS = 4% Fines = 4%	1.80	0.34
Average (standard deviation)		1480 (60.4)	0.80 (0.07)	0.48 (0.05)	N/A	2.77 (1.17)	0.32 (0.02)

\*FS = Fine sand, MS = Medium sand, CS = Coarse sand, Fines = Clay + silt

The variation in  $e_{max}$  is greater than that observed by Neal (2011) for the Witzand Formation sands near Big Bay ( $0.798 < e_{max} < 0.808$ ), which is expected when considering the greater geographical extent of sampling during the current research.

Comparison of  $e_{min}$ , estimated from  $e_{max}$  from existing correlations proposed by Cubrinovski and Ishihara (2002) and  $e_{min}$  obtained by the modified AASHTO compaction tests (Section 4.5), was attempted. No MDD data are available for the six samples for which the minimum index density was determined experimentally. For this reason, a general comparison between the estimated  $e_{min}$  values to the range of laboratory obtained  $e_{min}$  values was made. From the modified AASHTO compaction data,  $e_{min}$  values for Cape Flats sands (only Witzand and Springfontyn Formations) were found to mostly range between 0.37 and 0.73. Estimated  $e_{min}$  values range from 0.39 to

0.52. The difference in the upper limit can be ascribed to the disparity in the number of  $e_{min}$  values from laboratory compaction and the estimated  $e_{min}$  values respectively, included in the assessment. Similar average  $e_{min}$  values were obtained.

The relative densities of sands sampled from the Gatesville and Mfuleni sites were calculated from the tabulated results and in-situ densities from nuclear density tests. The relative density of the shallow site soils at the Gatesville site is in the order of 33%. At Mfuleni,  $e_{in-situ}$  is less than  $e_{min}$ , resulting in a relative density greater than 100%. The outcome can either be ascribed to inaccuracies in the on-site determination of dry density, or possibly the cemented nature of the site soils (evident during profiling), increasing in-situ compactness. The relative density can provide an approximate indication of the compressibility, shear strength and permeability of the sands at specific locations in the Cape Flats.

The influence of the shape, size and distribution of the soil particles on the  $\rho_{dmin}$  values was considered. In this regard, an increase in  $C_u$  is typically associated with an increase in  $\rho_{dmin}$  (refer to Table 4-8). The influence of fines content on  $\rho_{dmin}$  could not be evaluated as the combined silt and clay contents in the studied soils vary between the narrow limits of 3% and 5%. It is anticipated that, for a given sandy soil, an increase in the soil fines content will be associated with an increase in  $\rho_{dmin}$  as void spaces are filled with the smaller sized grains. A CT scan image of disturbed sands from the Mfuleni site – obtained from a past study by Sitela (2018) - is shown in Figure 4-20, illustrating the grain shapes associated with the predominant quartz sands (lesser feldspars). The scanned specimen was prepared by recompacting disturbed sands to a dry density of  $1500\text{kg/m}^3$  and extracting a small sample with a thin pipe. It is believed that significant disturbance occurred after re-compaction, destroying aspects such as pore size and distribution, particle pattern and contact relation.

From the figure it is evident that most particles are sub-rounded to sub-angular in shape, with a fair proportion of angular grains. Micro shells are also present. The shapes observed in the image deviates somewhat from the typical grain shape descriptions for aeolian sands. Amdurer (1956), described the Cape Flats sands as rounded and sub-rounded in shape. Particle shape is a function of several factors, such as transportation distance, grain sizes and mineralogy, and variation in the study area is likely. Typically, for a given  $C_u$ ,  $\rho_{dmin}$  will decrease with increasing particle angularity. Higher values of  $\rho_{dmin}$  can be achieved for clean fine sands (such as the Mfuleni sands) with rounded and/or sub-rounded particle shapes, compared to the  $\rho_{dmin}$  value of  $1422\text{kg/m}^3$  given in Table 4-8.

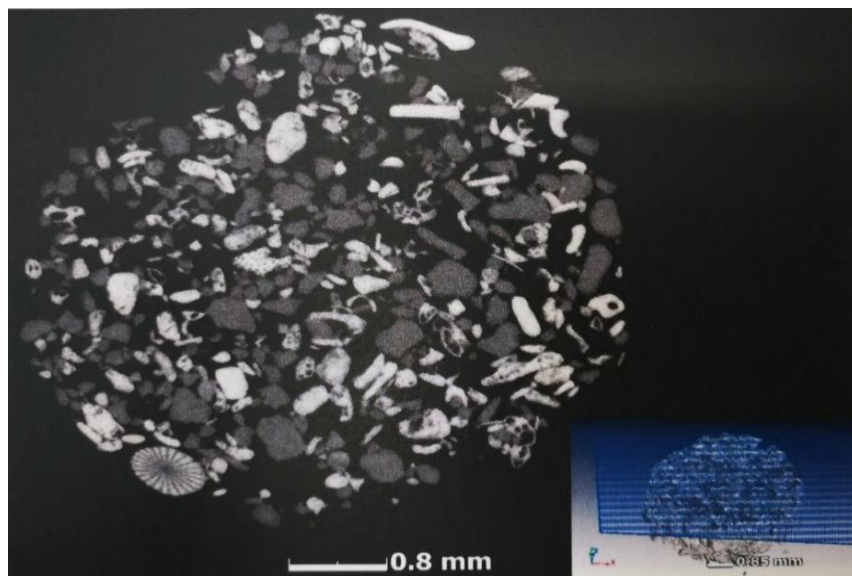


Figure 4-20: CT scan image of Mfuleni sand (Sitela, 2018)

## 4.9 Corrosivity

The corrosion risk posed by the sands and the groundwater on the Cape Flats to buried concrete and metal, was assessed by means of the following properties and indices: pH and resistivity, the Langelier saturation index, the aggressiveness index and the leaching-corrosion and spalling-corrosion sub-indices (Basson, 1989), as well as the aggressiveness chemical environment for concrete class (BRE, 2005a). All soils were collected from the upper 3m of the soil profile. The distribution of sites with corrosion risk information is shown in Figure C6 in Appendix C, with the corrosion assessment method (property, index or class) associated with each site indicated.

### 4.9.1 Corrosion influencing factors

pH and electrical conductivity (or resistivity) of soils and groundwater can provide a preliminary estimate of corrosion potential and rates in the study area. Special conditions such as excessive salts from seawater can increase corrosion rates, whereas corrosion rates will be slowed below the water table where free oxygen forming oxides is reduced (or absent) due to stagnant (or low flow velocity) water conditions.

#### 4.9.1.1 pH

The pH values of 85 soil samples and 16 groundwater samples from the study area were included in the assessment of the acidity/alkalinity of the Cape Flats subsurface environment and ultimately corrosion susceptibility. Soil pH was determined electrometrically by means of the KCL method (potassium chloride solution) and the pH of bottled groundwater by means of a pH meter (refer to Table 3-3 from Chapter 3). The distribution of acidity classes (USDA, 1998), in the Witzand, Springfontyn and Langebaan Formation sands, and in groundwater specimens is shown in Figures 4-21a and 4-21b (Where: Str = Strongly, Mod = Moderately, and Sl = Slightly).

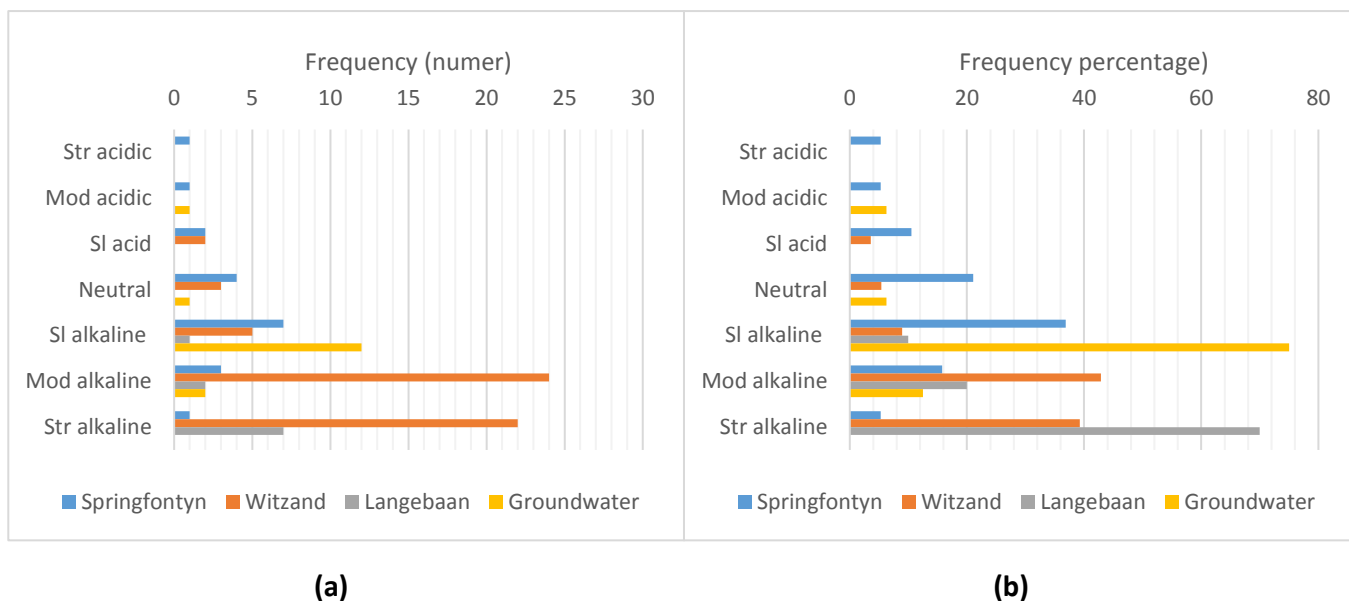


**Figure 4-21: Distribution of acidity classes in the Cape Flats in terms of a) number and b) percentage**

Because cementitious binders in concrete are soluble in acidic solutions, low pH values (below five) pose a corrosion risk to concrete. Alkaline solutions indicate non-corrosive environments or even protection from corrosion. Steel has higher corrosion rates in soils or solutions that are either highly acidic (pH less than 4.5) or alkaline with pH values between 8 and 10.5 (Clayton, 2013). In the Witzand Formation, most of the sampled soils (approximately 82%) are either moderately or strongly alkaline ( $7.9 < \text{pH} < 9.0$ ). The remainder of the soils from this formation is neutral or slightly alkaline ( $6.6 < \text{pH} < 7.8$ ), with only two slightly acidic soils ( $6.1 < \text{pH} < 6.5$ ). Soil pH may therefore be a dominant factor in the corrosion of buried steel in the moderately and strongly alkaline soils. The presence of calcium carbonate in the often-calcareous sands from this formation will contribute to the high level of alkalinity.

In the Springfontyn Formation, the soils typically display lower pH values compared to the Witzand Formation. Approximately 20% of the sampled soils are moderately and strongly alkaline, and potentially corrosive to steel components. These soils will pose no risk to buried concrete, and the elevated magnesium and calcium in the alkaline soils may provide corrosion protection. The lower pH values observed in this formation can probably be attributed to a lower calcium carbonate content and possibly the presence of peat, which is acidic in nature. The pH values associated with the moderately and strongly acidic soils ( $5.1 < \text{pH} < 6$ ) does not exceed the critical lower pH limits of 4.5 and 5 for corrosion of steel and concrete respectively, and soil pH will therefore not be a controlling factor in corrosion in these soils. The solutes responsible for the high level of acidity is unknown and may be, amongst others, from acidic salts or humic acid.

All soils collected from the Langebaan Formation are alkaline; ninety percent of the soils being moderately and strongly alkaline, thus presenting a corrosion risk to buried steel. As for the Witzand Formation soils, it is likely that the calcareous nature of the deposits from this formation is responsible for the raised alkalinity.

ANOVA statistical testing confirmed variances in pH between formations. Mean pH values of 7.2 in the Springfontyn Formation, 8.2 in the Witzand Formation and 8.6 in the Langebaan Formation, were obtained. Significant variation in the means of the pH data sets from the Witzand and Springfontyn Formations and the Springfontyn and Langebaan Formations was noted ( $P$  two-tail =  $3.7 \times 10^{-6}$  and  $1.8 \times 10^{-4}$  respectively). Analysis shows that the data sets from the Witzand and Langebaan Formations are relatively similar, both influenced by the presence of calcium carbonate.

It should be noted that all measured pH values are associated with a particular soil moisture content and temperature and will vary with these influences. Of the 16 groundwater samples collected from test pits in the study area, 14 originate from a single site in Strandfontein (Witzand Formation). Most of the pH values vary between 7 and 8 (slightly and moderately alkaline), and buried structures will not be susceptible to corrosion (based on pH alone) at the sampling sites.

#### 4.9.1.2 Resistivity

The ability of soil and groundwater from the Cape Flats to conduct electricity, referred to as electrical conductivity (EC), was determined by means of an EC meter (refer to Table 3-3) during past and current investigations, and evaluated to assign primary corrosivity ratings to the sampled soils and groundwater. The EC was determined for the same soil and groundwater samples for which the pH was determined. Conductivity is the reciprocal of resistivity, and all EC values were converted to resistivity (in ohm.cm) for classification. The resistivity based corrosivity classification table produced by Roberge (2008) is given in Section 2.5.7 of Chapter 2. Frequency bar charts showing the distribution of corrosivity ratings for the Witzand, Springfontyn and Langebaan Formation sands, and for groundwater specimens, are shown in Figures 4-22a and 4-22b (where Ext = extremely, Mod = moderately). The resistivities associated with the corrosivity ratings are included in the discussion of the results.

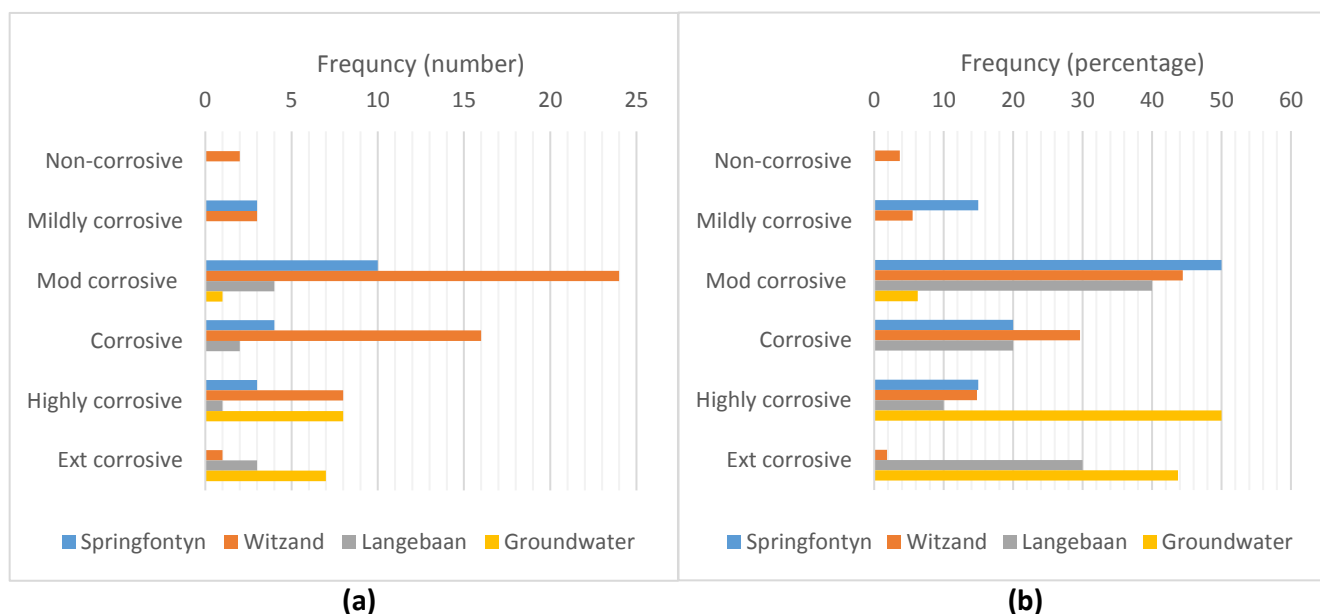


**Figure 4-22: Distribution of corrosivity ratings based on soil resistivity in the Cape Flats in terms of a) number and b) percentage**

Sandy soils typically have high electrical resistivity, indicating slowed corrosion reactions. It is the texture and water-holding capacity that distinguishes resistivity values between soil types. This was typically not reflected in the measured resistivities. In the Witzand Formation, approximately 45% of the sampled soils have resistivity values between 5 000 and 10 000ohm.cm, thus categorised as moderately corrosive. An additional 45% of the soils are either corrosive (3 000 – 5 000ohm.cm) or highly corrosive (1 000 – 3 000ohm.cm) based on soil resistivity. Only one soil is categorised as extremely corrosive (<1000ohm.cm). The grading results reveal an association between clay content and corrosivity, with higher clay contents associated with lower resistivities. A few soils have resistivity values exceeding 10 000ohm.cm and are mildly or non-corrosive. The Springfontyn Formation sands are typically moderately to highly corrosive. No appreciable difference in resistivity was observed between the Springfontyn Formation sands - typically with a higher fines content - and the Witzand Formation sands. Notwithstanding this, similar soil textures were noted (from the grading results) for the sampled soils from these formations. Corrosion ratings in the sands from the Langebaan Formation range from moderately to extremely corrosive. ANOVA statistical testing was undertaken to quantify variances in resistivity between formations. No significant variation in the resistivity data sets was recorded ( $F < F_{crit}$ ).

The electrical resistivity of the groundwater in the study area mostly ranged between 800ohm.cm and 2300ohm.cm (extremely and highly corrosive), with only one groundwater sample categorised as moderately corrosive.

Soil resistivity is influenced by the soil moisture content, with an increase in soil moisture associated with lower resistivity. Soils from the study area were typically sampled above the groundwater table and are partially saturated throughout the year, spanning approximately 20 years. The findings should therefore provide a general indication of soil resistivity in the Cape Flats. From the results it is evident that, based on resistivity alone, buried structural elements will be at risk of corrosion at many of the investigated sites. Notwithstanding this, the aggressiveness of the soil and groundwater should be evaluated in combination with all other influencing factors (including pH) to determine a more precise corrosion risk. Relationships between soil resistivity, pH and underground corrosion rate (steel loss) have been proposed by various researchers. However, usefulness of these relationships is limited as consideration of other influencing factors is necessary to accurately predict underground steel loss. When considering both pH and resistivity, a better indication of corrosion potential can be obtained (than considering resistivity alone). In this regard, approximately 30% of the soils have both pH and resistivity values in high corrosion risk categories (e.g.  $pH > 8.0$  and  $resistivity < 5000ohm.cm$ ).

#### **4.9.2 Corrosion indices and classes**

The Langelier saturation index (for metals) and the aggressiveness index (N), leaching-corrosion and spalling-corrosion sub-indices (LCSI and SCSi) (for concrete) were determined for two groundwater specimens sampled from the Cape Flats as described in Section 3.5.5 of Chapter 3. The results are presented in Table 4-9. The aggressive chemical environment for concrete (ACEC) classes obtained for 17 soil and groundwater specimens are discussed below the table.

**Table 4-9: Corrosion indices for metal and concrete**

Index	Langelier index		N, LCSI, SCSI	
Material	Steel		Concrete	
Sample	Sample 1	Sample 2	Sample 1	Sample 2
Sample type	Groundwater			
Location (Formation)	Mfuleni (Witzand)	Macassar (Langebaan)	Mfuleni (Witzand)	Macassar (Langebaan)
Properties for calculation	pH and calcium carbonate-saturated pH (pH <sub>s</sub> )		pH, pH <sub>s</sub> , calcium hardness, NH <sub>4</sub> , Mg, SO <sub>4</sub> , Cl and TDS	
Index value	0.89	-1.94	N = -2649 LCSI = -897 SCSI = 14.3	N = 6503 LCSI = 2163 SCSI = 5.0
Description	Non-aggressive	Aggressive	Non-aggressive	Very highly aggressive
Comments	Non-etching and non-scaling (or slightly protected from corrosion)	Undersaturated with calcium carbonate	No risk to concrete structures	Leaching is dominant mode of attack. Requires anti-corrosive measures
Recommendations	None	Refer to SANS 10064:2011 for coating of steel surfaces	Use concrete class required for structural design	Concrete class 3 or 4 (min. cement content of 420kg/m <sup>3</sup> and a min. cement to water ratio of 2.2. Coating type B, D or E which includes - but not limited to- polyethylene, vinyls and epoxy tars of varying min. thicknesses.

The calculated N, LCSI and SCSI indices are applicable to standard temperature conditions (20°C) and laminar flow conditions. In addition to the N, LCSI, and SCSI indices, Basson (1989) proposed a chloride corrosion sub-index. The presence of chloride ions in ground and groundwater (with oxygen and moisture also present) presents a significant corrosion risk to buried metal and reinforcement in concrete. Chloride ions are present in seawater, and its presence in the marine and aeolian Cape Flats sands and groundwater is expected. The chloride ion content of 16 groundwater specimens from the study area was determined, from which the chloride ion sub-index was calculated as described in Section 3.5.5 of Chapter 3. Fourteen of these samples originate from the site in Strandfontein referred to in Section 4.9.1.1, and the others form part of the groundwater collected from the two sites listed in Table 4-9. The index was used to identify the chloride corrosion risk in the sampled waters and to assess suitable countermeasures. The chloride ion content varies between 8mg/l and 190mg/l, and the chloride corrosion sub-index between 1.6 and 38. These values lie in the lowest risk category, requiring a minimum concrete cover (over reinforcement) of 25mm.

The aggressive chemical environment for concrete (ACEC) class encompasses the type of site (natural ground condition or brownfield), the sulfate concentration, and the acidity and mobility of the groundwater. Sulfates and acids are aggressive chemical agents, and the concentration of these agents and the rate they can be replaced at the concrete surface (dependent on the mobility of the groundwater), will determine the ACEC class. The aggressiveness of soils and groundwater

from the Mfuleni, Macassar and Strandfontein sites towards concrete, was assessed in terms of its ACEC class. The 17 sampling locations from the study area all received an AC-1 class designation, revealing non-aggressive soil and groundwater. The alkaline soils with low sulphate concentrations (below 80mg/l) present at the sites determined the outcome. The ACEC class is used to prescribe concrete quality in terms of a design chemical class. Design chemical class one (DC-1) is specified for the investigated sites for an intended working life of both > 50 and >100 years (BRE, 2005a). Concrete qualities to avoid chemical attack are given in BRE (2005a) for the allocated design class.

Although limited soil and groundwater chemical test results were available for the study area, the high percentage of moderately and strongly alkaline soils posing a risk to buried steel, the widespread presence of soils with low electrical resistivity aiding corrosion reactions, and the groundwater from the coastal area of Macassar posing a definitive corrosion risk to buried steel and concrete, proves that deterioration of buried structures via electrochemical processes will occur in certain areas of the Cape Flats. The assessment of the aggressive chemical environment through the ACEC class, revealed non-aggressive soils at all locations, including the Macassar site. The contradicting outcomes can be ascribed to the limitations of the ACEC class method, which restricts its assessment to the presence of sulfates and acids at natural ground locations.

The groundwater study conducted by Geohydrological and Spatial Solutions International (Pty) Ltd (GEOSS) at the Cape Town International Airport in 2014, revealed substantially higher concentrations of chloride ions and total sulfate compared to the remainder of the study, as well as resistivities below 1000ohm.cm (extremely corrosive waters). The higher sulfate concentration at the site produces a higher design sulfate class, which is associated with ACEC class designation AC-2. An increased risk of chemical attack is thus indicated in these soils. The chloride corrosion sub-index was calculated from the chloride ion content (2200mg/l), with the resulting index value of 440 illustrating the chloride corrosion risk, recommending a minimum concrete cover of 35mm. The aggressiveness of the ground and groundwater in the study area will vary widely, based on factors such as contamination, evaporation rates and the depositional history.

## **4.10 Erodibility**

The erodibility of the Cape Flats sands was evaluated in terms of its dominant erosion index (erosion hazard potential based on the Revised Universal Soil Loss Equation, RUSLE), the erodibility K-factor, and its performance as wearing course gravel. The outcomes of the assessments are presented below.

### **4.10.1 Erosion hazard potential**

The erosion hazard potential maps produced for ten sediment yield regions in South Africa by the Water Research Commission in 2010 (as described in Section 2.5.8 of Chapter 2), identifies erosion hazard classes from rainfall erosivity, soil erodibility, topography and land cover, and groups them in terms of an index scale, describing the water erosion risk. The map containing the Cape Flats area, known as Region 8 of 10, was used to establish the erosion hazard and to predict sediment yield in the study area. The relevant map is shown as Figure 4-23. The approximate boundaries of the study area are shown in red. The individual catchment boundaries (black area outlines) are also indicated.

From Figure 4-23 it is evident that erosion index (EI) 1 covers most of the Cape Flats study area. Portions of four catchments are present in the study area. The portions of three catchments occurring within the boundaries of the Cape Flats are uniform in terms of its erosion index (EI = 1), and only a small portion of the remaining catchment has a higher erosion index value (EI = 2). The total area of the Cape Flats is approximately 460km<sup>2</sup>; of which about 439km<sup>2</sup> has an erosion index equal to 1. Only the north eastern corner of the study area, representing 21km<sup>2</sup>, received an erosion index value of 2. The dominant erosion index for the Cape Flats, representing approximately 95% of the area, is therefore erosion index 1, representing a very low erosion hazard with minimal expected soil loss. A significant factor in this outcome is the soil erodibility, which is dependent upon soil texture, organic matter content, shearing resistance, infiltration and permeability. Soil erodibility, represented by the soil erodibility K-factor, is discussed in Section 4.10.2.

#### **4.10.2 Soil erodibility factor**

The soil erodibility factor (the K-factor), which provides an indication of the susceptibility of soil grains to detach and be transported by rainfall and runoff, was estimated for the Cape Flats sands using the soil erodibility nomograph proposed by Wischmeier and Smith (1978). The nomograph, which is based on soil texture, structure, organic matter content and permeability, is shown in Figure 3-23 in Chapter 3. As discussed in Section 3.5.6 of Chapter 3, ten soils with a range of textures - collected from the Witzand, Springfontyn and Langebaan Formations - were selected for evaluation of their erodibility. In this way, the probable limits within which the K-factor is likely to vary, will emerge. The range of soils included was limited to sandy soils for which the permeability is known or could be inferred from test results on similar soils from the study area (excluding clayey or calcretised soils), and to soils without organic matter (based on profile descriptions). The results are shown in Table 4-10 and the sampling locations in Figure C7 in Appendix C.

Structure code 1 for very fine granular soils (particle sizes <1mm) applies to all the investigated soils from the study area, and permeability class 1 for sandy soils (rapid flow) applies to all soils included in the current erodibility assessment. Permeability was estimated from both on-site permeameter readings and laboratory measurements for specimens compacted at densities ranging between 1540kg/m<sup>3</sup> and 1727kg/m<sup>3</sup>. Guiding values from Wischmeier and Smith (1963) were subsequently used to determine the permeability class. The soil organic matter content was zero throughout. For this reason, the K-values for the Cape Flats sands were separated only by soil texture. The K-factor varies from 0.01 to 0.31 (very low to moderate erodibility), with an increase in the K-value (and thus the soil erodibility) associated with higher silt and very fine sand percentages. The particles in this size range are more susceptible to detachment (less energy required to lift the smaller grains). A wide range of soil textures was selected, illustrating the probable outer limits of K-values in the sandy Cape Flats soils (with permeability class 1 and no organic matter). Notwithstanding this, low silt and fine sand contents (0.002mm to 0.1mm particle sizes) below 20% is the norm in the study area, and the K-factor will typically not exceed 0.1, comparing well with the erosion index (EI) from Section 4.10.1. The Cape Flats sands are mostly dominated by grain sizes in the 0.1mm to 0.425mm range.

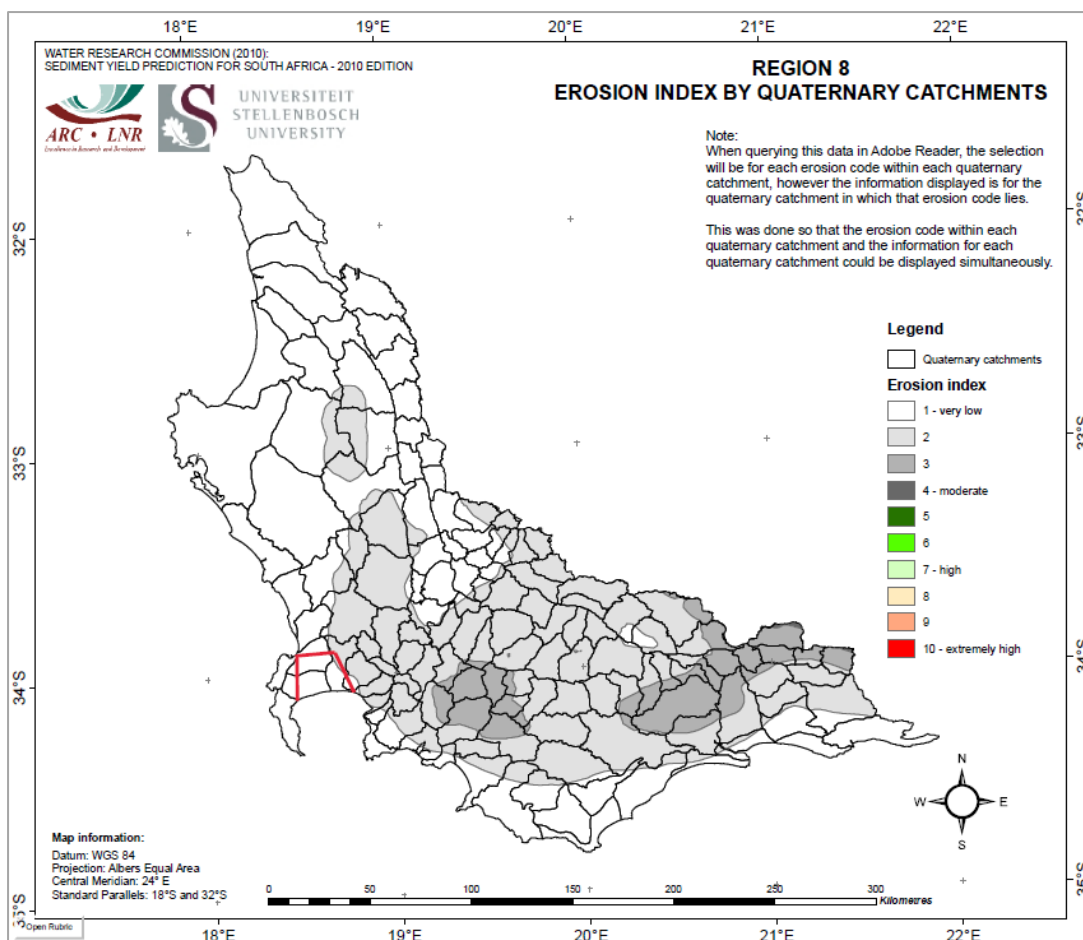


Figure 4-23: Erosion hazard potential map for Region 8, including the Cape Flats (WRC, 2010)

Table 4-10: Erodibility results based on the soil nomograph method

Sample code (sample depth, m)	Formation	Silt and very fine sand (0.002 – 0.1mm) (%)	Sand (0.1-2.0mm) (%)	Organic matter content (%)	Soil structure code*	Permeability class**	K-factor
Co54TP18 (1.8-2.4)	Witzand	23	61	0	1	1	0.08
SM2TP7 (0.5-1.8)		10	84				0.02
Co7TP2 (1.0-1.4)		2	96				0.01
CGBH2 (2.0-2.25)		48	49				0.31
Co11TP3 (0.3-0.9)	Springfontyn	14	83				0.02
Co33TP2 (1.0-1.3)		9	88				0.015
Co64TP2 (1.95)		33	46				0.13
A1TP4 (2.2-2.8)		22	69				0.08
KT13BH10 (2.0-2.45)	Langebaan	37	60				0.24
KT13TP4 (0.8-2.4)		17	80				0.05

\*1=Very fine granular (Predominant particle size <1mm)

\*\*1=Rapid in sandy soils

The K-factor is directly proportional to water erosion in the study area and represents the rate of erosion (A) (in t/ha/year) per erosion index (EI) unit from a standard plot (221.3m long, 9% length-wise slope). The typically very low estimated erosion rates for the Cape Flats sands can largely be attributed to the low silt and very fine sand content - representing particles vulnerable to detachment - and the high permeability resulting in rapid infiltration and less runoff. A decrease in soil permeability in the calcretised sands from the Langebaan and Witzand Formations, will be associated with an increase in soil erodibility. In this regard, a K-value of approximately 0.35 is expected for soils with moderate to slow flow rates (with the maximum silt and very fine sand content of 48). The presence of organic matter will bind particles and lower the erodibility. An increase in the mineral clay content will decrease soil permeability, but in contrast, will increase cohesion and impede the detachment of particles.

An additional factor which will influence soil erodibility, is particle shape. This characteristic is often neglected in the evaluation of the erodibility of cohesionless soils, but has been found to have a pronounced influence on grain detachment (Guo, Yang and Yu, 2017). Particles with angular shapes will provide better interlocking (compared to rounded grains) and will be more difficult to detach and transport (more energy required). The CT scan image of Cape Flats sands presented in Section 4.8, confirms the presence of sub-rounded, sub-angular and angular particle shapes at the specific location. The variation arises from the mineralogy, grain sizes present and the transportation distance. The degree of particle interlock, and its influence on the erodibility of the sands from the study area will vary, however, some resistance to detachment should mostly occur.

#### **4.10.3 Erosion of unpaved gravel wearing course**

The erodibility of the Cape Flats sands, when utilised as a wearing course in unpaved roads, was evaluated based on the classification system given in TRH20 (1990). To determine the likely performance of the sands as unpaved road material, the shrinkage product ( $S_p$ ) and grading coefficient ( $G_c$ ) were calculated for 333 soils as discussed in Section 3.5.2 of Chapter 3, and the  $S_p$ - $G_c$  data pairs plotted on the classification diagram shown in Figure 3-24. The linear shrinkage of most Cape Flats sands is zero, and so also the value of  $S_p$ . As a result, many of the data points plotted in the same region in the classification graph as shown in Figure 4-24. The results were therefore also presented in the form of frequency bar charts (see Figures 4-25a and 4-25b) (Where  $R_{av}$  = Ravels and  $corr$  = corrugates). The soils were mostly sampled from the upper 3m of the soil profile for index testing. The sampling localities are shown in Figure C7 in Appendix C.

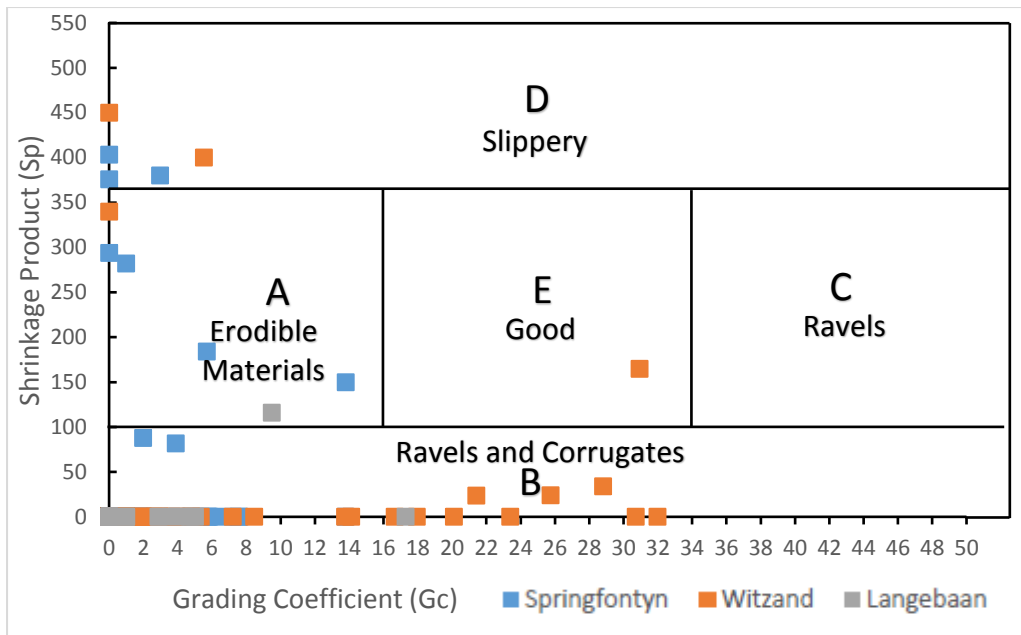


**Figure 4-24: Performance of Cape Flats sand as unpaved gravel wearing course**

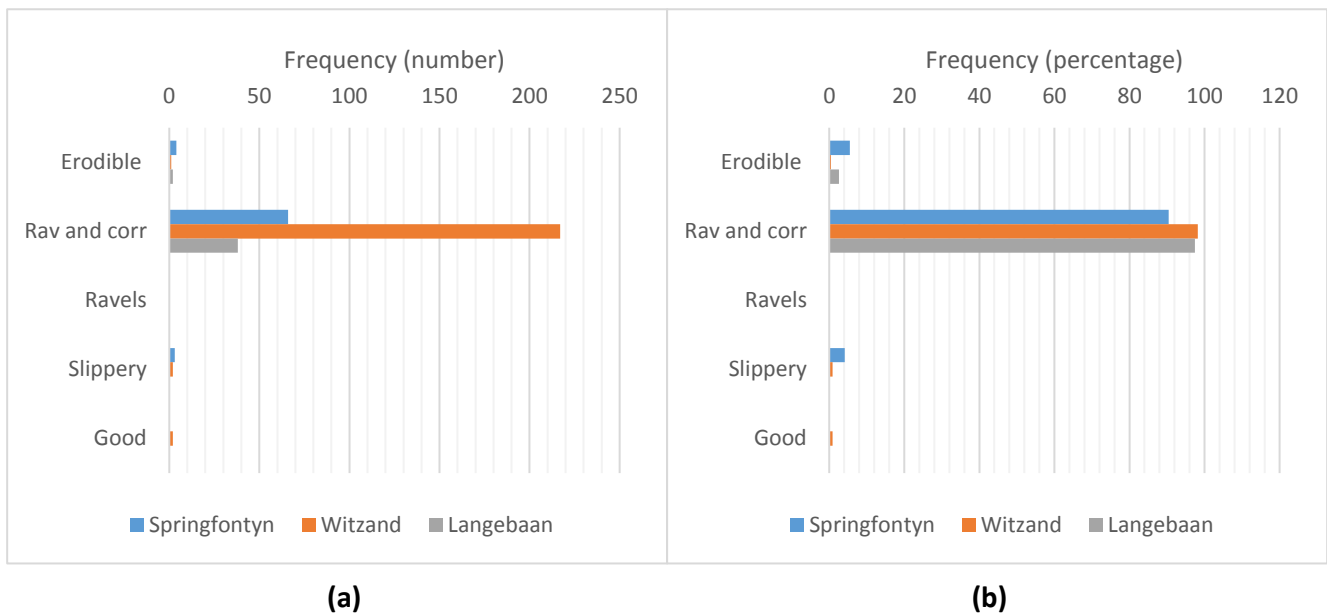


**Figure 4-25: Distribution of gravel wearing course performance in the Cape Flats in terms of a) number and b) percentage**

Unpaved roads using Cape Flats sand as a wearing course will be prone to corrugation, i.e. the formation of loose or fixed parallel crests and troughs, and ravelling, i.e. the generation of loose particles under traffic. It is the high sand content, with uniform gradation, and the general lack of fines and cohesion in the Cape Flats soils, that increases the susceptibility to these performance issues. Increased soil moisture during the wet months of the year will provide apparent cohesion, lessening material losses. Approximately 6% and 3% of the soils from the Springfontyn and Langebaan Formations respectively, were found to be prone to erosion by surface water flow. The grading results show that these are mainly fine-grained soils, containing between 21% and 37% clay and silt sized particles with minimal or no coarse fraction. An increase in cohesion and

plasticity will be associated with decreased erosion rates. The shrinkage product of these soils exceeds 100. The higher proportions of erodible soils in the Springfontyn Formation (compared to the other formations) agree with the known soil textures. The few slippery soils identified in the study area are soils with plastic fines and  $Sp > 365$ . Soils with considerable fines contents (with  $Sp > 100$ ), were only identified below depths of 0.5m in the study area.

Even though the Cape Flats sands aren't predominantly erodible, the sands will typically prove inadequate as an unpaved gravel wearing course by forming corrugates, and ravelling. Most sands have uniform gradations (in the fine and medium sand range), lacking plastic fines and cohesion. The sand particles are more susceptible to loosening and kick-back. Various safety concerns are associated with these soil types. The CBR and grading modulus values of the Cape Flats sands are typically too low for use as a wearing course gravel, and the addition of soil fines and/or compaction at appropriate moisture conditions are unlikely to result in satisfactory performance of the material.

#### 4.11 Specific gravity

The specific gravity ( $G_s$ ) of sands sampled from six sites in the study area was determined by means of a water pycnometer in accordance with ASTM test designation D 854-02 (refer to Section 3.3.2.2 from Chapter 3). The specific gravity of an additional 15 soils (from five sites), determined during previous investigations, completed the data set for interpretation. The sampling localities are shown in Figure C8 in Appendix C.

Because of the few  $G_s$  values available for interpretation, no differentiation based on soil formation was made. The findings are summarised as follows:

- The specific gravity of soils with predominantly sand-size grains (minor fines content <10%) ranges between 2.62 and 2.69 (average  $G_s = 2.65$ ). The range of values obtained for seemingly similar soil textures can be ascribed to the mineralogical makeup of these soils. The accompanying soil profiles did not provide explanations for the atypical upper and lower bound values (e.g. organic matter or pedogenic materials).
- The specific gravity of each soil represents the average specific gravity of the combined soil particles in the sample, reflecting the proportions of grains with different densities ( $\rho_s$ ). In this regard, it is anticipated that the Cape Flats sands contain varying combinations of minerals such as quartz, feldspar, kaolinite and illite, each with a characteristic particle density. The likely presence of potassium feldspar (with  $G_s = 2.57$ ) and/or sodium and calcium feldspar (with  $2.62 < G_s < 2.76$ ) (Das and Sobhan, 2018) in the sand and silt size fractions, may be responsible for the range of  $G_s$  values (refer to the 1<sup>st</sup> bullet point).
- No association between clay content and  $G_s$  is evident. It should be noted that the clay content (of the investigated soils) varied between narrow limits of zero and 6%, which is unlikely to have a significant influence on the overall  $G_s$  value. The clay size fraction in Cape Flats soils comprise the clay minerals kaolinite and illite (refer to Section 4.4). Lower values of  $G_s$  will be associated with Cape Flats sands containing significant quantities of kaolinite (with a typical  $G_s = 2.6$ ); presumably present in a few soils investigated during the current research. An increase in the amount of illite clay will, in contrast, increase the value of  $G_s$ .

- The  $G_s$  of soils containing organic matter (percentage unknown) was found to vary between 2.4 and 2.64 (average  $G_s = 2.58$ ). These soils were described as silty fine and medium sands.

## 4.12 In-situ density and moisture content

Field measurements of density and moisture content were obtained from four sites in the study area by means of the nuclear density gauge, as described in Section 3.3.2.1. All tests were conducted in the upper metre of the soil profile. Laboratory moisture content tests were also undertaken on 133 samples collected from test pits across the Cape Flats. The samples were collected from the upper 3m of the soil profile in the Witzand and Springfontyn Formations, and from the upper 2m in the Langebaan Formation. All sampling and testing sites are shown in Figure C9 in Appendix C.

### 4.12.1 Field measurements

In the upper metre of the soil profile, bulk density varies between  $1624\text{kg/m}^3$  and  $1951\text{kg/m}^3$  at the investigated sites. The in-situ moisture contents at the test sites ranged from 2.4% to 6.3% and were mostly confirmed by laboratory moisture content determinations. The calculated dry densities, varying between  $1571\text{kg/m}^3$  and  $1844\text{kg/m}^3$ , represent the characteristic loose, shallow sands, and the dense cemented sands regularly occurring close to the soil surface in the Witzand and Langebaan Formations. These dry densities are associated with void ratios in the order of 0.41 to 0.7 ( $G_s = 2.66$ ). Loose sands were identified below upper cemented soils, agreeing with the DCP test results, in which high penetration resistances were often noted at shallow depth, followed by lower resistances deeper down. An overall trend of increasing density with depth is anticipated as the soils consolidate. An increase in bulk density will also occur as the natural moisture content increases to the groundwater table. Soils with organic matter were mostly noted in the profile descriptions of Springfontyn Formation deposits, however, similar descriptions were also noted for some Witzand Formation sands. The low specific gravity of organic matter will result in lower densities in these soils (with no change in void ratio necessarily).

The obtained in-situ void ratios were used, together with  $e_{\min}$  and  $e_{\max}$  values, to determine the relative density of the site soils (refer to Section 4.8). The attained densities (and void ratios) were also used to estimate the permeability and collapse potential of the Cape Flats sands from existing transformation models (refer to Sections 4.13 and 4.14).

### 4.12.2 Laboratory moisture content test results

The results associated with the laboratory determination of soil moisture content are summarised in Table 4-11. The results are separated per formation and into 1m depth intervals. A limited number of moisture content values was available for the 2m to 3m depth range, which can be ascribed to the typically shallow water tables and test pit depths (often limited by collapse of the pit sidewalls). Most samples were collected above the water table. In-situ moisture content ( $w_n$ ) is dependent on factors such as grain size, density, organic matter content, soil structure, and impermeable/low permeability layers and topography which influences the water table level, and consequently the soil moisture content. A significant degree of spatial variation in soil moisture content will therefore occur. In addition, the level of the groundwater table (and thus the soil moisture content) will vary at any given location with seasonal changes. The summarised results should therefore be viewed in this context.

**Table 4-11: Summarised natural moisture content results**

In-situ moisture content, $w_n$ (%)						
Depth range (m)	Maximum	Minimum	25 <sup>th</sup> /75 <sup>th</sup> percentile	Average	Standard deviation	Number of values*
<b>Springfontyn Formation</b>						
0 - 1	17.1	0.5	6.7/15.3	11.0	5.5	20
1 - 2	20.0	1.0	12.0/15.5	13.0	4.5	27
2 - 3	21.3	1.2	13.6/18.5	15.1	5.4	11
<b>Witzand Formation</b>						
0 - 1	27.5	0.5	3.0/11.6	7.6	6.2	54
1 - 2	32.8	0.5	4.3/13.0	8.9	6.6	49
2 - 3	32.8	1.5	5.1/13.8	10.3	9.6	9
<b>Langebaan Formation</b>						
0 - 1	14.1	1.4	2.7/6.8	5.5	4.1	8
1 - 2	15.7	2.2	4.2/6.9	6.9	4.7	6
2 - 3	N/A					1 ( $w_n = 6.4$ )

\* Where a soil specimen (for testing) was taken from a bulk sample collected over a depth range spanning two depth intervals (say 0.5m to 1.5m depth), the moisture content values were included in both intervals (where the soil is uniform, i.e. unchanging moisture content description). The number of data values shown in the table are therefore more than the number of tests performed.

#### Springfontyn Formation

In this formation, an increase in the average natural moisture content from 11% in the upper metre of the soil profile, to about 15% between 2m and 3m depth, was documented for the investigated soils. The same trend is noted in the 25<sup>th</sup> and 75<sup>th</sup> percentile values. Notwithstanding this, significant scatter about a linear trendline was noted when plotting moisture content against depth ( $R^2 = 0.21$ ). The minimum values of moisture content ranging from 0.5% to 1.2% for the investigated depth intervals, reveals virtually dry to slightly moist sands. The maximum in-situ moisture content of 21.3% was attained for sands near the water table. Four samples were collected below the water table, with moisture contents ranging between 15.8% and 19.9%. The groundwater table was intersected at about 56% of the sampling locations at an average depth of 1.9m. This depth is comparable with the average water table depth of 1.63m recorded at the DCP test positions (refer to Section 4.7.2). The average in-situ moisture content in all three depth intervals exceeds corresponding values in the other formations. The higher moisture contents in this formation is possibly the result of grain size (higher fines content), organic matter content and impermeable clay layers. Notwithstanding this, in-situ moisture content is influenced by various factors, only some of which may be responsible for intra-formation variation. This aspect, together with the limited number of samples collected for moisture content determination in relation to the size of the study area, introduces some uncertainty with regards to the observed variation between formations.

### Witzand Formation

The average in-situ moisture content in the investigated depth intervals of the Witzand Formation varies from 7.6% to 10.3% (increasing with depth). The interquartile ranges also display a notable upwards shift with depth. The limited number of data values in the 2m to 3m depth range (compared to the upper 2m metres), may have affected the representativeness of the summary values in this lowest depth interval. Once again, a weak linear relationship between moisture content and depth ( $R^2 = 0.1$ ) is illustrative of the many influences on in-situ moisture content. Four soil samples were collected below the water table, their moisture contents varying between 20.8% and 35.4%. The dry density corresponding to the moisture content at saturation of 35.4% is  $1371\text{kg/m}^3$  ( $G_s = 2.66$ ), which is lower than all the obtained minimum index densities and therefore likely a disturbed sample. This moisture content value was excluded from the analysis. The higher saturated moisture contents in the Witzand Formation (compared to the Springfontein Formation) can probably be ascribed to the soil density (void ratio) at the specific locations. The groundwater table level was only recorded (or intersected) at approximately 28% of the sampling locations. At some positions, the water table level was not documented (rather than absent), and the calculated average water table depth of 1.7m may thus be unreliable in representing the investigated sites.

### Langebaan Formation

The in-situ moisture content in the soils sampled from the Langebaan Formation range between 1.4% and 14% in the upper metre and between 2.2% and 15.7% between 1m and 2m depth. These ranges, and the attained average in-situ moisture contents, are affected by the limited number of data values for the soils from this formation. The lower moisture contents associated with the shallow sands of the Langebaan Formation (compared to the Witzand and Springfontyn Formations) can possibly be ascribed to the depth to groundwater. In this regard, the groundwater table was only intersected in one test pit at a depth of 1.3m. No samples were collected below the water table.

### Variation with depth

It is uncertain how much of the variation in in-situ moisture content between the formations is due to soil properties characteristic of each formation and, as such, the data for the formations was combined, and a statistical summary of the data presented in the form of box and whiskers plots, as shown in Figure 4-26. Because of the few moisture content values obtained for the 2m to 3m depth range, only data from the upper 2m was analysed.

There is a slight increase in soil moisture with depth, however, it is unlikely to have a significant influence on aspects such as grain sliding friction, soil suction and compressibility.

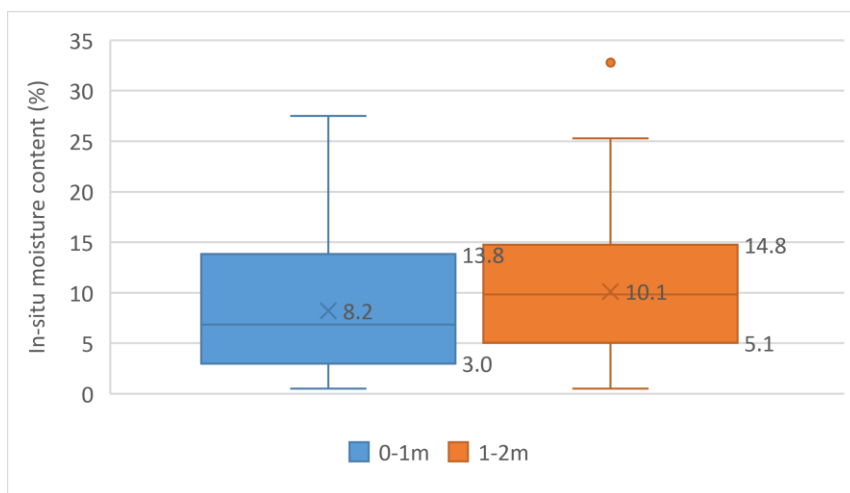


Figure 4-26: In-situ moisture content summary for all formations

### 4.13 Collapse settlement

The collapse potential of the Cape Flats sands was evaluated using the predictive methods by Brink (1985) and Prikloniski (1952) (refer to Howayek et al., 2011) based on dry density, and natural moisture content and soil plasticity properties respectively, and by means of collapse potential tests. All sampling and testing locations are shown in Figure C10 in Appendix C, including four in-situ density test sites, four sites from which undisturbed block samples were collected for oedometer testing, and seven sites at which plastic soils were sampled for index testing. The sites where potentially collapsible soils were identified, are shown in red.

#### 4.13.1 Empirical methods

Soils with dry densities below  $1672\text{kg/m}^3$  (the critical value proposed by Brink (1985) to distinguish potentially collapsible soils from non-collapsible soils), were identified at three of the four sites where nuclear density tests were performed. All in-situ density tests were performed in the upper metre of the soil profile. The soils with low dry densities occur both at the soil surface and at the maximum test depth of 0.8m to 1.0m. The dry densities range between  $1571\text{kg/m}^3$  and  $1664\text{kg/m}^3$ . According to the relationship proposed by Brink (refer to Equation 3-32 in Chapter 3) these densities correspond to collapse potentials between 0.5% and 4.6%. Soils described as “moderate trouble” in terms of collapse potential (1% - 5% collapse potential – see classification of severity classes in Section 3.5.7) were identified at two sites. The degree of saturation ( $S_r$ ) of the potentially collapsible soils varies between 13% and 25%, all well below the critical degree of saturation of about 50 to 60% for sands and silty sands above which collapse will not occur (Schwartz, 1985). The low-density soils from two of the three sites have no or negligible clay contents, and collapse settlement is unlikely in these soils. The limitations of this empirical method in ‘clean’ Cape Flats sands is thus evident. The presence of a chemical cementing agent may provide strength to these sands, which could be lost when inundated. Clay sized grains constitute approximately 7% of the low-density soil sampled from the third site. The formation of clay bridges between larger sands grains is thus possible. Very loose and loose soils with low dry densities are anticipated to cover large portions of the study area. Brink’s method, which relies solely on density, suggests that these soils will be collapsible. However, this method should not be used in isolation, but in combination with other properties such as grading and moisture

content. In this way, soils that are merely compressible can be distinguished from potentially collapsible soils.

The relation given by Prikloński (1952) (as cited in Howayek et al., 2011) was used to determine the liquidity index ( $K_D$ ) of 11 plastic soils sampled from seven sites in the study area, to provide an indication of the collapse potential of the soils. All soils sampled during previous investigations for which the plasticity properties and natural moisture contents are known, were included in the assessment. Most of these soils belong to the Springfontyn Formation.

The method is based on the field moisture condition relative to the plastic limit, and the plasticity index of the soil. The natural moisture contents ( $w_n$ ) of all sampled soils exceed the respective plastic limits (PL) resulting in values of  $K_D > 0$ . The soils are divided almost equally into the non-collapsible ( $K_D > 0.5$ ) and swelling soil ( $0 < K_D < 0.5$ ) categories. The plasticity index (relative to the moisture condition, i.e.  $W_n - PL$ ) determined the outcome. The plasticity indices of all soils varied between 3% and 10% (average of 7.3%) and the plastic limits between 9% and 27% (average of 15.7%). A reduction in the moisture content of these soils, which ranged from 13.7% to 21.3% above the water table, could ultimately reduce the value of  $K_D$  to below zero, marking the presence of highly collapsible soils. The soils below the water table will not be susceptible to collapse. Seasonal groundwater fluctuations must be considered. Soils deemed collapsible (using the Prikloński, 1952 criteria) at a certain point in time, may not be collapsible at other times.

Approximately 3.5% of all soils included in the current study (for which the index properties were determined) have measurable plasticity. Based simply on the possibility of the formation of colloidal bridging material between sand grains, this indicates the potential occurrence of some collapsible soils in the study area. The soils from the Springfontyn Formation contain, on average, more plastic fines compared to the other formations, and the development of a collapsible fabric is therefore more likely in these soils.

#### **4.13.2 Collapse potential tests**

This section considers the collapsibility of the Cape Flats sands as determined from 20 collapse potential tests in the oedometer. The  $e$ - $\log(p)$  curves associated with the tests undertaken during the investigative phase of the research are included in Appendix D. The limited number of collapse potential tests stems from the difficulty in obtaining undisturbed samples from these typically cohesionless soils. Some rearrangement of soil particles during the sampling and preparation procedures is however inevitable, which will have an effect on the test outcomes. The soils were all collected from the upper 3m of the soil profile (mostly the upper 1.5m) from Witzand and Springfontyn Formation deposits. The sampling methods used during previous investigations, and the orientation of samples in the oedometer cell relative to the likely preferred orientation of soil particles, is unknown.

The most recent collapse potential tests undertaken on Cape Flats sands at Stellenbosch University involved saturation of specimens in the oedometer apparatus at both 100kPa and 200kPa, as described in Section 3.3.2.2 of Chapter 3. Saturation at the non-standard pressure of 100kPa allows the collapse settlement associated with lower foundation pressures to be determined. All other collapse potential values from previous investigations are for soils saturated at 200kPa. The collapse potential test results are summarised in Table 4-12.

**Table 4-12: Summary of collapse potential test results on Cape Flats sands**

Collapse potential (%)					
Maximum	Minimum	Range	Average	Standard deviation	Number of tests
Saturation at 200kPa					
0.92	0.03	0.89	0.40	0.29	14
Saturation at 100kPa					
0.94	0.18	0.76	0.42	0.28	6

Based on the classification of the severity of collapse given by Schwartz (1985) (after Jennings, 1974), all soils were placed in the 'no problem' category ( $0\% < CP < 1\%$ ). From the void ratio-effective stress curves (see Figure 4-27), significant normal settlement occurred prior to saturation due to the reduction in void space in the absence of strong particle bonds providing apparent strength. Total soil settlement will include both the collapse settlement and the normal settlement. Note that only the results associated with saturation at 200kPa are shown in Figure 4-27. The raw data from some tests could not be obtained, and these results are therefore not included in the figure.

The natural moisture content of the sands varied from less than 1% to approximately 10% and the degree of saturation ( $S_r$ ) from 1.4% to 43%. For soils with similar initial void ratios, slightly higher collapse potentials were associated with lower in-situ moisture contents. The presence of soil moisture, giving rise to soil suction, enabled (largely) undisturbed sampling in the sandy soils. The initial dry densities of the sampled sands ranged from  $1245\text{kg/m}^3$  ( $e_0 = 1.13$ ) to  $1731\text{kg/m}^3$  ( $e_0 = 0.5$ ), with an average in-situ dry density of  $1433\text{kg/m}^3$ . Most of the initial dry densities are below the critical value of  $1672\text{kg/m}^3$  suggested by Brink (1985). The initial dry densities of a few soils sampled from a particular site (Mfuleni) are lower than corresponding values obtained from in-situ density testing at the same site. This could be due to variations in void ratio on the site or disturbance of the soils during the sampling. Colloidal bonds or bonds formed by chemical cementing agents, such as calcium carbonate, may also have been broken during the sampling process. The maximum fines content (silt and clay) in the investigated sands is 5%, and all soils are non-plastic. There are no hydrometer test results to differentiate between the clay and silt contents. It is suggested that weak bonds were formed by the soil fines (particularly the clay minerals) forming interparticle bonds, and thus providing some strength - that was lost during saturation. The results can also possibly be ascribed to other forms of bonding, including salts from precipitation (in the surficial soils) and  $\text{CaCO}_3$  or  $\text{Fe}_2\text{O}_3$ .

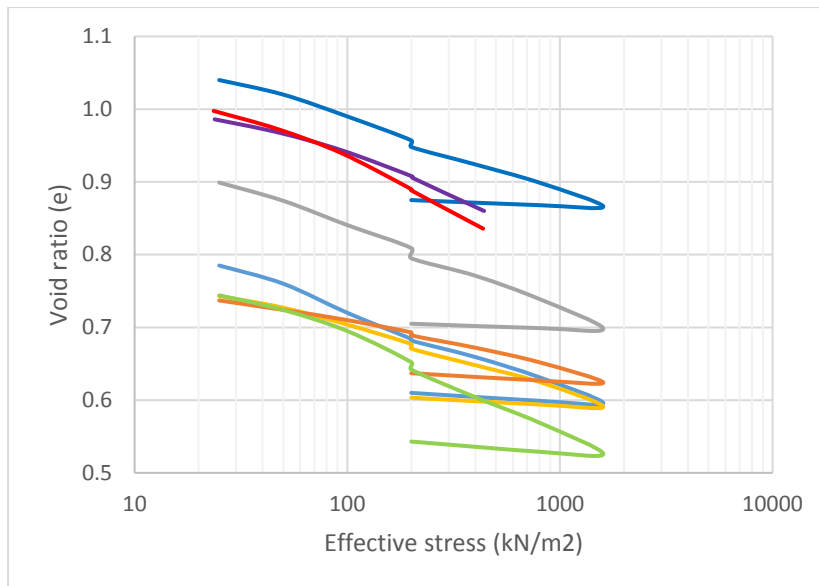


**Figure 4-27: Collapse potential test results for Cape Flats sands**

#### 4.13.3 Summary

The following conclusions are drawn from the results of the empirical methods and the laboratory tests:

- The low density, non-plastic sands included in the assessment of collapse potential are considered highly compressible (prior to saturation) and either non-collapsible or possessing a low collapse potential upon saturation.
- The presence of moderate amounts of plastic fines paired with low in-situ moisture contents increases the collapse potential. A high percentage of clay minerals filling void spaces will however decrease the susceptibility of the soil to collapse upon saturation.
- The collapse potential test results are considered representative of sands from the Witzand Formation. Exceptions include soils with plastic fines (which are uncommon) and soils with other bonding agents such as salts or calcium carbonates (particularly in the surficial soils).
- Disturbance of the sands during the sampling or preparation will break some or all of the interparticle bonds, resulting in inaccurate laboratory outcomes. On-site plate bearing tests are therefore considered superior in the identification of collapsible sands.
- The typically higher fines content of the sands from the Springfontyn Formation is likely to result in more soils with collapsible fabrics (from colloidal coatings), compared to the Witzand and Langebaan Formation sands.
- The calcareous soil horizons from the Langebaan Formation, with calcium carbonate as cementing agent, may be prone to collapse settlement.
- The criteria proposed by Brink (1985) is not valid in the predominantly clean sands of the Cape Flats.

#### 4.14 Hydraulic conductivity

The hydraulic conductivity of the Cape Flats sands was investigated from six constant head permeability tests, four CPTu pore water pressure dissipation tests and existing predictive methods by Carrier (2003) and Chapuis (2004) based on the grading and in-situ density of soils from four sites in the study area. Results were limited to sands from the Witzand and Springfontyn Formations and will be discussed alongside permeabilities obtained for the Langebaan Formation sands by Stapelberg (2009). The infiltration capacity of Witzand Formation deposits was also determined by means of six double ring infiltrometer tests undertaken at two sites. In some cases, more than one method was used to determine the hydraulic conductivity of soils sourced from the same location, allowing comparison of the experimental and empirical methods. All test and sampling sites are shown in Figure C11 in Appendix C.

As discussed in Section 3.5.8 of Chapter 3, CPTu dissipation tests were carried out on two sites. The results from one of the sites were excluded due to atypical dissipation readings thought to have been caused by problems during execution of the tests. The permeabilities obtained for the second site were three to four orders of magnitude smaller than the laboratory and empirically derived values for similar textures and densities. For this reason, all CPTu based permeabilities were discarded from further analysis and interpretation, as the outcomes were probably affected by procedural errors.

A summary of the hydraulic conductivity test results is given in Table 4-13. The sands were reconstituted by compacting specimens to predetermined densities. The alignment of elongated soil particles during compaction in the laboratory (to the predetermined densities) will create anisotropic behaviour (probably similar to the in-situ preferred orientation of grains). Vertical saturated permeability is given in Table 4-13.

**Table 4-13: Hydraulic conductivity test results**

Sampling Site (depth in m)	Formation	Constant head saturated k (m/s)	Laboratory dry density (kg/m <sup>3</sup> )	Estimated k from Chapuis (m/s)	Estimated k from Carrier (m/s)	In-situ dry density (kg/m <sup>3</sup> )	Grading*
Mfuleni (0 – 2m)	Witzand	$2.3 \times 10^{-5}$	1567	$2.6 \times 10^{-4}$	$2.5 \times 10^{-4}$	1829	FS = 99% CS = 1%
Blue Downs (0 – 0.8m)		$1.4 \times 10^{-5}$	1727	-	-	-	FS = 93% MS = 2% Fines = 5%
Mitchells Plain (0.9 – 1.3m)		$5.9 \times 10^{-4}$	1600	-	-	-	FS = 24% MS = 53% CS = 10% Gravel = 9% Silt = 1% Clay = 3%
Matroosfontein (0-1.5m)		$5.7 \times 10^{-6}$	1750	-	-	-	FS = 79% MS = 17% Fines = 4%
Capricorn (0.2-0.4)		-	-	$3.5 \times 10^{-4}$	$4 \times 10^{-4}$	1659	FS = 78% MS = 22%
Gatesville (0.7 – 2m)	Springfontyn	$2.8 \times 10^{-5}$	1560	$2.0 \times 10^{-4}$	$3.9 \times 10^{-4}$	1718	FS = 56% MS = 41% Clay = 3%

Sampling Site (depth in m)	Formation	Constant head saturated k (m/s)	Laboratory dry density (kg/m <sup>3</sup> )	Estimated k from Chapuis (m/s)	Estimated k from Carrier (m/s)	In-situ dry density (kg/m <sup>3</sup> )	Grading*
Bellville South (0.5 – 2m)	Springfontyn	$6.6 \times 10^{-6}$	1540	-	-	-	FS = 92% MS = 4% Fines = 4%
Bellville (0-0.2)		-	-	$9.9 \times 10^{-6}$	$2.8 \times 10^{-5}$	1598	FS = 75% MS = 9% Silt = 11% Clay = 5%
Average (standard deviation)		$1.1 \times 10^{-4}$ ( $2.3 \times 10^{-4}$ )	1629 (91)	$2.0 \times 10^{-4}$ ( $1.4 \times 10^{-4}$ )	$2.7 \times 10^{-4}$ ( $1.7 \times 10^{-4}$ )	1701 (98.4)	

\*FS = Fine sand, MS = Medium sand, CS = Coarse sand

At two of the sampling sites (Mfuleni and Gatesville), the assessment of permeability involved both laboratory testing and empirical methods. From the table it is evident that both predictive methods gave permeabilities higher than the laboratory determined values. For instance, if the hydraulic conductivity of the Mfuleni sands is determined at a compacted dry density of 1567kg/m<sup>3</sup> using the empirical formulae, the method by Chapuis produces a k-value of  $5.9 \times 10^{-4}$ m/s and Carrier's method a k-value of  $7.2 \times 10^{-4}$ m/s. These values are significantly higher than the laboratory obtained permeability of  $2.3 \times 10^{-5}$ m/s. As the fines content of the soil increases, the method proposed by Chapuis (relying on the effective size, D<sub>10</sub>), produces results closer to the laboratory determined values. The relationship by Carrier (2003) includes a shape factor, which was set equal to 6.6 (for rounded/sub-rounded grain shapes). For medium angularity, a shape factor of 7.5 is suggested (Carrier, 2003). Inserting this value in Carrier's formula, produces slightly decreased flow rates (still exceeding estimates from other methods).

The Springfontyn Formation sands have, in general, slightly higher fines contents compared to the Witzand and Langebaan Formations, which will decrease the permeability of these soils. Low permeability pedogenic layers of the Witzand and Langebaan Formations will significantly reduce vertical flow rates in these deposits. Stapelberg (2009) documented a wider range of permeabilities for the Cape Flats soils than obtained in the current study; the lower extreme likely reflecting flow rates in cohesive or peaty layers or cemented sands (refer to Table 2-13 in Section 2.5.13 of Chapter 2). The sands investigated in the current study were limited to unconsolidated aeolian deposits. In the Langebaan Formation, Stapelberg (2009) performed eight permeability tests, obtaining an average permeability of  $1.03 \times 10^{-4}$  m/s (<  $4 \times 10^{-8}$  m/s to  $5.84 \times 10^{-4}$  m/s). The lower bound value is likely representative of calcretisation in this formation.

The hydraulic conductivities in Table 4-13 translate to average saturated hydraulic conductivities between 9.5m/day and 20m/day. These values correspond to the lower end of the range of values (15 to 50m/day) obtained by Gerber (1981) in the Cape Flats aquifer (Adelana, Xu and Shafick, 2006).

Surface infiltration rates at the investigated sites (refer to Figure C11 in Appendix C), vary between  $1.2 \times 10^{-4}$  and  $5.5 \times 10^{-4}$  m/s (average of  $2.4 \times 10^{-4}$  m/s). All tests were conducted between surface and 0.2m depth in fine and medium sands. These moderate to high infiltration rates will result in generally minor runoff or ponding, thus aiding recharge of groundwater and the unconfined aquifer underlying the study area. Notwithstanding this, blinding of the surface with soil fines and detritus, and the presence of less permeable layers below surficial soils can hinder recharge rates,

and result in ponding and flooding on the ground surface during periods of heavy rainfall. As stated in GEOSS (2014), approximately 15% to 37% of the annual precipitation in the area recharges groundwater in the Cape Flats aquifer.

## 4.15 Shear strength

The shear strength parameters of Cape Flats sands were determined by consolidated drained direct shear tests (some from past investigations) and monotonic triaxial compression tests. In addition, shear strength was estimated using transformation models based on SPT and CPT/CPTu data. The findings are presented and interpreted in this section.

### 4.15.1 Shear strength of compacted sands

#### 4.15.1.1 Monotonic triaxial compression tests

Static load triaxial tests on 152mm diameter x 300mm specimens were carried out on modified Witzand Formation sand from Mfuleni (94% Mfuleni sand with 6% added non-plastic soil fines), following the Council for Scientific and Industrial Research protocol (CSIR, 2014). Soils were tested in a partially saturated state, and total stress strength parameters obtained. These tests were performed to obtain the peak shear strength parameters of the material and to determine the cyclic stresses to be applied during dynamic testing.

To establish the influence of density (compaction) and moisture content on the shear parameters, samples were prepared at dry densities of 1660kg/m<sup>3</sup> (100% of Mod AASHTO MDD) and 1560kg/m<sup>3</sup> (94% of Mod AASHTO MDD), each at a moisture content of 12% (OMC) and 9% (75% of OMC). Confining air pressures of 50kPa, 100kPa and 150kPa were applied. Note that during disturbed soil sampling, any interparticle bonds (from salts or CaCO<sub>3</sub>) would have been broken, thus affecting the cohesion. By determining the major principle stress at failure ( $\sigma_{1,f}$ ) at the three confining pressures ( $\sigma_3$ ),  $\phi_{max}$  and  $c_{max}$  were determined by linear regression following the procedure specified in the CSIR draft document of 2014. The results are shown in Table 4-14. The critical state was not reached during testing, and only peak values are provided. The stress states at failure were also represented by Mohr circles, and failure envelopes constructed to confirm the calculated shear parameters. The results for one specimen are displayed in Figures 4-28 and 4-29.

**Table 4-14: Triaxial test results**

Specimen number	Sample condition		Model constants		Shear parameters		Model R <sup>2</sup>
	Compaction	Moisture content	A	B	$\phi_{max}$ (°)	$c_{max}$ (kPa)	
1	1660kg/m <sup>3</sup>	12%	6.17	28.97	46.1	5.8	0.994
2	1660kg/m <sup>3</sup>	9%	5.93	0	45.4	0	0.999
3	1560 kg/m <sup>3</sup>	12%	4.80	107.61	41.0	24.6	0.999
4	1560 kg/m <sup>3</sup>	9%	3.68	90.77	35.0	23.6	0.989

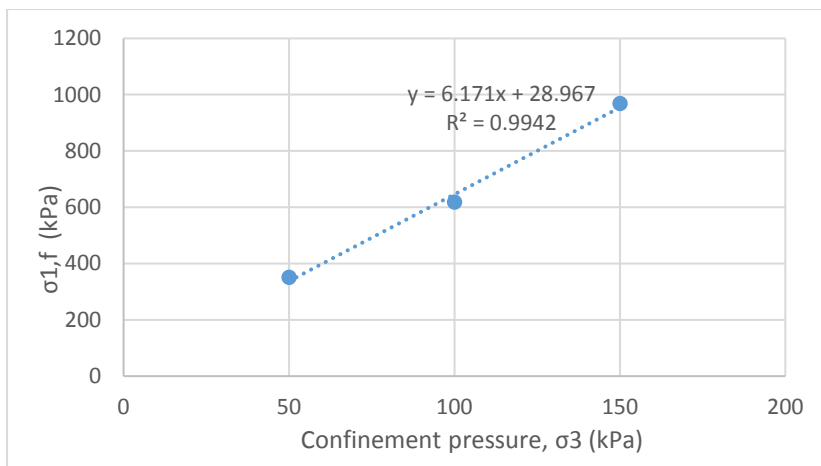


Figure 4-28:  $\sigma_{1,f}$  and  $\sigma_3$  relationship for Specimen 1 (CSIR, 2014 method)

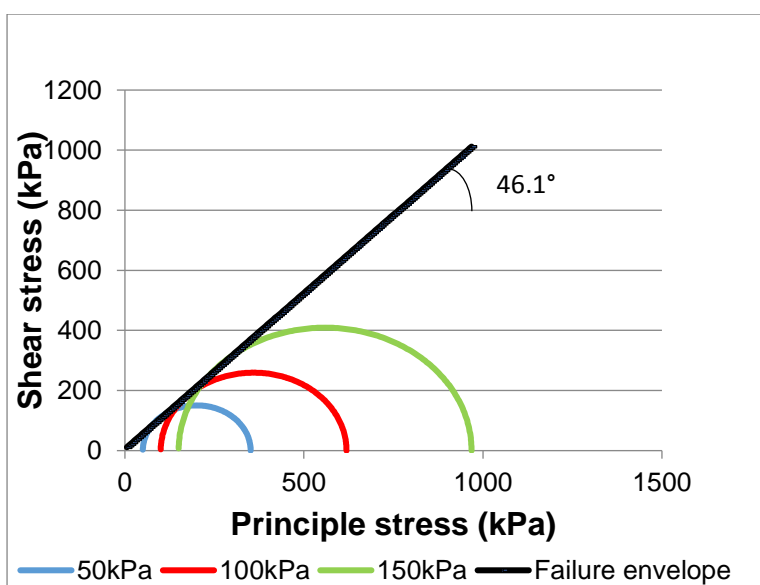


Figure 4-29: Mohr circle plot for Specimen 1

The friction angles of the sands are higher than expected for the material type and its compactness, particularly for the MDD specimens. Theyse (2008) found the effective friction angles of partially saturated compacted sands of G7 quality to vary between 37° and 40° in a moderate climatic condition (SAPEM, 2014). Direct shear tests (presented in Section 4.15.1.2), confirmed that the friction angles in Table 4-14 are higher than expected for the Cape Flats sands. The sands were however tested in a partially saturated state, (being total stress parameters), and are thus affected by the moisture condition (lack of lubrication for particle movement) and soil suction. Notwithstanding this, it is postulated that the rubber membrane which enclosed the triaxial test specimens restricted deformation (refer to Section 3.3.2.2: Monotonic triaxial tests). As explained in the aforementioned section, the influence of the membrane varies as it is re-used, and some specimens may have been influenced more than others. The influence of the membrane on the strength results was evaluated by performing direct shear tests on identical specimens. The findings are discussed in Section 4.15.1.2. The cohesion values obtained for specimens 3 and 4 are apparent cohesions which are the result of negative pore water pressures.

An increase in  $\phi_{\max}$  is noted with an increase in soil density at both 9% and 12% moisture. The increase in shearing resistance with increasing compactness is expected as the void ratio decreases, and the inter-particle contact areas increase. At both densities, an increase in moisture content results in higher friction angles, although marginal at MDD. The result is unexpected, as a decrease in soil moisture is usually accompanied by an increase in shear strength as soil suction increases. The result can possibly be explained by the compaction process. Compaction by means of the vibratory hammer, necessitated longer compaction times for the drier and less workable sands, thus possibly causing particle breakage and strength reduction. The observed trend should be verified by further tests.

The stress-strain diagrams will be considered in Section 4.17, with the presentation and interpretation of the stiffness properties of the Cape Flats sands from triaxial testing.

#### 4.15.1.2 Direct shear tests

Direct shear tests were undertaken on the same four sample types (density and moisture content variations) prepared from the modified sands used for the triaxial testing, to compare the shear parameters. Comparison of the triaxial and direct shear test peak friction angles for the modified Mfuleni sand is shown in Figure 4-30.

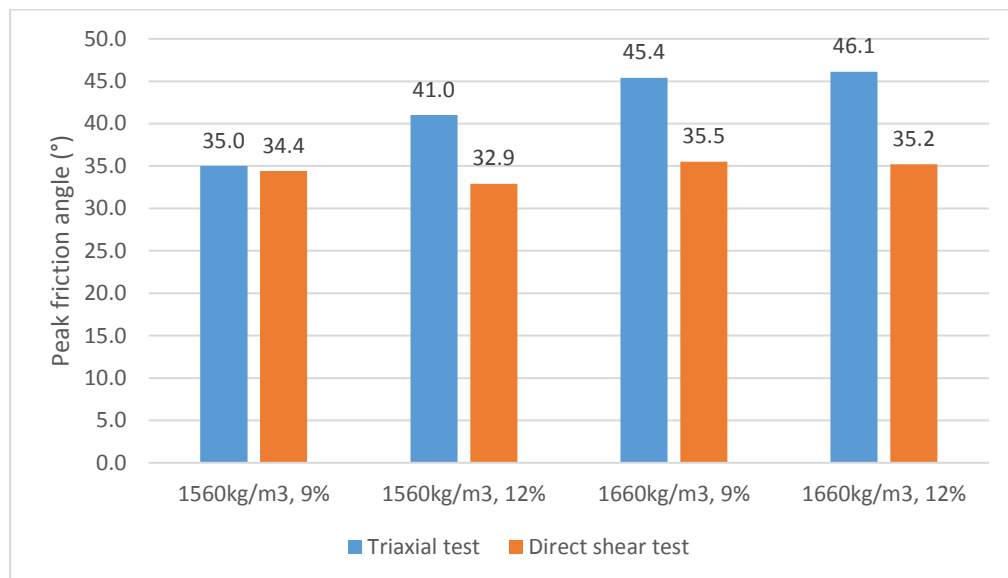


**Figure 4-30: Comparison of peak friction angles from triaxial and direct shear testing on compacted sands**

The friction angles from the direct shear test are consistently lower than the corresponding triaxial values. The friction angles from three of the four direct shear tests are approximately 20% (varying from 19.8% to 23.6%) lower than those from the triaxial tests. Similar friction angles were obtained for one specimen. The disparity in test outcomes is largely attributed to the latex membrane enclosing triaxial samples, providing additional confinement to the sample. Other, less prominent influences may include the presence of an anisotropic soil fabric (preferred particle orientation after compaction) and the position of the failure plane. The friction angles from the direct shear tests are considered more representative of the actual peak frictional strength of the soil, although lower than the values suggested by Theyse (2008) for G7 sand. The cohesion values for the modified sands vary between 13 and 16kPa. The direct shear test findings also illustrate the positive relationship between friction angle and density, although less pronounced than in

the triaxial test specimens. The increase in the friction angle as the moisture content decreases, is also more in line with expectations. The modified AASHTO compaction process followed during the preparation of the direct shear test specimens provides equal compaction energy to all samples, avoiding excessive particle damage in drier samples, which may have contributed to the strength reduction noted in the triaxial tests.

#### 4.15.2 Shear strength of reconstituted sands

Eleven direct shear tests results were obtained for Cape Flats sands sampled during past and current investigations. A summary of the conventional drained direct shear tests performed on soaked reconstituted sands is given in Table 4-15. The sampling locations are shown in Figure C12 in Appendix C and the failure envelopes (of the soils tested during the current study) given in Appendix G (Figures G4 to G8).

**Table 4-15: Summary of direct shear test results**

Sampling site (depth, m)	Formation	Dry density (kg/m <sup>3</sup> ) [Approximate density index] (%)	$\phi'_{max}$ [ $\phi'_{cv}$ ] (°)	$c'_{max}$ (kPa)	Model R <sup>2</sup>	Grading*
Gatesville (0.5-2.2)	Springfontyn	1600 [59]	37.8	8.0	0.999	FS = 56% MS = 41% Clay = 3%
Bellville South (0-1.0)		1600 [59]	35.1	4.0	0.998	FS = 92% MS = 4% Fines = 4%
Matroosfontein (0-1.0)	Witzand	1600 [44]	38.3	0	0.997	FS = 79% MS = 17% Fines = 4%
Blue Downs (0-0.8)		1600 [45]	35.3	7.8	0.999	FS = 93% MS = 2% Fines = 5%
Mitchells Plain (0.9-1.3)		1600 [38]	40.4 [39.9]	5	0.983	FS = 24% MS = 53% CS = 10% Gravel = 9% Silt = 1% Clay = 3%
Bellville (2-2.25)		Unknown (possible very low)	29.8	12.6	Unknown	FS = 75% MS = 19% Gravel = 3% Silt = 1% Clay = 2%
Bellville (3-3.5)		1650	31.2	5.5		FS = 80% MS = 9% CS = 1% Gravel = 3% Silt = 1% Clay = 6%
Macassar (7-7.45)		Langebaan	1430	35.2	0	FS = 91% MS = 3% Silt = 3% Clay = 3%
Macassar (6-6.45)	1350		34.3	0	FS = 93% MS = 1% Fines = 7%	

Sampling site (depth, m)	Formation	Dry density (kg/m <sup>3</sup> )	$\phi'_{\max}$ [ $\phi'_{cv}$ ] (°)	$c'_{\max}$ (kPa)	Model R <sup>2</sup>	Grading*
Khayelitsha (3.3-5.2)	Langebaan	1550	39.9	6.7	Unknown	FS = 82% MS = 11% Silt = 4% Clay = 3%
Khayelitsha (2.4-4.0)		1750	35.3	4.9		FS = 69% MS = 19% Silt = 6% Clay = 6%

For the sands with dry densities ranging from 1350kg/m<sup>3</sup> to 1750kg/m<sup>3</sup>,  $\phi'_{\max}$  varies between approximately 30° and 40°, with  $c'_{\max}$  values up to 12.6kPa. The average  $\phi'_{\max}$  for the sands is 35.9° (standard deviation of 3.2°). The influence of grain size and the distribution of the grain sizes on the effective friction angles is apparent. For soils compacted to similar dry densities, coarser soils and/or soils with a wider range of particle sizes are typically associated with higher values of  $\phi'_{\max}$ . A clear relationship between  $\phi'_{\max}$  and density for soils with similar textures did not emerge. Some of the measured cohesions are higher than expected for a sand.

The stress-strain curves obtained from the direct shear tests undertaken by the candidate, typically showed a gradual increase in shear stress to failure, indicative of loose contractive sands. A peak stress at moderately low strain, followed by a decrease in the shear stress as particle interlocking is overcome, was observed only for the sands from Mitchells Plan. These sands are thus dilative, increasing in volume during shear (as particles move up and over one another). The critical state friction angle for the sand from Mitchells Plain is shown in Table 4-15. Only the peak shear strength of the sands investigated during past investigations were provided in the investigation and laboratory reports.

### 4.15.3 Transformation models

#### 4.15.3.1 SPT-based methods

Standard penetration test (SPT) based transformation models proposed by Wolff (1989) (as cited in Hettiarachchi and Brown, 2009), Kulhawy and Mayne (1990) and Chen (2004) were used to obtain  $\phi'$  estimates for the Cape Flats sands. The transformation models predict peak friction angles (dependent on the density of the material). The effective friction angles were calculated from SPT N values (assumed to be  $N_{60}$  values) corrected for overburden stress for 1526 SPT's from 178 boreholes. Three sets of  $\phi'$  estimates were thus produced, extending from ground surface level to a maximum depth of approximately 42m, typically at 1m or 1.5m depth intervals. The results obtained from the three empirical methods were compared to find the one most suitable to the Cape Flats sands, i.e. providing the best prediction of  $\phi'$  in comparison with experimental  $\phi'$  values and typical values from literature.

The  $\phi'$  estimates from standard penetration resistances from a single Cape Flats borehole are given in Table 4-16. To identify the most accurate method for interpretation, the minimum and maximum index densities presented in Section 4.8 and the attained laboratory dry densities presented in Table 4-15 were used to calculate the density indices of the sands. Only the sands sampled and tested by the candidate were considered. The density index was also calculated from SPT  $(N_1)_{60}$  as shown in Table 4-16 (Cubrinovski and Ishihara, 1999). Experimental and predicted  $\phi'$  values were compared at similar density indices. For example, for the sands from Gatesville with

a density index of 60%, the friction angle was determined as 37.8° in the direct shear test. A slightly higher density index (63%) reveals  $\phi'$  estimates of 34.1°, 42.5° and 40.2° using the Wolff (1989), Kulhawy and Mayne (1990) and Chen (2004) formulas respectively. The predictive model proposed by Wolff (1989) typically underestimates the angle of internal friction of the Cape Flats sands. This observation was corroborated by Clayton (1993), highlighting its conservative approach. The methods by Kulhawy and Mayne (1990) and Chen (2004) produce closer estimates. Close comparison of the methods, noting variations with depth and overburden, shows Chen's method to provide more accurate estimates of  $\phi'$ , despite overestimation in loose soils. Consequently, only frictional resistances derived from Chen's model were interpreted.

**Table 4-16: Comparison of  $\phi'$  values from SPT based methods**

Average SPT depth (m)	SPT $N_{60}$	SPT $(N_1)_{60}$	Density index from SPT (%)	$\phi'$ Wolff (1989) (°)	$\phi'$ Kulhawy and Mayne (1990) (°)	$\phi'$ Chen (2004) (°)
1.8	8	14	48	31.1	36.7	37.9
2.8	9	12	45	30.7	36.1	37.6
3.3	18	24	63	34.1	42.5	40.2
4.3	27	32	73	36.2	45.2	41.4
5.2	26	29	70	35.3	44.1	40.9
6.3	17	18	55	32.3	39.3	39.0
7.3	25	25	65	34.1	42.2	40.3
8.8	15	14	48	31.1	36.4	37.9
12.3	34	27	67	34.9	42.6	40.7

The friction angles were plotted against the average test depth to evaluate the strength profiles and note any inter-formation variation (see Figure 4-31). The data was grouped into 2m depth intervals and the statistical parameters of the data in each interval calculated. The average  $\phi'$  varies between the narrow limits of 39.0° and 41.3° for all depth intervals (no pronounced increasing  $\phi'$  trend with depth is noted from the statistical parameters). The middle 50% of data values are mostly between lower and upper limits of 38.5° and 42° respectively. The outcome can largely be ascribed to the variations in moisture content, soil density, and grain characteristics with depth (reflected in the penetration resistance) and laterally across the study area. The overestimation of  $\phi'$  in the very loose and loose sands influences  $\phi'$  estimates mostly in the upper 2m of the soil profile (although all SPT  $(N_1)_{60}$  values below  $N=11$  produce overestimates). At shallow depths, low  $\phi'$  values (minimum of 28°) are representative of very loose and loose sands, and high  $\phi'$  values (maximum of 46.1°) are possibly associated with cemented soils. The range of  $\phi'$  values becomes narrower with depth in the predominantly dense and very dense sands. Normalisation of SPT N values for the effects of overburden pressure is also evident. When comparing the results for the different geological formations, slightly higher friction angles (reflected in the average, 25<sup>th</sup> and 75<sup>th</sup> percentile, maximum and minimum values) were noted for the soils from the Langebaan Formation. This can either be ascribed to the presence of soil cementation or due to the fewer data values available for the soils from this formation. ANOVA testing confirmed the notion, with the difference between the means of the Langebaan Formation ( $\phi' = 40.8^\circ$ ) and Witzand Formation ( $\phi' = 39.8^\circ$ ) in particular, being statistically significant ( $P$  two-tail =  $3.9 \times 10^{-6}$ ).

In the shallow soil profile, where very loose and loose sands are prevalent, Chen's method provides overestimates of the effective friction angle. For this reason, it is proposed that the predictive equation developed by Kulhawy and Mayne (1990) be applied to very loose and loose sands (SPT  $N < 11$ ), whereas Chen's (2004) method be used for medium dense to very dense sands with SPT  $N$  values exceeding 10.

Standard penetration resistance is a useful indicator of soil consistency. All SPT  $N_{60}$  values were plotted against the average test depth, illustrating soil consistency with depth in the Cape Flats (see Figure 4-32). The SPT  $N_{60}$ -values are not corrected for overburden pressure, thus also incorporating the effect of confinement on penetration resistance. Significant variation in soil consistency is noted both horizontally (at a specific depth) and vertically, with frequent trend reversal. Variation in penetration resistance with depth in normalised profiles [SPT  $(N_1)_{60}$  values] is mostly associated with changes in soil type and/or degree of cementation (i.e. density index variations). Notwithstanding this, an overall trend of increasing SPT  $N_{60}$  with depth is shown for all formations, mainly due to increasing confinement with depth. Average SPT blow counts of 28 in the Witzand Formation, 26 in the Springfontyn, and 33 in the Langebaan Formation were recorded. ANOVA testing revealed a significant variation in the means of all three data sets, in particular, variation between the Springfontyn and Langebaan Formations ( $P$  two-tail =  $1.4 \times 10^{-10}$ ). The distribution of sites with SPT data is shown in Figure C12 in Appendix C.

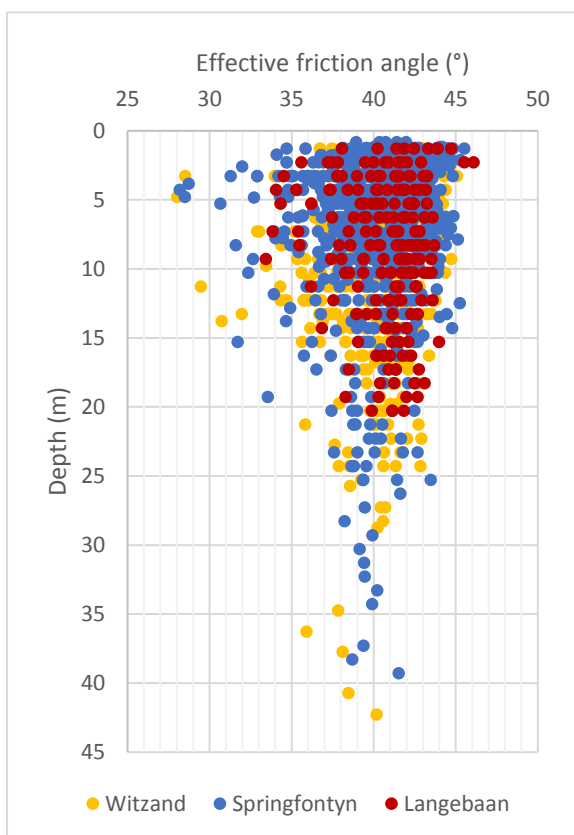


**Figure 4-31: SPT derived  $\phi'$  versus depth**

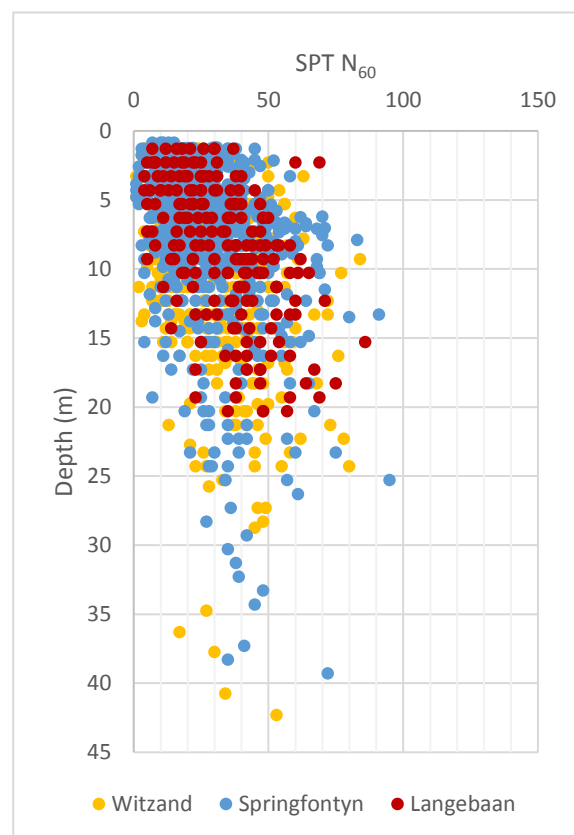


**Figure 4-32: SPT  $N_{60}$  versus depth**

#### 4.15.3.2 CPT/CPTu-based methods

Cone penetration test-based transformation models proposed by Durgunoglu and Mitchell (1975) (as cited in Meigh, 1987), Robertson and Campanella (1983) and Kulhawy and Mayne (1990) were used to predict frictional angles in Cape Flats sands. Cone penetration resistance data from 12

CPT's and four CPTu's, extending to maximum depths ranging from 3m to 11m, were utilised. All CPT's were performed in Springfontyn Formation sands, whereas the CPTu's were undertaken on sites underlain by Witzand Formation deposits. At three sites in the study area, both SPT's and CPT's were performed. However, the SPT and CPT were conducted at different locations on the site or limited or no association between the recorded penetration resistances was found, due to lateral variation in soil profile. The CPT and CPTu test sites are shown in Figure C12 in Appendix C.

The methods used all apply to uncemented quartz sand and require cone resistance ( $q_c$ ,  $q_t$  or  $Q_{tn}$ ) as input parameters. The graphical method by Durgunoglu and Mitchell (1975) and the predictive equation by Robertson and Campanella (1983) give similar approximations of  $\phi'$ . Durgunoglu and Mitchell's method is time-consuming and  $\phi'$  values were only determined at 0.5m depth intervals. In addition, the method requires interpolation between curves of equal  $\phi'$ . Robertson and Campanella's method was therefore preferred. Kulhawy and Mayne's method (which requires correction for pore water effects and water table depth) was the preferred CPTu method. The friction angles obtained using Durgunoglu and Mitchell (1975), Robertson and Campanella (1983) and Kulhawy and Mayne's (1990) methods using cone resistances from CPTu 1 in Capricorn, are shown in Table 4-17. As for the SPT based methods, the experimental and empirical  $\phi'$  values were compared at similar density indices. All three methods produced  $\phi'$  values higher than the direct shear test values, with Kulhawy and Mayne's method typically producing the closest estimates, particularly at shallower depths.

**Table 4-17: Comparison of  $\phi'$  values from CPTu data (Capricorn site)**

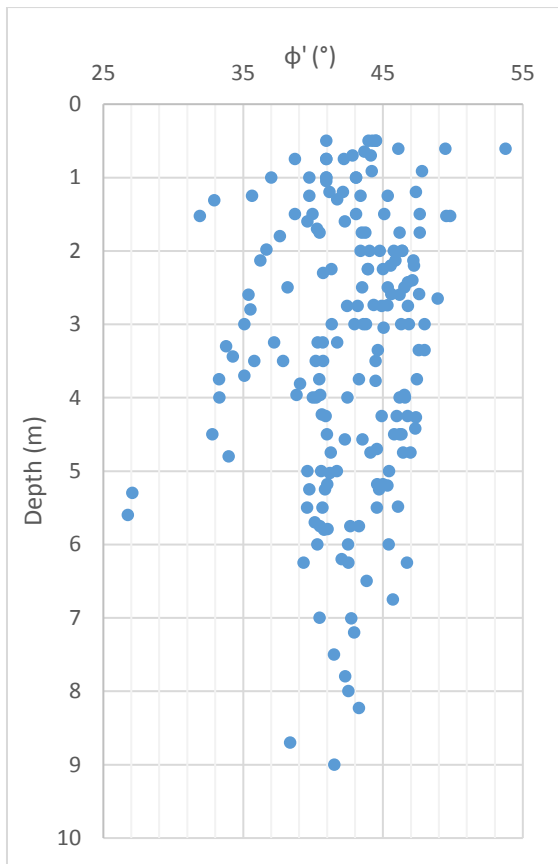
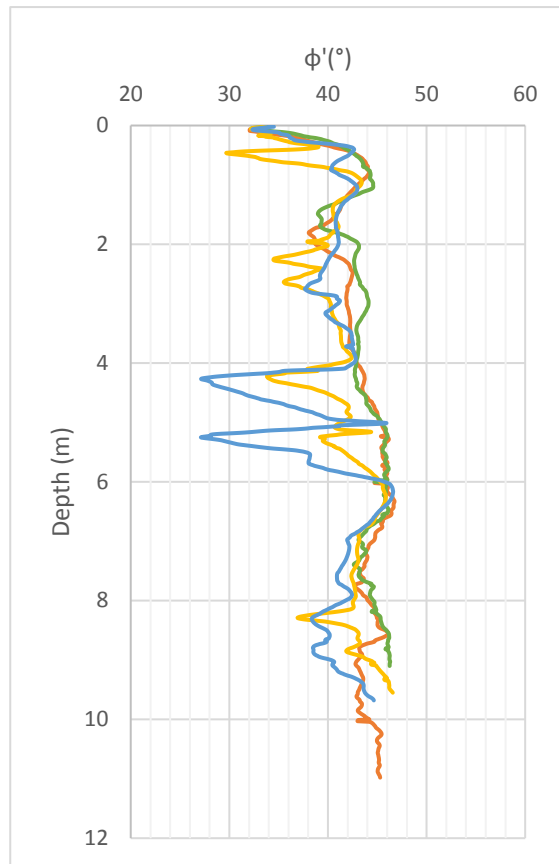
Depth (m)	Cone resistance, $q_t$ (MPa)	$Q_{tn}$ (MPa)	Density index from CPT (%)	$\phi'$ Durgunoglu and Mitchell (1975) ( $^\circ$ )	$\phi'$ Robertson and Campanella (1983) ( $^\circ$ )	$\phi'$ Kulhawy and Mayne's (1990) ( $^\circ$ )
1	9.1	204.3	38	46.0	48.2	43.0
2	4.8	83.7	45	41.0	41.9	38.7
3	12.1	161.7	50	42.5	44.6	41.9
4	16.5	200.2	52	43.0	45.2	42.9
5	29.7	335.5	55	45.0	47.2	45.4
6	28.9	311.9	59	44.5	46.5	45.0
7	27.5	283.4	58	43.5	45.7	44.6
8	25.8	254.3	59	43.0	44.9	44.1
9	21.9	204.7	61	42.0	43.7	43.0
10	28.9	261.6	62	43.0	44.6	44.2

Estimated peak effective friction angles from Robertson and Campanella's CPT based transformation model were plotted against depth as shown in Figure 4-33. The  $\phi'$  values range from 26.8° to 53.8°, with an average  $\phi'$  of 42.5°. The middle 50% of data values range between 40.5° and 45.4°. Although the peak shear strengths in Figure 4-33 are higher than those inferred from the SPT tests in Figure 4-31, both the CPT and SPT based methods show that the average strength remains relatively constant with depth. The presence of clay or peat layers, occurring intermittently with the Quaternary sands in the Springfontyn Formation, are possibly responsible for the low  $\phi'$  values documented between 5m and 6m depth, although the sleeve friction was

not measured and therefore the soil behaviour type could not be determined. It can be concluded that the CPT inferred results are higher than the SPT inferred results (at a similar density index), and that the latter are more in line with the results of the direct shear strength tests.

The CPTu-based  $\phi'$  estimates are shown in Figure 4-34. Normalised cone resistance ( $Q_{tn}$ ) and  $\phi'$  values were calculated at 1cm intervals from surface to between 9m and 11m depth. Effective friction angles mostly vary between  $35^\circ$  and  $45^\circ$ . As previously mentioned, comparison of the experimental and predicted  $\phi'$  values showed that Kulhawy and Mayne's (1990) method typically overestimates the frictional strength of the sands, however, the lower  $\phi'$  values recorded at shallow depths represents the shear strength of very loose and loose sands more accurately than the CPT and SPT methods. The abrupt and large decreases in  $\phi'$  noted between 4m and 6m at one CPTu position, marks the presence of soft clayey and silty soil layers (confirmed by SBT index plot). Penetration resistances ( $q_c$ ) with depth reveals very loose and loose sand to between 0.5m and 0.75m depth below surface. Below these depths, and extending to between 4m and 6m depth, are soils in the medium dense range, becoming dense and very dense further down. Layers of loose/soft soils occur intermittently with the denser/stiffer soils.

Overall comparison of SPT, CPT and CPTu derived friction angles shows that the means of the three data sets vary significantly ( $F > F_{crit}$ ). SPT derived  $\phi$  values have the lowest mean ( $40.2^\circ$ ) and was found to be significantly different from the CPT and CPTu derived data sets ( $P$  two-tail =  $2.6 \times 10^{-12}$ ). CPT and CPTu data sets have similar average  $\phi$  values of  $42.5^\circ$  and  $42.1^\circ$  respectively. The SPT derived  $\phi$  values are closest to the direct shear test values for Cape Flats sands. It should however be noted that penetration test data originates from different sites, and that limited CPT and CPTu data were available and compared to the SPT data. Data from the three formations were combined for the analyses as insufficient data are available to form adequate data subsets.

Figure 4-33: CPT derived  $\phi'$  versus depthFigure 4-34: CPTu derived  $\phi'$  profiles

#### 4.16 Dilative/Contractive behaviour (Liquefaction potential)

The volumetric response of the Cape Flats sands during shear was evaluated by means of a CPTu-based method published by Robertson (2016), to assess the potential for flow liquefaction of the Cape Flats sands (identifying loose, contractive soils). As the porewater pressure rises during undrained shear in a contractive soil, the effective stress and the shear resistance decrease until the shear resistance falls below the static shear stress – triggering flow in the soil. The cyclic liquefaction potential of dense, dilative sands was also assessed by means of an empirical SPT-based method put forward by Idriss and Boulanger (2004). The results of the penetration test-based methods for assessing both cyclic- and flow liquefaction potential are presented in this section.

One hundred and eighty-two in-situ test locations spread across the study area (comprising four CPTu's and 178 boreholes with SPT's), were evaluated. The in-situ test locations are shown in Figure C13 in Appendix C, which shows the distribution of the tests and liquefiable soils. Final standard penetration test depths in the boreholes range between 1.95m and 42.25m below ground level (average final test depth of 11.23m). The four CPTu's penetrated to between 9.5m and 11m below ground level. The depth to the water table in the study area, as recorded in the boreholes and from pore water pressure dissipation tests, varied between ground surface and a maximum depth of 6.0m (average water table depth of 2.3m).

#### 4.16.1 Cyclic liquefaction potential

The cyclic liquefaction potential of the Cape Flats sands was studied in terms of the triggering of liquefaction. Figure 4-35 shows the liquefaction triggering curve (blue curve) with  $CSR-(N_1)_{60cs}$  data points for a design earthquake with a moment magnitude of 6.0 and a PGA of 0.15g. The selection of the PGA value and the design earthquake moment magnitude for the study site are discussed in Section 3.5.10 of Chapter 3. At most of the test locations, the soils' resistance to cyclic liquefaction (CRR) exceeds the cyclic demand (CSR), thus providing a factor of safety greater than 1. Of the 1526 data pairs obtained from 178 boreholes plotted in the figure, only 19 pairs from 14 boreholes showed the potential to liquefy during an earthquake with the magnitude and acceleration mentioned above (see Figure C13 in Appendix C for the locations). Liquefiable soils were identified in the Witzand, Springfontyn and Langebaan Formations. Note that in calculating the CRR and CSR values, the water table levels at the time of each specific ground investigation were used (investigations undertaken over a period of approximately 30 years). Liquefaction can only occur in saturated soils and, as such, the outcome presented in Figure 4-35 may vary depending upon the depth of the phreatic surface.

The potential of the Cape Flats soils to liquefy under static conditions at the SPT locations could not be determined, as there is no appropriate SPT-based flow liquefaction method.

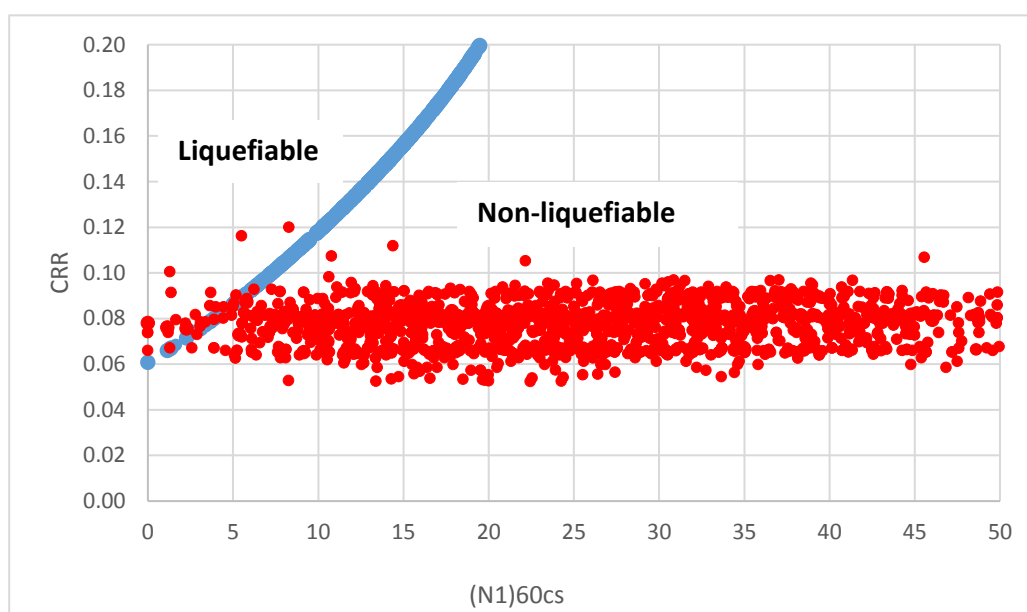


**Figure 4-35: Cyclic stress ratio plotted against clean sand equivalent SPT blow count for a design earthquake with  $M = 6.0$  and  $a_{max} = 0.15g$**

To illustrate the occurrence and thicknesses of liquefiable soil layers in the 14 boreholes in which liquefiable soils were identified, the CRR and CSR values were plotted relative to the average SPT depths (with linear interpolation between points). A continuous profile of the factor of safety against liquefaction is shown in Figure 4-36 for one such borehole located in Pinelands. At this position, liquefiable soil occurs between approximately 3m and 5m depth. At the time of the site investigation, a perched water table was located close to the surface, thus making liquefaction possible during a seismic event. At most borehole positions, only a single CSR value calculated at an individual SPT depth (midpoint of 300mm test depth) was higher than its corresponding CRR value. Interpolation between SPT depths introduces some uncertainty with regards to the exact boundaries of liquefiable soil layers. Liquefiable soils occur between upper and lower depth limits

of about 3.2m and 19m respectively, with layer thicknesses varying from approximately 0.3m to 2m. Rauch (1997), however notes that liquefaction is unlikely at depths exceeding 15m where confining stresses are large and frictional resistance is likely to prevent liquefaction. Liquefiable soils were identified as fine to coarse grained sands and silty sands in boreholes in Athlone, Philippi, Khayelitsha, Macassar, Pinelands and in the vicinities of the Cape Town International Airport in Matroosfontein and the Tygerberg Hospital in Bellville.

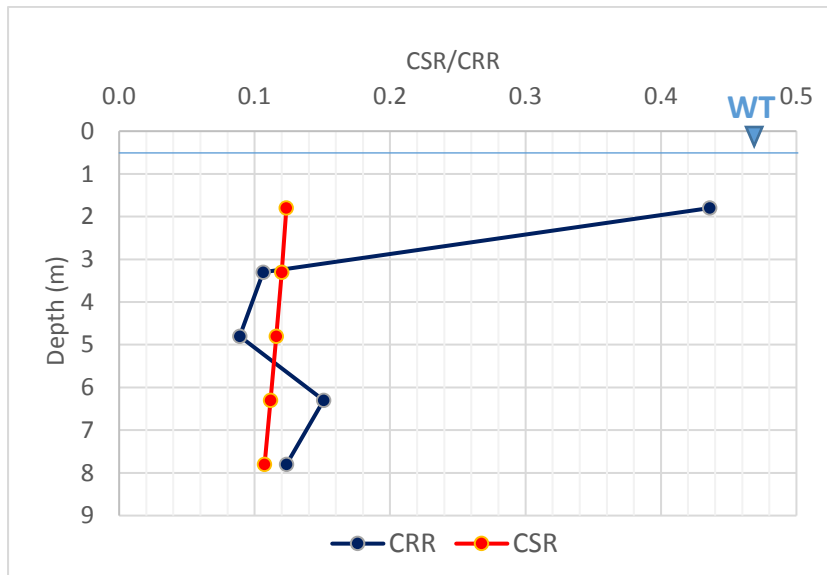


**Figure 4-36: Liquefaction analysis in a borehole in Pinelands**

To illustrate the effects of a larger magnitude earthquake producing higher PGA's on the triggering of cyclic liquefaction in the study area, the liquefaction triggering curve with  $CSR-(N_1)_{60cs}$  data points were generated for a design earthquake with moment magnitude of 7.5 and a PGA of 0.2g, as shown in Figure 4-37.

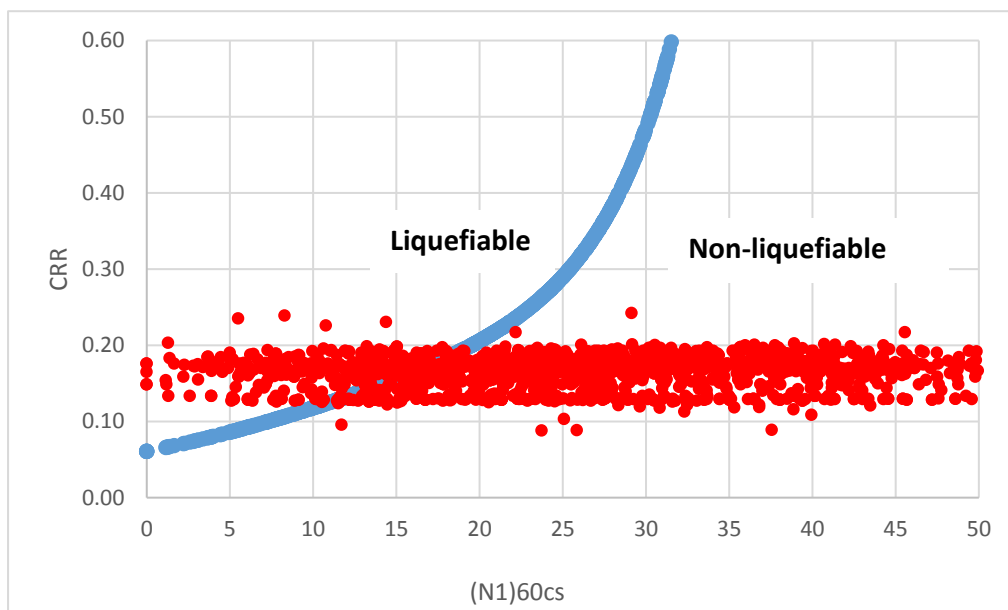


**Figure 4-37: Cyclic stress ratio plotted against clean sand equivalent SPT blow count for design earthquake with  $M = 7.5$  and  $a_{max} = 0.2g$**

A notable increase in potentially liquefiable soils is associated with the abovementioned design earthquake, with safety factors at about 15% of SPT locations being less than 1 (CSR>CRR). Liquefiable soils were identified at most of the borehole positions, but at many of these positions only one or a few of the CSR values exceeded corresponding CRR values.

#### 4.16.2 Flow liquefaction potential

Figure 4-38 shows Robertson’s normalised soil behaviour type (SBTn) chart (including the contractive – dilative boundary) with  $Q_{tn}$ - $F_r$  data points calculated from the field data of four CPTu’s (refer to Figure C13 in Appendix C for the test sites). Figures 4-38a and 4-38b show the results from a site in Capricorn (Southwest Cape Flats), and Figures 4-38c and 4-38d show the results from Airport Industria (near central Cape Flats). Both localities are underlain by Witzand Formation deposits, although the Airport Industria site is situated near the Springfontyn soil boundary. The soil behaviour types were determined as sand, silty sand and sandy silt with irregular layers of clay and silty clay underlying the site in Airport Industria.

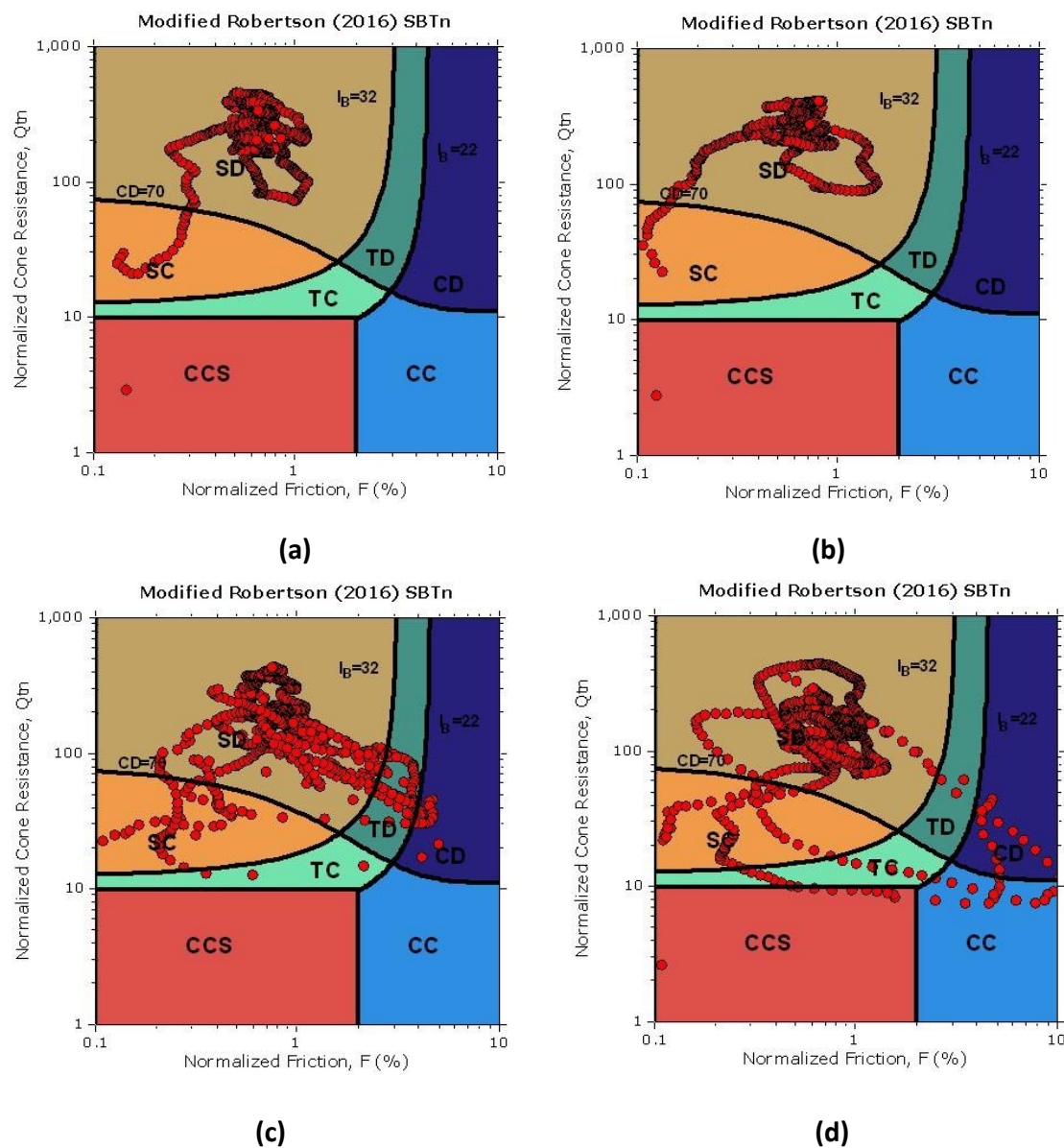
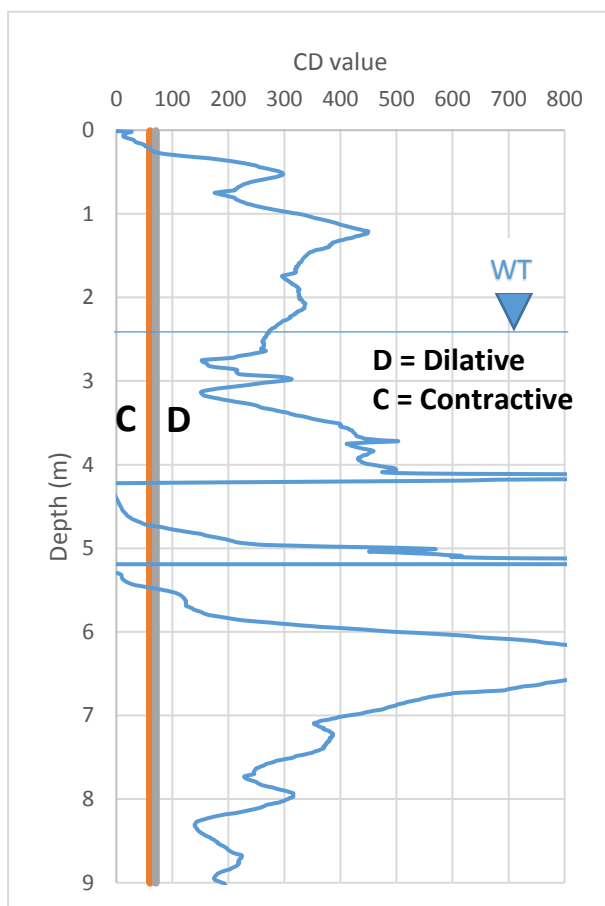


Figure 4-38: SBTn charts showing dilative/contractive response of Cape Flats soils during shear

From the SBTn charts it is evident that the soils from both sites mostly dilate during undrained shear (category SD: sand-like, dilative). These dilative soils, plotting above the contractive-dilative (CD) boundary, may be susceptible to cyclic liquefaction with deformations occurring during cyclic loading, when a brief loss in shear resistance occurs. Deformations will however stabilise when the cyclic loading ends.

Loose, contractive sands, in which  $Q_{tn}-F_r$  data pairs plot below the CD boundary, are also present at all four locations. A limited number of data points plot within the transitional or clay-like zones (some of which display contractive behaviour). To assess the depths and thicknesses of dilative and contractive soil zones, the contractive-dilative (CD) values were plotted against depth for each of the CPTu's. One such graph, for a CPTu in Airport Industria, is shown in Figure 4-39. Note the contractive/dilative boundary is transitional, the upper and lower boundaries of this zone represented by the grey and orange vertical lines respectively.



**Figure 4-39: Contractive-dilative chart for a CPTu in Airport Industria**

Examination of the 'CD' value versus depth graphs for the four CPTu's confirms the presence of contractive soils at shallow depths (extending to a maximum depth of 0.6m) at all four locations, and in zones between 4m and 5.5m depth at the Airport Industria CPTu locations. The shallow, unsaturated sands will not be susceptible to liquefaction. Between 4m and 5.5m depth, liquefiable layers vary in thickness from 0.1m to 0.5m. At these depths in the soil profiles, a complete loss of strength (leading to flow of the soil) can be triggered by monotonic or dynamic loading, occurring when the static shear stress exceeds the residual shear strength of the soil. The water table was recorded between 2.45m and 2.9m depth in the four CPTu's. It is the build-up of

pore water pressure during loading that leads to strength loss and, as such, flow liquefaction is only likely to occur in the saturated sands below the water table. The strain softening soils (prone to strength loss) can also experience cyclic liquefaction depending on ground geometry (Robertson and Cabal, 2012). A comparison of the outcomes of the SPT and CPTu-based liquefaction methods could not be made, as there are no sites with overlapping penetrometer test data.

The current assessment of the liquefaction potential of the Cape Flats sands is limited in extent. However, a predominance of dilative sands is indicated. Ground failures ascribed to soil liquefaction are expected to be mostly characterised by limited deformations during cyclic loading. The presence of contractive soils, prone to strength loss and liquid-like flow during undrained shear, is also established. Failure in these soils can be triggered by either cyclic or monotonic loading. The types of ground failures linked to soil liquefaction in earthquakes, and most likely to be associated with the Cape Flats deposits, include sand boils, lateral spreads, loss of bearing capacity, and settlement. The degree of the ground failure will be determined by the residual shear strength and the magnitude of the static shear stress. Notwithstanding the above, an assessment of the likelihood of cyclic liquefaction in the sands from the study area, revealed a general resistance to liquefaction for an earthquake with a moment magnitude of 6.0 and a PGA of 0.15g, which corresponds to the design earthquake typically assumed for the Cape Flats.

The stability of saturated sands at the Koeberg nuclear power station site, located on the West coast of South Africa, was studied by M.J. de Witt and O.B. Barker (refer to Brink, 1985). The site is underlain by sands from the Witzand and Langebaan Formations (although not within the bounds of the Cape Flats). The Milnerton fault, which extends in a north westerly to south easterly direction from about eight kilometres offshore of the Koeberg power station through the Cape Flats, exposes these areas to a possible seismic event. The cyclic strength characteristics of the sands were determined from stress-controlled cyclic triaxial tests, and strain-controlled cyclic triaxial and resonant column tests were undertaken to determine the variation of the shear modulus and damping with strain. The wave-propagation characteristics of the underlying bedrock were determined by means of seismic refraction, cross- and uphole velocity surveys. For an earthquake producing a peak horizontal ground acceleration (PGA) of 0.15g, it was found that the soils would remain stable. Liquefaction accompanied by loss of bearing resistance and gross deformations are possible at the higher PGA's for which some structures at the site were designed. The findings from the current research agree with the outcomes of this earlier study.

#### **4.17 Compressibility**

The modulus of compressibility of Cape Flats sand was obtained from the results of the monotonic triaxial compression tests undertaken on modified sands from Mfuleni (refer to Figure C12 in Appendix C for the site location). SPT and CPT-based transformation models were also used to estimate modulus values to a maximum depth of 42m in the study area. In addition, the resilient modulus of the sands was acquired from the results of the repeated load triaxial tests undertaken on the same soil specimens prepared for the monotonic triaxial tests, and mathematical models were used to characterise the stiffness behaviour of the sands. The small-strain stiffness of the Cape Flats sands was calculated from the results of the CSW tests, and the relationship between  $V_s$  and SPT N explored.

### 4.17.1 Soil elastic modulus

#### 4.17.1.1 Monotonic triaxial tests

Monotonic triaxial tests were performed on modified sands (94% fine sand with 6% soil fines added) prepared at two densities, each at OMC and 75% of OMC. The four sample types (density and moisture content variants) were subjected to all-round pressures of 50kPa, 100kPa and 150kPa, and a static vertical load applied until specimen failure occurred. The stress-strain plots are shown in Figures 4-40 to 4-43.

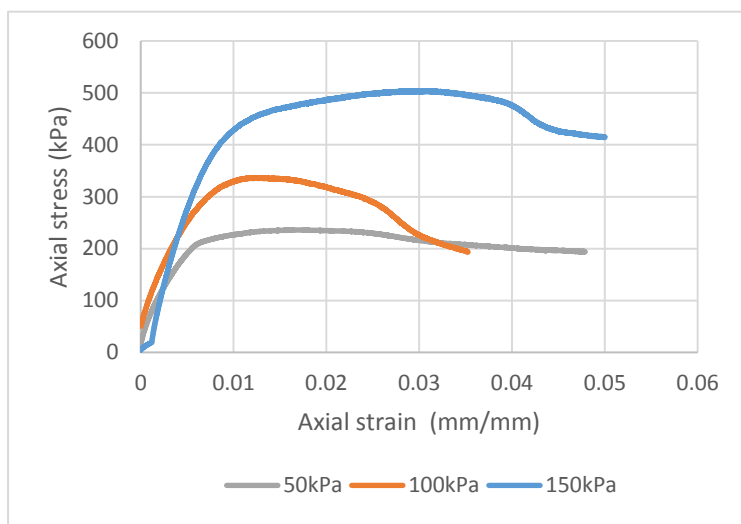


Figure 4-40: Stress-strain plot for  $\rho_d = 1560\text{kg/m}^3$ ,  $w = 9\%$  specimens

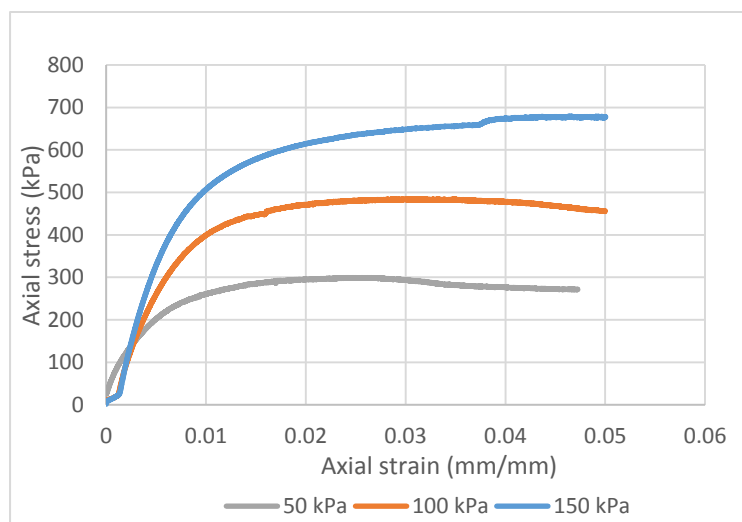
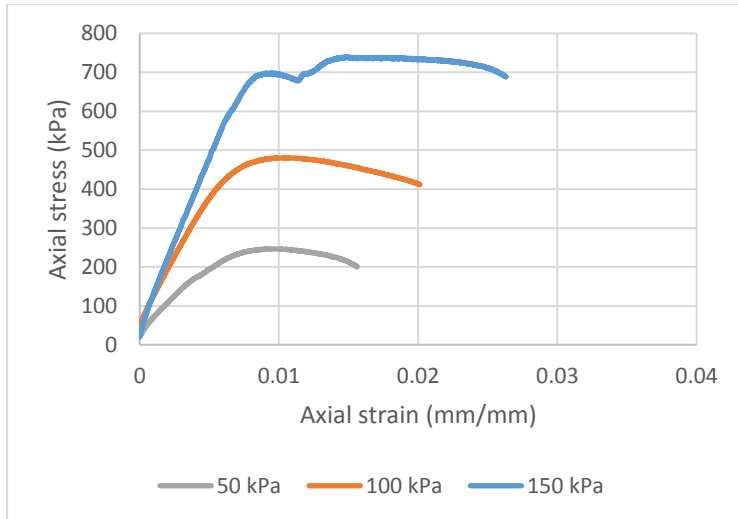
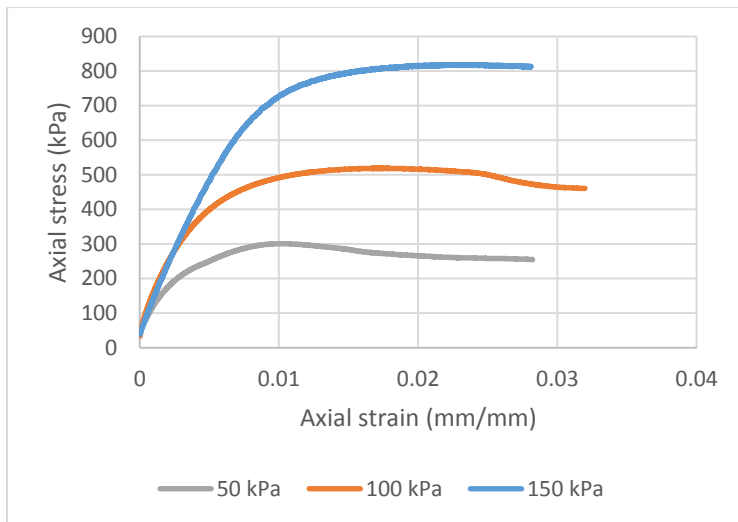


Figure 4-41: Stress-strain plot for  $\rho_d = 1560\text{kg/m}^3$ ,  $w = 12\%$  specimens



**Figure 4-42: Stress-strain plot for  $\rho_d = 1660\text{kg/m}^3$ ,  $w = 9\%$  specimens**



**Figure 4-43: Stress-strain plot for  $\rho_d = 1660\text{kg/m}^3$ ,  $w = 12\%$  specimens**

The following observations were made from the above plots of deviator stress versus axial strain:

- The 9% moisture content (75% of OMC) specimens demonstrate a dilative response to shear at both  $1560\text{kg/m}^3$  and  $1660\text{kg/m}^3$ . At 12% moisture (OMC) the stress-strain curves are indicative of a more ductile material (larger strains before failure occurs).
- The shear strength (and axial strain at failure) increases as the confining pressure rises due to an increase in particle crushing and frictional resistance, prevention of particle re-orientation, and the suppression of dilatancy which contributes significantly to soil strength.
- Lower peak stress was noted for the 9% moisture specimens (at both soil densities), indicating a reduction in strength with decreasing moisture content. Soil strength typically increases as soil moisture decreases due to reduced lubrication of interparticle contacts and an increase in suctions. The lower moisture content samples were however subjected to higher compaction energy (longer periods of compaction), likely leading to particle damage (abrasion and breakage) and reduced frictional resistance and strength.
- An increase in soil strength with increasing soil density was noted, once more the result of increased inter-grain sliding friction, interlocking friction and rolling friction.

The elastic modulus of the material was obtained from the gradient of the initial straight-line portion of each stress-strain curve. The results are shown graphically in Figure 4-44.

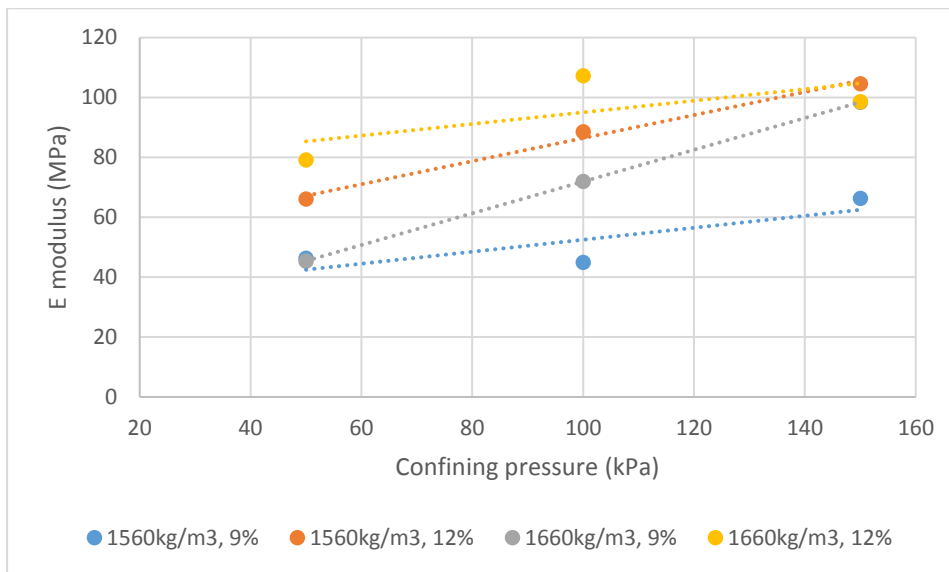


**Figure 4-44: Elastic modulus versus confining pressure**

Typically, an increase in soil stiffness is related to an increase in confining pressure, as indicated by the trendlines and noted in Figures 4-40 to 4-43 (gradients of the stress-strain curves). This result is expected as a rise in confining pressure increases the resistance to vertical pressure. For two sample types (1560kg/m<sup>3</sup>, 9% and 1660kg/m<sup>3</sup>, 12%) a single outlier in each at  $\sigma_3 = 100$ kPa reduces the  $R^2$  values to 0.45 and 0.70. An increase in soil stiffness is also noted as the degree of compaction and moisture content of the specimens increases. Typically, as soil moisture decreases and soil suction increases, voids are reduced and soil stiffness increases. The increased stiffness at higher moisture content can possibly be ascribed to particle breakage in drier samples during compaction (as previously described) and a change to the PSD curve and particle shapes.

At a confining pressure of 50kPa, the elastic modulus varies between about 45MPa and 80MPa. When the confining pressure is increased to 100kPa, the elastic modulus ranges from about 45MPa to 107MPa (although the upper value is likely overestimated). A confining pressure of 150kPa is associated with modulus values ranging from 66MPa to 105MPa. From the stress-strain plots, it can be seen that the shear strains over the linear portion of the curve are above the threshold value of 0.001% to 0.002%, below which small-strain stiffness (maximum stiffness values) is recorded. As such, some stiffness degradation has started, whereby stiffness decreases in a non-linear manner as strain levels rise. The triaxial elastic moduli values may be a slight overestimation of true stiffnesses as a result of the membrane which enclosed the specimens during testing.

A single plate load test (300mm diameter plate) was undertaken at shallow depth at a site in Springfontyn Formation sands in Epping during a previous investigation. The secant elastic moduli decreased from 40MPa to 27MPa as bearing pressures increased from 50kPa to 150kPa. The reduction in stiffness can be ascribed to increased shear strain levels at higher pressures and possibly breaking of interparticle cementitious bonds.

#### 4.17.1.2 Transformation models

##### SPT-based methods

The SPT-based method proposed by Stroud (1989) was applied in the current study as it recognises the influence of strain on stiffness. Stroud's graph of  $E/N_{60}$  versus degree of loading ( $q_{net}/q_{ult}$ ) is given in Section 3.5.11 of Chapter 3. The elastic modulus of the Cape Flats sands was determined for three  $q_{net}/q_{ult}$  ratios. Factors of safety of 3 ( $q_{net}/q_{ult} = 0.33$ ), 7 ( $q_{net}/q_{ult} = 0.14$ ) and 20 ( $q_{net}/q_{ult} = 0.05$ ) on bearing capacity were selected. The over-consolidated curve is considered best in representing the stress history of the site soils. Elastic moduli were calculated from 1521 SPT  $N_{60}$  values from 178 boreholes distributed across the study area as shown in Figure C12 of Appendix C. SPT N-values are not corrected for stress level as Stroud argued that both penetration resistance and stiffness increase with increasing overburden pressure. Of the 1521 SPT's carried out in the study area, 415 SPT's were undertaken in the Witzand Formation, 991 in the Springfontyn Formation, and 195 in the Langebaan Formation.

Plotting average SPT depth (midpoint of the 300mm test depth interval) against the estimated elastic moduli values for the abovementioned strain levels (separately per formation), illustrates a positive relationship between the elastic soil modulus and the test depth, as the overburden pressure and soil relative density increases (see Figures G9 to G11 in Appendix G). A large spread in the data about the plotted trendlines is noted, illustrative of the non-uniform stiffness profiles. By plotting trendlines through data sets associated with each  $q_{net}/q_{ult}$  ratio, the influence of strain on stiffness emerges. As the  $q_{net}/q_{ult}$  ratio rises and the safety factor decreases, there is a markable degradation in soil stiffness. Conversely, the stiffness of the over-consolidated sands increases considerably as the strain level decreases. The same trend is noted in Figures 4-45 to 4-47, where elastic moduli are grouped in 2m depth intervals and the average modulus value for each interval plotted against the  $q_{net}/q_{ult}$  ratios, per formation. Two-metre-thick intervals were considered the minimum thickness ensuring representative stiffness values. From the graphs, elastic moduli can be obtained at any strain level, read from one of the depth intervals curves (linear regression lines with  $R^2$  equal to 0.74). Due to the spread of data points observed in the elastic modulus versus depth plots, the restricted representativeness of the mean of the data should be noted. In this regard, standard deviations associated with average moduli values per 2m depth intervals vary between 14MPa and 90MPa. The spread of the modulus values in each depth interval (represented by the maximum, minimum, 25<sup>th</sup>, 50<sup>th</sup>, and 75<sup>th</sup> percentile values) is given in the form of box plots in Figures G12 to G20 in Appendix G and are discussed below. As mentioned, moduli were grouped into 2m depth intervals, from 1m to 15m in the Witzand and Springfontyn Formations and to 11m in the Langebaan Formation. In most boreholes, SPT's commenced from 1m or 1.5m depth and, as such, limited data is available for the top 1m of the soil profile. In addition, data points are infrequent below the abovementioned final depths included in the data analysis.

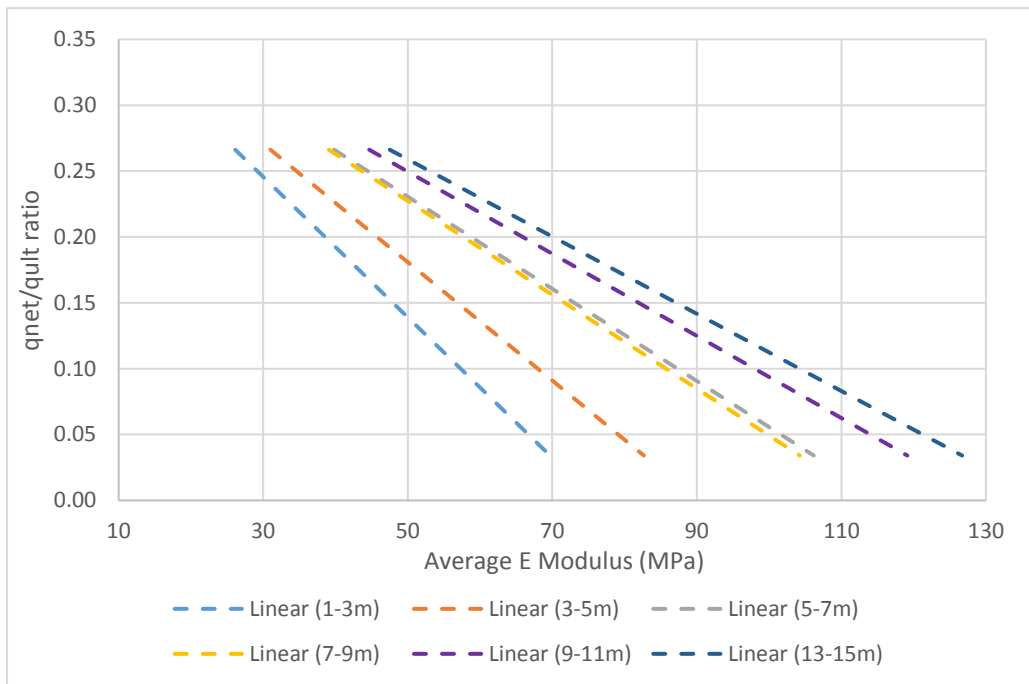


**Figure 4-45: Elastic modulus estimates for the Witzand Formation sands**

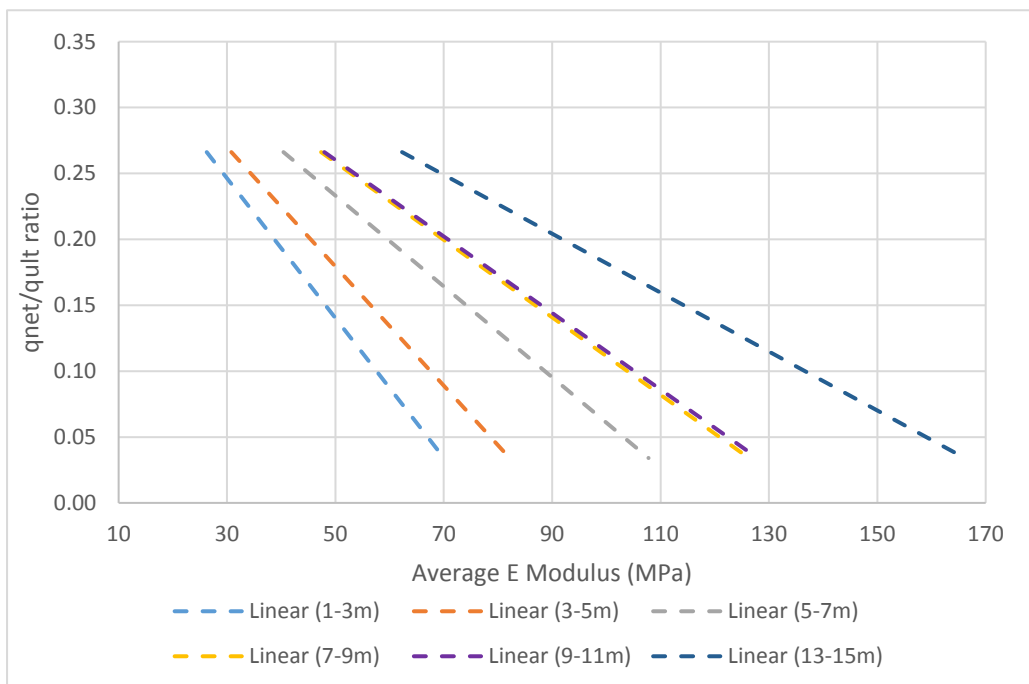


**Figure 4-46: Elastic modulus estimates for the Springfontyn Formation sands**

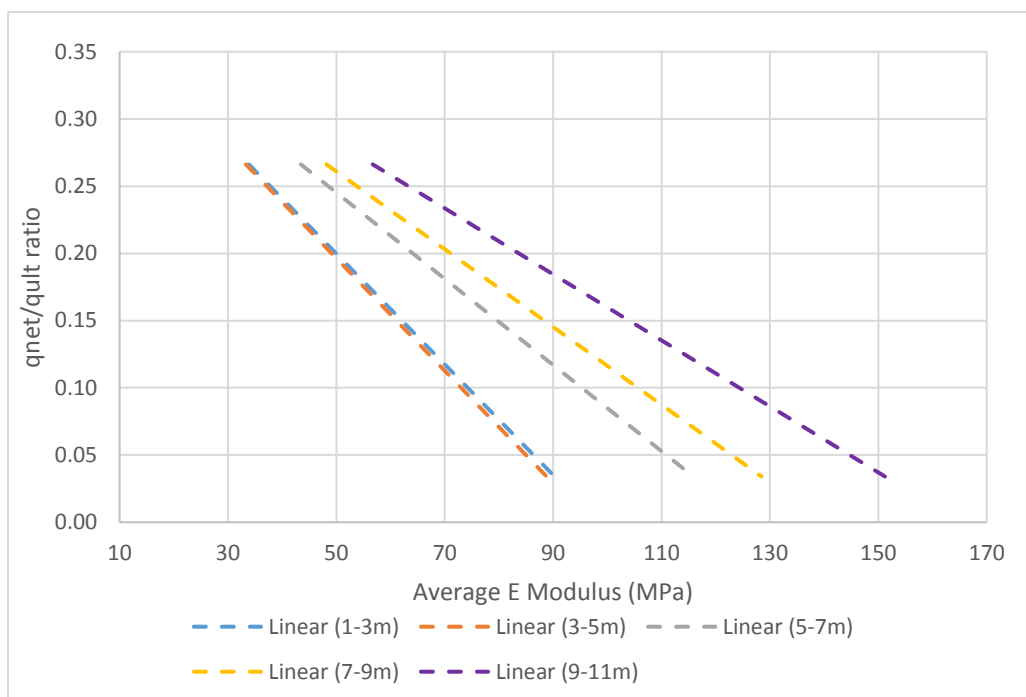


**Figure 4-47: Elastic modulus estimates for the Langebaan Formation sands**

Statistical parameters were determined per depth interval to study the spread of the soil compressibility data based on Stroud's method (refer to Figures G12 to G20 in Appendix G). Data analysis reveals trends in the data and allows comparison of stiffness profiles in the different soil formations. The following trends emerged:

- Similar stiffness profiles are observed for the Witzand and Springfontyn Formation soils to a depth of about 7m, with peak values between 59MPa (1-3m,  $q_{net}/q_{ult} = 0.33$ ) and 364MPa (13-15m,  $q_{net}/q_{ult} = 0.05$ ). Below 7m, a disparity in soil stiffness emerges, with the Springfontyn Formation soils consistently displaying greater stiffness at depth (shown in the average, 1<sup>st</sup> and 3<sup>rd</sup> quartile modulus values). The mean elastic modulus calculated for depth intervals between 7m and 15m is, on average, approximately 18% higher in the Springfontyn Formation (compared to the Witzand Formation). ANOVA testing confirms statistically significant variation between group means (P two-tail = 0.026).
- Soil stiffness in the Langebaan Formation constantly exceeds equivalent values in the Witzand and Springfontyn Formations, with the average elastic modulus between 4% and 22% higher, when compared with corresponding depth intervals in the upper 7m of the soil profile. Below this depth, the mean elastic modulus in the Langebaan Formation is, on average, about 20% and 8% higher than the average stiffnesses in the Witzand and Springfontyn Formations respectively. Peak soil stiffnesses in the Langebaan Formation range from about 55MPa (1-3m for  $q_{net}/q_{ult} = 0.33$ ) to 260MPa (between 9m and 11m for  $q_{net}/q_{ult} = 0.05$ ). Although lower peak stiffnesses were found in the Langebaan Formation, the greater overall stiffness is shown in the average, 25<sup>th</sup> and 75<sup>th</sup> percentile values. Cemented sands and limestone/calcarenite banks characteristic of this formation are considered responsible for the consistently higher stiffnesses.

- ANOVA testing reveals a significant statistical difference between data sets from the Langebaan Formation and both the Witzand and Springfontyn Formations, with P two-tail equal to  $1.1 \times 10^{-4}$  and  $8.3 \times 10^{-10}$ . The means of the data sets are as follows: Witzand Formation = 55, Springfontyn Formation = 51, and Langebaan Formation = 67.

As discussed in Section 3.5.11 in Chapter 3, both over-consolidated and normally consolidated sands occur in the study area. For this reason, elastic moduli were also estimated based on  $E/N_{60}$  ratios attained from Stroud's normally consolidated curve. Again, factors of safety of 3 ( $q_{net}/q_{ult} = 0.33$ ), 7 ( $q_{net}/q_{ult} = 0.14$ ) and 20 ( $q_{net}/q_{ult} = 0.05$ ) on bearing capacity were selected. As for the over-consolidated case, elastic moduli were grouped in 2m depth intervals and the average modulus value for each interval plotted against the  $q_{net}/q_{ult}$  ratios, per formation (refer to Figures G21 to G23 in Appendix G). A statistical summary of soil stiffness values is presented in the form of box plots in Figures G24 to G32 in Appendix G. From these figures it is evident that the looser, normally consolidated sands display lower stiffnesses at all strain levels, reaching peak values at an  $E/N_{60}$  ratio of approximately 2.

The moisture present in a soil impacts the soil stiffness, with softening occurring as the moisture content rises. SPT resistances were recorded during past investigations undertaken over a significant period. Penetration resistance and soil stiffness will vary over time at any site as the moisture content fluctuates. The above stiffnesses are therefore conditional and influenced by the in-situ moisture conditions prevalent at the time of investigation.

#### CPTu-based methods

The CPTu-based method proposed by Robertson (2009), was used to estimate soil stiffness from CPTu data from sites in Capricorn and near the Cape Town International Airport (refer to Figure C12 in Appendix C for the site locations). Both sites are underlain by Witzand Formation deposits. Porewater pressure measurements are required for correction of penetration resistances, and therefore CPT data could not be included. The method applies to young, uncemented silica sand and recognises the influence of strain on the elastic modulus. The elastic modulus was, once again, determined for  $q_{net}/q_{ult}$  ratios of 0.33, 0.14 and 0.05 corresponding to safety factors of 3, 7 and 20 respectively for comparison with the SPT-based findings.

The empirically derived elastic moduli were plotted against depth for the three strain levels, and a typical plot from each site is shown in Figures 4-48a and 4-48b. The influence of loading on stiffness once again emerges, with a notable stiffness degradation as the  $q_{net}/q_{ult}$  ratio increases. At the site in Capricorn, the sand is typically loose to 0.5m depth, medium dense from 0.5m to 3.5m, dense from 3.5m to 5m and dense and very dense below 5m. Soils of lower consistency underlie the Airport Industria site, with loose/soft soil pockets present between 4m and 5.5m depth. Using the method proposed by Robertson (2009), elastic moduli up to 60MPa and 140MPa are associated with medium dense sand for high and low strain levels respectively. In the dense sand range, elastic moduli peak at about 100MPa and 200MPa for high and low strain levels respectively, reaching a maximum of 300MPa in very dense soils. Loose/soft soil pockets are associated with stiffnesses of the order of 10MPa to 40MPa, depending on loading conditions. These moduli values are comparable to SPT-derived stiffnesses based on Stroud's method.

The small-strain elastic modulus,  $E_0$ , was also determined for the site soils from the CPTu data using the formulae put forward by Robertson (2009). Peak stiffnesses up to 525MPa were recorded. These small strain stiffnesses agree with values calculated from CSW shear wave velocity profiles (refer to Section 4.17.3). A strain level between 0.002% and 0.1% applies to the CPTu derived elastic moduli (Robertson, 2009), and in view of this, estimates based on piezocone penetrometer data are considered plausible.

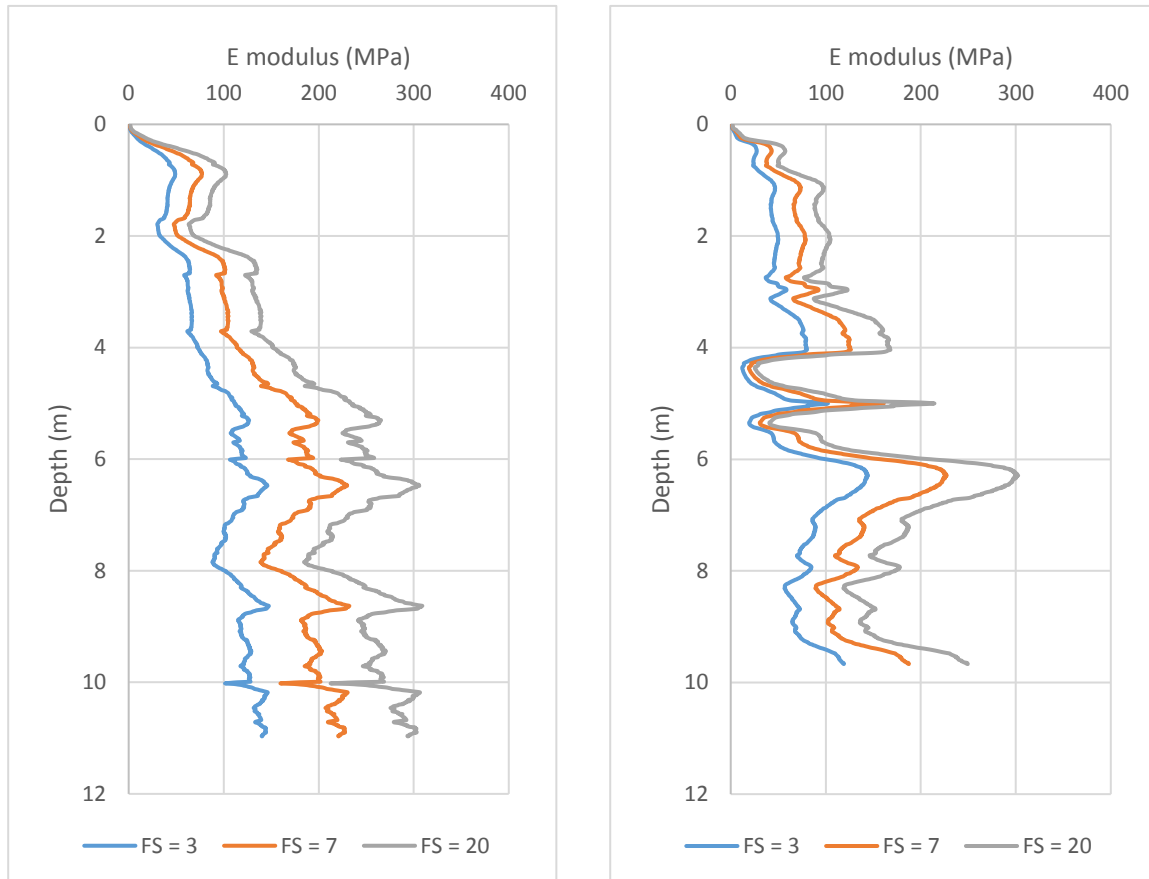


**Figure 4-48: Typical graphs of E modulus versus depth in (a) Capricorn and (b) Airport Industria**

#### 4.17.2 Resilient modulus

Cyclic loading resilient deformation tests were undertaken on the modified Cape Flats sands (94% fine sand and 6% soil fines) to determine its stress dependent resilient deformation behaviour. The four sample types of varying density (compaction) and moisture content prepared for the monotonic triaxial tests, were tested under dynamic conditions. Mathematical models were used to characterise the stiffness behaviour of the sands, and the influence of the study variables on resilient stiffness was examined.

The resilient response was defined by the resilient modulus, and the results presented by plotting the calculated resilient moduli ( $M_r$ ) against bulk stress ( $\sigma_1 + \sigma_2 + \sigma_3$ ), both on a logarithmic scale. Significant variability was observed in the axial deformation readings recorded at a deviator stress ratio (DSR) of 10%. This can be ascribed to inherent inaccuracies at the low loads. As a result, the resilient stiffness values at 10% DSR were excluded from the modelling, and only the 20%, 30% and 40% DSR results included. As discussed in Section 3.3.2.2 (dynamic triaxial testing), the actual forces (and thus the DSR's), were lower than the pre-entered force and the actual DSR values

ranged from 9% (entered 10%) to 35% (entered 40%). The lower forces were due to characteristic impreciseness in pressure control at these lower values. The DSR's were sufficiently consistent at each stress level, and the validity of the outcome and the  $M_r$ -bulk stress model will not be affected. For simplicity purposes, the presented results will refer to the pre-entered forces and the derived DSR's.

This section comprises of two main parts, namely:

- Fitting the  $M_r$ - $\Theta$  model and the  $M_r$ - $\sigma_3$ - $\sigma_d$  model to the resilient response results. The model parameters and  $R^2$  values are derived and the most fitting model identified.
- Studying the effect of moisture content and compaction on resilient stiffness.

#### 4.17.2.1 Modelling resilient deformation behaviour

Describing the noted stress dependency through suitable mathematical models allows prediction of the behaviour of the material under stress conditions other than those investigated. Using the relatively simple and extensively used models given in Equations 3-19 and 3-20 below (from Chapter 3), the best fit model parameters were determined from the test data. A peak stress level of approximately 40% of the failure level of the sand was applied during dynamic testing, which is considered "mild" and well below failure stress. The results are presented below per sample type.

$$M_r = k_1 \left( \frac{\theta}{\theta_0} \right)^{k_2} \quad \text{Equation 3-19}$$

$$M_r = k_1 \left( \frac{\sigma_3}{\sigma_{3,0}} \right)^{k_2} \cdot \left( \frac{\sigma_d}{\sigma_{d,0}} \right)^{k_3} \quad \text{Equation 3-20}$$

Where:

$M_r$  = Resilient modulus (MPa)

$\theta$  = Bulk stress =  $\sigma_1 + \sigma_2 + \sigma_3$  (kPa)

$\sigma_3$  = Confining pressure (kPa)

$\sigma_d$  = Deviator stress (kPa)

$\theta_0, \sigma_{3,0}, \sigma_{d,0}$  = Reference stresses = 1 kPa

$k_1, k_2, k_3$  = Material coefficients

#### **$P_d = 1660 \text{ kg/m}^3, w = 9\%$ resilient response testing**

The  $M_r$ - $\Theta$  model fits the data relatively reasonably, with an  $R^2$  of 0.72 (refer to Figure 4-49). The experimental data points are plotted on the graph, and the grey line represents the model (connecting the  $M_r$  estimates- $\Theta$  data points). Material constants  $k_1$ , which provides an indication of material stiffness, and  $k_2$ , the rate of stiffness increase with an increase in bulk stress, are given in Figure 4-49.

The stress dependency of the material is illustrated by the model, with the stiffness increasing as bulk stress and confinement increase. Notwithstanding this, there is a decrease in resilient stiffness as DSR increases (at a given confining pressure), illustrating the limitations on the model. This decrease is a result of a loss in integrity of the specimens as damage occurs. Additionally, the alignment of fine particles and a loss of shear strength may be partly responsible, as well as initial suction present in the specimen being dissipated during dynamic loading. Typically, "stress

stiffening” is observed in granular pavement materials followed by slight softening under severe stress regimes (Jenkins and Rudman, 2016).

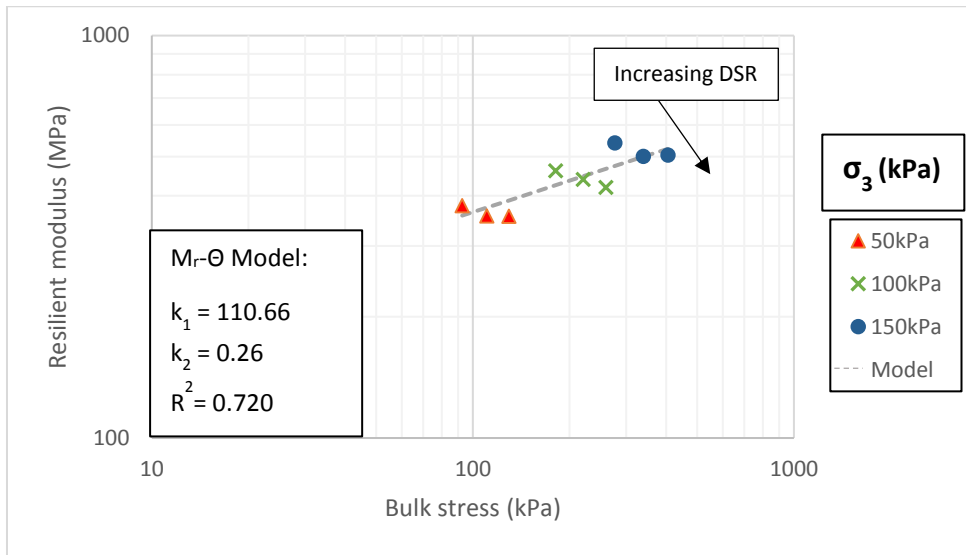


**Figure 4-49:  $M_r$ - $\theta$  model for  $\rho_d = 1660\text{kg/m}^3$ ,  $w = 9\%$  specimen**

The  $M_r$ - $\sigma_3$ - $\sigma_d$  model was also fitted to the resilient response results, as shown in Figure 4-50. In order to model stress dependence and not the change in  $M_r$  with DSR (due to stress-softening), the model was fitted to the overall positive  $M_r$ - $\theta$  relationship connecting the same DSR's. The dotted lines were plotted using the model parameters. The reduction in resilient stiffness with increasing DSR is noteworthy (and mainly due to sample damage) and to improve the prediction of  $M_r$ , the stress level should be considered.  $M_r$  can be estimated as an average of the three relationships or determined at a stress level. Notwithstanding this, all tests were done on the same material and, as such, the same model parameters should apply throughout. The model fails to account for the relevant model parameter of DSR. This approach (of separation into three different models accounting for DSR) will therefore not be followed and only the  $M_r$ - $\theta$  model, which provides a marginally improved fit to the overall trend, presented and explored.

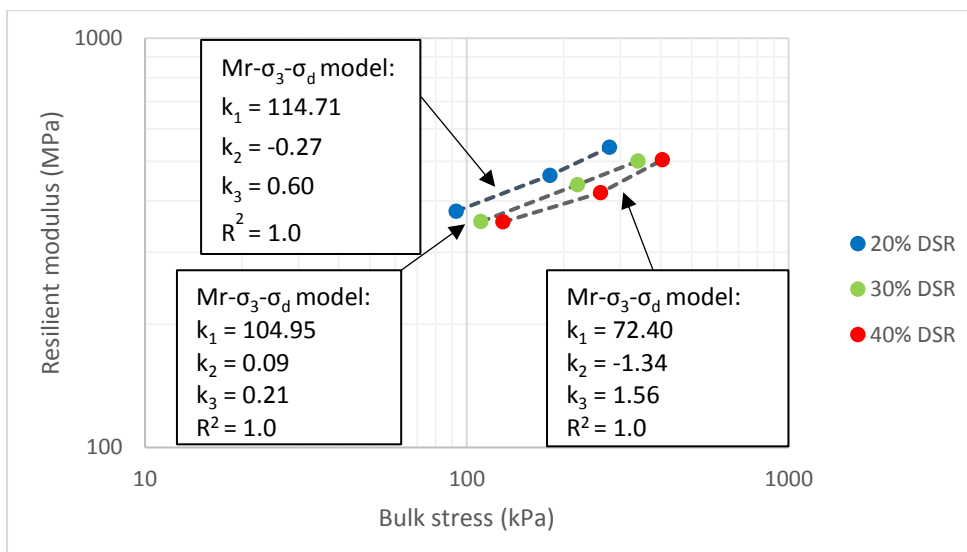


**Figure 4-50:  $M_r$ - $\sigma_3$ - $\sigma_d$  model for  $\rho_d = 1660\text{kg/m}^3$ ,  $w = 9\%$  specimen**

**$\rho_d = 1660\text{kg/m}^3$ ,  $w = 12\%$  resilient response testing**

At MDD and OMC the resilient stress dependency of the Cape Flats sand represented by the  $M_r$ - $\Theta$  model, produces an  $R^2$  value of 0.550 (see Figure 4-51). Stress-softening is more pronounced at the higher moisture content of 12% (compared to 9%), affecting the goodness of fit of the model.

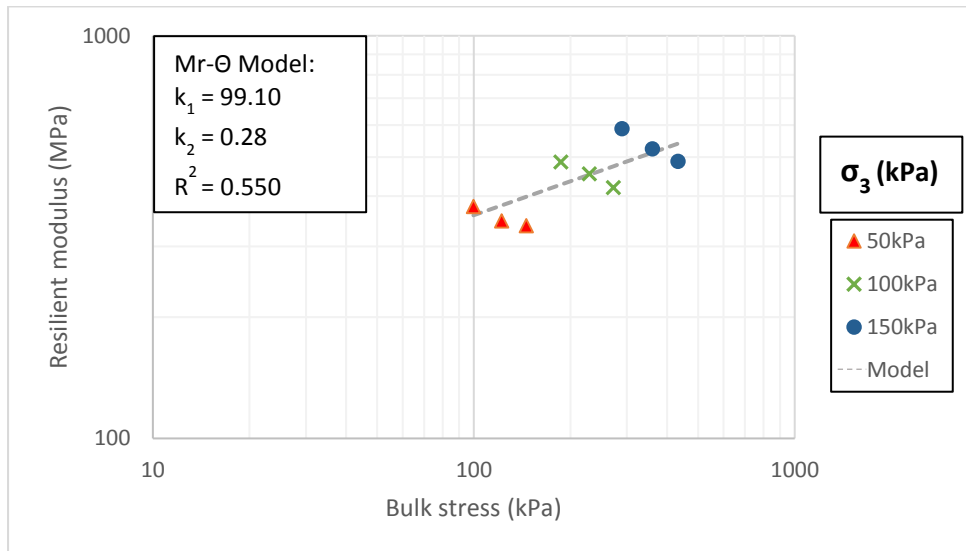


Figure 4-51:  $M_r$ - $\Theta$  model for  $\rho_d = 1660\text{kg/m}^3$ ,  $w = 12\%$  specimen

 **$\rho_d = 1560\text{kg/m}^3$ ,  $w = 9\%$  resilient response testing**

The  $M_r$ - $\Theta$  model yielded an  $R^2$  value of 0.49 for the lower density and moisture content specimen, as shown in Figure 4-52.

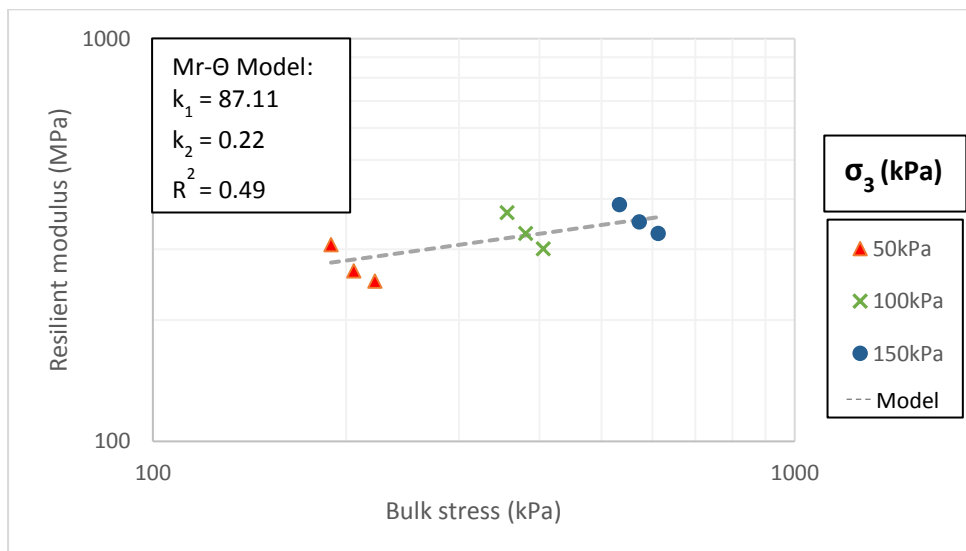
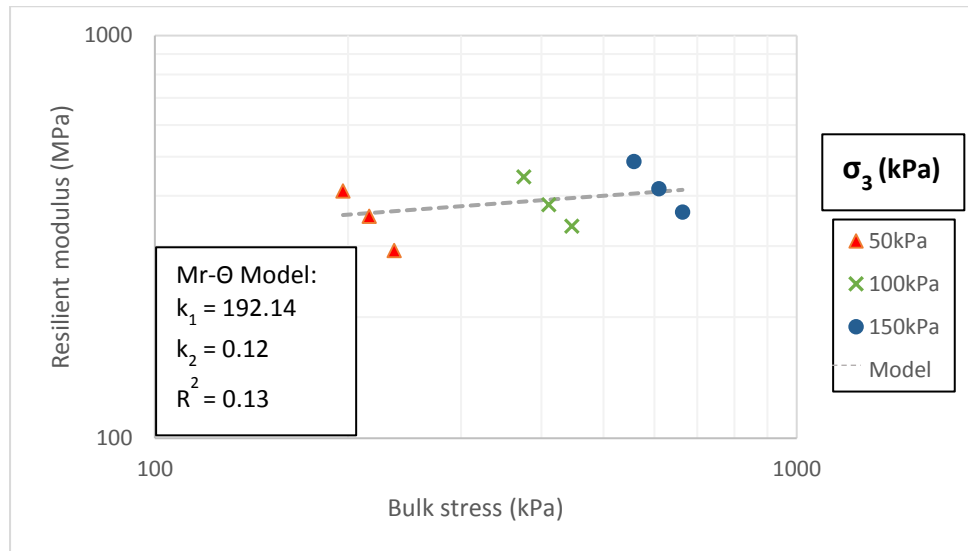


Figure 4-52:  $M_r$ - $\Theta$  model for  $\rho_d = 1560\text{kg/m}^3$ ,  $w = 9\%$  specimen

### **$P_d = 1560\text{kg/m}^3$ , $w = 12\%$ resilient response testing**

The resilient stiffness data of the Cape Flats sand compacted to a dry density of  $1560\text{kg/m}^3$  at OMC revealed a poor fit to the  $M_r$ - $\Theta$  model, with an  $R^2$  value of 0.13 (see Figure 4-53). The observed material softening with increasing DSR is significant, shown by the spread of data points about the curve. Softening appears to become more pronounced as the moisture content rises (comparison of 9% and 12% moisture specimen results).



**Figure 4-53:  $M_r$ - $\Theta$  model for  $\rho_d = 1560\text{kg/m}^3$ ,  $w = 12\%$  specimen**

The resilient modulus is a vital parameter in the determination of the response of a road pavement to traffic loadings. The above-given transformation models can be used to estimate the resilient modulus of the Cape Flats sands, once the in-situ stress state (and thus the bulk stress) in the pavement layers has been calculated. Limitation exists, governed by the loss in integrity of the sands as damage occurs during dynamic loading.

#### *4.17.2.2 Influence of compaction and moisture content on resilient response*

This section presents the results of the evaluated influence of moisture content and density on the resilient stiffness. In Figure 4-54,  $M_r$ - $\Theta$  model lines are shown for the four sample types (moisture and density variations).

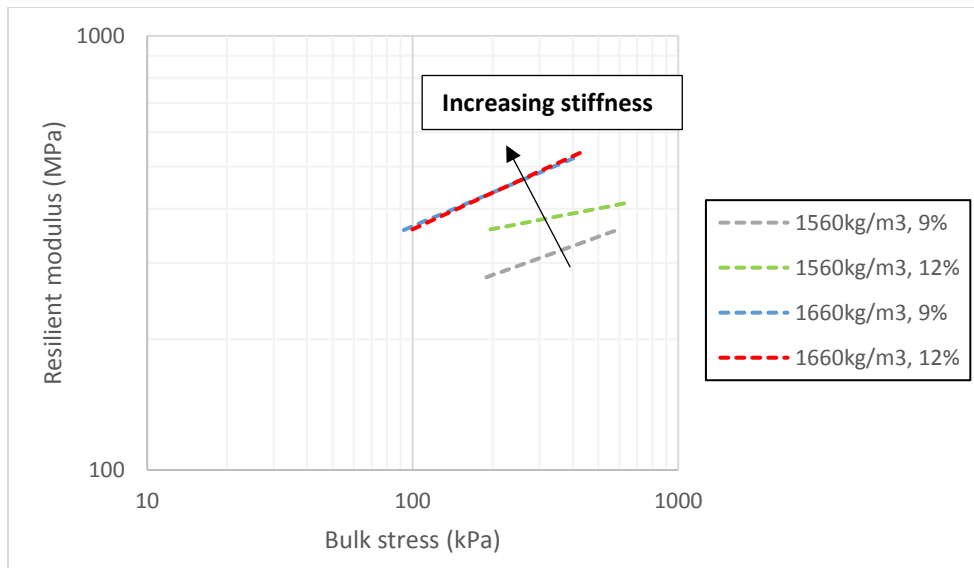


**Figure 4-54: Mr- $\Theta$  model lines showing influence of moisture and density on resilient response**

An upward shift in model lines is seen as the soil density increases (at both moisture contents), illustrating a clear increase in material stiffness with compaction. The effect of moisture content on resilient response is evident at the lower density (1560kg/m<sup>3</sup>), but with no differentiation at the higher density. Uncharacteristically, an increase in soil stiffness is accompanied by an increase in moisture content. Soil strength and stiffness typically decrease as the moisture content of a soil increases. Particle breakage during compaction of drier specimens, requiring extended periods of tamping, is a possible contributor to this atypical outcome. Notwithstanding this, only four sample types were tested (with limited repeats) and the observed trends should be confirmed by additional testing.

In the column chart shown in Figure 4-55, average  $M_r$  (combining 20%, 30% and 40% DSR) at 50kPa, 100kPa and 150kPa confining pressure, is shown for each sample type.

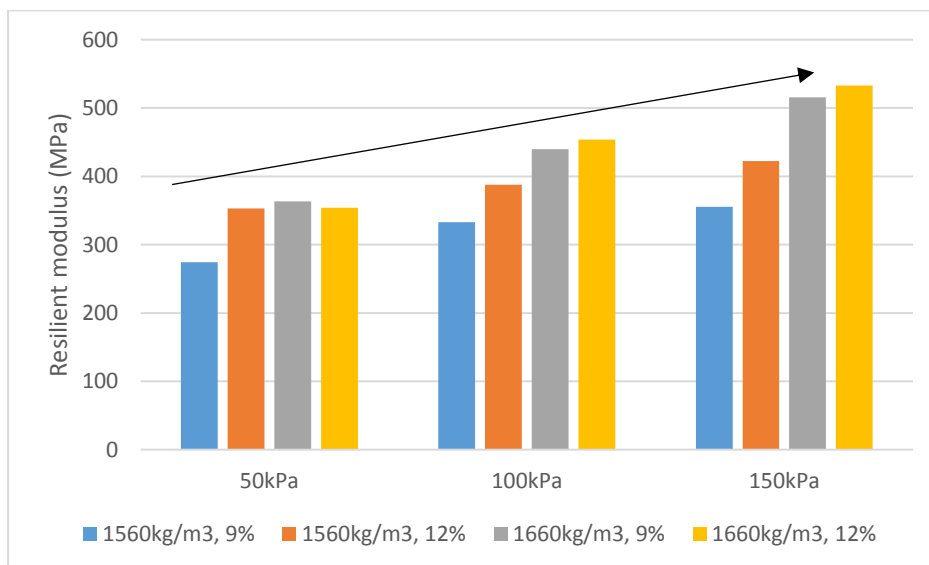


**Figure 4-55: Influence of moisture content and compaction on resilient stiffness**

Once more, soil stiffness is seen to be influenced by soil moisture and degree of compaction. Comparison of blue and red columns and grey and yellow columns independently, relating stiffnesses at 9% and 12% moisture, typically reveals higher values of  $M_r$  at 12% moisture at all confining pressures. Comparison of blue and grey columns, and red and yellow columns, illustrates the positive correlation between density and soil stiffness.

#### 4.17.3 Small-strain Stiffness

At very small values of strain, the small-strain stiffness is recorded. As strain values increase beyond the threshold shear strain of 0,001% to 0,002%, stiffness decreases in a non-linear manner. The non-linear stiffness behaviour of soil can be illustrated by a typical stiffness degradation or softening curve. A knowledge of the small-strain stiffness and existing strain levels enables the determination of soil stiffness for a variety of geotechnical applications, facilitating the prediction of ground movement.

Shear wave velocity and SPT blow count data were obtained from CSW tests and SPT's undertaken on sites in Athlone, Muizenberg and Atlantis. Refer to Figure C14 in Appendix C for the site locations. Plots of shear wave velocity and SPT N values from these sites are given in Appendix G (Figures G33 to G42). From this data, 80  $V_s$ -SPT N data pairs were generated. Vertical effective stress was considered in the regression of  $V_s$  and SPT N, which has often been neglected in previous studies. In this regard, a separate overburden term ( $P_a/\sigma'_v$ ) was included. In addition, values of  $N_{60}$  and  $V_s$  were corrected for overburden pressure to  $(N_1)_{60}$  and  $V_{s1}$  values, using equation 3-5 and 3-6 from Chapter 3 in a separate analysis. The execution of both analyses allows the emergence of the strongest correlation for the site soils. The influence of soil type, geological epoch, fines content, coefficient of uniformity and average particle size on shear wave velocity was excluded from analyses, as there were either insufficient differentiation with regards to a variable or inadequate data was obtainable to enable successful regression.

$V_s$ , rather than  $E_0$ , was preferred for regression analyses, as the calculation of  $E_0$  requires bulk density and Poisson's ratio with depth, which is likely to introduce some uncertainty. In addition, estimates of  $V_s$  could simply be converted to  $E_0$  estimates where site specific information is available. Notwithstanding this,  $E_0$  profiles were determined from  $V_s$  in order to study the stiffness profiles of Cape Flats sand. In Figures 4-56a and 4-56b below,  $E_0$  is plotted against depth, as obtained from the CSW tests undertaken at the Athlone and Cape Flats WWTW's sites and at Atlantis respectively. The data from the site in Atlantis is presented separately as the high stiffness moduli at this site affects the scale and readability of a combined plot.

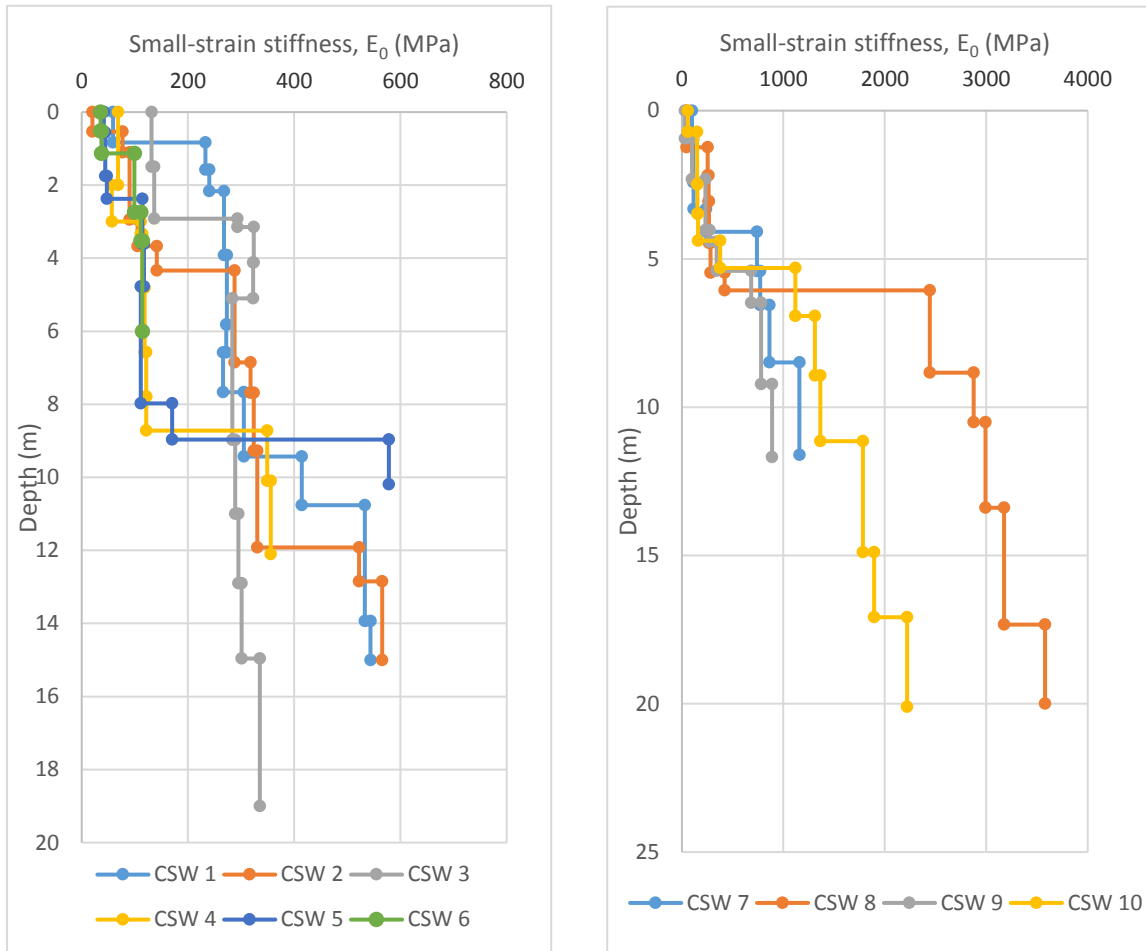


**Figure 4-56:  $E_0$ -depth profiles at the a) Cape Flats and Athlone WWTW's and b) Atlantis**

At the WWTW's sites  $E_0$  is typically below 100MPa to 3m depth and below 300MPa to about 9m depth. A maximum  $E_0$  of almost 600MPa was determined from  $V_s$  at the investigated sites. Borehole profile logs reveal sands, silty and clayey sand and sandy silt at the sites.  $E_0$  values up to 3500MPa were reached in the soils from Atlantis. Cemented sands, which is identified in the accompanying borehole profiles, is most likely responsible for the high stiffness values.

For the regression analyses, the following forms of regression equations were used, firstly expressing  $V_s$  as a function of  $N_{60}$  and  $P_a/\sigma'_v$ , and then expressing  $V_{s1}$  in terms of  $(N_1)_{60}$ :

$$V_s = A(N_{60})^B \cdot \left(\frac{P_a}{\sigma'_v}\right)^C \quad \text{Equation 4-5}$$

$$V_{s1} = A(N_1)_{60}^B \quad \text{Equation 4-6}$$

To obtain the functional form, equations are expressed in terms of natural logs, as shown for Equation 4-5:

$$\ln V_s = \beta_0 + \beta_1 \ln N_{60} + \beta_2 \ln \left(\frac{P_a}{\sigma'_v}\right) + \varepsilon \quad \text{Equation 4-7}$$

The constants were solved by means of least squares regression. The resultant regression equations and statistical parameters are shown in Table 4-18. Significant variation in relative density and stiffness with depth was noted at the WWTW sites (from the SPT N profiles). SPT and CSW test depths infrequently overlapped and, as such, the non-uniform profiles resulted in less accurate  $V_s$ -SPT N relations. In addition, the shear wave velocities increased monotonically with depth at these sites, whereas the SPT blow counts revealed softer layers below stiffer layers. The monotonic increase in  $V_s$  with depth is presumably the result of inversion routines used in the analysis of the CSW results, rather than a true reflection of the variation in stiffness with depth. The more uniformly increasing stiffness profiles at the Atlantis site, provided opportunity for the development of an accurate  $V_s$ -SPT N correlation for this site. The data from this site was analysed separately, and the results included as regression numbers 3 and 4 in Table 4-18.

**Table 4-18: Regression equations for predicting the shear wave velocity (m/s) of Cape Flats sand**

Regression number	Regression equations	Number of data pairs	Coefficient of determination ( $R^2$ )	Standard error (m/s)
1	$V_{s1} = 115.6(N_{160})^{0.221}$	80	0.07	118.0
2	$V_s = 139.8(N_{60})^{0.176}(P_a/\sigma_v')^{-0.259}$	80	0.42	113.6
3	$V_{s1} = 15.2(N_{160})^{0.936}$	32	0.46	110.8
4	$V_s = 64.1(N_{60})^{0.555}(P_a/\sigma_v')^{-0.344}$	32	0.83	83.5

The regression analysis revealed that the inclusion of a separate overburden term in the regression of  $V_s$  and  $N_{60}$ , produces improved fits, as opposed to the stress corrected equations in which the  $R^2$  of the regression is notably lower. It is the correction of  $V_s$  and  $N_{60}$  to  $V_{s1}$  and  $(N_{160})$  with empirical constants 'n' and 'm' prior to regression, that introduces bias with respect to overburden pressure. The expression of  $V_s$  in terms of  $N_{60}$  and  $P_a/\sigma_v'$  derived from the Atlantis data set reveals the best fit with  $R^2 = 0.83$  and a standard error of 83.5m/s.

When comparing the estimates of  $V_s$  obtained using the best fit model to existing  $V_s$ -SPT  $N_{60}$  models also considering overburden pressure or depth (Andrus, Piratheepan and Juang, 2007, Bellana, 2009 and Rollins et.al., 1998), the model proposed by the candidate produces estimates exceeding those proposed for Holocene aged sands, such as the sands from the Witzand Formation. A closer comparison can be drawn between  $V_s$  estimates for Pleistocene aged deposits, such as the sands from the Langebaan and Springfontyn Formations. According to Fumal and Tinsley (1985) (refer to Sykora, 1987), Pleistocene deposits have a higher dependence of shear wave velocity on void ratio than Holocene-age soils, resulting in higher shear wave velocities for similar SPT blow count values.

To examine the influence of the independent variables on  $V_s$ , plots of  $V_s$  versus  $N_{60}$  were created with trendlines through various  $P_a/\sigma_v'$  values, and  $V_s$  versus  $P_a/\sigma_v'$  with trendlines through various  $N_{60}$  values. Figures 4-57a and 4-57b include all data pairs, whereas only data pairs from the Atlantis site are shown in Figures 4-58a and 4-58b.

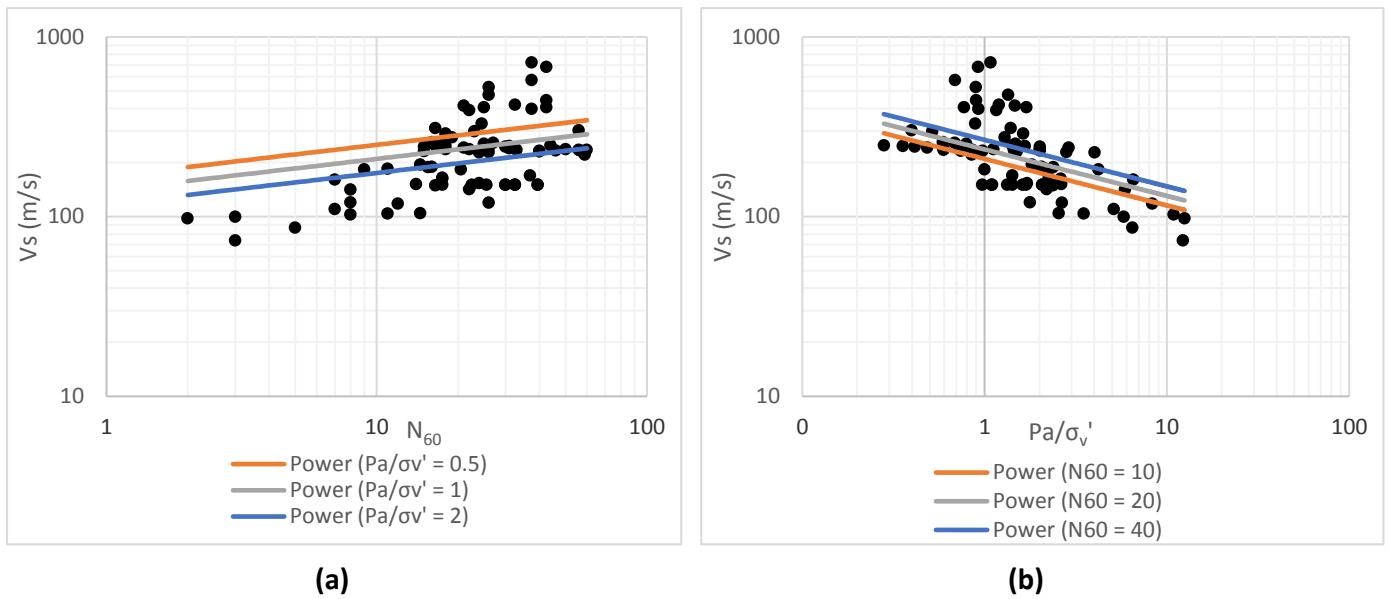


Figure 4-57: a)  $V_s$  versus  $N_{60}$  with  $P_a/\sigma_v'$  trendlines and b)  $V_s$  versus  $P_a/\sigma_v'$  with  $N_{60}$  trendlines

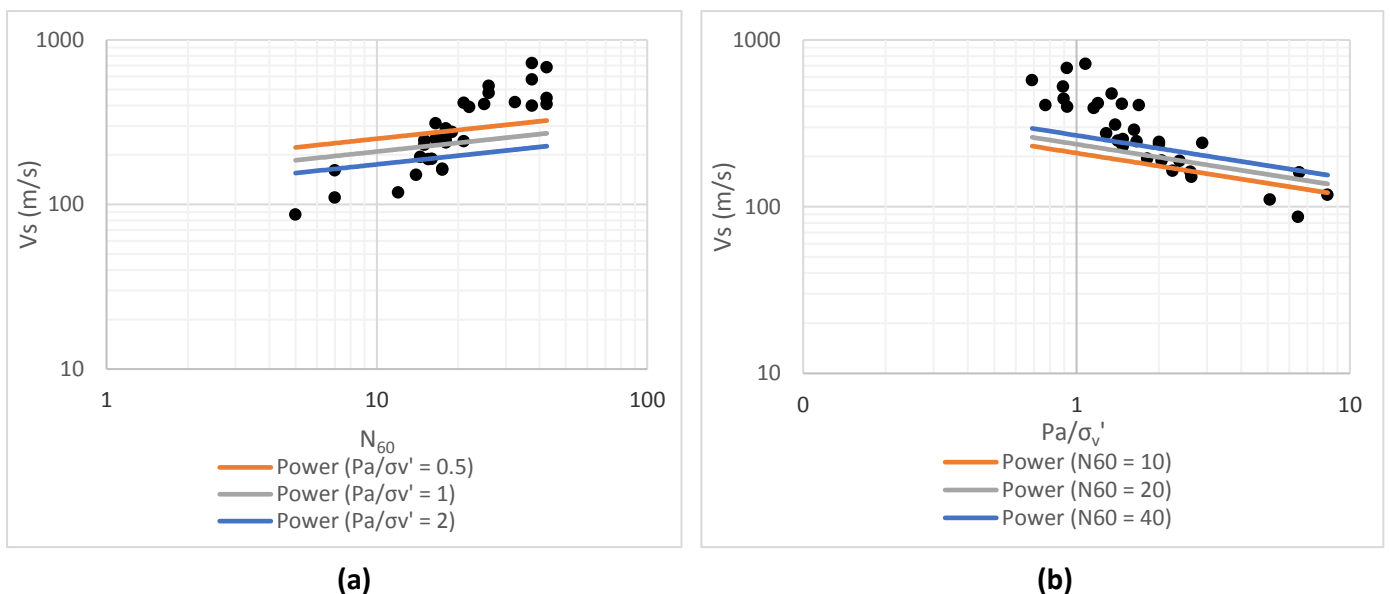
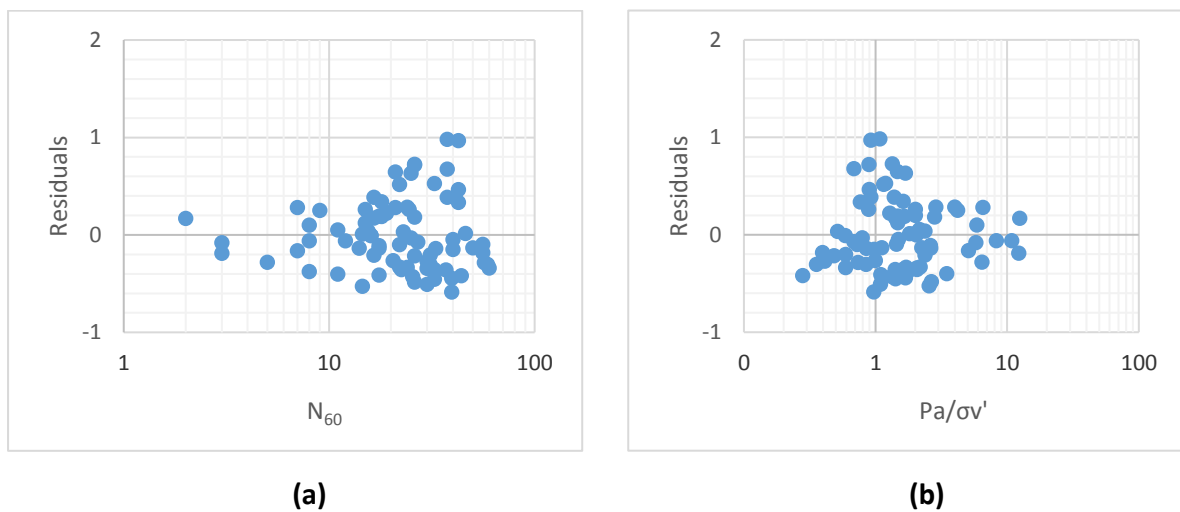


Figure 4-58: Atlantis soils regression results with a)  $V_s$  versus  $N_{60}$  with  $P_a/\sigma_v'$  trendlines and b)  $V_s$  versus  $P_a/\sigma_v'$  with  $N_{60}$  trendlines

Figures 4-57a and 4-58a illustrate the influence of overburden pressure on  $V_s$ . For a given  $N_{60}$  value, higher effective vertical stress corresponds to increased wave velocity. Conversely, for a given value of  $P_a/\sigma_v'$ , higher relative densities ( $N_{60}$  values) return higher values of  $V_s$ , as shown in Figures 4-57b and 4-58b. The results show a stronger correlation between  $V_s$  and  $P_a/\sigma_v'$ , than between  $V_s$  and  $N_{60}$ , which verifies the importance of including overburden in the regression of  $V_s$  and  $N_{60}$ . Notwithstanding this, the large scatter of the data shows that  $N_{60}$  and  $P_a/\sigma_v'$  are not very efficient predictors of  $V_s$ .

Residuals associated with the regression of  $V_s$ - $N_{60}$  data pairs (regression numbers 2 and 4) - producing best-fitting regression models - are plotted against  $N_{60}$  and  $P_a/\sigma_v'$  to examine the appropriateness of the two models (see Figures 4-59 and 4-60). The standard deviations of the regression residuals are 0.220 and 0.361 for regression numbers 2 and 4 respectively. No trends

are observed in the residuals and there are positive and negative values, mostly centred on zero, throughout the range of  $N_{60}$  and  $P_a/\sigma_v'$  values. The regression has therefore removed bias with regards to these independent variables.



**Figure 4-59: Regression residuals versus a)  $N_{60}$  and b)  $P_a/\sigma_v'$  for all data pairs**

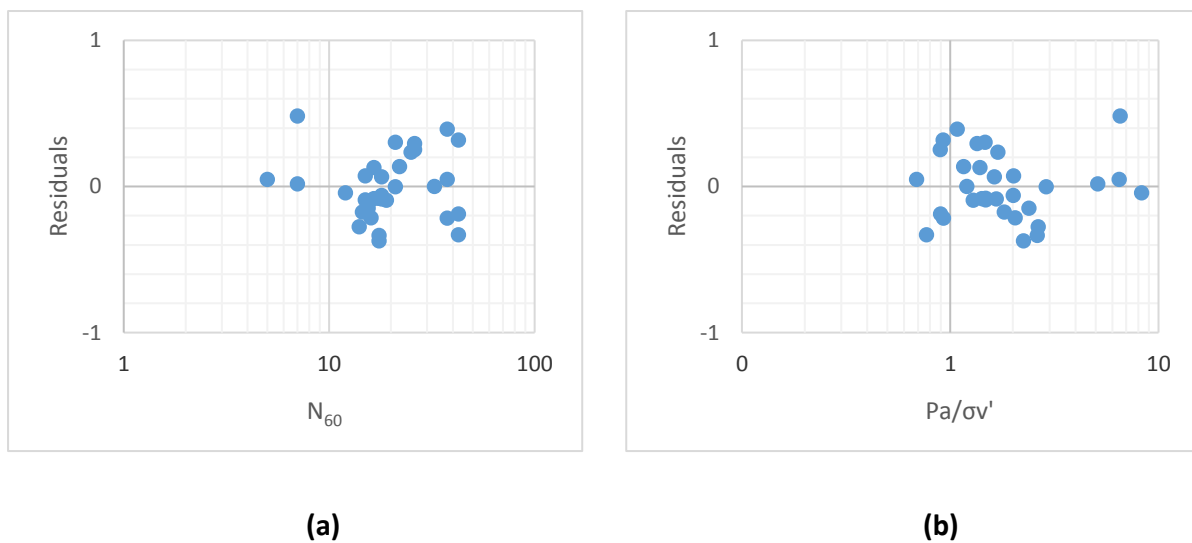


**Figure 4-60: Regression residuals versus a)  $N_{60}$  and b)  $P_a/\sigma_v'$  for Atlantis data**

To assess whether the error terms are normally distributed, the regression residuals were plotted against the theoretical residuals for an assumed normal error distribution (normal scores or Z-scores) (see Figures 4-61a and 4-61b). An approximate straight line should be formed by the residuals, with nonconformity indicating deviations from normality. Deviation from normality is more pronounced in the distribution plot associated with regression of all data points. A near linear plot with minor deviations from normality is shown by the regression errors from the Atlantis data set. Nonetheless, both plots indicate that the errors are reasonably close to normal distributions.

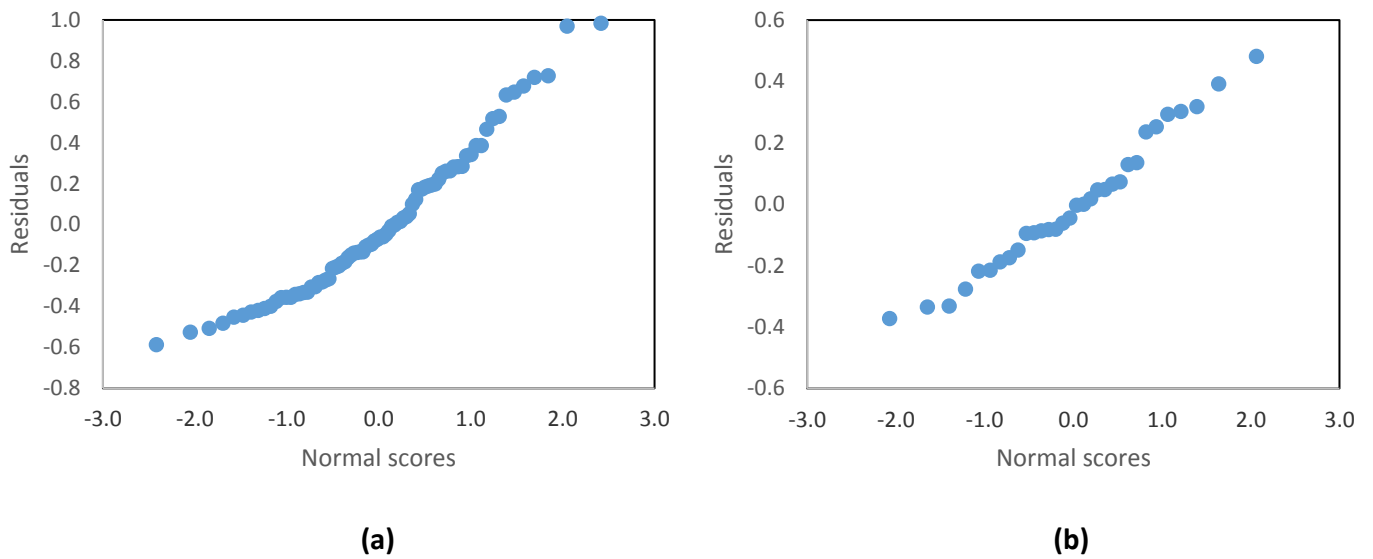


**Figure 4-61: Distribution of regression errors based on a) all data and b) Atlantis data**

Elastic settlement analysis was undertaken for the Cape Flats sands, using a non-linear stepwise method based on estimates of  $G_0$ , which was obtained from the best  $V_s-N_{60}$  model (regression number 4) for typical loose, medium dense and dense soil profiles. The settlement analysis is addressed in Chapter 5.

## 5. Settlement Analysis

### 5.1 Introduction

For granular materials such as the Cape Flats sands, the allowable bearing pressures of foundations will typically be determined by settlement rather than bearing capacity. In the study area, differential settlement may be significant where the consistency of the sands below footings of the same structure vary substantially; for example, compressible sands (possibly with intermittent highly compressible peaty layers in the Springfontyn Formation) and hard calcretised horizons. According to Simons and Menzies (1975), bearing capacity in sands will only become more critical than settlement in instances where shallow footings, less than 1.5 m wide, are founded in loose soils with a shallow water table.

The settlement of shallow foundations on Cape Flats sands is commonly predicted using the results of in-situ tests such as the SPT, DPSH or CPT, due to the difficulty of retrieving undisturbed samples for laboratory testing. Varying degrees of accuracy and reliability are associated with these methods. According to Giddings (1984, as cited in Brink, 1985), settlement predictions from penetrometer results in medium dense or dense sands below spot footings are poorly correlated with observed settlements.

More recently, shear wave velocity profiles obtained from seismic testing are being used for settlement prediction. Such predictions have the advantage of considering non-linear stress-strain behaviour of soil and the degradation of stiffness with increasing strain. However, the tests required to obtain shear wave velocity profiles are seldom undertaken in the study area.

The use of elastic theory, small strain stiffness profiles (obtained from seismic tests) and stiffness degradation data (see Section 2.5.16.3 in Chapter 2), is likely to provide more realistic estimates of soil settlement by considering variations in soil stiffness with depth and strain level. For this reason, a non-linear stepwise method of settlement estimation proposed by Archer (2014) was used to determine the expected foundation settlement in Cape Flats sands using small-strain stiffness data from a  $V_s$ - $N_{60}$  model for Cape Flats sands proposed by the candidate in Section 4.17.3 of Chapter 4. The aim was to demonstrate that it is possible to take account of the non-linear stress-strain behaviour of soils in a simple and practical way, and that the developed correlation allows application of the method even when shear wave velocity measurements are unavailable. Furthermore, and most significantly, comparative settlement calculations are undertaken, with the aim of assessing the outcomes from the abovementioned non-linear stepwise method incorporating stiffness degradation, and other methods of settlement prediction by 1) taking into account strain level indirectly and 2) not taking account of the variation in elastic modulus with strain. All three methods used stress distributions derived from a flexible load on the surface of a semi-infinite elastic half-space (i.e. Boussinesq's method). The differences lie in the method of estimating the stiffness of the profile.

In this chapter, the settlement methodologies are discussed, including the procedures followed to obtain the input data. The settlement prediction results for shallow foundations on Cape Flats sands are presented in graphical form and the outcomes discussed. The settlements given in Section 5.3 should be viewed as examples and not design charts. Site-specific conditions should be considered when predicting the settlement of footings in Cape Flats sand.

## 5.2 Settlement analysis methods

### 5.2.1 Non-linear stepwise method using small-strain stiffness data

The data required for the non-linear stepwise method proposed by Archer (2014) include the small strain shear stiffness ( $G_0$ ) profile, Poisson's ratio ( $\nu$ ), foundation shape and geometry, and the applied load. The application of the method can be summarised as follows:

1. Determine  $G_0$  with depth using an appropriate method.
2. Divide the soil within the zone of influence into layers and assign an  $E_0$  value to each layer ( $E_0$  can be calculated from  $G_0$  using Equation 3-3 from Chapter 3).
3. Determine the contact stress between the foundation and the soil.
4. Select a number of load steps (increments in which the final load is applied).
5. Calculate the vertical and horizontal effective stress increase at the centre of each layer for the first load step using Boussinesq's method. Uniform contact stress distribution (i.e. a flexible loaded area) is assumed.
6. Calculate the vertical and shear strain increments for each layer for the first load step using the appropriate values of  $E_0$ . Plane strain conditions are assumed for strip footings and axis-symmetrical conditions for other foundation shapes.
7. Use a softening function (stiffness degradation curve) to calculate Young's Modulus at the end of the load step, which will also be the new stiffness value for the successive load step.
8. Repeat the process until the maximum contact stress is reached.
9. For each layer, multiply the layer thickness by the vertical strain for the layer to obtain the change in thickness. The sum of the change in thickness of all layers gives the total settlement.

The idea behind this method is to provide a simple and practical way of taking account of small strain stiffnesses and stiffness degradation, without having to resort to numerical analysis, thereby increasing the usefulness of seismic methods of settlement determination in general practice.

The above method has been computerised, with development of the Versak<sup>1</sup> 1.0 and 2.0 settlement software programs. To use the programme, appropriate values of  $G_0$  and  $\nu$  must be assigned to a maximum of eight soil layers and the foundation information (geometry, shape and contact stress) provided. One hundred load increments are used. Versak 2.0 uses, amongst others, stiffness reduction functions developed by Archer and Heymann (2015) for loose ( $D_r = 20\%$ ), medium dense ( $D_r = 50\%$ ) and dense ( $D_r = 80\%$ ) sand. The properties of the sand used by Archer and Heymann (2015) are similar to those of the Cape Flats sands and the proposed stiffness reduction functions are considered appropriate for the current analysis.

Archer and Heymann (2015) used the following hyperbolic relationship proposed by Oztoprak and Bolton (2013) as a softening function:

$$\frac{G}{G_0} = \frac{1}{\left[1 + \left(\frac{\gamma - \gamma_e}{\gamma_r}\right)^n\right]} \quad \text{Equation 5-1}$$

<sup>1</sup> Versak is the Afrikaans word for settle

Where:

$G$  = Shear modulus

$G_0$  = Small strain shear modulus

$\gamma$  = Shear strain (current)

$\gamma_e$  = Elastic threshold shear strain

$\gamma_r$  = Reference shear strain

$n$  = Curvature parameter

The variables for the softening functions determined for the three densities are shown in Table 5-1 and softening curves are shown in Figure 5-1.

**Table 5-1: Softening function variables**

Loose sand		Medium dense sand		Dense sand	
$\gamma_e$	0.001	$\gamma_e$	0.001	$\gamma_e$	0.001
$\gamma_r$	0.005	$\gamma_r$	0.015	$\gamma_r$	0.03
$n$	0.35	$n$	0.35	$n$	0.35

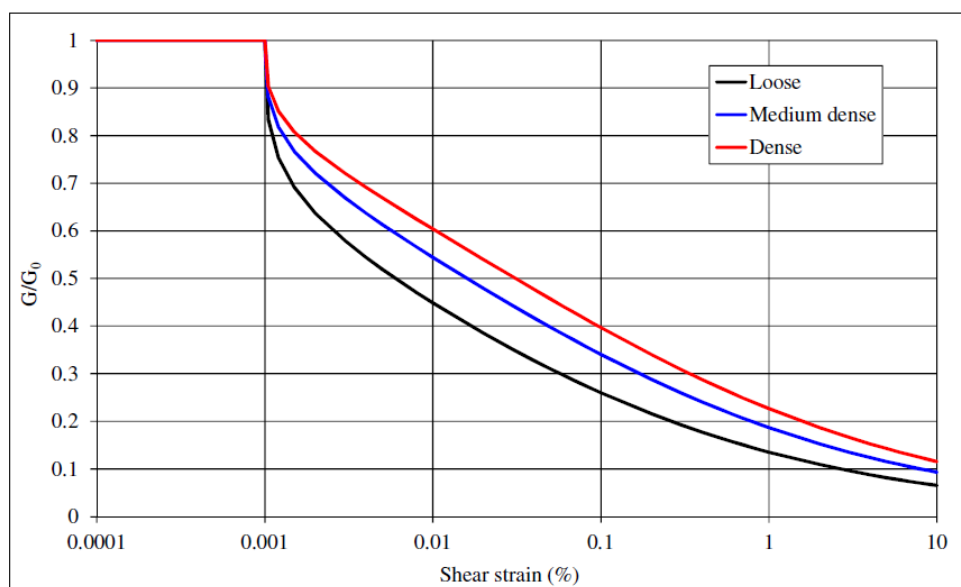


**Figure 5-1: Softening functions proposed by Archer and Heymann (2015)**

Archer and Heymann (2015) caution that the accuracy of the method decreases as the density index increases, being within 12% for loose sand, 22% for medium dense sand, and 30% for dense sand. In addition, the proposed  $V_s$ - $N_{60}$  model used in the analysis achieved an  $R^2$  value of 0.83, introducing additional uncertainty. The settlements plots presented in Section 5.3 should therefore be viewed in this context.

#### 5.2.1.1 Input data

The expected settlement of a series of shallow foundations on Cape Flats sand was estimated using Versak 2.0 settlement analysis software. The soil input parameters and foundation information required for analysis are discussed below.

### **Soil parameters**

The non-linear stepwise settlement prediction method requires  $G_0$  profiles as well estimates of  $v$  (to calculate  $E_0$ ). The following method was used to obtain these parameters:

1. From the candidate's SPT database, three individual SPT profiles from the study area were selected; that is, a typical loose, medium dense and dense sand profile (note that the loose profile was formed by combining SPT data from two boreholes – 0 to 8.45m and 8.45m to 12.45m). The aim was to apply the softening functions proposed by Archer and Heymann (2015) for soils with similar densities. For the loose, medium dense and dense sands, the density index ranged from 15% to 35%, 35% to 65%, and 65% to 85% respectively (Das and Sivakugan, 2019). The selected SPT  $(N_1)_{60}$  profiles for soils from Athlone (loose Springfontyn Formation sand), Airport Industria (medium dense Witzand Formation sand) and Mitchell's Plain (dense Langebaan Formation sand) are shown in Figure 5-2. The maximum depth of the profiles was aligned with the deepest profile in loose sand.
2. The following regression equation proposed by the candidate for Cape Flats sands was used to obtain estimates of  $V_s$  (in m/s) from the SPT blow counts:

$$V_s = 64.1(N_{60})^{0.555}(P_a/\sigma'_v)^{-0.344} \quad \text{with } R^2 = 0.83 \quad \text{Equation 5-2}$$

Where:

$P_a$  = Atmospheric pressure (taken as 101kPa)

$\sigma'_v$  = Overburden pressure at test depth (kN/m<sup>2</sup>)

3.  $G_0$  profiles were subsequently obtained from the  $V_s$  estimates using Equation 3-2 from Chapter 3. The density and Poisson's ratio were estimated from the corrected SPT profiles. The  $G_0$  profiles associated with the loose, medium dense and dense sands are shown in Figure 5-3.
4. The soil within the foundation zone of influence was then divided into uniform layers, each with a  $G_0$  and  $v$  estimate.

In addition, and as discussed in Section 4.17.3 of Chapter 4, comparison of the abovementioned model with similar models for Holocene aged sands, reveals higher estimates of  $V_s$  with the proposed model. A closer comparison can be drawn between  $V_s$  estimates for Pleistocene aged deposits. It is thus more suited to cemented Cape Flats sands and the older Springfontyn Formation deposits, in which the soils have a higher dependence of shear wave velocity on void ratio than Holocene-age soils (Fumal and Tinsley, 1985 as cited in Sykora, 1987).

### **Foundation information**

The expected settlement was calculated for different sizes of square ( $L/B=1$ ) and strip footings ( $L/B \geq 10$ ) for a range of bearing pressures. The depth to groundwater was taken into account when calculating  $V_s$  from the SPT blow counts via its effect on overburden pressure. The Versak programme calculates the settlement at the centre of a flexible loaded area and does not include any correction factors. The settlement estimates were corrected for founding depth ( $D$ ) using the correction proposed by Fox (1948) (as cited in Lutenegger and DeGroot, 1995), and a correction factor of 0.8 applied for foundation rigidity. The foundation sizes and other varied parameters are

given in Table 5-2. The width of the strip footing was restricted to 4m, ensuring the depth of influence does not exceed the depth to which there are available SPT data.

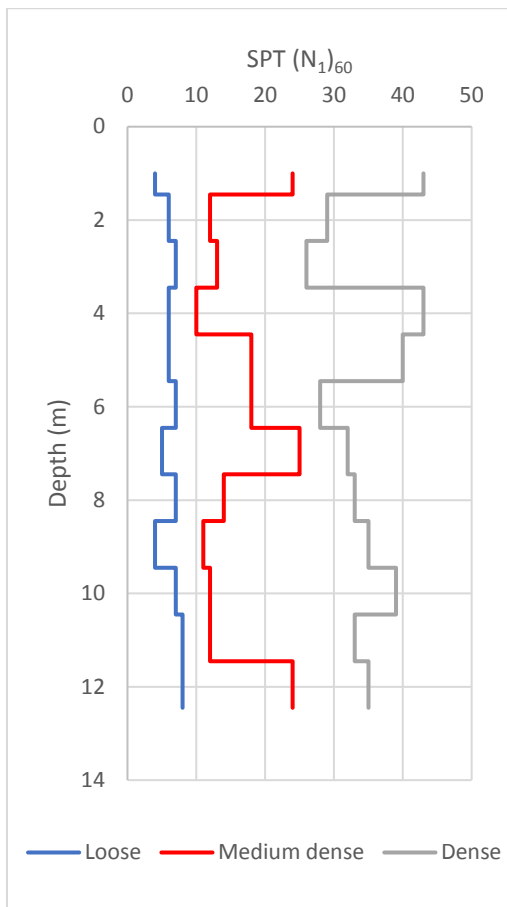


Figure 5-2: SPT ( $N_1$ )<sub>60</sub> profiles

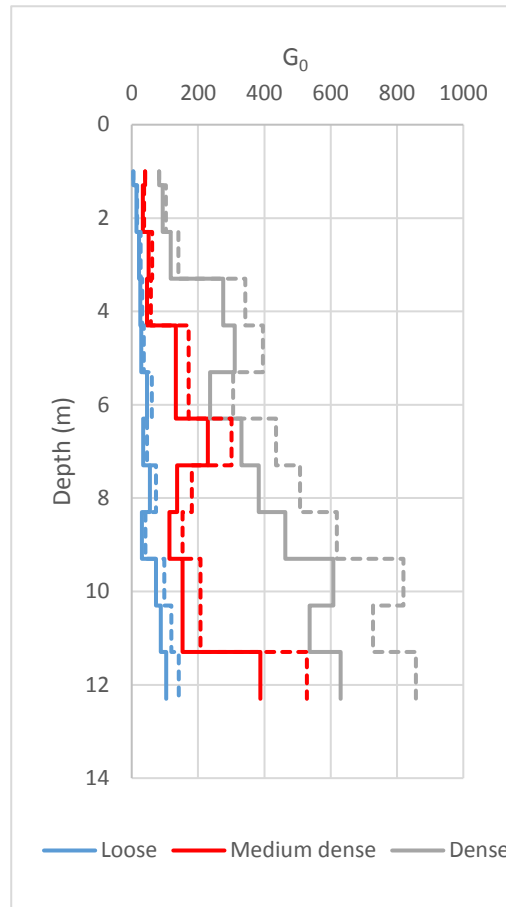


Figure 5-3:  $G_0$  profiles (solid line: WT = 1.5m, dotted line: no WT)

Table 5-2: Variables of analysis (non-linear stepwise method)

Variable	Range
Foundation width (m)	0.5 to 5 (Strip footing limited to 4m)
Foundation shape	Square and strip
Net bearing pressure, $q_n$ (kPa)	50 to 500 (limited to 250 in loose sand)
Founding depth, $D$ (m bgl)	1.0 and 2.0
Water table depth (m bgl)	1.5 and no WT

### 5.2.2 General elastic solution using SPT $N_{60}$ -E transformation models

For the same three SPT profiles (loose, medium dense and dense sands), the foundation settlement was calculated using the general elastic solution with stiffness profiles determined using Stroud's (1989) and Webb's (1969) SPT  $N_{60}$ -E transformation models. The equation on which the analyses are based, is as follows:

$$S = F_R \cdot F_D \int_0^z \frac{\Delta\sigma'_v}{E} dz \quad \text{Equation 5-3}$$

Where:

S = Total settlement (mm)

$F_R$  = Rigidity correction (0.8 for rigid loaded area)

$F_D$  = Depth correction factor (Fox, 1948 as cited in Lutenege and DeGroot, 1995)

E = Soil elastic modulus (MPa)

$\Delta\sigma'_v$  = Vertical stress increment (kPa) based on a Boussinesq-type stress distribution.

### 5.2.2.1 Input data

For the comparative study, a 2m square and a 2m wide strip footing, both at 1m depth with the water table at 1.5m depth, are analysed. The soil input parameters and foundation information required for analysis using the general elastic solution are discussed below.

#### Soil parameters

The soil elastic modulus was estimated using the SPT-based transformation models proposed by Stroud (1989), which recognises the influence of strain and stiffness, and Webb (1969), which does not consider the influence of strain. Stroud's plot of ratio  $E/N_{60}$  (in  $\text{MN/m}^2$ ) versus degree of loading,  $q_{\text{net}}/q_{\text{ult}}$ , are shown as Figure 3-30 in Section 3.5.11 of Chapter 3, and Webb's SPT  $N_{60}$ -E relationship is presented as Equation 2-14 in Section 2.5.16.1 of Chapter 2.

The following steps were followed to determine the foundation settlement:

1. Estimate the friction angle of the founding soil (within the influence bulb) based on the average SPT blow count. An appropriate value was selected based on the  $[(N_1)_{60}-\phi']$  transformation models proposed by Chen (2004), Kulhawy and Mayne (1990) and Wolff (1989) (as cited in Hettiarachchi and Brown, 2009). These models are given as Equations 3-40 to 3-42 in Chapter 3.
2. Determine the ultimate bearing capacity using the following soil parameter values (based on Meyerhof's, 1963 method):  
 Loose sand:  $\phi' = 32^\circ$ ,  $c' = 0\text{kPa}$ ,  $\gamma = 16\text{kN/m}^3$ ,  $\gamma_{\text{sat}} = 18\text{kN/m}^3$ .  
 Medium dense sand:  $\phi' = 35^\circ$ ,  $c' = 0\text{kPa}$ ,  $\gamma = 17\text{kN/m}^3$ ,  $\gamma_{\text{sat}} = 19\text{kN/m}^3$   
 Dense sand:  $\phi' = 38^\circ$ ,  $c' = 0\text{kPa}$ ,  $\gamma = 18\text{kN/m}^3$ ,  $\gamma_{\text{sat}} = 20\text{kN/m}^3$
3. Determine the  $q_{\text{net}}/q_{\text{ult}}$  ratios for use in Stroud's transformation model using the selected net foundation pressures (50 to  $500\text{kN/m}^2$ ).
4. Obtain the  $E/N_{60}$  ratio from Stroud's plot, reading from the over-consolidated sand and gravel soil curve.
5. Determine the elastic modulus profiles corresponding to the selected SPT  $N_{60}$  profiles based on Stroud's and Webb's transformation models.
6. Perform elastic settlement analysis based on a Boussinesq-type stress distribution, corrected for depth of founding and foundation rigidity.

## **Foundation information**

The foundation information is summarised in Table 5-3.

**Table 5-3: Variables of analysis (general elastic solution)**

Variable	Range
Foundation width (m <sup>2</sup> )	2
Foundation shape	Square and strip
Net bearing pressure, $q_n$ (kPa)	50 to 500 (limited to 250 in loose sand)
Founding depth, D (m bgl)	1.0
Water table depth (m bgl)	1.5

## **5.3 Predicted settlements**

### **5.3.1 Versak analysis results**

The expected settlements in the loose, medium dense, and dense sands, calculated from the small strain stiffness data (linear stepwise method) are shown graphically in Figures 5-4 to 5-9. Note the different y-axis scales used for the loose, medium dense and dense sand plots. The results of the analysis of the strip footings are shown on the graphs as dotted lines. The settlements associated with the range of footing sizes and net bearing pressures are shown at founding depths of 1m and 2m below ground level. The depth to groundwater typically has minimal influence on the calculated settlements (only influencing the  $G_0$  values via the overburden pressure). Within the zone of influence, the difference in  $G_0$  with varying water level (as shown in Figure 5-3), resulted in minor differences in estimated settlements, and only the results associated with a water table level of 1.5m bgl are shown. From Figures 5-4 to 5-9 it is evident that for footings carrying the same pressure, an increase in footing size, and hence the depth of the zone of influence, results in an increase in settlement. The settlement of the deeper foundation is less than that of the shallower one, which can be ascribed to the increase in lateral confining pressure with depth. The magnitude of settlement below a footing is strongly dependent on the density index of the sand. This is evident in the results, with the magnitude of settlement decreasing rapidly as the relative density increases and there is less scope for particle rearrangement.

For footings on sand, maximum settlements are generally limited to 25mm. In the loose sands, the maximum expected settlements often exceed this limit. Where the net bearing pressure is limited to 50kPa in the loose sand, footing widths up to 3m (at 1m bgl) and 4m (at 2m bgl) give acceptable settlements (<25mm). As the bearing pressure increases, only smaller footing sizes meet the limiting settlement criterion. For the smallest square footing (0.5m x 0.5m in size), settlements are within acceptable limits up to 250kPa, reducing to approximately 125kPa in the case of a strip footing. The analyses show that the strip footings in loose sand settle by as much as 2.4 times more than the square footings with the same width. As the foundation size increases, this difference in estimated settlement diminishes (to zero for the 3m and 4m wide footings), a function of the stress distribution below the different footing shapes as well as soil consistency.

In the medium dense sand, expected settlements are greatly reduced (compared to the loose sand). For all footing sizes, net bearing pressures up to approximately 270kPa are associated with settlements below 25mm. For the 0.5 and 1m wide footings, the expected settlements are less than 25mm for all considered foundation pressures. The estimated settlement below the strip footings is between  $\pm 1.1$  and 3 times more than the settlement below corresponding (same width) square footings. Where the depth to groundwater is below the depth of influence, the settlement of the 5x5m footing with  $q_n = 500\text{kPa}$  decreases by about 15%.

In the dense sands, the estimated settlement below the strip footings is up to 2.5 times greater compared to the square footings. The settlement of footings founded  $\geq 1\text{m}$  below ground is less than 25mm for all square and strip foundation sizes and bearing pressures.

### 5.3.2 Comparative analyses results

In this section, the results for the 2m wide square and strip footings from the non-linear stepwise method are compared to the results obtained using Stroud and Webb's correlations between SPT  $N_{60}$  and the soil elastic modulus. The results are shown in Figures 5-10, 5-11 and 5-12 for the loose, medium dense and dense sands respectively. The elastic moduli from Stroud's and Webb's transformation models, are tabulated in Appendix H.

For the loose sand, similar settlement estimates are obtained with the general elastic solution using Stroud's and Webb's transformation models, with the lower estimates associated with Webb's method. As the strain level increases, the settlement estimates associated with Stroud's method increase more rapidly than the estimates obtained using Webb's method, showing the effect of disregarding strain in the determination of soil stiffness. The settlement estimates from the non-linear stepwise method, based on small strain (using Versak), are notably higher than the settlements obtained using the general elastic solution. For the square and strip footings respectively, settlement estimates using Versak are  $\pm 2$  and 3.5 times greater than estimates using Stroud's method. These higher estimates are expected due to the large strains associated with footings on loose sands.

For the medium dense sand, similar settlement estimates are once again achieved using Stroud's and Webb's transformation models, but now with the lower estimates associated with Stroud's method. The elastic moduli obtained using Webb's method (single E modulus profile, irrespective of soil consistency) is lower than the stiffnesses at corresponding depths at all strain levels obtained from Stroud's method. As the net pressure increases, the percentage difference between the settlement estimates decreases as the soil stiffness profiles draw closer together. The settlement estimated using Versak is about half of the settlement determined using the other methods. The difference between the settlement of the square and strip footings for Stroud's and Webb's methods is greater than obtained using Versak.

In dense sand, the effect of increased stiffness at small strains is clearly evident with the estimates from Versak and Stroud's method being significantly lower than those from Webb's method. However, it appears that even the high ratios of  $E'$  to  $N_{60}$  at low values of  $q_{\text{net}}/q_{\text{ult}}$  in the Stroud model are insufficient to match the high stiffnesses predicted by the small strain stiffness model at low strains.

### 5.3.3 General comments

Most of the settlement in the Cape Flats sands will occur during construction and initial loading. The magnitude of differential settlement will be determined by variations in the homogeneity of the sand within the zone of influence below the footing, the geometry of the footing and the applied loads. The depth of the water table has a lesser effect. In the study area, significant lateral variability in consistency was noted, even over very short distances. This is due to both inherent spacial variability and the presence of cemented layers or compressible peat and soft clay. In extreme cases, the differential settlement may be almost equal to the total settlement. The profiles selected for the settlement analysis comprised only of aeolian sands. The presence of soft clay and peat layers in the sandy soil profile will have a significant influence on the maximum anticipated settlement.

Both Stroud's method and the small strain stiffness method predict higher stiffnesses for medium dense and dense profiles than Webb's method, which takes no account of strain level in the determination of soil stiffness. Webb's method appears to be suitable for loose sands only.

The Versak software appears to underestimate differences in settlement between square and strip footings of similar width.

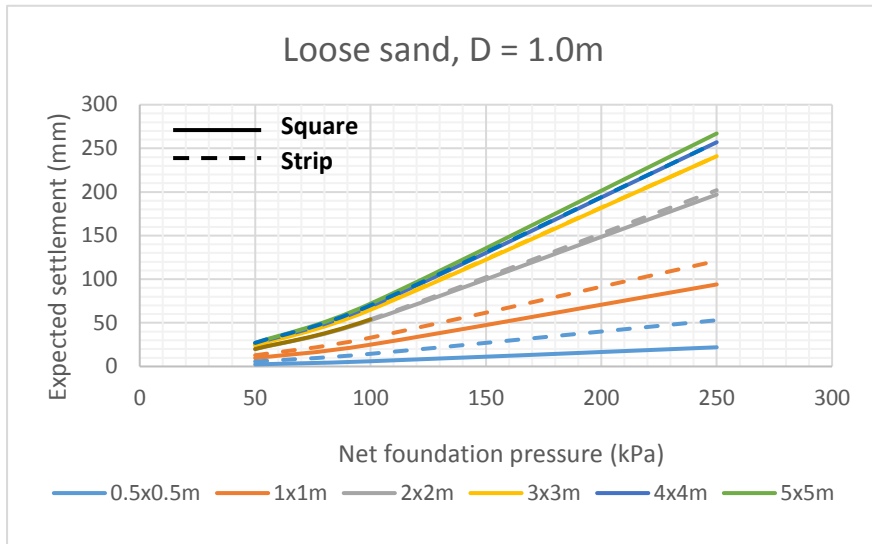


Figure 5-4: Settlement of square and strip footings at 1m in loose sand

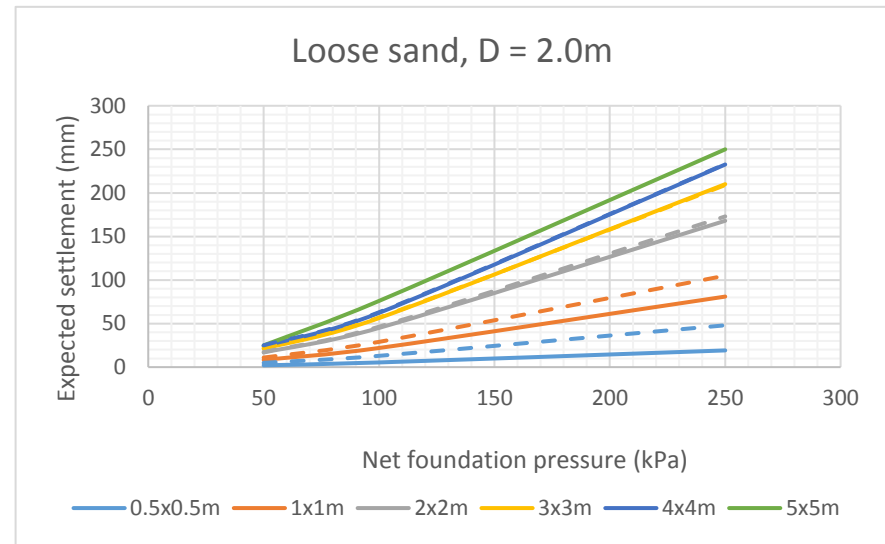


Figure 5-5: Settlement of square and strip footings at 2m in loose sand

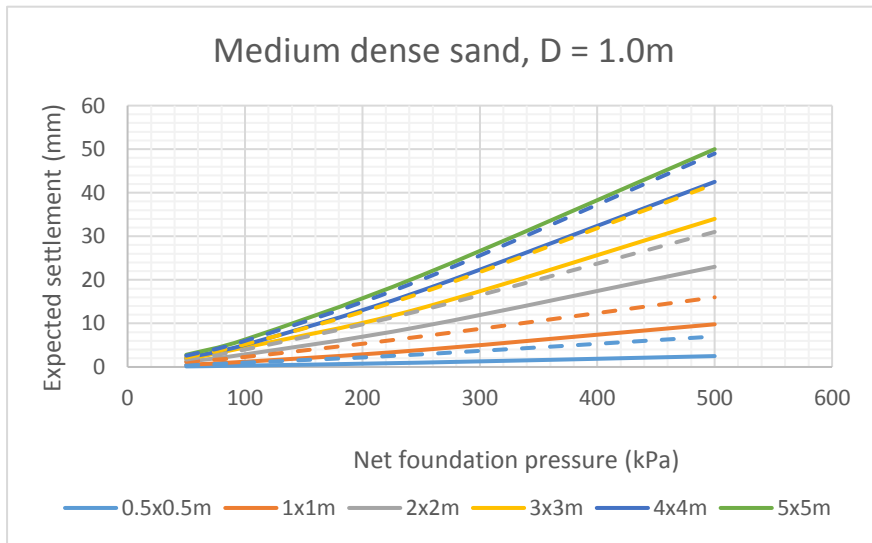


Figure 5-6: Settlement of square and strip footings at 1m in med dense sand

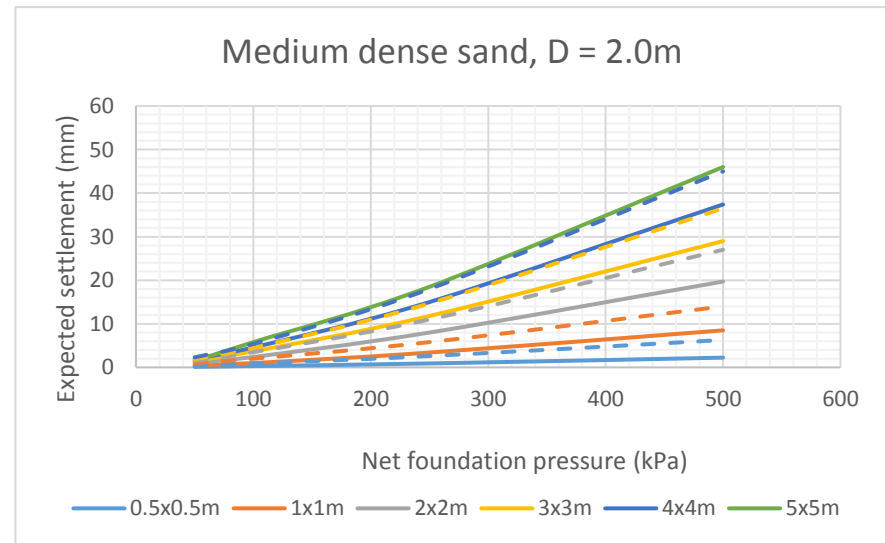


Figure 5-7: Settlement of square and strip footings at 2m in med dense sand

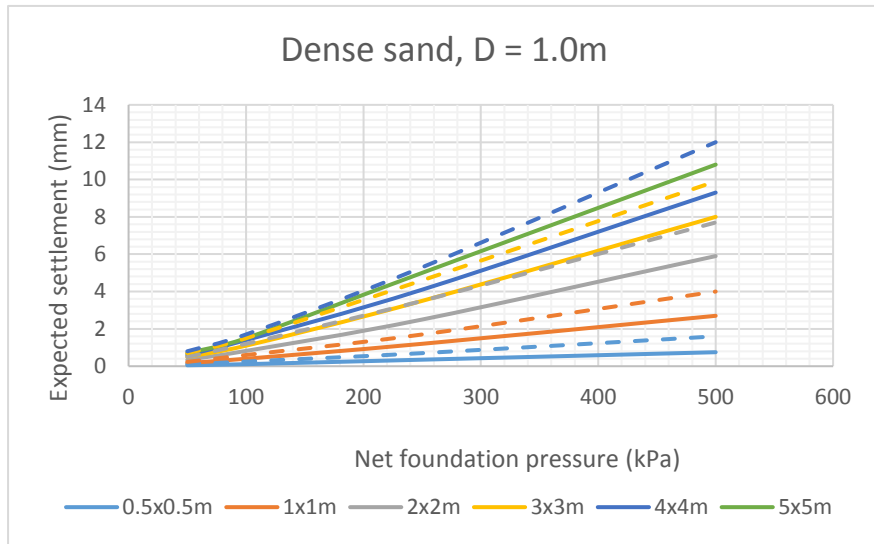


Figure 5-8: Settlement of square and strip footings at 1m in dense sand

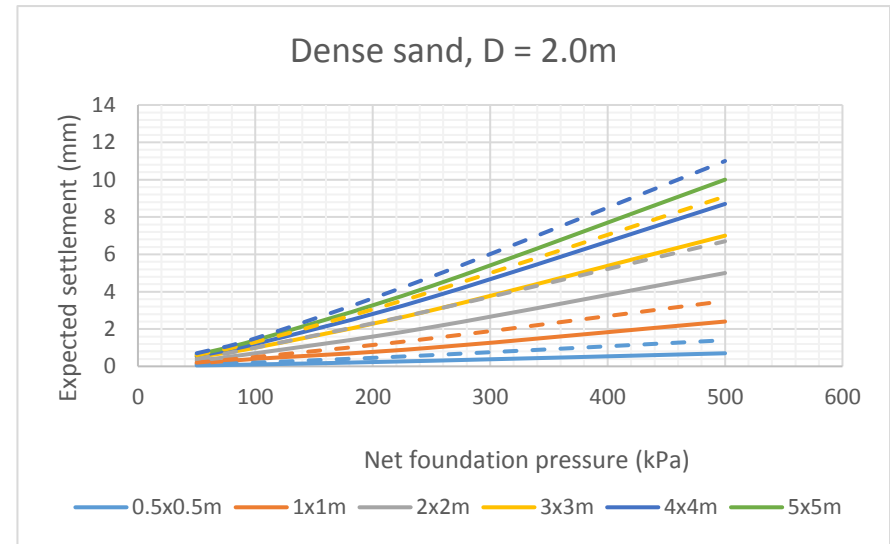


Figure 5-9: Settlement of square and strip footings at 2m in dense sand

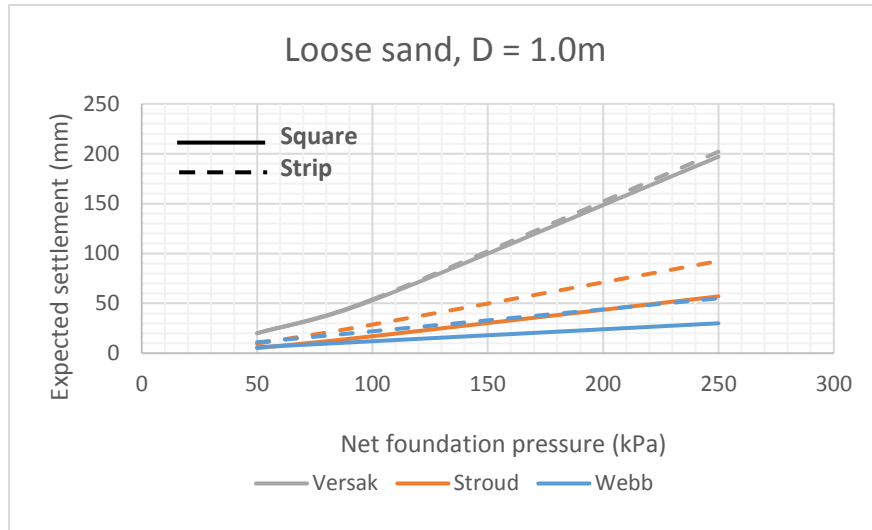


Figure 5-10: Settlement comparison in loose sand (B = 2m and WT = 1.5m)

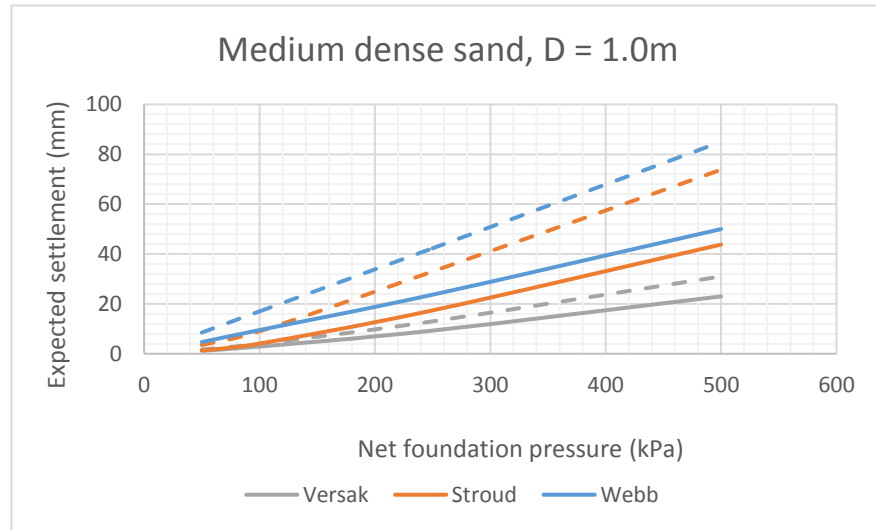


Figure 5-11: Settlement comparison in medium dense sand (B = 2m and WT = 1.5m)

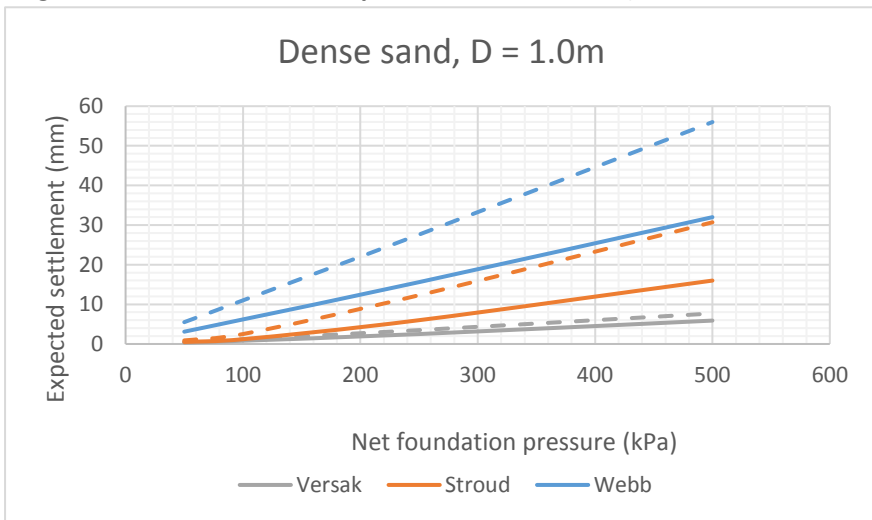


Figure 5-12: Settlement comparison in dense sand (B = 2m and WT = 1.5m)

## 6. Conclusions, Summary of Properties and Recommendations

### 6.1 Introduction

As stated in the introductory and literature chapters, there are very few publications on the geotechnical and engineering geological properties of the upper Quaternary age sands of the Cape Flats. Many geotechnical investigations have been undertaken in the area; however, the valuable geotechnical data from these investigations has largely remained uninvestigated and unpublished. The aim of the research was to present the first major contribution towards classifying and describing the recent aeolian sands covering the entire Cape Flats area in terms of their physical properties and engineering behaviour. In-situ and laboratory data from 155 site investigations undertaken in the study area - including 953 soil investigation points - were collected and documented. In addition, methods of investigation and testing not commonly used in the area were included in this research, including, piezocone penetrometer testing (CPTu), continuous surface wave (CSW) testing, double ring infiltrometer testing and monotonic and repeated load triaxial tests.

The sands from the Witzand, Springfontyn and Langebaan Formations were classified based on their grading properties, Atterberg limits, maximum dry density and optimum moisture content, minimum dry density, California Bearing Ratio (CBR), erodibility and corrosivity, and characterised in terms of their compressibility, shear strength, permeability, volumetric behaviour during shear including liquefaction potential, in-situ density, moisture content and specific gravity. The geotechnical properties that characterise the distinctive sand formations were explored to produce statistical results, revealing underlying patterns, distinctive trends, distributions and correlations, and the resultant practical importance and probable implications were explored. Focus was placed upon determining the nature of the relationships between the soil parameters, specifically for the sands of the Cape Flats, and any inter-formation variation in such relationships. One such relationship between  $V_s$  and SPT  $N_{60}$  enabled elastic settlement analysis using small-strain stiffness data, and subsequent comparative settlement analyses.

The objectives of the research are set out in Section 1.3 of Chapter 1 and the methods used to achieve these objectives are presented in Chapter 3. The results associated with the classification and characterisation of the Cape Flats sands are presented, interpreted and evaluated in Chapter 4, and the settlement analysis is addressed in Chapter 5. In the current chapter, the important findings discussed in detail in Chapters 4 and 5 are highlighted to emphasise the findings of the research and the main research questions are addressed. For each formation, a summary of the soil properties is tabulated (see Tables 6-1 to 6-3). To avoid outliers detracting from specific properties and behaviours, soil properties were further divided into classes of the Unified Soil Classification System. Recommendations are also made for future research.

## 6.2 Conclusions

### 6.2.1 Soil classification properties

Based on the results of this study, various conclusions can be drawn concerning the classification properties of the Cape Flats sands. Focus is placed on highlighting inter-formation variation in these properties.

- The typically steep particle size distribution (PSD) curve associated with the shallow Cape Flats sands reflects the predominance of particle sizes between 0.075mm and 0.6mm (fine and medium sand). The sands are typically “clean” sands with fines contents (silt and clay) of around 5%. The Springfontyn Formation has a slightly higher fines content than the Witzand and Langebaan Formations. ANOVA testing confirmed significant differences between the Witzand and Springfontyn Formations in terms of fine sand and fines contents.
- The findings indicate a slight decrease in the average fine sand content from surface to 3m depth in all formations. A slight increase in the average clay and silt content is noted from surface to 3m depth in all formations. Although these trends can possibly be explained by geological processes (e.g. fine sands remaining mobile whilst coarser fraction settles under gravity) data become much sparser with depth and these findings are therefore inconclusive.
- The narrow grading of the sands is reflected in the soil gradation coefficients, showing predominantly uniformly graded deposits, which do not satisfy the criteria for a well graded soil ( $C_u > 6$  and  $1 < C_z < 3$ ). Sands from the Witzand Formation have a higher degree of uniformity than those from the Springfontyn and Langebaan Formations, reflected in both the soil textures and gradation results. ANOVA testing confirmed statistically significant variation of the  $C_u$  and  $C_z$  values between the Witzand and Springfontyn Formations.
- The aeolian sands of the Cape Flats are typically non-plastic or slightly plastic in nature. The lower clay contents characteristically associated with the soils from the Witzand and Langebaan Formations are reflected in the low percentage of soils with measurable PI.
- When comparing individual clay content – PI pairs for soils from the Witzand, Springfontyn and Langebaan Formations, similar clay contents consistently produce higher PI's in the Witzand Formation. This is most likely due to clay mineral type, with kaolinite likely being dominant in the Springfontyn and Langebaan Formations, and Illite (or potentially a smectite clay) presumably present in the Witzand Formation.
- Compacted dry densities above 1850kg/m<sup>3</sup> were seldom achieved using Modified AASHTO compaction effort. The predominance of fine sand sized particles (uniform gradation) hinders proper densification, possibly exacerbated by the presence of angular carbonate shells.
- Soils from the Langebaan Formation typically achieved the lowest compacted densities at the highest OMCs and the Springfontyn Formation showed the highest compacted densities and lowest OMCs. ANOVA statistical testing revealed that the variation between the means of all three MDD data sets are significant.
- Higher compaction densities were often associated with an increase in the range of particle sizes (wider PSD curve). The controlling factor is the distribution of the grain sizes and the difference in average particle size. However, variability between seemingly similar soils was noted as well as anomalous results such as similar gradings producing differing maximum dry densities. These anomalies could be due to variation in particle shape or differences in the quality of results from different testing laboratories.

- Grading parameters were found to be relatively poor predictors of MDD and OMC, particularly at the upper and lower end of the achieved densities and OMCs. It is advised that the proposed transformation models be used cautiously and that MDD and OMC values be determined directly using the Modified AASHTO test.
- Despite the compacted densities characteristically being highest in the Springfontyn Formation and lowest in the Langebaan Formation, the CBR results show an opposite trend; the bearing strength of the Langebaan Formation sands are typically the highest, followed by the Witzand Formation sands. ANOVA statistical analysis showed that, overall, the variation in CBR between formations is not well defined and varies with compaction level. The outcome is likely to differ (and possibly become more distinct) with larger data sets.
- As expected, a decrease in bearing strength (CBR) was noted with decreasing percentage compaction. Despite this, a strong relationship between individual CBR and dry density values did not emerge. Soil coarseness, as measured by the grading modulus, was found to influence CBR, although not the main determining factor. Including the grading modulus in the analysis provided only a marginal improvement in the prediction of CBR.
- In the Witzand and Langebaan Formations, refusal of the DCP probe often occurred at shallow depth (<1m), presumably on calcretised sands, which reflected in the DCP CBR values. Below the calcretised sands, soils of lower density were often intersected. The gradual decrease in DN (and increase in DCP CBR) with depth noted in the Springfontyn Formation probably reflects the effect of friction on the rods in the fine sands and silty and/or clayey sands.
- The soils in the study area were classified mainly as G7, G8 and G9 quality materials according to the TRH14 system. The highest percentage of low quality G10 soils was recorded in the Springfontyn Formation.
- The estimated material G classes from DCP CBR (using the proposed relationship by Paige-Green and Du Plessis, 2009), were found to be lower than those presented above (typically G10 or worse quality). This could be due to the in-situ density being lower than that used in the TRH14 classification.
- Most of the investigated soils from all three formations were classified as non-plastic, fine sandy materials (class A-3), according to the AASHTO classification system. In the Springfontyn Formation, a higher percentage of the soils fell in groups A-2-4 (silty or clayey gravel sand) and A-4 (silty soils), compared to the other formations. This outcome was expected and agrees with the grading results. The assigned classes are typically associated with good to excellent subgrade material quality.
- The USCS classified most of the soils from all three formations as SP (poorly graded sand with less than 6% fines). Most of the remaining soils fell into the SM, SC, or SM-SC categories (silty and/or clayey sand) or SP-SM or SW-SM (combination soils).
- The minimum index density varies from approximately 1420kg/m<sup>3</sup> to 1590kg/m<sup>3</sup>. Higher minimum densities are typically associated with higher  $C_u$  values, (often soils with an appreciable medium sand, coarse sand, and/or gravel fraction).
- The high percentage of moderately and strongly alkaline soils, the widespread presence of soils with low electrical resistivity, and the saline groundwater from the coastal area of Macassar, pose a corrosion risk to buried steel and concrete.
- The aggressiveness of the ground and groundwater in the study area will vary widely, based on factors such as contamination, evaporation rates and the depositional history.

- The susceptibility of soil grains to detach and be transported by rainfall and runoff in the study area is typically very low, which can be attributed to the low silt and very fine sand content (0.002mm to 0.1mm particle sizes) - representing particles vulnerable to detachment - and the high permeability resulting in rapid infiltration and less runoff.
- Unpaved roads using Cape Flats sand as a wearing course will be prone to corrugation and ravelling. A small percentage of soils from the Springfontyn and Langebaan Formations was found to be prone to erosion by surface water flow (based on its shrinkage product and grading coefficient).

### 6.2.2 Soil characterisation properties

Based on the results of this study, the following conclusions can be drawn concerning the characterisation properties of the Cape Flats sands:

- The specific gravity of soils with predominantly sand-size grains, ranges between 2.62 and 2.69. The range of values obtained for seemingly similar soil textures can be ascribed to the mineralogical makeup of the soils, which contain varying combinations of quartz, feldspar, kaolinite and illite, each with a characteristic particle density. Soils containing organic matter were associated with lower values of  $G_s$ .
- In-situ dry densities in the upper 1m of the soil profile range from 1571kg/m<sup>3</sup> and 1844kg/m<sup>3</sup>, representing the characteristic loose, shallow sands and the dense cemented sands of the Witzand and Langebaan Formations.
- Significant variation in the depth to groundwater is expected in the study area, possibly over short distances. The main influencing factors are the topography and the formation of perched water tables above low permeability layers and lenses of pedogenic material or clay. Seasonal fluctuations at any specific location can be significant. The influence of shallow groundwater on settlement and bearing capacity of the sands should be considered in all instances.
- The low density, non-plastic sands are compressible but are either non-collapsible or possessing a low collapse potential when saturated. Exceptions include soils with plastic fines (which are uncommon) and soils with other bonding agents such as salts. Sands from the Springfontyn Formation with higher fines content and from the Langebaan Formation with calcium carbonate as cementing agent may be susceptible to collapse settlement.
- The unconsolidated aeolian sands from the study area are mostly semi-pervious ( $10^{-4}$  to  $3 \times 10^{-7}$  m/s), as determined by constant head permeability tests. The associated soil types range from clayey silty fine sand to well-graded sand. The wider range of hydraulic conductivities previously documented for Cape Flats deposits reflect the presence of cohesive soils, peaty layers and cementation.
- The permeability prediction methods by Carrier (2003) and Chapuis (2004), based on grading and in-situ density, produce higher estimates of soil permeability than laboratory determined values. These predictive methods are therefore considered unsuitable for use with the Cape Flats sands.
- Surface infiltration rates in the study area are typically moderate to high, which will result in generally minor runoff or ponding, aiding recharge of the unconfined aquifer underlying the study area.
- For sands with a range of textures (e.g. clayey silty sands, fine uniform sands and well-graded sands) and densities, the peak friction angles vary from about 30° to 40°, with cohesion values

up to about 13kPa. For soils compacted to similar dry densities, coarser soils and/or soils with a wider range of particle sizes are typically associated with higher values of  $\phi'_{\max}$ . No clear relationship emerged between  $\phi'_{\max}$  and density for soils with similar textures.

- CPT inferred  $\phi'_{\max}$  values were found to be higher than the SPT inferred values at a similar density indices. The SPT derived results are more in line with, but still higher than the results of the direct shear strength tests.
- Significant variation in soil consistency was noted, both horizontally and vertically in the study area, with frequent trend reversals. Variation in penetration resistance with depth in normalised profiles [SPT  $(N_1)_{60}$  values] is mostly associated with changes in soil type and/or degree of cementation. ANOVA testing revealed a significant variation in the means of the SPT data sets from the three formations, with the Langebaan Formation sands having the highest consistencies followed by the Witzand Formation sands.
- The limited assessment of the liquefaction potential of the Cape Flats sands showed a predominance of dilative sands. However, contractive soils, prone to strength loss and liquid-like flow during undrained shear, are present. Ground failures ascribed to soil liquefaction are expected to be characterised by limited deformations during cyclic loading.
- Notwithstanding the above, there is a general resistance to liquefaction during an earthquake with a moment magnitude of 6.0 and a PGA of 0.15g, which corresponds to the design earthquake typically assumed for the Cape Flats.
- Monotonic triaxial testing of modified Cape Flats sands (94% Mfuleni sand and 6% added fines) subjected to all-round pressures of 50kPa, 100kPa and 150kPa during monotonic triaxial testing produced elastic moduli varying between approximately 45MPa and 100MPa. An increase in soil stiffness occurred as the degree of compaction and moisture content of the specimens increased. The reduced stiffness at low moisture contents can possibly be ascribed to particle breakage during compaction of drier samples and a change to the PSD curve and particle shape.
- Based on SPT derived elastic moduli, soil stiffness in the Langebaan Formation consistently exceeds that in the Witzand and Springfontyn Formations (variation confirmed by statistical testing). Cemented sands and limestone/calcarenite banks characteristic of this formation are considered responsible for the higher stiffnesses.
- The stress dependency of the dynamic stiffness of the Cape Flats sand was illustrated by the  $M_r-\Theta$  and  $M_r-\sigma_3-\sigma_d$  models, with the stiffness increasing as bulk stress and confinement increase. However, stress-softening occurred (with increasing DSR), especially at a higher moisture content, affecting the goodness of fit of the models. This decrease in stiffness is a result of a loss in integrity of the specimens as damage occurs. The models therefore fail to account for the relevant model parameter of DSR.
- The prediction of shear wave velocity,  $V_s$ , from SPT tests is improved by the inclusion of the overburden term ( $P_a/\sigma'_v$ ) and this produces a better fit than stress corrected equations (correction of  $V_s$  and  $N_{60}$  to  $V_{s1}$  and  $(N_1)_{60}$ ). Nonetheless,  $N_{60}$  and  $P_a/\sigma'_v$  are not very efficient predictors of  $V_s$ , as shown by the large scatter of the data in Figures 4.57 and 4.58 of Chapter 4.
- The proposed  $V_s-N_{60}$  model for Cape Flats sands combined with the non-linear stepwise settlement analysis method proposed by Archer (2014) provides a simple and practical method of taking account of the non-linear stress-strain behaviour of soils.

- Comparison of settlements predicted using small strain stiffness and using the general elastic solution with Stroud's (1989) and Webb's (1969) SPT  $N_{60}$ -E transformation models showed that both Stroud's method and the small strain stiffness method predict lower settlements for medium dense and dense profiles than Webb's method which takes no account of strain level in the determination of soil stiffness. Webb's method appears to be suitable for loose sands only.
- The Versak software developed by Archer (2014) for settlement prediction based on small strain stiffness appears to underestimate the difference in settlement between square and strip footings of similar width.
- The magnitude of differential settlement in the sands will largely be determined by non-homogeneity of the sand within the zone of influence below the footing. In the study area, significant lateral variability in consistency was noted, even over very short distances. This is mostly due to the presence of pedogenic layers and lenses with varying degrees of cementation particularly in the Langebaan and Witzand Formation, and the presence of intermittent highly compressible peat and soft clay layers in the Springfontyn Formation.

### **6.2.3 Horizontal and vertical variation of soil properties**

The study aimed to investigate both horizontal and vertical variation in the soil properties in the study area. In Section 6.2.2 the findings associated with the classification and characterisation properties were summarised, focusing on inter-formation variation. As mentioned in Section 1.5 of Chapter 1, data from depths exceeding 3m are typically sparse (aside from penetration test results). Observed changes with depth were mostly deemed inconclusive as data become sparser with depth. Statistical analysis of depth interval data sets was therefore considered pointless. For many soil properties, studying variation with depth was not possible due to insufficient data. Penetration test data revealed dense, cemented deposits close to surface, often underlain by softer soils. Despite this, an overall increase in SPT resistance with depth was noted, mostly the result of increasing confinement with depth. Variation in penetration resistance is mostly associated with changes in soil type and/or degree of cementation. When studying individual SPT  $(N_1)_{60}$  profiles, significant variation in soil consistency was noted vertically, with frequent trend reversal.

### **6.2.4 Soil properties for the various formations**

The entire Cape Flats database is summarised in Tables 6-1, 6-2 and 6-3 below, divided into the Witzand, Springfontyn and Langebaan Formations and further into USCS classes.

**Table 6-1: Summary of soil properties in the Witzand Formation per USCS class**

Property	Value				
<b>Grading (ASTM D422:2007 size boundaries) (soils mostly sampled from upper 3m of the soil profile)</b>					
<b>SP: Poorly graded sand Fines 0-5%</b>	<b>Maximum</b>	<b>Minimum</b>	<b>Average</b>	<b>No. of values</b>	<b>Standard deviation</b>
Gravel and coarse sand (%)	19	0	0.7	158	2.3
Medium sand (%)	70	0	18	158	14.9
Fine sand (%)	99	24	78	158	15.2
Silt and clay (%)	5	0	3	158	1.5
Coefficient of uniformity (Cu)	6.5	1.43	2.7	157	0.8
Coefficient of curvature (Cz)	1.56	0.02	0.98	157	0.2
<b>SP – SM: Poorly graded sand - silty sand combination soil Fines 6 – 12%</b>					
Gravel and coarse sand (%)	40	0	4	92	9.0
Medium sand (%)	46	1	14	92	9.3
Fine sand (%)	93	36	75	92	14.2
Silt and clay (%)	12	6	8	92	1.9
Coefficient of uniformity (Cu)	27.5	1.93	4.1	91	4.5
Coefficient of curvature (Cz)	9.6	0.25	1.1	91	1.0
<b>SM/SC/SM-SC: Silty and/or clayey sands Fines &gt;12%</b>					
Gravel and coarse sand (%)	2	0	0.6	7	0.8
Medium sand (%)	18	4	13	7	4.9
Fine sand (%)	82	44	64	7	14.0
Silt and clay (%)	46	13	23	7	13.1
Coefficient of uniformity (Cu)	88	2.9	37.9	5	39.5
Coefficient of curvature (Cz)	47	0.7	16.2	5	21.1
<b>Atterberg limits (soils mostly sampled from upper 3m of the soil profile)</b>					
<b>SP: Poorly graded sand Fines 0-5%</b>	<b>Maximum</b>	<b>Minimum</b>	<b>Average</b>	<b>No. of values</b>	<b>Standard deviation</b>
Liquid limit (%)	Non-plastic			148	-
Plastic limit (%)					
Plasticity index (%)					
Linear shrinkage (%)					
<b>SP – SM: Poorly graded sand - silty sand combination soil Fines 6 – 12%</b>					
91 No. samples in total. Of which 83 No. non-plastic, 6 No. slightly plastic (with linear shrinkage between 0 and 0.5%) and 2 No. samples with the following plasticity properties:					
Liquid limit (%)	24	19	22	2	3.5
Plastic limit (%)	14	10	12	2	2.8
Plasticity index (%)	14	5	10	2	6.4
Linear shrinkage (%)	5	2.5	4	2	1.8
<b>SM/SC/SM-SC: Silty and/or clayey sands Fines &gt;12%</b>					
Liquid limit (%)	36	24	30	2	8.5
Plastic limit (%)	27	15	21	2	8.5
Plasticity index (%)	9		9	2	0
Linear shrinkage (%)	4.5	4	4	2	0.4
Note: An additional 4 samples are: non-plastic (3. No) and slightly plastic (1 No.)					

<b>Maximum dry density and OMC (soils sampled from upper 4m of the soil profile)</b>					
<b>SP: Poorly graded sand Fines 0-5%</b>	<b>Maximum</b>	<b>Minimum</b>	<b>Average</b>	<b>No. of values</b>	<b>Standard deviation</b>
Maximum dry density (kg/m <sup>3</sup> )	2000	1530	1717	57	98.5
OMC (%)	19.3	7.5	12.5	57	2.7
<b>SP – SM: Poorly graded sand - silty sand combination soil Fines 6 – 12%</b>					
Maximum dry density (kg/m <sup>3</sup> )	1969	1598	1756	54	88.2
OMC (%)	16.2	8	12.4	54	1.6
<b>SM/SC/SM-SC: Silty and/or clayey sands Fines &gt;12%</b>					
Maximum dry density (kg/m <sup>3</sup> )	1816	1675	1746	2	99.7
OMC (%)	14.4	13.7	14.0	2	0.5
<b>California bearing ratio (CBR) (soils sampled from upper 3m of the soil profile)</b>					
<b>SP: Poorly graded sand Fines 0-5%</b>	<b>Maximum</b>	<b>Minimum</b>	<b>Average</b>	<b>No. of values</b>	<b>Standard deviation</b>
CBR at 98% MDD	51	8	26	57	10.8
CBR at 95% MDD	42	8	20	58	8.2
CBR at 93% MDD	36	7	16	58	6.6
CBR at 90% MDD	28	4	2	58	5.2
<b>SP – SM: Poorly graded sand - silty sand combination soil Fines 6 – 12%</b>					
CBR at 98% MDD	38	12	18	53	5.8
CBR at 95% MDD	25	8	13	54	4.0
CBR at 93% MDD	20	6	11	54	3.2
CBR at 90% MDD	17	3	9	54	2.7
<b>SM/SC/SM-SC: Silty and/or clayey sands Fines &gt;12%</b>					
CBR at 98% MDD	30	13	22	2	12.0
CBR at 95% MDD	21	9	15	2	8.5
CBR at 93% MDD	18	8	13	2	7.1
CBR at 90% MDD	12	7	10	2	3.5
<b>Minimum index density (soils sampled from upper 2m of the soil profile)</b>					
<b>SP: Poorly graded sand Fines 0-5%</b>	<b>Maximum</b>	<b>Minimum</b>	<b>Average</b>	<b>No. of values</b>	<b>Standard deviation</b>
Dry density (kg/m <sup>3</sup> )	1492	1422	1464	4	29.8
<b>Corrosivity (soils sampled from upper 3m of the soil profile)</b>					
<b>All sands (SP/SP-SM/SM/ SC/SM-SC)</b>	<b>Maximum</b>	<b>Minimum</b>	<b>Average</b>	<b>No. of values</b>	<b>Standard deviation</b>
pH	9.1	6.1	8.2	56	0.65
Resistivity (ohm.cm)	33333	333	6334	54	5371
<b>Erodibility (soils sampled from upper 2.5m of the soil profile)</b>					
<b>All sands (SP/SP-SM/SM/ SC/SM-SC)</b>	<b>Maximum</b>	<b>Minimum</b>	<b>Average</b>	<b>No. of values</b>	<b>Standard deviation</b>
K-factor (Wischmeier and Smith, 1978)	0.31	0.01	0.11	4	0.14

<b>Specific gravity (soils sampled from upper 3m of the soil profile)</b>					
<b>SP/SP-SM: Poorly graded sand and poorly graded sand - silty sand combination soil (no organic matter)</b>	<b>Maximum</b>	<b>Minimum</b>	<b>Average</b>	<b>No. of values</b>	<b>Standard deviation</b>
G <sub>s</sub> (laboratory determined)	2.63	2.62	2.63	3	0.006
<b>SP/SP-SM: Poorly graded sand and poorly graded sand - silty sand combination soil (contains organic matter)</b>					
G <sub>s</sub> (laboratory determined)	2.64	2.43	2.58	9	0.08
<b>In-situ density (density measurements in upper 1m of the soil profile)</b>					
<b>SP/SP-SM: Poorly graded sand and poorly graded sand - silty sand combination soil</b>	<b>Maximum</b>	<b>Minimum</b>	<b>Average</b>	<b>No. of values</b>	<b>Standard deviation</b>
Dry density (kg/m <sup>3</sup> )	1895	1664	1814	7	80.2
<b>In-situ moisture content (soils sampled from upper 2.1m of the soil profile)</b>					
<b>All sands (SP/SP-SM/SM/SC/SM-SC)</b>	<b>Maximum</b>	<b>Minimum</b>	<b>Average</b>	<b>No. of values</b>	<b>Standard deviation</b>
Laboratory determined moisture content (%)	32.8	0.5	8.3	76	6.5
<b>Collapsibility (undisturbed soil sampled from upper 3m of the soil profile)</b>					
<b>SP: Poorly graded sand Fines 0-5%</b>	<b>Maximum</b>	<b>Minimum</b>	<b>Average</b>	<b>No. of values</b>	<b>Standard deviation</b>
Collapse potential (%) (Standard collapse potential test: saturation at 200kPa)	0.92	0.05	0.42	13	0.28
<b>Permeability (soils sampled from upper 2m of the soil profile) (density ranging from 1567 to 1750kg/m<sup>3</sup>)</b>					
<b>SP: Poorly graded sand Fines 0-5%</b>	<b>Maximum</b>	<b>Minimum</b>	<b>Average</b>	<b>No. of values</b>	<b>Standard deviation</b>
Saturated hydraulic conductivity (k in m/s) (Constant head test)	5.9 x 10 <sup>-4</sup>	5.7 x 10 <sup>-6</sup>	1.6 x 10 <sup>-4</sup>	4	2.9 x 10 <sup>-4</sup>
<b>Shear strength</b>					
<b>SP/SP-SM: Poorly graded sand and poorly graded sand - silty sand combination soil</b>	<b>Maximum</b>	<b>Minimum</b>	<b>Average</b>	<b>No. of values</b>	<b>Standard deviation</b>
Effective friction angle (°) (Drained direct shear test: dry density ranging from <1600 to 1650kg/m <sup>3</sup> )	40	30	35	5	4.5
Effective cohesion (kPa) (Drained direct shear test: dry density ranging from <1600 to 1650kg/m <sup>3</sup> )	13	0	6	5	4.6
<b>All sands (SP/SP-SM/SM/SC/SM-SC)</b>					
Effective friction angle (°) (Chen, 2004 SPT based transformation model)	45	28	40	416 [SPT N (and φ') values]	2.6

<b>Consistency</b>					
<b>All sands (SP/SP-SM/SM/SC/SM-SC)</b>	<b>Maximum</b>	<b>Minimum</b>	<b>Average</b>	<b>No. of values</b>	<b>Standard deviation</b>
SPT N (blow count) (Max test depth of 42m)	84	1	28	416	16.3
CPTu $q_c$ (MPa) (Max test depth = 11m)	45	0.1	17	3930 (from 4 CPTu's: reading taken every 1cm)	11.2
<b>Compressibility (Stroud, 1989 SPT based method) (Max depth = 42m)</b>					
<b>All sands (SP/SP-SM/SM/SC/SM-SC)</b>	<b>Maximum</b>	<b>Minimum</b>	<b>Average</b>	<b>No. of values</b>	<b>Standard deviation</b>
Elastic modulus (MPa) ( $q_{net}/q_{ult} = 0.33$ , FS = 3)	126	1.5	42	408	24.5
Elastic modulus (MPa) ( $q_{net}/q_{ult} = 0.14$ , FS = 7)	168	2	55		32.7
Elastic modulus (MPa) ( $q_{net}/q_{ult} = 0.05$ , FS = 20)	336	4	111		65.4

**Table 6-2: Summary of soil properties in the Springfontyn Formation per USCS class**

Property	Value				
<b>Grading (ASTM D422:2007 size boundaries) (soils mostly sampled from upper 3m of the soil profile)</b>					
<b>SP: Poorly graded sand Fines 0-5%</b>	<b>Maximum</b>	<b>Minimum</b>	<b>Average</b>	<b>No. of values</b>	<b>Standard deviation</b>
Gravel and coarse sand (%)	7	0	0.5	69	1.5
Medium sand (%)	83	0	24	69	15.0
Fine sand (%)	100	11	73	69	15.1
Silt and clay (%)	5	0	3	69	1.4
Coefficient of uniformity (Cu)	4.5	1.67	2.8	58	0.7
Coefficient of curvature (Cz)	1.6	0.66	0.95	58	0.2
<b>SP – SM: Poorly graded sand - silty sand combination soil Fines 6 – 12%</b>					
Gravel and coarse sand (%)	13	0	2	22	4.0
Medium sand (%)	41	2	16	22	11.2
Fine sand (%)	90	50	73	22	11.6
Silt and clay (%)	12	6	8	22	2.1
Coefficient of uniformity (Cu)	7.8	2.4	3.6	18	1.3
Coefficient of curvature (Cz)	3.6	0.81	1.6	18	0.7
<b>SM/SC/SM-SC: Silty and/or clayey sands Fines &gt;12%</b>					
Gravel and coarse sand (%)	16	0	3	24	4.9
Medium sand (%)	18	1	7	24	4.0
Fine sand (%)	78	46	64	24	9.7
Silt and clay (%)	48	13	26	24	11.8
Coefficient of uniformity (Cu)	46.7	3.0	22.7	10	16.6
Coefficient of curvature (Cz)	31.4	0.82	8.5	10	9.0
<b>Atterberg limits (soils mostly sampled from upper 3m of the soil profile)</b>					
<b>SP: Poorly graded sand Fines 0-5%</b>	<b>Maximum</b>	<b>Minimum</b>	<b>Average</b>	<b>No. of values</b>	<b>Standard deviation</b>
Liquid limit (%)	Non-plastic			68	-
Plastic limit (%)					
Plasticity index (%)					
Linear shrinkage (%)					
<b>SP – SM: Poorly graded sand - silty sand combination soil Fines 6 – 12%</b>					
Liquid limit (%)	Non-plastic (20 No.) and slightly plastic (1 No.). For SP sample: linear shrinkage = 1.5%.			21	-
Plastic limit (%)					
Plasticity index (%)					
Linear shrinkage (%)					
<b>SM/SC/SM-SC: Silty and/or clayey sands Fines &gt;12%</b>					
Liquid limit (%)	28	17	22	11	3.4
Plastic limit (%)	19	9	15	11	2.6
Plasticity index (%)	4.5	1	3	11	1.1
Linear shrinkage (%)	10	3	8	11	2.3
Note: An additional 10 samples (48% of total tested) are non-plastic (6. No) and slightly plastic (4 No.)					

<b>Maximum dry density and OMC (soils sampled from upper 3m of the soil profile)</b>					
<b>SP: Poorly graded sand Fines 0-5%</b>	<b>Maximum</b>	<b>Minimum</b>	<b>Average</b>	<b>No. of values</b>	<b>Standard deviation</b>
Maximum dry density (kg/m <sup>3</sup> )	1864	1606	1776	27	54.8
OMC (%)	11.8	7.8	10	27	1.3
<b>SP – SM: Poorly graded sand - silty sand combination soil Fines 6 – 12%</b>					
Maximum dry density (kg/m <sup>3</sup> )	1920	1735	1796	9	53.8
OMC (%)	12.8	9.2	11	9	1.2
<b>SM/SC/SM-SC: Silty and/or clayey sands Fines &gt;12%</b>					
Maximum dry density (kg/m <sup>3</sup> )	1701		-	1	-
OMC (%)	8.7		-	1	-
<b>California bearing ratio (CBR) (soils sampled from upper 3m of the soil profile)</b>					
<b>SP: Poorly graded sand Fines 0-5%</b>	<b>Maximum</b>	<b>Minimum</b>	<b>Average</b>	<b>No. of values</b>	<b>Standard deviation</b>
CBR at 98% MDD	36	9	21	23	7.9
CBR at 95% MDD	31	2	14	27	7.6
CBR at 93% MDD	27	2	12	23	6.3
CBR at 90% MDD	22	1	9	20	5.6
<b>SP – SM: Poorly graded sand - silty sand combination soil Fines 6 – 12%</b>					
CBR at 98% MDD	45	14	25	8	9.1
CBR at 95% MDD	27	10	15	9	5.3
CBR at 93% MDD	32	7	14	8	8.0
CBR at 90% MDD	17	4	10	7	4.6
<b>SM/SC/SM-SC: Silty and/or clayey sands Fines &gt;12%</b>					
CBR at 98% MDD	14				
CBR at 95% MDD	10				
CBR at 93% MDD	8				
CBR at 90% MDD	5				
			-	1	-
<b>Minimum index density (soils sampled from upper 2m of the soil profile)</b>					
<b>SP: Poorly graded sand Fines 0-5%</b>	<b>Maximum</b>	<b>Minimum</b>	<b>Average</b>	<b>No. of values</b>	<b>Standard deviation</b>
Dry density (kg/m <sup>3</sup> )	1590	1431	1511	2	112
<b>Corrosivity (soils sampled from upper 3m of the soil profile)</b>					
<b>All sands (SP/SP-SM/SM/ SC/SM-SC)</b>	<b>Maximum</b>	<b>Minimum</b>	<b>Average</b>	<b>No. of values</b>	<b>Standard deviation</b>
pH	8.9	5.3	7.2	19	0.92
Resistivity (ohm.cm)	18 748	1065	6629	18	4610
<b>Erodibility (soils sampled from upper 3m of the soil profile)</b>					
<b>All sands (SP/SP-SM/SM/ SC/SM-SC)</b>	<b>Maximum</b>	<b>Minimum</b>	<b>Average</b>	<b>No. of values</b>	<b>Standard deviation</b>
K-factor (Wischmeier and Smith, 1978)	0.13	0.015	0.06	4	0.05

<b>Specific gravity (soils sampled between 1m and 3m depth)</b>					
<b>SP/SC: Poorly graded sand and clayey sand (no organic matter)</b>	<b>Maximum</b>	<b>Minimum</b>	<b>Average</b>	<b>No. of values</b>	<b>Standard deviation</b>
G <sub>s</sub> (laboratory determined)	2.67	2.65	2.66	2	0.01
<b>In-situ density (density measurements in upper 1m of the soil profile)</b>					
<b>All sands (SP/SP-SM/SM/SC/SM-SC)</b>	<b>Maximum</b>	<b>Minimum</b>	<b>Average</b>	<b>No. of values</b>	<b>Standard deviation</b>
Dry density (kg/m <sup>3</sup> )	1776	1571	1665	6	83.6
<b>In-situ moisture content (soils sampled from upper 3m of the soil profile)</b>					
<b>All sands (SP/SP-SM/SM/SC/SM-SC)</b>	<b>Maximum</b>	<b>Minimum</b>	<b>Average</b>	<b>No. of values</b>	<b>Standard deviation</b>
Laboratory determined moisture content (%)	21.3	0.5	12.6	46	5.4
<b>Collapsibility (undisturbed soil sampled between 1m and 2m depth)</b>					
<b>SP: Poorly graded sand Fines 0-5%</b>	<b>Maximum</b>	<b>Minimum</b>	<b>Average</b>	<b>No. of values</b>	<b>Standard deviation</b>
Collapse potential (%) (Standard collapse potential test: saturation at 200kPa)	0.03		-	1	-
<b>Permeability (soils sampled from upper 2m of the soil profile) (density ranging from 1540 to 1560kg/m<sup>3</sup>)</b>					
<b>SP: Poorly graded sand Fines 0-5%</b>	<b>Maximum</b>	<b>Minimum</b>	<b>Average</b>	<b>No. of values</b>	<b>Standard deviation</b>
Saturated hydraulic conductivity (k in m/s) (Constant head test)	2.8 x 10 <sup>-5</sup>	6.6 x 10 <sup>-6</sup>	1.7 x 10 <sup>-5</sup>	2	1.5 x 10 <sup>-5</sup>
<b>Shear strength</b>					
<b>SP: Poorly graded sand Fines 0-5%</b>	<b>Maximum</b>	<b>Minimum</b>	<b>Average</b>	<b>No. of values</b>	<b>Standard deviation</b>
Effective friction angle (°) (Drained direct shear test: Sands compacted to 1600kg/m <sup>3</sup> )	38	35	37	2	1.9
Effective cohesion (kPa) (Drained direct shear test: Sands compacted to 1600kg/m <sup>3</sup> )	8	4	6	2	2.8
<b>All sands (SP/SP-SM/SM/SC/SM-SC)</b>					
Effective friction angle (°) (Chen, 2004 SPT based transformation model)	46	28	40	897 [SPT N (and φ') values]	2.4
<b>Consistency</b>					
<b>All sands (SP/SP-SM/SM/SC/SM-SC)</b>	<b>Maximum</b>	<b>Minimum</b>	<b>Average</b>	<b>No. of values</b>	<b>Standard deviation</b>
SPT N (blow count) (Max test depth of 39.5m)	(95)	1	26	897	15.0
CPT q <sub>c</sub> (MPa) (Max test depth = 9m)	30	1	10	187 (from 12 CPT's)	7.1

<b>Compressibility (Stroud, 1989 SPT based method) (Max test depth = 39.5m)</b>					
<b>All sands (SP/SP-SM/SM/SC/SM-SC)</b>	<b>Maximum</b>	<b>Minimum</b>	<b>Average</b>	<b>No. of values</b>	<b>Standard deviation</b>
Elastic modulus (MPa) ( $q_{net}/q_{ult} = 0.33$ , FS = 3)	158	1.5	39	897 [SPT N (and E) values]	23.1
Elastic modulus (MPa) ( $q_{net}/q_{ult} = 0.14$ , FS = 7)	210	2	51		30.8
Elastic modulus (MPa) ( $q_{net}/q_{ult} = 0.05$ , FS = 20)	420	4	103		61.6

Table 6-3: Summary of soil properties in the Langebaan Formation per USCS class

Property	Value				
<b>Grading (ASTM D422:2007 size boundaries) (soils mostly sampled from upper 3m of the soil profile)</b>					
<b>SP: Poorly graded sand Fines 0-5%</b>	<b>Maximum</b>	<b>Minimum</b>	<b>Average</b>	<b>No. of values</b>	<b>Standard deviation</b>
Gravel and coarse sand (%)	20	0	3	20	6.0
Medium sand (%)	53	1	24	20	13.7
Fine sand (%)	96	24	70	20	12.7
Silt and clay (%)	5	1	3	20	1.3
Coefficient of uniformity (Cu)	4.6	2.1	2.9	20	0.82
Coefficient of curvature (Cz)	1.3	0.7	0.95	20	0.18
<b>SP – SM: Poorly graded sand - silty sand combination soil Fines 6 – 12%</b>					
Gravel and coarse sand (%)	5	0	0.4	16	1.3
Medium sand (%)	47	1	15	16	15.1
Fine sand (%)	93	41	77	16	15.7
Silt and clay (%)	11	6	7	16	1.7
Coefficient of uniformity (Cu)	5.4	1.4	3.0	16	1.24
Coefficient of curvature (Cz)	2.1	0.7	1.1	16	0.38
<b>SM/SC/SM-SC: Silty and/or clayey sands Fines &gt;12%</b>					
Gravel and coarse sand (%)	23	0	12	2	16.3
Medium sand (%)	19	7	13	2	8.5
Fine sand (%)	69	29	49	2	28.3
Silt and clay (%)	29	24	27	2	3.5
<b>Atterberg limits (soils mostly sampled from upper 3m of the soil profile)</b>					
<b>SP: Poorly graded sand Fines 0-5%</b>	<b>Maximum</b>	<b>Minimum</b>	<b>Average</b>	<b>No. of values</b>	<b>Standard deviation</b>
Liquid limit (%)	Non-plastic			20	-
Plastic limit (%)					
Plasticity index (%)					
Linear shrinkage (%)					
<b>SP – SM: Poorly graded sand - silty sand combination soil Fines 6 – 12%</b>					
Liquid limit (%)	Non-plastic			15	-
Plastic limit (%)					
Plasticity index (%)					
Linear shrinkage (%)					
<b>SM/SC/SM-SC: Silty and/or clayey sands Fines &gt;12%</b>					
Liquid limit (%)	20	-		1	-
Plastic limit (%)	15				
Plasticity index (%)	5				
Linear shrinkage (%)	2				
Note: 1 No. additional sample is non-plastic					

<b>Maximum dry density and OMC (soils sampled from upper 3m of the soil profile)</b>					
<b>SP/SP-SM: Poorly graded sand and poorly graded sand - silty sand combination soil</b>	<b>Maximum</b>	<b>Minimum</b>	<b>Average</b>	<b>No. of values</b>	<b>Standard deviation</b>
Maximum dry density (kg/m <sup>3</sup> )	1765	1483	1615	12	92.9
OMC (%)	20.4	9.2	15.1	12	3.1
<b>California bearing ratio (CBR) (soils sampled from upper 3m of the soil profile)</b>					
<b>SP/SP-SM: Poorly graded sand and poorly graded sand - silty sand combination soil</b>	<b>Maximum</b>	<b>Minimum</b>	<b>Average</b>	<b>No. of values</b>	<b>Standard deviation</b>
CBR at 98% MDD	47	17	29	12	7.8
CBR at 95% MDD	36	12	21	12	6.4
CBR at 93% MDD	30	10	17	12	5.6
CBR at 90% MDD	23	7	12	12	5.2
<b>Corrosivity (soils sampled from upper 2.5m of the soil profile)</b>					
<b>All sands (SP/SP-SM/SM/SC/SM-SC)</b>	<b>Maximum</b>	<b>Minimum</b>	<b>Average</b>	<b>No. of values</b>	<b>Standard deviation</b>
pH	9	7.7	8.6	10	0.38
Resistivity (ohm.cm)	8333	388	4153	10	3082
<b>Erodibility (soils sampled from upper 2.5m of the soil profile)</b>					
<b>SP-SM/SM: Poorly graded sand - silty sand combination soil and silty sand</b>	<b>Maximum</b>	<b>Minimum</b>	<b>Average</b>	<b>No. of values</b>	<b>Standard deviation</b>
K-factor (Wischmeier and Smith, 1978)	0.24	0.05	0.15	2	0.13
<b>In-situ moisture content (soils sampled from upper 3.0m of the soil profile)</b>					
<b>All sands (SP/SP-SM/SM/SC/SM-SC)</b>	<b>Maximum</b>	<b>Minimum</b>	<b>Average</b>	<b>No. of values</b>	<b>Standard deviation</b>
Laboratory determined moisture content (%)	15.7	1.4	6.7	10	4.8
<b>Shear strength</b>					
<b>SP-SM: Poorly graded sand - silty sand combination soil</b>	<b>Maximum</b>	<b>Minimum</b>	<b>Average</b>	<b>No. of values</b>	<b>Standard deviation</b>
Effective friction angle (°) (Drained direct shear test: dry density ranging from 1350 to 1750kg/m <sup>3</sup> )	40	34	36	4	2.5
Effective cohesion (kPa) (Drained direct shear test: dry density ranging from 1350 to 1750kg/m <sup>3</sup> )	7	0	3	4	3.4
<b>All sands (SP/SP-SM/SM/SC/SM-SC)</b>					
Effective friction angle (°) (Chen, 2004 SPT based transformation model)	46	33	41	194	2.2

Consistency					
All sands (SP/SP-SM/SM/SC/SM-SC)	Maximum	Minimum	Average	No. of values	Standard deviation
SPT N (blow count) (Max test depth of 20m)	86	4	33	194	16.6
Compressibility (Stroud, 1989 SPT based method) (Max depth = 20m)					
All sands (SP/SP-SM/SM/SC/SM-SC)	Maximum	Minimum	Average	No. of values	Standard deviation
Elastic modulus (MPa) ( $q_{net}/q_{ult} = 0.33$ , FS = 3)	129	6	50	194	24.9
Elastic modulus (MPa) ( $q_{net}/q_{ult} = 0.14$ , FS = 7)	172	8	67		33.2
Elastic modulus (MPa) ( $q_{net}/q_{ult} = 0.05$ , FS = 20)	344	16	133		66.4

### 6.2.5 Compressibility and foundation performance in the Cape Flats

The shallow Cape Flats sands are often highly compressible and may be potentially collapsible where the presence of clay or chemical bonds form a collapsible fabric. According to Yates (personal communication, 2020) the sands are often loose and compressible in the upper 1.0m to 1.5m of the surface. Below this depth, the density of the sands typically increases. The current research confirms the widespread presence of loose shallow sands and a general exceedance of the maximum allowable settlement in these sands. Within the upper 1m of the soil profile in the Witzand and Langebaan Formations, dense cemented deposits (hardpan calcrete) are often intersected. In the study area, differential settlement may therefore be significant (close to total settlement) where the consistency of the sands below footings of the same structure vary substantially. Typically, denser soils were found to be associated with the Langebaan Formation (compared to the Witzand and Springfontyn Formations). The depth to groundwater was found to vary substantially in the study area. Seasonal fluctuations at any specific location can also be significant. The presence of shallow groundwater will influence the compressibility of soils below shallow footings, and its variation over time (seasonal) should be taken into consideration when predicting the performance of foundations in the study area.

General foundation performance in the Cape Flats sands is relatively good, provided due cognisance is taken of loose layers within the soil profile. One way of doing so is the compaction of any compressible layers below foundation level and within the zone of influence of foundations to at least 95% of Modified AASHTO MDD (Yates, personal communication, 2020). A small amount of long-term creep-settlement can be expected. Modified construction methods such as additional steel reinforcement in footings and jointing in walls are sometimes used to accommodate expected total and differential movements.

Currently, the prediction of settlement for small scale projects relies on empirically correlated elastic modulus values, most often from SPT-based methods such as those proposed by Webb (1969) and Stroud (1989). To minimise project costs, DCP tests are regularly performed and DN (DCP number in mm/blow) used as an intermediate parameter. The average DCP value of each sand layer is crudely converted to an SPT N-value, from which the elastic modulus is determined using the abovementioned relations. Foundation settlement is then calculated using the general elastic solution with rigidity and depth correction factors. This method of estimating the stiffness

of the profile will negatively influence the accuracy of the calculated settlements, only providing a rough measure of foundation performance. To predict the performance of shallow foundations in moderately or highly compressible sands more accurately, the use of the SPT or CPT, or vertical plate load tests are considered essential. Settlement analysis using small-strain stiffness data from the proposed  $V_s$ - $N_{60}$  model for Cape Flats sands provides a way to take account of the non-linear stress-strain behaviour of the sands when calculating settlement.

## 6.3 Recommendations

### 6.3.1 Geotechnical Investigations

The Cape Flats sands have been found to be highly variable, with a wide range in many material properties. The findings of this research may be used to form initial appreciation of the likely properties of the material and potential problem areas. This will guide the planning and execution of appropriate site-specific investigations and aid the interpretation of results.

This research has shown that there is merit in broadening the current approach to site investigations of the Cape Flats, which traditionally rely heavily on shallow test pits and dynamic penetrometer testing. In particular, increased use of CPTu testing and the determination of shear wave velocity by means of CSW or MASW testing should be considered.

### 6.3.2 Further Research

After completing the research, and in view of the limitations stipulated in Section 1.5 of Chapter 1, the following general recommendations can be made for future research:

- The research was concerned with the recent aeolian deposits which typically underlie the study area, including the Witzand, Springfontyn and Langebaan Formations. As an extension to the research by Amdurer (1956), further investigation should be carried out into the geotechnical properties and engineering behaviour of the cohesive transported soils, found interlayered with the sandy horizons of the Springfontyn Formation, and of the residual Malmesbury soils.
- This research focused on the geographic area of the Cape Flats. However, the sand formations found on the Cape Flats extend well beyond this geographic location, particularly along the West Coast where many comprehensive geotechnical investigations have been undertaken for industrial development. The results of these investigations should be compared with the findings of current research.
- Multiple investigation methods, i.e. a variety of in-situ test methods and/or laboratory tests should be undertaken for many sites to establish more reliable interrelationships between soil properties.
- A layered GIS database producing maps with the distribution of typical properties for the three formations should be created as a practical contribution of the work.

The following specific areas of research are identified:

- From the limited number of clayey sands with measurable PI sampled from the study area during past investigations, the dominant clay mineral type seems to vary between the soil formations. Further research is necessary to investigate this possibility.

- Aeolian sands are typically described as rounded and sub-rounded in shape, often the roundness being a function of travel distance. A CT scan image of Cape Flats sands from Mfuleni revealed mostly sub-angular sand grains, with a fair proportion of angular grains. Since many material properties, such as density, shear strength, CBR, and erodibility are influenced by particle shape, investigation into particle shape (including form, roundness and surface texture), and possible variations influencing soil parameter values to varying extents, has the potential to add value.
- Uncharacteristically, the monotonic triaxial compression tests on compacted samples showed an increase in soil stiffness and shear strength as the moisture content increased. Particle breakage during compaction of drier specimens (requiring extended periods of tamping) is a possible contributor to this atypical outcome. This phenomenon should be confirmed by additional testing.
- The accuracy of the collapse potential test results was possibly influenced by disturbance of the sands during sampling or preparation. In addition, no calcareous soil horizons from the Langebaan Formation were sampled and tested during the current research. On-site plate bearing tests are considered superior in the identification of collapsible sands and should be undertaken on a range of soils from the Witzand, Springfontyn and Langebaan Formations to quantify the risk associated with the different soil types/textures and bonding agents.
- The influence of soil type, geological epoch, fines content, coefficient of uniformity and average particle size on shear wave velocity was excluded from the current analyses. Including these parameters as additional independent variables in the regression of  $V_s$  and SPT  $N_{60}$  may improve the obtained correlations.

## References

- Adelana, S. & Xu, Y. 2006. Contamination and protection of the Cape Flats aquifer, South Africa. Groundwater pollutions in Africa. 1<sup>st</sup> Edition. Edited by Xu, Y and Usher, B. London: Taylor and Francis.
- Adelana, S., Xu, Y. & Shafick, A. 2006. Identifying sources and mechanisms of groundwater recharge in the Cape Flats, South Africa: Implications for sustainable resource management. Proceedings, Congress of the International Association of Hydrogeologists. 9 – 13 October. Beijing, China.
- Adelana, S. & Xu, Y. 2008. Impacts of land-use changes on a shallow coastal aquifer, South-Western Cape, South Africa. Proc. XXXVI Congress of the International Association of Hydrogeologists (IAH). 28 Oct - 2 Nov 2008. Toyama, Japan.
- Adelana, S., Xu, Y. & Vrbka, P. 2010. A conceptual model for the development and management of the Cape Flats aquifer, South Africa. *Water SA*. 36(4).
- Alao, O.O. 2015. Refinement of air-borne chloride exposure classes for RC structures in the Cape Peninsula. M.Sc. thesis. University of Cape Town.
- Alias, R., Kasa, A. & Taha, M.R. 2014. Particle size effect on shear strength of granular materials in direct shear test. *International Journal of Civil, Environmental, Structural, Construction and Architectural Engineering*. 8(11): 1144-1147.
- Amdurer, S.S. 1956. The engineering geology of the Cape Flats. Unpublished doctoral thesis. Cape Town: University of Cape Town.
- American Association of State Highway and Transportation Officials (AASHTO) M145-91. 2008. Standard specification for classification of soils and soil-aggregate mixtures for highway construction purposes. Washington: AASHTO.
- Andrus, R.D., Piratheepan, P. & Juang, C.H. 2007. Shear wave velocity – penetration resistance correlations for ground shaking and liquefaction hazards assessment. *USGS Grant Report*. Department of Civil Engineering, Clemson University.
- Archer, A. 2014. Using small-strain stiffness to predict the settlement of shallow foundations on sand. MEng dissertation. University of Pretoria.
- Archer, A. & Heymann, G. 2015. Using small-strain stiffness to predict the load-settlement behaviour of shallow foundations on sand. *Journal of the South African Institution of Civil Engineering*. 57(2): 28-35.
- ASTM D854. 2002. *Standard test methods for specific gravity of soil solids by water pycnometer*. West Conshohocken, Pennsylvania: American Society for Testing and Materials.
- ASTM D5333. 2003. *Standard test method for measurement of collapse potential of soils (withdrawn 2012)*. West Conshohocken, Pennsylvania: American Society for Testing and Materials.
- ASTM D422. 2007. *Standard test method for particle- size analysis of soils (withdrawn 2016)*. West Conshohocken, Pennsylvania: American Society for Testing and Materials.

ASTM D3080. 2011. *Standard Test Method for Direct Shear Test of Soils Under Consolidated Drained Conditions (Withdrawn 2020)*. American Society for Testing and Materials. West Conshohocken, Pennsylvania.

ASTM D698. 2012. *Standard test methods for laboratory compaction characteristics of soil using standard effort (12 400ft-lbf/ft<sup>3</sup> 600kN-m/m<sup>3</sup>)*. West Conshohocken, Pennsylvania: American Society for Testing and Materials.

ASTM D1557. 2012. *Standard test methods for laboratory compaction characteristics of soil using modified effort (56 000ft-lbf/ft<sup>3</sup> 2700kN-m/m<sup>3</sup>)*. West Conshohocken, Pennsylvania: American Society for Testing and Materials.

ASTM D1556. 2015. *Standard test method for density and unit weight of soil in place by sand-cone method*. West Conshohocken, Pennsylvania: American Society for Testing and Materials.

ASTM D2167. 2015. *Standard test method for density and unit weight of soil in place by the rubber balloon method*. West Conshohocken, Pennsylvania: American Society for Testing and Materials.

ASTM D2850. 2015. *Standard Test Method for Unconsolidated-Undrained Triaxial Compression Test on Cohesive Soils*. American Society for Testing and Materials. West Conshohocken, Pennsylvania.

ASTM D1883. 2016. *Standard test method for California bearing ratio (CBR) of laboratory-compacted soils*. West Conshohocken, Pennsylvania: American Society for Testing and Materials.

ASTM D4253. 2016. *Standard test methods for maximum index density and unit weight of soils using a vibratory table*. West Conshohocken, Pennsylvania: American Society for Testing and Materials.

ASTM D4254. 2016. *Standard test methods for minimum index density and unit weight of soils and calculation of relative density*. West Conshohocken, Pennsylvania: American Society for Testing and Materials.

ASTM D2487. 2017. *Standard practice for classification of soils for engineering purposes (Unified Soil Classification System)*. West Conshohocken, Pennsylvania: American Society for Testing and Materials.

ASTM D4318. 2017. *Standard test methods for liquid limit, plastic limit, and plasticity index of soils*. West Conshohocken, Pennsylvania: American Society for Testing and Materials.

ASTM D6913. 2017. *Standard test methods for particle size distribution (gradation) of soils using sieve analysis*. West Conshohocken, Pennsylvania: American Society for Testing and Materials.

ASTM D7928. 2017. *Standard test methods for particle size distribution (gradation) of fine-grained soils using the sedimentation (hydrometer) analysis*. West Conshohocken, Pennsylvania: American Society for Testing and Materials.

ASTM D3385. 2018. *Standard test method for infiltration rate of soils in-field using double-ring infiltrometer*. West Conshohocken, Pennsylvania: American Society for Testing and Materials.

- ASTM D4943. 2018. *Standard test method for shrinkage factors of cohesive soils by the water submersion method*. West Conshohocken, Pennsylvania: American Society for Testing and Materials.
- ASTM D2216. 2019. *Standard test methods for laboratory determination of water (moisture) content of soil and rock by mass*. West Conshohocken, Pennsylvania: American Society for Testing and Materials.
- ASTM D4767. 2020. *Standard Test Method for Consolidated Undrained Triaxial Compression Test for Cohesive Soils*. American Society for Testing and Materials. West Conshohocken, Pennsylvania.
- ASTM D5778. 2020. *Standard Test Method for Electric Friction Cone and Piezocone Penetration Testing of Soils*. American Society for Testing and Materials. West Conshohocken, Pennsylvania.
- ASTM D7181. 2020. *Standard Test Method for Consolidated Drained Triaxial Compression Test for Soils*. American Society for Testing and Materials. West Conshohocken, Pennsylvania.
- ASTM D7382. 2020. Standard test methods for determination of maximum dry unit weight of granular soils using a vibrating hammer. West Conshohocken, Pennsylvania: American Society for Testing and Materials.
- Atkinson, J.H. 2000. Non-linear soil stiffness in routine design. *Geotechnique*. 50(5): 487-508.
- Atkinson, J.H. & Bransby, P.L. 1978. *The mechanics of soils: An introduction to critical state soil mechanics*. England: McGraw-Hill book company (UK) Limited.
- Auerswald, K., Fiener, P., Martin, W. & Elhaus, D. 2014. Use and misuse of the K factor equation in soil erosion modelling: An alternative equation for determining USLE nomograph soil erodibility values. *Catena*. 118:220-225.
- Baldi, G. & Nova, R. 1985. Closure to “membrane penetration effects in triaxial testing”. *Journal of Geotechnical Engineering*. 111(8): 1048–1049.
- Bareither, C.A., Edil, T.B., Benson, C.H. & Mickelson, D.M. 2008. Geological and physical factors affecting the friction angle of compacted sands. *Journal of Geotechnical and Geoenvironmental Engineering*. 134(10): 1476-1489.
- Barwis, J.H. & Tankard, A.J. 1983. Pleistocene shoreline deposition and sea-level history at Swartklip, South Africa. *Journal of Sedimentary Petrology*. 53(4): 1281 – 1294.
- Basson, J.J. 1989. Deterioration of concrete in aggressive waters – measuring aggressiveness and taking countermeasures. South Africa: Concrete-Durability Bureau of the Portland Cement institute.
- Been, K. & Jefferies, M.G. 1985. A state parameter for sands. *Geotechnique*. 35(2): 99-112.
- Bellana, N. 2009. Shear wave velocity as function of SPT penetration resistance and vertical effective stress at California bridge sites. MSc.Eng thesis. University of California.
- Berardi, R. & Lancellotta, R. 1991. Stiffness of granular soils from field performance. *Géotechnique*. 41(1): 149-57.

- Bolton, M.D. & Whittle, R.W. 1999. A non-linear elastic/perfectly plastic analysis for plane strain undrained expansion tests. *Geotechnique*. 49(1): 133-141.
- Bowles, J.E. 1997. *Foundation analysis and design*. 5<sup>th</sup> Ed. Singapore: McGraw-Hill.
- Brandt, M. 2011. *Seismic hazard in South Africa*. Council for Geoscience report No. 2011-0061. Cape Town: Council for Geoscience.
- Bredenkamp, Z. 2018. *The performance properties of recycled concrete in road pavement materials*. M.Sc thesis. Stellenbosch University.
- Breytenbach, I.J. 2009. *The relationship between index testing and California Bearing Ratio values for natural road construction materials in South Africa*. M.Sc. thesis. University of Pretoria.
- Brink, A.B.A. 1985. *Engineering Geology of Southern Africa, Volume 4 Post-Gondwana Deposits*. Pretoria: Building Publications.
- Brink, A.B.A. & Bruin, R.M.H (eds). 1990. *Guidelines for soil and rock logging in South Africa*, 2<sup>nd</sup> impression, 2002. *Proceedings of the Geoterminology Workshop*. Pretoria: AEG – SAIEG – SAICE.
- Brink, A.B.A., Partridge, T.C. & Williams, A.A.B. 1982. *Soil survey for engineering*. Oxford, U.K: Clarendon Press.
- British Standard 1377. 1990. *Methods of test for soils for civil engineering purposes*. London: British Standards Institution.
- Bruand, A., Hartmann, C. & Lesturgez, G. 2005. *Physical properties of tropical sandy soils: A large range of behaviours*. Symposium on management of tropical sandy soils for sustainable agriculture: A holistic approach for sustainable development of problem soils in the tropics, Session 4. 27 Nov – 2 Dec 2005. Bangkok.
- Building Research Establishment (BRE). 2005a. *Special Digest 1*. 3<sup>rd</sup> ed. *Concrete in aggressive ground*. Part C: Assessing the aggressive chemical environment. Watford: Building Research Establishment.
- Building Research Establishment (BRE). 2005b. *Special Digest 1*. 3<sup>rd</sup> ed. *Concrete in aggressive ground*. Part D: Specifying concrete for general cast-in-situ use. Watford: Building Research Establishment.
- Byrne, G. & Berry, A.D. 2008. *A Guide to Practical Geotechnical Engineering in Southern Africa*. 4th ed. South Africa: Frankipile South Africa (Pty) Ltd.
- Cabalar, A.F. & Akbulut, N. 2016. Evaluation of actual and estimated hydraulic conductivity of sands with different gradation and shape. *SpringerPlus* 5(820). Available: <https://springerplus.springeropen.com/articles/10.1186/s40064-016-2472-2>.
- Campanella, R.G., Robertson, P.K., Gillespie, D.G. & Grieg, J. 1985. Recent developments in in-situ testing in soils. 11<sup>th</sup> International Conference on Soil Mechanics and Foundation Engineering. Volume 2 pp. 849 - 854. San Francisco.
- Carrier, W.D. 2003. Goodbye, Hazen; Hello, Kozeny-Carman. *Journal of Geotechnical and Geoenvironmental Engineering*. 6(3): 287-326.

Cerato, A.B. & Lutenegeger, A.J. 2006. Specimen size and scale effects of direct shear box tests of sands. *Geotechnical Testing Journal*. 29(6): 1-10.

Cetin, K.O., Seed, R.B., Der Kiureghian, A., Tokimatsu, K., Harder, L.F., Kayen, R.E. & Moss, R.E.S. 2004. Standard penetration test-based probabilistic and deterministic assessment of seismic soil liquefaction potential. *Journal of Geotechnical and Geoenvironmental Engineering*. 130(12): 1314-1340.

Chapuis, R.P. 2004. Predicting the saturated hydraulic conductivity of sand and gravel using effective diameter and void ratio. *Canadian Geotechnical Journal*. 41(5): 787-795.

Chapuis, R.P. & Aubertin, M. 2003. Predicting the coefficient of permeability of soils using the Kozeny-Carman equation. Département des génies civil, géologique et des mines. École Polytechnique de Montréal.

Chen, J.R. 2004. Axial behaviour of drilled shafts in gravelly soils. PhD thesis. Cornell University, New York.

Chen, W.F. & Mizuno, E. 1990. Nonlinear analysis in soil mechanics: Theory and implementation. Amsterdam: Elsevier Science.

Ching, J., Arroyo, M., Chen, J., Jorge, C., Lansivaara, T., Li, D., Mayne, P. & Phoon, K (Discussers). 2017. Chapter 1 Transformation models and multivariate soil databases. Joint TC205/TC304 Working group on “discussion statistical/reliability methods for Eurocodes” - Final report. Available: <http://140.112.12.21/issmge/tc304.htm>.

City of Cape Town (CoCT). 2011. *Cape Flats draft district plan: Volume 1*. Spatial development plan and environmental management framework: Baseline information and analysis report. Spatial Planning and Urban Design Department. Available: [https://www.capetown.gov.za/en/sdf/Documents/Draft\\_Vols\\_2011/Cape\\_Flats\\_District%20VOL1\\_SDP.EMF.pdf](https://www.capetown.gov.za/en/sdf/Documents/Draft_Vols_2011/Cape_Flats_District%20VOL1_SDP.EMF.pdf).

City of Cape Town (CoCT). 2012a. Cape Flats district plan: Final draft. Spatial development plan and environmental management framework: Technical report. Spatial Planning and Urban Design Department. Available: [http://resource.capetown.gov.za/documentcentre/Documents/City%20research%20reports%20and%20review/Cape\\_Flats\\_District\\_Plan\\_Technical\\_Report.pdf](http://resource.capetown.gov.za/documentcentre/Documents/City%20research%20reports%20and%20review/Cape_Flats_District_Plan_Technical_Report.pdf).

City of Cape Town (CoCT). 2012b. *Khayelitsha, Mitchell's Plain, greater Blue Downs final draft district plan*. Spatial development plan and environmental management framework: Technical report. Spatial Planning and Urban Design Department. Available: [http://resource.capetown.gov.za/documentcentre/Documents/City%20research%20reports%20and%20review/Khayelitsha\\_MitchellsPlain\\_Technical\\_Report.pdf](http://resource.capetown.gov.za/documentcentre/Documents/City%20research%20reports%20and%20review/Khayelitsha_MitchellsPlain_Technical_Report.pdf).

Clayton, C.R.I. 1993. *The standard penetration test (SPT) – methods and use*. Construction Industry Research and Information Association, Funder Report / CP/7. CIRIA, London.

Clayton, D.J. 2013. Design and technical service manual. 9<sup>th</sup> ed. Kansas: Earth Contact Products, LLC.

Clayton, C.R.I. & Heymann, G. 2001. Stiffness of geomaterials at very small strains. *Geotechnique*. 51(3): 245-255.

- Coetzee, L.L. 2015. Evaluating the influence of end conditions and membrane thickness on triaxial tests and results. FYP418 (skripsie) Project report. Stellenbosch University.
- Committee of Land Transport Officials (COLTO). 1998. Standard Specification for Road and Bridge Works for State Road Authorities. The South African Institution of Civil Engineering.
- Council for Scientific and Industrial Research (CSIR). 2014. Proposed protocol for resilient/cord modulus and permanent deformation characteristics of unbound and bound granular materials. 2<sup>nd</sup> Draft. Draft contract report SARDM-B1C-2014-01. South Africa: CSIR, Stellenbosch University.
- Cubrinovski, M. & Ishihara, K. 1999. Correlation between penetration resistance and relative density of sandy soils. International Society for Soil Mechanics and Geotechnical Engineering. Available: <https://www.issmge.org/publications/online-library>.
- Cubrinovski, M. & Ishihara, K. 2002. Maximum and minimum void ratio characteristics of sand. *Soils and Foundations*. 42(6): 65-78.
- Dakshanamurthy, V. & Raman, V. 1973. A simple method of identifying expansive soil. *Soils and foundations*. Japanese Society of Soil Mechanics and Foundation Engineering. 13(1):91-104.
- Das, B.M. 2000. Fundamentals of geotechnical engineering. USA: Brooks/Cole.
- Das, B.M. 2008. Introduction to Geotechnical Engineering. International student edition. USA: Cengage Learning.
- Das, B.M. 2011. Principles of Foundation Engineering. 7th ed. Stamford: Cengage Learning.
- Das, B.M. & Sivakugan, N. 2007. Settlements of shallow foundations on granular soils – An overview. *International Journal of Geotechnical Engineering*. 1(1):19-29.
- Das, B.M. & Sivakugan, N. 2019. Principles of foundation engineering. 9<sup>th</sup> ed, SI. Boston, USA: Cengage Learning.
- Das, B.M. & Sobhan, K. 2018. *Principles of geotechnical engineering*. 9<sup>th</sup> ed, SI. USA: Cengage Learning.
- Day, P.W. 2016. Settlement of shallow foundations. Foundation design 811: A practical perspective. Course notes for postgraduates [Class notes]. Department of Civil Engineering, University of Stellenbosch.
- De la Harpe, C.W.H. 2015. The development of a seismic risk reduction procedure for the prioritization of low cost, load bearing masonry buildings. M.Sc. Thesis. University of Stellenbosch.
- Department of Water Affairs and Forestry (DWAF). 2008. Updated manual for the identification and delineation of wetlands and riparian areas, prepared by M. Rountree, A. L. Batchelor, J. MacKenzie & D. Hoare. Pretoria: Stream Flow Reduction Activities, Department of Water Affairs and Forestry.
- Di Buo, B., D'Ignazio, M., Selänpää, J., Haikola, M., Länsivaara, T. & Di Sante, M. 2019. Investigation and geotechnical characterization of Periö Clay, Finland. *AIMS Geosciences*. 5(3): 591-616.

- Eijkelkamp. 2018. Double ring infiltrometer: Operating instructions. Eijkelkamp Soil and Water. Available: <https://en.eijkelkamp.com/products/field-measurement-equipment/double-ring-infiltrometer.html> [2019, June 10].
- Elhakim, A.F. 2016. Estimation of soil permeability. *Alexandria Engineering Journal*. 55: 2631-2638.
- ESOPT I. 1974. Various authors. Proceedings of the Conference on the Settlement of Structures. Cambridge, UK: Pentech Press.
- Ezeabasili, A.C.C., Okoro, B.U. & Emengini, E.J. 2014. Relative erodibilities of some soils from Anambra basin. *Sky Journal of Soil Science and Environmental Management*. 3(8): 083-090.
- Farouk, A., Lamboj, L. & Kos, J. 2004. A numerical model to predict matric suction inside unsaturated soils. *Acta Polytechnica*. 44(4): 3-10.
- Franceschini, G.2003. Geology of aeolian and marine deposits in the Saldanha Bay region, Western Cape, South Africa. PhD thesis. University of Cape Town.
- Geohydrological and Spatial Solutions International (GEOSS). 2014. Groundwater specialist study – Cape Town International Airport runway re-alignment and associated infrastructure project. Report No. 2014/06-10.
- Geological Survey of South Africa. 1990. Theron, J.N (compiled). 1:25 000 geological series [South Africa]. 3318, Cape Town. Pretoria: Government Printer.
- GeoLogismiki. 2014. CPeT-IT User's Manual v.1.4. GeoLogismiki. Available: <https://www.geologismiki.gr/Documents/CPeT-IT/CPeT-IT%20manual.pdf>.
- Gerber, A. 1981. A digital model of groundwater flow in the Cape Flats. CSIR contract report. C WAT 46. Pretoria: CSIR.
- Germaine, J.T. & Germaine, A.V. 2009. Geotechnical laboratory measurements for engineers. New Jersey: John Wiley and Sons, Inc.
- Giljam, R. 2002. The effect of the Cape Flats aquifer on the water quality of False Bay. M.Sc. Thesis. University of Cape Town.
- Gill, K.S., Jha, J.N. & Choudhary, A.K. 2010. CBR value estimation using dynamic cone penetrometer. Proceeding of the Indian Geotechnical Conference. GEOtrendz. 16-18 December 2010. Mumbai.
- Goktepe, A.B. & Sezer, A. 2011. Effect of particle shape on density and permeability of sands. *Geotechnical Engineering*. 163(EG6): 307-320.
- Gomaa, Y. & Abdel-rahman, G. 2007. Correlations between relative density and compaction test parameters. In 12<sup>th</sup> international colloquium on structural and geotechnical engineering. Pg.1-8.
- Google Earth Pro 7.3.3.7786. 2012. Cape Flats region, Western Cape, South Africa. [Map July, 21]. 34° 00'45.58''S; 18 34'27.88'' E, eye alt. 43.68km.

- Guo, Y., Yang, Y. & Yu, X. 2017. Influence of particle shape on the erodibility of non-cohesive soil: Insights from coupled CFD-DEM simulations. *Particuology*. Available: <https://daneshyari.com/article/preview/7061567.pdf>.
- Ham, T.G., Nakata, Y., Orense, R. & Hyodo, M. 2010. Influence of water on the compression behaviour of decomposed granite soil. *Journal of Geotechnical and Geoenvironmental Engineering*. 136 (5).
- Harison, J.A. 1986. Correlation of CBR and dynamic cone penetrometer strength measurement of soils. *Australian Road Research*. 16(2): 130-136.
- Hatanaka, M. & Uchida, A. 1996. Empirical correlation between penetration resistance and internal friction angle of sandy soils. *Soils and Foundations*. 36(4): 1-9.
- Hay, R., McGibbon, D., Botha, F. & Riemann, K. 2015. Cape Flats aquifer and False Bay - Opportunities to change. *Proceedings of the 79<sup>th</sup> IMESA conference on "Changing the Face of the Municipal Engineer"*. 27-30 October 2015. Cape Town.
- Head, K.H. 1992. *Manual of soil laboratory testing*. Volume 1. Soil classification and compaction tests. 2<sup>nd</sup> ed. London: Pentech.
- Henkel, D.J. & Gilbert, G.D. 1952. The effect measured of the rubber membrane on the triaxial compression strength of clay samples. *Geotechnique*. 3(1): 20-29.
- Henzen, M. 1973. The reclamation, storage and abstraction of purified sewage effluents in the Cape Peninsula. D.Sc. Thesis. University of the Free State, Bloemfontein.
- Hettiarachchi, H. & Brown, T. 2009. Use of SPT blow counts to estimate shear strength properties of soils: Energy balance approach. *Journal of Geotechnical and Geoenvironmental Engineering*. 135: 25-32.
- Heymann, G. 2007. Ground stiffness measurement by the continuous surface wave test. *Journal of the South African Institution of Civil Engineering*. 49(1):25–31.
- Hill, R.S. & Theron, J.N. 1981. *Silica sand of the Cape Flats*. Bulletin Vol 69. Pretoria: Geological Survey of South Africa.
- Hoffman, K. 2019. Determination of pullout resistance of galvanized-steel strips within select South African soils based on their free draining potential in mechanically stabilized earth wall backfill conditions. M.Sc. thesis. Stellenbosch University.
- Houlsby, G.T. & Teh, C.I. 1988. Analysis of the piezocone in clay. *Proceedings of the 1<sup>st</sup> International Symposium on Penetration Testing, ISOPT-1*. De Ruiter (ed.). 20-24 March 1988. Orlando.
- Houston, S.L., Houston, W.N. & Spadola, D.J. 1988. Prediction of field collapse of soils due to wetting. *Journal of Geotechnical Engineering*. 114(1): 40-59.
- Howayek., A.E., Huang, P.T., Bisnett, R. & Santagata, M.C. 2011. Identification and behaviour of collapsible soils. Report No. FHWA/IN/JTRP-2011/12. Joint transportation research program. Indiana Department of Transportation and Purdue University.

- Idriss, I.M. & Boulanger, R.W. 2004. Semi-empirical procedures for evaluating liquefaction potential during earthquakes. Proceedings of the 11<sup>th</sup> ICSDEE and 3<sup>rd</sup> ICEGE. pp. 32-56. California, USA.
- Idriss, I.M. & Boulanger, R.W. 2008. Soil liquefaction during earthquakes. Monograph MNO-12. Earthquake Engineering Research Institute, Oakland, California. pp. 261.
- Idriss, I.M. & Boulanger, R.W. 2010. SPT-based liquefaction triggering procedures. Report No. UCD/CGM-10-02. Center for Geotechnical Modelling. University of California. Available: [https://faculty.engineering.ucdavis.edu/boulanger/wpcontent/uploads/sites/71/2014/09/Idriss\\_Boulanger\\_SPT\\_Liquefaction\\_CGM-10-02.pdf](https://faculty.engineering.ucdavis.edu/boulanger/wpcontent/uploads/sites/71/2014/09/Idriss_Boulanger_SPT_Liquefaction_CGM-10-02.pdf).
- Indian Standard (IS): 2720. 2007. Methods of test for soils. Part 29. Determination of dry density of soils in-place by the core-cutter method. 1<sup>st</sup> revision. New Delhi: Bureau of Indian Standards.
- Jamiolkowski, M. & Presti, D.C.F. 2003. Geotechnical characterisation of Holocene and Pleistocene Messina sand and gravel deposits. Characterisation and engineering properties of natural soils: Volume 2 – Tan et al. (eds.). Tokyo: A.A. Balkema Publishers.
- Jenkins, K.J. & Rudman, C.E. 2016. Hitchhikers guide to pavement engineering. Course notes for postgraduates [Class notes]. Department of Civil Engineering, University of Stellenbosch.
- Jennings, J.E.B. 1974. Contribution by Jennings to Newsletter No. 2 of the SAICE Geotechnical Division, August, 1974.
- Jennings, J.E., Brink, A.B.A. & Williams, A.A.B. 1973. Revised guide to soil profiling for civil engineering purposes in Southern Africa. *The Civil Engineer in South Africa*. 15(1): 236-246.
- Johnson, M.R., Anhaeusser, C.R. & Thomas, R.J. Ed. 2006. The Geology of South Africa. Pretoria: Council for Geoscience.
- Jones, G. & Rust, E. 1983. Piezometer probe (CUPT) for subsoil identification. Proceedings, International Symposium, in-situ testing. Volume 2:303-398. Paris.
- Jones, G. & Rust, E. 1995. Piezocone settlement prediction parameters for embankments on alluvium. *Proceedings of the International Symposium on Cone Penetration Testing*. Volume 2. 4-5 October 1995. Sweden.
- Kalumba, D. 1998. Effect of grading and grain size on the friction characteristics of a sand/geotextile interface. M.Sc. Eng. Thesis. University of Cape Town.
- Kara, E.M., Meghachou, M. & Aboubekr, N. 2013. Contribution of particle size ranges to soil friction. *Engineering, Technology and Applied Science Research*. 4(3): 497-501.
- Knappett, J.A. & Craig, R.F. 2012. *Craig's soil mechanics*. 8<sup>th</sup> ed. Oxon, U.S: Spon Press.
- Korfiatis, G.P. & Manikopoulos, C.N. 1982. Correlation of maximum dry density and grain size. *Journal of geotechnical engineering*. 108(9): 1171-1176.
- Krige, A.V. 1927. An examination of the Tertiary and Quaternary changes of sea level in South Africa, with special stress on the evidence in favour of a recent world-wide sinking ocean level. *Annals of the University of Stellenbosch*. Vol 5, Sect A, No.1. Cape Town: National Press Limited.

- Kulhawy, F.H. & Mayne, P.W. 1990. Manual on estimating soil properties for foundation design. Final report, Project 1493-6, EL-6800. California: Electric Power Research institute.
- Kusumandari, A. 2013. Soil erodibility of several types of green open space areas in Yogyakarta City, Indonesia. *Procedia Environmental Sciences*. 20: 732 -736.
- Lade, P.V., Liggio, C.D. & Yamamuro, J.A. 1998. Effects of non-plastic fines on minimum and maximum void ratios of sand. *Geotechnical testing journal, ASTM*. 21(4):336-347.
- Latha, G.M. & Sitharam, T.G. 2008. Effect of particle size and gradation on the behaviour of granular material simulated using DEM. *Indian Geotechnical Journal*. 38(1): 68-88.
- Le Roux, J.J., Morgenthal, T.L., Malherbe, J., Smith, H.J., Weepener, H.L. & Newby, T.S. 2006. Improving spatial soil erosion indicators in South Africa. ISCW Report No. GW/A/2006/51. ARC – Institute for Soil, Climate and Water, Pretoria, South Africa.
- Le Roux, J.J., Morgenthal, T.L., Malherbe, J., Pretorius, D.J. & Sumner, P.D. 2008. Water erosion prediction at a national scale for South Africa. *Water SA*. 34(3): 3015-314.
- Liao, S. & Whitman, R.V. 1986. Overburden correction factor for SPT in sand. *Journal of Geotechnical Engineering, ASCE*. 112(3): 373 – 37.
- Lunne, T., Long, M. & Forsberg, C.F. 2003. Characterisation and engineering properties of Holmen, Drammen sand. Characterisation and engineering properties of natural soils: Volume 2 – Tan et al. (eds.). Tokyo: A.A. Balkema Publishers.
- Lunne, T., Robertson, P.K. & Powell, J.J.M. 1997. Cone penetration testing in geotechnical practice. New York: Blackie Academic, EF Spon/Routledge Publishers.
- Lutenegger, A. & DeGroot, D. 1995. *Settlement of shallow foundations on granular soils*. Research report, Boston, MA, US: Massachusetts Highway Department.
- MacRobert, C.J. 2009. Correlations between the Dynamic Probe Super Heavy test and the Standard Penetration Test and their application within South Africa. BSc.Eng. Thesis. University of Cape Town.
- Mavis, F.T. & Wilsey, E.F. 1936. A study of the permeability of sand. Bulletin 7. University of Iowa studies in engineering. Iowa: University of Iowa.
- Mayne, P.W. & Poulos, H.G. 1999. Approximate displacement influence factors for elastic shallow foundations. *Journal of Geotechnical and Geoenvironmental Engineering*. 125(6): 453-460.
- Mayne, P.W., Uzielli, M. & Illingworth, F. 2012. Shallow footing response on sands using a direct method based on cone penetration tests. Full scale testing and foundation design. Proceedings GSP 227 honouring Bengt Fellenius, ASCE. Virginia: 664 – 679.
- Mehta, P.J. & Gandhi, A. 2016. Influence of particle size gradation and relative density on shear parameters for cohesionless soils. *International Journal of Advanced Research and Innovative Ideas in Education*. 2(3): 869-878.
- Meigh, A.C. 1987. *Cone penetration testing – methods and interpretation*. Construction Industry Research and Information Association, Ground Engineering Report: In-Situ Testing. CIRIA, London.

- Meisina, C. 2006. Characterisation of weathered clayey soils responsible for shallow landslides. *Natural Hazards and Earth System Sciences*. 6:825-838.
- Meriggi, R., Paronuzzi, P. & Simeoni, L. 2000. Engineering geological characterization of lacustrine overconsolidated clays in an alpine area of Italy. *Canadian Geotechnical Journal*. 37(6):1241-1251.
- Metcalf, J.B. & Romanoschi, S.A. 2009. Predictions of maximum dry density and optimum moisture content from simple material properties. Available: <https://www.scribd.com/document/136638513/Predictions-of-Maximum-Dry-Density-John-Metcalf-Australia>.
- Mitchell, J.K. 1993. *Fundamentals of soil behaviour*. 2<sup>nd</sup> ed. Canada: John Wiley & Sons, Inc.
- Mitchell, J.K., Guzikowski, F. & Villet, W.C.B. 1978. The measurement of soil properties in-situ: Present methods – their applicability and potential. U.S. Department of Energy Report, Department of Civil Engineering, University of California, Berkeley.
- Moxhay, A., Tinsley, R., Redgers, J. & Gravell, D. 2008. The prediction of ground settlement from continuous surface wave data. *Ground Engineering*, July. pp.34-38.
- Murray, W.A. 1976. Erodibility of coarse sand/clayey silt mixtures. Fritz engineering laboratory report No. 411.2. Available: [https://digital.lib.lehigh.edu/fritz/pdf/411\\_2.pdf](https://digital.lib.lehigh.edu/fritz/pdf/411_2.pdf).
- National Center for Earthquake Engineering Research (NCEER). 1997. Proceedings of the NCEER workshop on evaluation of liquefaction resistance of soils. Youd, T.L. & Idriss, I.M (Eds.). Technical report NCEER-97-022. New York.
- Neal, P.M. 2011. Correlation of liquefaction and settlement in windblown sands using the flat plate dilatometer. M.Sc. Thesis. Cape Peninsula University of Technology, Cape Town.
- Novak-Szabo, T., Sipos, A.A., Shaw, S., Bertoni, D., Pozzebon, A., Grottoli, E., Sarti, G. & Ciavola, P. 2018. Universal characteristics of particle shape evolution by bed-load chipping. *Science advances*. 4:1-11. Available: <https://www.ncbi.nlm.nih.gov/pmc/articles/PMC5903904/>.
- Odong, J. 2007. Evaluation of empirical formulae for determination of hydraulic conductivity based on grain-size analysis. *Journal of American Science*. 3(3): 54-60.
- Oztoprak, S. & Bolton, M.D. 2013. Stiffness of sands through a laboratory test database. *Geotechnique*. 63(1): 54-70.
- Paige-Green, P. & Du Plessis, L. 2009. The use and interpretation of the dynamic cone penetrometer (DCP) test. Pretoria: CSIR Built Environment.
- Parker, R.J. 1991. A study of the liquefaction potential of sandy soils with specific reference to the Cape Flats. M.Sc.Eng. Thesis. University of Stellenbosch.
- Peck, R.B., Hanson, W.E. & Thorburn, T.H. 1974. *Foundation engineering*. 2<sup>nd</sup> ed. Canada: John Wiley & Sons, Inc.
- Prasad, A. & Pandey, B. 2013. Effect of fines on the mechanical behaviour of sand. *International Journal of Structural and Civil Engineering Research*. 2(2): 40-47.

- Rauch, A.F. 1997. EPOLLS: An empirical method for predicting surface displacements due to liquefaction-induced lateral spreading in earthquakes. PhD thesis. Virginia Polytechnic Institute and State University.
- Reznik, Y.M. 1993. Plate-load tests of collapsible soil. *Journal of Geotechnical Engineering*. 119(3): 608-615.
- Rhoades, J.D., Chanduvi, F. & Lesch, S. 1999. Soil salinity assessment: Methods and interpretation of electrical conductivity measurements. FAO irrigation and drainage paper 57. Rome: FAO (Food and Agriculture Organization of the United Nations).
- Roberge, P.R. 2007. Corrosion inspection and monitoring: Volume 2. New Jersey: John Wiley and Sons Inc.
- Roberge, P.R. 2008. Corrosion engineering. The McGraw-Hill companies, Inc. Available: <http://accessengineeringlibrary.com.ez.sun.ac.za/browse/corrosionengineering/p200144759970385001#p200144759970385003>.
- Roberts, D.L. 2001. *The geology of Melkbosstrand and Environs. Explanation of Sheet 3318CB*. Pretoria: Geological Survey of South Africa.
- Robertson, P.K. 1990. Soil classification using the cone penetration test. *Canadian Geotechnical Journal*. 27: 151-158.
- Robertson, P.K. 2009. Interpretation of cone penetration tests – a unified approach. *Canadian Geotechnical Journal*. 46: 1337-1355.
- Robertson, P.K. 2010a. Soil behaviour type from the CPT: an update. 2nd International Symposium on Cone Penetration Testing, CPT'10, Huntington Beach, CA, USA. Available: [https://www.geoengineer.org/storage/publication/18399/publication\\_file/2638/56RobSBT.pdf](https://www.geoengineer.org/storage/publication/18399/publication_file/2638/56RobSBT.pdf).
- Robertson, P.K. 2010b. Estimating in-situ soil permeability from CPT and CPTu. 2nd International Symposium on Cone Penetration Testing, CPT'10, Huntington Beach, CA, USA. Available: [https://www.geoengineer.org/storage/publication/18394/publication\\_file/2633/51Robehc.pdf](https://www.geoengineer.org/storage/publication/18394/publication_file/2633/51Robehc.pdf).
- Robertson, P.K. 2010c. Evaluation of Flow Liquefaction and Liquefied Strength Using the Cone Penetration Test. *Journal of Geotechnical and Geoenvironmental Engineering*. 136 (6): 842-853.
- Robertson, P.K. 2016. Cone penetration test (CPT)-based soil behaviour type (SBT) classification system: an update. *Canadian Geotechnical Journal*. 53: 1910-1927.
- Robertson, P.K. & Cabal, K.L. 2012. Guide to Cone Penetration Testing for Geotechnical Engineering. 5<sup>th</sup> Edition. California: Gregg Drilling and Testing, Inc.
- Robertson, P.K. & Campanella, R.G. 1983. Interpretation of cone penetration tests. Part I: Sand. *Canadian Geotechnical Journal*. Volume 20: 718-733.
- Robertson, P.K. & Wride, C.E. 1998. Evaluating cyclic liquefaction potential using the cone penetration test. *Canadian Geotechnical Journal*. 35: 442-459.
- Rogers, J. 1980. First report on the Cenozoic sediments between Cape Town Eland's Bay: Unpublished report. Geological Survey of South Africa, 136pp.

- Rollins, K.M., Evans, M.D., Diehl, N.B. & Daily III, W.D. 1998. Shear modulus and damping relationships for gravels. *Journal of Geotechnical and Geoenvironmental Engineering*. 124(5): 396-405.
- Rust, E., Heymann, G. & Jones, G.A. 2005. Collapse potential of partly saturated sandy soils from Mozal, Mozambique. *Journal of the South African Institute of Civil Engineering*. 47(1): 8-14.
- Sampson, L.R. 1984. Investigation of the correlation between CBR and DCP. Technical note TS/33/84. Pretoria: National Institute for Transport and Road Research, CSIR.
- Schalke, H.J.W.G. 1973. The upper quaternary of the Cape Flats area (Cape Province, South Africa). *Scripta Geologica*. 15: 1-57.
- Schmertmann, J.H. 1978. Guidelines for cone penetration test: Performance and design. FHWA-TS-78-209 (report). Springfield: U.S. Department of Transportation.
- Schoeman, J.J. 2018. The liquefaction potential of soils on the Cape Flats established by means of empirical correlation. M.Sc.Eng. Thesis. University of Stellenbosch.
- Schofield, A.N. & Wroth, C.P. 1968. Critical state soil mechanics. Great Britain: McGraw-Hill Publishing Company.
- Schwartz, K. 1985. Problem soils in South Africa: Collapsible soils. *The Civil Engineer in South Africa*, pp 378-391.
- Schwartz, K. & Yates, J.R.C. 1980. Engineering properties of aeolian Kalahari sands. 7<sup>th</sup> Regional Conference for Africa, SMFE, Vol 1.
- Schwartz, K., Yates, J.R.C. & Tromp, B.E. 1981. In-situ compaction of aeolian Kalahari sand. Proceedings of the 10<sup>th</sup> International Conference on Soil Mechanics and Foundation Engineering. Stockholm: 15 to 19 June 1981.
- Seed, R.B., Cetin, K.O., Moss, R.E.S., Kammerer, A.M., Wu, J., Pestana, J.M., Riemer, M.F. & Sancio, R.B. 2013. Recent advances in soil liquefaction engineering: A unified and consistent framework. Report No. EERC 2003-06. Earthquake engineering research center. University of California, Berkeley.
- Shipeng, Q., Zhonghui, W., Chengpeng, L., Longcang, S., Jianwei, S., Yin, H., Shuo, Z. & Yixin, H. 2015. A new empirical model for estimating the hydraulic conductivity of low permeability media. Remote Sensing and GIS for Hydrology and Water Resources. Proceedings, RSHS14 and ICGRHWE14, Guangzhou, China. August 2014.
- Simons, N.E. & Menzies, B.K. 1975. *A short course in foundation engineering*. United Kingdom: IPC Science and Technology Press.
- Sitela, V. 2018. Determining the collapsibility of Cape Flats soil. FYP458 (skripsie) Project report. Stellenbosch University.
- Sivadass, T. & Lee, C. 2008. Simple shear testing of residual soils with high silt content. International Conference on Construction and Building Technology. Vol 38: 469-484.

- South African Institute of Civil Engineering (SAICE) Geotechnical Division. 2010. Site Investigation Code of Practice.
- South African National Standard. 1996. SANS 1200M: Roads (general) 1996. *Standardized specification for civil engineering construction*. Pretoria: SABS.
- South African National Standard. 2010. SANS 10160-4:2010. *Basis of structural design and actions for buildings and industrial structures. Part 4. Seismic actions and general requirements for buildings*. Pretoria: SABS.
- South African National Standard. 2011. SANS 10064:2011. *The preparation of steel surfaces for coating*. Pretoria: SABS.
- South African National Standard. 2013. SANS 10100-2: 2013 (Draft SA standard). *The structural use of concrete. Part 2. Materials and execution of work*. Pretoria: SABS.
- South African Pavement Engineering Manual (SAPEM). 2014. Chapter 3: Materials testing. 2<sup>nd</sup> edition. South African National Roads Agency Ltd.
- Stapelberg, F.D.J. 2009. *The engineering geology of Bellville and environs: Explanation: Sheet 3318DC. The engineering geology of Bellville and environs, Western Cape South Africa (1:50 000)*. Bellville: Council for Geoscience.
- Stroud, M.A. 1989. The standard penetration test: Its application and interpretation. Proceedings of the Institute of Civil Engineers Conference on Penetration Testing in the U.K. 6-8 July 1988. Birmingham.
- Sykora, D.W. 1987. Examination of existing shear wave velocity and shear modulus correlations in soils. *Department of the Army, Waterways Experiment Station, Corps of Engineers, Miscellaneous Paper GL-87-22*.
- Sykora, D.E. & Stokoe, K.H. 1983. Correlations of in-situ measurements in sands of shear wave velocity. *Soil Dynamics and Earthquake Engineering Journal*. 20:125-136.
- Taylor, H.C. 1972. Notes on the vegetation of the Cape Flats. *Bothalia*. 10(4): 637-646.
- Technical methods for highways (TMH) 1. 1986. Standard methods of testing road construction materials. Committee of State Road Authorities. Pretoria: National Institute for Transport and Road Research.
- Technical recommendations for highways (TRH) 14. 1985. Guidelines for road construction materials. Pretoria: Department of Transport.
- Technical recommendations for highways (TRH) 20. 1990. The structural design, construction and maintenance of unpaved roads. Pretoria: Department of Transport.
- Terzaghi, K., Peck, R.B. & Mesri, G. 1996. Soil mechanics in engineering practice. 3<sup>rd</sup> ed. New York: John Wiley & Sons, Inc.
- Theron, J.N. 1984. *The geology of Cape Town and surroundings. Explanation of Sheet 3318 CD, 3418 AB, AD, and BA*. Pretoria: Geological Survey of South Africa.

- Theron, J.N., Gresse, P.G., Siegfried, H.P. & Rogers, J. 1992. *The geology of the Cape Town area: Explanation of Sheet 3318*. Pretoria: Geological Survey of South Africa.
- Theyse, H.L. 2008. A mechanistic-empirical design model for unbound granular pavement layers. PhD thesis. University of Johannesburg.
- Tomlinson, M.J. 1994. *Pile design and construction practice*. 4<sup>th</sup> ed. UK: E & FN Spon.
- Transport Research Laboratory (TRL). 1993. *A guide to the structural design of bitumen-surfaced roads in tropical and sub-tropical countries*. Crownthorn: TRL.
- Van der Merwe, D.M. 1964. The prediction of heave from plasticity index and percentage clay fraction of soils. *The Civil Engineer in South Africa*. 6(6): 103-107.
- Van Niekerk, A.A. 2002. Mechanical behaviour and performance of granular bases and sub-bases in pavements. Ph.D thesis. Technical University Delft.
- Vermaak, J.J.G. 2000. Geotechnical and hydrogeological characterization of residual soils in the vadose zone. Ph.D thesis. University of Pretoria.
- Viana da Fonseca, A. 2003. Characterising and deriving engineering properties of a saprolitic soil from granite, in Porto. *Characterisation and Engineering Properties of Natural Soils: Vol 2*. Tan et al., Eds. Lisse: Swetz & Zeitlinger. 1341-1378.
- Vinod, P. & Bindu, J. 2010. Compression index of highly plastic clays – an empirical correlation. *Indian Geotechnical Journal*. 40(3): 174-180.
- Wair, B.R., DeJong, J.T. & Shantz, T. 2012. Guidelines for estimation of shear wave velocity profiles. *Pacific Earthquake Engineering Research Center PEER Report*. University of California.
- Wanasinghe, G.I. & Suzuki, K. 2012. Gradation effect on the peak friction angle of granular soil under different confining pressures. *Annual Research Journal of SLSAJ*. 12: 23-26.
- Water Research Commission (WRC). 2010. Msadala, V., Gibson, L., Le Roux, J., Rooseboom, A. & Basson, G.R (authors). *Sediment yield prediction for South Africa: 2010 edition*. Water Research Commission Report K5/765. Prepared by: Institute for Water and Environmental Engineering, University of Stellenbosch.
- Webb, D.L. 1969. Settlement of structures on deep alluvial sandy sediments in Durban, South Africa. *Proceedings of the Conference on In-Situ Site Investigations in Soils and Rocks*, BGS. Pp 181-187.
- Webb, D.L. 1974. *Penetration Testing in South Africa*. State of the Art Report. European Symposium on Penetration Testing 1. Stockholm.
- Weinert, H.H. 1980. *The natural road construction materials of Southern Africa*. Cape Town: H&R Academica.
- Wils, L., Van Impe, P.O. & Haegeman, W. 2015. Triaxial compression tests on a crushable sand in dry and wet conditions. *Proceedings of the XVI ECSMGE. Geotechnical engineering for infrastructure and development*. p.3449-3454. London, UK: ICE publishing.

Wischmeier, W.H. & Smith, D.D. 1978. Predicting rainfall erosion losses. A guide to conservation planning. Agriculture handbook No. 537. U.S. Department of Agriculture.

Yasin, S.J.M. & Safiullah, A.M.M. 2003. Effect of particle characteristics on the strength and volume change behaviour of sand. *Journal of Civil Engineering. The Institution of Engineers, Bangladesh*. 31(2): 127-148.

Yongqing, H. 2011. Settlement of shallow foundations on cohesionless soil considering modulus degradation of soil. PhD Thesis. Nanyang Technological University.

## Appendix A: Geological map

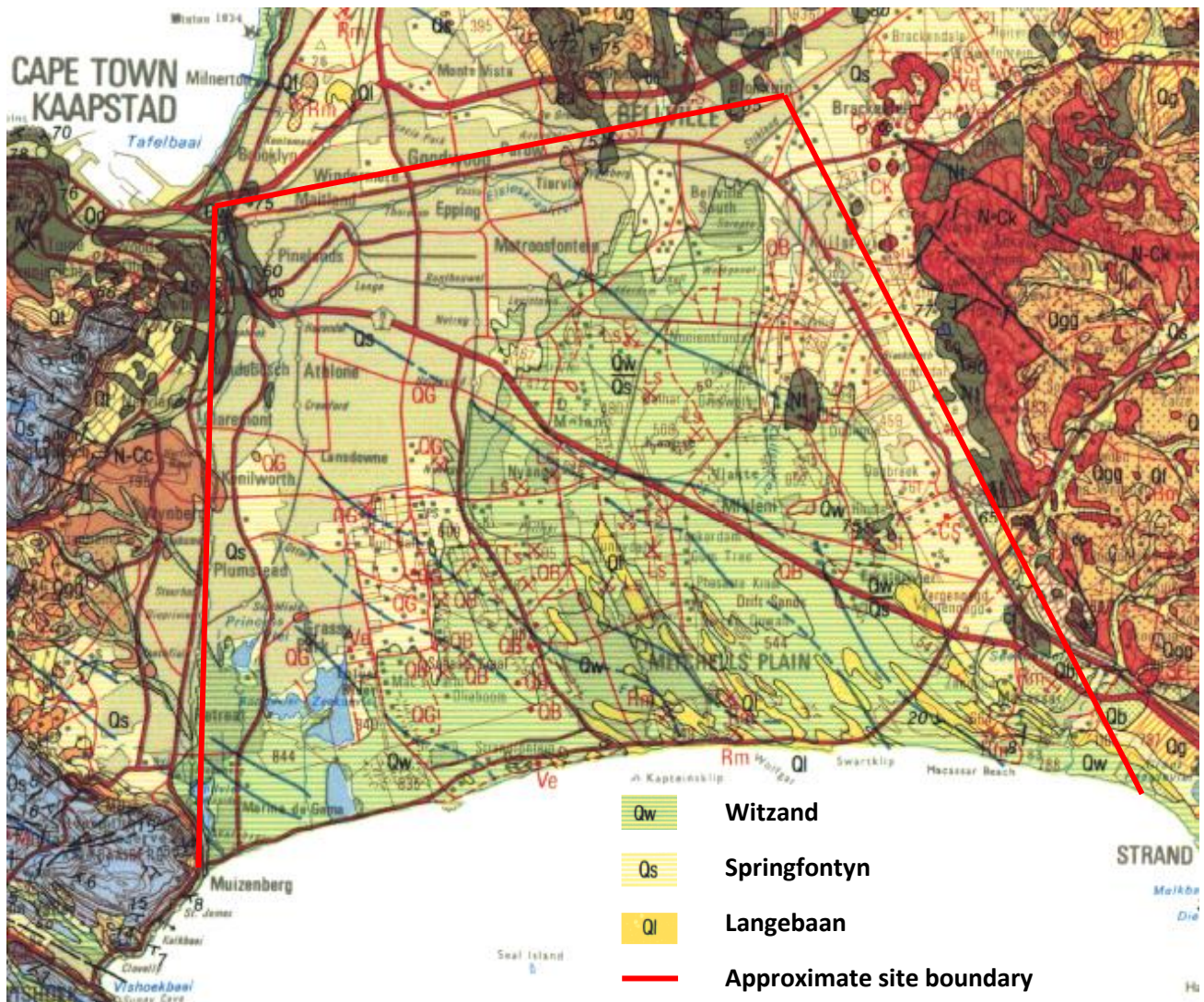


Figure A1: Geological map of the Cape Flats (1:250 000 geological series, 3318 Cape Town) (Geological Survey of South Africa, 1990).

## Appendix B: Classification systems

Groups	G1, G2, G3: Graded Crushed Stone			G4, G5, G6: Natural Gravels			G7, G8, G9, G10: Gravel Soil			
Description	G1 Crushed unweathered rock	G2, G3 Crushed rock, boulders or coarse gravel		Natural gravel; may be mixed with crushed rock such as boulders. May be cementitiously or mechanically modified.			Categorised in terms of properties below.			
Material Class	G1	G2	G3	G4	G5	G6	G7	G8	G9	G10
GRADING										
Sieve Size (mm)	Nominal max size 37.5 mm <sup>1</sup>	Nominal max size 28 (26.5) mm <sup>1</sup>					Max size, in place, after compaction, shall not be greater than two-thirds of the layer thickness.	No grading requirements		
50 / 53	100			100						
37.5	100			85 – 100						
28 / 26.5	84 – 94	100		–						
20 / 19	71 – 84	85 – 95		60 – 90						
14 / 13.2	59 – 75	71 – 84		–						
5 / 4.75	36 – 53	42 – 60		30 – 65						
2	23 – 40	27 – 45		20 – 50						
0.425	11 – 24	13 – 27		10 – 30						
0.075	4 – 12	5 – 12		5 – 15						
Grading Modulus (min)	n/a			n/a	1.5	1.2	n/a			
Flakiness Index	Max 35% on weighted average of -28 (26.5) and -20 (19) mm fractions		n/a	n/a			n/a			
Crushing Strength	10% FACT (min) 110 kN or ACV (max) 29%		n/a	n/a			n/a			
ATTERBERG LIMITS										
Liquid Limit (max)	25	25		25	30	n/a	n/a	No Atterberg Limit requirements		
Plasticity Index, PI (max)	4	6		6	10	12 or 3 GM <sup>2</sup> + 10	12 or 3 GM <sup>2</sup> + 10			
Linear shrinkage, % (max)	4	3		3	5	n/a	n/a			
Linear shrinkage x -0.425 mm sieve (max) <sup>3</sup>	n/a			170	170	n/a	n/a			
BEARING STRENGTH AND SWELL										
CBR, % (min) at MDD <sup>4</sup>	n/a	80 at 98%		80 at 98%	45 at 95% <sup>5</sup>	25 at 93%	15 at 93%	10 at in situ	7 at in situ	3 at in situ
Swell, % (max) at MDD	n/a	0.2 at 100%		0.2 at 100%	0.5 at 100%	1.0%	1.5%			
Material Class	G1	G2	G3	G4	G5	G6	G7	G8	G9	G10

**Notes:**

- G1 adjustments to the grading can only be made using crusher dust or other fractions from the parent rock. Only in exceptional cases can a maximum 10% non-plastic fines be added. G2 and G3 materials may be a blend of crushed stone and other fine aggregate to adjust the grading.
- GM is the grading modulus (see Chapter 3, Section 2.3.2)
- Only applicable to nodular calcrites
- MDD is the maximum dry density determined by the modified AASHTO method.
- In dry areas (Weinert N > 10) and AADT < 300 vpd CBR can be reduced to 25% @ 95% MDD if subbase cover is at least 150 mm.

**Figure B1: TRH14 classification system for granular materials, gravels and soils (SAPEM, 2014)**

General Classification	Granular Materials (35% or less passing the 0.075 mm sieve)							Silt-Clay Materials (>35% passing the 0.075 mm sieve)			
Group Classification	A-1		A-3	A-2				A-4	A-5	A-6	A-7
	A-1-a	A-1-b		A-2-4	A-2-5	A-2-6	A-2-7				A-7-5 A-7-6
<b>Sieve Analysis (% passing)</b>											
2 mm	50 max										
0.425 mm	30 max	50 max	51 min								
0.075 mm	15 max	25 max	10 max	35 max	35 max	35 max	35 max	36 min	36 min	36 min	36 min
<b>Characteristics of fraction passing 0.425 mm</b>											
Liquid Limit				40 max	41 min	40 max	41 min	40 max	41 min	40 max	41 min
Plasticity Index	6 max		NP	10 max	10 max	11 min	11 min	10 max	19 max	11 min	11 min <sup>1</sup>
<b>Significant constituent materials</b>	stone fragments gravel sand		fine sand	silty or clayey gravel sand				silty soils	clayey soils		
<b>General rating as a subgrade</b>	excellent to good							fair to poor			

Note:

1. Plasticity Index of A-7-5 subgroup is equal to or less than the liquid limit (LL) – 30. Plasticity Index of A-7-6 subgroup is greater than LL – 30.

**Figure B2: AASHTO soil classification system (SAPEM, 2014)**

Major Divisions			Group Symbol	Group name	
<b>Coarse grained soils:</b> more than 50% retained on 0.075 mm sieve	Gravel: > 50% of coarse fraction retained on 5 mm sieve	clean gravel < 5% passes 0.075 mm sieve	<b>GW</b>	well graded gravel fine to coarse gravel	
		gravel with > 12% fines	<b>GP</b>	poorly graded gravel	
			<b>GM</b>	silty gravel	
	Sand: > 50% of coarse fraction passes 5 mm sieve	clean sand	<b>GC</b>	clayey gravel	
			<b>SW</b>	well graded sand	
			<b>SP</b>	poorly graded sand	
		sand with > 12% fines	<b>SM</b>	silty sand	
			<b>SC</b>	clayey sand	
			<b>ML</b>	Silt	
<b>Fine grained soils:</b> more than 50% passes 0.075 mm sieve	Silt and clay: Liquid Limit < 50	inorganic	<b>CL</b>	Clay	
		organic	<b>OR</b>	organic silt organic clay	
	Silt and clay: Liquid Limit > 50	inorganic	<b>MH</b>	silt of high plasticity elastic silt	
			<b>CH</b>	clay of high plasticity fat clay	
		organic	<b>OH</b>	organic clay organic silt	
	<b>Highly organic soils</b>			<b>Pt</b>	peat

**Figure B3: Unified soil classification system (SAPEM, 2014)**

## Appendix C: Locations of soil investigation points

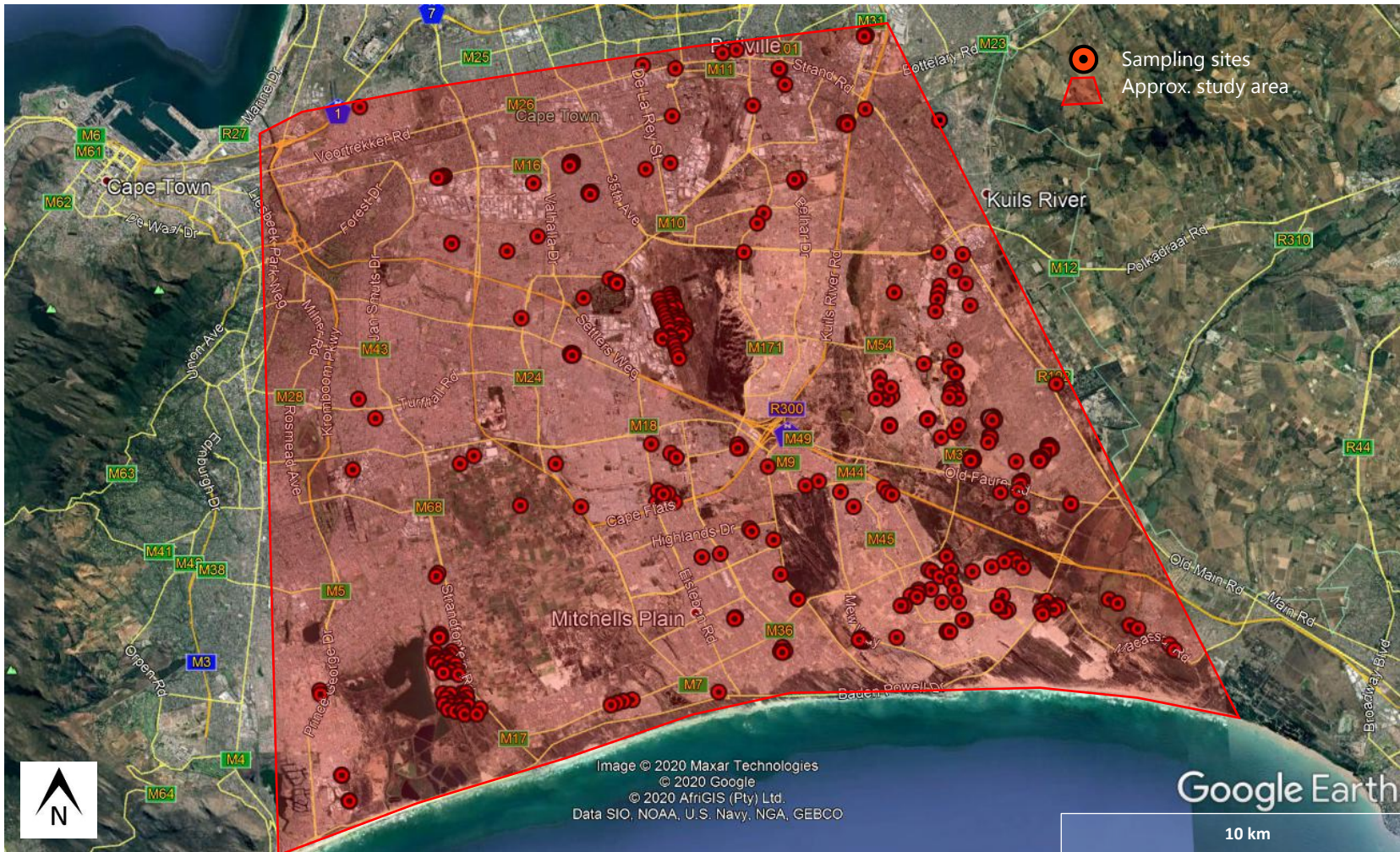


Figure C1: Sites with known grading data (base map Google Earth Pro, 2020). Due to large geographical extent of the study area (and the scale of the map), sampling sites in close proximity plot in an overlapping manner.

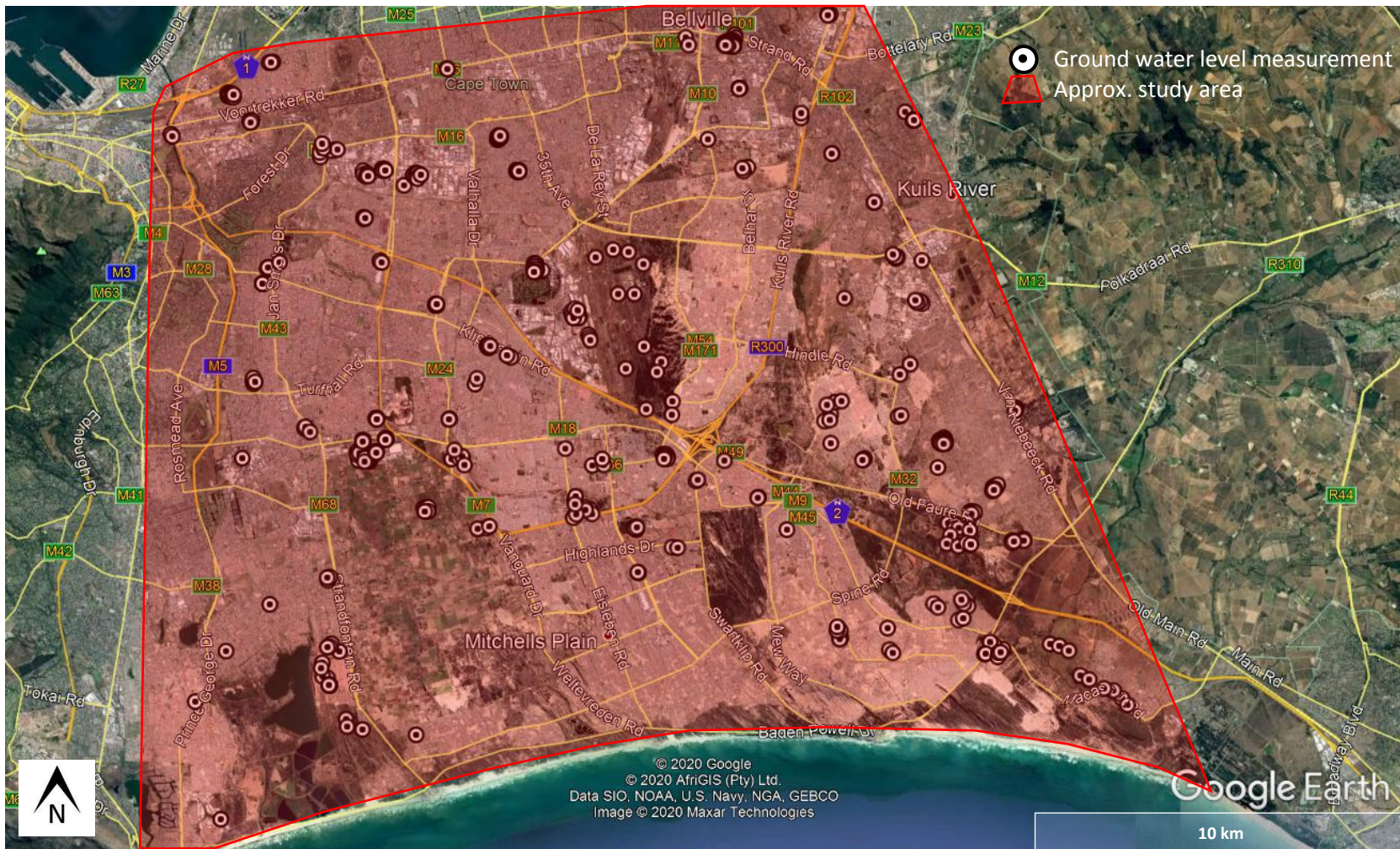


Figure C2: Sites with ground water level data (base map Google Earth Pro, 2020)

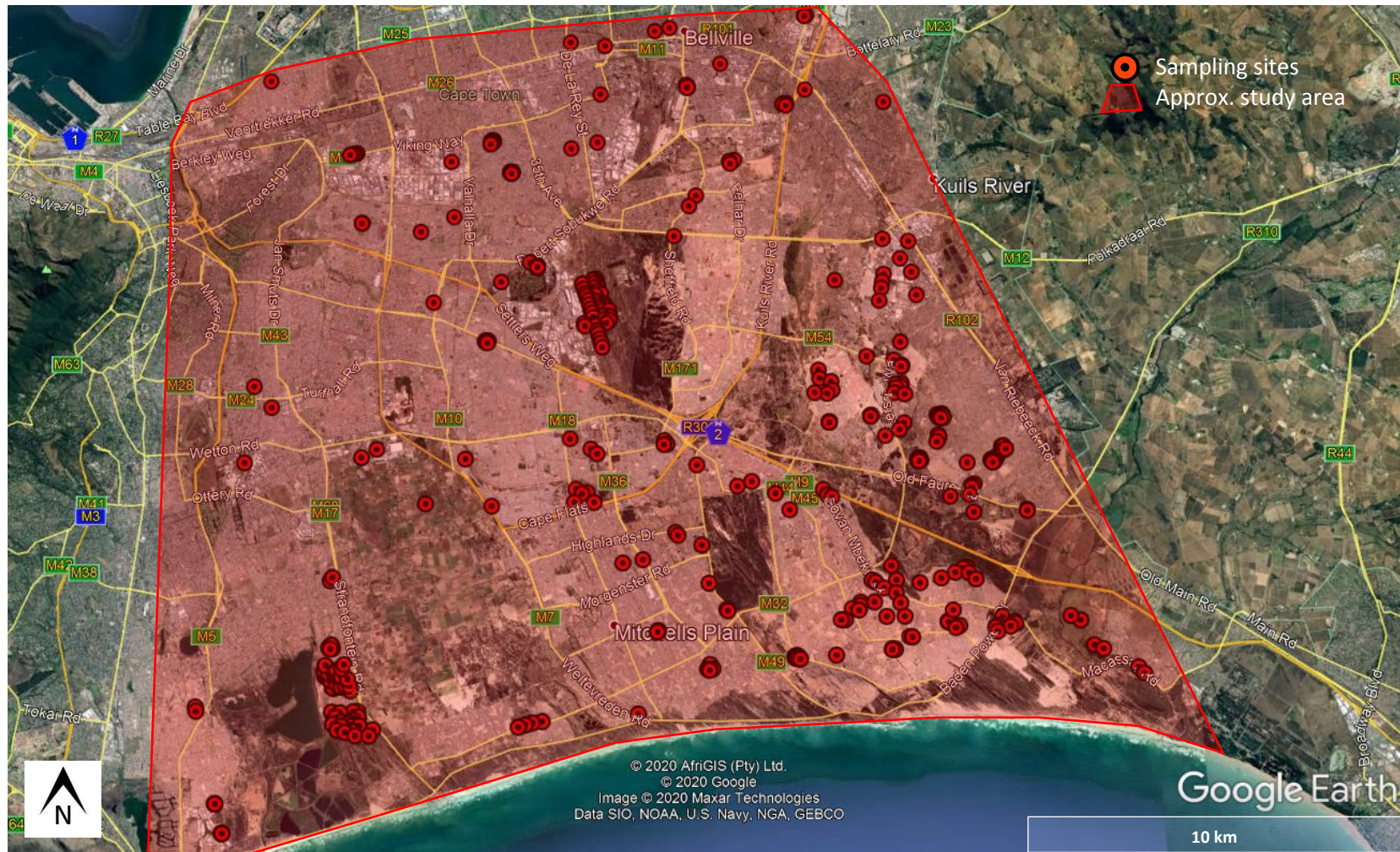


Figure C3: Sites with soil plasticity data and USCS and AASHTO classification (base map Google Earth Pro, 2020)







Figure C6: Sites with corrosivity data (base map Google Earth Pro, 2020)

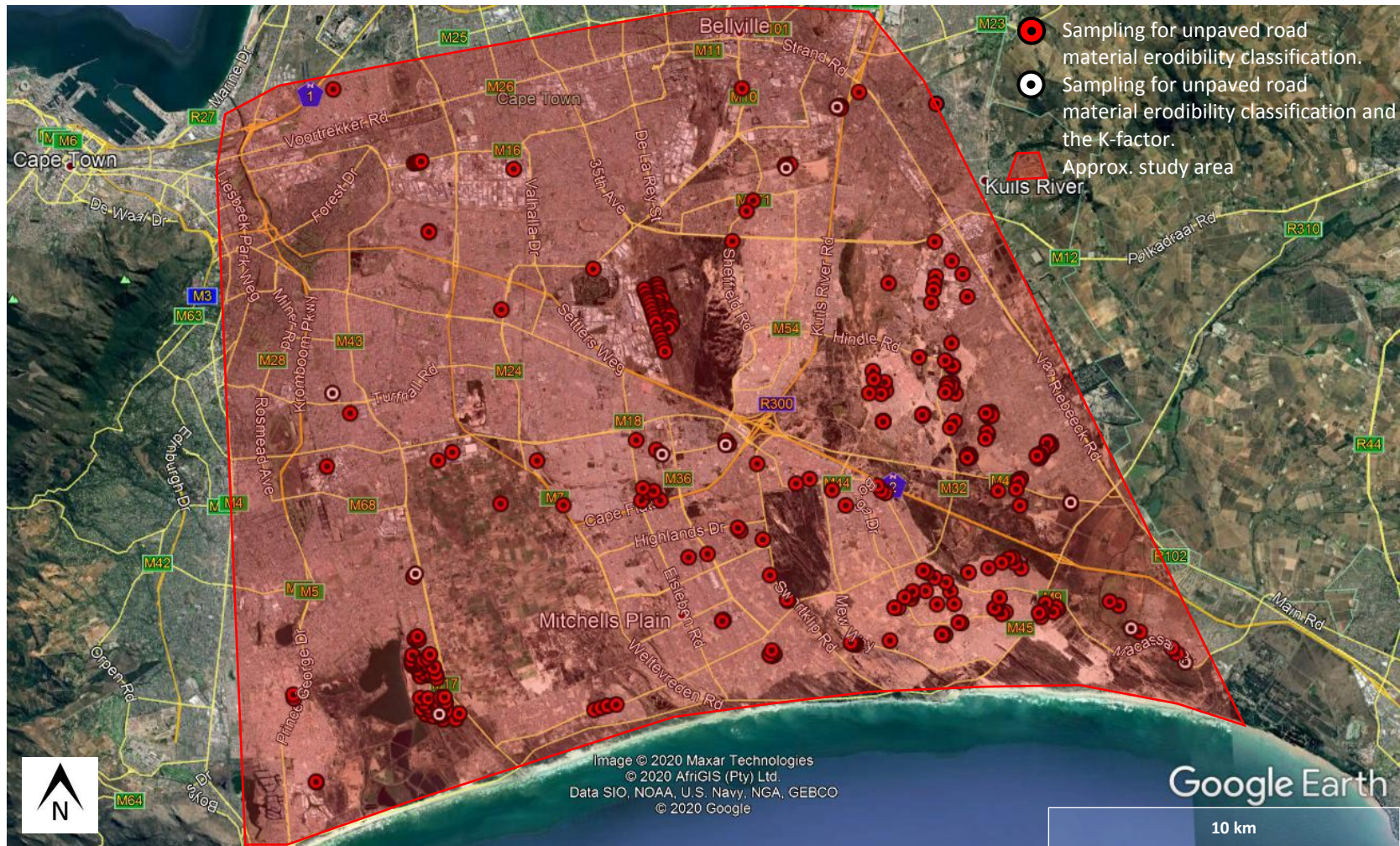


Figure C7: Sites with erodibility data (base map Google Earth Pro, 2020)

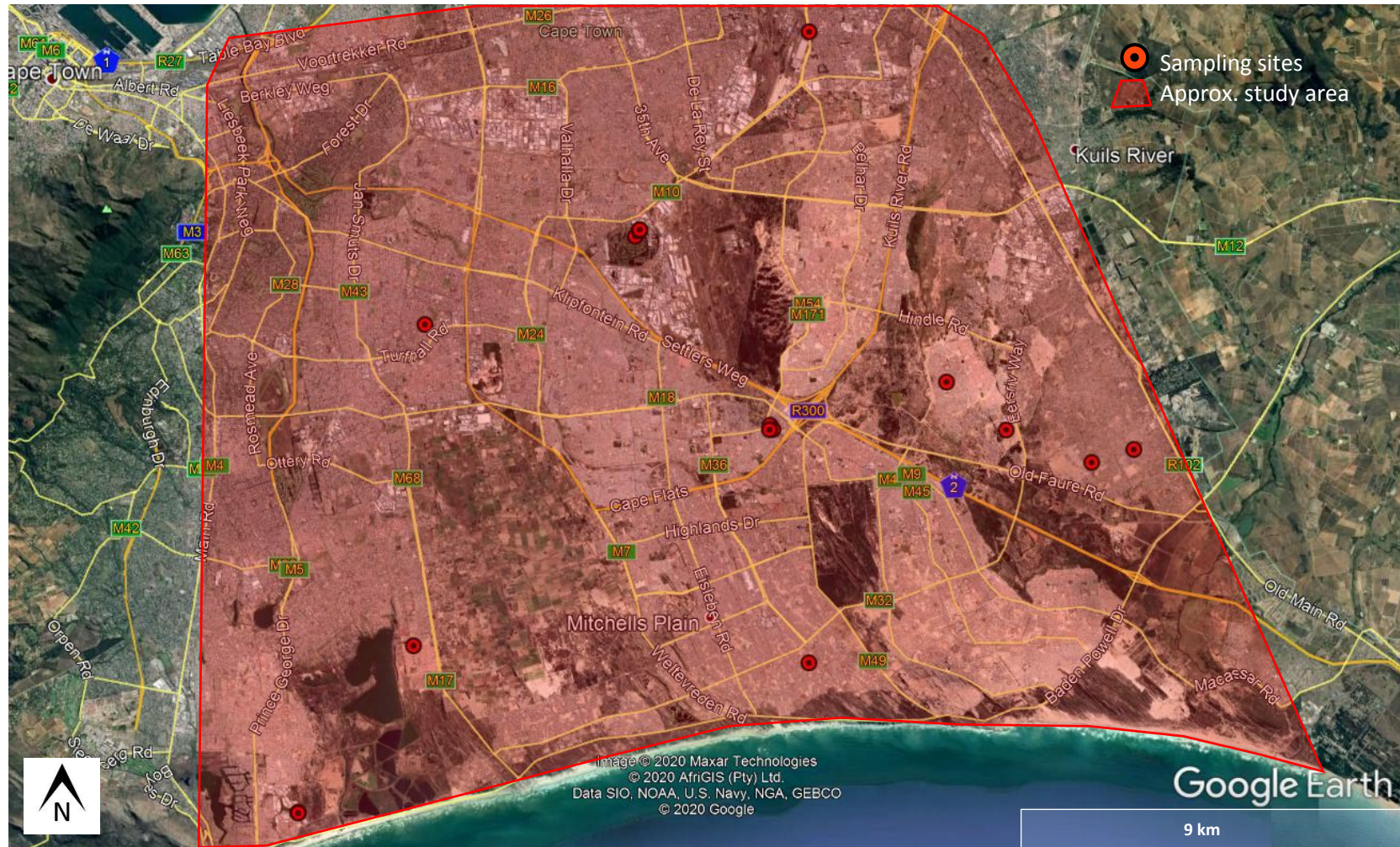


Figure C8: Sites with specific gravity data (base map Google Earth Pro, 2020)

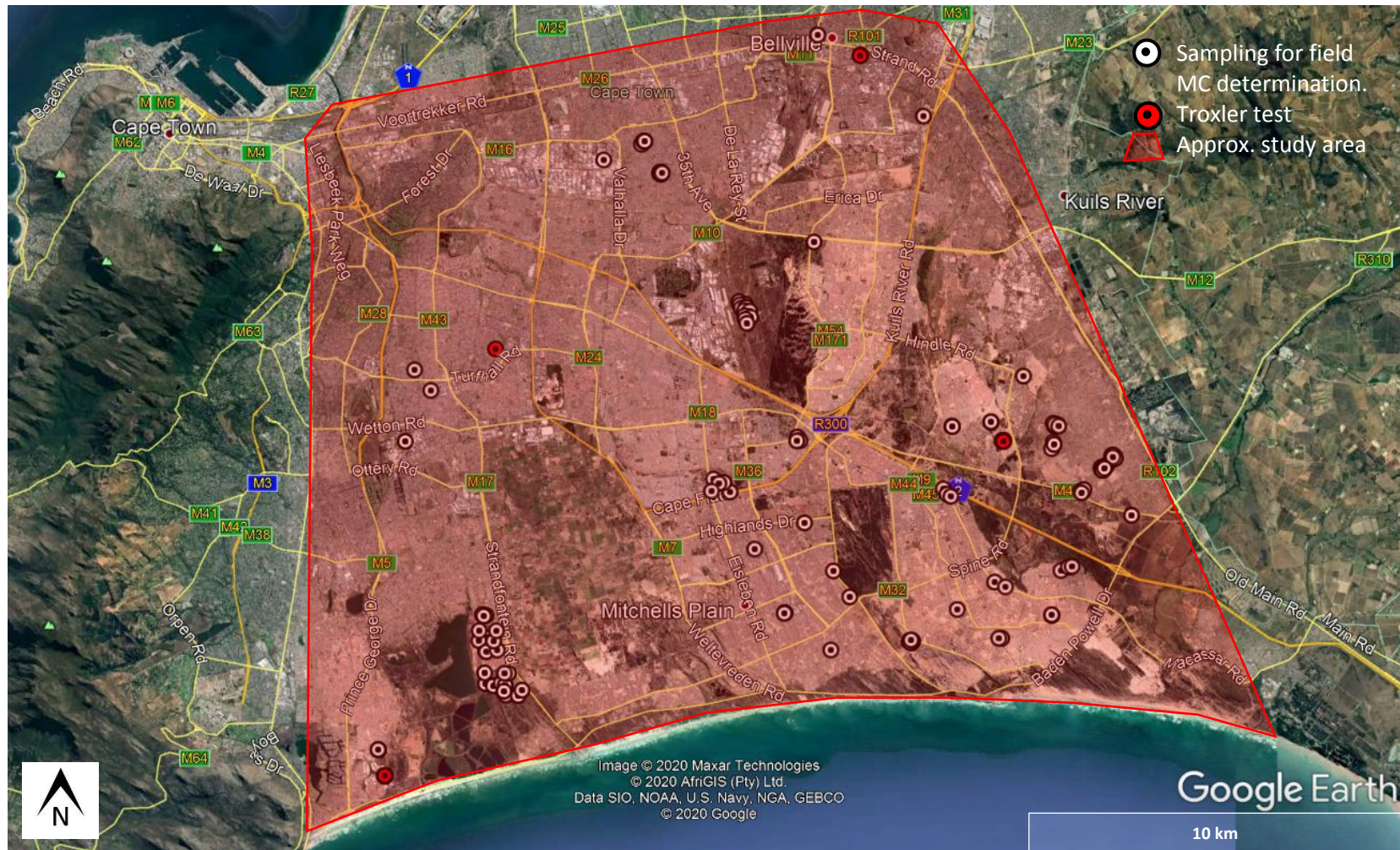


Figure C9: Sites with in-situ density and moisture content data (base map Google Earth Pro, 2020)



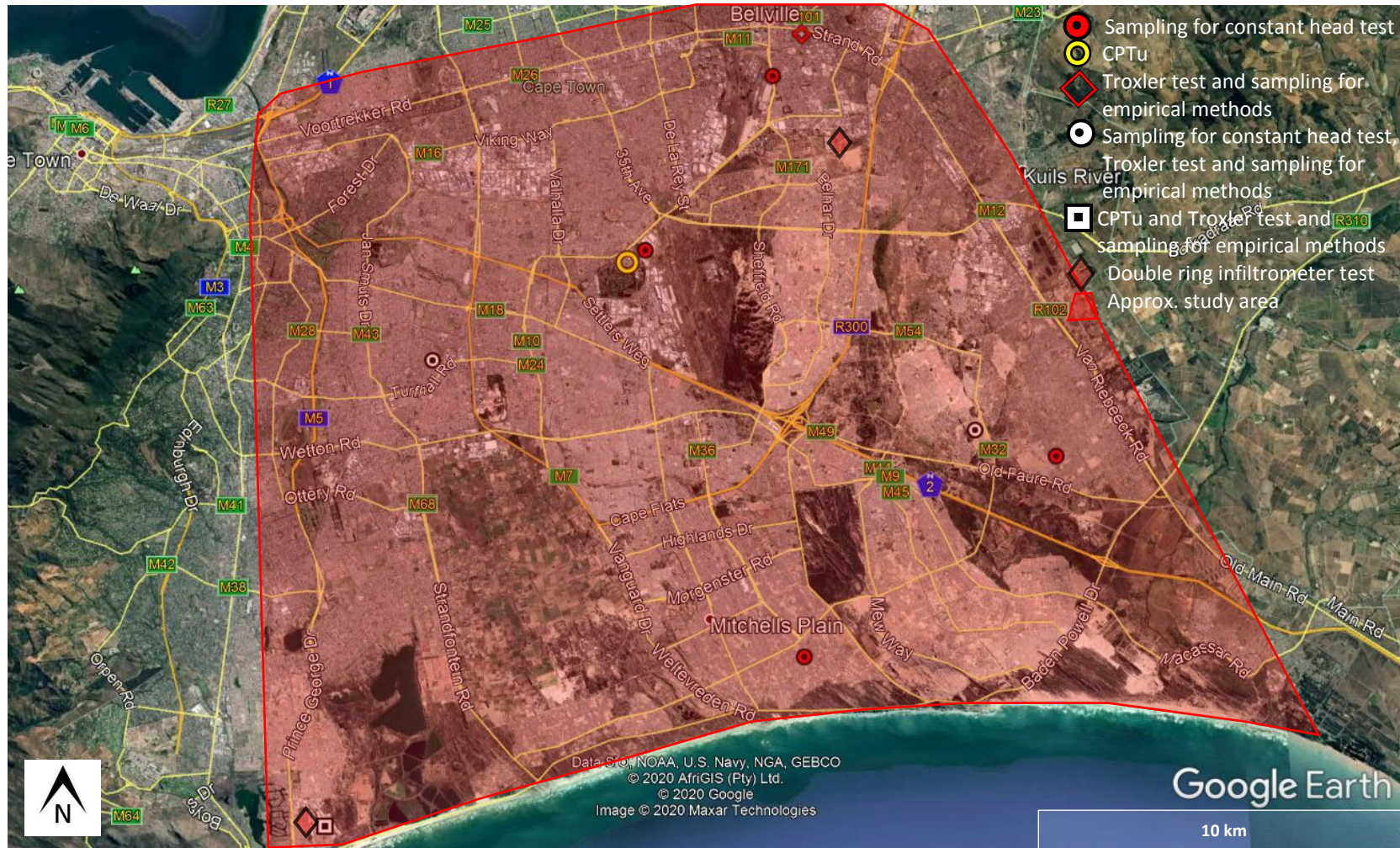


Figure C11: Sites with known hydraulic conductivities (base map Google Earth Pro, 2020)

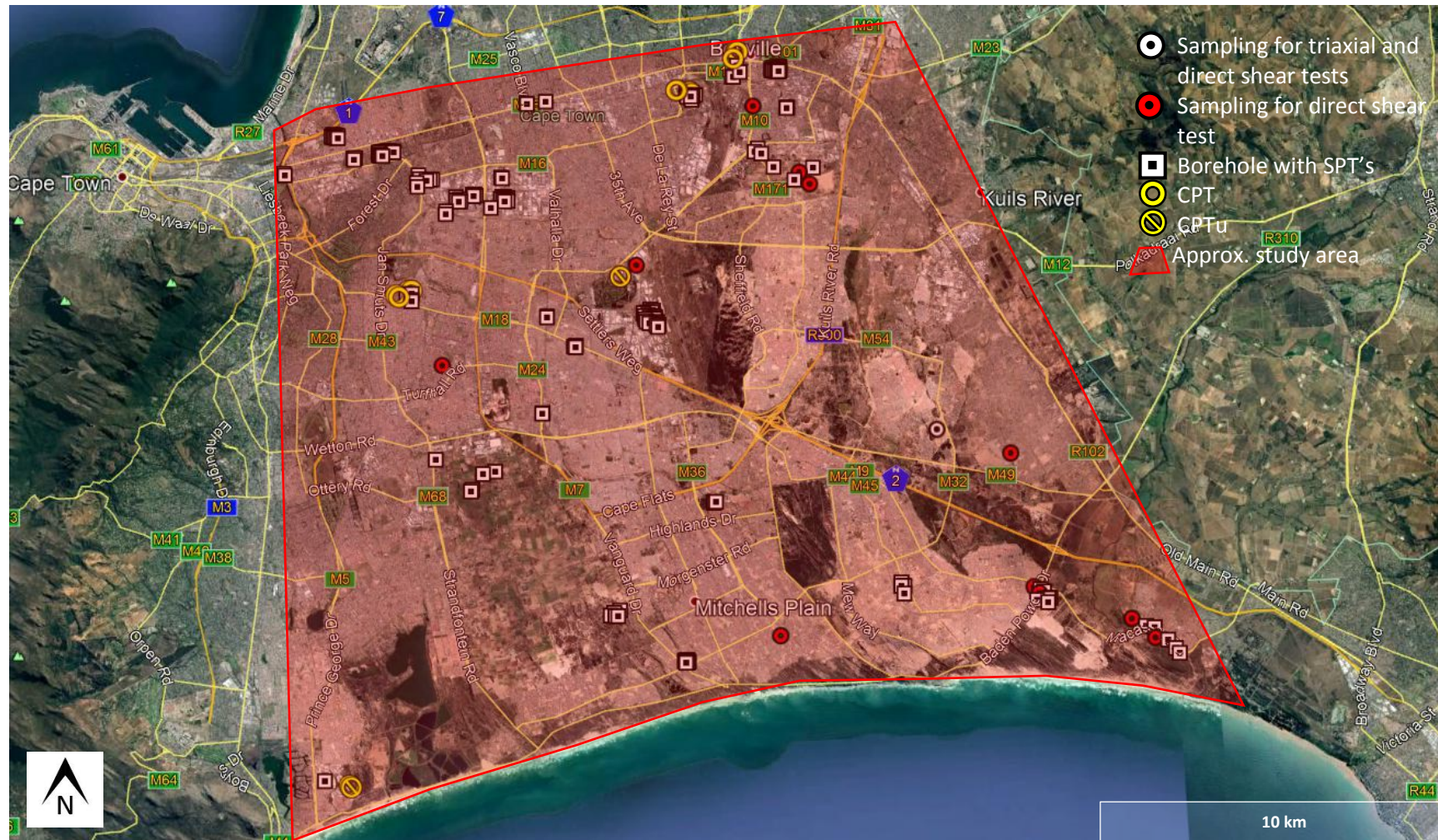


Figure C12: Sites with shear strength and compressibility data (base map Google Earth Pro, 2020)

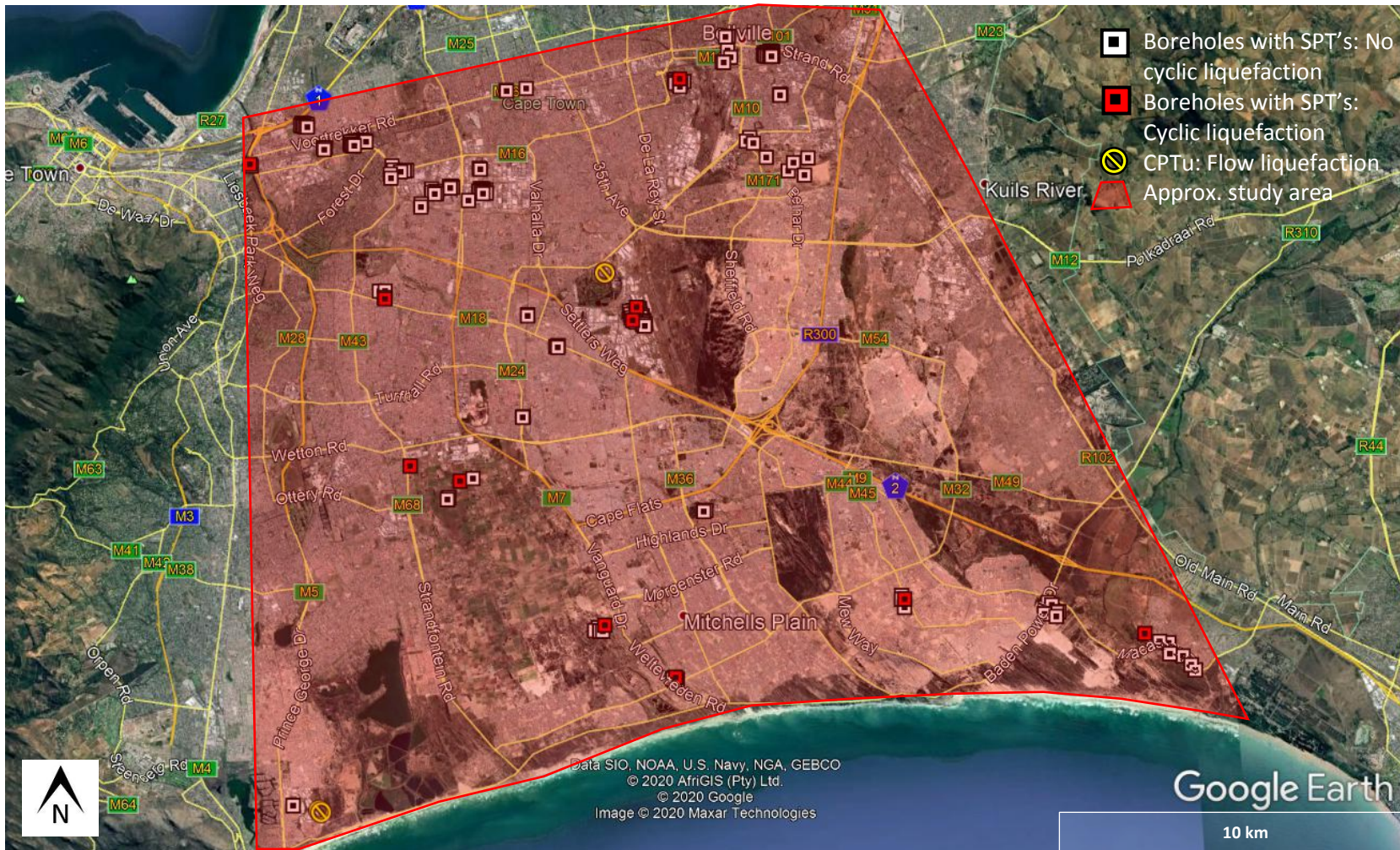


Figure C13: Sites with liquefiable and non-liquefiable soils (base map Google Earth Pro, 2020)

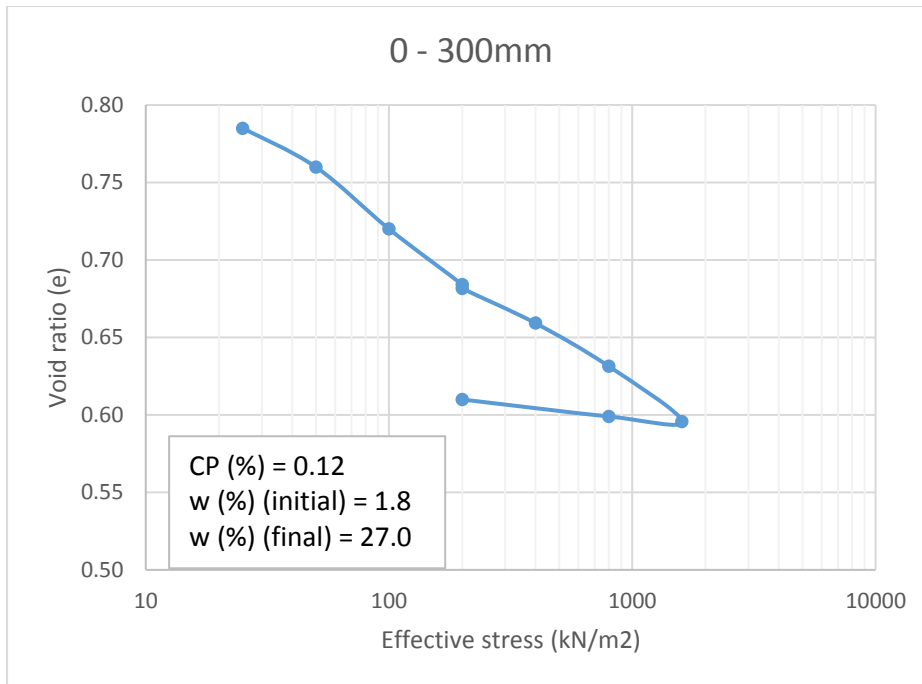


Figure C14: Sites with CSW and SPT data (base map Google Earth Pro, 2020)

## Appendix D: Collapse potential test results

**200kPa saturation test information: Test Pit 1**

**Test date: 18 June 2018**



**Figure D1: Collapse potential (CP) test result for TP1 0 to 300mm at 200kPa saturation**

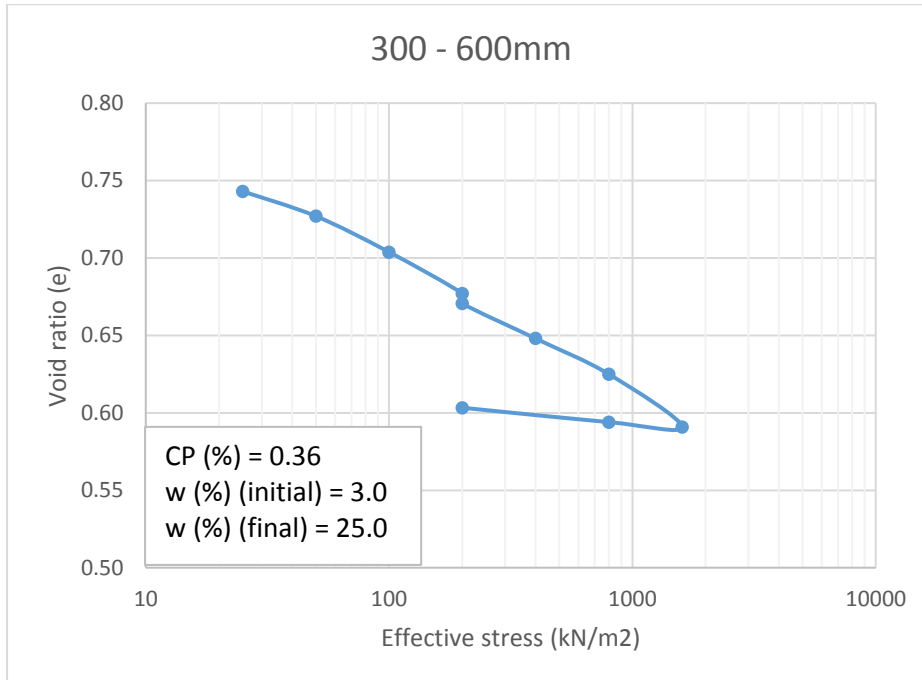


**Figure D2: Collapse potential (CP) test result for TP1 300 to 600mm at 200kPa saturation**

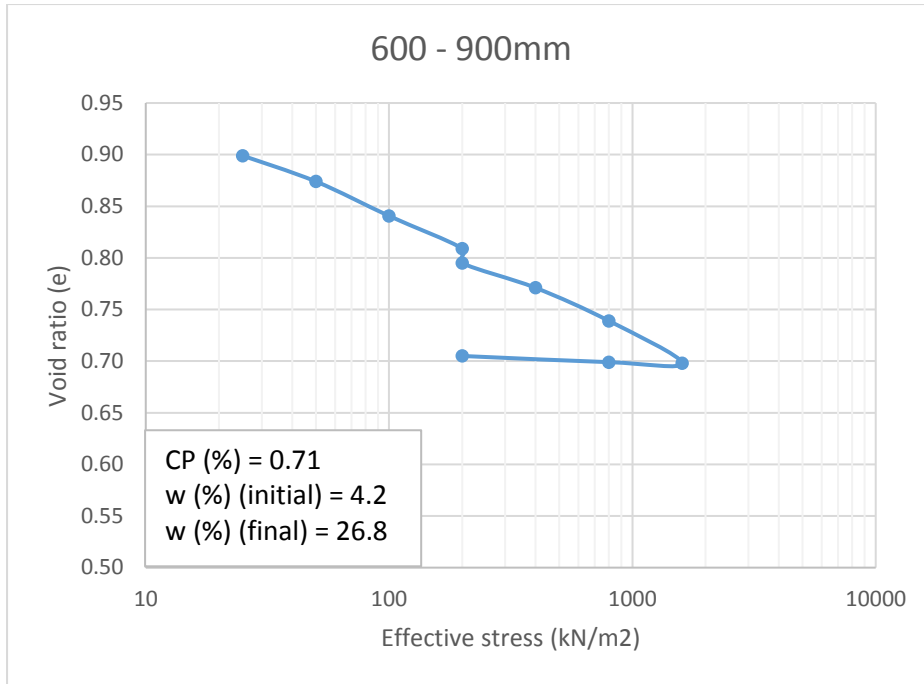


Figure D3: Collapse potential (CP) test result for TP1 600 to 900mm at 200kPa saturation

**200kPa saturation test information: Test Pit 2**

**Test date: 18 June 2018**

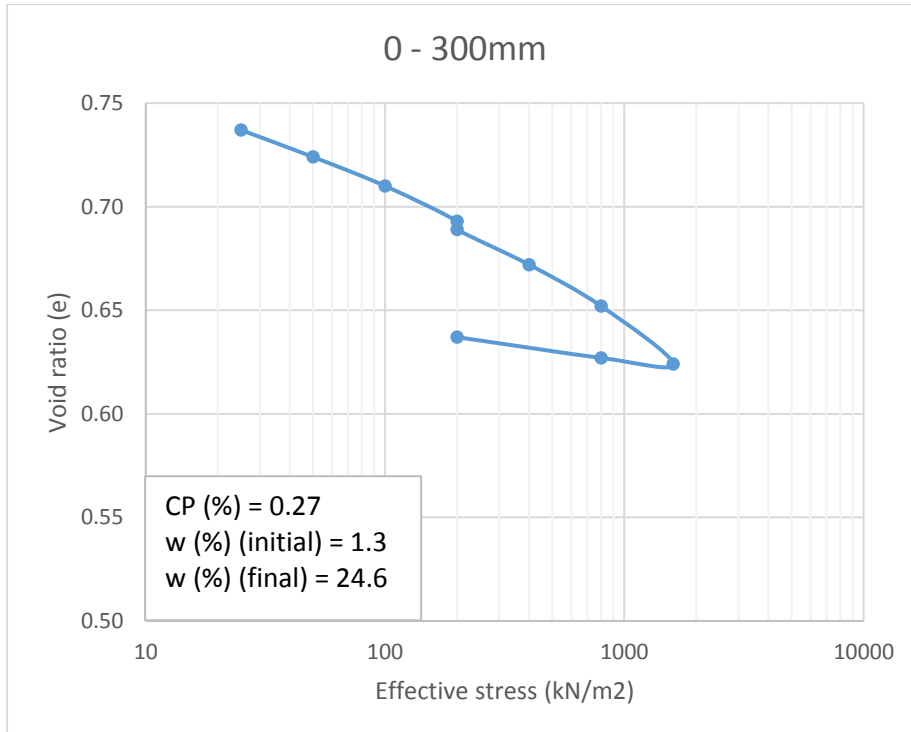


Figure D4: Collapse potential (CP) test result for TP2 0 to 300mm at 200kPa saturation

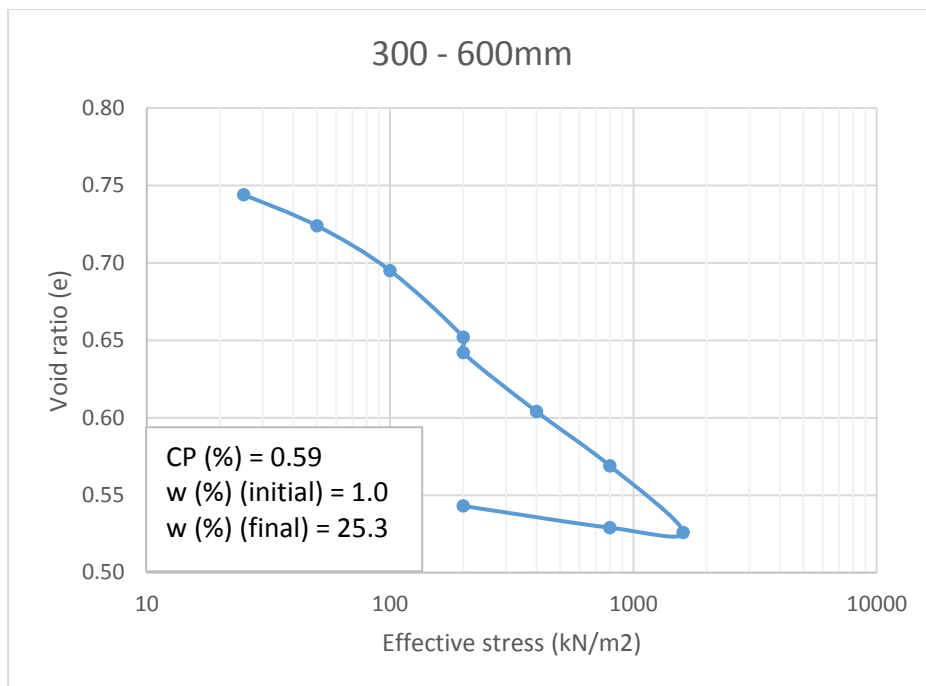


Figure D5: Collapse potential (CP) test result for TP2 300 to 600mm at 200kPa saturation

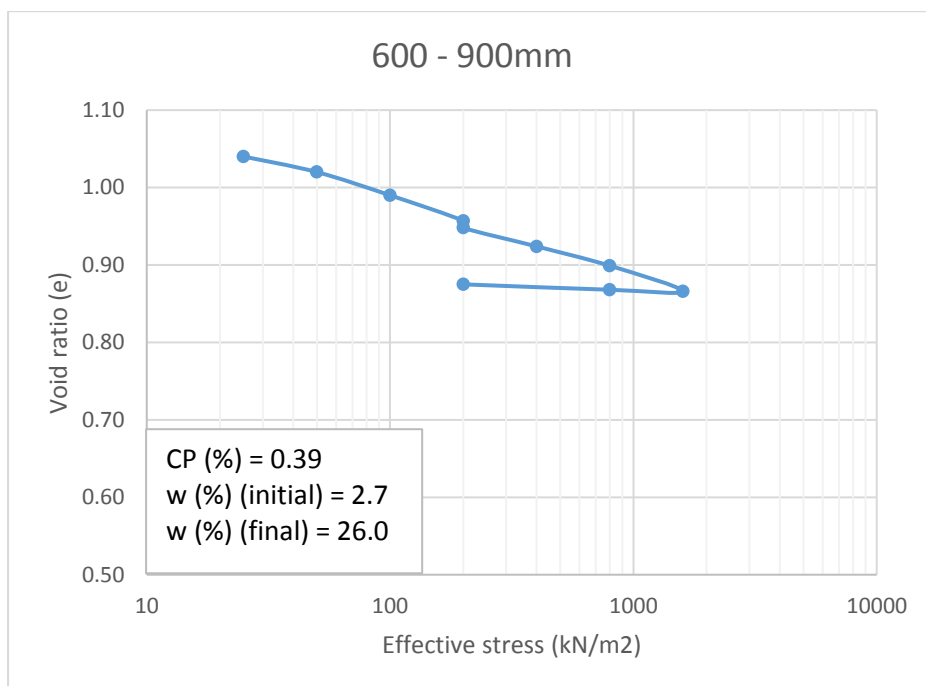
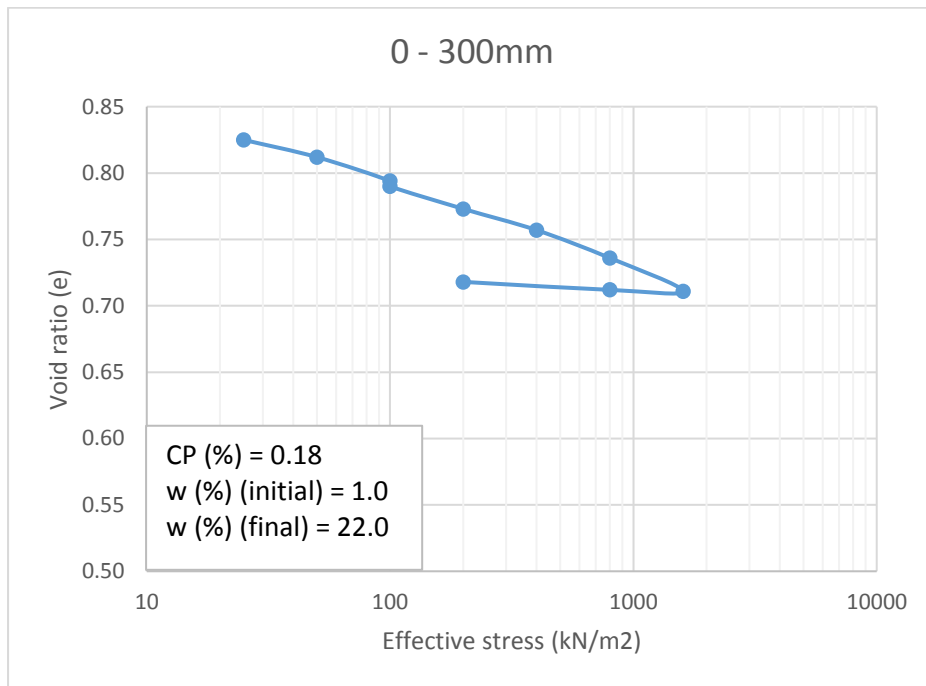


Figure D6: Collapse potential (CP) test result for TP2 600 to 900mm at 200kPa saturation

**100kPa saturation test information: Test pit 1**

**Test date: 2 July 2018**



**Figure D7: Collapse percentage (CP) for TP1 0 to 300mm at 100kPa saturation**

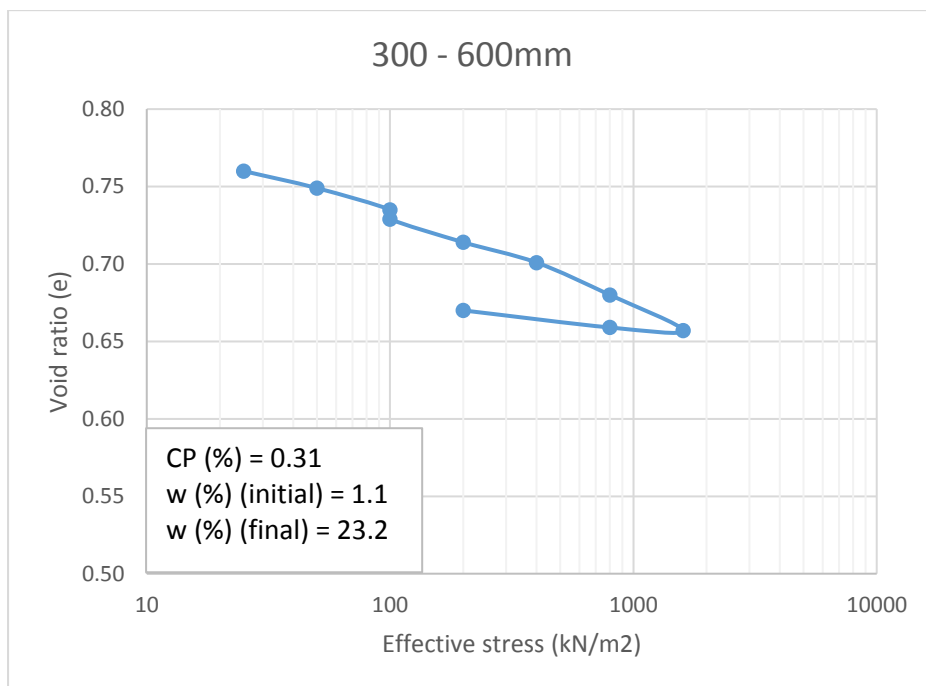


**Figure D8: Collapse percentage (CP) for TP1 300 to 600mm at 100kPa saturation**

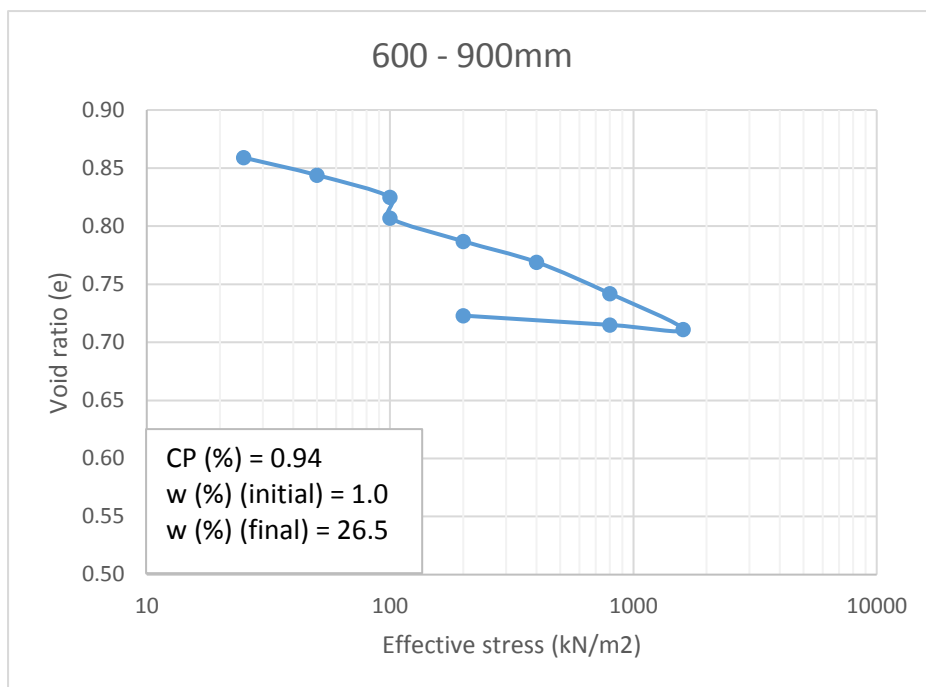


Figure D9: Collapse percentage (CP) for TP1 600 to 900mm at 100kPa saturation

100kPa saturation test information: Test pit 2

Test date: 2 July 2018

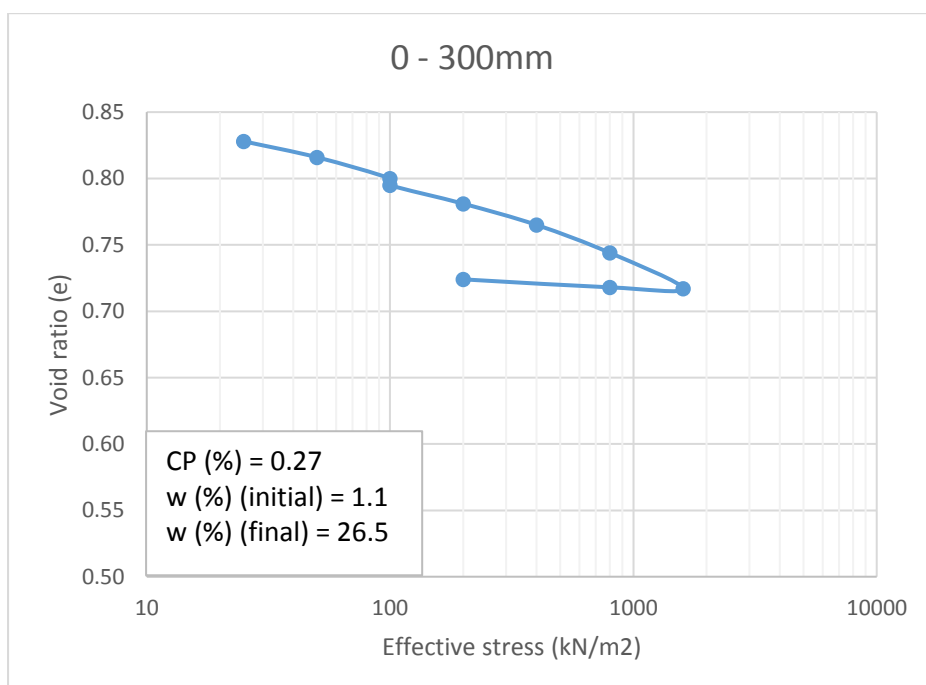


Figure D10: Collapse percentage (CP) for TP2 0 to 300mm at 100kPa saturation

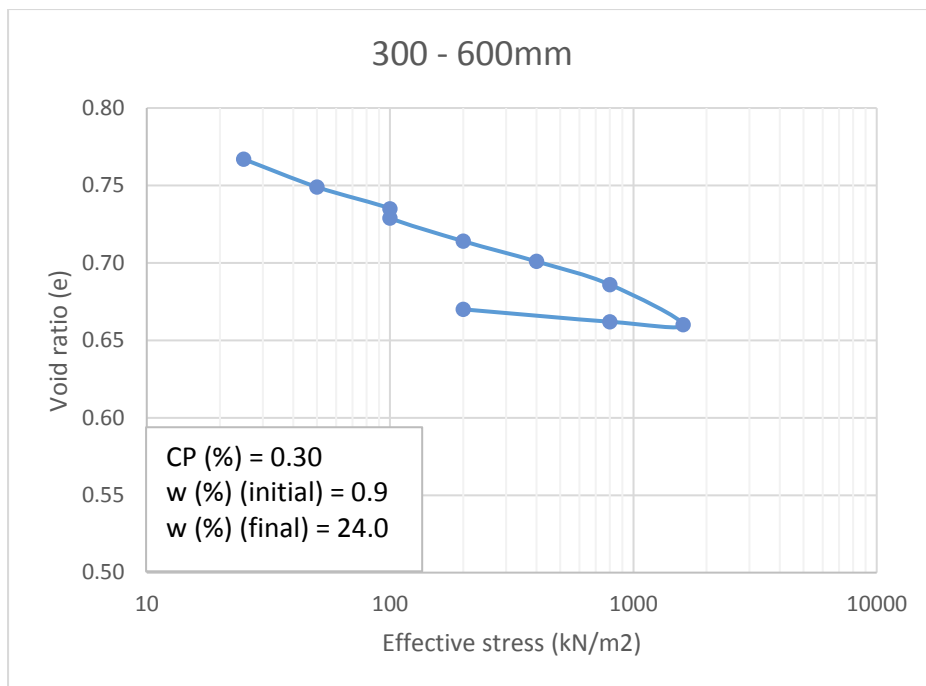


Figure D11: Collapse percentage (CP) for TP2 300 to 600mm at 100kPa saturation

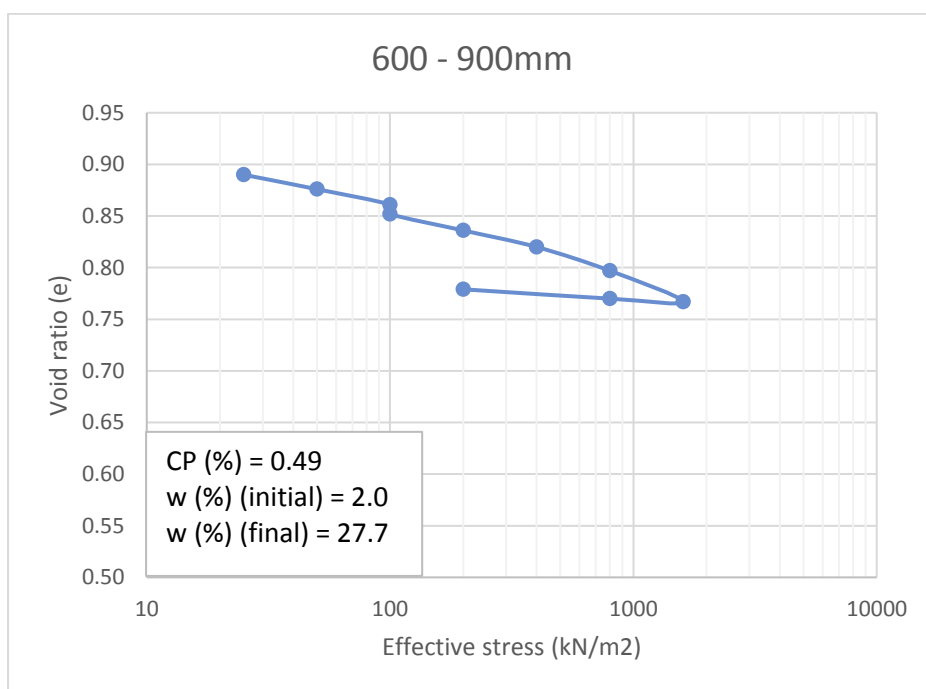


Figure D12: Collapse percentage (CP) for TP2 600 to 900mm at 100kPa saturation

## Appendix E: Dynamic triaxial test data

Table E1: Dynamic triaxial testing loading regime

Phase	Confinement Pressure (kPa)	Static force at failure (kN)	$\sigma_{d,f}$ (kPa)	$\sigma_{1,f}$ (kPa)	Deviator stress Ratio (DSR) (%)	$\sigma_d$ (kPa)	$\sigma_1$ (kPa)	Dynamic force (kN)
<b>Specimen: <math>P_d = 1560\text{kg/m}^3</math>; <math>w = 9\%</math> Test 1</b>								
1	50	4.28	236	286	10	23.38	73.4	0.42
					17	39.48	89.5	0.72
					24	55.54	105.5	1.01
					30	71.77	121.8	1.30
2	100	6.11	336.7	436.7	9	30.71	130.7	0.56
					17	56.39	156.4	1.02
					24	80.99	181.0	1.47
					31	105.61	205.6	1.92
3	150	9.15	504.2	654.2	9	44.42	194.4	0.81
					17	83.43	233.4	1.51
					24	122.29	272.3	2.22
					32	162.45	312.5	2.95
<b>Specimen: <math>P_d = 1560\text{kg/m}^3</math>; <math>w = 9\%</math> Test 2</b>								
1	50	4.28	236	286	10	22.91	72.9	0.42
					18	41.54	91.5	0.75
					24	57.30	107.3	1.04
					31	74.15	124.1	1.35
2	100	6.11	336.7	436.7	10	33.22	133.2	0.60
					17	56.84	156.8	1.03
					24	82.44	182.4	1.50
					32	108.05	208.1	1.96
3	150	9.15	504.2	654.2	9	45.51	195.5	0.83
					17	84.57	234.6	1.53
					25	124.25	274.3	2.25
					33	164.86	314.9	2.99
<b>Specimen: <math>P_d = 1560\text{kg/m}^3</math>; <math>w = 12\%</math> Test 1</b>								
1	50	5.43	299.4	349.4	8	23.54	73.5	0.43
					15	46.35	96.4	0.84
					22	65.79	115.8	1.19
					29	85.94	135.9	1.56
2	100	8.79	484.5	584.5	8	40.95	140.9	0.74
					16	75.61	175.6	1.37
					23	110.63	210.6	2.01
					30	146.08	246.1	2.65
3	150	12.33	679.7	829.7	8	56.11	206.1	1.02
					16	107.57	257.6	1.95
					24	159.88	309.9	2.90
					31	213.67	363.7	3.88

Phase	Confinement Pressure (kPa)	Static force at failure (kN)	$\sigma_{d,f}$ (kPa)	$\sigma_{1,f}$ (kPa)	Deviator stress Ratio (DSR) (%)	$\sigma_d$ (kPa)	$\sigma_1$ (kPa)	Dynamic force (kN)
<b>Specimen: <math>P_d = 1560\text{kg/m}^3</math>; <math>w = 12\%</math> Test 2</b>								
1	50	5.43	299.4	349.4	8	24.62	74.6	0.45
					16	49.24	99.2	0.89
					23	68.91	118.9	1.25
					30	89.60	139.6	1.63
2	100	8.79	484.5	584.5	9	44.32	144.3	0.80
					16	78.76	178.8	1.43
					24	114.12	214.1	2.07
					31	150.20	250.2	2.73
3	150	12.33	679.7	829.7	9	58.81	208.8	1.07
					16	110.74	260.7	2.01
					24	164.23	314.2	2.98
					32	219.24	369.2	3.98
<b>Specimen: <math>P_d = 1660\text{kg/m}^3</math>; <math>w = 9\%</math> Test 1</b>								
1	50	4.48	246.7	296.7	9	22.16	72.2	0.40
					18	45.54	95.5	0.83
					25	60.63	110.6	1.10
					31	77.19	127.2	1.40
2	100	8.72	480.4	580.4	10	46.12	146.1	0.84
					17	80.30	180.3	1.46
					24	117.11	217.1	2.13
					32	153.12	253.1	2.78
3	150	13.43	739.9	889.9	9	66.45	216.4	1.21
					17	124.35	274.3	2.26
					25	183.75	333.7	3.33
					33	244.48	394.5	4.44
<b>Specimen: <math>P_d = 1660\text{kg/m}^3</math>; <math>w = 9\%</math> Test 2</b>								
1	50	4.48	246.7	296.7	9	21.01	71.0	0.38
					17	42.62	92.6	0.77
					25	60.61	110.6	1.10
					32	79.46	129.5	1.44
2	100	8.72	480.4	580.4	9	42.83	142.8	0.78
					17	81.38	181.4	1.48
					25	120.89	220.9	2.19
					33	160.06	260.1	2.90
3	150	13.43	739.9	889.9	9	64.86	214.9	1.18
					17	127.23	277.2	2.31
					26	190.22	340.2	3.45
					34	255.16	405.2	4.63

Phase	Confinement Pressure (kPa)	Static force at failure (kN)	$\sigma_{d,f}$ (kPa)	$\sigma_{1,f}$ (kPa)	Deviator stress Ratio (DSR) (%)	$\sigma_d$ (kPa)	$\sigma_1$ (kPa)	Dynamic force (kN)
<b>Specimen: <math>P_d = 1660\text{kg/m}^3</math>; <math>w = 12\%</math> Test 1</b>								
1	50	5.46	301.1	351.1	8	25.07	75.1	0.45
					17	50.63	100.6	0.92
					24	73.49	123.5	1.33
					32	96.33	146.3	1.75
2	100	9.42	518.9	618.9	9	46.22	146.2	0.84
					17	87.44	187.4	1.59
					25	129.07	229.1	2.34
					33	171.38	271.4	3.11
3	150	14.85	818.2	968.2	9	70.99	221.0	1.29
					17	139.50	289.5	2.53
					26	208.68	358.7	3.79
					34	281.11	431.1	5.10
<b>Specimen: <math>P_d = 1660\text{kg/m}^3</math>; <math>w = 12\%</math> Test 2</b>								
1	50	5.46	301.1	351.1	7	22.02	72.0	0.40
					17	49.72	99.7	0.90
					24	72.22	122.2	1.31
					32	95.68	145.7	1.74
2	100	9.42	518.9	618.9	9	45.78	145.8	0.83
					17	86.86	186.9	1.58
					25	129.24	229.2	2.35
					33	172.09	272.1	3.12
3	150	14.85	818.2	968.2	9	71.19	221.2	1.29
					17	139.66	289.7	2.53
					26	209.91	359.9	3.81
					35	282.88	432.9	5.13

## Appendix F: Oedometer test results

STATE OF SAMPLE	: Undisturbed	SPECIFIC GRAVITY (EST)	= 2.65
DRY DENSITY	= 1476 Kg/m <sup>3</sup>	FINAL SATURATION	= 0.78
INITIAL SATURATION	= 0.69	FINAL MOISTURE CONTENT	= 22.43 %
INITIAL MOISTURE CONTENT	= 20.77 %	FINAL VOID RATIO	= 0.7575
INITIAL VOID RATIO	= 0.7945		

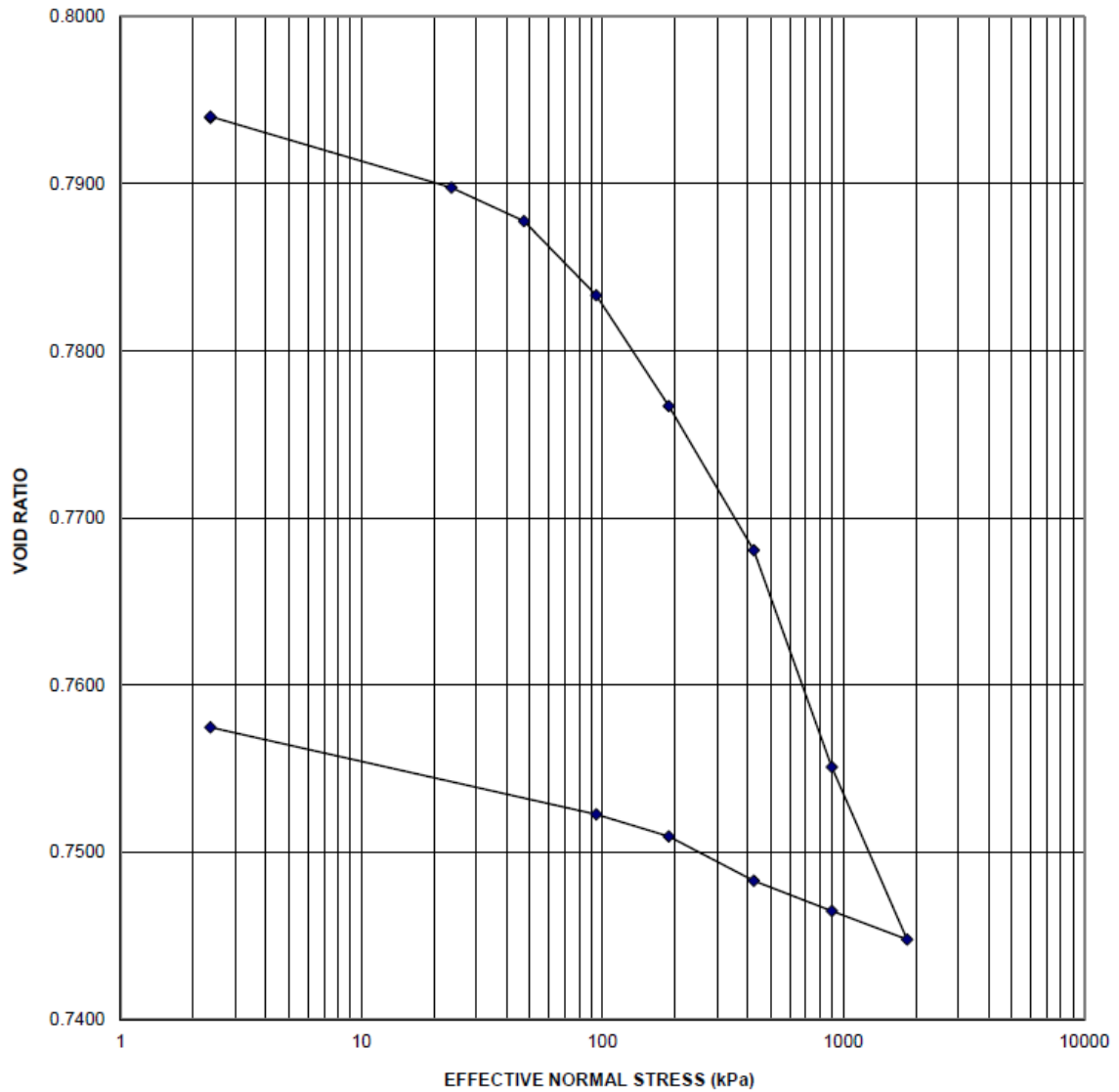


Figure F1: Oedometer test on Blue Downs sand

STATE OF SAMPLE	: Undisturbed	SPECIFIC GRAVITY (EST)	= 2.65
DRY DENSITY	= 1792 Kg/m <sup>3</sup>	FINAL SATURATION	= 0.90
INITIAL SATURATION	= 0.80	FINAL MOISTURE CONTENT	= 12.11 %
INITIAL MOISTURE CONTENT	= 14.47 %	FINAL VOID RATIO	= 0.3584
INITIAL VOID RATIO	= 0.4789		

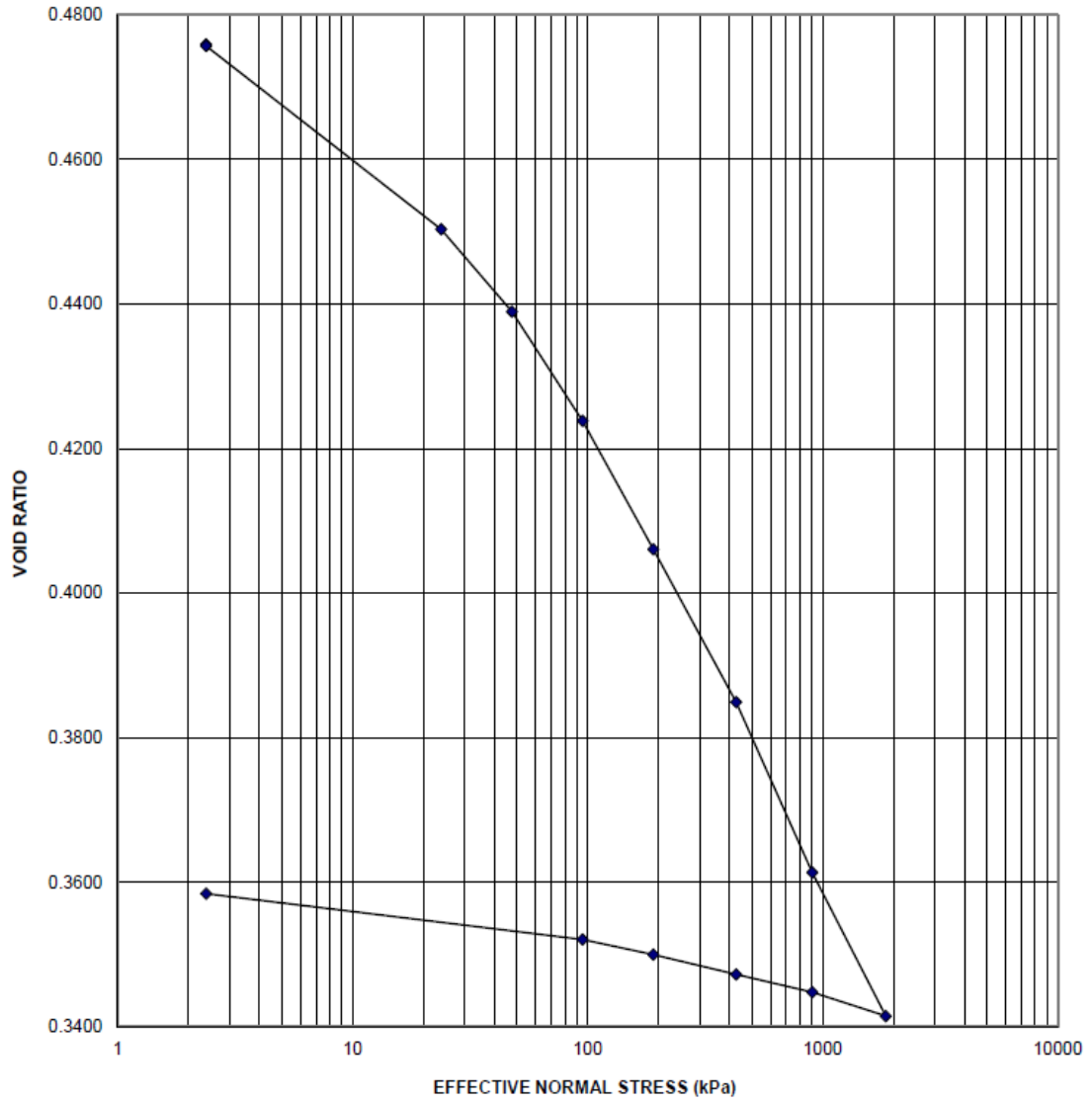


Figure F2: Oedometer test on Blue Downs clayey sand

## Appendix G:

### Results - Summary tables and graphs

Table G1: Grading summary table

Springfontyn Formation						
Fine sand (0.075mm - 0.425mm)						
Depth range (m)	Maximum (%)	Minimum (%)	25 <sup>th</sup> /75 <sup>th</sup> percentile (%)	Average (%)	Standard deviation (%)	Number of values
0 - 1	93	11	65/84	71.3	13.5	66
1 - 2	100	28	61/85	70.5	15.5	64
2 - 3	86	44	62/79	68.6	12.0	16
3 - 4	82	77	-	79.5	3.5	2
Medium sand (0.425mm – 2mm)						
0 - 1	83	1	9/29	20.0	14.7	66
1 - 2	70	0	7/29	19.7	15.4	64
2 - 3	55	2	8/17	14.7	12.8	16
3 - 4	21	16	-	18.5	3.5	2
Coarse sand (2mm – 4.75mm)						
0 - 1	8	0	0	0.5	1.2	66
1 - 2	8	0	0	0.6	1.4	64
2 - 3	8	0	0/1.25	1.2	2.1	16
3 - 4	0	0	-	0	0	2
Gravel (>4.75mm)						
0 - 1	8	0	0	0.8	1.9	66
1 - 2	11	0	0	0.8	2.2	64
2 - 3	11	0	0/3	1.8	3.3	16
3 - 4	0	0	-	0	0	2
Silt (0.005mm – 0.075mm)						
0 - 1	11	0	2/5	3.9	2.7	36
1 - 2	29	0	2/6	5.0	6.0	37
2 - 3	18	0	2/10	6.4	5.0	13
Clay (<0.005mm)						
0 - 1	15	0	0/3.5	3.2	3.6	36
1 - 2	30	0	3/7	6.2	7.3	37
2 - 3	28	0	5/14	10.2	8.7	13
Fines (silt and clay) (no hydrometer test)						
0 - 1	38	1	3/8.5	7.9	9.4	30
1 - 2	38	0	2/5	5.4	7.7	27
2 - 3	2	2	-	2.0	0	3
3 - 4	2	2	-	2.0	0	2
Witzand Formation						
Fine sand (0.075mm - 0.425mm)						
Depth range (m)	Maximum (%)	Minimum (%)	25 <sup>th</sup> /75 <sup>th</sup> percentile (%)	Average (%)	Standard deviation (%)	Number of values
0 - 1	99	20	71/87	76.1	14.9	184
1 - 2	99	24	69/87	75.1	16.2	125
2 - 3	95	42	53/88	72.8	18.0	33
3 - 13	91	70	74/84	79.2	6.9	10
Medium sand (0.425mm – 2mm)						
0 - 1	70	0	8/22	17.1	13.2	184
1 - 2	62	0	7/22	16.7	13.1	125
2 - 3	54	1	6/35	19.6	16.9	33
3 - 13	25	2	4.5/18	12.1	8.2	10
Coarse sand (2mm – 4.75mm)						
0 - 1	10	0	0	0.3	1.1	184

1 - 2	10	0	0	0.6	1.6	125
2 - 3	3	0	0	0.1	0.5	33
3 - 13	1	0	0	0.1	0.3	10
<b>Gravel (&gt;4.75mm)</b>						
0 - 1	32	0	0	1.1	4.3	184
1 - 2	36	0	0	2.1	6.2	125
2 - 3	14	0	0	0.6	2.5	33
3 - 13	3	0	0	0.3	0.9	10
<b>Silt (0.005mm – 0.075mm)</b>						
0 - 1	43	0	1/3	2.6	4.4	105
1 - 2	43	0	1/3	3.0	5.6	72
2 - 3	43	0	1/3	4.3	9.3	23
3 - 13	3	1	1/2	1.7	1.2	3
<b>Clay (&lt;0.005mm)</b>						
0 - 1	15	0	0/3	2.1	2.3	105
1 - 2	16	0	1.5/3	2.7	2.4	71
2 - 3	16	0	2/3	3.3	3.3	23
3 - 13	13	2	4/9.5	7.0	5.6	3
<b>Fines (silt and clay) (no hydrometer test)</b>						
0 - 1	33	0	3/8.5	5.9	4.6	79
1 - 2	33	0	2/9	5.4	5.4	53
2 - 3	33	0	1.5/9.5	8.1	9.7	10
3 - 5	10	6	7.5/9	8.1	1.5	7
<b>Langebaan Formation</b>						
<b>Fine sand (0.075mm - 0.425mm)</b>						
Depth range (m)	Maximum (%)	Minimum (%)	25 <sup>th</sup> /75 <sup>th</sup> percentile (%)	Average (%)	Standard deviation (%)	Number of values
0 - 1	96	47	63/83	73.6	13.4	27
1 - 2	96	24	61/83	70.1	18.9	21
2 - 3	86	69	68/81	74.6	7.7	7
3 - 9	93	41	69/82	76.4	15.8	9
<b>Medium sand (0.425mm – 2mm)</b>						
0 - 1	47	1	13/28	19.5	13.0	27
1 - 2	53	1	13/28	21.0	14.0	21
2 - 3	32	4	14/27	19.6	9.8	7
3 - 9	47	1	9/19	16.0	14.8	9
<b>Coarse sand (2mm – 4.75mm)</b>						
0 - 1	1	0	0	0.2	0.4	27
1 - 2	10	0	0	0.6	2.2	21
2 - 3	0	0	0	0	0	7
3 - 9	5	0	0	0.6	1.7	9
<b>Gravel (&gt;4.75mm)</b>						
0 - 1	20	0	0/1	1.4	4	27
1 - 2	21	0	0/1	1.9	6.3	21
2 - 3	0	0	0	0	0	7
3 - 9	0	0	0	0	0	9
<b>Silt (0.005mm – 0.075mm)</b>						
0 - 1	15	0	0/4	2.7	3.7	18
1 - 2	15	0	0/4	3.1	3.7	17
2 - 3	7	3	3/6	4.6	1.8	5
3 - 9	6	3	3.75/4	4.0	0.9	8
<b>Clay (&lt;0.005mm)</b>						
0 - 1	9	1	3/5	3.8	2.0	18

1 - 2	14	1	3/3	3.8	2.9	17
2 - 3	6	1	3/3	3.2	1.8	5
3 - 9	6	3	3/3.75	3.8	1.4	8
<b>Fines (silt and clay) (no hydrometer test)</b>						
0 - 1	5	1	1/4	2.9	1.6	9
1 - 2	1	1	1/1	1	0	4
2 - 3	1	1	-	1	0	2
3 - 4			-			1 (1)

Note: Where soil was sampled from a uniform soil layer spanning two depth intervals (e.g. 0 to 2m), the grading data were included in both depth intervals. The number of data values shown in the table are therefore more than the number of tests performed.

Table G2: Gradation summary table

<b>Springfontyn Formation</b>						
<b>Coefficient of Uniformity, Cu</b>						
Depth range (m)	Maximum	Minimum	25 <sup>th</sup> /75 <sup>th</sup> percentile	Average	Standard deviation	Number of values
0 - 1	24.4	2.0	2.5/3.4	4.6*	4.6	47
1 - 2	46.7	1.7	2.4/3.6	4.6*	7.0	47
2 - 3	46.7	2.3	2.9/5.5	7.6*	12.4	14
3 - 4	3.2	2.9	-	3.1	0.2	2
<b>Coefficient of Curvature, Cz</b>						
0 - 1	9.9	0.7	0.8/1.3	1.7*	2.1	47
1 - 2	13.4	0	0.9/1.2	1.6*	2.2	47
2 - 3	31.4	0.8	1.0/3.2	5.9*	9.6	14
3 - 4	0.9	0.8	-	0.85	0	2
<b>Witzand Formation</b>						
<b>Coefficient of Uniformity, Cu</b>						
0 - 1	21.4	1.4	2.4/3.1	3.1*	2.4	184
1 - 2	24.7	1.4	2.3/3.1	3.4*	3.2	124
2 - 3	18.8	1.9	2.3/3.1	3.6*	3.2	31
3 - 4	3.1	2.5	2.6/2.8	2.8	0.2	6
4 - 13	27.5	2.9	-	11.3*	14.1	3
<b>Coefficient of Curvature, Cz</b>						
0 - 1	29.5	0	0.8/1.1	1.1*	2.1	184
1 - 2	3.0	0	0.8/1.2	1.0	0.3	124
2 - 3	2.6	0.6	0.9/1.3	1.2	0.4	31
3 - 4	0.8	0.7	0.75/0.78	0.8	0	6
4 - 13	9.6	0.8	-	3.9*	5.0	3
<b>Langebaan Formation</b>						
<b>Coefficient of Uniformity, Cu</b>						
0 - 1	5.4	2.1	2.4/3.2	3.0	0.9	27
1 - 2	5.4	2.1	2.3/3.4	3.0	1.0	21
2 - 3	6.3	1.4	2.6/3.0	3.1*	1.5	7
3 - 9	6.3	1.4	2.4/2.9	3.1*	1.6	9
<b>Coefficient of Curvature, Cz</b>						
0 - 1	24	0.7	0.9/1.2	2.8*	4.4	27
1 - 2	9.6	0.7	0.9/1.2	1.5*	1.9	21
2 - 3	1.4	0.9	1.0/1.2	1.1	0.2	7
3 - 9	1.4	1.0	0.9/1.0	1.1*	0.3	9

\*Average skewed by few large values

Note: Where soil was sampled from a uniform soil layer spanning two depth intervals (e.g. 0 to 2m), the gradation data were included in both depth intervals. The number of data values shown in the table are therefore more than the number of tests performed.

Table G3: MDD and OMC summary table

Springfontyn Formation						
Maximum dry density (kg/m <sup>3</sup> )						
Depth range (m)	Maximum	Minimum	25 <sup>th</sup> /75 <sup>th</sup> percentile	Average	Standard deviation	Number of values
0 - 1	1920	1606	1748/1819	1783	60.8	33
1 - 2	1888	1701	1729/1789	1768	48.4	19
2 - 3	N/A					1 (Value: 1797)
Optimum moisture content (%)						
0 - 1	12.6	7.8	8.9/11.2	10.2	1.4	33
1 - 2	12.8	7.8	9.5/11.6	10.5	1.4	19
2 - 3	N/A					1 (Value: 9.5)
Witzand Formation						
Maximum dry density (kg/m <sup>3</sup> )						
0 - 1	2000	1530	1658/1782	1729	94.3	81
1 - 2	2000	1563	1670/1788	1746	108.1	48
2 - 3	1760	1563	1599/1715	1654	79.9	6
3 - 4	1776	1674	1741/1771	1746	38.1	6
Optimum moisture content (%)						
0 - 1	19.3	7.5	11.3/13.8	12.5	2.3	81
1 - 2	17.7	8	10.4/13.4	12.2	2.3	48
2 - 3	17.7	8.8	12.1/16.4	13.9	3.4	6
3 - 4	13	11.5	12.5/12.9	12.6	0.5	6
Langebaan Formation						
Maximum dry density (kg/m <sup>3</sup> )						
0 - 1	1756	1483	1537/1673	1602	94.7	10
1 - 2	1765	1497	1550/1716	1629	98.3	8
2 - 3	1632	1557	N/A	1599	38.4	3
Optimum moisture content (%)						
0 - 1	20.4	9.9	14.4/16.8	15.6	2.8	10
1 - 2	17.2	9.2	12.5/16.5	14.3	3.2	8
2 - 3	17.2	15.3	N/A	16.4	0.7	3

Note: Where soil was sampled from a uniform soil layer spanning two depth intervals (e.g. 0 to 2m), the MDD and OMC values were included in both intervals. The number of data values shown in the table are therefore more than the number of tests performed.

Table G4: CBR summary table

Springfontyn Formation							
Compaction level	Property	Maximum	Minimum	25 <sup>th</sup> /75 <sup>th</sup> percentile	Average	Standard deviation	Number of values
MDD	CBR (%)	62	10	20/34	29	10.9	39
	DD (kg/m <sup>3</sup> )	1920	1606	1750/1814	1782	56.7	39
98% MDD	CBR	45	9	15/26	21.9	8	36
	DD	1850	1566	1712/1777	1738	61.3	36
97% MDD	CBR	22	9	13/18	15.1	3.8	11
	DD	1802	1558	1677/1759	1707	68	11
95% MDD	CBR	31	2	10/17	14.4	6.8	39
	DD	1824	1526	1662/1723	1693	53.9	39
93% MDD	CBR	32	2	8/15	12.3	6.4	34
	DD	1756	1494	1630/1688	1657	50.6	34
90% MDD	CBR	22	1	6/13	9.4	5.1	30
	DD	1699	1445	1578/1636	1606	51	30
Witzand Formation							
MDD	CBR	70	9	17/31	25	12.3	115
	DD	2000	1530	1675/1783	1736	94.2	115
98% MDD	CBR	51	8	14/26	22.1	9.6	113
	DD	1960	1499	1642/1747	1701	92.7	113
97% MDD	CBR	48	8	12/22	18	8.7	84
	DD	1940	1540	1639/1729	1695	81.2	84
95% MDD	CBR	42	7.6	11/20	17	7.2	115
	DD	1900	1454	1591/1694	1649	90	115
93% MDD	CBR	36	6	9/16	14	5.8	115
	DD	1860	1423	1558/1658	1614	88	115
90% MDD	CBR	28	3	7/13	11	4.5	115
	DD	1800	1377	1508/1605	1562	84.7	115
Langebaan Formation							
MDD	CBR	55	21	31/42	36	9.5	12
	DD	1765	1483	1550/1700	1615	92.9	12
98% MDD	CBR	47	17	24/30	29	7.8	12
	DD	1730	1453	1519/1664	1583	91.2	12
95% MDD	CBR	36	12	17/23	21	6.4	12
	DD	1677	1409	1473/1614	1534	88.2	12
93% MDD	CBR	30	10	12/20	17	5.8	11
	DD	1641	1379	1436/1547	1493	85.3	11
90% MDD	CBR	23	7	8/17	12	5.2	12
	DD	1589	1335	1395/1529	1453	83.8	12

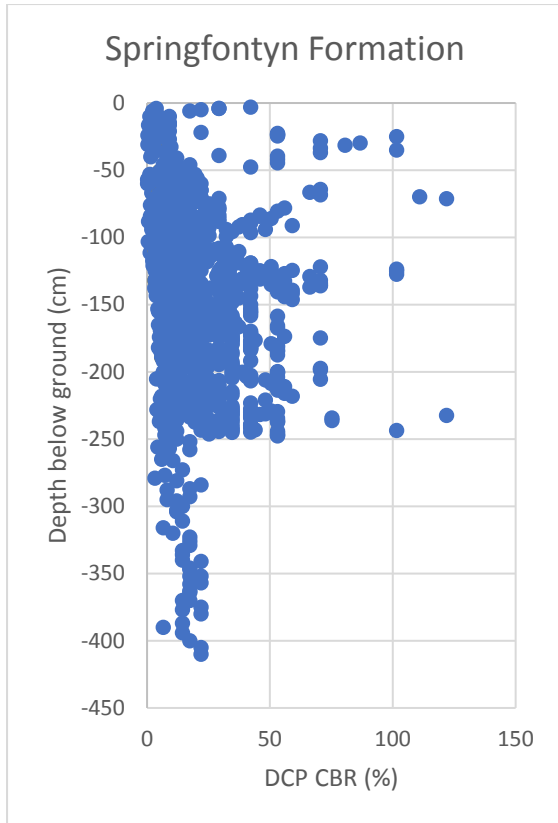


Figure G1: Springfontyn DCP CBR versus depth

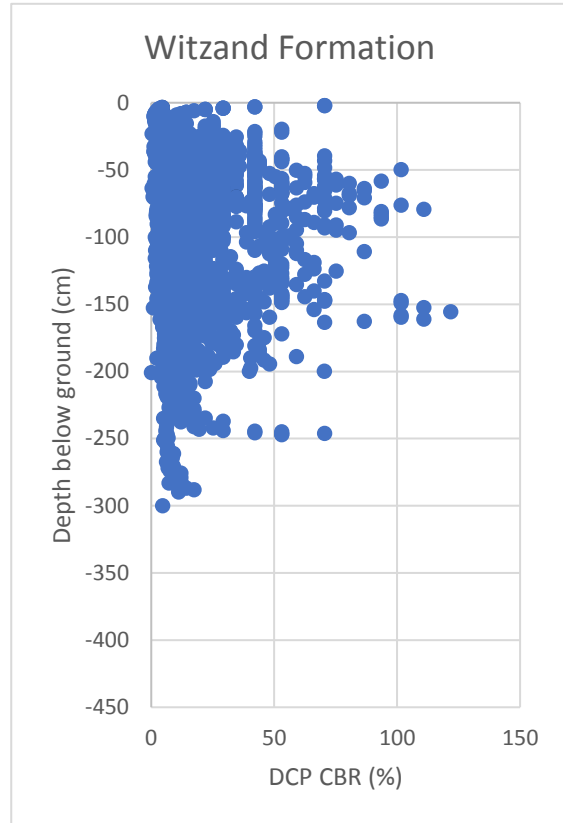


Figure G2: Witzand DCP CBR versus depth

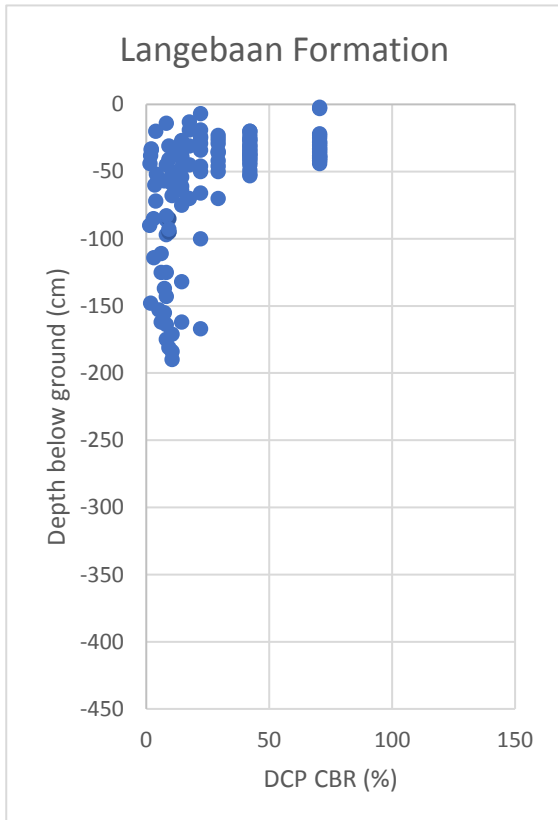
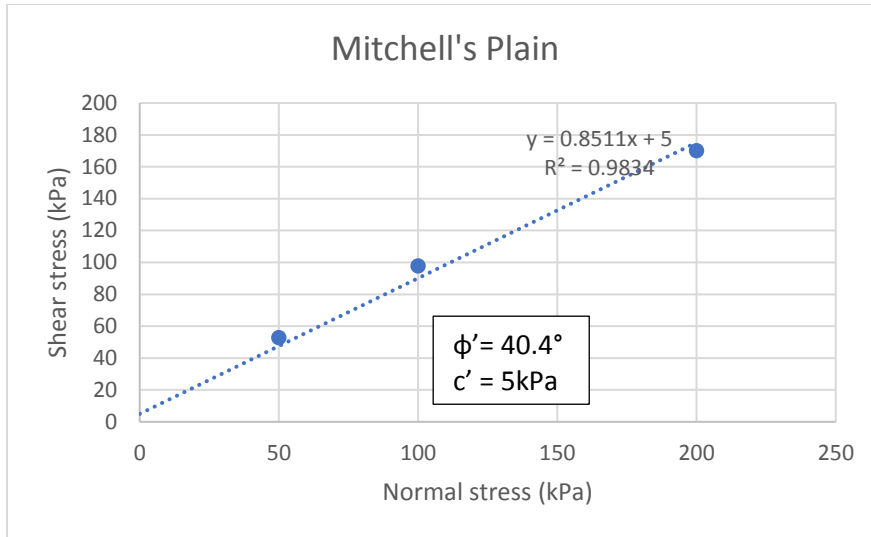
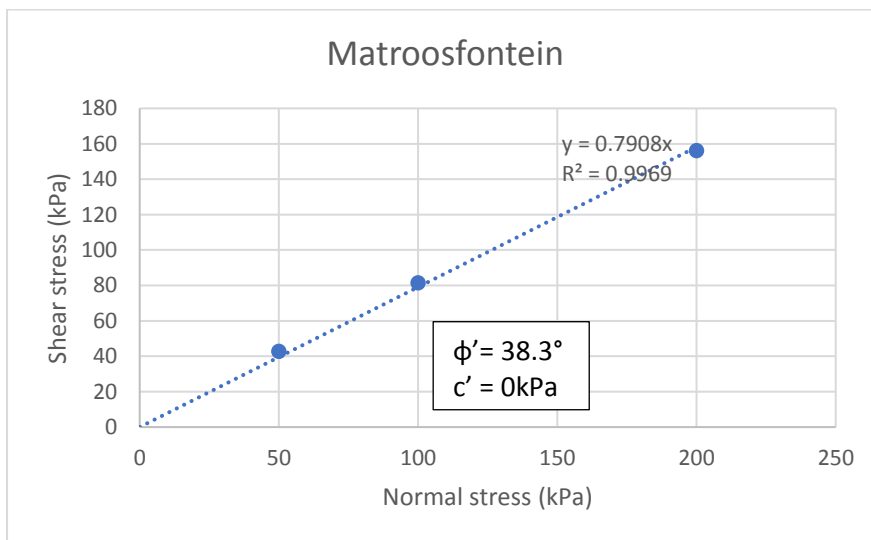


Figure G3: Langebaan DCP CBR versus depth



**Figure G4: Failure envelope of Mitchell's Plain sand**



**Figure G5: Failure envelope of Matroosfontein sand**

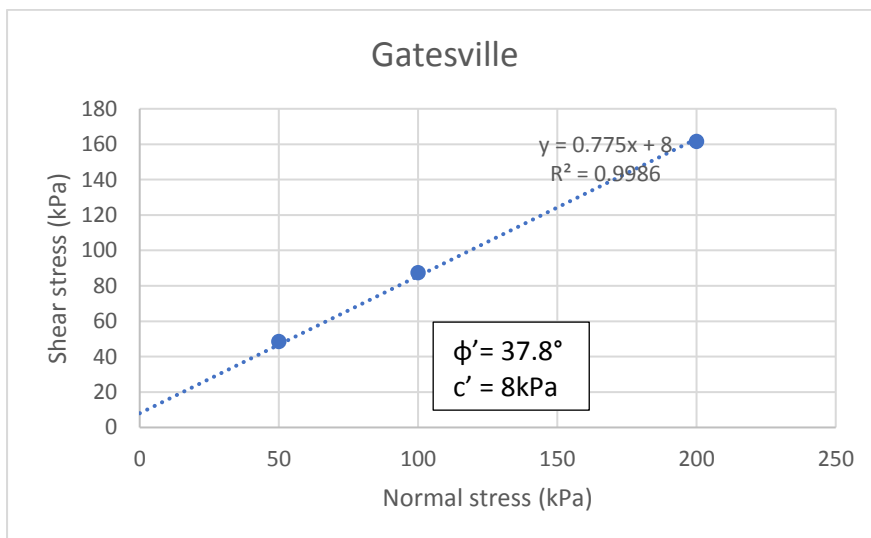


**Figure G6: Failure envelope of Gatesville sand**

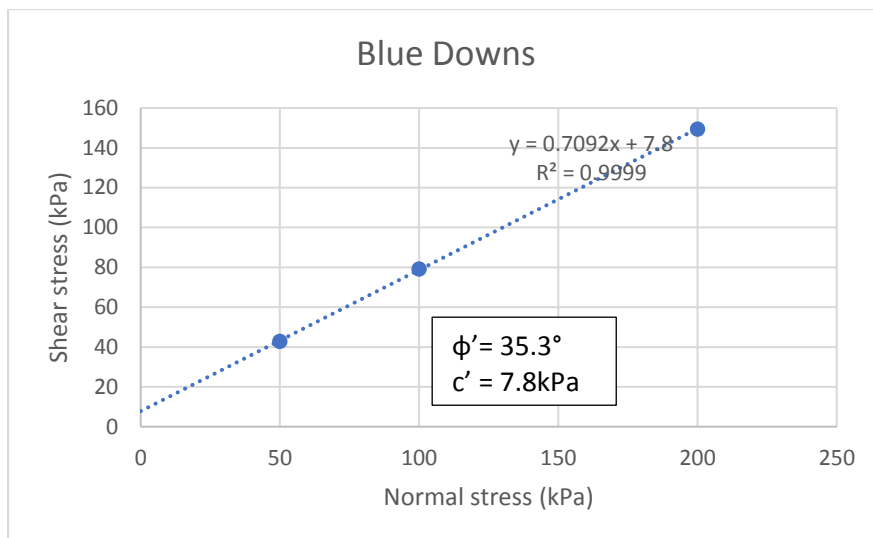


**Figure G7: Failure envelope of Blue Downs sand**

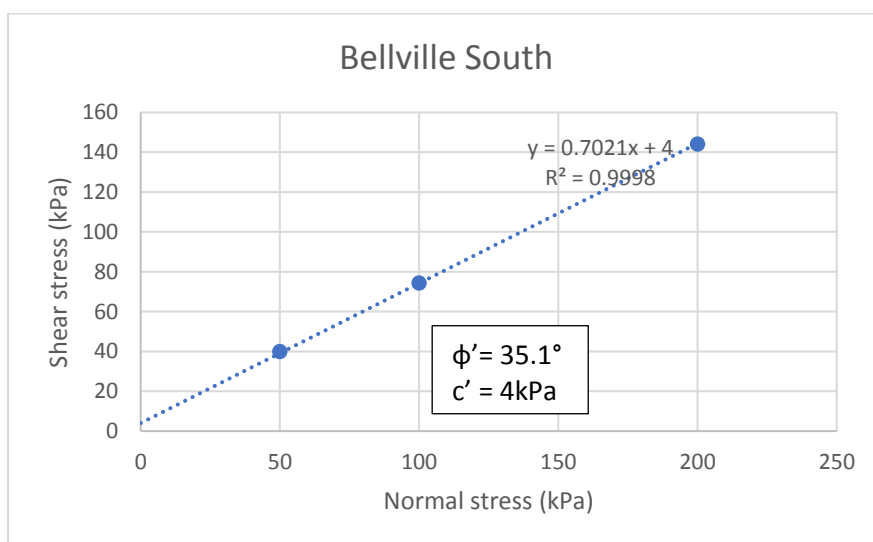


**Figure G8: Failure envelope of Bellville South sand**

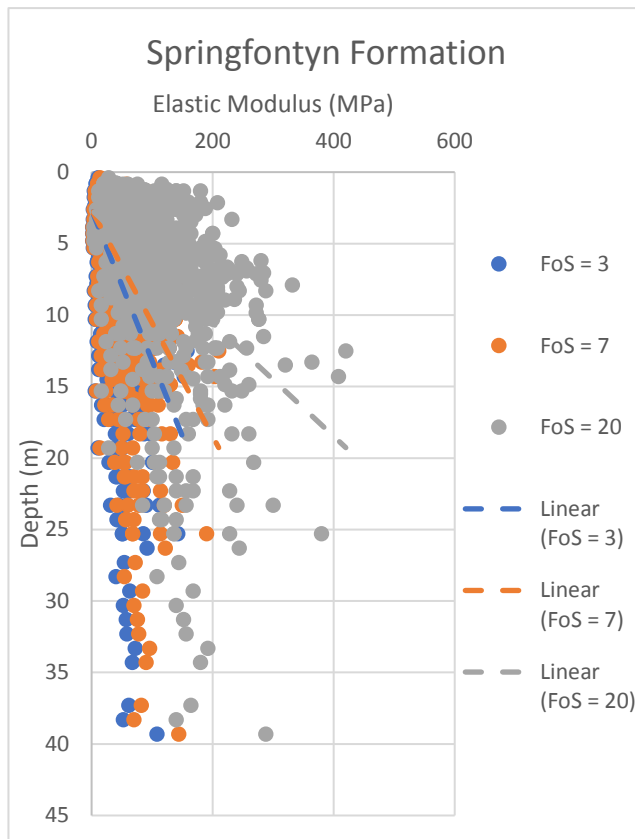


Figure G9: Sprinfontyn E modulus (Stroud, 1989)

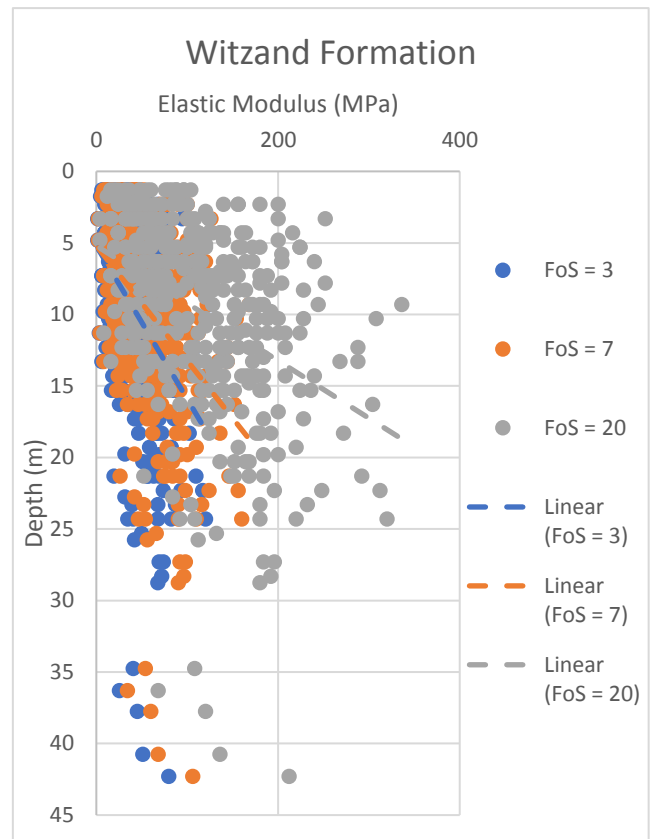


Figure G10: Witzand E modulus (Stroud, 1989)

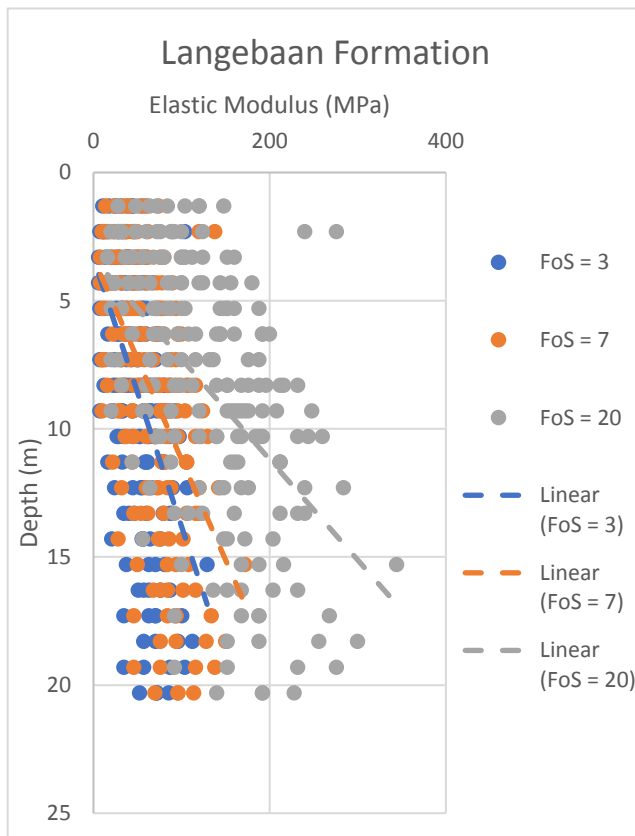


Figure G11: Langebaan E modulus (Stroud, 1989)

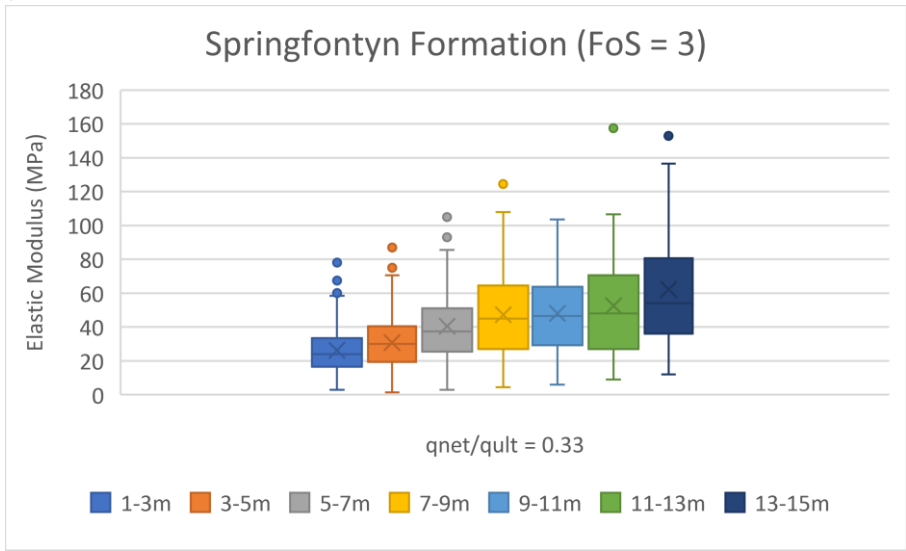


Figure G12: Overconsolidated sand: E modulus summary (Stroud, 1989), Springfontyn Formation (FoS = 3)

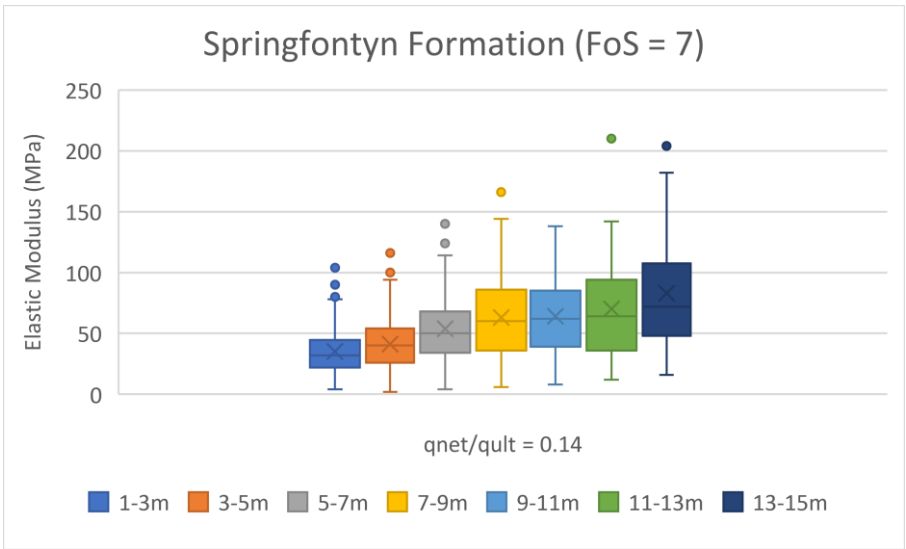


Figure G13: Overconsolidated sand: E modulus summary (Stroud, 1989), Springfontyn Formation (FoS = 7)

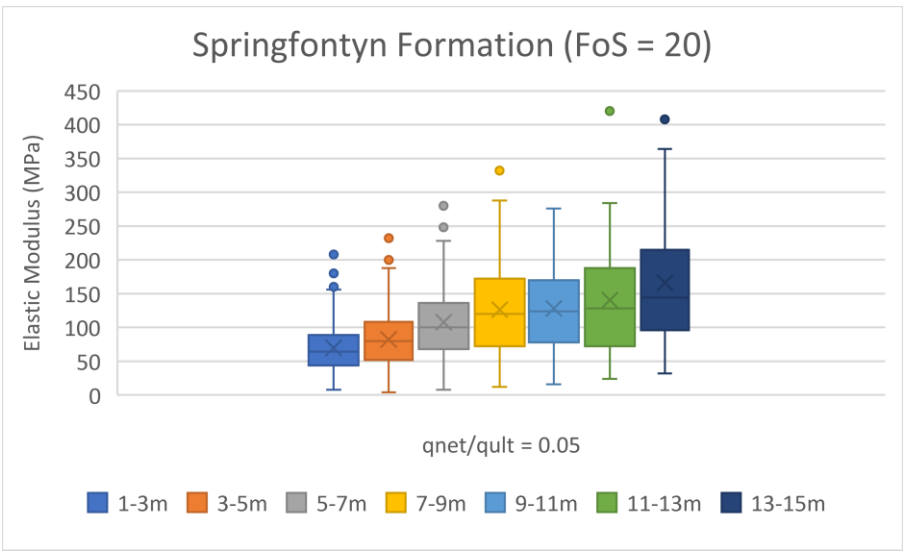


Figure G14: Overconsolidated sand: E modulus summary (Stroud, 1989), Springfontyn Formation (FoS = 20)

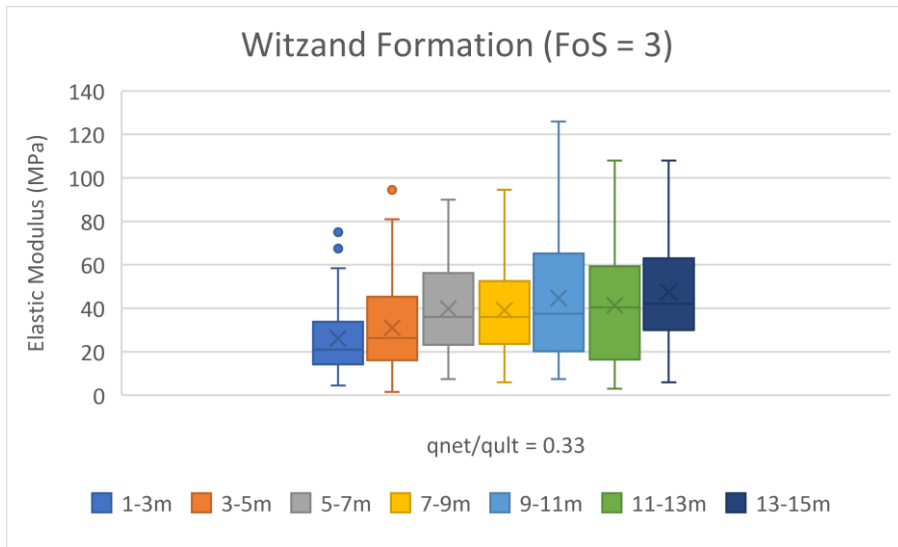


Figure G15: Overconsolidated sand: E modulus summary (Stroud, 1989), Witzand Formation (FoS = 3)

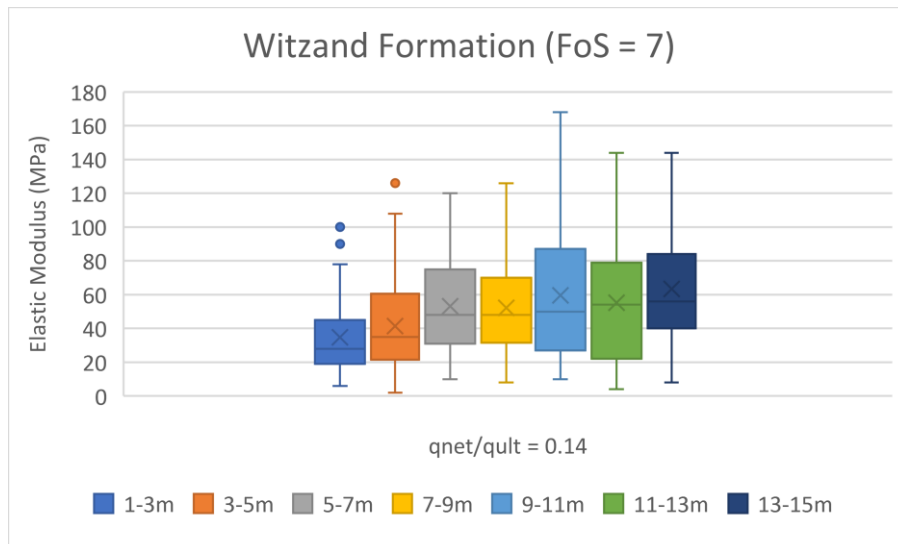


Figure G16: Overconsolidated sand: E modulus summary (Stroud, 1989), Witzand Formation (FoS = 7)

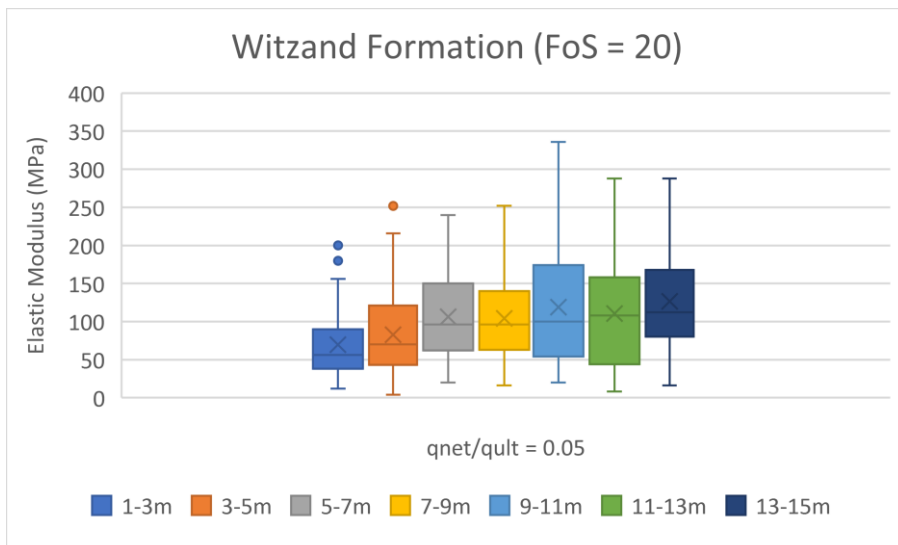
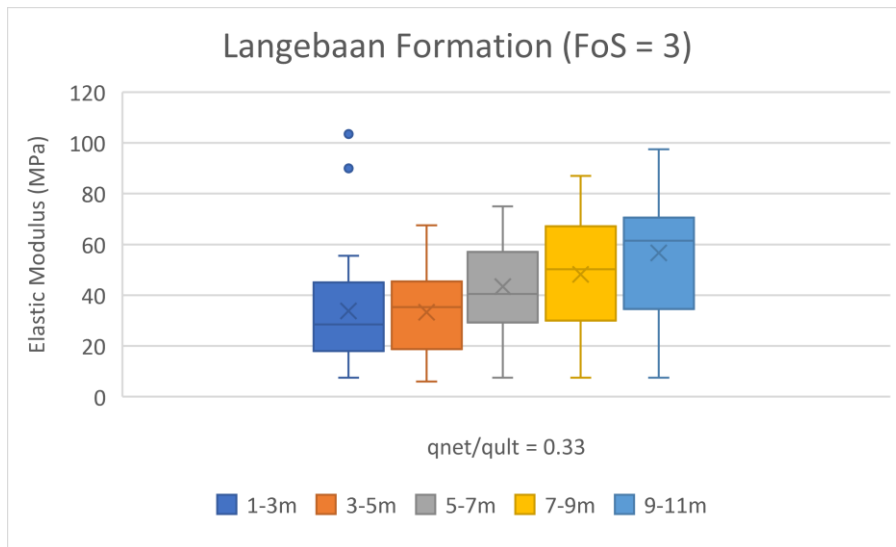
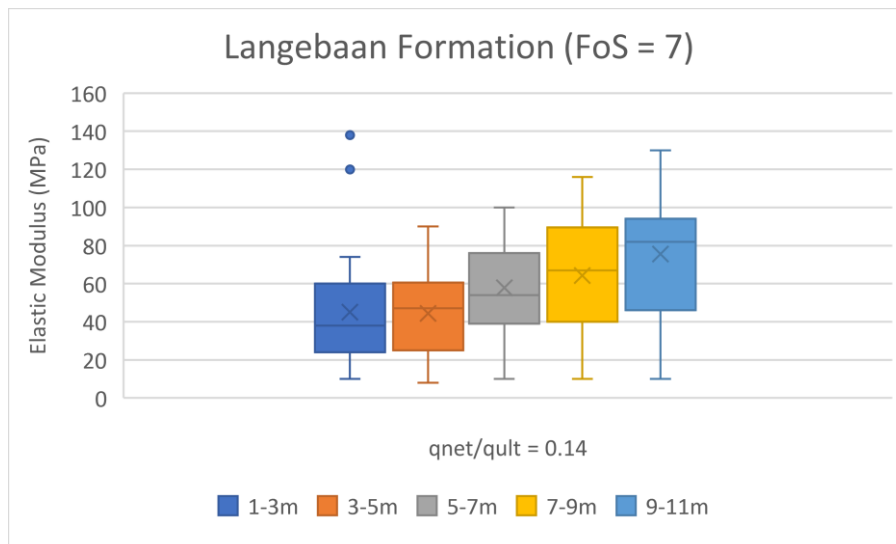


Figure G17: Overconsolidated sand: E modulus summary (Stroud, 1989), Witzand Formation (FoS = 20)



**Figure G18: Overconsolidated sand: E modulus summary (Stroud, 1989), Langebaan Formation (FoS = 3)**



**Figure G19: Overconsolidated sand: E modulus summary (Stroud, 1989), Langebaan Formation (FoS = 7)**

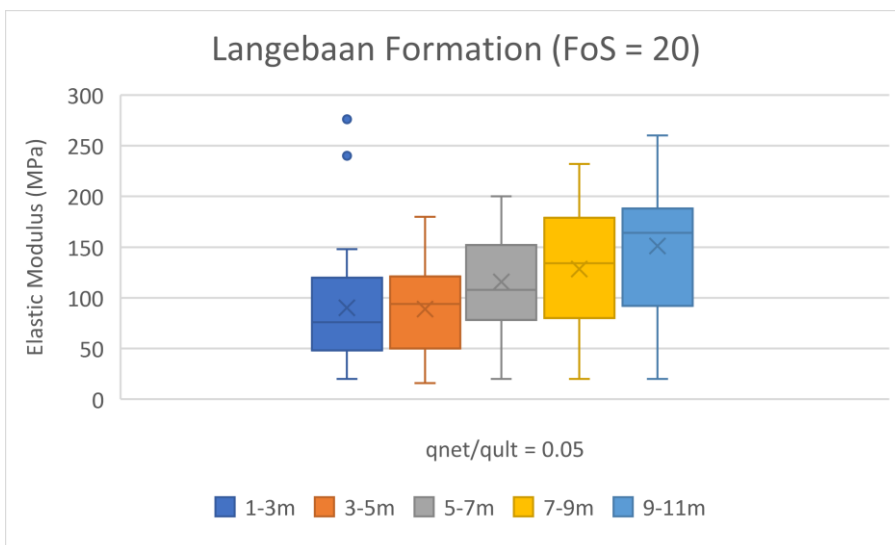


**Figure G20: Overconsolidated sand: E modulus summary (Stroud, 1989), Langebaan Formation (FoS = 20)**

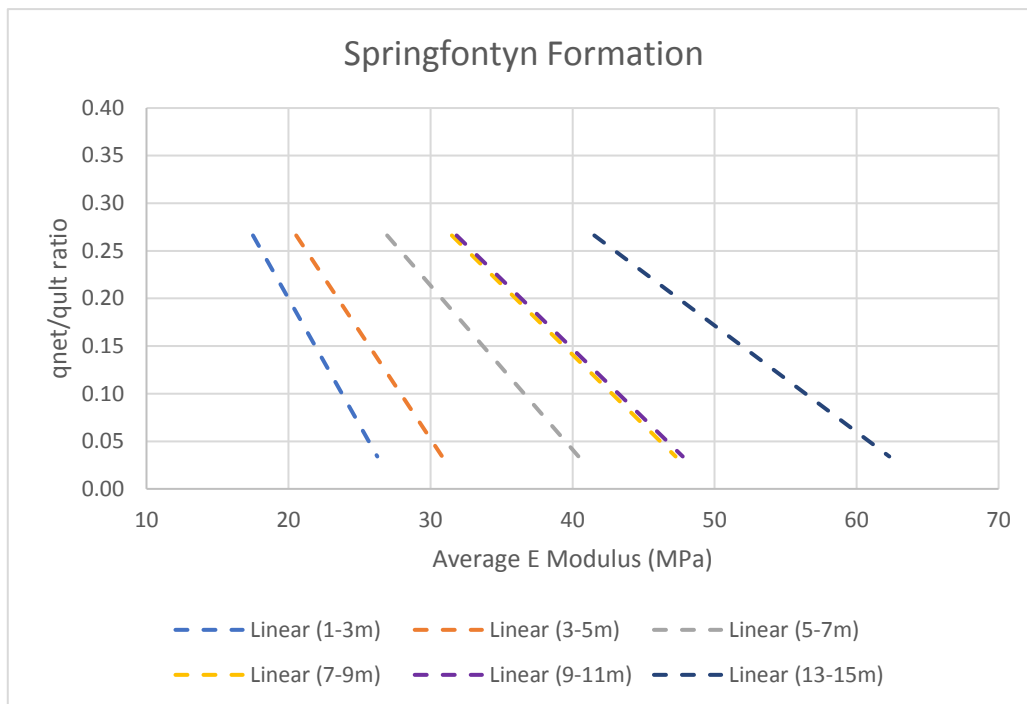


**Figure G21: Normally consolidated sand: Elastic modulus estimates for the Springfontyn Formation sands using Stroud’s (1989) method**

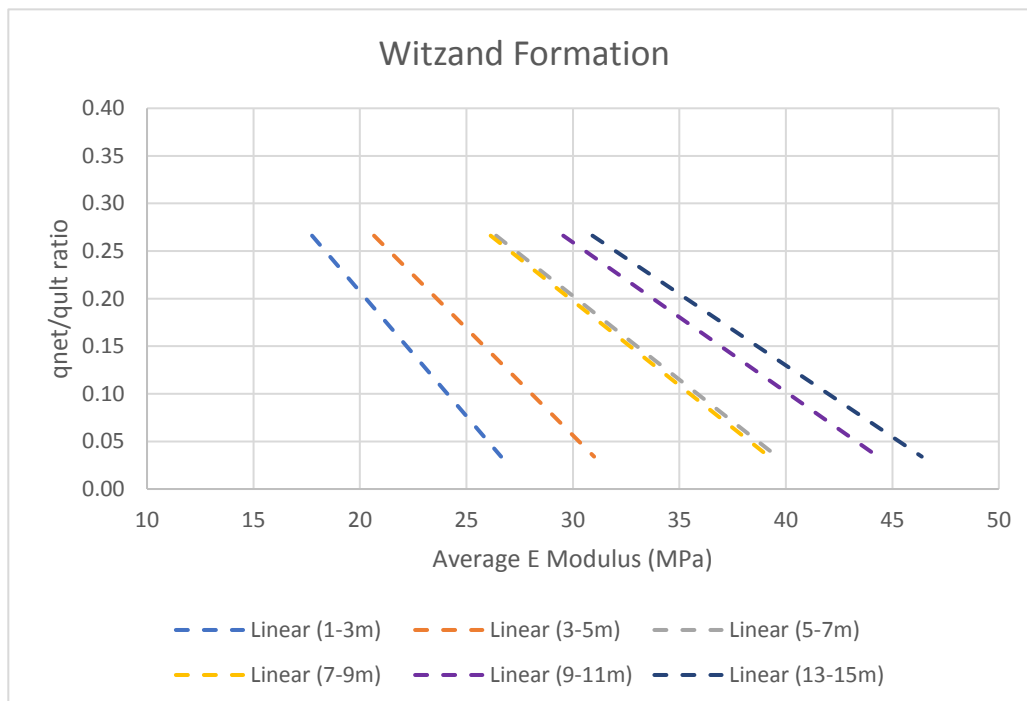


**Figure G22: Normally consolidated sand: Elastic modulus estimates for the Witzand Formation sands using Stroud’s (1989) method**

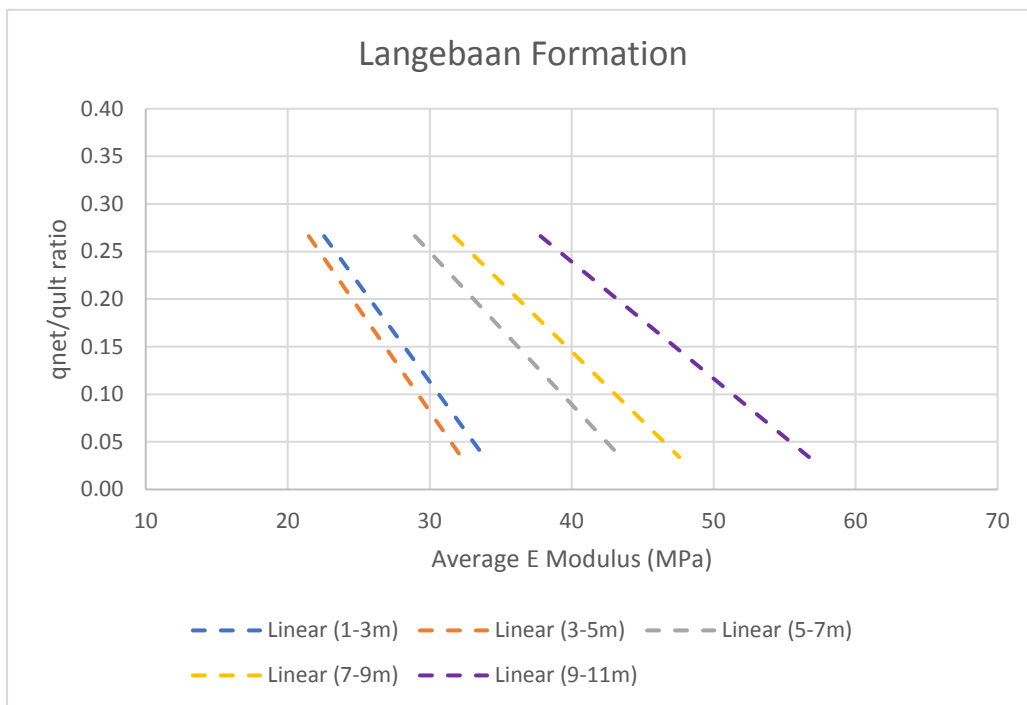


**Figure G23: Normally consolidated sand: Elastic modulus estimates for the Langebaan Formation sands using Stroud's (1989) method**

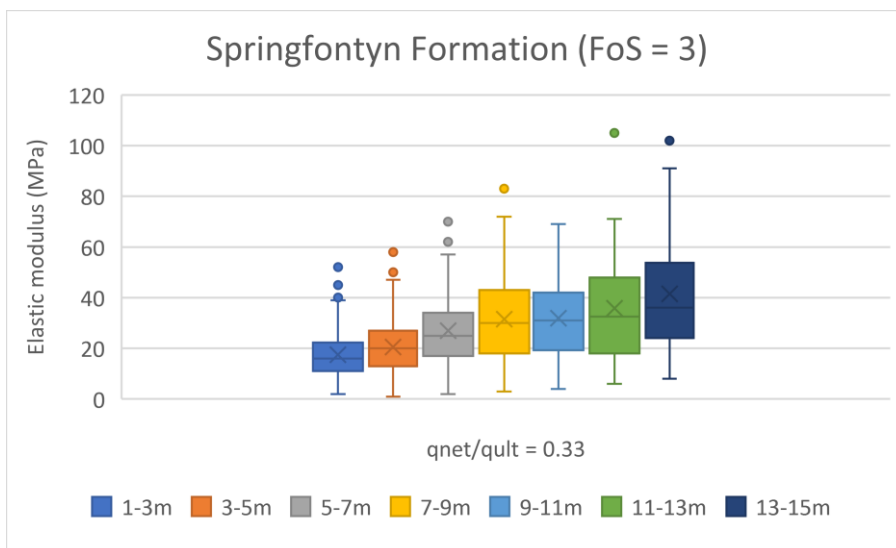


**Figure G24: Normally consolidated sand: E modulus summary (Stroud, 1989), Springfontyn Formation (FoS = 3)**

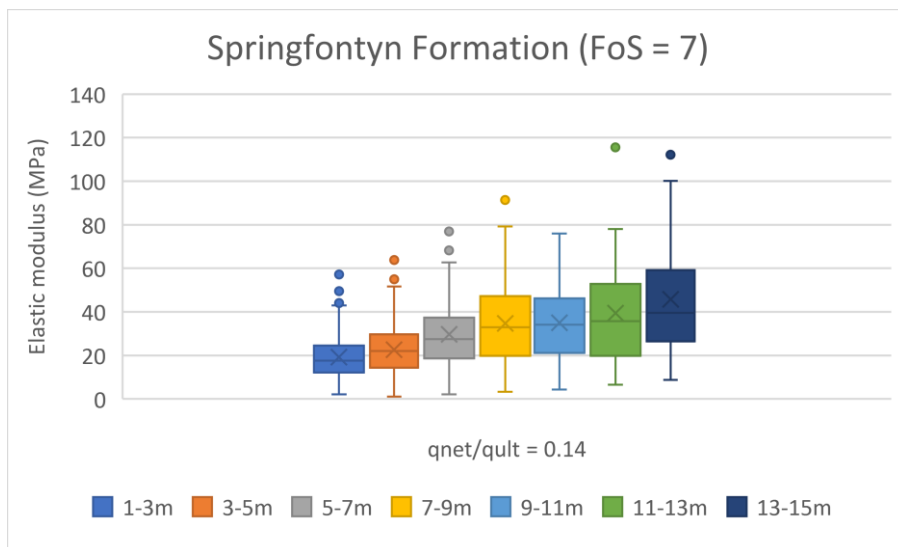


Figure G25: Normally consolidated sand: E modulus summary (Stroud, 1989), Springfontyn Formation (FoS = 7)

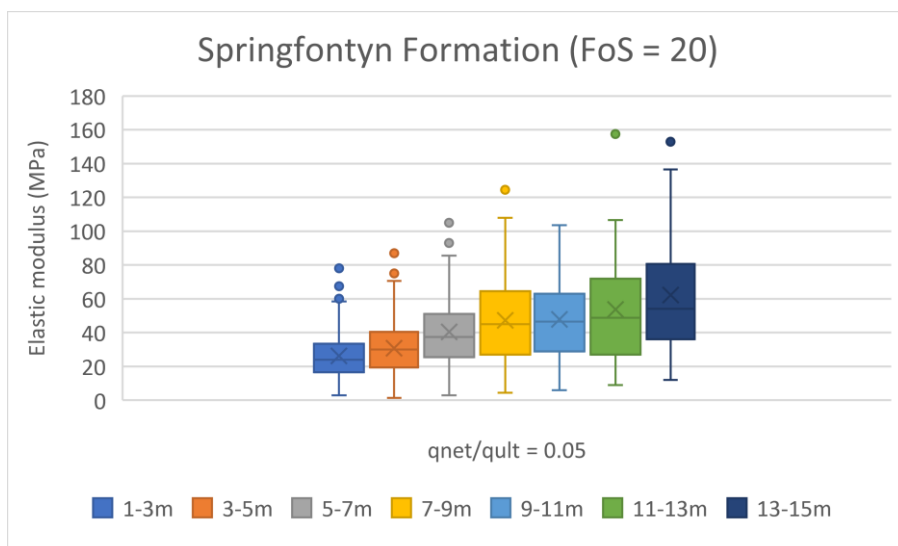


Figure G26: Normally consolidated sand: E modulus summary (Stroud, 1989), Springfontyn Formation (FoS = 20)

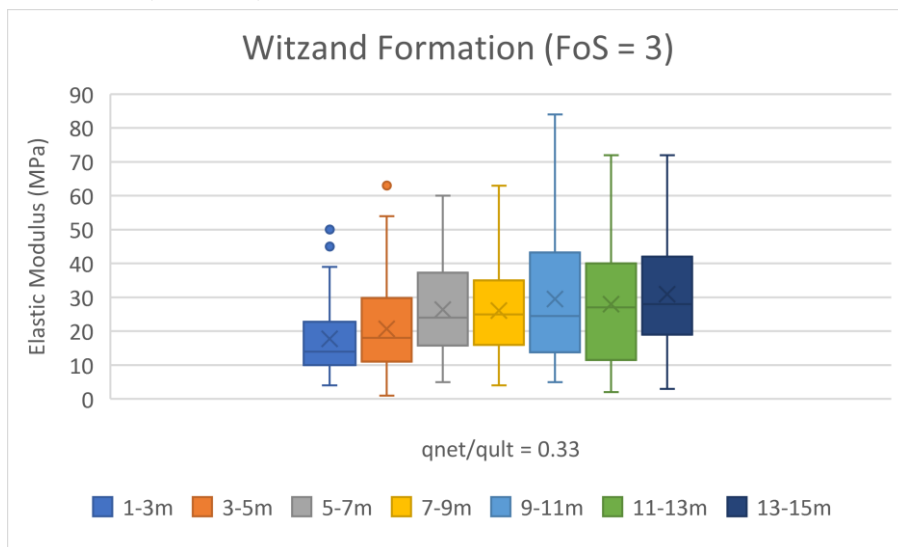


Figure G27: Normally consolidated sand: E modulus summary (Stroud, 1989), Witzand Formation (FoS = 3)

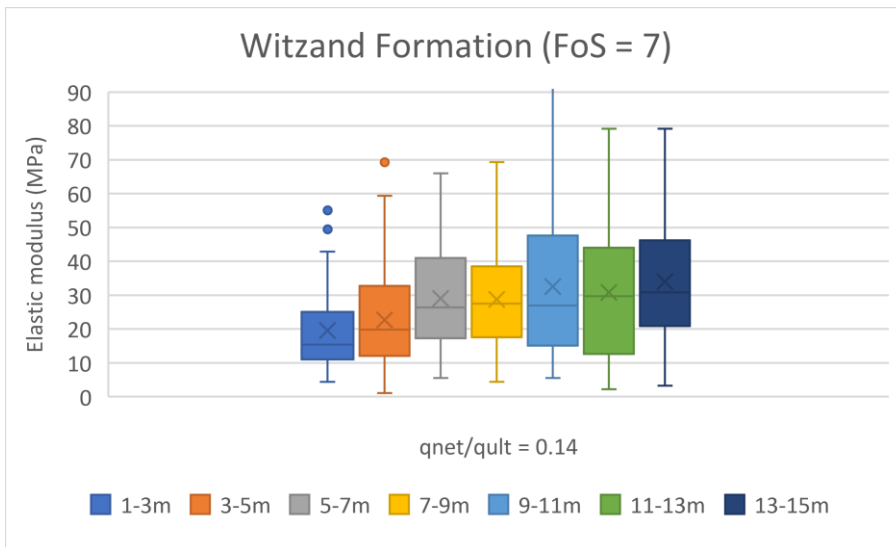


Figure G28: Normally consolidated sand: E modulus summary (Stroud, 1989), Witzand Formation (FoS = 7)

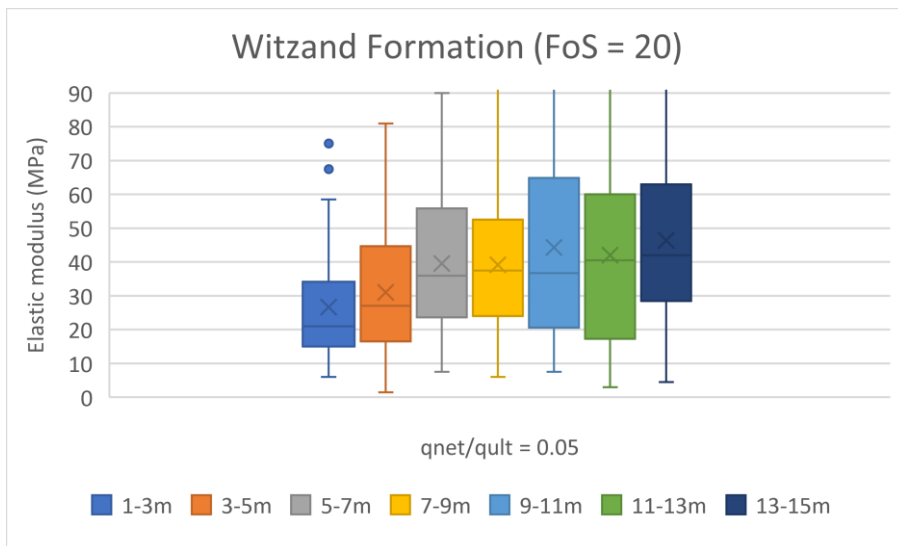


Figure G29: Normally consolidated sand: E modulus summary (Stroud, 1989), Witzand Formation (FoS = 20)

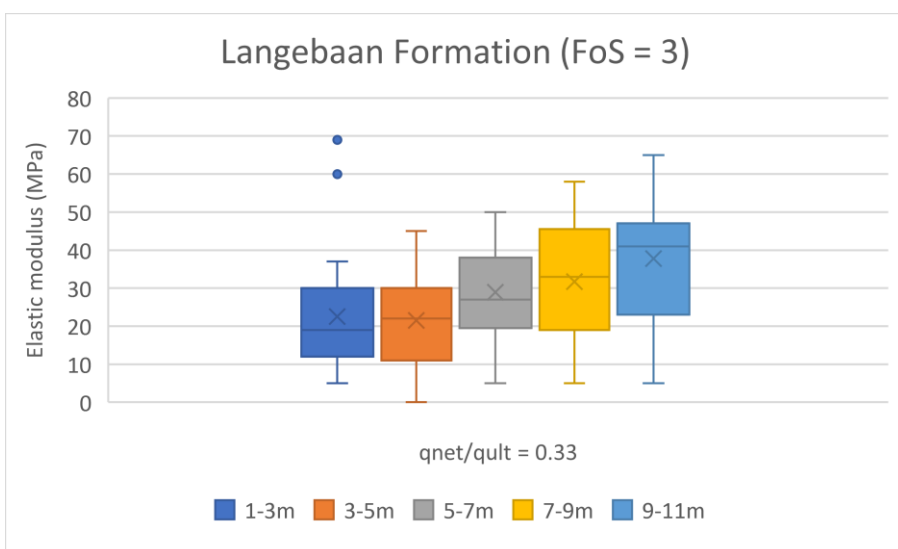
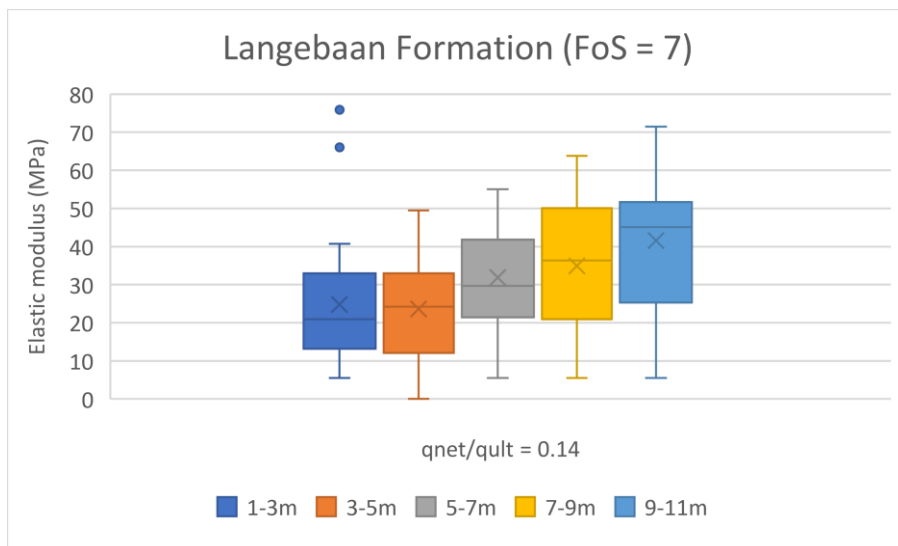
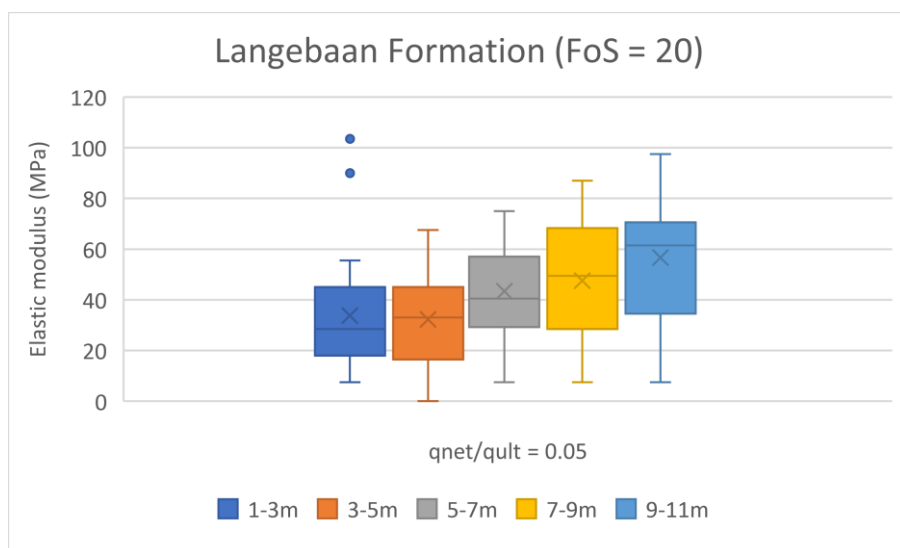


Figure G30: Normally consolidated sand: E modulus summary (Stroud, 1989), Langebaan Formation (FoS = 3)



**Figure G31: Normally consolidated sand: E modulus summary (Stroud, 1989), Langebaan Formation (FoS = 7)**



**Figure G32: Normally consolidated sand: E modulus summary (Stroud, 1989), Langebaan Formation (FoS = 20)**

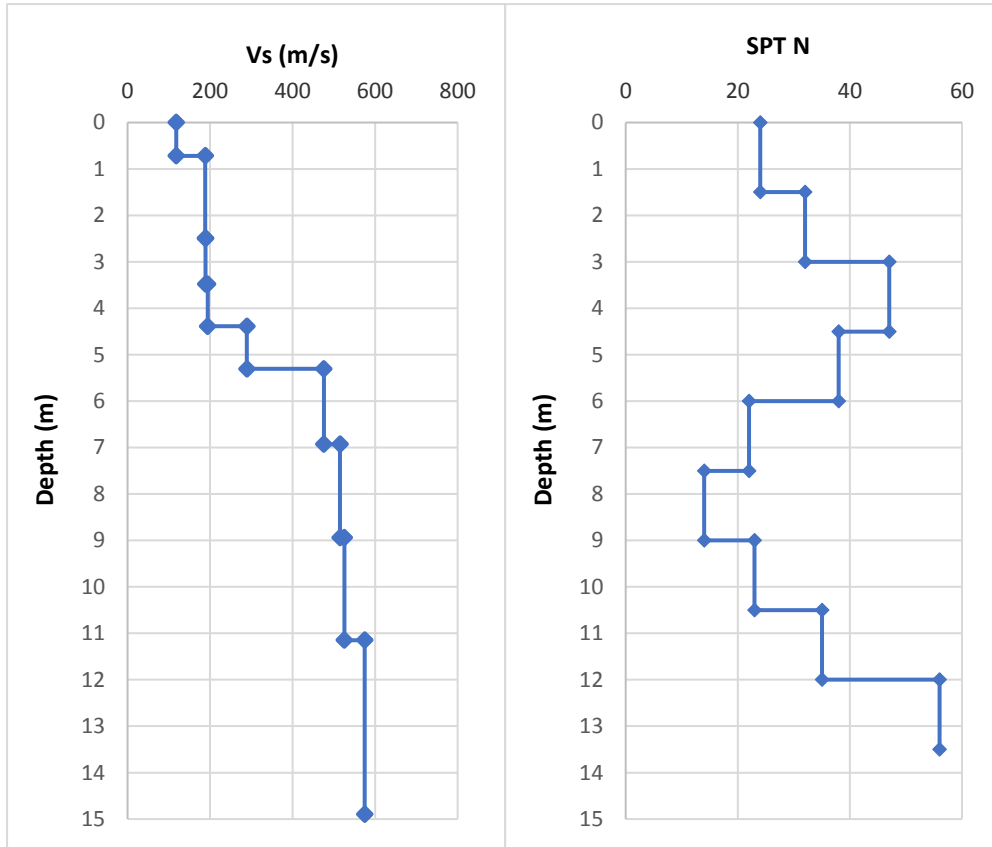


Figure G33: Cape Flats WWTW CSW 1 and SPT 1

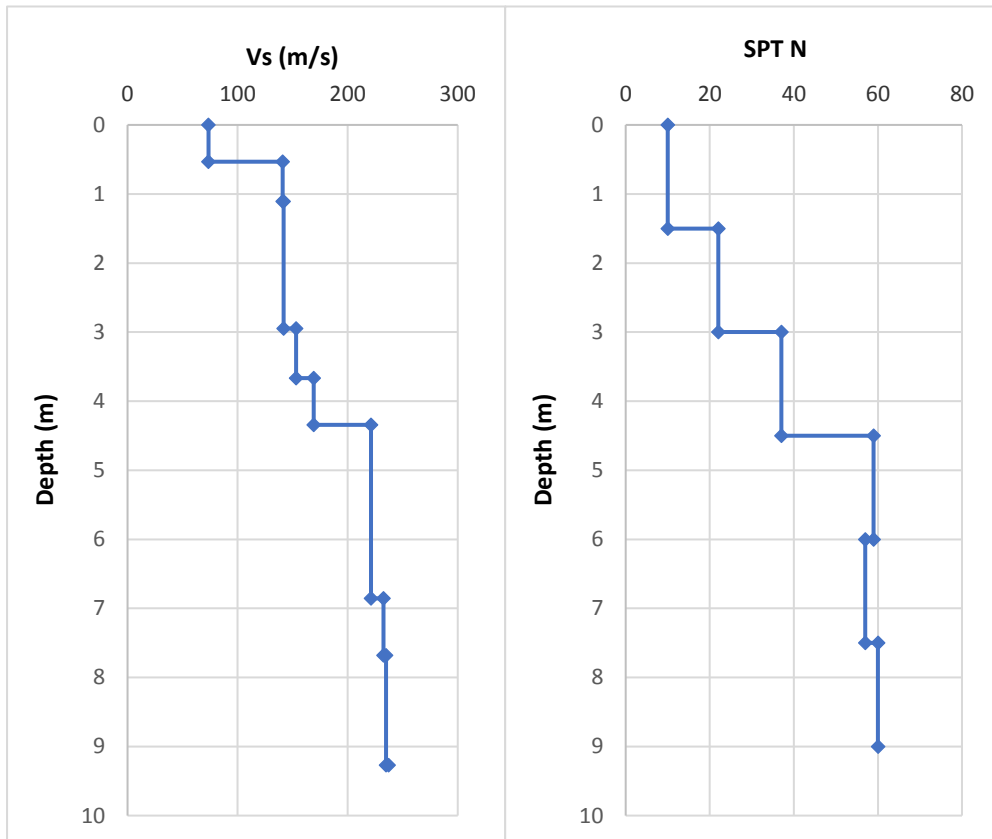


Figure G34: Cape Flats WWTW CSW 2 and SPT 2

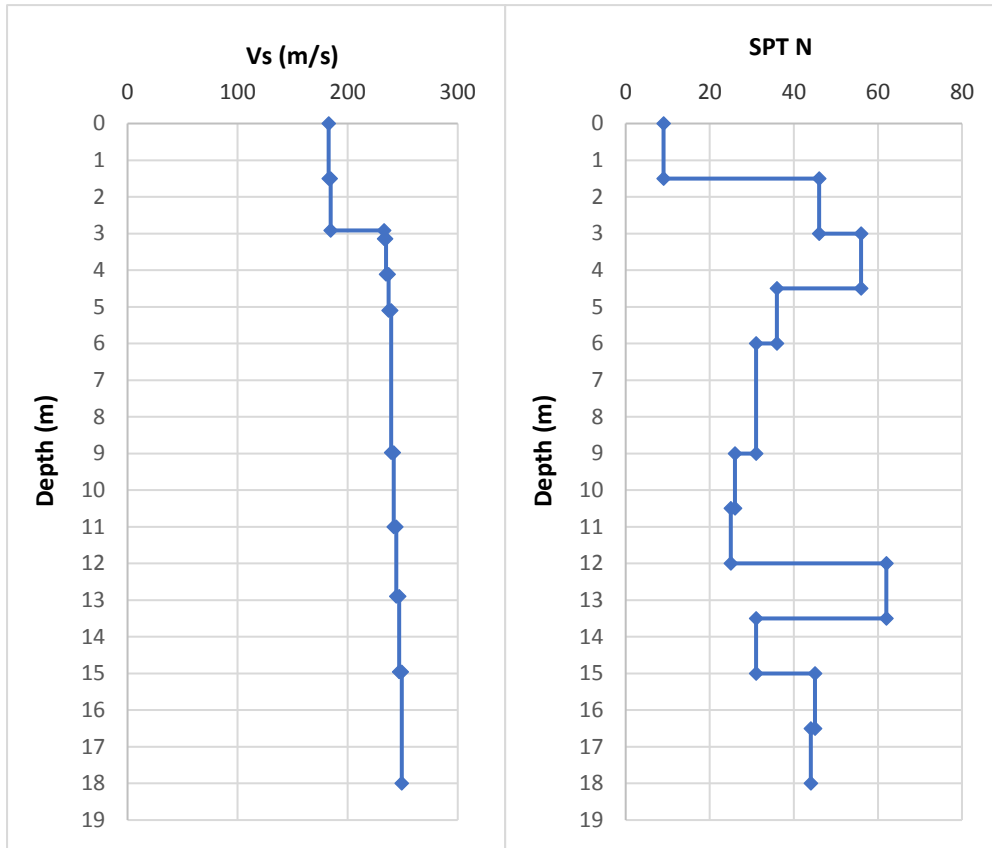


Figure G35: Cape Flats WWTW CSW 3 and SPT 3

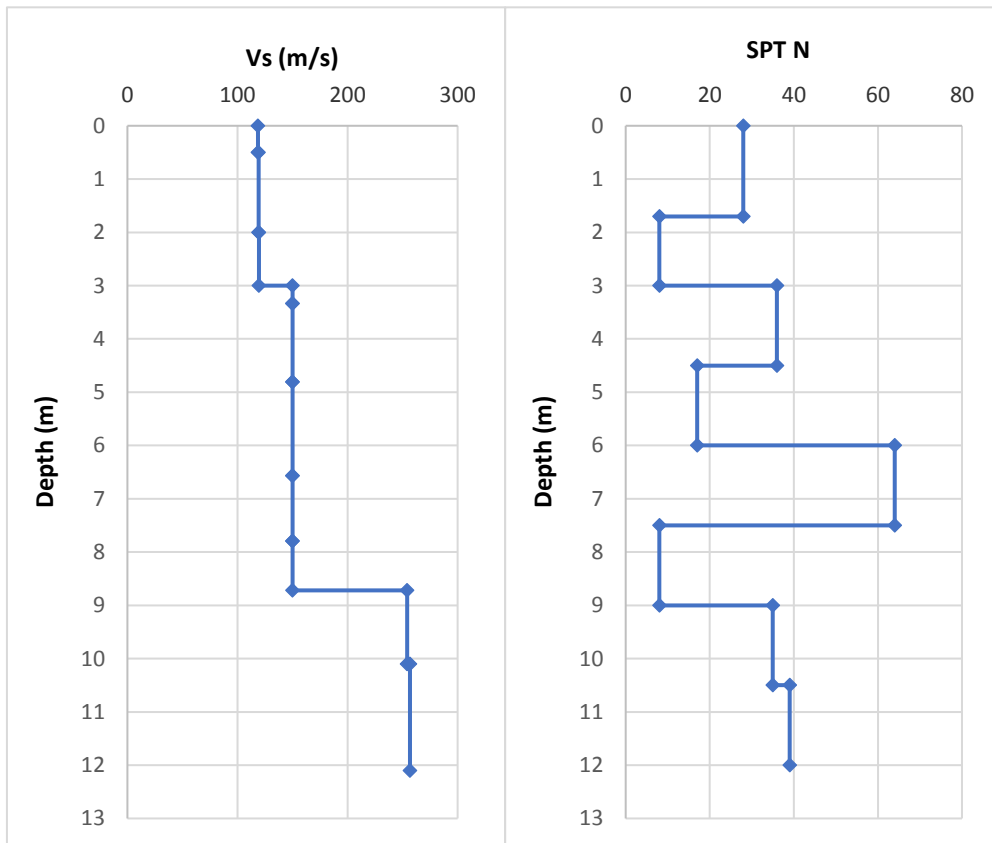


Figure G36: Athlone WWTW CSW 4 and SPT 4

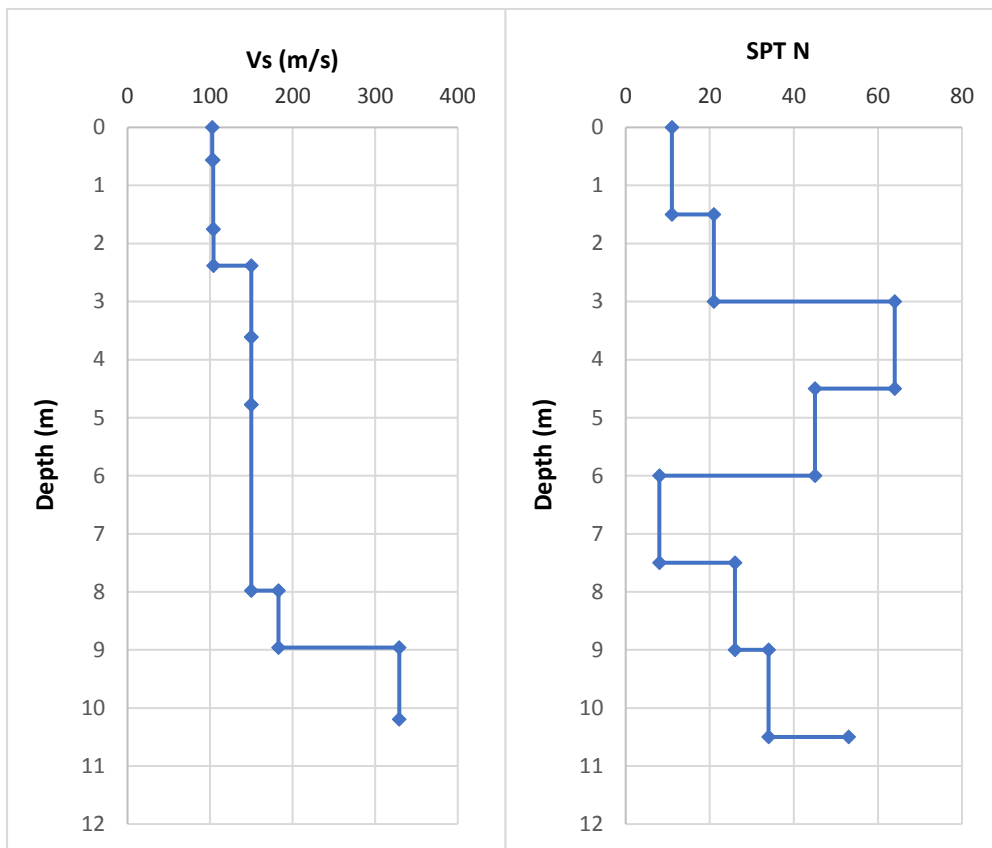


Figure G37: Athlone WWTW CSW 5 and SPT 5

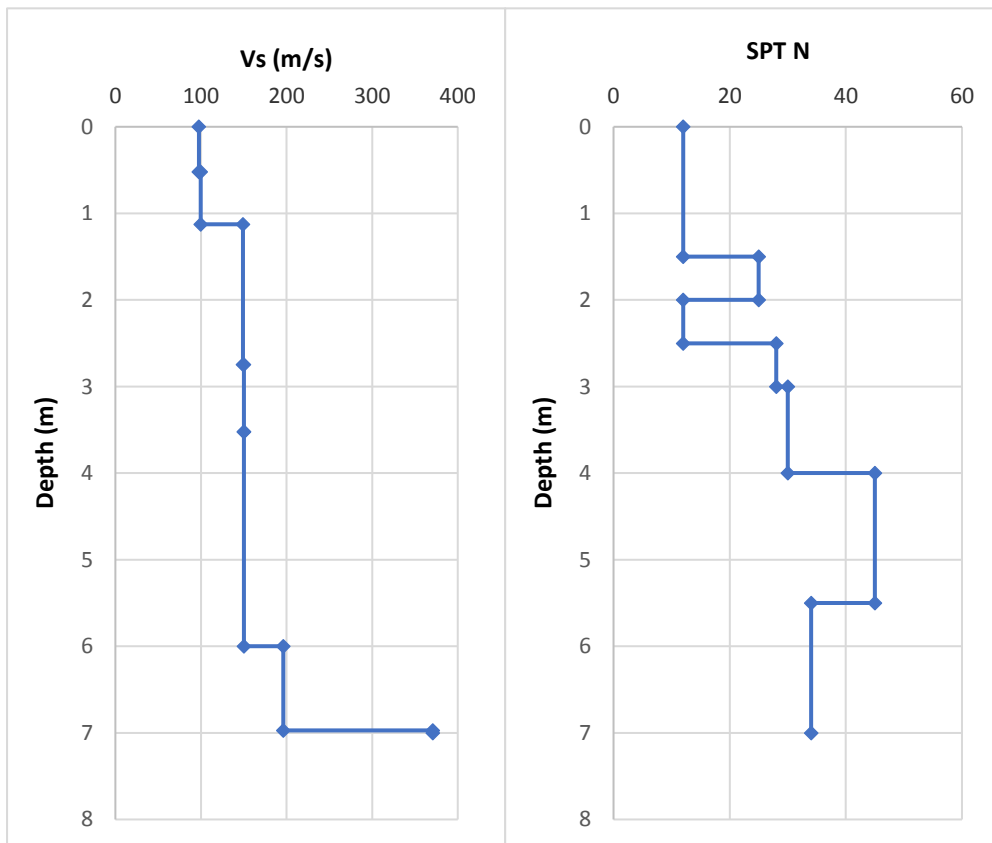


Figure G38: Athlone WWTW CSW 6 and SPT 6

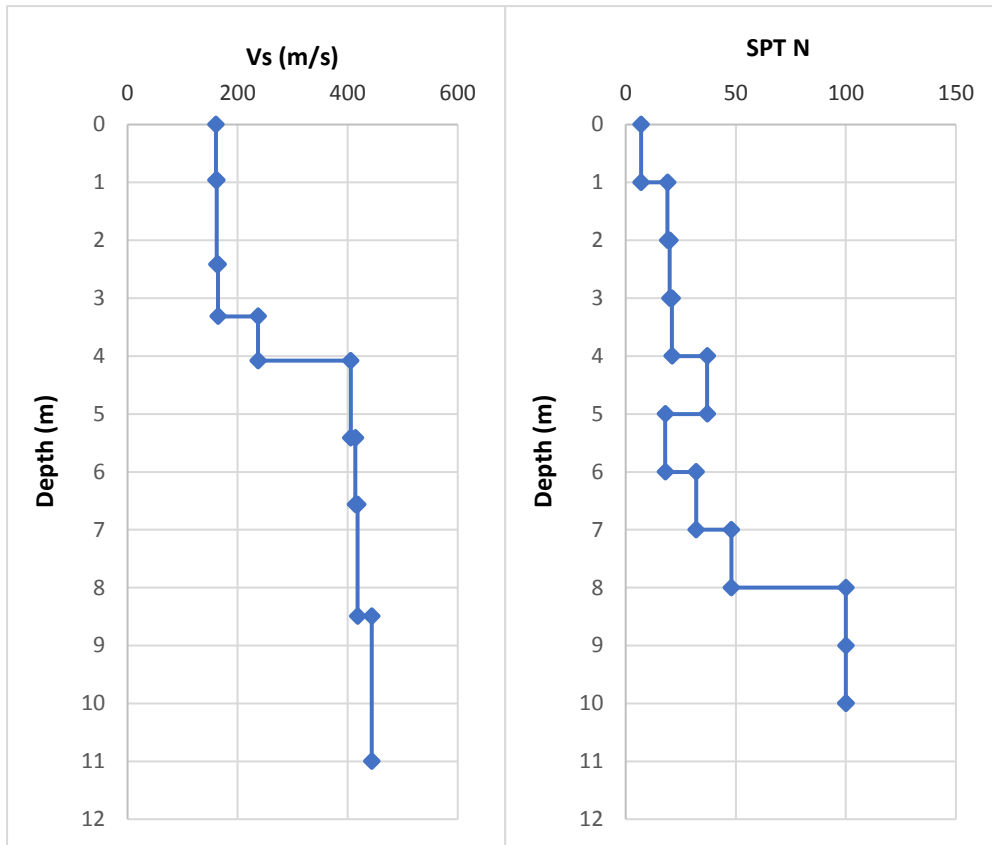


Figure G39: Atlantis CSW 7 and SPT 7

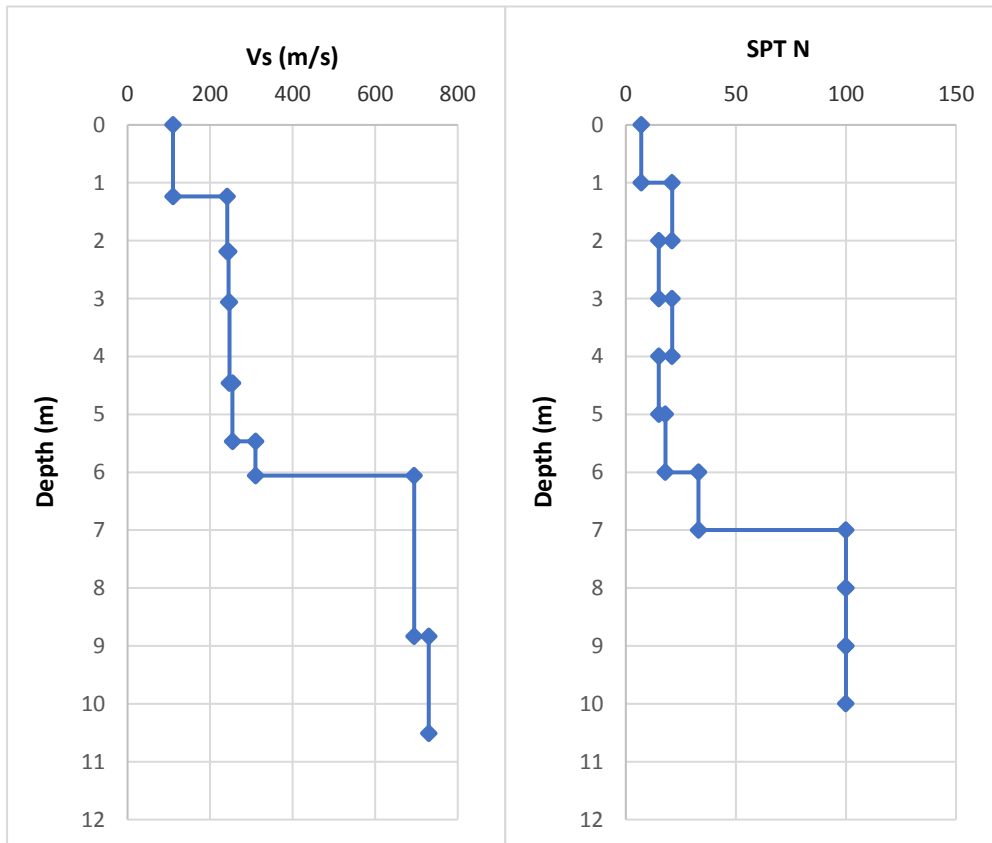


Figure G40: Atlantis CSW 8 and SPT 8

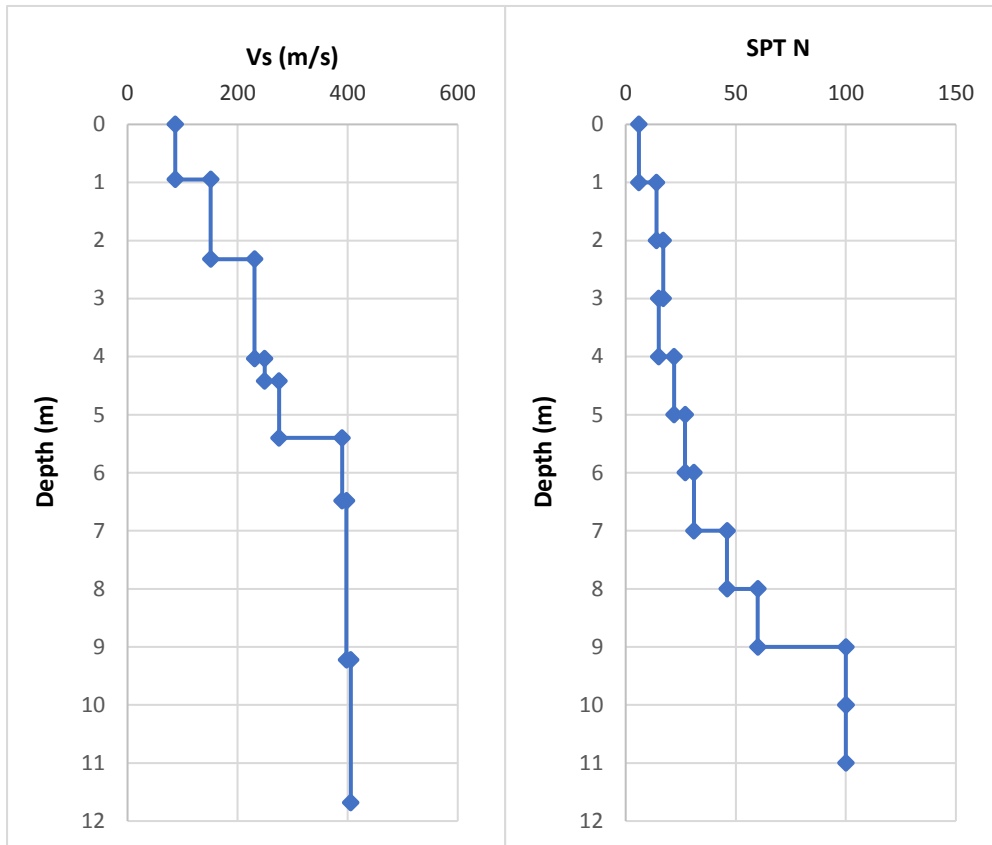


Figure G41: Atlantis CSW 9 and SPT 9

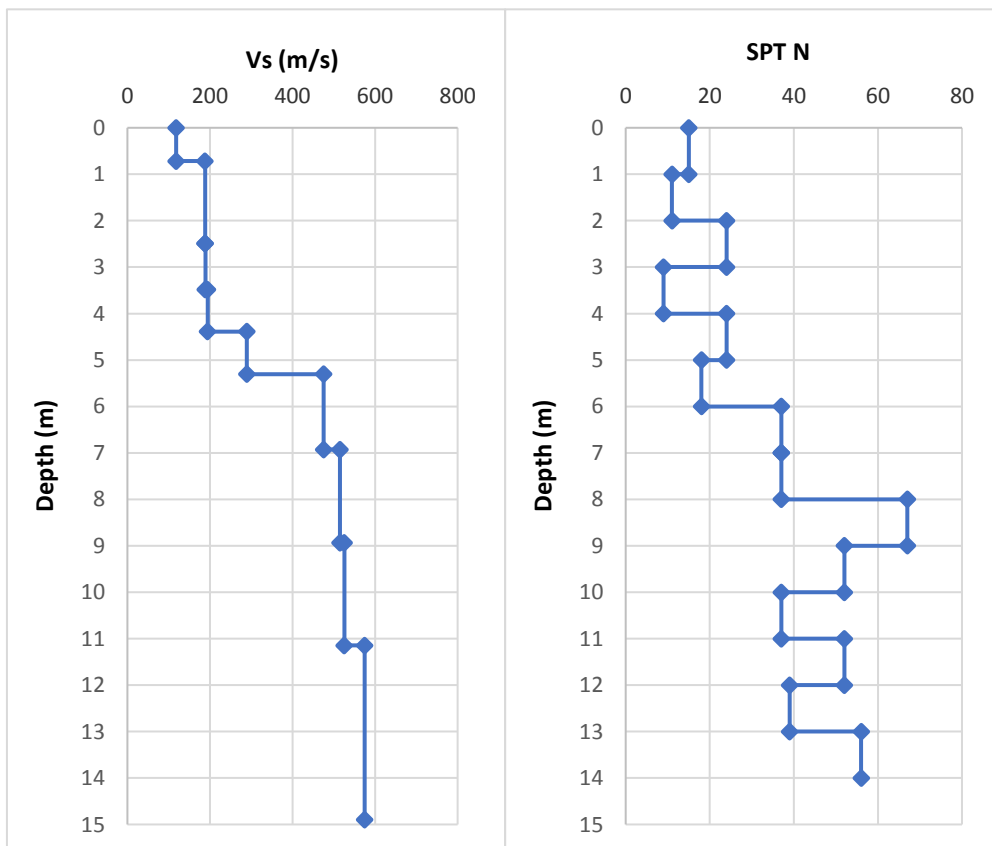


Figure G42: Atlantis CSW 10 and SPT 10

## Appendix H: Elastic moduli - Stroud (1989) and Webb (1969)

**Stroud (1989)**Loose profile

	Net pressure (qn) (kPa)	50		100		250	
	Foundation shape	Square	Strip	Square	Strip	Square	Strip
	E/N ratio	3.3	2.9	2	1.9	1.5	1.5
Depth (m)	SPT N60	Elastic modulus (MPa)					
1.3	2	7	6	4	4	3	3
2.3	4	13	12	8	8	6	6
3.3	5	17	15	10	10	7.5	8
4.3	5	17	15	10	10	7.5	8
5.3	5	17	15	10	10	7.5	8
6.3	7	23	20	14	13	10.5	11
7.3	5	17	15	10	10	7.5	8
8.3	7	23	20	14	13	10.5	11
9.3	4	13	12	8	8	6	6
10.3	8	26	23	16	15	12	12
11.3	9	30	26	18	17	13.5	14
12.3	10	33	29	20	19	15	15

Medium dense profile

	Net pressure (qn) (kPa)	50		100		250		500	
	Foundation shape	Square	Strip	Square	Strip	Square	Strip	Square	Strip
	E/N ratio	5	4	3.2	2.7	1.9	1.6	1.5	1.5
Depth (m)	SPT N60	Elastic modulus (MPa)							
1.3	12	60	48	38	32	23	19	18	18
2.3	8	40	32	26	22	15	13	12	12
3.3	10	50	40	32	27	19	16	15	15
4.3	8	40	32	26	22	15	13	12	12
6.3	17	85	68	54	46	32	27	26	26
7.3	25	125	100	80	68	48	40	38	38
8.3	15	75	60	48	41	29	24	23	23
9.3	12	60	48	38	32	23	19	18	18
11.3	14	70	56	45	38	27	22	21	21
12.3	30	150	120	96	81	57	48	45	45
13.3	32	160	128	102	86	61	51	48	48

Dense profile

	Net pressure (qn) (kPa)	50		100		250		500	
	Foundation shape	Square	Strip	Square	Strip	Square	Strip	Square	Strip
	E/N ratio	6	5.2	4.8	4	2.4	2	1.8	1.6
Depth (m)	SPT N60	Elastic modulus (MPa)							
1.3	21	126	109	101	84	50	42	38	34
2.3	19	114	99	91	76	46	38	34	30
3.3	20	120	104	96	80	48	40	36	32
4.3	36	216	187	173	144	86	72	65	58
5.3	36	216	187	173	144	86	72	65	58
6.3	27	162	140	130	108	65	54	49	43
7.3	33	198	172	158	132	79	66	59	53
8.3	35	210	182	168	140	84	70	63	56
9.3	39	234	203	187	156	94	78	70	62
10.3	46	276	239	221	184	110	92	83	74
11.3	40	240	208	192	160	96	80	72	64
12.3	44	264	229	211	176	106	88	79	70
13.3	56	336	291	269	224	134	112	101	90

**Webb (1969)**Loose profile

Depth (m)	SPT N60	E Modulus (MPa)
1.3	2	9
2.3	4	10
3.3	5	11
4.3	5	11
5.3	5	11
6.3	7	12
7.3	5	11
8.3	7	12
9.3	4	10
10.3	8	12
11.3	9	13
12.3	10	13

Medium dense profile

Depth (m)	SPT N60	E Modulus (MPa)
1.3	12	14
2.3	8	12
3.3	10	13
4.3	8	12
6.3	17	17
7.3	25	21
8.3	15	16
9.3	12	14
11.3	14	16
12.3	30	24
13.3	32	25

Dense profile

Depth (m)	SPT N60	E Modulus (MPa)
1.3	21	19
2.3	19	18
3.3	20	19
4.3	36	27
5.3	36	27
6.3	27	23
7.3	33	26
8.3	35	27
9.3	39	29
10.3	46	33
11.3	40	30
12.3	44	32
13.3	56	38